THIS DOCUMENT PROVIDED BY THE ABBOTT AEROSPACE
TECHNICAL LIBRARY
ABBOTTAEROSPACE.COM

LEVEL II

AGARD-CP-288

AGARD-CP-288

AGARD

ADVISORY GROUP FOR AEROSPACE RESEARCH & DEVELOPMENT

7 RUE ANCELLE 92200 NEUILLY SUR SEINE FRANCE

AD A090311

AGARD Conference Proceedings No.288

Effect of Service Environment on Composite Materials

DISTRIBUTION STATEMENT A
Approved for public release;
Distribution Unlimited

DTIC
ELECTE
OCT 15 1980

NORTH ATLANTIC TREATY ORGANIZATION

DDC FILE COPY

DISTRIBUTION AND AVAILABILITY
ON BACK COVER

80 10 00 001

THIS DOCUMENT PROVIDED BY THE ABBOTT AEROSPACE
TECHNICAL LIBRARY
ABBOTTAEROSPACE.COM

AGARD-CP-288

NORTH ATLANTIC TREATY ORGANIZATION

ADVISORY GROUP FOR AEROSPACE RESEARCH AND DEVELOPMENT

(ORGANISATION DU TRAITE DE L'ATLANTIQUE NORD)

DTIC
ELECTE
OCT 15 1980
S
C
D

AGARD Conference Proceedings No.288

EFFECT OF SERVICE ENVIRONMENT ON COMPOSITE MATERIALS

Conference proceedings

Aug 80

326

DISTRIBUTION STATEMENT A
Approved for public release;
Distribution Unlimited

Papers presented at the 50th Meeting of the AGARD Structures and Materials Panel, held in Athens, Greece on 14–17 April 1980.

JOB

TECHNICAL LIBRARY
ABBOTTAEROSPACE.COM

THE MISSION OF AGARD

The mission of AGARD is to bring together the leading personalities of the NATO nations in the fields of science and technology relating to aerospace for the following purposes:

- Exchanging of scientific and technical information;
- Continuously stimulating advances in the aerospace sciences relevant to strengthening the common defence posture;
- Improving the co-operation among member nations in aerospace research and development;
- Providing scientific and technical advice and assistance to the North Atlantic Military Committee in the field of aerospace research and development;
- Rendering scientific and technical assistance, as requested, to other NATO bodies and to member nations in connection with research and development problems in the aerospace field,
- Providing assistance to member nations for the purpose of increasing their scientific and technical potential;
- Recommending effective ways for the member nations to use their research and development capabilities for the common benefit of the NATO community.

The highest authority within AGARD is the National Delegates Board consisting of officially appointed senior representatives from each member nation. The mission of AGARD is carried out through the Panels which are composed of experts appointed by the National Delegates, the Consultant and Exchange Programme and the Aerospace Applications Studies Programme. The results of AGARD work are reported to the member nations and the NATO Authorities through the AGARD series of publications of which this is one.

Participation in AGARD activities is by invitation only and is normally limited to citizens of the NATO nations.

The content of this publication has been reproduced
directly from material supplied by AGARD or the authors.

Published August 1980

Copyright © AGARD 1980
All Rights Reserved

ISBN 92-835-0273-6

Printed by Technical Editing and Reproduction Ltd
Harford House, 7–9 Charlotte St, London, W1P 1HD

TECHNICAL LIBRARY
ABBOTTAEROSPACE.COM

RESUME DU PRESIDENT

par

Georges Jubé
Sous-Directeur Technique
Aérospatiale
37 Boulevard de Montmorency
75781 Paris, Cedex 16

L'objectif ambitieux de ce Congrès était de faire le point du niveau des connaissances sur le comportement des matériaux composites soumis aux divers types d'agressions que l'on recouvre aujourd'hui du vocable d'"environnement".

On doit admettre que cette revue était particulièrement opportune au moment où se situe la charnière entre la période de développement technologique, déjà accomplie, et l'application en service dont des résultats significatifs sont maintenant disponibles.

On peut constater que ce Congrès a mis successivement en évidence deux tendances que l'on pourrait, à première vue, qualifier d'opposées.

Les Spécialistes de la Recherche et de l'expérimentation en laboratoire ont décrit un ensemble de phénomènes qui indiquent clairement que l'usage des composites comporte un certain nombre de limitations. L'influence de l'humidité, des chocs, leur combinaison défavorable avec les autres facteurs de l'environnement, la sensibilité particulière de la sollicitation en compression, sont autant de sujets qui n'auraient pas manqué de freiner le dévelopement des matériaux composites s'ils avaient été connus à ce point il y a une dizaine d'années.

Auprès de ces facteurs d'inquiétude, l'expérience en service se traduit d'une façon assez contradictoire par la satisfaction, l'optimisme, l'absence de difficultés majeures et en fin de compte une vigoureuse poussée en avant, dans laquelle les utilisateurs emboîtent le pas aux promoteurs.

Il est difficile de ne pas être tenté, dans ce dilemme, de rejeter les avertissements des scientifiques et de consacrer le triomphe de la pratique sur la spéculation théorique.

La question n'est pas aussi simple, car les phénomènes mis en évidence en laboratoire sont indéniables. Il leur manque simplement les données statistiques qui permettraient de définir leur degré de probabilité.

D'un autre côté, il est vraisemblable que les éléments mis en service avaient bénéficié d'une fabrication relativement bien surveillée, effectuée dans des ateliers travaillant dans des conditions de fabrication prototype. Qu'en sera-t-il lorsque le composite sera produit en série avec des défauts à la limite des conditions d'acceptation, lesquelles auront bien dû, entre temps, être quelque peu libéralisées?

La solution finale se trouve donc à la convergence des deux cheminements, lorsque les deux tendances se rejoindront et se compléteront dans une appréciation raisonnée du risque.

Un nouveau rendez-vous est déjà pris; entre-temps, tous les éléments sont réunis pour que le matériaux composite poursuive, sous surveillance, sa croissance et son développement.

Accession For
NTIS GRA&I ☐
DTIC TAB ☐
Unannounced ☐
Justification
By
Distribution/
Availability Codes
Dist | Avail and/or Special
A

TECHNICAL LIBRARY
ABBOTTAEROSPACE.COM

CONTENTS

	Page
RESUME DU PRESIDENT par Georges Jubé	iii
	Reference
SESSION I – PHYSICO-CHEMICAL EFFECTS OF ENVIRONMENT	
THE IMPLICATIONS OF LABORATORY ACCELERATED CONDITIONING OF CARBON FIBRE COMPOSITES by E.C.Edge	1
EFFECT OF VARIOUS ENVIRONMENTAL CONDITIONS ON POLYMER MATRIX COMPOSITES by R.C.Tennyson	2
PREDICTABILITY OF MOISTURE ABSORPTION IN GRAPHITE/EPOXY SANDWICH PANELS by H.W.Bergmann and P.Nitsch	3
EFFECTS CONNECTED WITH THE SPACE ENVIRONMENT ON COMPOSITE MATERIALS by R.Barboni, M.Marchetti and I.Peroni	4
RECORDER'S REPORT, Session I by M.F.Card	R1
SESSION II – ENVIRONMENT SUPERIMPOSED ON STRESSING	
CONSTANT-AMPLITUDE AND FLIGHT-BY-FLIGHT TESTS ON CFRP SPECIMENS by F.J.Arendts, K.O.Sippel and D.Weisgerber	5
FATIGUE STRENGTH OF CFRP UNDER COMBINED FLIGHT-BY-FLIGHT LOADING AND FLIGHT-BY-FLIGHT TEMPERATURE CHANGES by J.J.Gerharz and D.Schütz	6
FATIGUE TEST RESULTS OF CARBON FIBRE REINFORCED PLASTIC F28 AIRCRAFT COMPONENT AND ITS STRUCTURAL DETAILS by J.A.A.M.Dijns	7
EFFECTS OF TEMPERATURE AND MOISTURE ON THE CREEP COMPLIANCE OF GRAPHITE-EPOXY COMPOSITES by K.G.Kibler	8
RECORDER'S REPORT, Session II by G.Dorey	R2
SESSION III – MECHANICAL EFFECTS AND HAZARDS	
RELATIONSHIPS BETWEEN IMPACT RESISTANCE AND FRACTURE TOUGHNESS IN ADVANCED COMPOSITE MATERIALS by G.Dorey	9
EROSION ET IMPACTS SUR LES PALES D'HELICOPTERES EN COMPOSITES par M.Torres	10
GRAPHITE-EPOXY PANEL COMPRESSION STRENGTH REDUCTION DUE TO LOCAL IMPACT by M.F.Card and M.D.Rhodes	11
THE INFLUENCE OF DEFECTS ON THE BEHAVIOUR OF COMPOSITES by R.Aoki and K.Stellbrink	12

THIS DOCUMENT PROVIDED BY THE AUTHOR FOR
TECHNICAL LIBRARY
ABBOTTAEROSPACE.COM

Reference

RECORDER'S REPORT, Session III
by K.Brunsch R3

SESSION IV – PHYSICAL HAZARDS

EVALUATION DU COMPORTEMENT A LA FOUDRE DE STRUCTURES EN MATERIAUX COMPOSITES HAUT MODULE
par J.Rouchon et D.Gall 13

LIGHTNING PROTECTION CONSIDERATIONS FOR GRAPHITE/EPOXY AIRCRAFT STRUCTURE
by S.D.Schneider 14

THE POTENTIAL FOR DAMAGE FROM THE ACCIDENTAL RELEASE OF CONDUCTIVE CARBON FIBERS FROM AIRCRAFT COMPOSITES
by V.L.Bell 15

EROSION OF COMPOSITE MATERIALS
by G.S.Springer 16

RECORDER'S REPORT, Session IV
by R.Barboni R4

SESSION V – CASE STUDIES OF SERVICE EXPERIENCE

FATIGUE AND DAMAGE PROPAGATION IN COMPOSITE ROTOR BLADES
by A.J.Barnard 17

SERVICE EXPERIENCE WITH GRC HELICOPTER BLADES (BO-105)
by K.Brunsch 18

COMPOSITE COMPONENTS ON COMMERCIAL AIRCRAFT
by H.Benson Dexter 19

AIR FORCE APPLICATIONS AND IN-SERVICE EXPERIENCE WITH COMPOSITE STRUCTURES
by F.J.Fechek 20

U.S. NAVY SERVICE EXPERIENCE WITH ADVANCED COMPOSITES
by A.Somoroff, M.Dubberly, J.M.McGinn, M.Tarricone and A.Manno 21

RECORDER'S REPORT, Session V
by J-M.Fehrenbach R5

TECHNICAL LIBRARY
ABBOTTAEROSPACE.COM

THE IMPLICATIONS OF LABORATORY ACCELERATED CONDITIONING OF CARBON FIBRE COMPOSITES

by
E. C. Edge
Principal Engineer
Advanced Structural Applications Department,
British Aerospace, Aircraft Group,
Warton Aerodrome
PRESTON PR4 1AX
Great Britain

SUMMARY

The available evidence on the effects of long term natural weathering of carbon fibre composites is examined and its implications with regard to the conditioning of test specimens discussed.

The effects of laboratory accelerated tests on the properties of some composite materials are considered in conjunction with the relevance of data thus acquired to real life situations and the need to generate the data with reasonable speed for design considerations.

The changes in conditioning procedure which have taken place are outlined along with the factors which have influenced these changes.

1. INTRODUCTION

Since the adverse effect of absorbed moisture on the material properties of carbon fibre composites was first noted, those concerned with the design of aircraft structures using these new materials have been considering the problem of including a realistic assessment of this loss of property in the determination of design allowables.

In military aircraft applications, which are the main consideration of this paper, the most severe design condition is usually taken to be the "hot wet" case. A simple view of this condition is the simultaneous occurrence of the maximum moisture content and a high (often >100°C) design temperature. Two problems present themselves here. There is the need to assess the level of moisture content likely to be experienced in service life. (Discussion of temperature levels is outside the scope of this article). There is also the need in the planning of experimental procedure to decide on the best method of achieving this representative level of moisture, bearing in mind that the real life timescale is in most cases much too slow (8 months - 3 years) to be capable of integration into the design process. Clearly laboratory accelerated conditioning will continue to be used in the foreseeable future. Accepting this, in order to prevent incorrect assessment of the experimental results thus obtained, it is necessary to assess how the state of the material to be expected after such accelerated conditioning relates to that likely to be encountered in service.

In this paper consideration is first given to the evidence now accumulating on a worldwide basis on the moisture levels likely to be found in CFC components, and the effect which this natural weathering, which includes among other things exposure to ultra-violet rays, thermal gradients between surfaces exposed and sheltered from sunlight, precipitation of various types, wind and sand, is expected to have on the condition and strength and stiffness properties of the material.

In Section 3, three methods of accelerated conditioning which have commonly been used are compared. Attention is given to the total level of moisture uptake, the distribution of moisture through the thickness of the material, the relationship between moisture content and loss of material property and the mechanisms of degradation occurring. An attempt is made to assess how these effects produced under these artificial "hot house" conditions are representative of real life situations. In Section 4 consideration is given to the need to know with some precision the actual moisture levels obtaining in test specimens and the evolution of experimental practice in this area within British Aerospace is outlined.

2. REAL TIME WEATHERING OF CFC

Before it is possible to decide on the merits and demerits of the various possible forms of accelerated laboratory conditioning, it is necessary to consider what level of moisture uptake should be the target. This can only be fixed with confidence when the required amount of information has been gained from real time weathering experiments. In addition to revealing the moisture content these tests will also provide information on the property and state of the material to be expected in service. The timescale of these experiments must of necessity be several years although useful intermediate results can be obtained by periodic withdrawal of exposed material.

Although it can not yet be honestly stated that the available information is adequate, test results are now beginning to come in and certain trends are appearing. Material has been exposed on various sites round the world, with measurements of moisture uptake, loss due to ultraviolet, and residual strength. In Hangar 32 at British Aerospace, Warton, which houses Jaguar BOR, regular measurements of temperature and humidity have been taken since July 1978.

Predictive calculations based on these measurements are illustrated in Fig. 1. These calculations are compared with moisture uptakes deduced by dessicating coupon specimens cut from discs attached to the aircraft, and these practical measurements are also given in Fig. 1. The actual flying time during the period under consideration is small and has been ignored in the predictive calculations, but it should be

THIS DOCUMENT PROVIDED BY THE TECHNICAL LIBRARY
ABBOTTAEROSPACE.COM

borne in mind that the effect of flight is generally to dry the material, at least near the surface, and this may account for some of the difference between the theoretical and practical results.

Roylance and Roylance[1] give results of exposure at open field sites in Panama of specimens from a 3M 1009-26 Scotchply glass/epoxy laminate. Exposure was in an unloaded condition facing south and 45 deg. to the vertical. As samples are returned for analysis increasing degradation of the outer surfaces, especially those facing the sun, is noticed. Resin is lost from the surface, leaving behind exposed fibres. Fig. 2 shows the results of glass transition temperature measurements plotted against months of exposure. The relatively undegraded state of the middle laminate layers should be noted.

Trabocco and Stander[2] give results of open field exposure in Pennsylvania and Panama. Degradation was measured by tension, compression and short beam shear tests. Unfortunately none of these property tests were at elevated temperature and no measurements of moisture uptake are available. However it must be remembered that this and other real time exposures were programmed several years ago when the need for such measurements had not been fully recognised. The exposed material included coated and uncoated panels, and a number of different fibre/resin combinations which produced a considerable variety of behaviour. The greatest effect was observed on material exposed in Panama. Modulite 5206 (Modmor II fibres) actually appeared to benefit from 18 months tropical exposure, it being suggested that post-curing was stimulated by the conditions. AS/3501 appeared to be little affected in mechanical properties. In contrast T400/2544 panels showed pronounced warping, loose fibres and loss of resin as was the case with the glass-epoxy material[1]. Additionally this material suffered considerable loss of tensile strength and ultimate strain properties. This system, however, is not a contender for British aircraft applications. Fig. 3 and 4 show the loss of ultimate strain and tensile strength by T400/2544. However, more typical are Fig. 5 and 6 showing negligible loss of compression strength by AS/3501 and 3002T after 18 months exposure at Warminster (Pennsylvania) and Panama.

Pride[3] gives the results of experiments in which specimens have been mounted on racks which are placed on rooftops of airline buildings at a number of locations round the world. Fig. 7 shows the weight change with exposure time for a 4-ply T300-5209 laminate exposed unstressed at Langley USAF. Va.. The specimens initially gained weight then began to lose weight under the influence of solar ultra-violet exposure. After 140 days the exposure was terminated and the moisture content determined by dessication. The ultra-violet loss is taken to be the difference between final dry weight and the initial pre-exposure measurement. The ultra-violet loss is assumed to be linear with time and the curve of moisture uptake is constructed on this basis. Fig. 8 summarises the results of moisture content measurements on various material combinations, these values being corrected for ultra-violet loss as previously described. Also taken from this reference is Fig. 9 which compares measured moisture contents with those predicted with and without allowance for solar effects. Residual mechanical property tests were conducted at ambient only. These revealed some scatter but no significant change in strength.

There have been a number of papers in recent years which have given the results of calculations of moisture uptake based on appropriate meterological information. Typical of these is Unman and Tenney[4]. They used weather bureau data for Langley AFB and Norfolk, Va. to calculate the amount of moisture a T300/5208 composite panel would contain if exposed outdoors. Solar radiation data along with cloud and wind information were used. Results are quoted with and without the solar effect. Good agreement was found between the calculated moisture content and published data for T300/5208 composite. Fig. 10 and 11 are reproduced from this reference. Fig. 10 illustrates the effect of solar radiation on the moisture content of a 12-Ply T300/5208 horizontal panel exposed at Norfolk Va. Fig. 11 gives the calculated moisture contents for 12-Ply T300/5208 laminates using monthly average weather data for five different sites.

Fig. 12 shows the results of calculations performed at B.Ae Warton, without solar effects, for XAS/914C material with an effective skin thickness of 2mm, based on meterological information for Gemert (Netherlands). Fig. 13 shows the through the thickness moisture distribution at the times of maximum and minimum total concentration in the quasi-steady state.

Considering the available information there would appear to be little justification for conditioning test pieces to a greater level of moisture uptake than 1% when due allowance is made for solar and flight drying effects, indeed for temperate climates 0.8% might be nearer the mark. This level is however fairly evenly distributed through the thickness. The damaging effect of ultra-violet in the surface layers, an apparent feature of natural weathering, will not of course be reproduced in laboratory experiments, but as it is confined to the outermost layers the loss of structural integrity is expected to be small.

3. METHODS OF ACCELERATED CONDITIONING IN COMMON USE

An attempt is made to compare three methods of accelerated conditioning:

(a) Immersion in Boiling Water

(b) Humidity cabinet exposure at 50°C and 95%-100% R.H.

(c) Ambient exposure at 21°C and 65% R.H.

These exposures were used in a joint programme conducted by B.Ae Warton and the Royal Aircraft Establishment, Farnborough. Exposure (b) is now used at Warton as a "slow" chamber, while exposure at 95°C and 95-100% R.H. is used as a "fast" chamber. The timescales of the design process largely dictate the use of the "fast" exposure when ideally a somewhat less severe conditioning would be preferred. The inclusion of exposure (c) may cause some surprise, but despite its mild appearance the results were considered unexpectedly severe at the time, and equilibrium moisture levels are apparently somewhat higher than those to be expected in service.

In the joint RAE/B.Ae programme moisture ingress levels and ILSS were measured for the three exposures on two fibre-resin combinations, HTS/BSL914C and AS/3501/5A. Results from this programme are used in this

TECHNICAL LIBRARY
ABBOTTAEROSPACE.COM

comparison, but it emphasised that the inferences drawn from these results are those of the author, and do not necessarily represent the views of the RAE or other parties. In carrying out this comparison, attention has been concentrated on three areas:

(i) Equilibrium concentration

(ii) Relationship between moisture content and loss of ILSS strength

(iii) Recovery of property after drying out from a moisturised condition.

Fig. 14 shows the equilibrium concentrations measured in or deduced from these experiments plotted against relative humidity. It will be observed that the concentrations recorded in the boiling water immersions are much greater than would be expected by extrapolating the relationship between concentration and humidity obtaining at lower levels. This was also noted by McKague et.al.[5] and is in harmony with other results[6] which show total immersion giving higher concentrations than exposure in a chamber to maximum humidity.

Fig. 15 and 16 illustrate the relationship between moisture content and ILSS strength at 130°C. This feature is perhaps better shown in Table 1, which gives the results of a linear regression analysis performed on the test points. A linear best fit is obtained for the equation,

$$S = AM + B$$

where S = ILSS (Mn/m^2)

M = moisture content %

A and B are constants,

and the computed values of A and B are given in Table 1. A fair amount of scatter is evident but there appears to be basically a similar relationship between ILSS and moisture content at all exposure conditions. This can be definitely seen in the case of HTS/914C laminate 2545.

Fig. 17 and 18 show the relationship between moisture content and ILSS strength at R.T. In this case there is a somewhat different relationship than at 130°C. For exposure (c) no significant change is apparent. For exposure (b), up to about the maximum level achieved with exposure (c), there is also no significant change; at higher moisture levels there is a small, erratic loss of property. For exposure (a), boiling water immersion, there is a drop of property at all levels, erratic for small uptakes, but more pronounced at higher levels.

Unfortunately not many tests where specimens, having been exposed, were dried out and tested to investigate recovery properties, have been performed after exposures (b) and (c). However, such as have been carried out have indicated complete or nearly complete recovery of ILSS at 130°C. Tables 2 and 3 show the results for exposure (a) and these generally show poor recovery of property.

This comparison suggests that exposure (a) leads to unrealistically severe specimen degradation, and despite the interesting results obtained with it in the past it would appear, bearing in mind other evidence[6] also, that when rapid results are required it is better to expose at a condition similar to that of the Warton "fast" chamber (95°C and 95% R.H.) rather than go to total immersion. Exposure (b) would appear to give somewhat excessive degradation at higher values of moisture content, but only when the expected maximum content in service has been exceeded. The timescale of exposure (c) is too slow to be much used in the design process. Fig. 19 illustrates the theoretical through the thickness distributions for each of the three exposures corresponding to the point where the total moisture content is 1.0%. Comparing these to the expected real life situation (Fig. 13) reinforces the remarks just made about the relative severity of the exposure conditions.

With particular reference to the poor recovery properties, it would appear that the boiling water exposure, in contrast to less severe tests, leads to a considerable degree of irreversible degradation. The distinction between irreversible and reversible degradation is of course not clear cut. However effects due to the plasticisation of the resin resulting from moisture content in the form of solution appear to be practically completely reversible at least as far as static strength is concerned. This may not be true to the same extent for stress-strain and fatigue. Microcracking of the resin due to moisture and thermal gradients and ultra-violet exposure would in contrast appear to be largely irreversible. The degradation of the fibre-resin interface is more complex. The bond between fibre and matrix appears to be part chemical and part friction. A friction bond would be expected to weaken in the presence of moisture and to reform on drying out provided the local fibre resin alignment had not been greatly disturbed. However once chemical bonds are ruptured then at best it would appear that a much longer timescale would be necessary for these to be reformed so that this type of debonding can probably be classed as irreversible. This may also be the case where water molecules appear to become permanently bound in the resin[7,8].

If it is accepted that apart from the ultra-violet effects on the surface layers, degradation to be expected in service is if anything less severe than that observed under exposure (c), then this would appear to imply that property loss will be largely reversible. Thus at the very least care will be required in reading across from results where it is considered that significant irreversible effects may have occurred.

4. MONITORING OF MOISTURE UPTAKE

Until fairly recently testing for material property within British Aerospace[9, 10] was done for "dry" and "wet" conditions without actual measurements of moisture content. It was at RAE[11] that the first British experiments took place in which the moisture uptake was systematically monitored. To obtain the

TECHNICAL LIBRARY
ABBOTTAEROSPACE.COM

"wet" condition specimens were given a standard conditioning of 2000 hours at 50°C and 95-100% R.H. The "dry" specimens were not dried to any predetermined datum. They were not given any conditioning and clearly had absorbed moisture during the inevitable dwells between manufacture and test.

A combination of circumstances have led to a change of attitude. The RAE work and the earliest results from real time exposure tests showed that the standard "wet" condition would give pessimistic results from the design point of view, at least for the thinner specimens. The earliest attempts at predictive calculations(12) drew attention to the need to give different exposures according to thickness, to the rate of absorption in ambient conditions (typically more than a quarter at 20°C of that at 50°C) and to the possible significant difference in through the thickness distribution between laboratory conditioned specimens and real life situations.

These considerations have led to a change in procedure at B.Ae Warton, where the "dry" condition is now obtained by drying test pieces to constant weight in an oven and the "wet" condition is 0.9%-1.0% measured moisture uptake. Simple predictive calculations are used to give guidance on exposure conditions and timings, with attention to the evenness of uptake where necessary, as for instance in the case of fatigue specimens. Fairly sophisticated models are now used, particularly in the U.S.A., which include attempted simulation of thermal and moisture cycling.

5. CONCLUSIONS

(a) Moisture uptakes to be expected in service life appear to be considerably lower than the equilibrium concentration produced in CFC material by a high humidity environment.

(b) While it would obviously be desirable to reproduce real life rates of moisture absorption, these are much too slow to be integrated into the design process.

(c) The excessive moisture contents produced by earlier standards of conditioning are now recognised, but the danger of inducing excessive degradation by over-acceleration remains even when the actual moisture level corresponds to real life expectations.

(d) Total immersion in water, particularly boiling water, does appear to give over severe effects, with an unduly high proportion of irreversible damage and unrealistic through the thickness distributions.

(e) Increased knowledge and experience, allied with improvements in predictive techniques and leading to a greater degree of control over the conditioning process, is reducing the danger of incorrect design decisions arising from misinterpretation of experimental results.

6. REFERENCES

1. D. Roylance & M. Roylance. "Influence of Outdoor Weathering of Dynamic Mechanical Properties of Glass/Epoxy Laminate." 1976. Environmental Effects on Advanced Composite Materials, ASTM STP 602, pp.85-94.

2. R. E. Trabocco and M. Stander. "Effect of Natural Weathering on the Mechanical Properties of Graphite/Epoxy Composite Materials." 1976. Environmental Effects on Advanced Composite Materials, ASTM STP 602, pp.67-84.

3. R. A. Pride. "Environmental Effects on Composites for Aircraft". NASA Technical Memorandum 78716.

4. J. Unman and D. R. Tenney. "Analytical Prediction of Moisture Absorption/Desorption in Resin Matrix Composites Exposed to Aircraft Environments". Paper presented at AIAA Conference, San Diego, March 24-25, 1977.

5. E. L. McKague, J. D. Reynolds and J. E. Halkias. "Life Assurance of Composite Structures." May 1975. AFML-TR-75-51. Vol. 1- Moisture effects.

6. E. R. Long, Jr. "Moisture Diffusion Parameter Characteristics for Epoxy Composites and Neat Resins". 1979. NASA Technical Paper 1474.

7. H. G. Carter and K. G. Kibler. "Langmuir-Type Model for Anomalous Moisture Diffusion in Composite Resins". 1978. Journal of Composite Materials, Vol. 12 (1978), p. 118.

8. Y. A. Tajima and P. E. Sandorff. "Experimental Determination of Moisture Distribution and Diffusion Parameters in Graphite-Epoxy Laminates". 1978. A.S.C.E. Annual Convention, Chicago, Illinois.

9. J. P. Prestwich. B.Ae Manchester Division. "Unidirectional Properties of Carbon Fibre Composites." 1978. MSA-MSM-R-GEN-0295.

10. J. Eastham. B.Ae Warton Division. "Final Report on M.O.D. Contract K/LA32B/2126. In Depth Evaluation of C.F.R.P." 1979. MDR 0182.

11. M. C. W. Judd. RAE (Farnborough). "The Effect of Water on Carbon Fibre Composites. Part IV". 1973. RAE Tech. Memo. MAT 225.

12. J. Crank. "The Mathematics of Diffusion." 2nd Edition. 1975. Clarendon Press. Oxford

TECHNICAL LIBRARY
ABBOTTAEROSPACE.COM

7. ACKNOWLEDGEMENTS

Thanks are due to the Directors of British Aerospace for permission to publish this paper, and to the Royal Aircraft Establishment, Farnborough, for permission to use experimental results from the joint B.Ae/RAE programme. In his work on moisture absorption of CFC and related phenomena the author is grateful for the encouragement of Mr. T. Sharples, Technical Manager, Advanced Structural Applications Department, British Aerospace, Warton Division.

TECHNICAL LIBRARY
ABBOTTAEROSPACE.COM

APPENDIX

TABLE 1

The coefficient A and B given in the table below are those given by the linear regression analysis described in Section 3. Graphical presentation of some of the results is given in Fig. 15 and 16.

The values of A and B have been deduced for which the equation

$$S = AM + B$$

where S = ILSS (Mn/m^2)

M = moisture content %

A and B are constants

is a best fit to the test results for ILSS at 130°C, based on minimum r.m.s. deviation.

Material	Exposure	A	B
AS/3501/5A	Boiling Water	-23.6	76.1
	50°C 95% R.H.	-21.6	72.9
	21°C 65% R.H.	-32.7	80.0
HTS/914C Lam. 0177S	50°C 95% R.H.	-16.7	52.7
	21°C 65% R.H.	- 7.65	53.2
HTS/914C Lam. 2545	Boiling Water	-19.0	60.0
	50°C 95% R.H.	-18.1	53.7
	21°C 65% R.H.	-18.2	57.1

TABLE 2

Table 2 following gives the results of ILSS tests conducted at 130°C in the joint BAe/RAE programme on AS/3501/5A specimens which had been immersed in boiling water then dried to constant weight in an oven set at 50°C.

Immersion Time hr.	Mean ILSS after immersion Mn/m^2	Moisture * Absorption %	Mean ILSS after immersion and drying Mn/m^2	Recovery percentage %
Control	80.7	-	-	-
3	74.2	0.17	77.9	56.8
5	73.5	0.10	76.4	40.4
8	70.6	0.24	74.9	42.4
15	69.9	0.29	73.3	31.3
24	64.1	0.58	70.1	36.4
72	48.1	0.95	62.5	44.2
168	35.4	1.78	56.4	46.4

*Measured absorption during experiments - no allowance made for unmonitored absorption prior to immersion.

TECHNICAL LIBRARY
ABBOTTAEROSPACE.COM

TABLE 3

Table 3 following gives the results of ILSS tests conducted at 150°C in the joint BAe/RAE programme on HTS/914C specimens from laminate 2545 which had been immersed in boiling water then dried to constant weight in an area set at 50°C.

Immersion Time hr.	Mean ILSS after immersion Mn/m^2	Moisture * Absorption %	Mean ILSS after immersion and drying Mn/m^2	Recovery percentage %
Control	60.0	-	-	-
3	55.3	0.30	55.3	0.0
5	52.3	0.47	53.4	14.3
8	49.0	0.58	55.7	60.9
15	39.6	0.90	50.4	52.9
24	35.9	1.19	43.0	29.5
72	25.9	1.93	48.7	66.9
168	24.6	1.79	47.1	63.6

*Measured absorption during experiments - no allowance made for unmonitored absorption prior to immersion.

TECHNICAL LIBRARY
ABBOTTAEROSPACE.COM

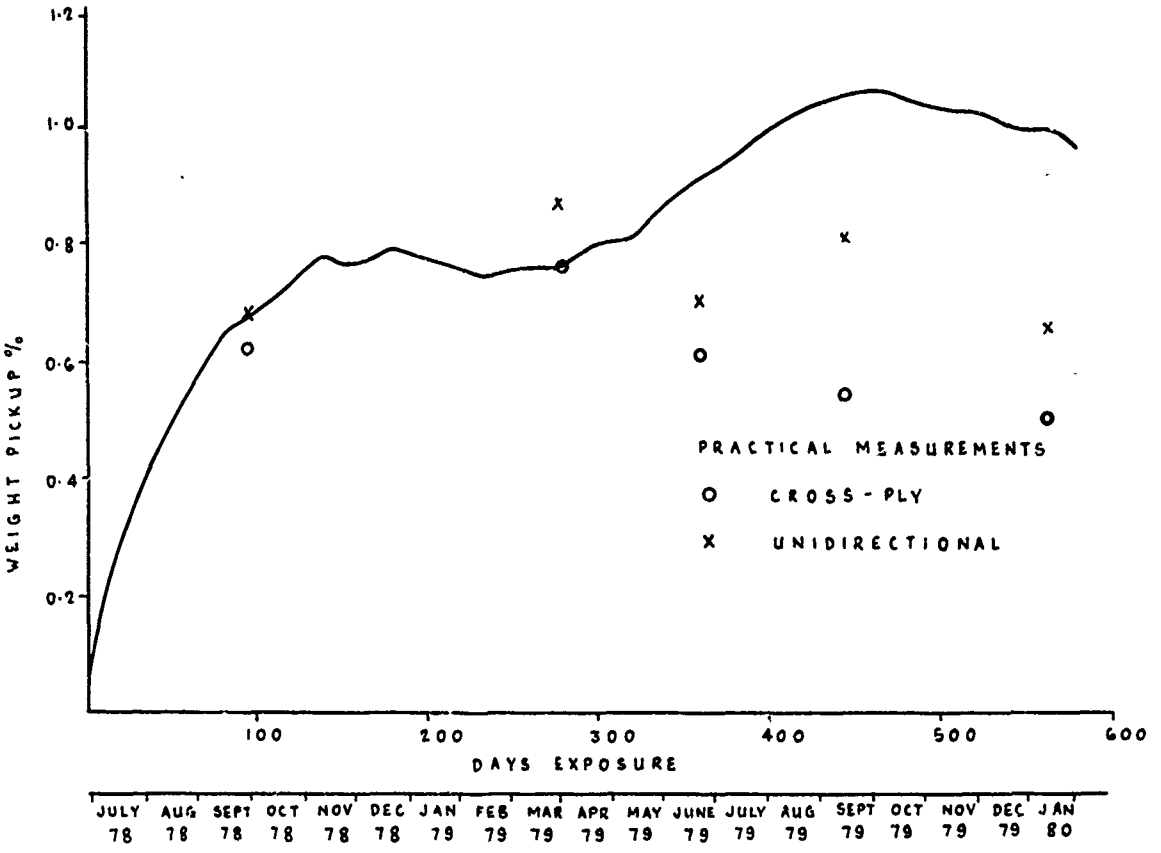

Fig.1 Moisture uptake prediction for Jaguar B08 based on temperature and humidity readings in Hanger 32 BAe Warton

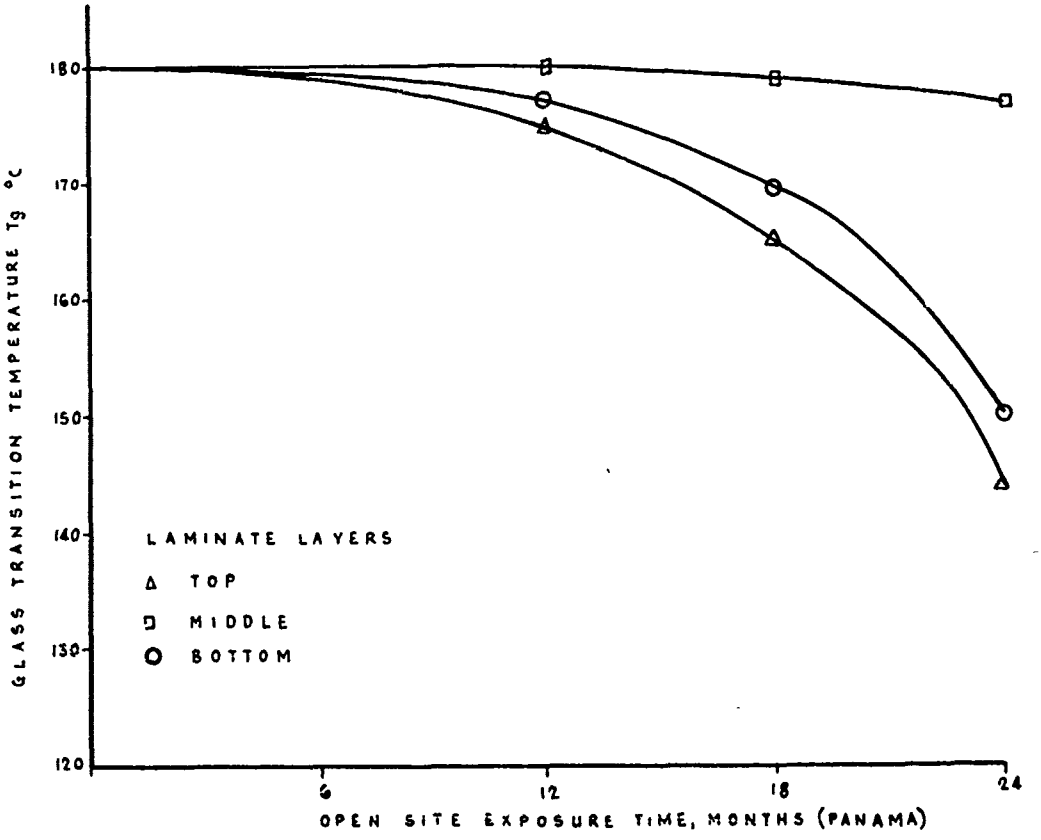

Fig.2 Measured glass transition temperatures after real time exposure (Ref.1, Fig.6)

TECHNICAL LIBRARY
ABBOTTAEROSPACE.COM

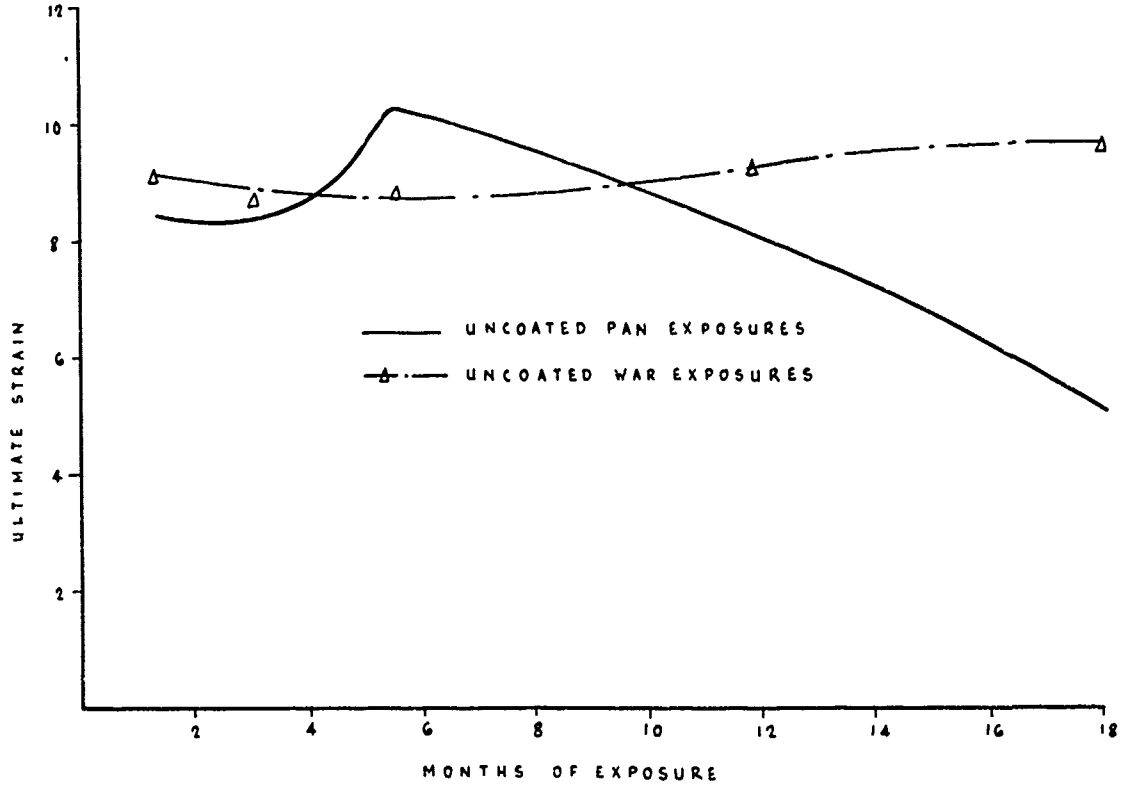

Fig.3 Ultimate strain of coated Panama and Warminster Pa T400/2544 Gr/Ep exposures (Ref.2, Fig.11)

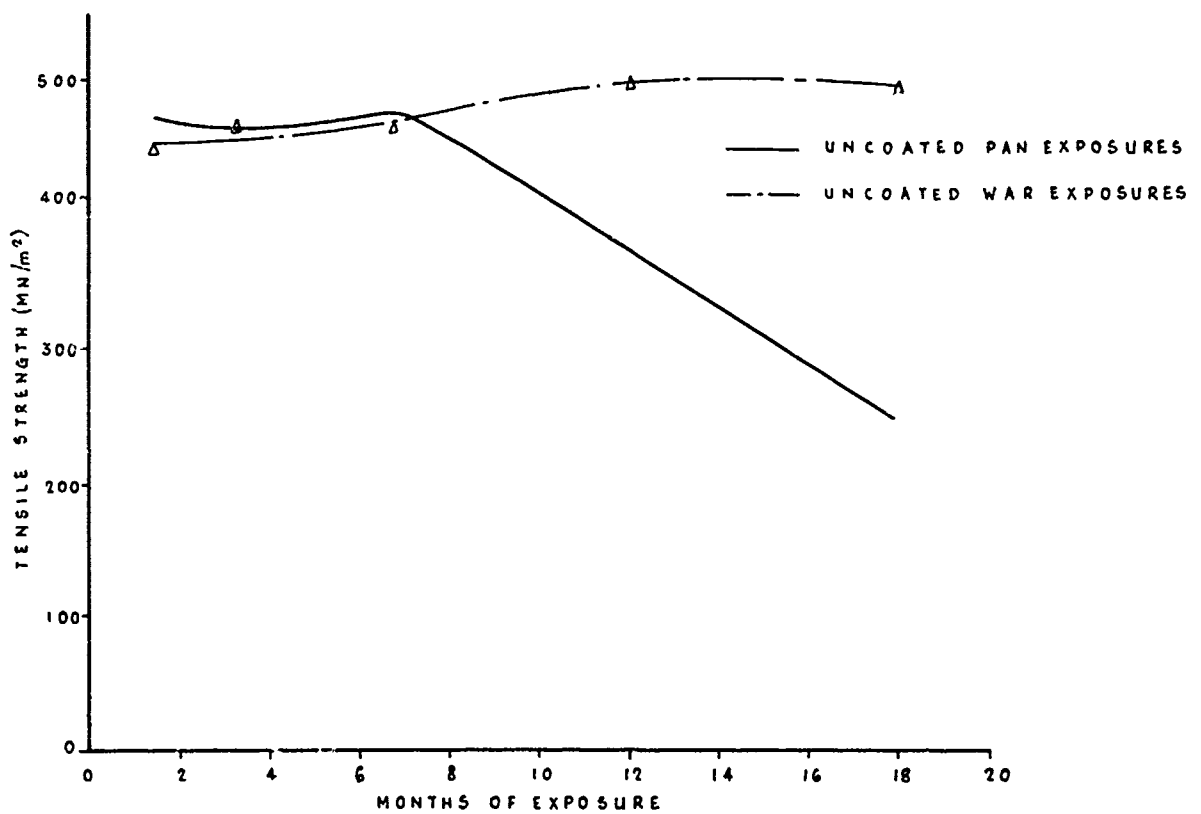

Fig.4 Tenile strength of uncoated Panama and Warminster Pa T400/2544 Gr/Ep exposures (Ref.2, Fig.12)

TECHNICAL LIBRARY
ABBOTTAEROSPACE.COM

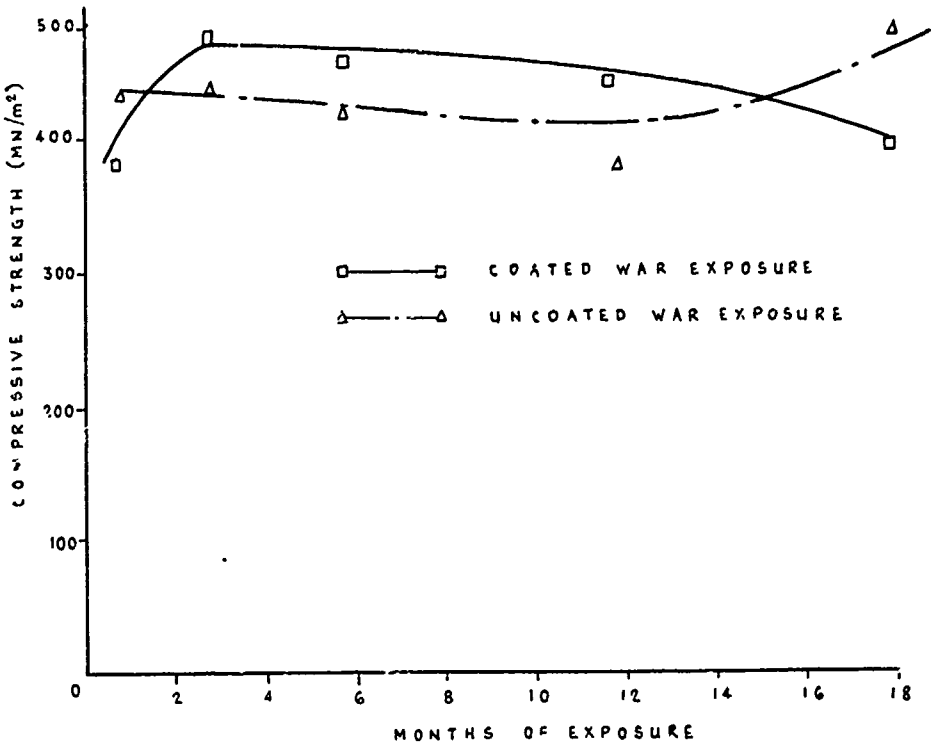

Fig.5 Compressive strength of AS 3501 Gr/Ep exposure at Warminster Pa (Ref.2, Fig.4)

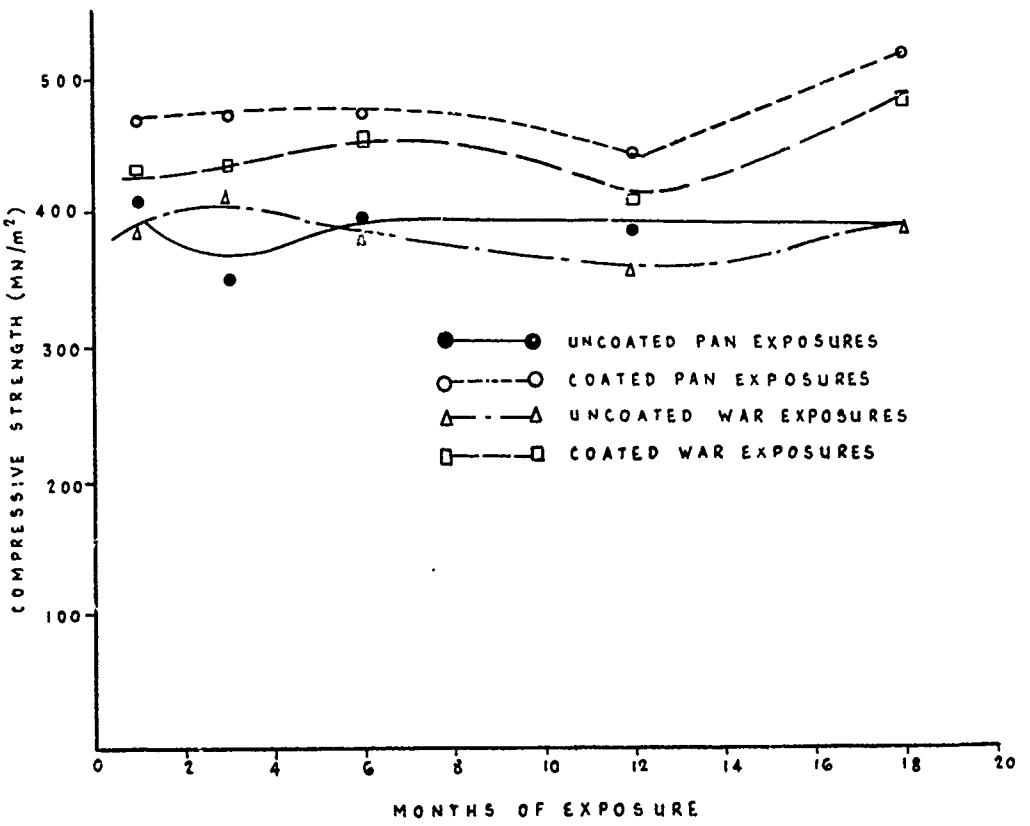

Fig.6 Compressive strength of 3002T Gr/Ep exposures at Panama, Warminster, Pa (Ref.2, Fig.3)

TECHNICAL LIBRARY
ABBOTTAEROSPACE.COM

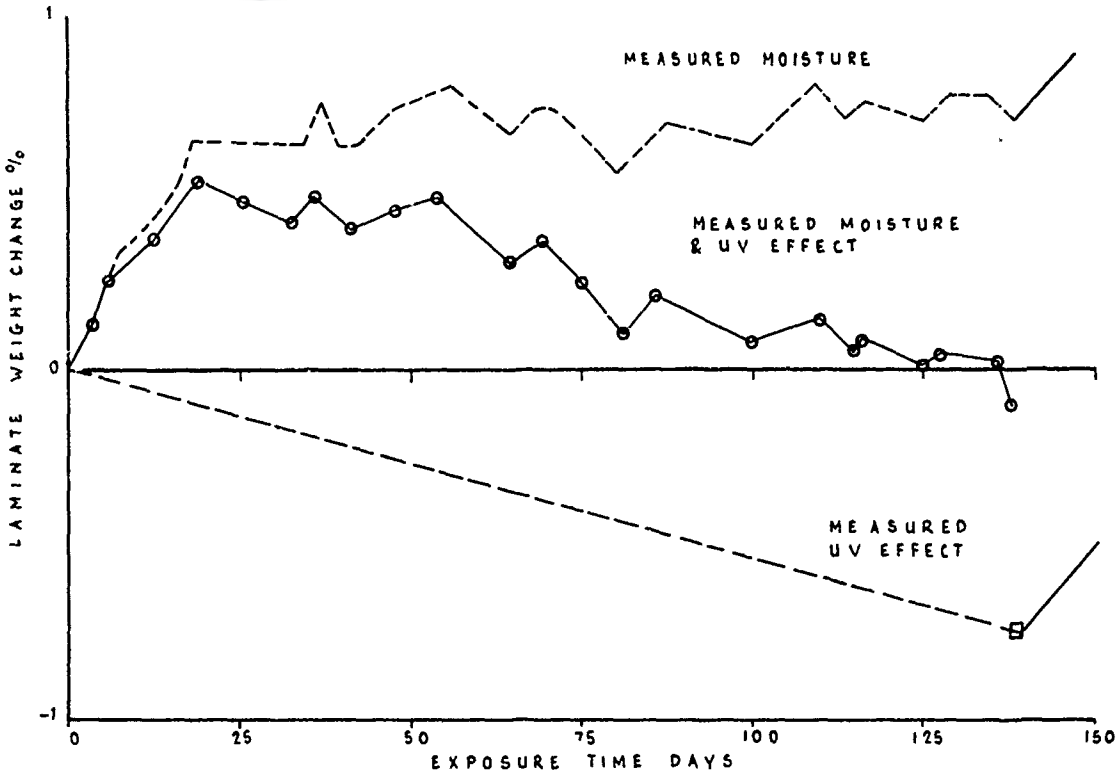

Fig.7 Weight change in outdoor exposure, 4 ply laminate, T300-5209 (Ref.3, Fig.10)

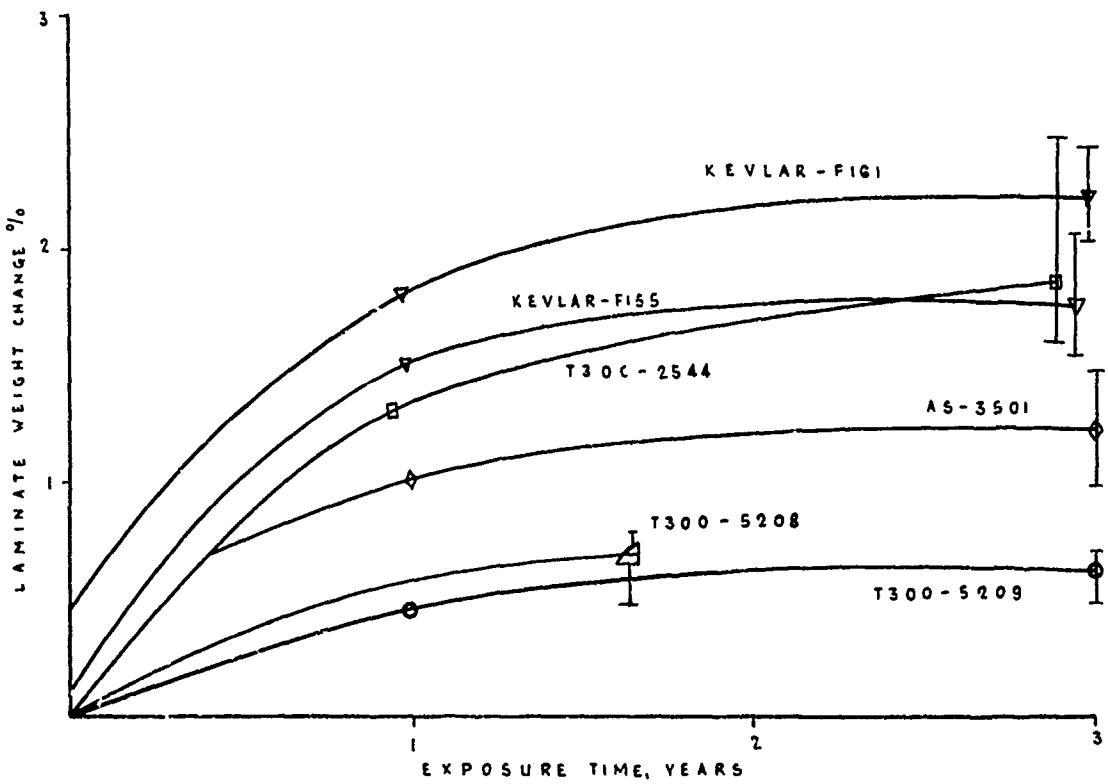

Fig.8 Moisture pickup after worldwide exposures (Ref.3, Fig.13)

THIS DOCUMENT WAS PRESENTED AT AGARD CONFERENCE
TECHNICAL LIBRARY
ABBOTTAEROSPACE.COM

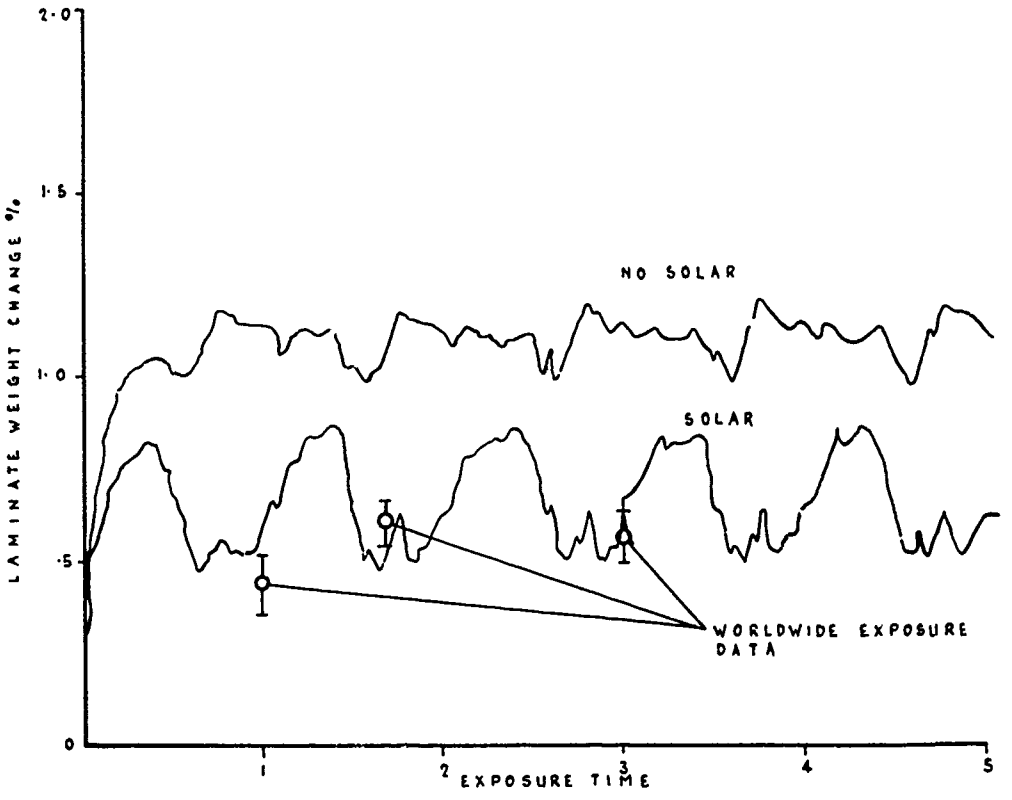

Fig.9 Comparison of predicted and measured moisture contents T300-5208, 12 ply laminate ground exposure (Ref.3, Fig.14)

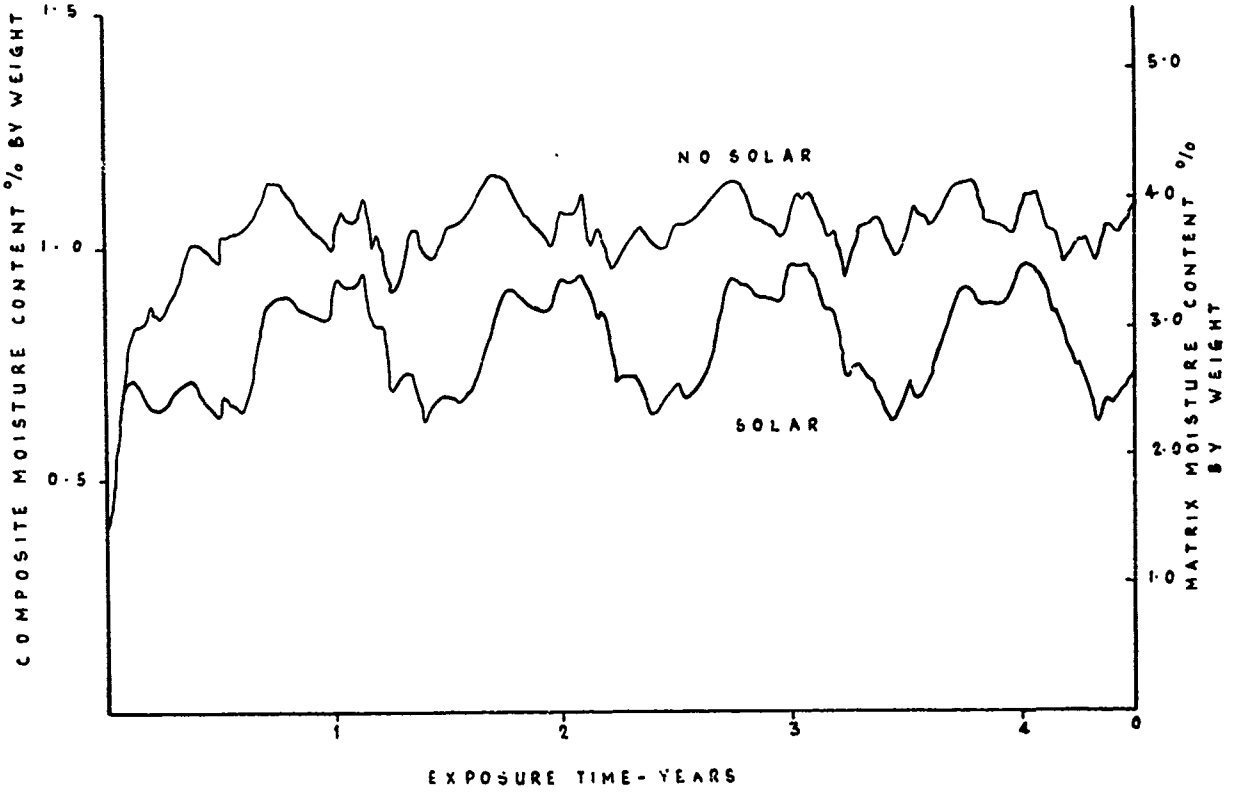

Fig.10 Effect of solar radiation on moisture content of a horizontal panel 12 ply T300-5208 horizontal panel exposed at Norfolk, Va (predicted response) (Ref.4, Fig.10)

TECHNICAL LIBRARY
ABBOTTAEROSPACE.COM

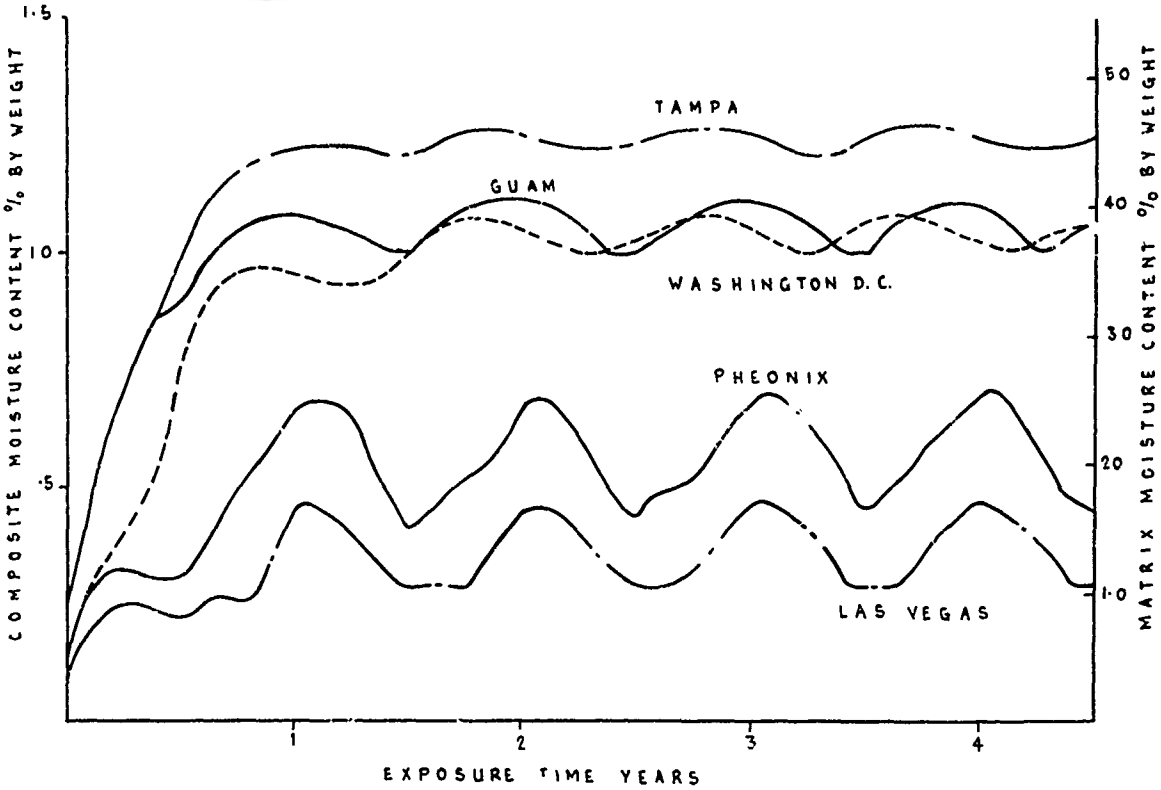

Fig.11 Calculated moisture contents using monthly average weather data (Ref.4, Fig.8) 12 ply T300-5208

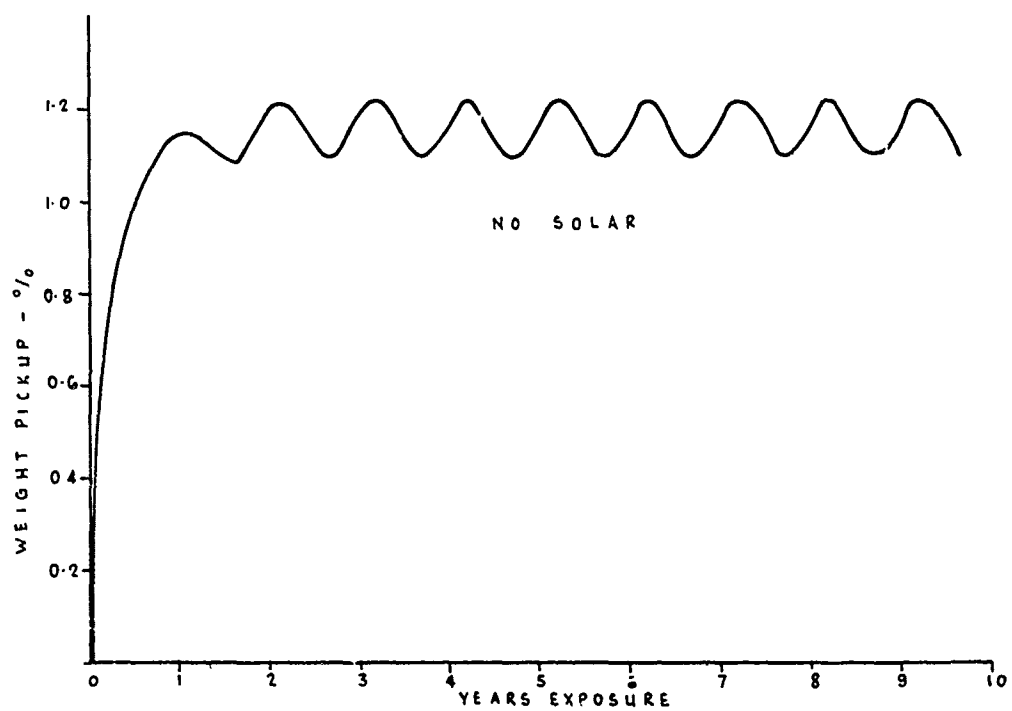

Fig.12 Moisture uptake prediction for RAF Bruggen based on information for Gemert (Netherlands) equivalent skin thickness = 2mm

TECHNICAL LIBRARY
ABBOTTAEROSPACE.COM

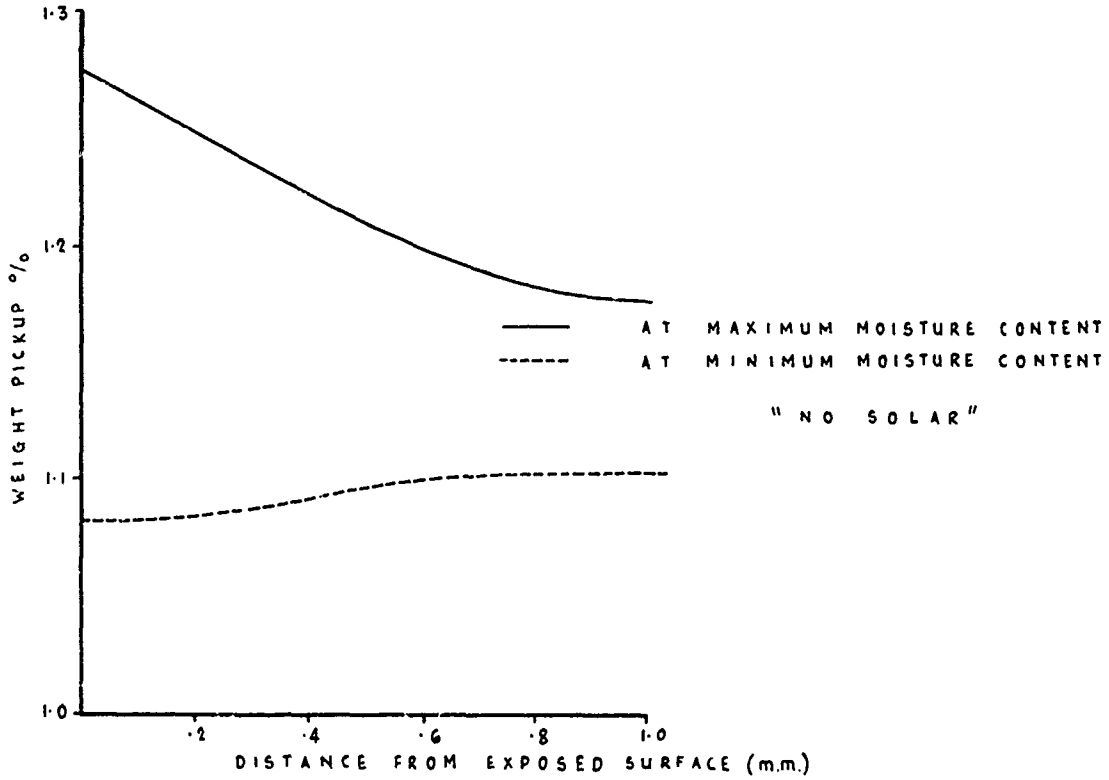

Fig.13 Through the thickness moisture uptake prediction for RAF Bruggen based on information for Gemert (Netherlands). Predictions for times of maximum and minimum total moisture content. Equivalent skin thickness = 2mm

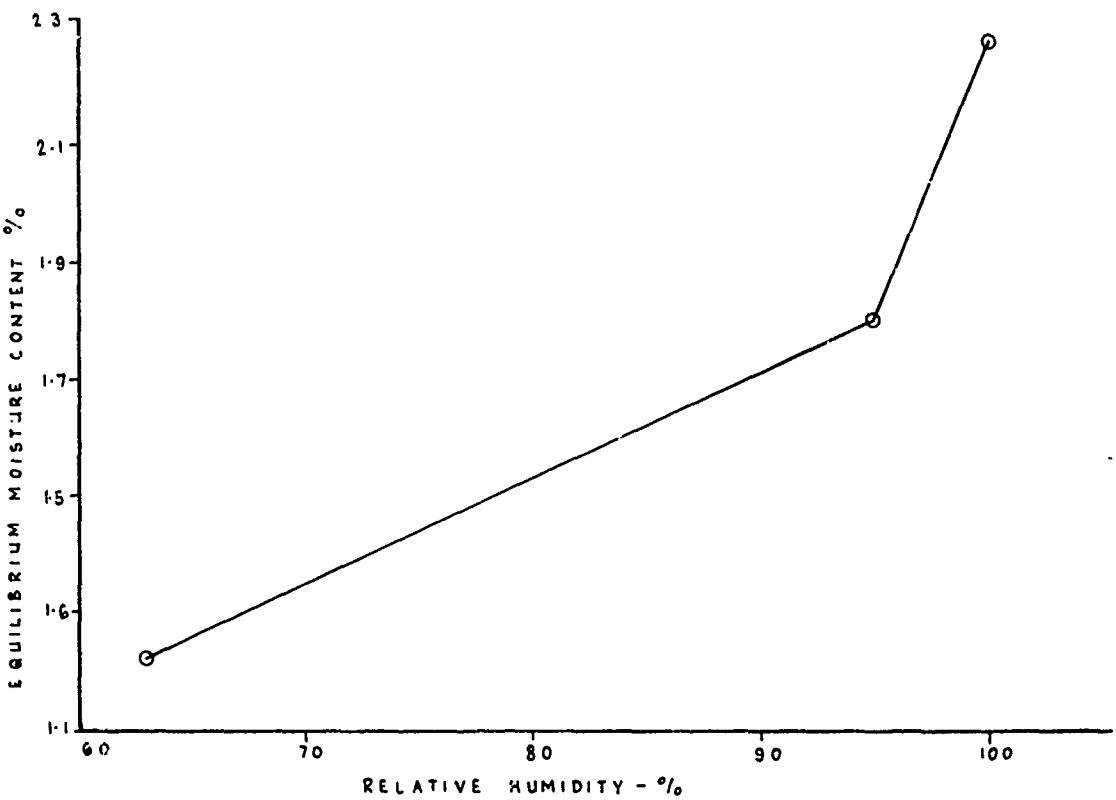

Fig.14 Measured equilibrium concentrations for HTS/914C plotted against relative humidity

THIS DOCUMENT IS PROVIDED BY THE
TECHNICAL LIBRARY
ABBOTTAEROSPACE.COM

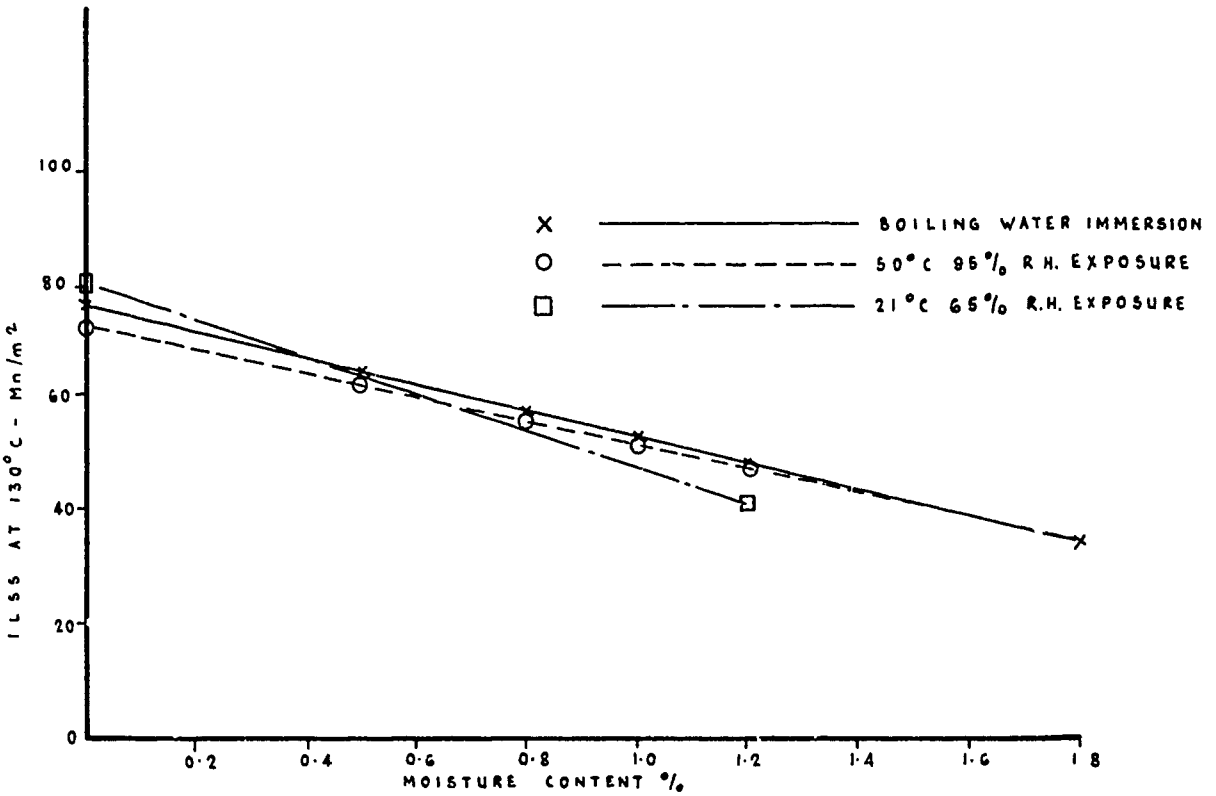

Fig.15 Relationship between ILSS at 130°C and moisture content for AS/3501/5A based on linear regression analysis of results from joint RAE/BAe programme

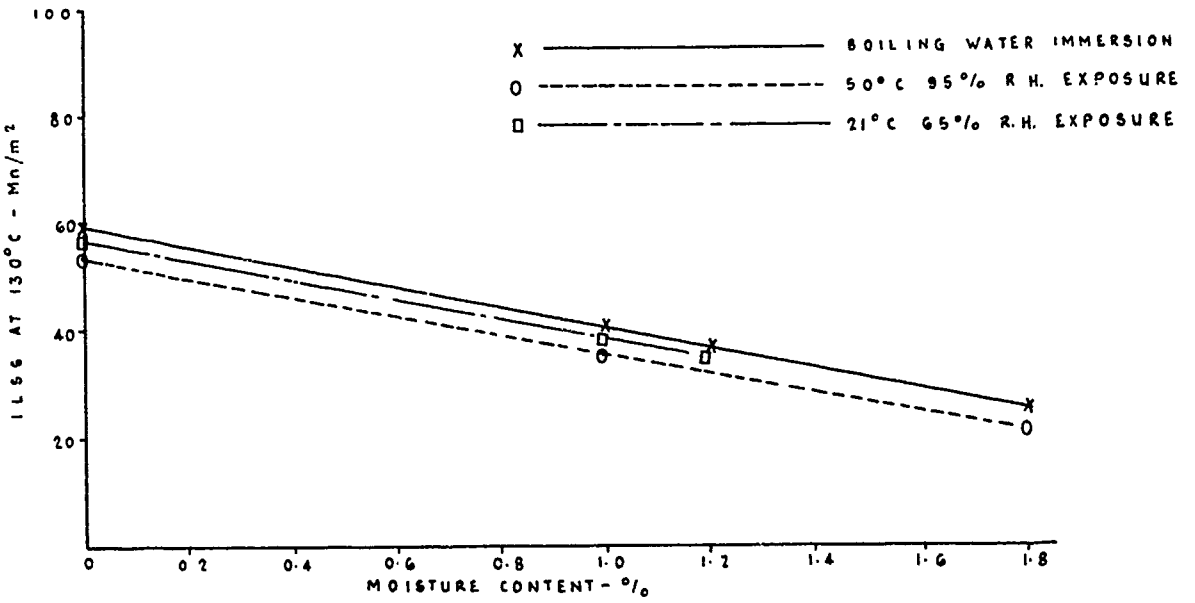

Fig.16 Relationship between ILSS at 130°C and moisture content for HTS/914, based on linear regression analysis of results from joint RAE/BAe programme (laminate 2545)

TECHNICAL LIBRARY
ABBOTTAEROSPACE.COM

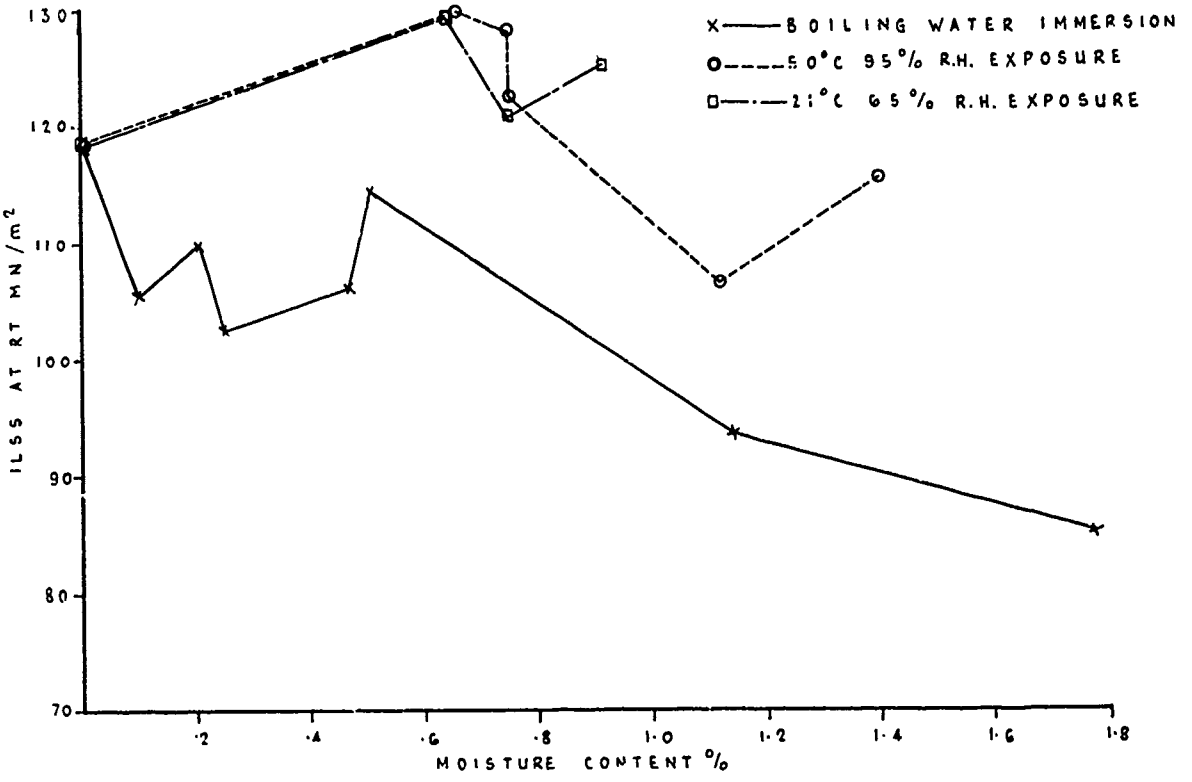

Fig.17 Relationship between ILSS at RT and moisture content for AS/3501/5A using results of joint RAE/BAe programme

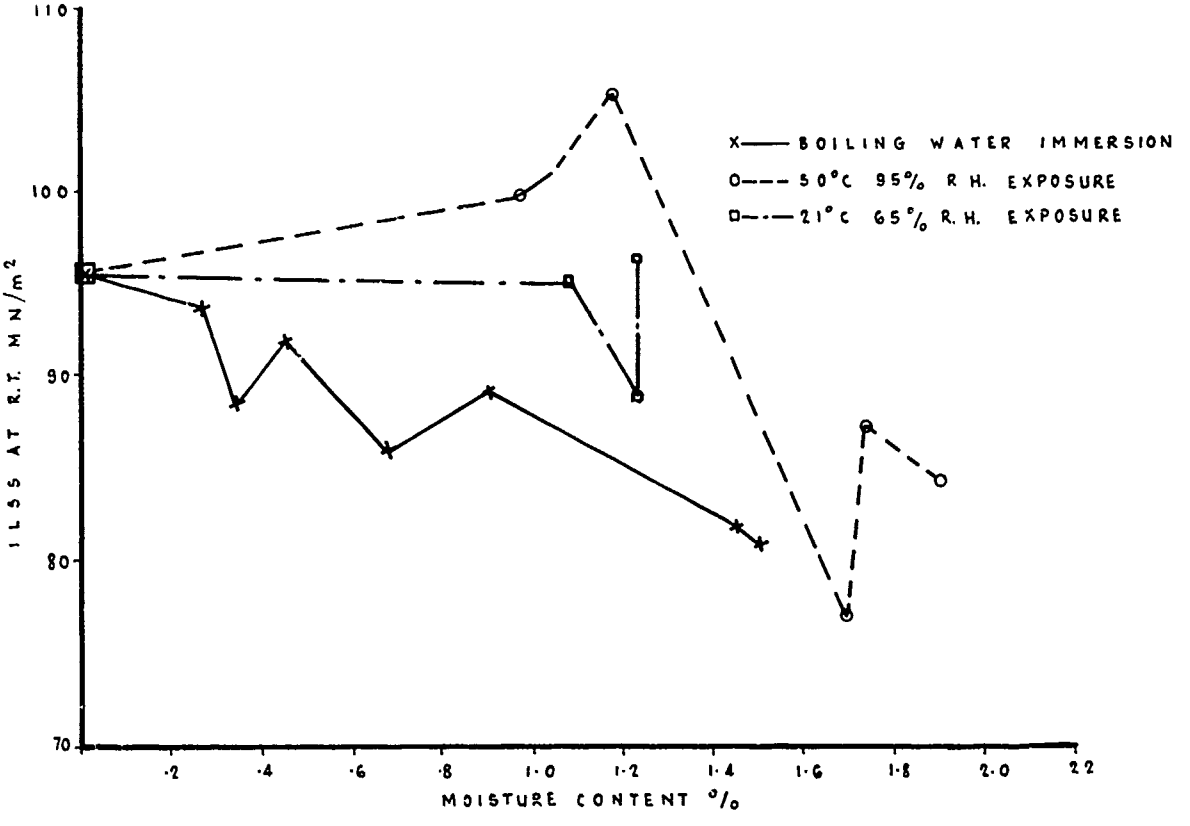

Fig.18 Relationship between ILSS at RT and moisture content for HTS/914C (laminate 0177S) using results of joint RAE/BAe programme

THIS DOCUMENT PROVIDED BY THE ABBOTT AEROSPACE
TECHNICAL LIBRARY
ABBOTTAEROSPACE.COM

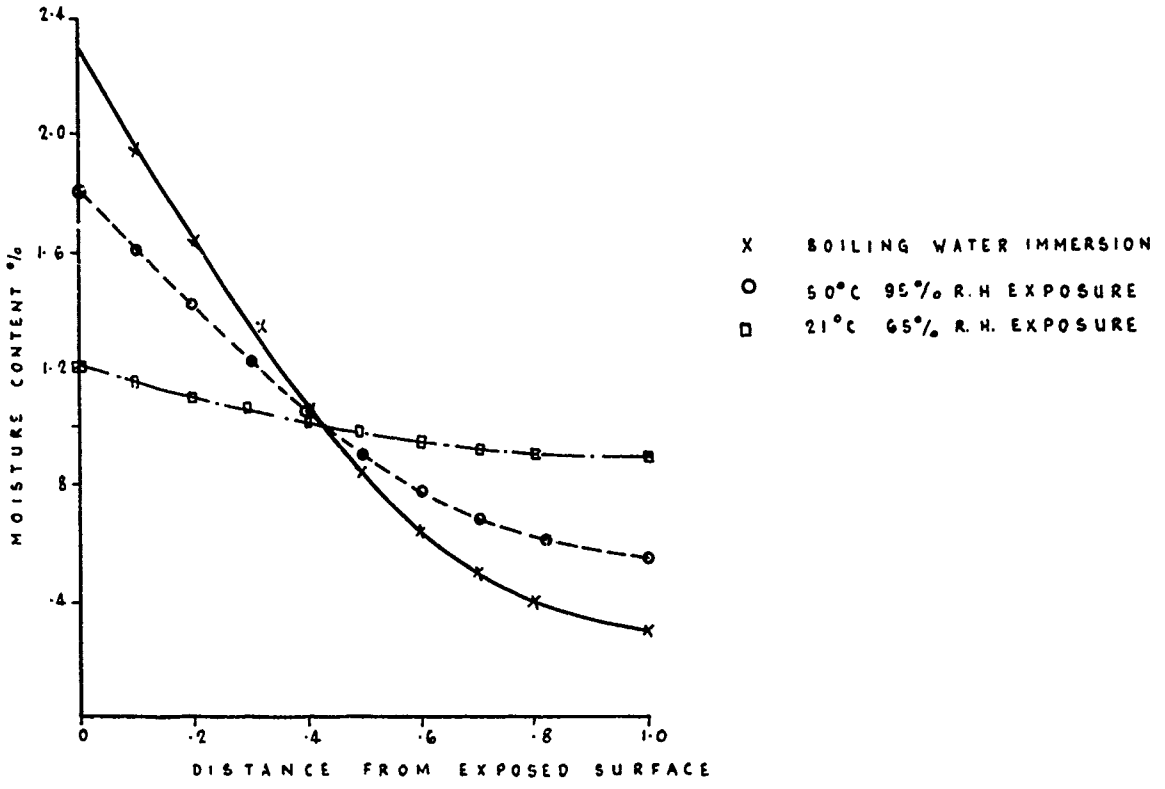

Fig.19 Through the thickness moisture prediction for ILSS specimens conditioned to 1.0% total moisture content under the three exposure conditions used in joint RAE/BAe programme

THIS DOCUMENT PROVIDED BY THE ABBOTT AEROSPACE
TECHNICAL LIBRARY
ABBOTTAEROSPACE.COM

EFFECT OF VARIOUS ENVIRONMENTAL CONDITIONS ON POLYMER MATRIX COMPOSITES

R. C. Tennyson
University of Toronto, Institute for Aerospace Studies
4925 Dufferin Street
Downsview, Ontario, Canada
M3H 5T6

SUMMARY

This report presents experimental results obtained on the short and long term behaviour of polymer matrix composites subjected to various environmental conditions. Changes in mechanical stiffness, strength and coefficient of thermal expansion were measured under ambient pressure and thermal vacuum conditions ($10^{-6} \sim 10^{-8}$ torr). It should be noted that in all tests involving the vacuum environment, measurements were made in-situ, thus necessitating the use of mechanical loading fixtures acting through flexible bellows to provide stiffness and strength data. Results are also given on the effects of varying some fabrication parameters (length of post-cure time and rate of cool-down in autoclave) on the changes observed in strength and stiffness. The materials investigated include: graphite/epoxy, boron/epoxy, PRD-49/epoxy and E glass/epoxy.

NOMENCLATURE

A_{ij}, B_{ij}, D_{ij}	$\int_{-\frac{h}{2}}^{\frac{h}{2}} (\bar{Q}_{ij})_k \, (1, z, z^2)dz$, respectively
E_{11}, E_{22}	orthotropic moduli of elasticity measured in the 1 and 2 directions, respectively
F_i, F_{ij}, F_{ijk}	lamina strength tensors of the 2nd, 4th and 6th ranks, respectively
G_{12}	shear modulus of elasticity measured in 1-2 plane
h	total laminate thickness
m, n	$\cos\theta$, $\sin\theta$, respectively
$\bar{n}$	total number of laminae in laminate
N_x, N_y	normal laminate stress resultants acting along x, y axes, respectively
N_{xy}	shear laminate stress resultant acting in x-y plane
$\bar{Q}_{11}$	$Q_{11}m^4 + 2(Q_{12} + 2Q_{66})n^2m^2 + Q_{22}n^4$
$\bar{Q}_{22}$	$Q_{11}n^4 + 2(Q_{12} + 2Q_{66})n^2m^2 + Q_{22}m^4$
$\bar{Q}_{12}$	$(Q_{11} + Q_{22} - 4Q_{66})n^2m^2 + Q_{12}(m^4 + n^4)$
$\bar{Q}_{66}$	$(Q_{11} + Q_{22} - 2Q_{12} - 2Q_{66})n^2m^2 + Q_{66}(m^4 + n^4)$
$\bar{Q}_{16}$	$(Q_{11} - Q_{12} - 2Q_{66})nm^3 + (Q_{12} - Q_{22} + 2Q_{66})n^3m$
$\bar{Q}_{26}$	$(Q_{11} - Q_{12} - 2Q_{66})n^3m + (Q_{12} - Q_{22} + 2Q_{66})nm^3$
Q_{11}	$E_{11}/(1 - \nu_{12}\nu_{21})$
Q_{22}	$E_{22}/(1 - \nu_{12}\nu_{21})$
Q_{12}	$\nu_{21}E_{11}/(1 - \nu_{12}\nu_{21}) = \nu_{12}E_{22}/(1 - \nu_{12}\nu_{21})$
Q_{66}	G_{12}
S, S'	positive and negative lamina shear strengths measured in 1-2 plane
T	temperature
X, X'	tensile and compressive lamina strengths measured in 1 direction
Y, Y'	tensile and compressive lamina strengths measured in 2 direction
z	distance from mid-surface normal to x-y plane

Subscripts

k	lamina number
L	laminate
o	midplane value

TECHNICAL LIBRARY
ABBOTTAEROSPACE.COM

x, y	orthogonal in-plane structural axes
1, 2	lamina material axes parallel and orthogonal to fiber (or filament) reinforcement
6	refers to shear value measured in 1-2 plane

Greek Symbols

α	coefficient of thermal expansion
γ	shear strain
ϵ	normal strain
κ	curvature
θ	fiber orientation relative to x-axis
ν	Poisson's ratio
σ	normal stress
τ	shear stress

1. INTRODUCTION

Aerospace applications of composite materials are increasing every year. One of the major concerns in the use of composites, particularly for primary structure and hardware components, is the effect of various environmental conditions on the material properties. This is especially true for polymer matrix systems which can be quite sensitive to temperature, moisture and radiation for example. Although in some cases extensive environmental test data can be found in the literature, a scarcity of information exists on space environment effects.

During the life cycle of a structure that must operate full or part-time in space, it will experience an exceedingly harsh environment composed of temperature extremes, ultra hard vacuum, a broad spectrum of intense radiation, micro-meteorite impact and impingement by various atomic and molecular species. Thus one is faced with the difficult task of assessing the degree to which such an environment will affect material properties over a prolonged period.

By necessity, one must either transport the materials in question to the space environment and retrieve them for examination (such as is planned in the NASA Long Duration Exposure Facility for example) or test these materials in a simulated space environment. Although a complete ground simulation is virtually impossible, the combined effects of temperature and vacuum are quite readily obtained. Additional features such as ultraviolet radiation and high energy particle and molecular beam bombardment can also be attained.

If one considers the effect of vacuum alone, loss of adsorbed and absorbed gases as well as sublimation or evaporation of the more volatile constituents of the material can occur. This is particularly evident for many organic/polymeric materials which are used as matrix or bonding agents in composite materials, as illustrated in Fig. 1. Using a mass spectrometer capable of resolving species in the range of 13 ~ 80 AMU and partial pressures of the order of 10^{-10} torr, it was found that the dominant outgassing component was H_2O^+. Furthermore it can be observed that it took about two weeks for the chamber vacuum pressure to drop from ~ 10^{-6} torr to ~ 10^{-8} torr due to material outgassing. Moreover, if these same materials are then exposed to ambient conditions, re-absorption occurs, as shown in Fig. 2. The excess in weight above the initial sample value (prior to vacuum exposure) is probably due to moisture diffusion into the composite, occupying molecular sites vacated by other lower mass number polymer molecules.

In addition to vacuum and temperature, the cumulative effects of radiation and thermal fatigue pose serious questions regarding the long term behaviour of polymer matrix composites in space. Recourse to special protective coatings may well be necessary to prevent significant material degradation.

The assessment of property changes resulting from exposure in a simulated space environment is best done with the samples remaining in the vacuum state. This is desirable to eliminate possible ground handling effects and re-absorption of atmospheric moisture and contaminants, as previously noted. Thus special facilities and test fixtures are required to provide in-situ loading, as will be described later. By necessity, one must obtain ambient pressure reference data which are also of value for 'non-space' applications.

Figure 3 summarizes the environmental and material parameters currently being investigated. To provide a comparison for the space simulation results, a composite experiment (Fig. 4) has also been assembled for inclusion in a forthcoming NASA LDEF mission. Since this satellite is scheduled to be retrieved after about 9 ~ 12 months exposure, it will be possible to compare property changes, as outlined in Fig. 5. The purpose of this report is to present results obtained from one phase of the program involving ground-based simulation. Material parameters of interest include strength, stiffness, coefficient of thermal expansion (CTE) and damping.

TECHNICAL LIBRARY
ABBOTTAEROSPACE.COM

2. STRENGTH AND STIFFNESS

2.1 General Strength Criterion

The usefulness of composite strength test data is governed by the failure criteria one employs to analyse individual laminae and laminates. The author has shown (Refs. 1 and 2) that the cubic form of the tensor polynomial lamina failure criterion provides the best correlation with experiments, particularly under biaxial load conditions. For a lamina subject to a plane stress the strength equation can be written in the form,

$$\begin{aligned} &F_1\sigma_1 + F_2\sigma_2 + F_{11}\sigma_1^2 + F_{22}\sigma_2^2 + F_{66}\sigma_6^2 \\ &+ 2F_{12}\sigma_1\sigma_2 + 3F_{112}\sigma_1^2\sigma_2 + 3F_{221}\sigma_2^2\sigma_1 \\ &+ 3F_{166}\sigma_1\sigma_6^2 + 3F_{266}\sigma_2\sigma_6^2 = 1 \end{aligned} \tag{1}$$

where it has been assumed that certain material property symmetry conditions hold true and odd order terms in σ_6 vanish. This requires the lamina to exhibit identical strength for both positive and negative shear (relative to the principal axes). The principal strength tensor components are defined by

$$\begin{aligned} F_1 &= \frac{1}{X} - \frac{1}{X'} \qquad F_2 = \frac{1}{Y} - \frac{1}{Y'} \qquad F_6 = \frac{1}{S} - \frac{1}{S'} \\ F_{11} &= \frac{1}{XX'} \qquad F_{22} = \frac{1}{YY'} \qquad F_{66} = \frac{1}{SS'} \end{aligned} \tag{2}$$

and the interaction terms (F_{12}, F_{112}, F_{221}, F_{166}, F_{266}) are described in Refs. 1 and 3.

Although the quadratic form of Eq. (1) is most often employed, one only has to examine the case of biaxial loading to realize how deficient it is. For example, one can consider a symmetric balanced laminate of $\pm\theta$ construction and calculate the failure condition for varying biaxial tensile stress ratios defined by N_x/N_y with $N_{xy} = 0$. Solutions were obtained in Ref. 2 for a graphite/epoxy material using both the quadratic and cubic formulations. If one plots the maximum strength ($\sigma_{Y_{LMAX}}$) and corresponding optimum fiber angle 'θ_o' for each value of the biaxial stress ratio, substantial differences between the two failure model predictions can be seen in Fig. 6. Note that the stress axis ($\sigma_{Y_{LMAX}}$) has been nondimensionalized by the uniaxial tensile strength measured in the fiber direction, $X \approx 185.63$ KSI for SP-288 T-300 (Ref. 1). One interesting feature which emerges is that not only does the quadratic criterion underestimate the strength, but the optimum fiber angle can be off as much as 10°, although generally the difference is less. This fact suggests that the quadratic equation cannot be used reliably in strength design for selecting an optimum laminate configuration. Note that when $\alpha = 0.5$, corresponding to internal pressure loading for example, both formulations give the same angle. Figure 7 presents a comparison of both failure models with experiments for this particular load case. It is readily apparent that the cubic equation provides the best correlation with test data. Let us now demonstrate the effect of a lamina failure criterion on the overall strength of a composite structure laminated in such a way that first ply failure does not constitute total failure. Clearly, once a ply (or set of plies) has suffered partial or total failure, a change in the stress/strain response should be evident. Referring to the diagram of Fig. 8, several failure modes are possible: (i) matrix crazing or fracture with fiber reinforcement intact; (ii) interlamina shear separation from adjacent plies; (iii) fiber/matrix fracture. Consequently, after initial "failure", assumptions have to be made regarding the effect of the "failed" ply (or plies) on the stiffness of the remaining structure. In Ref. 2, internal pressure tests were carried out on circular cylindrical graphite/epoxy tubes of $(\pm\theta_1, \pm\theta_2)_s$ symmetric construction. The results from one particular experiment for an 8 ply $(\pm 30°, \pm 55°)_s$ tube are shown in Fig. 9. Multi-mode failures occurring at ~ 2 KSI and ~ 3 KSI agree rather well with the cubic model predictions. Note that for this case the quadratic equation gives an overall ultimate strength of only ~ 2 KSI.

Having developed a failure analysis, it now remains to investigate the effect of various environmental factors on the strength and stiffness parameters. For completeness, one should include the four lamina orthotropic elastic 'constants' (E_{11}, E_{22}, ν_{12} and G_{12}) as well as the five principal strength terms (X, X', Y, Y', S). In general, knowledge of these parameters is sufficient tocalculate all of the tensor polynomial strength coefficients [see Eq. (1)] using the methods outlined in Ref. 1, and all of the lamina stresses, assuming linear elastic behaviour. However, up to this point, environmental data have only been obtained for E_{22} and Y, although one might expect that E_{11}, X and X' may not change appreciably anyway.

2.2 Effect of Post-Cure Time and Cool-Down Rate

Prior to studying environmental effects on material strength and stiffness, it was decided to investigate the influence of manufacturing variables. Tests were carried out on 4 ply 90° tubes for varying autoclave post-cure times and cool-down rates.

In the first phase involving post-cure times ranging from zero (i.e., no additional post-cure beyond manufacturer's specifications) to 24 hours, a glass/epoxy prepreg was used (3M SP 1002). It was found that no significant changes in E_{22} occurred, although some ambient strength increases (Y) were obtained, as shown in Fig. 10 in terms of F_2 and F_{22}.

Another interesting parameter from a manufacturing point of view is the rate at which the composite structure is cooled after the required cure cycle time in the autoclave. Varying rates of cool-down were achieved and recorded by thermocouples mounted on graphite/epoxy specimens. Typical rates of temperature reduction are shown in Fig. 11 where it is indicated how the values of (dT/dt) were estimated. Again it was observed that E_{22} did not change significantly, but some minor reduction in ambient strength (Y) with increasing dT/dt was found, as shown in Fig. 12.

This Document Provided by
TECHNICAL LIBRARY
ABBOTTAEROSPACE.COM

2.3 Effect of Thermal-Vacuum Environment

Stiffness and strength data were obtained at ambient pressure as a function of temperature for a graphite/epoxy material and are plotted in Figs. 13 and 14. The scatter bars indicate the range of maximum deviations found when three or more tests were conducted at a given temperature. It should be noted that the ambient data were obtained from specimens stored under "normal" laboratory conditions, with no regard for moisture content.

Based on the ambient pressure strength results, it was possible to calculate the thermal variation in the graphite/epoxy strength tensor coefficients F_2, F_{22} as shown in Figs. 15 and 16, respectively. From a design viewpoint, although this parameter is the "lowest" of the strength tensor components, its effect on the ultimate strength of any laminate configuration can be quite severe depending of course on the nature of the loading.

As stated earlier, in-situ vacuum testing of polymer matrix composites is regarded as a necessity. Thus space simulator facilities such as that shown in Fig. 17 have been developed at UTIAS capable of in-situ loading to determine the stiffness and strength parameters. The vacuum system is composed of several major components for pumping, valving, pressure measurement, baking, trapping and piping, a complete description of which can be found in Ref. 4. The stainless steel test chamber is cylindrical in shape, measuring 51 cm in diameter x 117 cm in length. Combined action of roughing and oil diffusion pumps with a liquid nitrogen cryogenic trap above the diffusion pump permits 10^{-6} torr to be achieved in about one hour. Of particular interest is the mechanical loading fixture attached to the chamber door (Fig. 18) which can supply in-situ uniaxial or torsional loading of specimens. Universal gimbals ensure alignment of the load which is transmitted via hydraulic pistons acting through flexible stainless steel bellows.

It is fairly certain that for most fiber reinforced polymer matrix materials, the existence of any thermal-vacuum effect should be most pronounced in terms of the matrix response. Consequently, test configurations were selected consisting of graphite/epoxy 90° layups (i.e., circumferential fiber orientation) using thin-walled tubes (0.38 mm ~ 0.58 mm thick) manufactured in-house with a belt-wrapper apparatus. Using bonded foil strain gauges, the variation in E_{22} was measured under vacuum conditions for varying temperatures (Fig. 13). If one now compares the mean results, it would appear that an increase in stiffness occurs in the vacuum state. Because of the limited test data for $T > 200°F$, it is premature to speculate on whether the large differences in E_{22} exist or not. However, it is well known that moisture content within the epoxy matrix can result in drastic strength reduction as one approaches the glass transition temperature for the resin system. Since no precautions were taken with the "ambient" specimens to limit or reduce their moisture absorption, there may well be a significant effect in terms of E_{22} as indicated. Confirmation of this behaviour must await tests which will be performed on specimens currently being studied in another facility.

Ultimate tensile strengths were also determined for the same specimens. A comparison between ambient pressure and vacuum strength data for varying temperatures is given in Fig. 14, where the results have been nondimensionalized by the ambient pressure, room temperature strength (Y_{RT}). Based on the mean values shown, it would appear that an increase in the matrix strength parameter occurs in vacuum, although substantial scatter in the test data is evident. Despite this scatter, three anomalous failure loads were obtained in the vacuum environment that fell well below the "scatter" range. From a design point of view, the rather limited results available indicate a 20% probability of the occurrence of such low loads within a group of test specimens fabricated at the same time, from the same material batch under highly controlled conditions. Since this anomalous behaviour has never been observed in our multitudinous ambient pressure tests conducted over the past five years using various batches of materials, it means that some random "flaw" characteristic might be present whose effect is amplified under vacuum conditions. However, elucidation of this effect should be forthcoming based on the number of specimens presently residing in the long term thermal-vacuum facility. They should provide statistically valid data when strength tests are carried out in the near future.

3. COEFFICIENT OF THERMAL EXPANSION (CTE)

One of the main design considerations associated with the use of composites is the possibility of achieving dimensional stability over a wide temperature range. For example, materials such as graphite/epoxy and Kevlar /epoxy provide the opportunity to design structural components with essentially a zero value of CTE in prescribed directions. Consequently, an extensive program was undertaken to obtain CTE data for three materials: graphite/epoxy (3M SP288 T300), Kevlar /epoxy (3M SP306, PRD-49-III) and and boron/epoxy (3M SP290). Up to present, emphasis has been placed on determining the variation in CTE with "number of thermal cycles under both ambient pressure and vacuum conditions. It is of value at this stage to present the theoretical CTE equation (refer to Appendix A for the derivation) for a given composite laminate. It should be emphasized that the structural CTE matrix $[\alpha]$ is dependent on the principal lamina stiffness and CTE parameters as well as the particular filament orientation (θ). Thus, for the special case of $\pm\theta$ symmetric laminates, the following equation can be used:

$$[\alpha] = [A_{ij}]^{-1} \sum_{k=1}^{\bar{n}} [\tilde{T}]_k^{-1} [Q]_k [\tilde{\alpha}] (h_k - h_{k-1}) \tag{3}$$

where

$$[\alpha] \equiv \begin{bmatrix} \alpha_x \\ \alpha_y \\ \alpha_{xy} \end{bmatrix} \quad \text{and} \quad [\tilde{\alpha}] \equiv \begin{bmatrix} \alpha_1 \\ \alpha_2 \\ 0 \end{bmatrix}$$

TECHNICAL LIBRARY
ABBOTTAEROSPACE.COM

3.1 CTE Test Procedure and Calibration

All thermal response data were obtained using bonded foil strain gauges (type EA-06-250-BB120, Micro-Measurements, USA) after extensive calibration under ambient pressure and vacuum conditions. The apparent response of a strain gauged structure or material sample undergoing a temperature change (ΔT) (i.e., the reading one obtains from a strain indicator) is given by

$$\epsilon_A = \epsilon_M - \epsilon_g \tag{4}$$

where 'M' and 'g' refer to the 'material' and strain 'gauge', respectively. If the material and gauge strains vary linearly over the temperature range of interest, then we can re-write Eq. (4) as

$$\alpha_m = \frac{\epsilon_A}{\Delta T} + \alpha_g \tag{5}$$

where α_m and α_g denote the material and strain gauge coefficients of thermal expansion, respectively. The determination of an average value for α_g at ambient pressure was made by bonding three gauges on separate metal tubes: steel, copper and aluminum, subjecting each sample to uniform heating and measuring the axial displacement as a function of temperature. This was done in a small oven (containing a glass window) mounted in a travelling microscope. At the same time, the apparent strains were recorded to correlate with the actual strains at different temperature increments. After many repeat tests, a least squares fit yielded an average value of $\alpha_g = 6.93 \times 10^{-6}$ in/in/°F (Fig. 19). The next step involved calibrating the strain gauge-metal tube system in vacuum. As shown in Fig. 20, the calibration for α_g shifted due to outgassing and the final value used throughout the remainder of this report was taken as $\sim 6.55 \times 10^{-6}$ (in/in/°F) under vacuum conditions.

Most of the subsequent test data are based on continuous thermal cycling ($75°F \leq T \leq 200°F$) at $10^{-7} \sim 10^{-8}$ torr over a period exceeding 6 months using the facility shown in Fig. 21. This ultra high vacuum chamber has a working volume of approximately 66 cm diameter x 76 cm in height. Employing a roughing pump, two Zeolite adsorption pumps and an ion getter pump yields a vacuum close to 10^{-8} torr in a fully loaded state. Currently, 158 composite specimens (120 flats + 38 tubes) are mounted in a tray structure slung below the top chamber closure plate (see Fig. 22). Of this number, 33 were strain gauged for monitoring thermal response of the materials. Both levels of the tray contain 3 thermocouples each to record temperature. Note that throughout this experiment, a calibrated steel tube containing the same type of bonded strain gauge was inside the facility undergoing the same thermal-vacuum cycling as the composite samples. It was found that no significant deviation in the measuring system occurred, thus providing the necessary confidence for interpreting the composite materials' response.

3.2 CTE Results

Figures 23, 24 and 25 present the CTE data obtained on 4 ply $\pm\theta$ symmetric balanced laminates as a function of the number of thermal cycles for varying vacuum exposure times. The three materials investigated include Kevlar/epoxy, graphite/epoxy and boron/epoxy

It is quite apparent that substantial changes occur in CTE due to the combined effects of vacuum and thermal cycling. Since the development and accumulation of microcracks together with bulk material outgassing probably account for this behaviour, it is reasonable to expect that the 'drift' in CTE's should level off with time. Clearly knowledge of the asymptotic values is required for design purposes. Independent measurements on a $\pm 43°$ graphite/epoxy tube confirm the vacuum effect change (see Fig. 23) after only two thermal cycles for 48 hrs at $\sim 10^{-7}$ torr.

To assess test data consistency, it is possible to calculate the theoretical variation in CTE [Eq. (3)] with fiber angle based on knowing α_1 ($\equiv \alpha_{0°}$), α_2 ($\equiv \alpha_{90°}$) and the four elastic orthotropic constants, E_{11}, E_{22}, G_{12}, ν_{12}. This was done for ambient pressure and vacuum conditions, the latter corresponding to 167 days at $10^{-7} \sim 10^{-8}$ torr after 31 thermal cycles. Figures 26 and 27 provide comparisons of the experimental results with predictions and it can readily be seen that excellent correlation was achieved. Note that for the graphite/epoxy vacuum tests, only one set of data at $\pm 43°$ (other than α_1 and α_2) was available for comparative purposes. One other factor that should be considered in these calculations is the variation in orthotropic elastic constants with temperature and vacuum. However, at present, we have only been able to accumulate graphite/epoxy test results on the change in E_{22} with temperature at $10^{-6} \sim 10^{-7}$ torr up to ~ 214 hrs (see Fig. 13). Nonetheless, using this value at $\sim 200°F$, curves were constructed to compare with the room temperature (75°F) modulus analysis, as shown in Fig. 26. From a design viewpoint, no significant effect occurs at the zero CTE crossing.

REFERENCES

1. R. C. Tennyson, D. MacDonald and A. P. Nanyaro, "Evaluation of the Tensor Polynomial Failure Criterion for Composite Materials", J. Composite Materials, Vol. 12, 1978.

2. R. C. Tennyson, A. P. Nanyaro and G. E. Wharram, "Application of the Cubic Polynomial Strength Criterion to the Failure Analysis of Composite Materials", to be published, J. Composite Materials, 1980.

3. S. W. Tsai and E. M. Wu, "A General Theory of Strength for Anisotropic Materials", J. Composite Materials, Vol. 5, 1971.

4. R. C. Tennyson, J. S. Hansen, R. P. Holzer, B. T. Uffen and G. Mabson, "Thermal-Vacuum Facility with In-Situ Loading", Proc. AIAA/IES/ASTM 10th Space Simulation Conf., Bethesda, Md., Oct. 1978.

THIS DOCUMENT PROVIDED BY
TECHNICAL LIBRARY
ABBOTTAEROSPACE.COM

ACKNOWLEDGEMENT

The author wishes to acknowledge the financial support for various phases of this program received from the National Research Council of Canada (Grant No. A-2783), the U.S. National Aeronautics and Space Administration (NSG-7409) and the U.S. Air Force Office of Scientific Research (AFOSR-78-3694). The NASA work is concerned with the composite strength studies whereas the AFOSR project involves space simulation effects on CTE. Research associates and assistants participating in the composites program include: Prof. J. S. Hansen, Mr. J. Catalano, Mr. G. Mabson, Mr. D. Morison, Mr. B. Uffen and Mr. G. Wharram.

APPENDIX A: DERIVATION OF COEFFICIENTS OF THERMAL EXPANSION

In general, if one considers a temperature change ΔT acting on a thin laminate composed of an assembly of linear elastic 'homogeneous' orthotropic laminae, the thermal stresses (referenced to some arbitrary set of structural axes X, Y) in the k-th lamina are given by:

$$\begin{bmatrix}\sigma_x\\ \sigma_y\\ \tau_{xy}\end{bmatrix}_{T_k} = [\bar{Q}_{ij}]_k \begin{bmatrix}\epsilon_x\\ \epsilon_y\\ \gamma_{xy}\end{bmatrix}_{T_k} - [\tilde{T}]_k^{-1}[Q]_k \begin{bmatrix}\alpha_1\\ \alpha_2\\ \cdot\end{bmatrix}_k \Delta T \qquad (A\text{-}1)$$

where

$$[\bar{Q}_{ij}] = \begin{bmatrix}\bar{Q}_{11} & \bar{Q}_{12} & \bar{Q}_{16}\\ \bar{Q}_{12} & \bar{Q}_{22} & \bar{Q}_{26}\\ \bar{Q}_{16} & \bar{Q}_{26} & \bar{Q}_{66}\end{bmatrix}$$

$$[Q] = \begin{bmatrix}Q_{11} & Q_{12} & 0\\ Q_{12} & Q_{22} & 0\\ 0 & 0 & Q_{66}\end{bmatrix}$$

$$[\tilde{T}] = \begin{bmatrix}m^2 & n^2 & 2mn\\ n^2 & m^2 & -2mn\\ -mn & mn & m^2-n^2\end{bmatrix}$$

Substituting for the k-th lamina in-plane strains in terms of the laminate mid-plane strains and curvatures, Eq. (A-1) becomes:

$$\begin{bmatrix}\sigma_x\\ \sigma_y\\ \tau_{xy}\end{bmatrix}_{T_k} = [\bar{Q}_{ij}]_k \begin{bmatrix}\epsilon_{x_o}\\ \epsilon_{y_o}\\ \gamma_{xy_o}\end{bmatrix}_{T_k} + Z[\bar{Q}_{ij}]_k \begin{bmatrix}\kappa_x\\ \kappa_y\\ \kappa_{xy}\end{bmatrix}_{T_k} - [\tilde{T}]_k^{-1}[Q]_k \begin{bmatrix}\alpha_1\\ \alpha_2\\ 0\end{bmatrix}_k \Delta T \qquad (A.2)$$

where Z is the + distance from the laminate mid-plane to the k-th lamina.

One can now integrate through the total laminate thickness to obtain the stress and moment-resultant matrix [N/M], assuming compatibility of strain deformation between laminae and ΔT = a constant. This yields the following equations for [N/M] = [O/O]:

$$\begin{aligned}[A_{ij}]\begin{bmatrix}\epsilon_{x_o}\\ \epsilon_{y_o}\\ \gamma_{xy_o}\end{bmatrix}_T + [B_{ij}]\begin{bmatrix}\kappa_x\\ \kappa_y\\ \kappa_{xy}\end{bmatrix}_T &= \Delta T \sum_{k=1}^{\bar{n}} [\tilde{T}]_k^{-1}[Q]_k \begin{bmatrix}\alpha_1\\ \alpha_2\\ 0\end{bmatrix}_k (h_k - h_{k-1})\\ [B_{ij}]\begin{bmatrix}\epsilon_{x_o}\\ \epsilon_{y_o}\\ \gamma_{xy_o}\end{bmatrix}_T + [D_{ij}]\begin{bmatrix}\kappa_x\\ \kappa_y\\ \kappa_{xy}\end{bmatrix}_T &= \frac{\Delta T}{2} \sum_{k=1}^{\bar{n}} [\tilde{T}]_k^{-1}[Q]_k \begin{bmatrix}\alpha_1\\ \alpha_2\\ 0\end{bmatrix}_k (h_k^2 - h_{k-1}^2)\end{aligned} \qquad (A.3)$$

Solving these equations for the mid-plane thermal strains and curvatures gives:

$$[\kappa]_T = \Delta T \left\{[D_{ij}] - [B_{ij}][A_{ij}]^{-1}[B_{ij}]\right\}^{-1} \left\{\frac{1}{2}\sum_{k=1}^{\bar{n}} [\tilde{T}]_k^{-1}[Q]_k \begin{bmatrix}\alpha_1\\ \alpha_2\\ 0\end{bmatrix}_k (h_k^2 - h_{k-1}^2) - [B_{ij}][A_{ij}]^{-1} \sum_{k=1}^{\bar{n}} [\tilde{T}]_k^{-1}[Q]_k \begin{bmatrix}\alpha_1\\ \alpha_2\\ 0\end{bmatrix}_k (h_k - h_{k-1})\right\} \qquad (A.4)$$

$$[\epsilon_o]_T = \Delta T [A_{ij}]^{-1} \sum_{k=1}^{\bar{n}} [\tilde{T}]_k^{-1}[Q]_k \begin{bmatrix}\alpha_1\\ \alpha_2\\ 0\end{bmatrix}_k (h_k - h_{k-1}) - [A_{ij}]^{-1}[B_{ij}][\kappa]_T$$

THE DIGITAL PROVIDER OF THE ABBOTT AEROSPACE
TECHNICAL LIBRARY
ABBOTTAEROSPACE.COM

where

$$[\kappa]_T = \begin{bmatrix} \kappa_x \\ \kappa_y \\ \kappa_{xy} \end{bmatrix}_T$$

and

$$[\epsilon_o]_T = \begin{bmatrix} \epsilon_{x_o} \\ \epsilon_{y_o} \\ \gamma_{xy_o} \end{bmatrix}_T$$

Note that for the special case of a symmetric laminate, $[B_{ij}] = 0$ and the above equations reduce to:

$$[\kappa]_T = \frac{\Delta T}{2} [D_{ij}]^{-1} \sum_{k=1}^{\bar{n}} [\tilde{T}]_k^{-1} [Q]_k \begin{bmatrix} \alpha_1 \\ \alpha_2 \\ 0 \end{bmatrix}_k (h_k^2 - h_{k-1}^2) = 0$$

$$[\epsilon_o]_T = \Delta T [A_{ij}]^{-1} \sum_{k=1}^{\bar{n}} [\tilde{T}]_k^{-1} [Q]_k \begin{bmatrix} \alpha_1 \\ \alpha_2 \\ 0 \end{bmatrix}_k (h_k - h_{k-1})$$

Defining a matrix of thermal expansion coefficients by

$$\begin{bmatrix} \alpha_x \\ \alpha_y \\ \alpha_{xy} \end{bmatrix} \equiv \begin{bmatrix} \epsilon_{x_o}/\Delta T \\ \epsilon_{y_o}/\Delta T \\ \epsilon_{xy_o}/\Delta T \end{bmatrix}$$

one then obtains

$$\begin{bmatrix} \alpha_x \\ \alpha_y \\ \alpha_{xy} \end{bmatrix} = [A_{ij}]^{-1} \sum_{k=1}^{\bar{n}} [\tilde{T}]_k^{-1} [Q]_k \begin{bmatrix} \alpha_1 \\ \alpha_2 \\ 0 \end{bmatrix}_k (h_k - h_{k-1})$$

TECHNICAL LIBRARY
ABBOTTAEROSPACE.COM

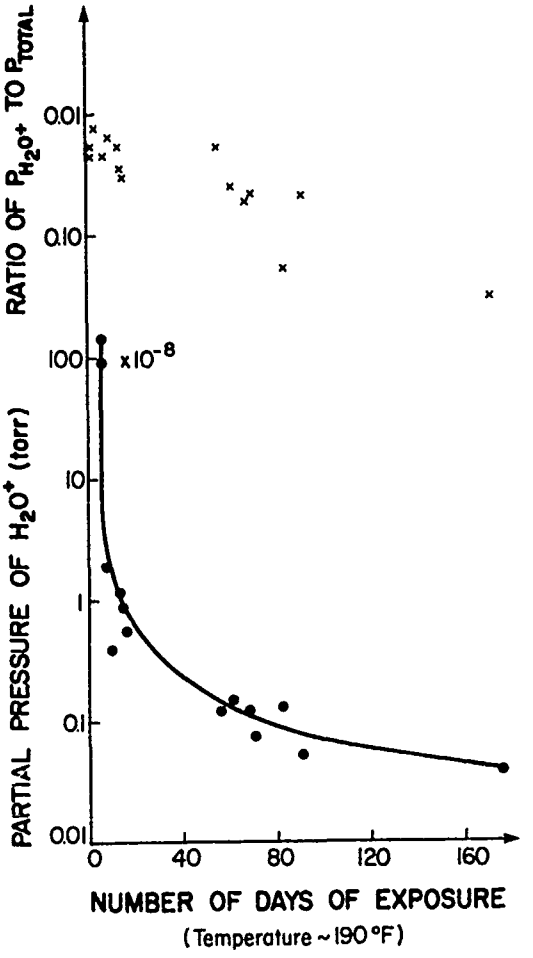

Fig.1 Mass spectrometer data on H_2O^+ as a function of vacuum duration for epoxy matrix composite

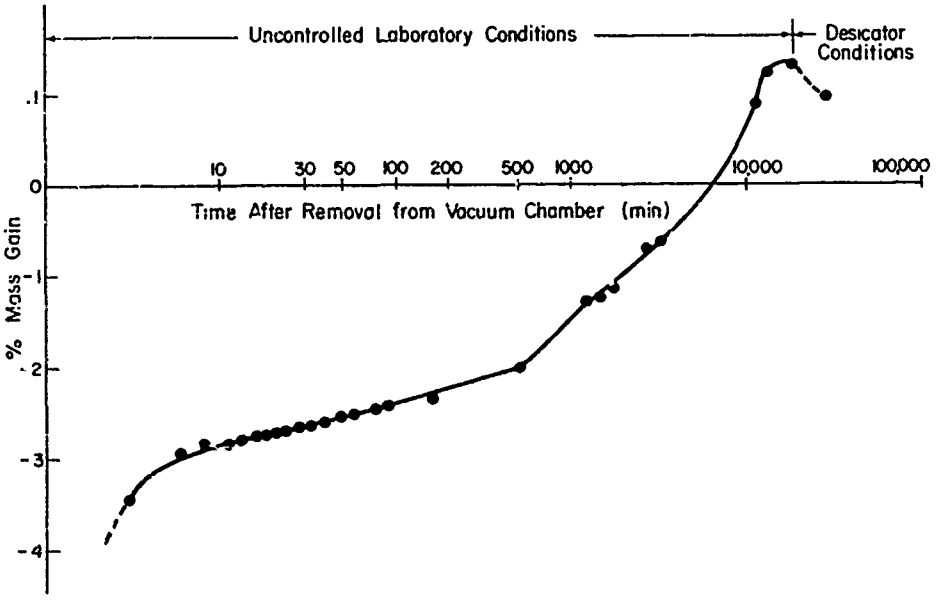

Fig.2 Variation in % mass gain for graphite/epoxy after removal from vacuum (3M SP 288 T-300)

THIS DOCUMENT PROVIDED COURTESY OF AN ABBOTT AEROSPACE
TECHNICAL LIBRARY
ABBOTTAEROSPACE.COM

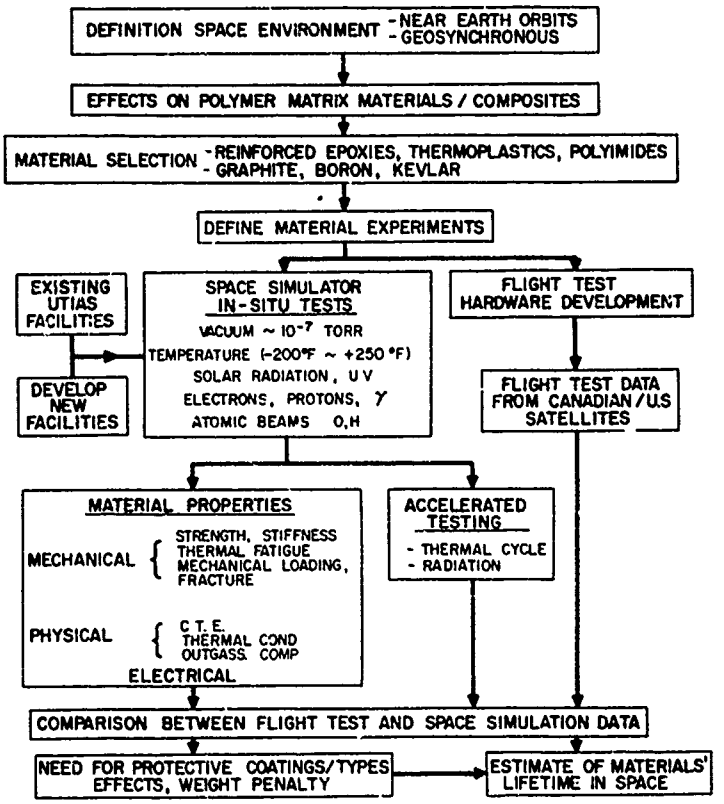

Fig.3 Flow chart illustrating research program at UTIAS

COMPOSITE MATERIALS SELECTED (3M Co.)

Graphite / Epoxy (SP 288 T 300)
Boron / Epoxy (SP 290)
Kevlar (PRD - 49 - III) / Epoxy (SP 306)
Glass / Epoxy (SP 1003)

CONFIGURATIONS (Tubes and Flat Plates)

4 Ply $\theta = 90°$
4 Ply $\theta = 0°$
4, 8, 12 Ply Sym. $\pm\theta$, Including Zero C.T.E. Quasi - Isotropic

NUMBER OF TEST SPECIMENS

63 Tubes, 4.5 cms ϕ x 10.2 cms L
45 Flats, 5 cms W x 12.7 cms L

Fig.4 UTIAS composite experiment for the NASA long duration exposure facility

TECHNICAL LIBRARY
ABBOTTAEROSPACE.COM

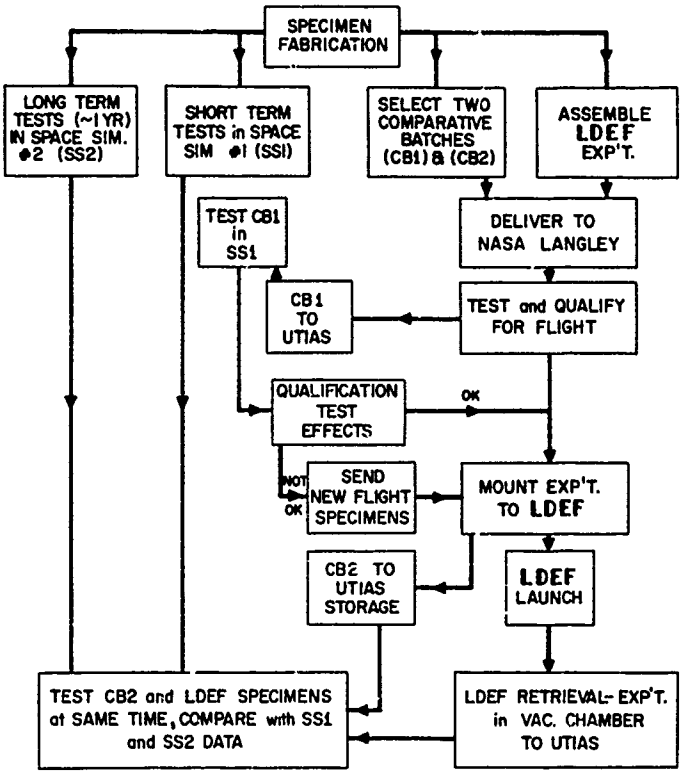

Fig.5 LDEF test programme

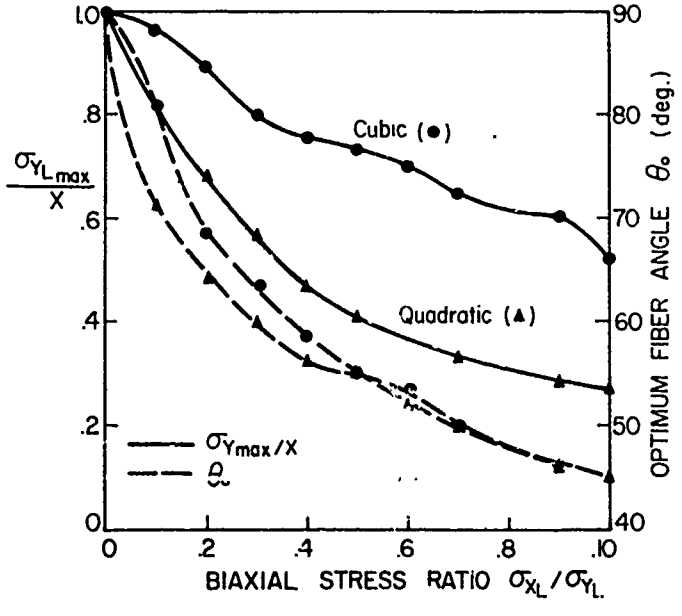

Fig.6 Locus of maximum strength and optimum fiber angle for varying values of the biaxial stress ratio

THIS DOCUMENT PROVIDED BY THE ABBOTT AEROSPACE
TECHNICAL LIBRARY
ABBOTTAEROSPACE.COM

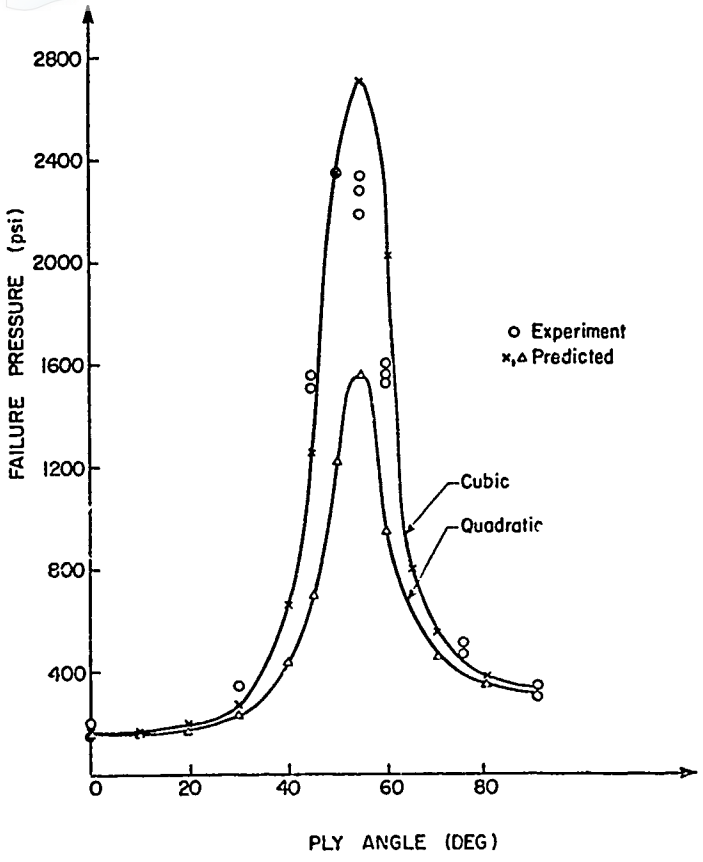

Fig.7 Failure of symmetric laminated tubes under pressure (graphite/epoxy)

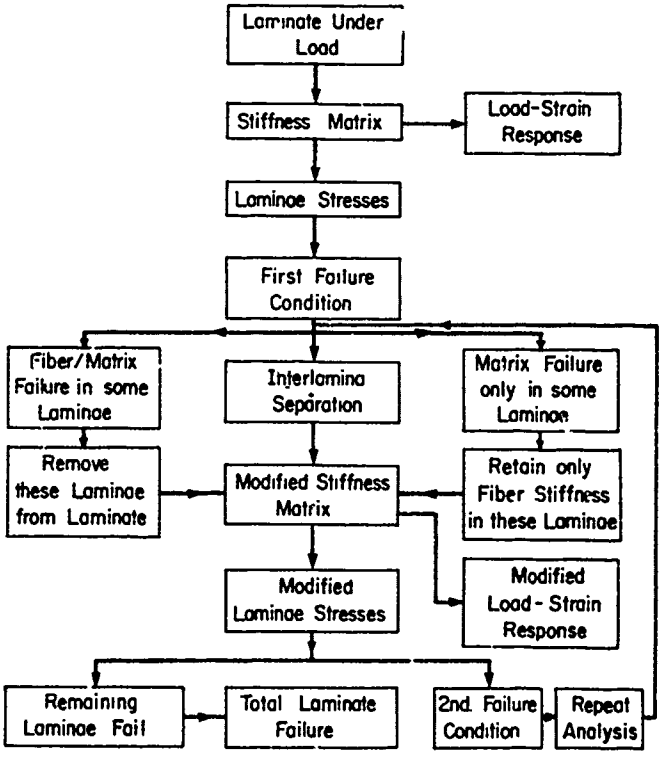

Fig.8 Procedure for calculating the load-strain response and ultimate strength of a laminate

TECHNICAL LIBRARY
ABBOTTAEROSPACE.COM

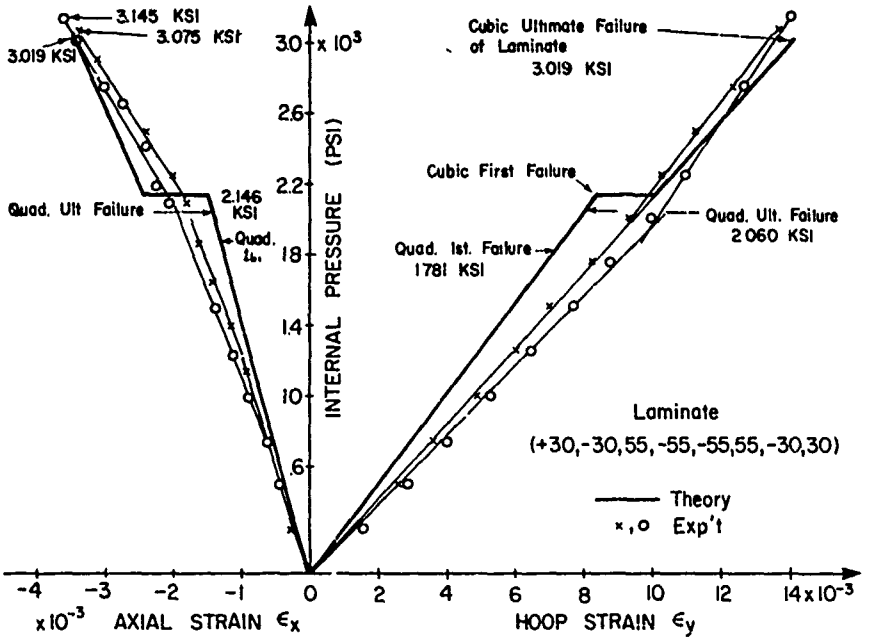

Fig.9 Comparison of cubic and quadratic failure models with experiment (SP-288 T300 3M)

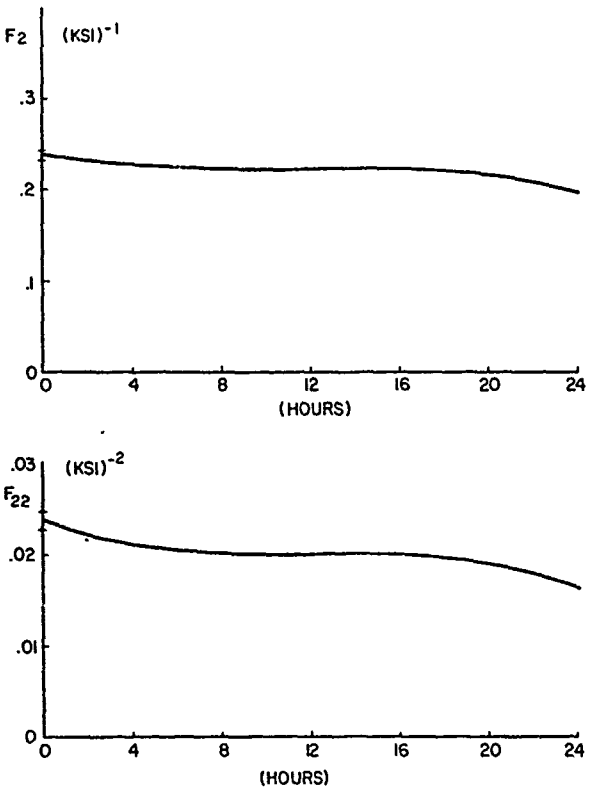

Fig.10 The variation in strength tensor component with post-cure time (glass/epoxy)

TECHNICAL LIBRARY
ABBOTTAEROSPACE.COM

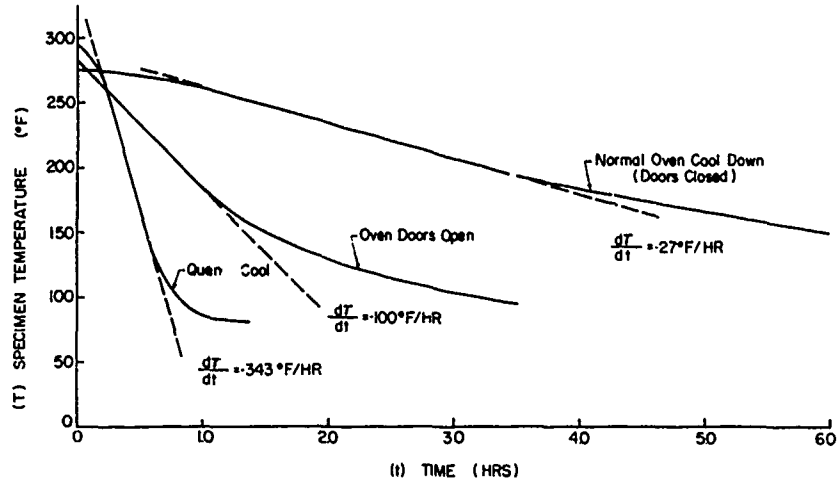

Fig.11 Varying rates of post-cure cool down for graphite-epoxy specimens in autoclave

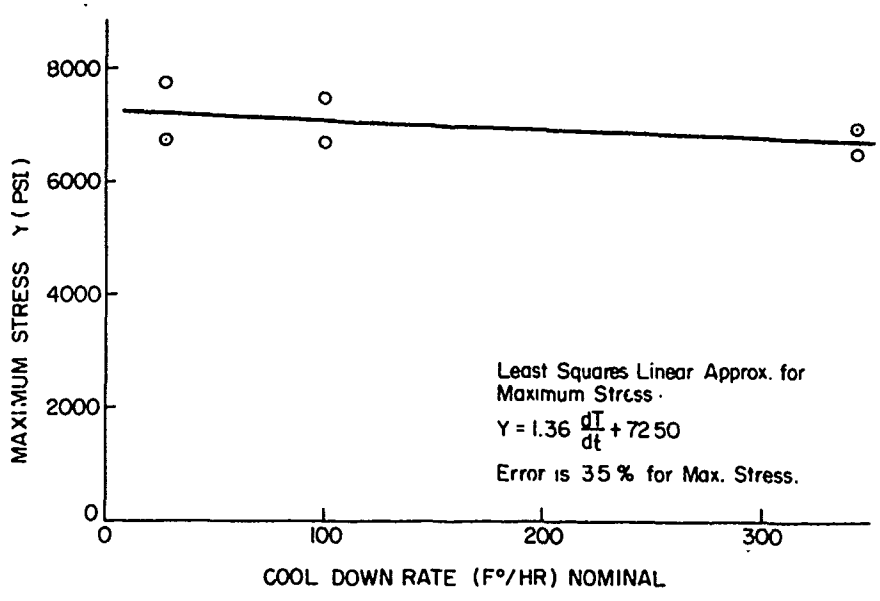

Figure 12

TECHNICAL LIBRARY
ABBOTTAEROSPACE.COM

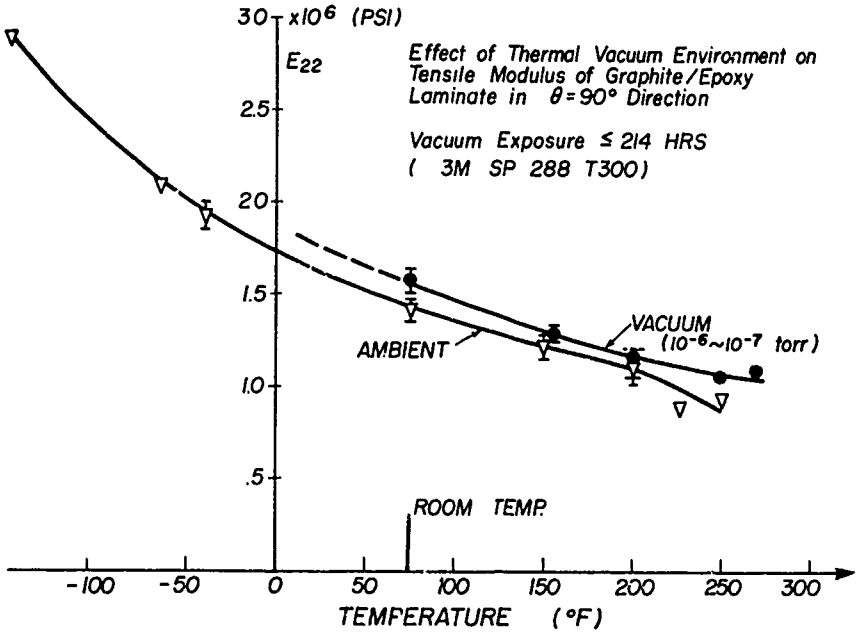

Figure 13

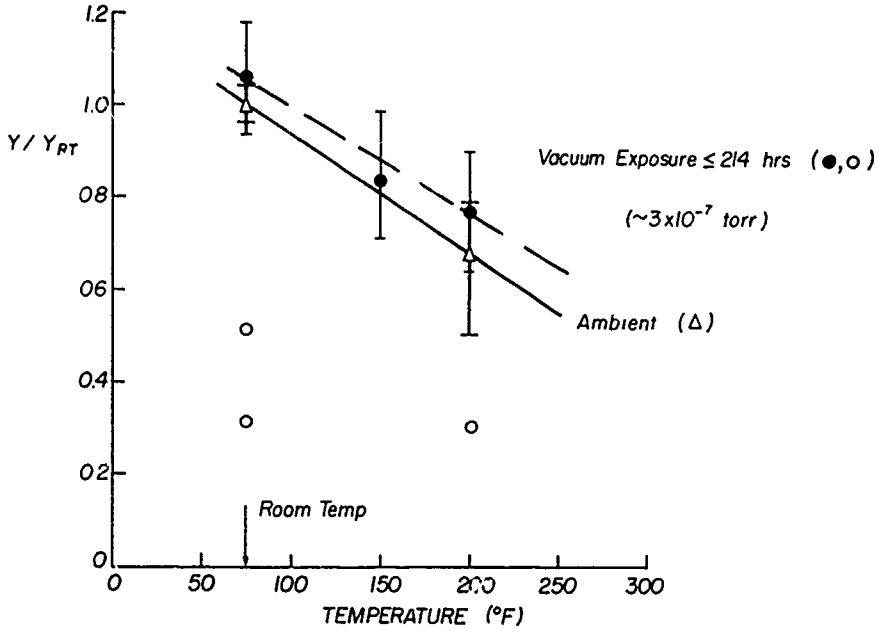

Effect of Thermal-Vacuum Environment on Tensile Strength of Graphite/Epoxy Laminates (θ=90° Configuration)

Figure 14

THIS DOCUMENT PREPARED BY
TECHNICAL LIBRARY
ABBOTTAEROSPACE.COM

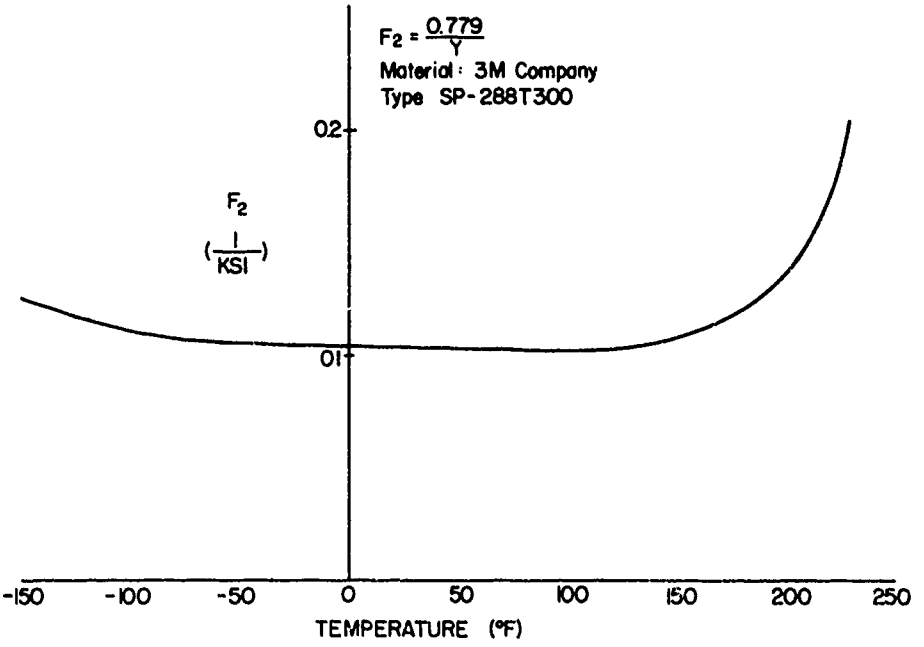

Figure 15

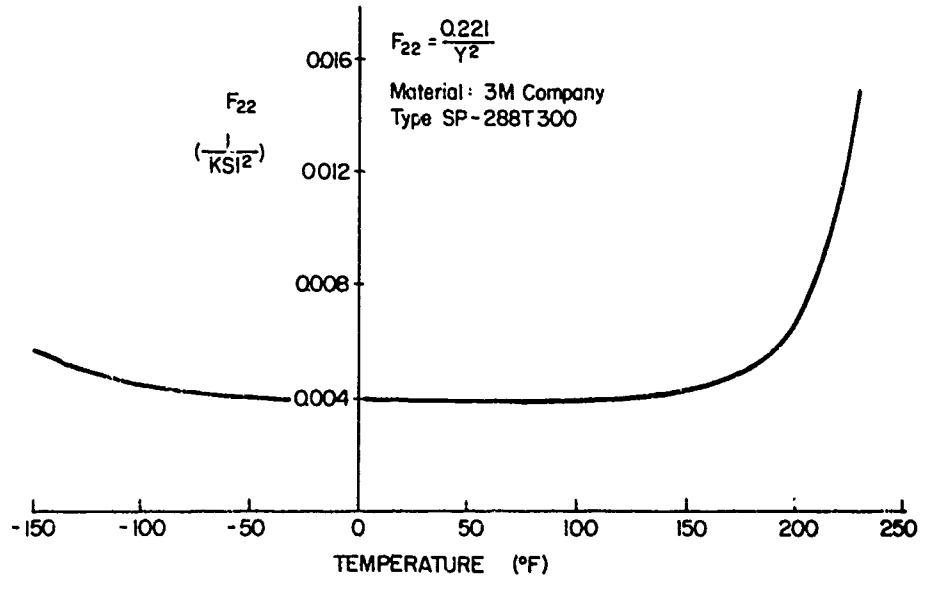

Figure 16

THIS DOCUMENT PROVIDED BY THE ABBOTT AEROSPACE
TECHNICAL LIBRARY
ABBOTTAEROSPACE.COM

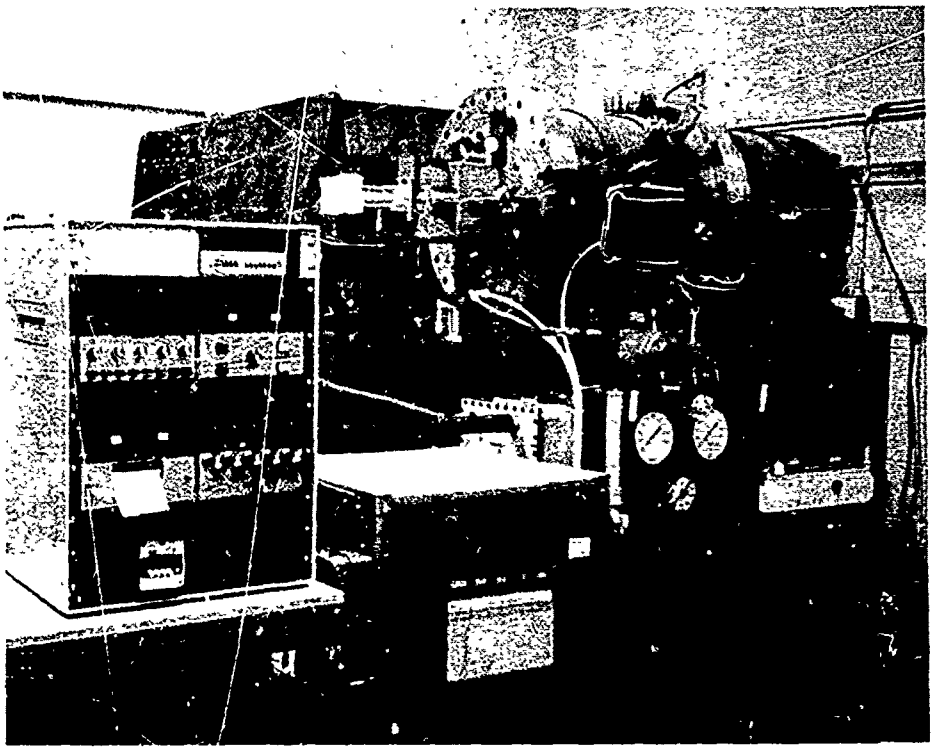

Fig.17 Thermal-vacuum chamber with in-situ mechanical loading

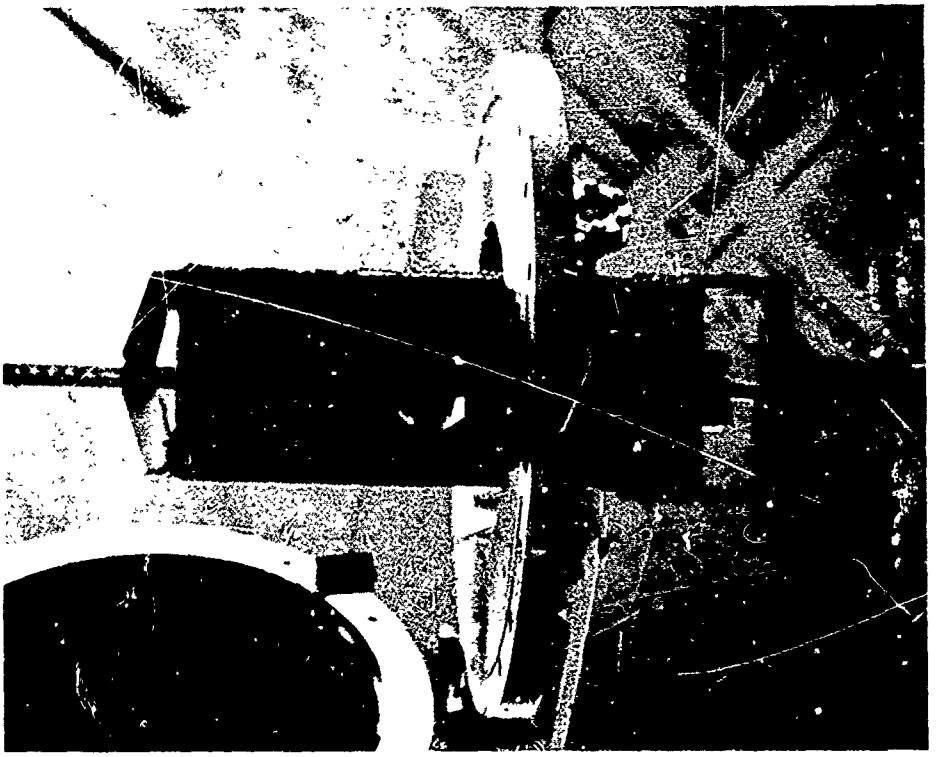

Fig.18 Chamber door with load fixture

THIS DOCUMENT PROVIDED BY THE ABBOTT TECHNICAL LIBRARY
TECHNICAL LIBRARY
ABBOTTAEROSPACE.COM

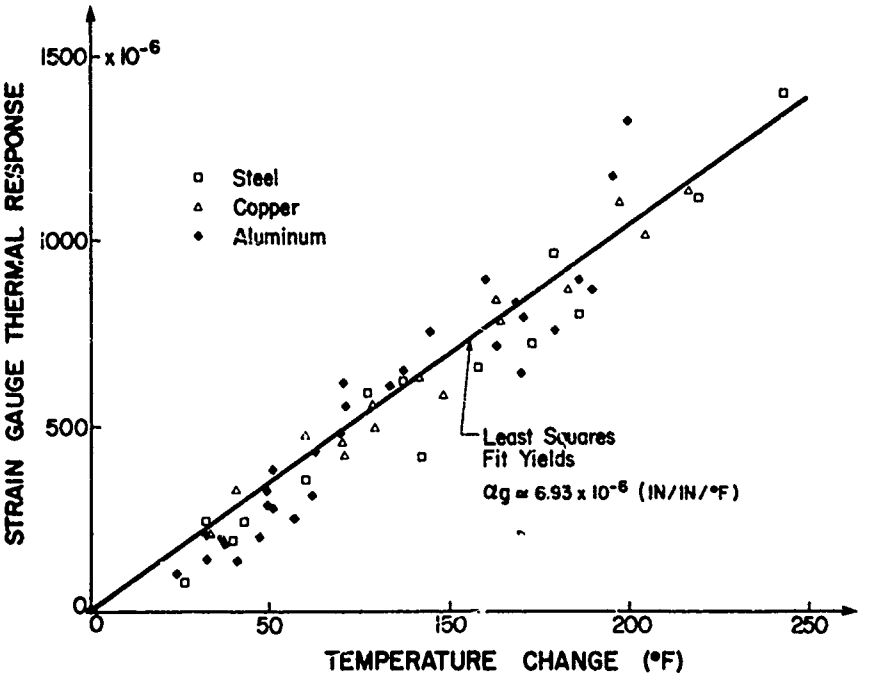

Figure 19

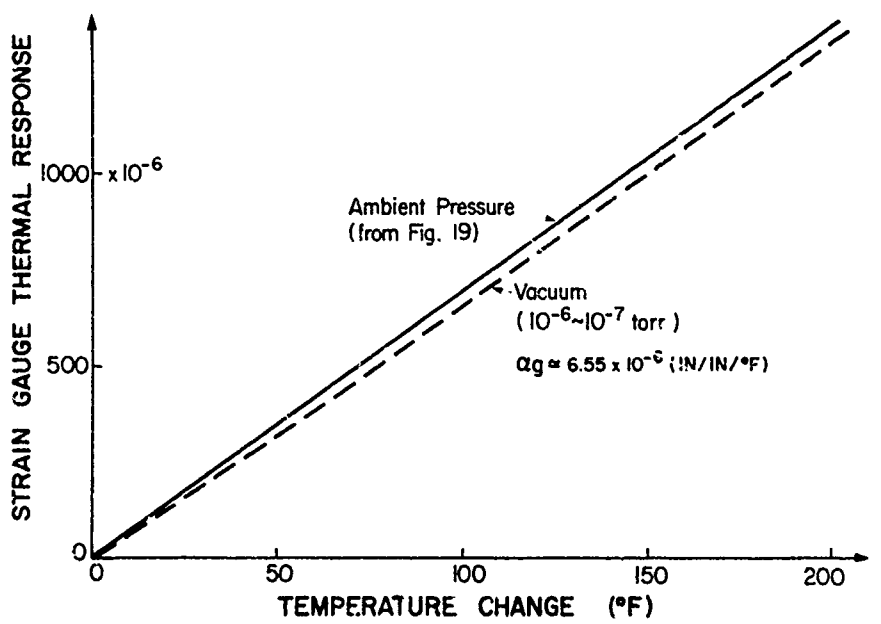

Figure 20

THIS DOCUMENT PROVIDED BY THE ABBOTT AEROSPACE
TECHNICAL LIBRARY
ABBOTTAEROSPACE.COM

Fig.21 Long term thermal vacuum test facility

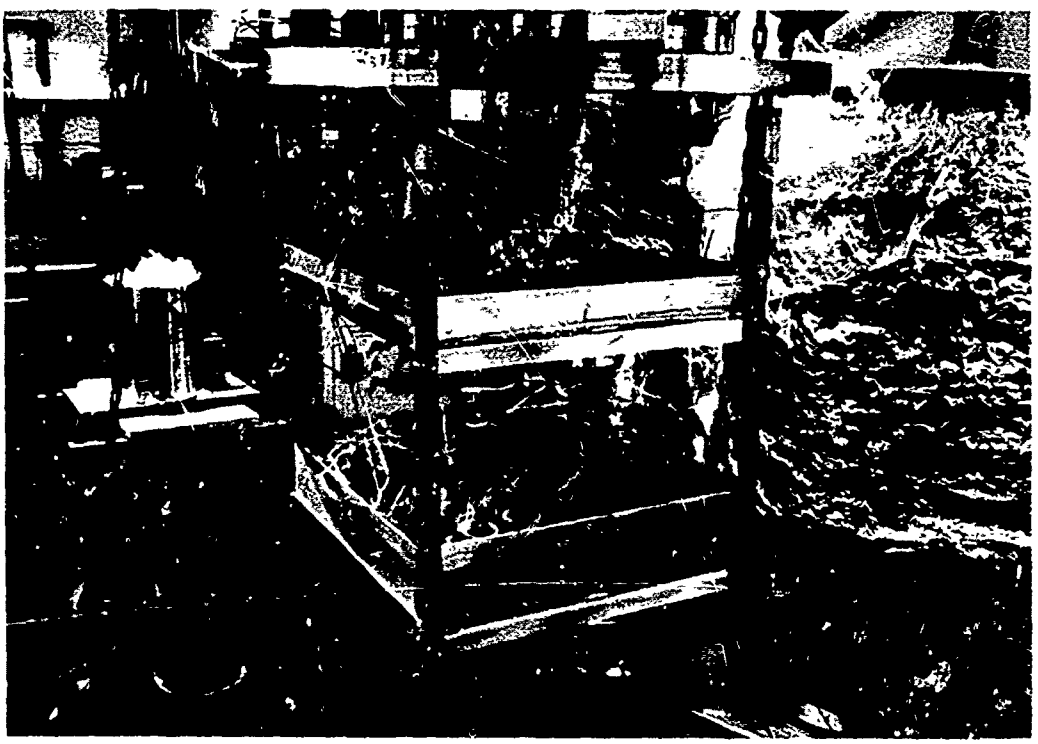

Fig.22 Tray containing composite samples

TECHNICAL LIBRARY
ABBOTTAEROSPACE.COM

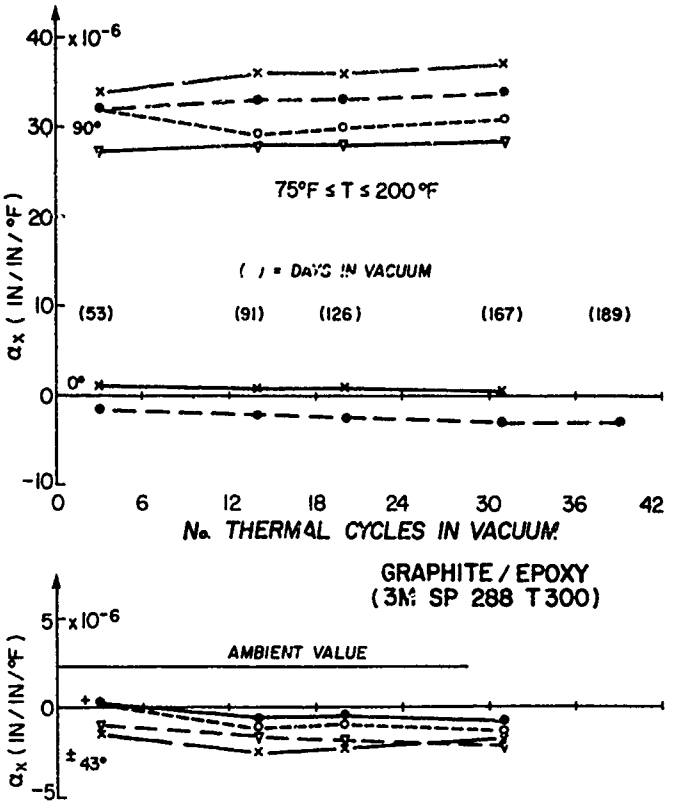

Figure 23

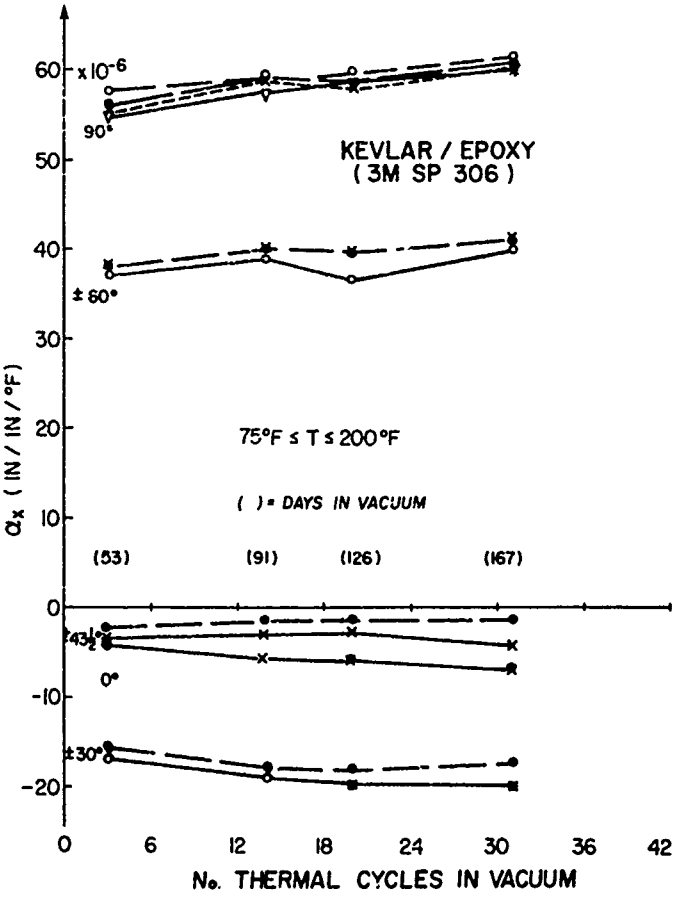

Figure 24

THIS DOCUMENT PROVIDED BY THE ABBOTT AEROSPACE
TECHNICAL LIBRARY
ABBOTTAEROSPACE.COM

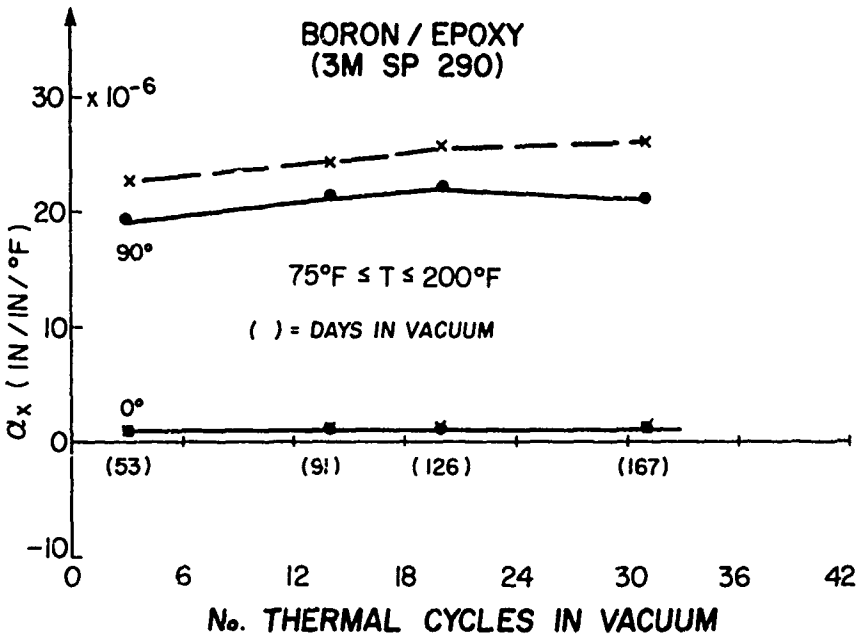

Figure 25

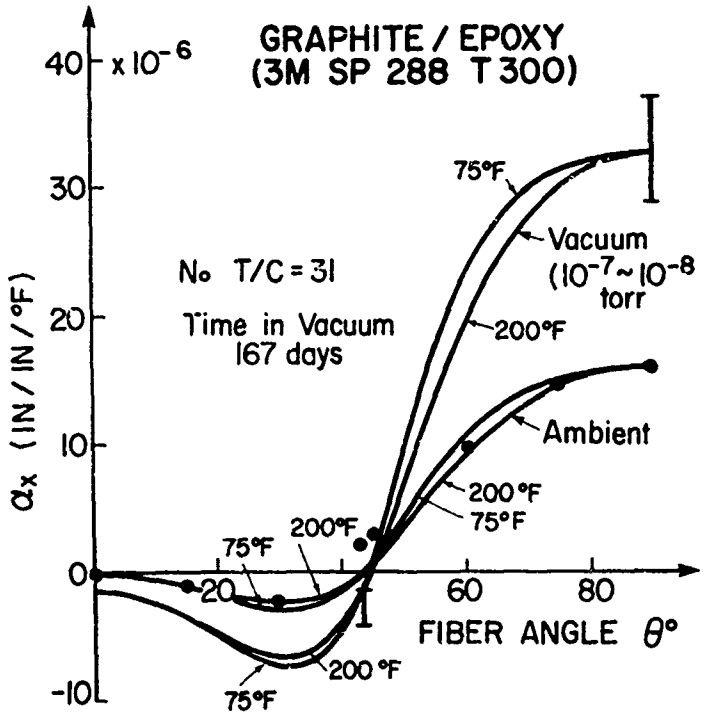

Figure 26

TECHNICAL LIBRARY
ABBOTTAEROSPACE.COM

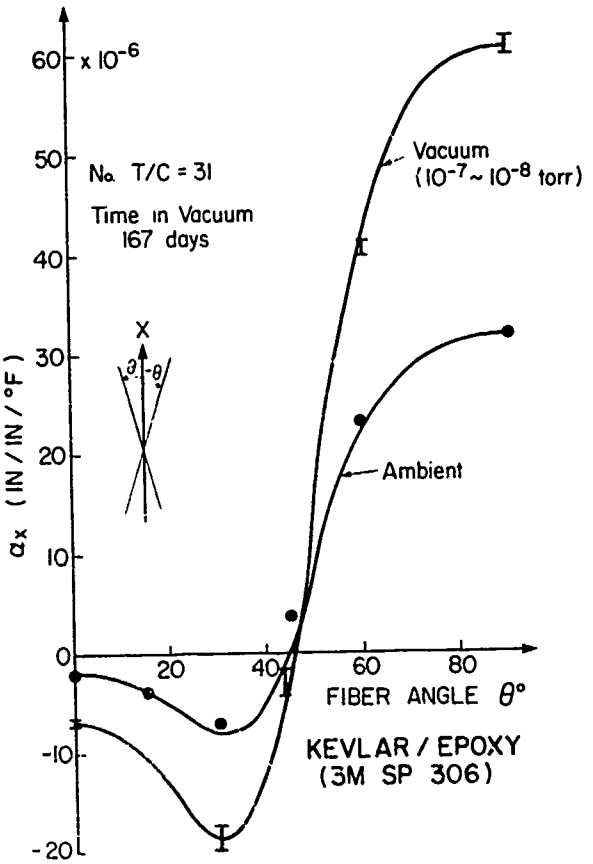

Figure 27

TECHNICAL LIBRARY
ABBOTTAEROSPACE.COM

PREDICTABILITY OF MOISTURE ABSORPTION IN GRAPHITE/EPOXY SANDWICH PANELS

By
H.W. Bergmann and P. Nitsch
Institute for Structural Mechanics
German Aerospace Research Establishment (DFVLR)
P.O. Box 32 67, D-3300 Braunschweig
Federal Republic of Germany

Summary

Graphite/epoxy materials are finding widening acceptance in the aircraft industry. Their generally attractive strength properties, however, tend to degrade in hot and moist environments. The high dependence of the strength loss on the moisture content demands an assessment of the amount and distribution of absorbed moisture, particularly in the case of light-weight sandwich panels. The reliability of such predictions hinges on the formulation of theoretical considerations, the accuracy of numerical processes, the definition of material constants and a proper interpretation of the environmental conditions. The impact of errors in these parameters on predicted moisture contents, and comparisons of analytical forecasts with experimentally determined values, are the topic of this paper.

1. Introduction

Graphite/epoxy laminates tend to absorb moisture from the atmosphere, principally by diffusion through the epoxy matrix. The bonding of the water molecules to the hydroxyl groups of the epoxy polymers leads to a swelling of the matrix and to changes in the state of stress in the laminates. The presence of moisture also lowers the glass transition temperature of the matrix, i.e., it softens the resin and thereby degrades the matrix-dependent laminate porperties at elevated temperatures. The severity of the degradation depends on the amount and the distribution of the moisture which are continually affected by changing temperature and humidity conditions. Drying of the moist laminates seems to restore the laminate properties fully unless permanent damage to the matrix material is caused by thermal shocks.

Apart from temperature and moisture, the properties of graphite/epoxy laminates depend, of course, on the characteristics of the epoxy, the fibers and the fiber treatment, on ply orientation, resin content, curing procedure, etc., so that a prediction of their actual strengths or stiffnesses under given conditions is difficult. An evaluation of a multitude of test data from different sources[1] for T 300/934, T 300/5208 and AS/3501-5 materials, however, leads to the interesting observation that the degradation of their compressive strength under hot and moist conditions can be approximated, in general terms, as percentages of their initial dry strength at room temperature. The data leading to the failure surface depicted in Figure 1 were reasonably compatible in the sense that all test specimens had comparable ply orientations and thicknesses, were cured in accordance with the supplier's recommendations, and were tested in the form of sandwich beams under four-point loading. These data indicate a uniform trend of several materials towards alarmingly reduced strength properties when exposed to moisture and heat.

The moisture problem is particularly sensitive in the case of graphite/epoxy sandwich panels with moisture-absorbent cores. Here, the structural safety at elevated temperatures is threatened not only by the degradation of the faceshents but by internal pressures generated by the vaporization of moisture contained in the core material as well. Figure 2 shows calculated vapor pressure intensities developing inside a sandwich panel with Nomex core after saturation at 40 % and 100 % relative humidity, and subsequent heating to 175°C. Corresponding tests have shown that, under adverse conditions, such panels will explode due to internal pressure alone.

Considering the critical nature of the moisture-induced degradation, it is obvious that the design and the qualification of graphite/epoxy structures destined for operation at high temperatures mandates a quantitative evaluation of these effects. Such an evaluation, generally, requires a forecast of the worst expected moisture state by analytical means, and a subsequent determination of the remaining margins of safety by test.

It is commonly agreed that the accuracy of analytical estimates depends on four factors:

- o The applicability of the classical theory of diffusion to fibrous composites;
- o The adequacy of mathematical models and their computational aspects;
- o The realistic definition of the environmental conditions;
- o The reliable determination of material properties affecting diffusion.

The following discussion attempts to describe the significance and limitations of these factors, and to assess the accuracy of moisture predictions based upon them.

2. Applicability of Classical Diffusion Theory

The diffusion equations in the form of Fick's first and second law are universally accepted for the response of homogeneous and isotropic materials. Their applicability to fibrous composites is not obvious but has been repeatedly claimed by several investigators[2],[3], for the one-dimensional flow of moisture through the thickness of laminates of large lateral dimensions.

TECHNICAL LIBRARY
ABBOTTAEROSPACE.COM

The corresponding form of Fick's first law

$$\Phi = -D \frac{\partial c}{\partial x} \tag{1}$$

states that the moisture flux is proportional to the concentration gradient, the constant of proportionality being the diffusion coefficient, D, and x denoting the thickness direction. Fick's second law treats the transient condition and for the one-dimensional case assumes the form

$$\frac{\partial c}{\partial t} = \frac{\partial}{\partial x} \left[D_{(c,T)} \frac{\partial c}{\partial x} \right] \tag{2}$$

where T and t represent temperature and time, respectively. The diffusion coefficient, strictly speaking, is a function of both the concentration and the temperature, but in graphite/epoxy materials the dependence on concentration has been considered slight [2], and generally ignored. The temperature dependence of the diffusion coefficients is, of course, quite pronounced. It is nevertheless permissible to ignore the temperature gradients in the thickness direction of the laminates since the rate of heat transfer is faster than that of the moisture transport by several orders of magnitude. Retaining with some reservation the assumption of negligible concentration effects, Equation (2) can be simplified to

$$\frac{\partial c}{\partial t} = D_{(T)} \frac{\partial^2 c}{\partial x^2} \tag{3}$$

It may be found practical to work in terms of weight percentages of moisture, M, relative to the dry weight of a laminate, rather than of concentration, c. The corresponding forms of Fick's laws are

$$\Phi = - \frac{D \varrho}{100} \frac{\partial M}{\partial x} \tag{4}$$

and

$$\frac{\partial M}{\partial t} = D_{(T)} \frac{\partial^2 M}{\partial x^2} \tag{5}$$

Recent experiments with T300/Code 69at the DFVLR question the supposition of negligible concentration dependence. According to Figure 3 the diffusion coefficients measured at room temperature varied from 1.4×10^{-8} mm^2 s^{-1} at 27.5 % relative humidity to 3.3×10^{-8} s^{-1} at 95 % relative humidity. Apart from this aspect, unresolved problems exist in regard to the influence of ply orientation, fiber treatment, surface conditions, and others. On the whole, however, it may be stipulated that the theoretical basis for the prediction of one-dimensional moisture flow in graphite/epoxy laminates, while far from being exact, leads to useful approximations of the moisture state.

3. Mathematical Models and computational Aspects

The differential equations governing the one-dimensional flow of moisture can be solved in closed form only under highly restrictive boundary conditions. The boundary limitations can be removed by a conversion of the differential to finite-difference equations, requiring a computerized solution of the resulting sets of algebraic equations. The degree of accuracy depends on the fineness of the mathematical model and on the magnitude of computational error which can be minimized by proficient programming. Figure 4 shows, as a function of time, the amount of moisture absorbed in a fictitious, initially dry laminate exposed to a constant climate on both sides. The solid line represents the closed-form solution, and the broken lines finite-difference solutions, indicating the numerical accuracy and sensitivity of step-size. The comparisons show that the computer solutions, with sufficiently small step-sizes, differ from the exact solution by less than 1 %.

It should be noted that for the purpose of program verification, a comparison of computed values to test results is improper since the objective of the verification is that of proving equivalence between the classical and numerical solution of the problem formulation. Test results may reflect additional influences such as variations from nominal thickness, nominal resin content, or nominal diffusion properties. The effect of small variations in the laminate thickness, as they frequently occur in practice, is quite significant as shown in Figure 5.

The analysis of moisture diffusion becomes more complicated if several dissimilar materials are joined in a multilayered slab [3] . While the principles developed before apply for the treatment of any of the individual layers, two additional conditions must be satisfied at each of the internal interfaces between adjacent layers. The first of these conditions demands that the flux of moisture leaving material i be equal to the flux entering i+1, i.e.,

$$(D \varrho)_{i+1} \cdot \left(\frac{\partial M}{\partial x} \right)_{i+1} = (D \varrho)_i \cdot \left(\frac{\partial M}{\partial x} \right)_i \tag{6}$$

The second condition requires compatibility of the moisture levels at the interface of the two materials. Defining, as percentage of the laminate dry weight, as $M_{100\%}$ the moisture saturation at RH = 100 %, the moisture saturation at values of RH < 100 % can be expressed in the form

TECHNICAL LIBRARY
ABBOTTAEROSPACE.COM

$$(7) \qquad M_{RH} = M_{100\%} \left(\frac{RH\%}{100} \right)^b$$

where the exponent b is a material property. On the condition that $(RH)^b$ has the same value for the two adjacent materials i and i+1, it follows that

$$(8) \qquad \left(\frac{M_{RH}}{M_{100\%}} \right)_{i+1} = \left(\frac{M_{RH}}{M_{100\%}} \right)_i$$

The equality of $(RH)_{i+1}$ and $(RH)_i$ at the interface has been deduced by the assumption of a fictitious airspace between the materials of infinitesimal width [3] but has yet to be proven by a more rigorous argument.

Sandwich panels, in a general sense, can be analyzed as multilayered slabs if the core material is regarded as a homogeneous layer with uniformly distributed densities and diffusion characteristics. In the case of honeycomb cores, this idealization is inadequate because the predominant portion of the moisture transfer occurs normal to the surfaces of the core ribbons through the entrapped air in the cells. A more realistic treatment of the problem is the coupling of the adhesive layers to both sides of the core by means of an internal moisture balance [3]. A welcome by-product of this approach is the calculability of the amount of moisture in the entrapped air space, and the corresponding vapor pressure. Figure 6 shows the physical and mathematical models of a honeycomb-type core with layers of adhesive on both sides. The difference of the fluxes during the time interval Δt represents the weight of moisture absorbed by the core, W_c, and that of residing vapor in the cavity, W_v. Introducing as w the weight and as v the volume of the core per unit area of the panel surface, then with $W_c = w\, M_{100\%}\, H^b$ and $W_v = p_s V/RT$ it can be shown that

$$(9) \qquad \Phi_{res}\, \Delta t = \frac{p_s V}{RT} \left(\bar{H}_i - H_i \right) + w\, M_{100\%} \left(\bar{H}_i^b - H_i^b \right)$$

where $\bar{H}$ relates to the end, and all other quantities to the beginning of the time interval, Δt. The resulting equation can be solved by Newton's method.

The accuracy of computer solutions predicting moisture contents and distributions in sandwich panels cannot be validated by comparison to classical solutions for lack of their existence even under idealized conditions. The proof of their acceptibility, therefore, must be based on experimental evidence. Such evaluations should be preceded by a discussion of the reliability with which the properties of the materials affecting the moisture transport can be established.

4. Material Properties

The prediction of moisture contents and distributions in graphite/epoxy sandwich panels depends critically on the correct identification of material properties which affect the moisture response, i.e.,

- o Maximum absorptivity at 100 % relative humidity, $M_{100\%}$;
- o Maximum absorptivity at relative humidities <100 %, M_{RH}, characterized in Equation (7);
- o Diffusion coefficients as functions of temperature and concentration.

Several investigators have in recent years attempted to identify the parameters M and b for various materials. Figure 7 summarizes some of the reported values for T 300/934, AS 3501-5, T 300/5208, T 300/Code 69 and T 300/914 C materials, partially taken from Reference [4] . It can be seen that the maximum absorptivity, $M_{100\%}$, for different materials ranges from 1.4 % to 2.0 %. Considerable variations occur even for a given material evaluated by different investigators. The reasons for the inconsistencies may be traced to changes in material composition from batch to batch, differences in the curing process, variations of the resin content, as well as to different test procedures and to human error. The exponent b also varies considerably but it is believed that most of the variations reflect difficulties in the measuring process, and that the most likely value is unity, so that the saturation moisture content, M_{RH} varies linearly with the relative humidity from zero at RH = 0 % to $M_{100\%}$ at RH = 100 %.

The temperature dependence of the diffusion coefficients can be expressed in the form $D = D_o \exp\left(\frac{C}{T}\right)$, where D_o and C are constants, and T is the temperature in °Kelvin. Accepting this relationship as valid, the values of diffusion coefficients, plotted on a log D versus $\frac{1}{T}$ graph, ought to fall on straight lines, so that from a limited number of test data the constants D_o and C can be evaluated. Figure 8, also taken from Reference [4] , displays diffusion coefficients experimentally determined by several investigators. The data scatter is appreciable and the prediction of moisture levels will vary accordingly. Figure 9 shows the sensitivity of the predicted moisture absorption at 21 °C with respect to different values of diffusion coefficients reported for T 300/934, and a comparison to actual absorption values determined by weighing.

It follows from Fick's laws that absorption and desorption are governed by the same prin-

TECHNICAL LIBRARY
ABBOTTAEROSPACE.COM

ciples and differ only with respect to their direction, i.e., the diffusion coefficients for absorption and desorption should be numerically equal. For graphite/epoxy laminates substantial evidence exists that this is approximately correct for temperatures up to 100 °C, while contradictory test data were obtained for T 300/934, T 300/5208 and T 300/F-263 in Reference [11] for temperatures above 100°C. The shape of drying curves observed during 24 hours of drying of saturated specimens at 120 °C, is not consistent with the standard diffusion laws. The problem is illustrated in Figure 10. At 120 °C, a diffusion coefficient of 600×10^{-8} mm^2/sec fits only the first part of the drying curve reasonably well. Beyond that the drying curve corresponds more to a diffusion coefficient of 300×10^{-8} mm^2/sec.

This observation is baffling but perhaps explainable by the fact that the drying temperature of 120 °C lies above the glass transition temperature of a saturated epoxy matrix, and that different diffusion coefficients may associate with the crystalline and the amorphous phases of the epoxy. Figure 11 shows that good agreement between theory and experimental data can be obtained with the assumption of a moving boundary between the two phases which, effectively, requires a numerical solution of Fick's equation in which the diffusion coefficient D is a function of concentration.

5. Initial and Environmental Conditions

Analytical approaches for the prediction of the moisture content in graphite/epoxy laminates are bound to commence from assumed initial conditions. The subsequent moisture flux then depends on the nature of the environment, i.e., on the temperature and the relative humidity to which the laminates are exposed. Since the heat transfer rates are much higher than the moisture transfer, it is customary to assume as environmental temperature the average of the actual temperatures on both sides of the laminate as a function of time. With respect to humidity, however, the actual time-dependent variations on both sides are significant factors and must be considered individually.

In experimental work the initial conditions are usually well defined by saturating the laminates at a constant humidity environment or by drying in an oven, so that no moisture gradient exists across the thickness of the laminate. The subsequent history of environmental changes can than be defined as required and simulated in humidity chambers.

6. Moisture Distribution in Sandwich Panels

Based on these premises the moisture distribution in sandwich panels designed for spacecraft applications was determined both by analysis and test. The sandwich panels consisted of 0.04 cm thick T 300/934 facesheets, bonded with a Nomex 329-7 film adhesive to a light Nomex core of 1.5 cm thickness. The facesheets were precured at 5.5 bar pressure and had a resin content of 32 % by weight. They were subsequently bonded to the core and postcured for 12 hours at 193 °C. The moisture properties of the constituent parts were experimentally determined and are summarized in Figure 12.

One panel of this configuration was completely dried in a 120 °C oven and then placed into a 95 % humidity chamber at 60 °C for 408 hours. Another panel was completely saturated at 95 % relative humidity and then dried at 120 °C for 96 hours. At the end of the time intervals, part of the facesheets and the core were removed from the panel and their moisture contents determined as the difference between their weights then, and after drying in a 120 °C oven. The moisture level in the adhesive was established indirectly as the difference between the weight loss of connected parts of the panel and that of the isolated facesheets and the core. The analytical predictions and the test results are shown in Figure 13. In view of the close control of the environment their comparison cannot be considered satisfactory but, in the light of an additional experiment, it must be doubted that more accuracy is attainable because of inconsistencies in the material response.

In this experiment a total of 14 test panels, 30x36 cm wide, were manufactured as identically as possible. After determining the dry weights of the panels after exposure under vacuum to 120 °C, all panels were placed into a 95 % humidity chamber at 60 °C. The panels were removed from the chamber after time intervals varying between 15 and 70 days. The recorded moisture absorption of the panels in terms of weight gain versus exposure time is shown in Figure 14. It is evident that the lack of consistency can hardly be attributed to human or experimental error and reflects more likely an inherent lack of uniformity in the material response. Parts of it may be due to thickness variations in the facesheets, or to the irregularity of the fillet formation in the adhesive.

7. Recommendations

The preceding arguments were stimulated by the senior author's experience with graphite/epoxy sandwich components of the Space Shuttle Orbiter. There, the tracking of the moisture flow led to useful approximations of the residual material properties because the initial condition was known in the sense that, after six months exposure to the rather constant climate prevailing at Palmdale, California, moisture equilibrium at 30 % relative humidity could be assumed. The subsequent conditions were also well defined by a precise time-line in controlled environments.

In the majority of aerospace systems, however, this situation does not exist. Especially with respect to aircraft structures designed for long life-time in variable climates, calculated predictions are hazardous. Apart from other imponderables the uncontrollable cli-

THIS DOCUMENT PROVIDED BY THE AEROSPACE TECHNICAL LIBRARY
ABBOTTAEROSPACE.COM

matic fluctuations encountered in regular service defy any sensible analytical attempt.

The thought lies near to circumvent the entire issue of moisture degradation by covering the exposed surfaces of the sandwich panels with a sealant. Since organic substances cannot be expected to provide an effective seal over extended time periods because of their own inherent diffusivity, the only feasible alternative are thin metal foils. Their attachment without tears or wrinkles is difficult especially on large surfaces, and the likelihood of externally caused damage must be accepted. The gradual entrance of moisture through small openings in the foil and the ensuing lateral distribution over extended time spans is dangerous. It is possible that in hot environments the accumulated moisture cannot escape quickly enough and that the developing vapor pressure will cause a separation of the foil from the sandwich facesheet. Figure 15 is a vivid example of foil separation under admittedly severe conditions. The thin aluminum foil was bonded to the previously cured sandwich panel by a hot-temperature-curing adhesive. The panel containing a perforated Nomex core was subsequently saturated in a 95 % relative humidity chamber and then exposed to 175 °C. The formation of the resulting blisters is solely due to the expanding vapor from the moisture contained in the adhesive and the sandwich facesheet, and questions the wisdom of applying metal foil seals.

The currently emerging trend deals with the moisture problem by anticipating complete saturation at the worst average humidity level to which the aircraft is exposed during its life-time. This maximum average must be defined judiciously and with the recognition that the moisture distribution will not be uniform in the thickness direction of the laminate but will exhibit gradients commensurate with the fluctuations of the environment. This point is illustrated in Figure 16 which shows, for the same total moisture content, different distributions inside the laminate. It ought to be expected that such variations from a uniform distribution significantly affect the matrix-dependent properties of graphite/epoxy laminates. Recent tests at the DFVLR indicate, however, that such effects seem to be quite moderate. In the case of laminates made from T300/914 C material with the ply sequence $[\pm 45°]_8$ and subjected to tension loading at 130 °C, no substantial strength differences were noted in test specimens with similar moisture contents of approximately 1 % but different distributions. The test results summarized in Figure 17 are encouraging although it must be recognized that the test points are averages of three replicates only, and that no conclusions can be drawn from such a limited data base. The importance of this issue, whose as yet uncertain consequences force the adoption of perhaps unduly conservative safety factors, suggests further testing of different ply sequences under various environmental and mechanical loading conditions.

8. References

[1] Collected heat data (1974-76) from Rockwell International (Los Angeles and Tulsa), McDonnel-Douglas (St. Louis), Lockheed (Sunnyvale) and ITTRI.

[2] C.H. Shen and G.S. Springer, "Effects of Moisture and Temperature on the Tensile Strength of Composite Materials", J. Composite Materials, Vol. 11 (1977).

[3] D.J. Zigrang and H.W. Bergmann, "The Response of the Space Shuttle Orbiter Graphite/Epoxy Sandwich Panels to Exposure to Moisture and Heat", Proceedings, 11th Congress ICAS, September 1978, Lisbon.

[4] A.C. Loos and G.S. Springer, "Moisture Absorption of Graphite/Epoxy Composites Immersed in Liquids and in Humid Air", J. Composite Materials, Vol. 13(1979).

[5] R.E. Bohlmann and E.A. Derby, "Moisture Diffusion in Graphite/Epoxy Laminates: Experimental and Predicted", Presented at the 18th Structures, Structural Dynamics and Materials Conference, and at the Conference on Aircraft Composites: The Emerging Methodology for Structural Assurance, San Diego, Calif., March 1977, AIAA Technical Papers. Vol. A (A77-25726, 10 39), pp. 219-226 (1977).

[6] R.De Iasi and J.B. Whiteside, "Effect of Moisture on Epoxy Resins and Composites", Advanced Composite Materials - Environmental Effects, ASTM STP 658, J.R. Vinson, Ed., American Society for Testing and Materials, 1978, pp. 2-20.

[7] J.M. Whitney and C.E. Browning, "Some Anomalies Associated with Moisture Diffusion in Epoxy Matrix Composite Materials", Advanced Composite Materials-Environmental Effects, ASTM STP 658, J.R. Vinson, Ed., Americar Society for Testing and Materials, 1978, pp. 43-60.

[8] C.D. Shirrell, "Diffusion of Water Vapor in Graphite/Epoxy Composites", Advanced Composite Materials - Environmental Effects, ASTM STP 658, J.R. Vinson, Ed., American Society for Testing and Materials, 1978, pp. 21-42.

[9] E.L. McKague, Jr., J.E. Halkias and J.D. Reynolds, "Moisture in Composites: The Effect of Supersonic Service on Diffusion", J. Composite Materials, Vol. 9 (1975), pp. 2-9.

TECHNICAL LIBRARY
ABBOTTAEROSPACE.COM

[10] G.E. Husman, "Characterization of Wet Composite Laminates", Proceedings of Mechanics of Composite Review, Air Force Materials Laboratory Non-Metallic Materials Division, Bergamo Center, Dayton, Ohio, 28-29 January 1976.

[11] J.H. Powell and D.J. Zigrang, "The Moisture Absorption and Desorption Characteristics of three Epoxy/Graphite Systems", 8th National SAMPE Technical Conference, Vol. 8, October 1976.

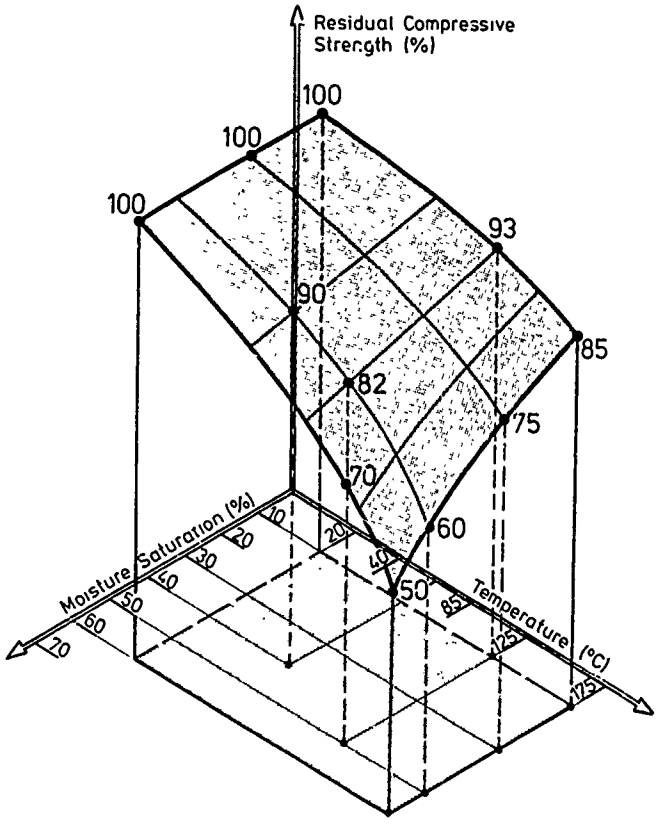

Fig. 1 DEGRADATION OF COMPRESSIVE STRENGTH

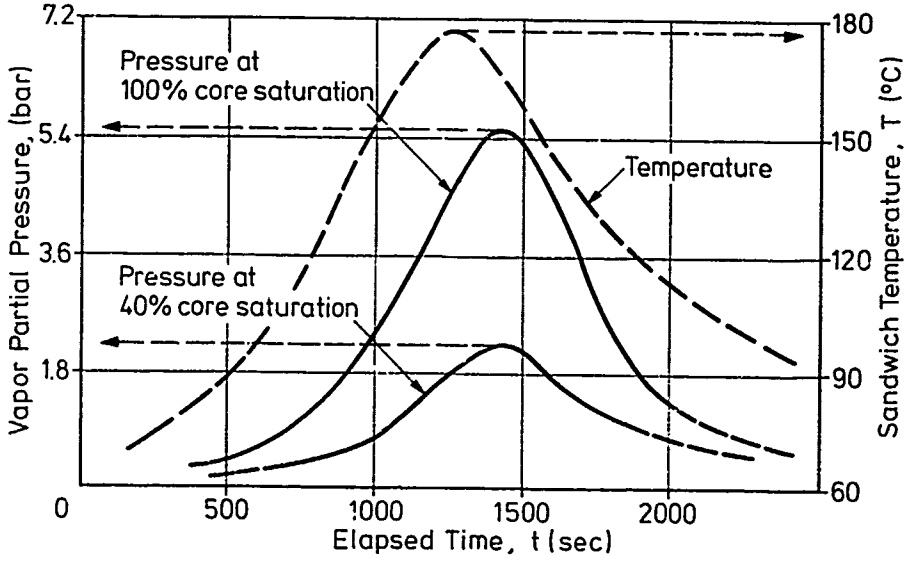

Fig. 2 INTERNAL PRESSURE IN MOIST SANDWICH PANEL

TECHNICAL LIBRARY
ABBOTTAEROSPACE.COM

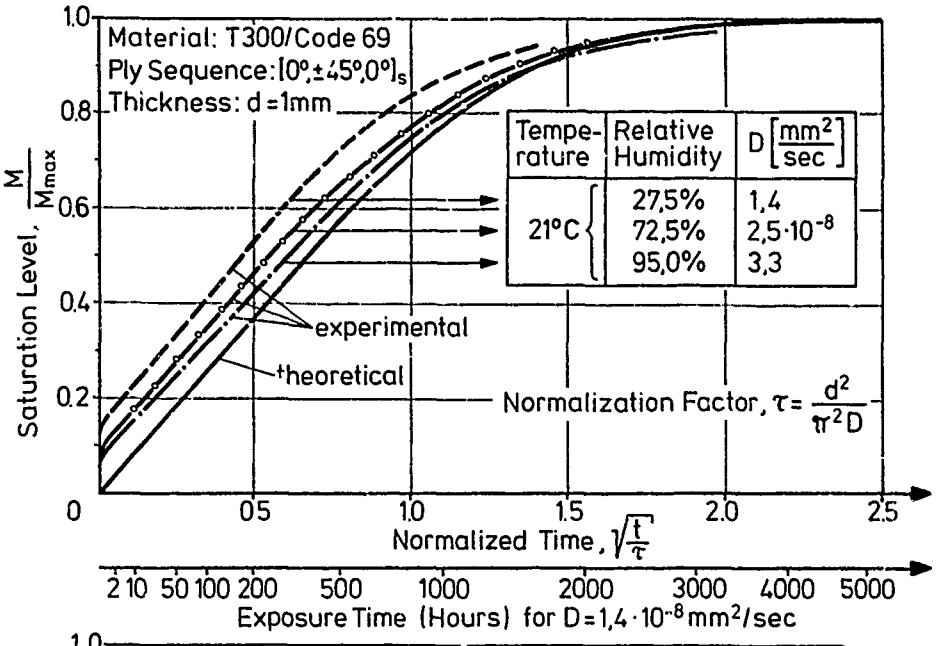

Fig. 3
Concentration Dependence of Diffusion Coefficient, D

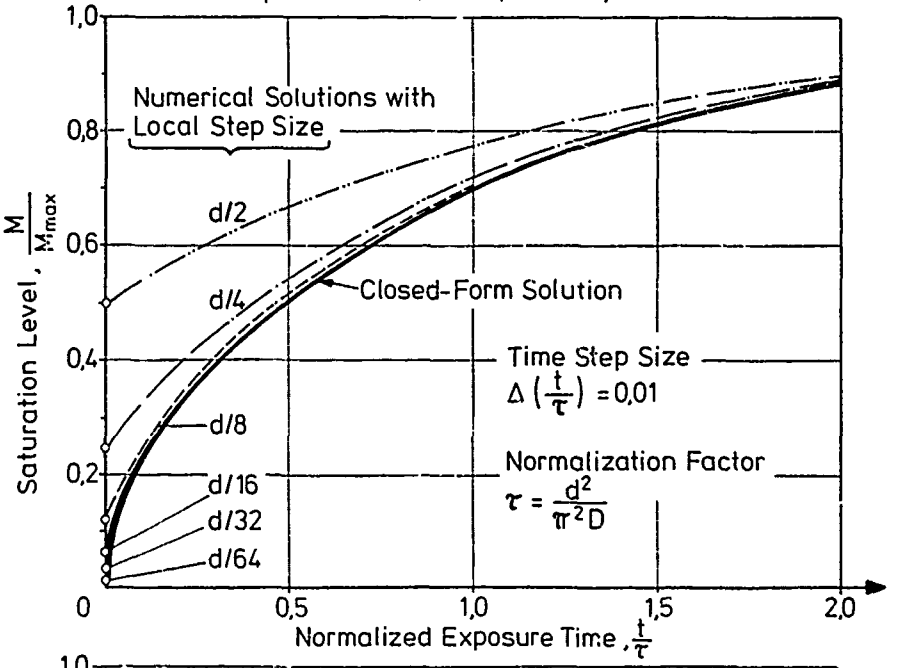

Fig. 4
Computational Accuracy

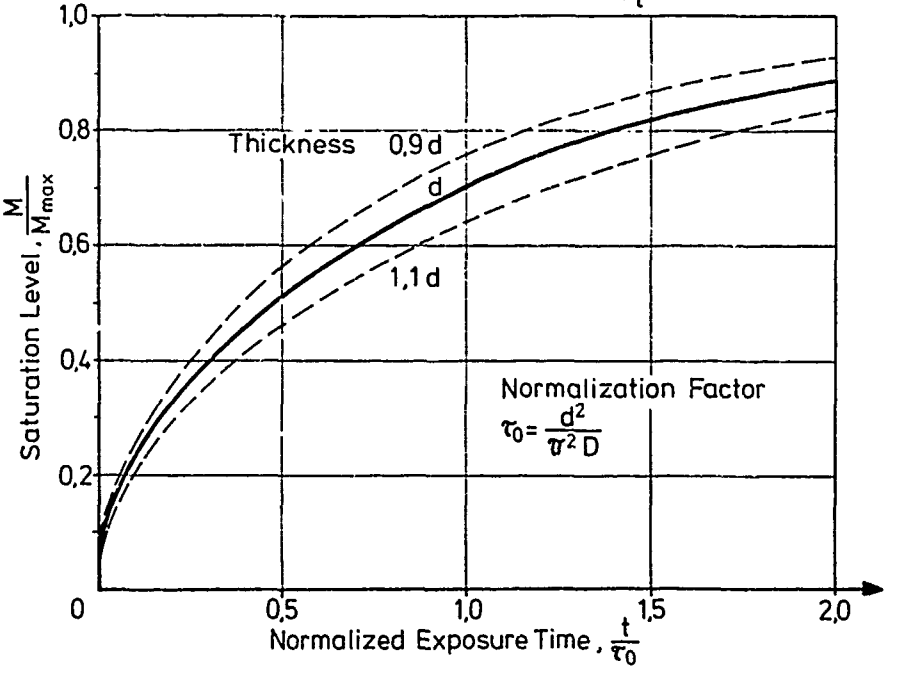

Fig. 5
Influence of Thickness Variation

TECHNICAL LIBRARY
ABBOTTAEROSPACE.COM

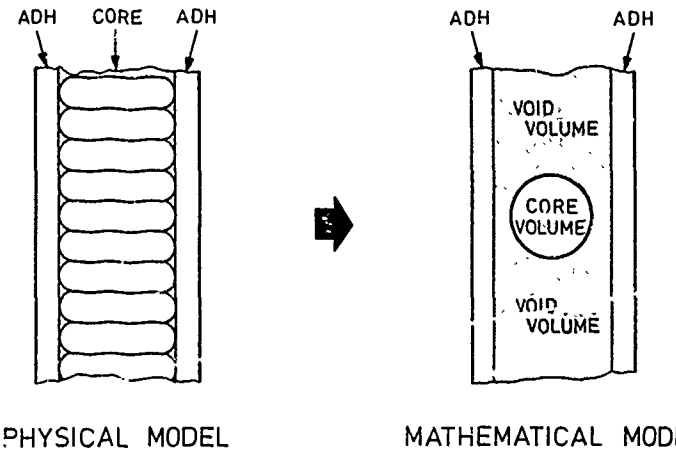

Fig. 6
Core Representation

MATERIAL	INVESTIGATOR	$M_{(100\%)}$	b
T300/1034	LOOS AND SPRINGER (4)	1,7	1
	SHEN AND SPRINGER (2)	1,4	-
	BOHLMANN AND DERBY (5)	1,8	-
T300/934	ZIGRANG AND BERGMANN (3)	2,0	1
AS/3501-S	LOOS AND SPRINGER (4)	1,9	1
	DE IASI AND WHITESIDE (6)	1,86	1,6, RH<60% 1,9; RH>60%
	WHITNEY AND BROWNING (7)	1,6	1,1
T300/5208	LOOS AND SPRINGER (4)	1,5	1
	SHIRRELL (8)	1,55	1
	MCKAGUE ET AL (9)	1,46	1
	HUSMAN (10)	1,5	1,81
T300/CODE69	DFVLR (unpublished)	1,6	1
T300/914C	DFVLR (unpublished)	2,0	1,2
T300/913C	DFVLR (unpublished)	1,4	1

Fig. 7
Reported Values for Maximum Absorptivity, $M_{(100\%)}$, and Exponent b

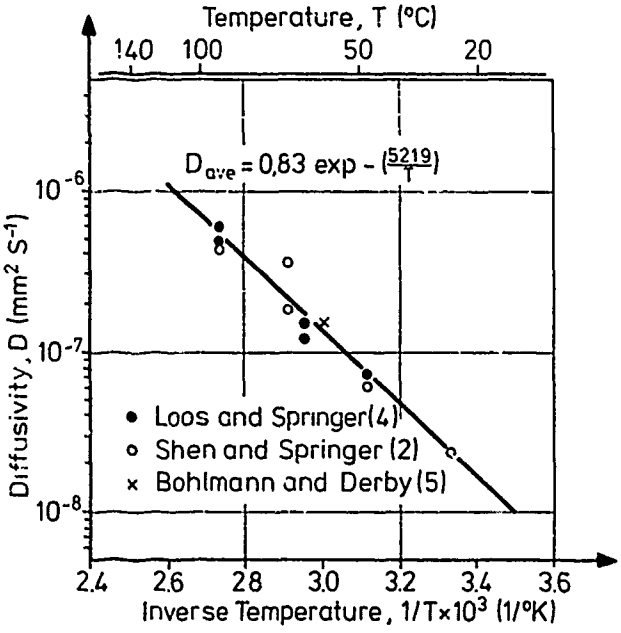

Fig. 8
Diffusivity as Function of Temperature for T300/1034

TECHNICAL LIBRARY
ABBOTTAEROSPACE.COM

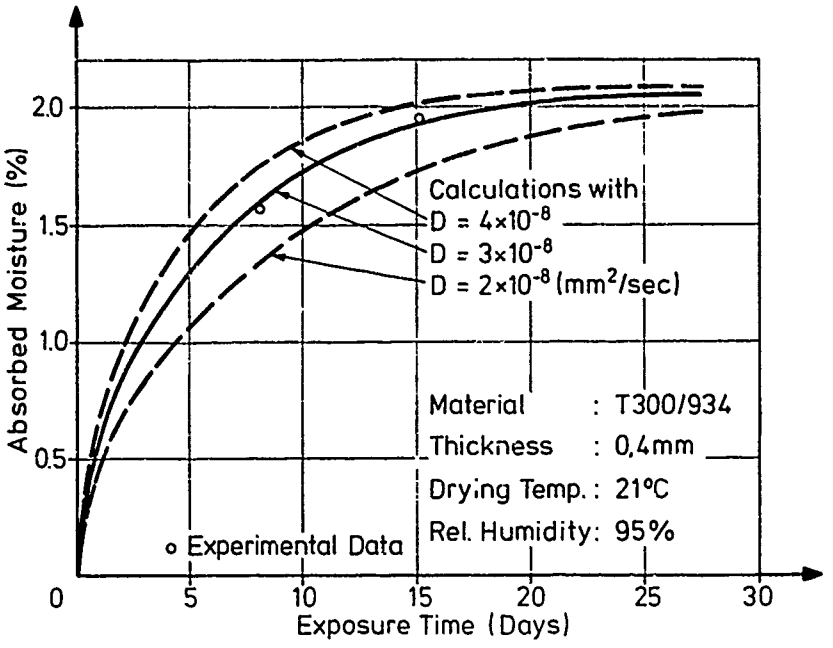

Fig. 9
Effect of Variation of Diffusivity

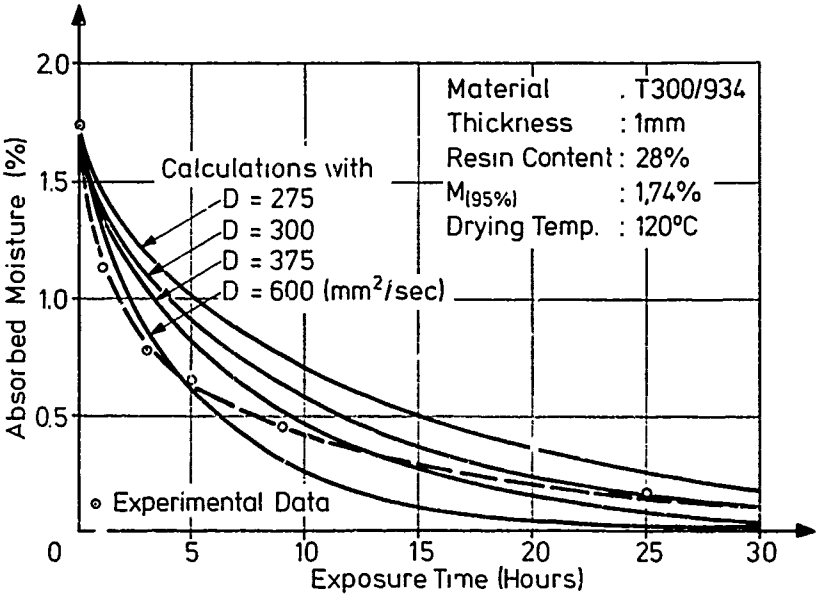

Fig. 10
Experimental and Calculated Drying Curves

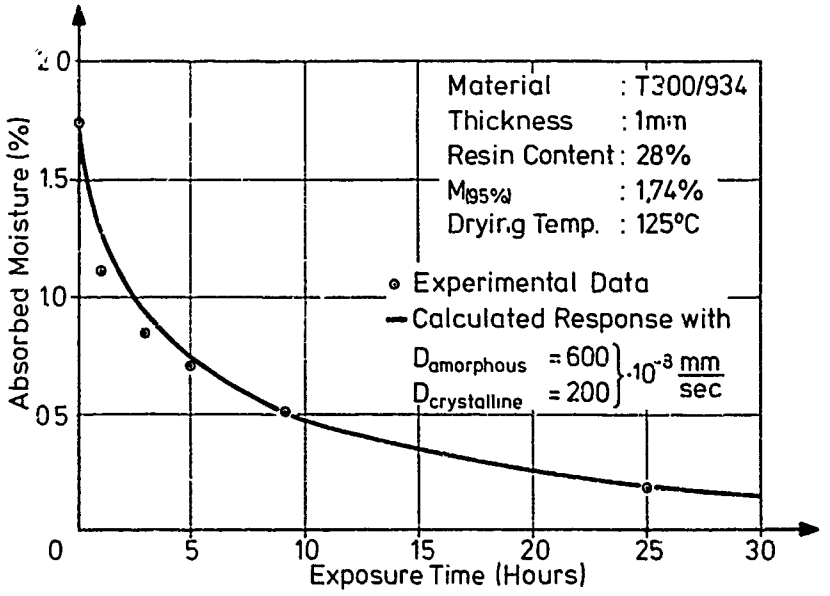

Fig. 11
Adjusted Drying Curve

TECHNICAL LIBRARY
ABBOTTAEROSPACE.COM

	DIFFUSION COEFFICIENTS ($mm^2/sec \times 10^{-8}$)				$M_{(100\%)}$ (%)	WEIGHT (kp/m^2)
	24°C	60°C	121°C	177°C		
GRAPHITE/EPOXY (32% RESIN BY WT) (52% FIBER BY VOL)	3,1	17	320	6500	2,0	0,268
NARMCO 329-7 FILM ADHESIVE	1,36	183	518	4880	3,5	0,336
NOMEX CORE (T = 1,5 CM)	3,1	17	320	6500	9,0	0,720

Fig. 12 MOISTURE PROPERTIES OF PANEL COMPONENTS

		TEST	ANALYSIS
PANEL NO 1	F/S	1,6%	1,5%
DRY PANEL, EXPOSED 408 HOURS TO 95% RH AT 60°C	ADH	2,3%	1,7%
	CORE	3,0%	4,1%
PANEL NO 2	F/S	0,4%	0,2%
SATURATED PANEL, DRIED AT 120°C FOR 96 HOURS	ADH	1,0%	1,0%
	CORE	2,0%	2,6%

Fig. 13 COMPARISON OF MOISTURE CONTENTS IN PANEL COMPONENTS

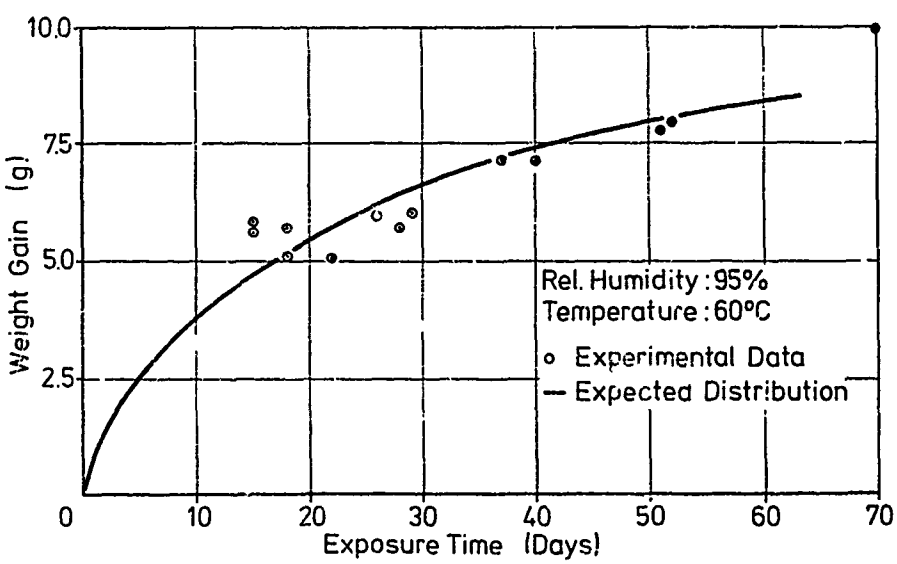

Fig. 14 WEIGHT GAIN OF SANDWICH PANELS

THIS DOCUMENT IS FROM THE ABBOTT AEROSPACE
TECHNICAL LIBRARY
ABBOTTAEROSPACE.COM

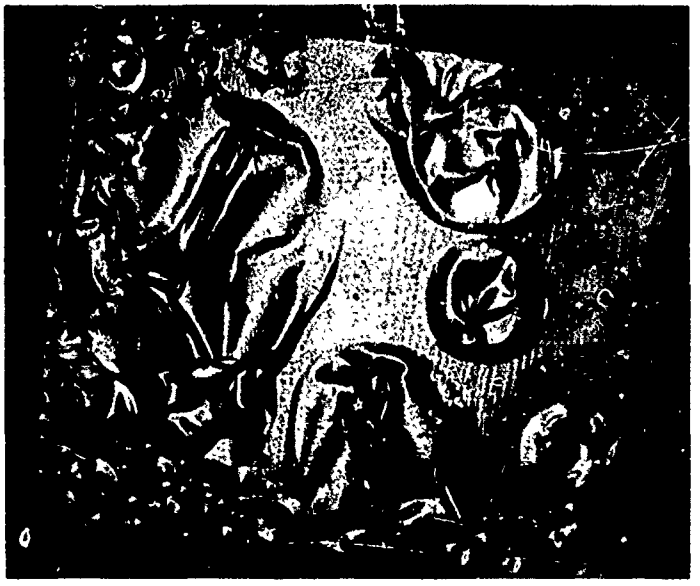

Fig. 15
SANDWICH PANEL
WITH BLISTERED
ALUMINIUM FOIL

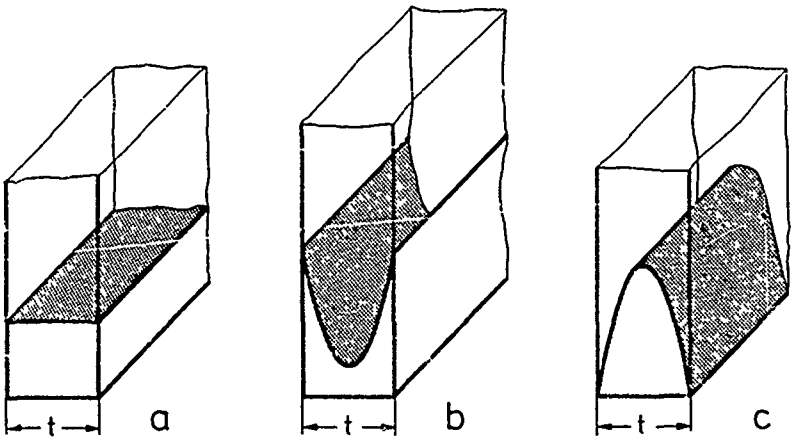

Fig. 16 DIFFERENT DISTRIBUTIONS
OF SAME MOISTURE CONTENT

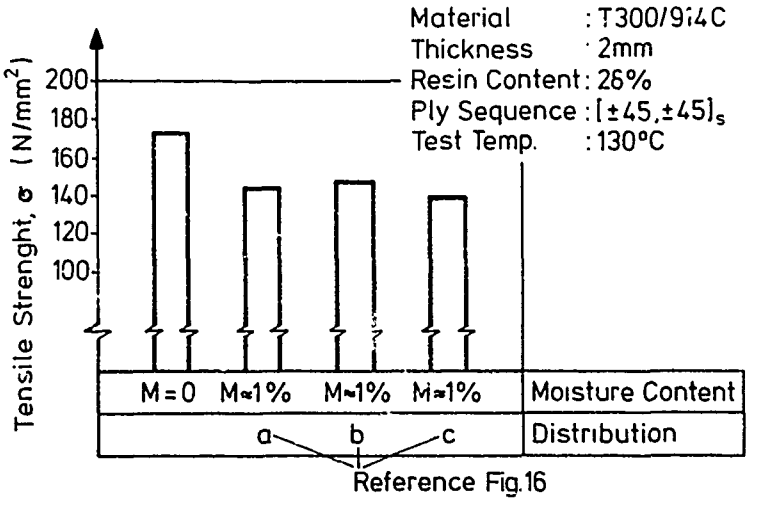

Fig. 17 TENSILE TEST WITH DIFFERENT
MOISTURE DISTRIBUTIONS

TECHNICAL LIBRARY
ABBOTTAEROSPACE.COM

EFFECTS CONNECTED WITH THE SPACE ENVIRONMENT ON COMPOSITE MATERIALS

by

Renato Barboni
Mario Marchetti
Isidoro Peroni
Istituto di Tecnologia Aerospaziale
dell'Università di Roma
Via Eudossiana, 16 – 00184 Roma – Italy

SUMMARY

Experimental and analytical results are presented for the mechanical and thermal behavior of carbon fibre pultrusion and laminate. Particular attention is paid to the temperature effects on the static mechanical characteristics and their non hookean behavior for the range 300 ÷ 450 K.

Dynamic tests in order to find the internal damping are also carried out. The linear coefficients of thermal expansion, α, are reported for the temperature range 150 ÷ 400 K.

It is shown that calculated values of thermal expansion are in close agreement with those measured.

1. INTRODUCTION

As carbon fiber composites are still, by engineering standards, a relatively new material, there are serious problems in the knowledge of their characteristics primarly the variability between apparently identical composites and everybody operating in the field of materials should endeavor to exploit their properties as much as possible.

The paper deals with the composite material consisting of continuous carbon fibers arranged with the long fiber axes aligned in resin matrix (CFRP).

Classical laminating theory and different models [1], [2], [3] has been applied for predicting the elastic and thermal properties of CFRP from properties of the layers and of the constituents too. Nevertheless the prevision of the real values is complicated by many factors such as the variation of carbon fibers in the cross sectional [4] and the variability of the constituent material properties to environmental effects [5], [6], [7].

At same time the experimental characterization of CFRP is generally complicated due to macroscopic anisotropic effects and various coupling effects.

Only a comparison of the results predicted by theoretical approaches and experimental tests can give a better understanding of the CFRP behaviour.

In Aerospace Technology Institute of Rome are available computer programmes to predict the mechanical properties (Young's moduli, Poisson's ratios, shear modulus, ultimate strength) and thermal properties (thermal expansion coefficient and thermal conductivity) relating to the lamina and the laminate too from the raw material properties of matrix and fiber [8].

In order to check the theoretical results on the mechanical properties at room temperature an experimental research was carried out last year [9].

The main purpose of the present paper is to reveal certain temperature dependent behavior of mechanical and thermal properties of the CFRP.

The necessity of this research derived by considering satellites which are at present in early development stage and the italian industry SELENIA, have examined the opportunity to design some of their structural member in CFRP.

As a matter of fact the high thermal stability and specific stiffness make CFRP an obvious material choice for antenna dishes and struts [10].

An analytical and experimental investigation on temperature effects of pultrusion and lay-up laminates is carried out.

It is shown that calculated values are in close agreement with those measured.

TECHNICAL LIBRARY
ABBOTTAEROSPACE.COM

2. SPECIMENS

For the present purpose two fundamental set of composite type was utilized:

a) **Pultrusion compounds:** the specimens source was bars of rectangular cross-section prepared by Courtaulds with fibers first passed through an impregnating bath of matrix material, and then pulled through a heated die of the rectangular cross-section where the composite is cured.

Micrographs of transverse and longitudinal sections of typical bar is given in fig. 1, which show uniforme fiber distribution, absence of voids or cracks and excellent fiber alignement.

The epoxy resin is designed by the manufacturer Epikote 828/MNA/K61B and the fibers GRAFIL A-S.

The values of the physical and mechanical properties are reported in Table I.

TABLE I: Physical and Mechanical Properties of the Pultrusion Components

Property	GRAFIL A - S	Epikote
Fiber Volume Fraction (%)	~ 60	~ 40
Density (g/cm^3)	1.8	1.2
Ultimate Tensile Strength (GPa)	2.30 ÷ 2.64	0,07
Elastic Modulus (GPa)	175 ÷ 205	3.5
Thermal expansion coefficient ($10^{-6}/K$)	− 1.0 (L) + 17 (T)	66

b) **Laminate:** the specimens were cut out of two sets of source plates made in Rome with prepregs delivered from two different suppliers:

B – Courtaulds: the preimpregnated fibre was prepared containing GRAFIL A-S fibre in Shell DX 210 epoxy.

C – Carboform: the prepregs with code 87 resin system and with GY - 70 carbon fibre was utilized.

The plates were fabricated by the following autoclave moulding process: a charge of different layer orientations was placed in an autoclave which was pressurized to 300 mm of mercury, the composite panel was heated to 120 ÷ 125 °C with rate of 2°C/min and a pressure of 600 ÷ 650 K Pa was applied, the heating was continued to 170 ± 3 °C; this temperature was holded for 60 ± 5 mins and the autoclave was cooled to 100 ± 5 °C; at least the pressure was released and the laminate removed.

Electronic microscope enlargements of transverse and oblique sections of one obtained laminate are shown in Fig. 2.

The elastic and thermal constants for the cast resin and fiber are listed in Table II.

TECHNICAL LIBRARY
ABBOTTAEROSPACE.COM

TABLE II: Elastic and thermal constants of the Laminate Components

Property	GY - 70	CODE 87	Shell DX 210
Fiber Volume Fraction (%)	~ 60	~ 40	~ 40
Density (g/cm^3)	1.87	–	–
Ultimate Tensile Strength (GPa)	2.35	–	–
Elastic Modulus (GPa)	345	3.5	3.5
Thermal expansion coefficient ($10^{-6}/K$)	– 1 (L) + 17 (T)	~ 65	~ 65
Temp. max (°C)		150	

3. THEORETICAL PREVISION

Analytical studies of the mechanical behavior of a layer via micromechanical formulation were developed. This calculation permitted us to perform subsequent numerical analyses in which the actual heterogeneous material was conceptually represented as a homogeneous, anisotropic solid via classical laminate theory.

In a preceding paper [8] a description of the background to micromechanics and macromechanics was followed by the computer program in which particular attention was paid to the influence of fibre type and orientation. For the present purpose in order to asses the influence of the temperature the programme was implemented to take into account the variability of the constituent materials properties.

The properties of the carbon fibres were assumed to be unaffected by temperature and those of the matrix only were assumed to be temperature dependent, over the range considered in the analytical prevision.

Numerical results of the computer program will be presented later in comparison with experimental values.

4. STATIC PROPERTIES

The tensile test data reported in this paper was determined using the testing machine shown in fig. 3, equipped with a specially constructed electric oven, in the temperature range of 300 ÷ 400 K.

The dimensions of the heating cylinder were such that all the specimens were completely inside the box. Termocouples placed inside the oven showed variations in temperature of the order of ± 0,5° C from top to bottom of the specimen.

Four fundamental group of specimens were tested A/a, B1/a, B1/b, C1/a, C2/a, summarized in Table III.

TABLE III: Type of Specimens.

Composite Type	Fibre	Resin	Lay - up sequence	Measurement angle (ϑ)	Sample Group
A – Pultrusion	GRAFIL A-S	Epikote 828	0	0°	A/a
B – Laminate	GRAFIL A-S	Shell DX 210	90 / 0 / 90	90° 45°	B1/a B1/b
C – Laminate	GY - 70 (Carboform)	Code 87	0 / 0 / 0 / 0 / 0/90/ 90/ 0 /	0° 0°	C1/a C2/a

Dimension of test specimens are shown in fig. 4, with effective variation within ± 1 percent. All the samples were the straight sided specimens but only the laminates with end aluminium tabs.

TECHNICAL LIBRARY
ABBOTTAEROSPACE.COM

Each specimen was instrumented with two biaxial strain-gauges on opposite faces and the tensile stress-strain curves were plotted.

Procedures for temperature testing consisted of mounting the specimen in the load frame with end connections of serrated jaw type, [11], a few minutes (5 ÷ 15) to raise the temperature to the desired level, an approximately equal number of minutes temperature soak to uniformly distribute the temperature, and then since composites may behave visco-elastically the load was applied linearly to rich the maximum value in 20 ÷ 30 seconds.

Young's modulus and Poisson's ratio were determined by tensile tests which were carried out to approximately 20% of the tensile strength.

It has been observed that, with regard to each sample group, the specimens tested have been show, with very small scatter (< 8%) a non linear stress-strain relation [12].

This non hookean behavior, that increases with temperature, can be one of the most important reason for the remarkable scatter found in the results of tensile tests from various reserchers.

In order to give a reference point the Young's modulus and Poisson's ratio reported in this paper as function of temperature was obtained at σ = 0.1 GPa.

A more detailed analysis of the results is given in the followings:

Type A/a : For pultrusion compound the temperature effect on Young's modulus can be seen neglegible and the theoretical prediction agrees very well with experimental results, fig. 5.

All tensile tests show a non linear stress-strain relation fig. 6, and the relation between Young's modulus and stress is plotted in fig. 7.

Type B : The value of Young's modulus as function of the measurement angles at room temperature is shown in fig. 8 as a comparison between experimental and theoretical results.

The temperature effect was neglegible for tensile test on samples with measurement angle $\vartheta = 90°$ but for samples with measurement angle $\vartheta = 45°$ was significant as it is shown in fig. 9. The same consideration is valid for Poisson's ratio fig. 10.

The variation of E with respect to stress for the samples of B1/b group is shown in fig. 11.

The Young modulus first increases with stress then decreases; this can be imputate to opposite effect of fiber and resin; the effect of resin becomes predominant with increasing of stress and temperature.

The variation of Poisson's ratio vs. stress is given in fig. 12.

Type C : All tensile tests show non linear stress-strain relation, fig. 13. With respect to this non-linear relation, the relation beetween Young's modulus and stress was found to be linear as shown in fig. 14 - 15.

The values of Young's modulus vs. the temperature for samples of the groups C1/a are plotted in fig. 16.

A most important effect of temperature on E results for samples of the group C2/a, where the lay-up orientation is not parallel, is shown in fig. 17.

The variation of Poisson's ratio vs. temperature for the group C2/a is given in fig. 18.

5. DYNAMIC PROPERTIES

We present experimental results obtained from a series of free and sinusoidally forced vibration tests of pultrusion compound in order both to verify the validity of the previous results and to find the internal damping [13].

Specimens were clamped at the ends and excited in first resonant flexural vibration by an electromagnetic shaker while measurements of frequency response were made and recorded. Since one of our objectives was to study the effect of the vacuum, specimen were tested in a small vacuum chamber, fig. 19, at various pressure in the range from room pressure to 10^{-7} mm Hg.

Measured values of specimens resonant frequency (380 Hz) and specimen geometry were used to find the longitudinal Young's modulus by utilizing Behrens correction [11].

The obtained value at room temperature was E = 109.7 GPa; the scattering results less then 5% with respect to data shown in fig. 7.

The experimental values of the dimensionless damping ratios ζ, as function of response amplitude at room condition are given in fig. 20.

The importance of the vacuum is shown in fig. 21; the effect can be estimated as a reduction of 15% in the dimensionless damping ratio.

TECHNICAL LIBRARY
ABBOTTAEROSPACE.COM

6. THERMAL EXPANSION BEHAVIOR

The thermal expansion coefficients were determined over a temperature range of ~ 150 ÷ 450 K utilizing an electronic dilatometer in which the measuring device reaction not exert a stress of more than 6.10^{-2} N/mm^2 on the specimen so that the specimen is not intended.

The samples were cut from pultrusion bar so that the fiber axis was at $\vartheta = 0°, 15°, 30°$ and 45° with the edge of the source bar. The final sample measured 25 mm in length and 5 x 5 mm^2 in cross-sectional area.

Each specimen was heated at the approximate rate of 1.3 °C/min in the dilatometer, fig. 19, from room temperature to 450 K and then cooled to initial value at same temperature rate. A small amount of hysteresis was observed between the heating and cooling curves of the first cycles. Further heating followed very closely the cooling curve and the behavior become essentially reversible. A minimum of four cycles without stoppage of work were recorded for each sample so that reproducible expansion curves were obtained.

The some procedure was followed in the range ~ 150 ÷ 370 K due to hysteresis; in those thermal cycles, temperature higher then room temperature was reached to verify the continuity of the behavior below and above room temperature.

In general, three specimens were run for each determination of expansion coefficient and a variation in individual values was less there 10% .

In order to compare the experimental values, the prediction of pultrusion thermoelastic properties from constituent properties has been carried out.

The material properties vs. temperature of the epoxy as the input data to the computer program are shown in fig. 20 in agreement with [14]. Unfortunately these properties concern only to the temperature range between 300 ÷ 450 K so that the prevision not was carried out outside this range.

The experimental and theoretical data on the linear thermal expansion are summarized in fig. 21, for the four angle orientations. In the temperature range subjected to inspection the linear thermal coefficient can be considered approximatly constant for angles $\vartheta \cong -30° \div 30°$.

As matter of fact the role of the resin becames predominant with the increase of the angle of the fiber orientation, ϑ, as might be expected [14], [15].

It can be observed that agreement between the experimental and the corresponding numerical results is good.

Off-axis experimental thermal expansion coefficients as a function of angle with the fiber orientation are shown in fig. 22.

The measured values at different temperatures and those calculated are plotted in fig. 23; the experimental results agree the numerical results very well.

7. CONCLUSION

It is hoped that this report has touch some of the most important problems connected with the exposed surface and struts of satellite structures.

It is not the complete answer to all satellite structural problems but other aspects such as various environmental condition, fatigue and impact resistance, implication of laboratory accelerated tests ... are discuss at this specialist meeting.

Grateful acknowledgement must be given to responsables of the AGARD Structures and Material Panel for the meeting arranged to cover both theoretical and practical aspects of the composite materials behavior.

At the Institute of Aerospace Technology of Rome is already begin a very extensive research, supported by ESA, in order to validate a general numerical program by an intensive program of experimental tests.

More then 500 specimens will be tested and this is the right way to realize the advantage of the material and to introduce it into satellites.

TECHNICAL LIBRARY
ABBOTTAEROSPACE.COM

REFERENCES

[1] G.P. SENDECKYJ: "Elastic Behavior of Composites". – Composite Materials, Vol. 2. Academic Press 1974.

[2] C.W. BERT: "Analysis of Plates". – Composite Materials: Vol. 7. Academic Press 1975.

[3] E. REISSNER and Y. STAVSKY: "Bending and Stretching of Certain Types of Heterogeneous Aeolotropic Elastic Plates". -- J. of A.M. September 1961 p. 402.

[4] HAWKER SIDDELEY DYNAMICS Lt - SPACE DIVISION: "Final Report for Phase 1 of a study on the use of Carbon Fibre Reinforced Plastics in Satellite Structures". TP 7427 - 1973.

[5] C.H. SHEN and G.S. SPRINGER: "Environmental Effects on the Elastic Moduli of Composite Materials". J.C.M. Vol. 11 / July 1977 pg. 250.

[6] C.Y. LUNDEMO and S.E. THOR: "Influence of Environmental Cycling on the Mechanical Properties of Composite Materials". J.C.M. Vol. 11 / July 1977 p. 276.

[7] C.H. SHEN and G.S. SPRINGER: "Effects of Moisture and Temperature on the Tensile Strength of Composite Materials". – J.C.M. Vol. 11 / January 1977 pg. 2.

[8] R. BARBONI and I. PERONI: "Mechanical and Thermal Coefficients in Composite Materials". – Istituto Tecnoiogia Aerospaziale – Q.C.E. n. 23 – Roma 1979.

[9] AA.VV.. "Studio di strutture a tecnologia avanzata e ad alta stabilità per antenne di un satellite di telecomunicazioni". – Research supported by CNR/SAS – GLIS-SCAS Final Report – Rome Oct 1979.

[10] P. SANTINI:"Thermostructural Problems of High Accuracy Antennas Mounted on Telecomunication Satellites." I.A.F. XXVIII Congress 77-737 – 1977.

[11] C.W. BERT: "Experimental Characterization of Composites". – Composite Materials, Vol. 8 Academic Press 1975.

[12] W.H.M. Van DREUMEL and J.L. M. KAMP: "Non Hookean Behaviour in the Fibre Direction of Carbon - Fibre Composites and the Influence of Fibre Waviness on the Tensile Properties". – J.C.M. Vol. 11 October 1977, p. 461.

[13] P. SANTINI, A. CASTELLANI and A. NAPPI: "An Introduction to the Problem of Dynamic Structural Damping". Agard – R - 663 - 1977.

[14] T. ISHKAWA, K. KOYAMA and S. KOBAYASHI: "Thermal Expansion Coefficients of Unidirectional Composites" J.C.M., Vol. 12 April 1978, p. 153.

[15] B. YATES, M.J. OVERY, J.P. SARGENT, B.A. Mc CALLA, D.M. KINGSTON-LEE, L.N. PHILIPS and K.F. ROGERS: "The Thermal Expansion of Carbon Fibre-Reinforced Plastics". J.M.S. Vol. 13, p. 433, 1578.

ACKNOWLEDGEMENTS

The authors wish to acknowledge the help of Mr. Siclari for his technical assistance in performing the experiments and the Selenia Spa for the preparation of the specimens.

THIS DOCUMENT PROVIDED BY THE ABBOTT AEROSPACE
TECHNICAL LIBRARY
ABBOTTAEROSPACE.COM

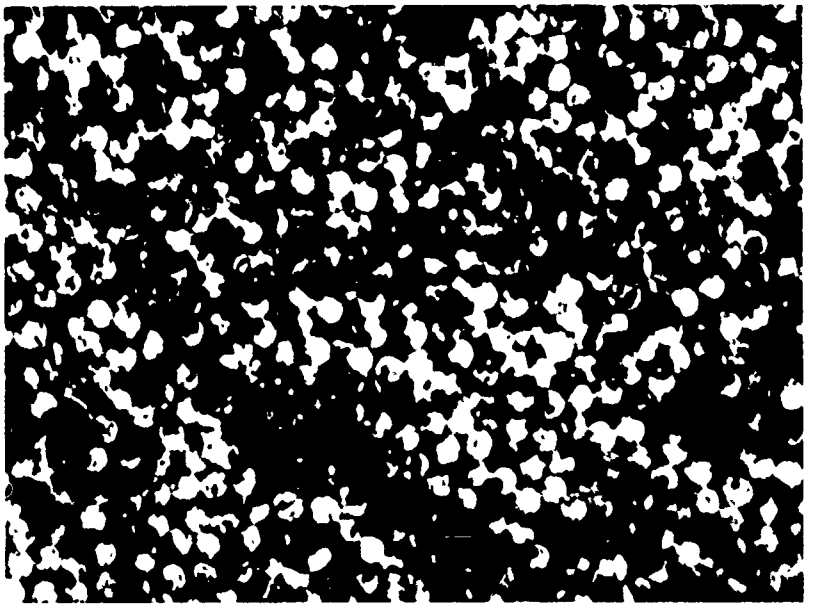

a) Trasversal section (x225)

b) Longitudinal section (x80)

Fig.1 Micrographs of pultrusion compound

THIS DOCUMENT PROVIDED BY THE ABBOTT AEROSPACE
TECHNICAL LIBRARY
ABBOTTAEROSPACE.COM

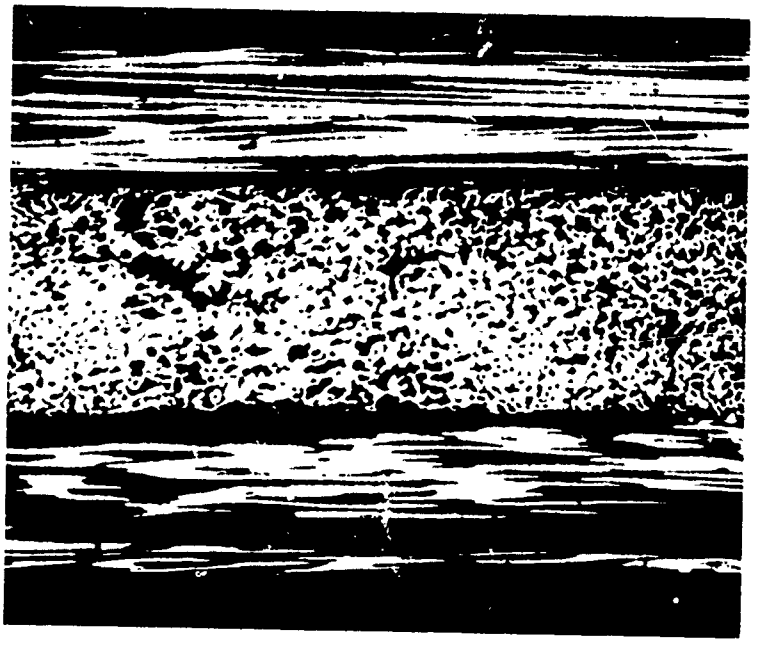

Longitudinal section (x80)

Longitudinal section (x225)

Fig.2 Micrographs of (0/90/90/0) laminate

TECHNICAL LIBRARY
ABBOTTAEROSPACE.COM

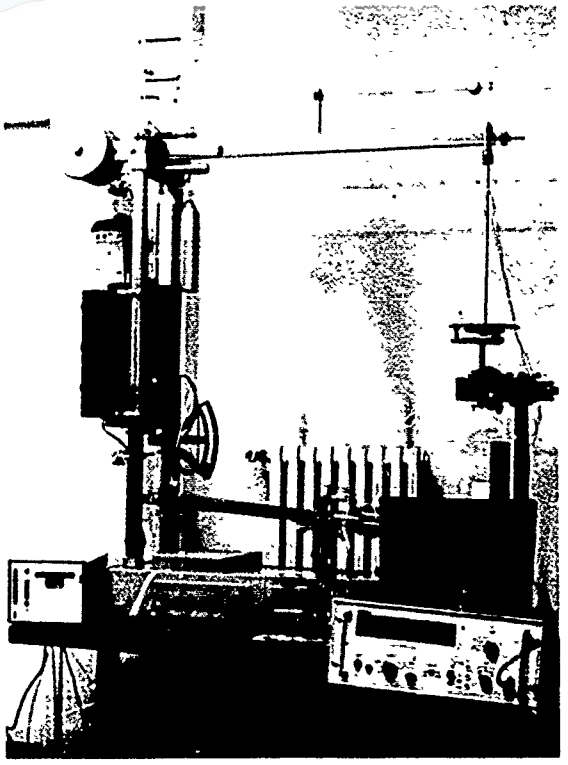

Fig.3 The tensile test machine

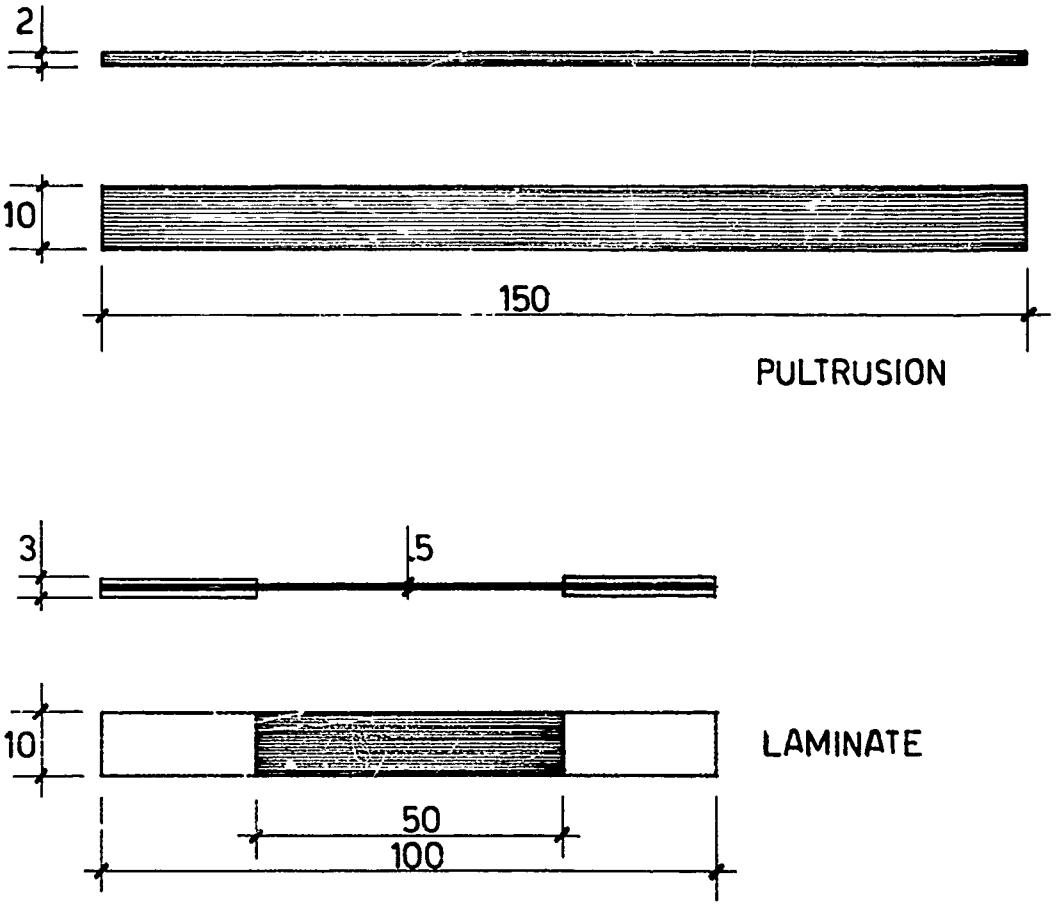

Fig.4 Geometry of the test specimens (mm)

TECHNICAL LIBRARY
ABBOTTAEROSPACE.COM

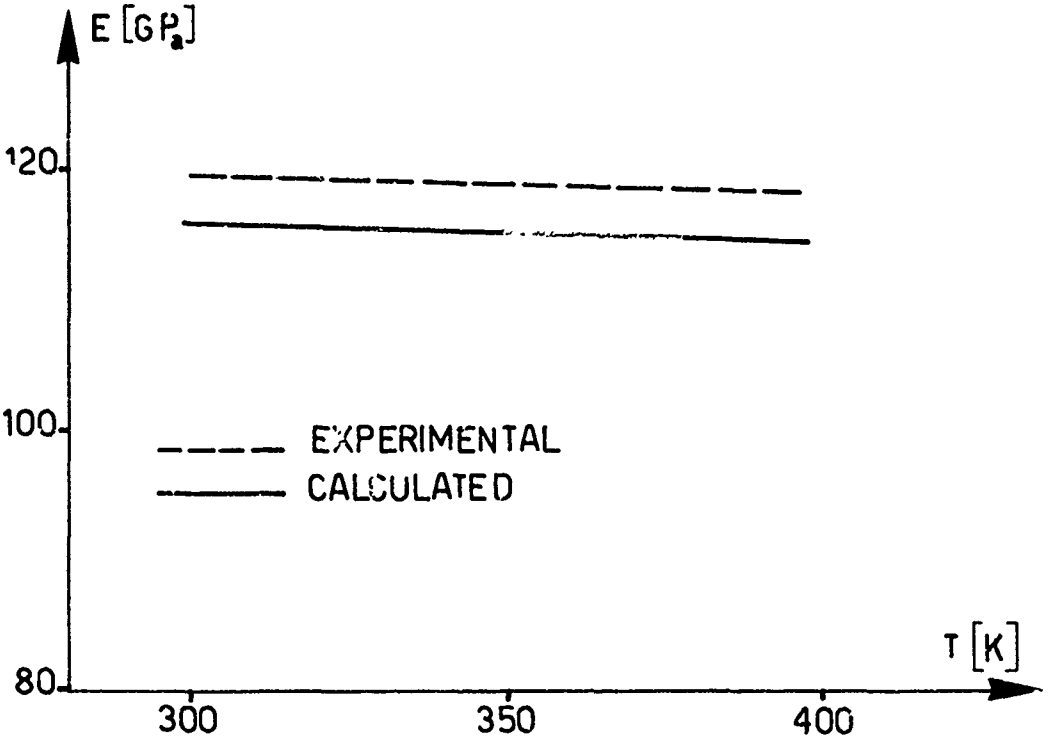

Fig.5 Young's modulus vs. temperature (specimens A/a)

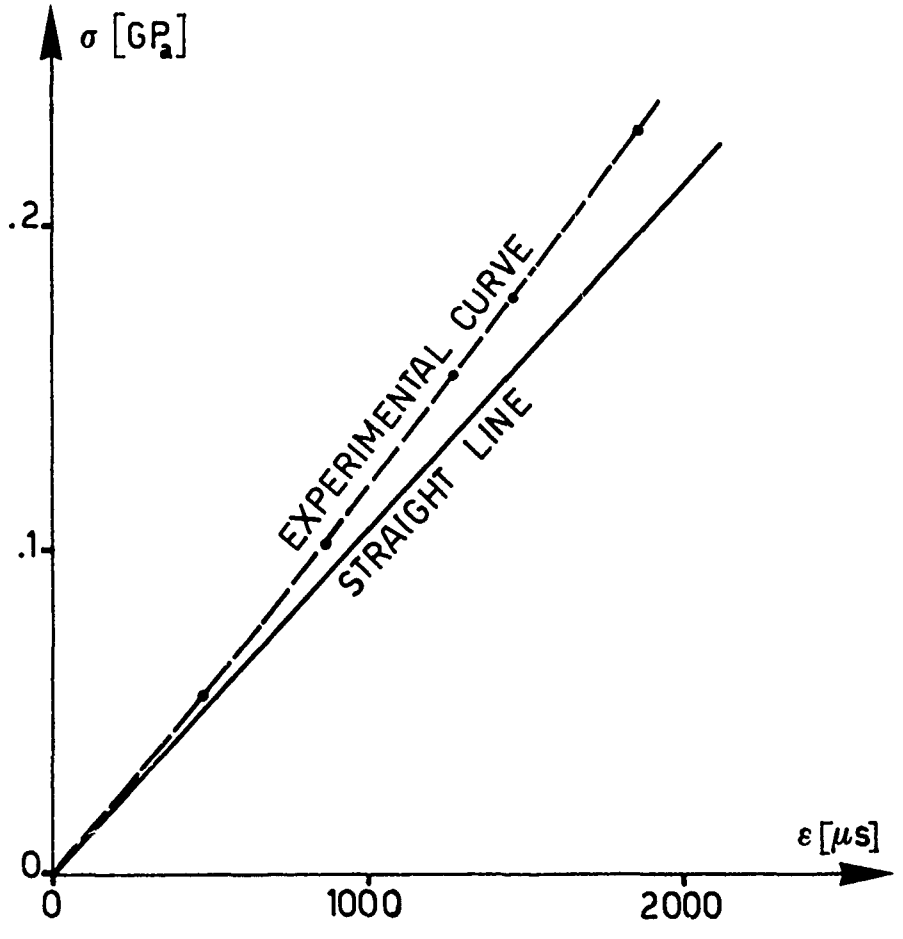

Fig.6 The stress-strain curve (specimens A/a)

THIS DOCUMENT PROVIDED BY THE AEROSPACE
TECHNICAL LIBRARY
ABBOTTAEROSPACE.COM

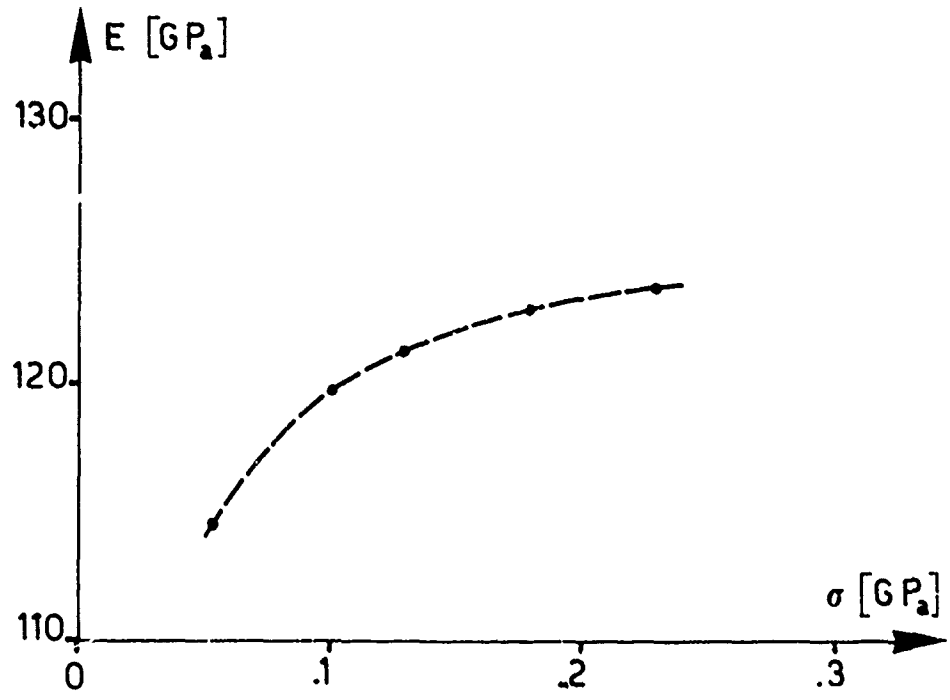

Fig.7 Young's modulus vs. stress (specimens A/a)

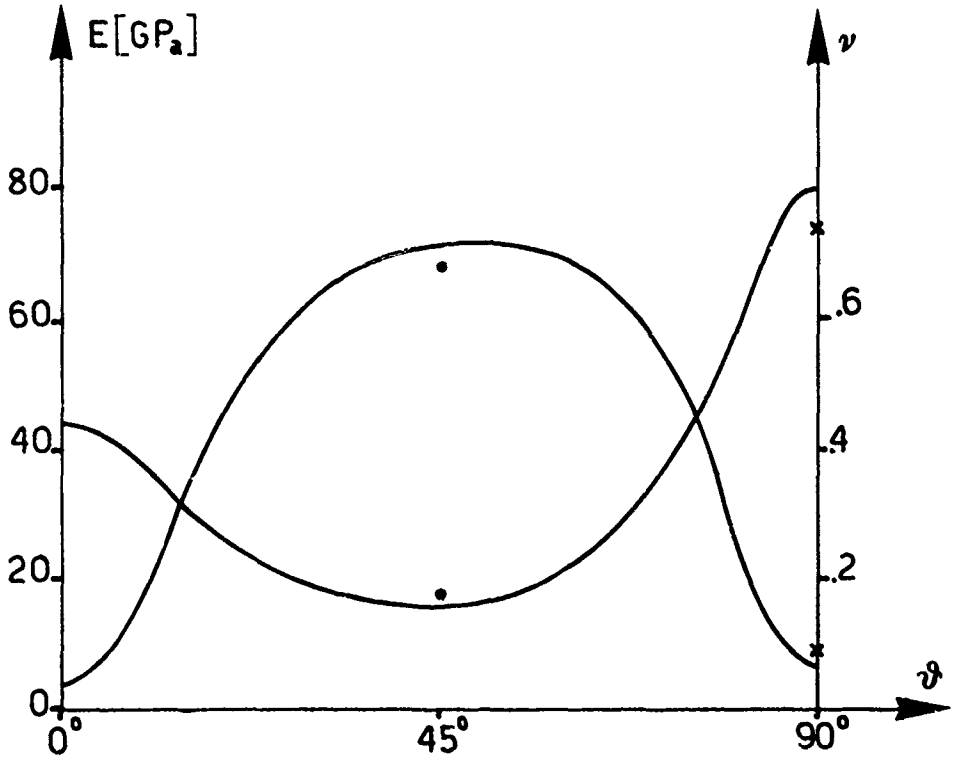

Fig.8 Comparison between experimental and numerical results (laminate B1)

THIS DOCUMENT PROVIDED BY ABBOTT AEROSPACE
TECHNICAL LIBRARY
ABBOTTAEROSPACE.COM

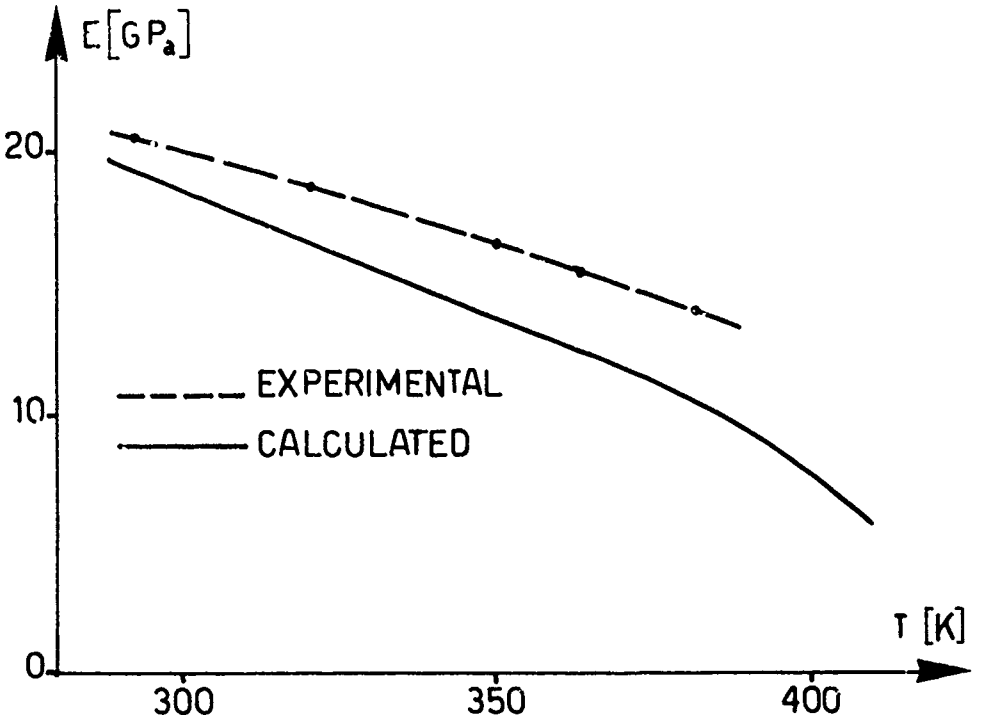

Fig.9 Young's modulus vs. temperature (specimens B1/b)

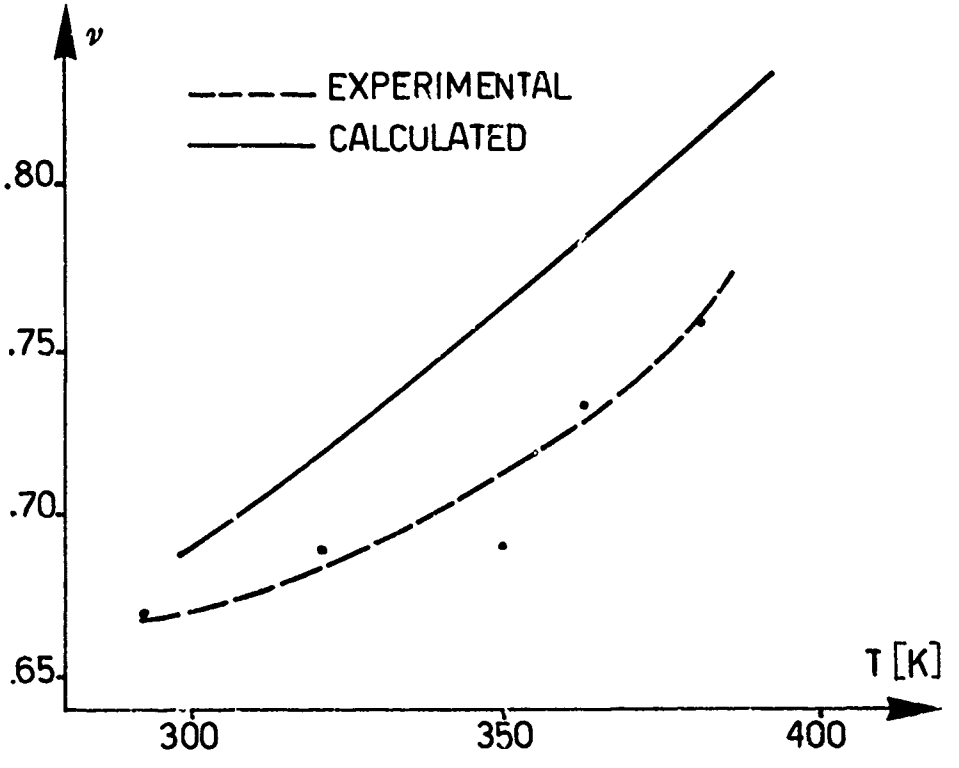

Fig.10 Poisson's ratio vs. temperature (specimens B1/b)

TECHNICAL LIBRARY
ABBOTTAEROSPACE.COM

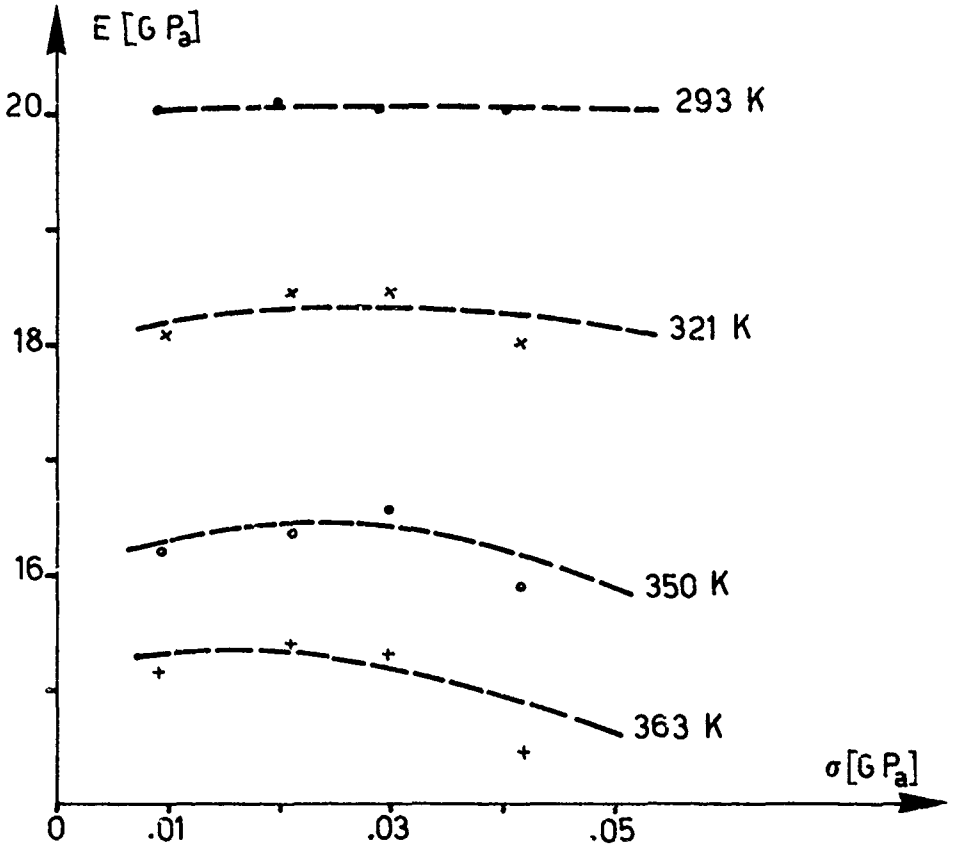

Fig.11 Young's modulus vs. stress (specimens B1/b)

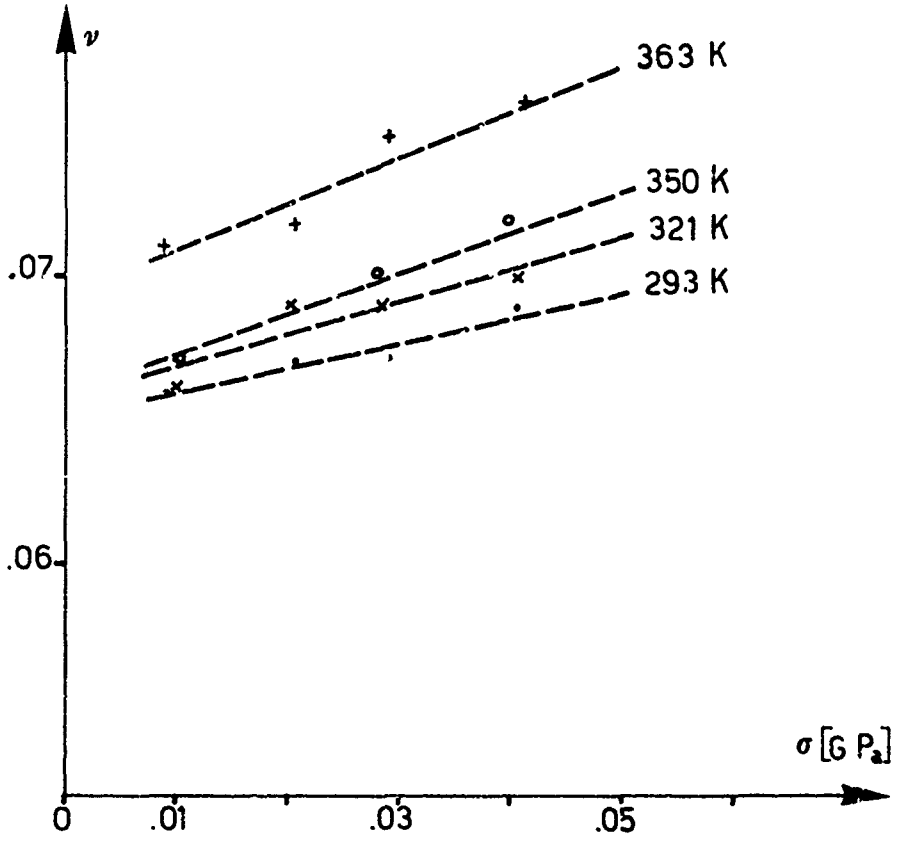

Fig.12 Poisson's ratio vs. stress (specimens B1/b)

TECHNICAL LIBRARY
ABBOTTAEROSPACE.COM

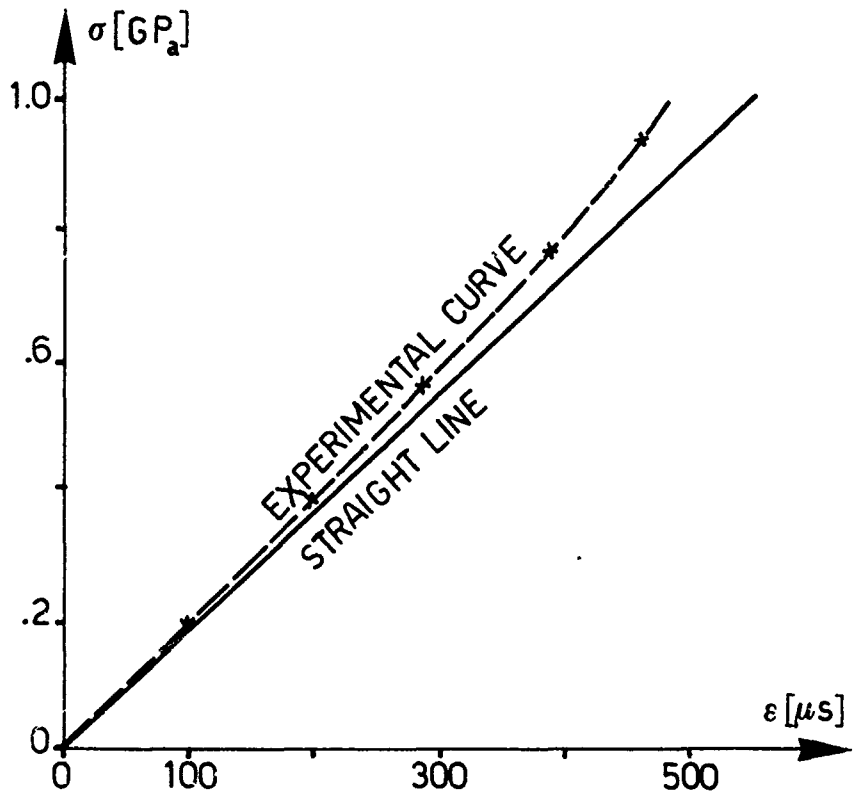

Fig.13 The stress-strain curve (specimens C)

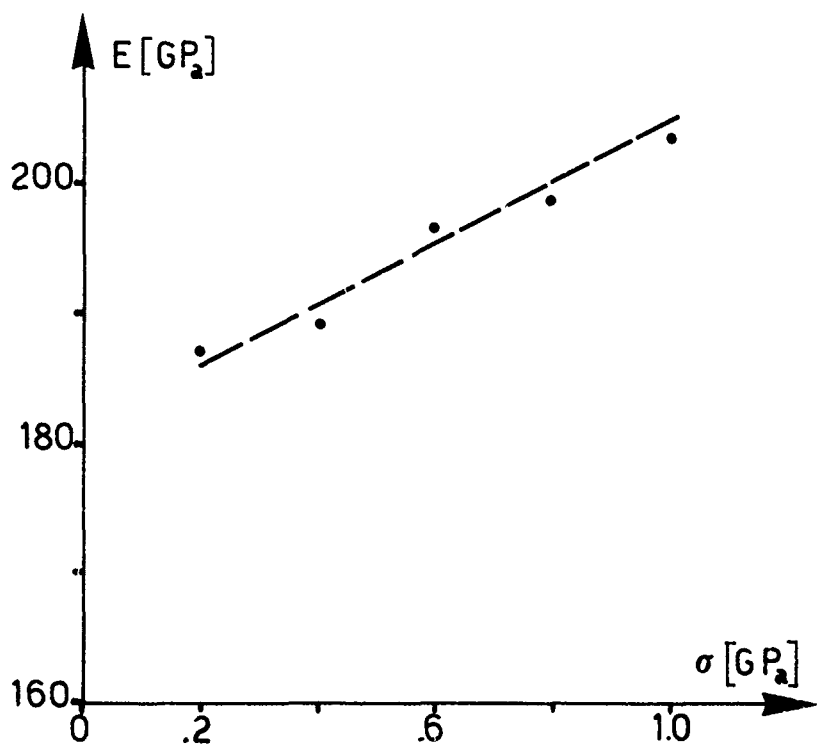

Fig.14 Young's modulus vs. stress (specimens C1/a)

THIS DOCUMENT PROVIDED BY THE ABBOTT AEROSPACE
TECHNICAL LIBRARY
ABBOTTAEROSPACE.COM

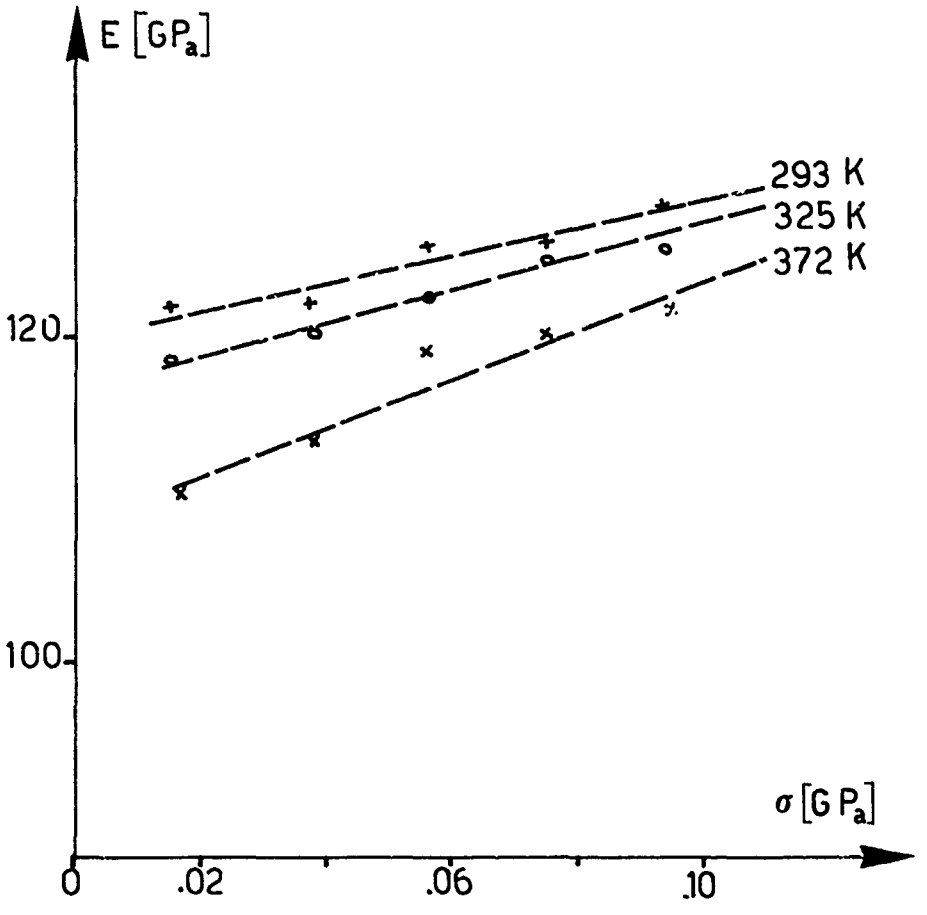

Fig.15 Young's modulus vs. stress (specimens C2/a)

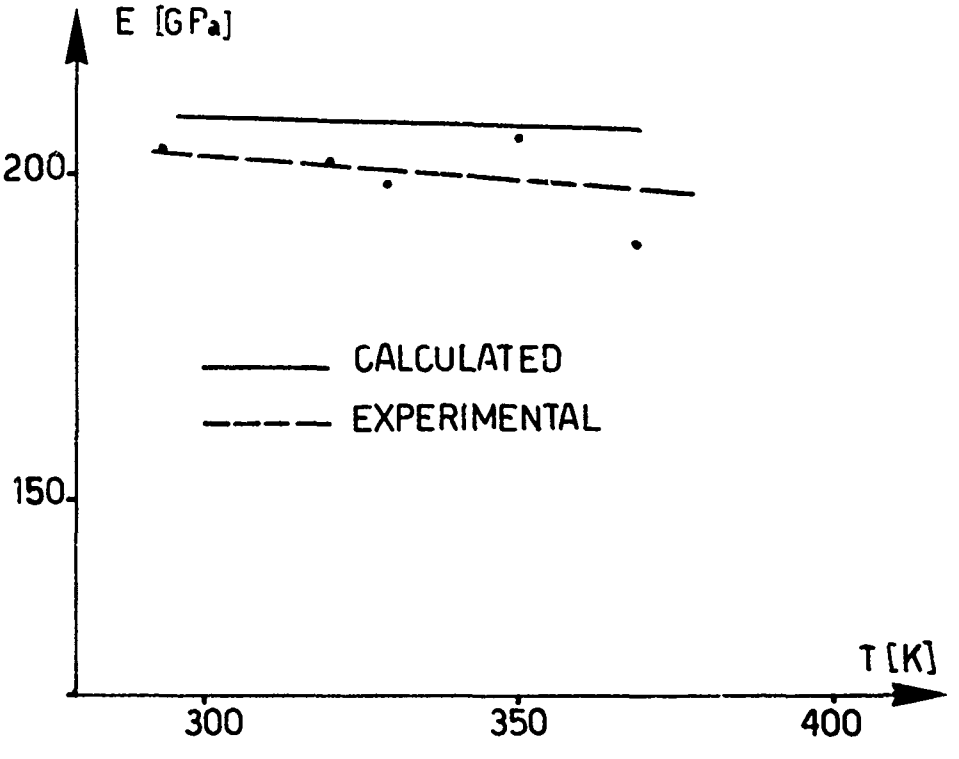

Fig.16 Young's modulus vs. temperature (specimens C1/a)

THIS DOCUMENT PROVIDED BY THE ABBOTT AEROSPACE
TECHNICAL LIBRARY

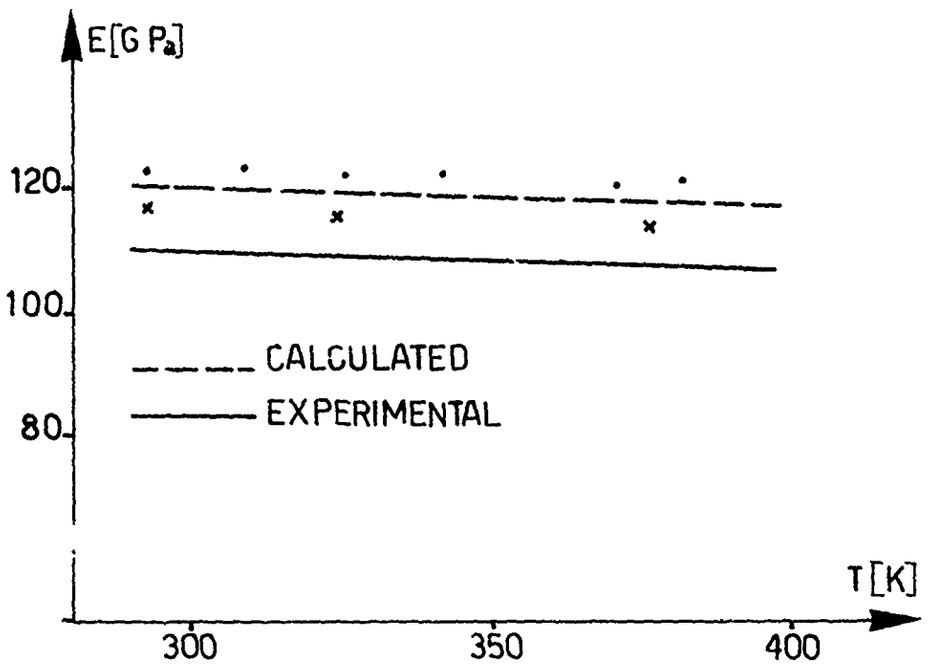

Fig.17 Young's modulus vs. temperature (specimens C2/a)

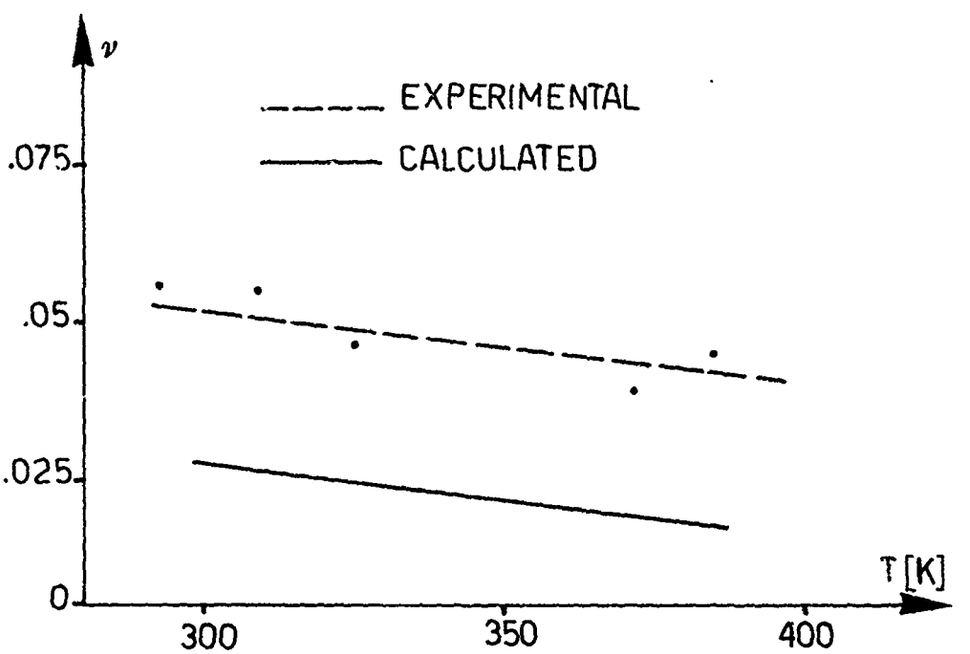

Fig.18 Poisson's ratio vs. temperature (specimen C2/a)

TECHNICAL LIBRARY
ABBOTTAEROSPACE.COM

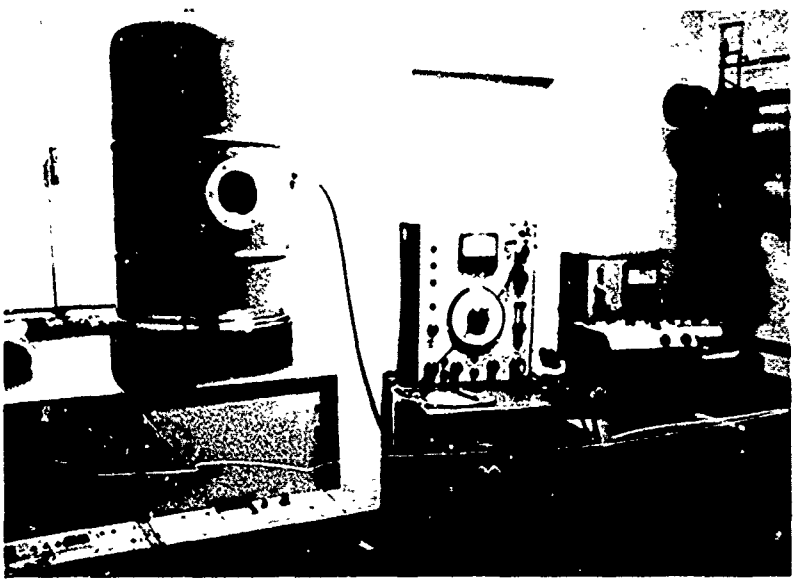

Fig.19 Equipment for dynamic tests

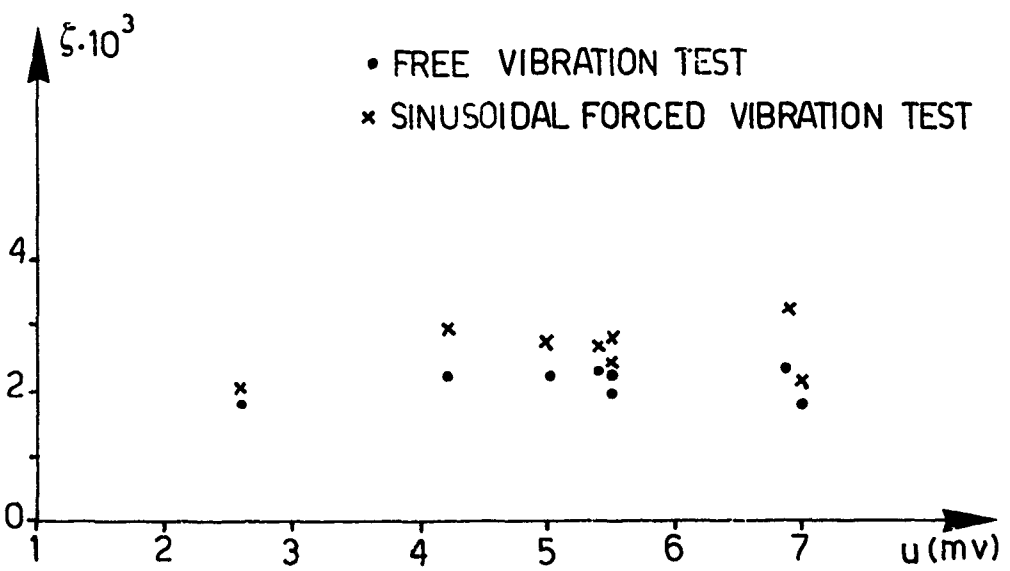

Fig.20 Dimensionless damping ratios (ξ) vs. the response amplitude

TECHNICAL LIBRARY
ABBOTTAEROSPACE.COM

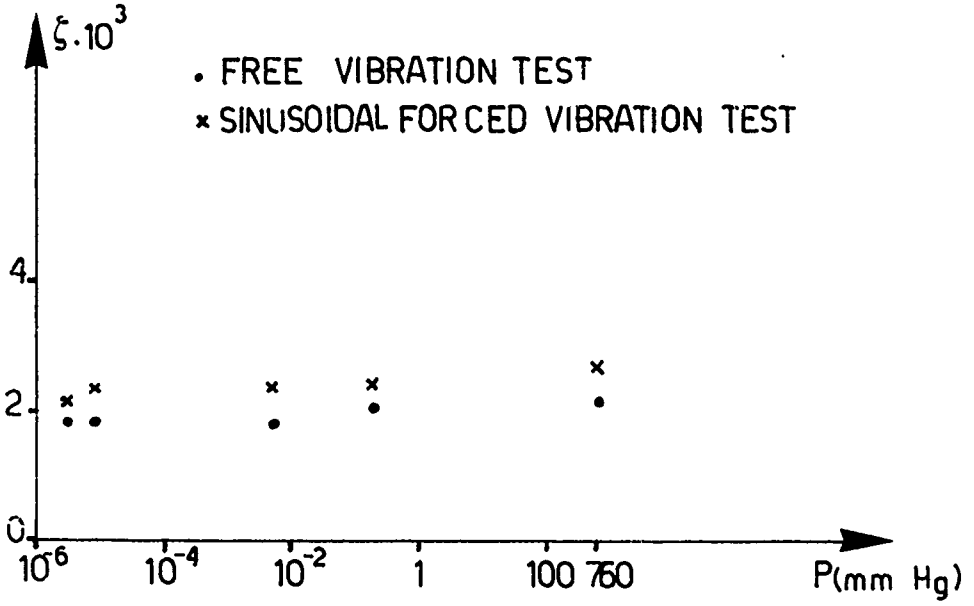

Fig.21 Dimensionless damping ratios (ζ) vs. chamber pressure

Fig.22 The dilatometer

TECHNICAL LIBRARY
ABBOTTAEROSPACE.COM

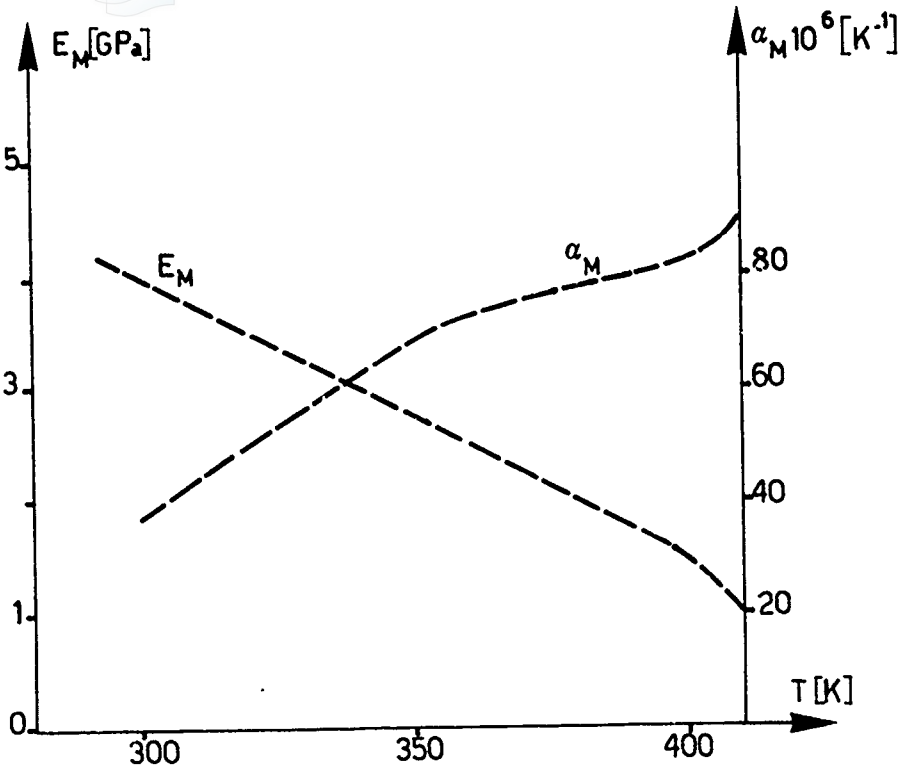

Fig.23 Resin epoxy characteristics

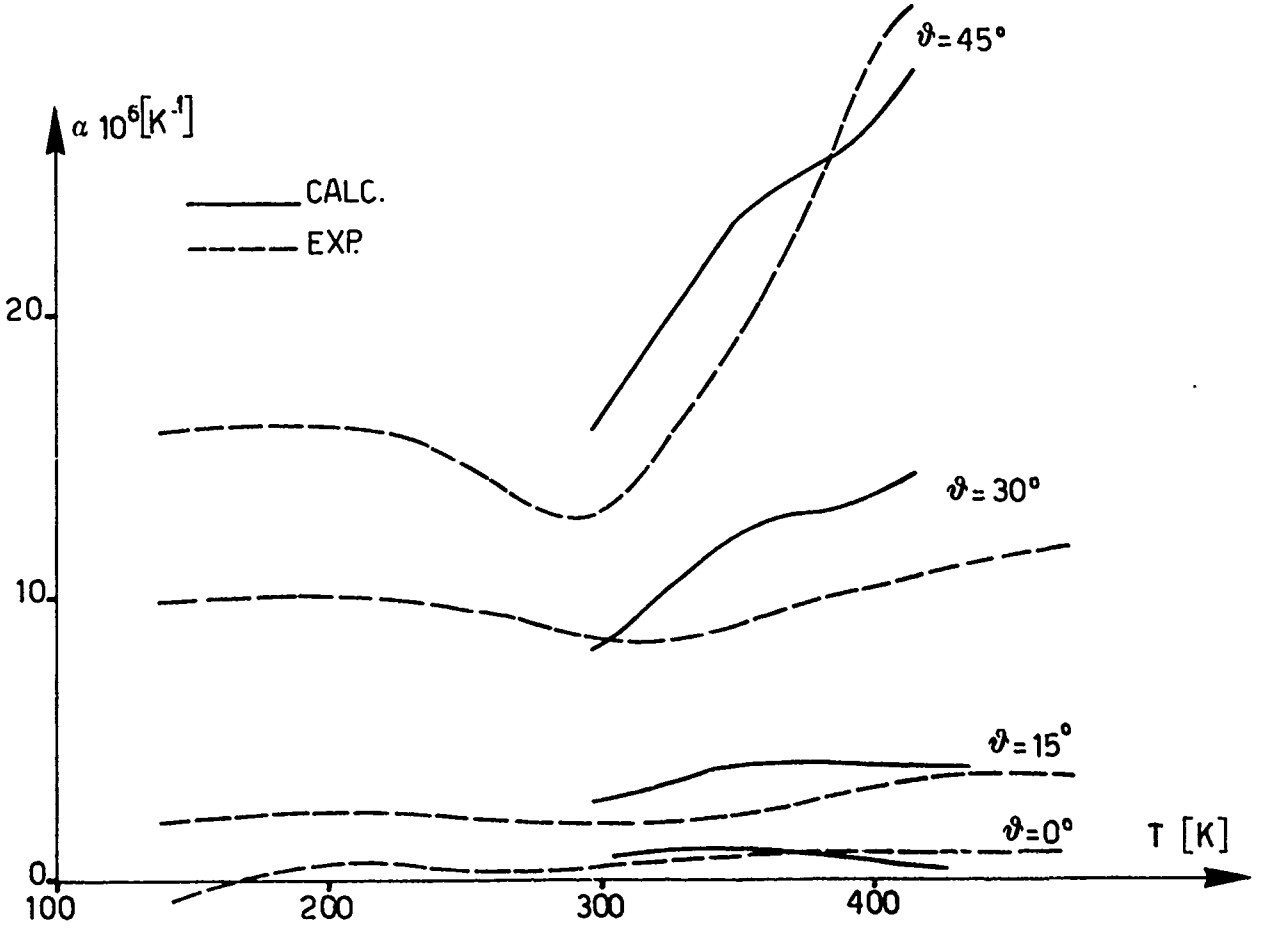

Fig.24 Pultrusion: linear thermal expansion α vs. temperature

THIS DOCUMENT PROVIDED BY THE
TECHNICAL LIBRARY
ABBOTTAEROSPACE.COM

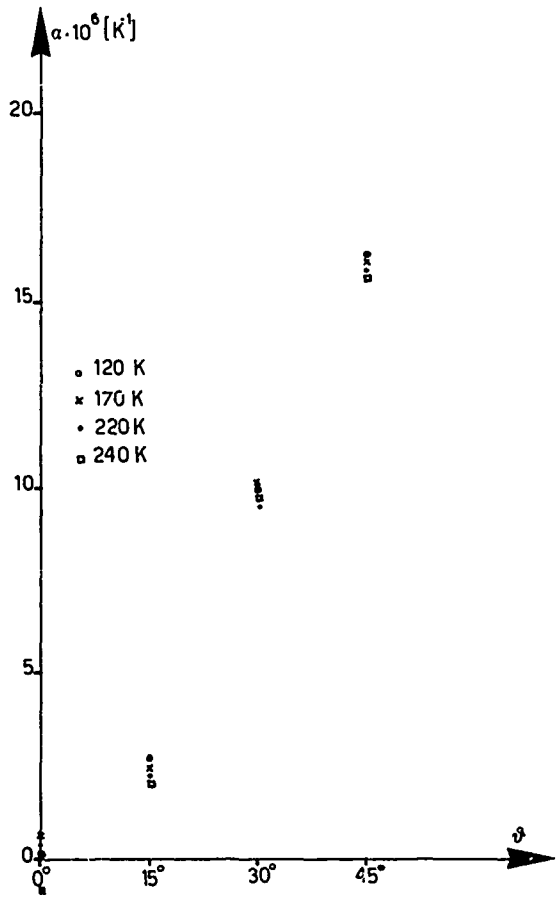

Fig.25 Pultrusion: experimental values of off-axis α (ϑ)

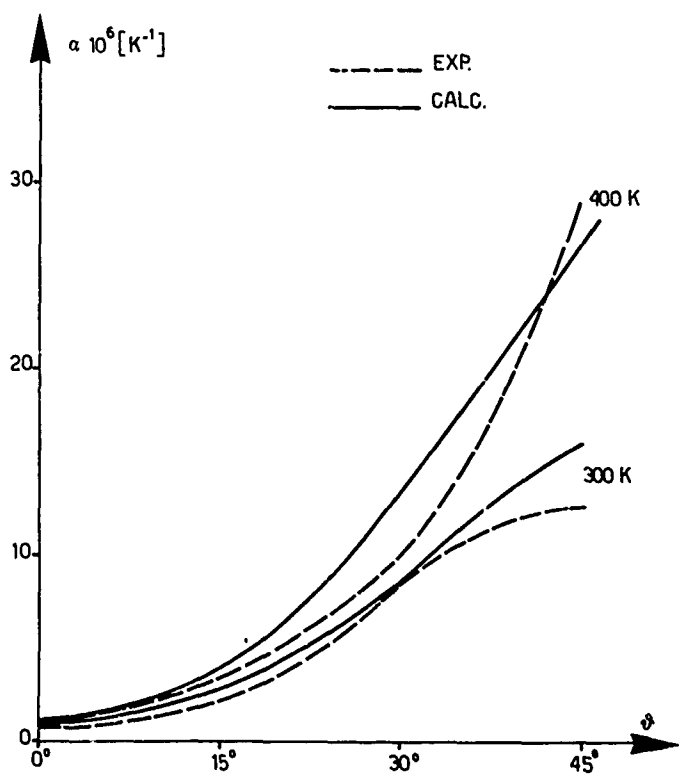

Fig.26 Comparison between theoretical and experimental α

THIS DOCUMENT PROVIDED BY THE ABBOTT AEROSPACE
TECHNICAL LIBRARY
ABBOTTAEROSPACE.COM

RECORDER'S REPORT

SESSION I – PHYSICO-CHEMICAL EFFECTS OF ENVIRONMENT

by

M.F.Card
NASA-Langley Research Center
Hampton, Virginia 23665
USA

Four papers were presented on physico-chemical effects of environment on composite materials. Mr Edge compared moisture absorption data obtained from aircraft exposure tests with accelerated laboratory tests. Data suggests that in most cases, moisture pickup in unaccelerated tests was less than one-percent over periods of time as long as five years. Comparisons of laboratory measures of accelerated testing indicate that immersion in boiling water gives excessive degradation results compared to real life expectations. Humidity and constant temperature exposures appear to give reasonable results except when maximum moisture content for unaccelerated exposures is exceeded. For ambient conditions, reductions in strength due to moisture pickup of less than one-percent are small. However, there still is concern for excessive degradation, particularly when hot, wet environmental exposures occur.

Mr Tennyson presented experimental results on short- and long-term behavior of composites subjected to various environmental conditions. A space environment test facility was described with provisions for mechanical loading under vacuum, temperature, solar radiation, and electron or proton exposures. Results were presented for outgassing of composite-epoxy material indicating that water was the principal outgassing component and that in situ testing is needed to truly characterize material behavior in space. Results of studies of material failure criteria were also presented. The superiority of a cubic strength criterion was illustrated for biaxial strength predictions as well as prediction of successive failures in internal pressure tests. Strength and stiffness changes in graphite-epoxy laminates due to vacuum and temperature changes were presented, as well as analytical predictions, of strength tensor coefficients. Finally, coefficient of expansion data for graphite-epoxy, Kevlar-epoxy, and boron-epoxy laminates under thermal cycling showed some changes due to microcracking and outgassing. Predictions of coefficient of expansion changes for angle plies for ambient versus vacuum conditions were in good agreement with test data.

Dr Bergmann discussed problems in predicting moisture absorption in graphite-epoxy sandwich panels. He indicated that moisture could reduce strength by 50% and that vapor pressures could cause explosions. He reviewed the assumptions inherent in one-dimensional diffusion theory. He indicated that the effects of moisture concentration were generally small, but that other material properties often varied. Some scatter was observed in material coefficients such as maximum absorptivity, the diffusion coefficient-temperature relation, and diffusion coefficients for absorption and desorption. Moisture distribution predictions for 14 thin graphite-epoxy panels were compared with experimental results. Although agreement between analysis and test was fair, Mr Bergmann stressed that these panels were exposed to a well-controlled environment, and that uncontrollable environmental changes would make analysis very difficult. He showed the fallacy of trying to circumvent the moisture problem by sealing, and proposed that conservative maximum saturation estimates be used for design.

Dr Barboni presented experimental and theoretical results for mechanical and thermal behavior of a graphite-epoxy pultrusion and three types of graphite laminates. The pultrusion exhibited a nonlinear stress-strain curve whose linear slope region was insensitive to temperature. Similar behavior was observed in the laminates with the largest temperature effect observed in measurements of a 90/0/90 ply along a 45-degree angle. Calculated values of Young's modulus and Poisson's ratio were in reasonable agreement with test. Free and sinusoidal forced vibration tests of the pultrusion, in and out of vacuum, showed small effects on modulus, but a 15% reduction in ambient damping results. Thermal expansion results for the pultrusion showed good agreement between theory and test.

Subsequent general discussions focused on how important moisture distribution was and how it could be more accurately simulated relative to aircraft exposure tests. Mr Edge reiterated the need for study of tropical (wet, hot) conditions. The practicality of analytical models for stiffness and strength was discussed. Mr Tennyson indicated that with known or measured principal values of stiffness or strength, analysis could be used to handle the variety of laminate configurations encountered in design.

THIS DOCUMENT PROVIDED BY THE ABBOTT AEROSPACE
TECHNICAL LIBRARY
ABBOTTAEROSPACE.COM

CONSTANT-AMPLITUDE AND FLIGHT-BY-FLIGHT TESTS ON CFRP SPECIMENS

BY

F.J. ARENDTS
K.O. SIPPEL
D. WEISGERBER

MESSERSCHMITT-BÖLKOW-BLOHM GMBH
AIRCRAFT DIVISION
8000 MÜNCHEN 80, P.O.BOX 801160
W-GERMANY

ABSTRACT

Constant-amplitude and flight-by-flight tests with five different load spectra were done with unnotched CFRP specimen. Also the influence of overloads was investigated. The test results were compared with fatigue life predictions based on "Miner's Rule" applied for different conditions.

The results show that overloads in all cases cause a significant reduction of the fatigue life. It turned out that fatigue life estimations based on "Miner's Rule" are on the unsafe side in some cases by more than a factor 10, getting a big scatter among the cases investigated.

1. INTRODUCTION

The new generation of fighter aircraft will have an increasing amount of CFRP structural components, which in many cases are subject to fatigue. Whilst comparatively reliable predictions of the service life of metallic components can now be made with the aid of damage accumulation theories based on available test results such as flight-by-flight tests, there is not yet any reliable method of assessing the service life of CFRP components.

Tests were therefore performed, initially on unnotched CFRP specimens, using the results of flight-by-flight fatigue tests to investigate to what extent the Palmgren/Miner linear damage accumulation hypothesis /1,2/ is applicable in assessing the service life of CFRP structures. A further aim was to examine the influence of overloads on the service life, and to determine the probable scatter of the test results.

2. TESTS

2.1 Test Programme

The test programme comprised the following investigations with unnotched specimens performed at RT:

Part A:

- Determining the static compressive and tensile strength of the specimens
- Load-controlled constant-amplitude fatigue tests
- Load-controlled flight-by-flight fatigue tests, varying the following parameters:
  - o load spectrum, or load sequence
  - o maximum spectrum load, or overload.

Part B:

The strength scatter of CFRP material was examined with the aid of further static tensile and compressive tests, each on 14 specimens, and flight-by-flight fatigue tests with a n_z spectrum on 24 specimens. All these specimens were taken from 7 different sheets which had been manufactured from 6 prepreg batches, and produced and cured at different times.

All the tests conducted are shown at a glance in Fig. 1.

2.2 Test Material and Specimens

The sheets from which the specimens were taken were made of prepreg material T300/914C, supplied by Ciba.

The sheets were cured in an autoclave at 180°C for 140 minutes. All the sheets, which were ultrasonically tested, measured 900 x 500 x 2.13 mm. The thickness of 2.13 mm, at a fibre content of 60 % by volume, is made up of 17 prepreg layers in the following proportion:

THIS DOCUMENT PROVIDED BY THE AEROSPACE TECHNICAL LIBRARY
ABBOTTAEROSPACE.COM

8 layers in 0° direction (proportion 47.5 %)
8 layers in ±45° direction (proportion 47.5 %)
1 layer in 90° direction (proportion 5 %)

The exact set up of the layers, and the specimen used for the tests, will be seen from Fig. 2. The longitudinal axis of the specimens was always in 0° direction, which was the direction in which the sheets had the maximum strength.

The specimens used for tests under part A had an GRP reinforcement bonded in the clamping area. This requires an additional tempering cycle of 110 minutes at 170°C. Since tests showed that this reinforcement was not necessary, it was omitted from the specimens used for part B of the programme. An influence on the material properties caused from the then given omission of the GRP reinforcement bonding cycle does not exist as earlier tests have shown.

2.3 Test Spectrum and Sequences Used in the Flight-by-Flight Fatigue Tests

The flight-by-flight tests were based on the following five typical spectra:

- Fighter aircraft horizontal tail spectrum HLW-1 (No.1) /3/
- Mini-Twist (No.2) /4/
- Fighter aircraft n_z spectrum (g-spectrum) (No.3) /5/
- Spectrum for SLAT operation (No.4) /6/
- Spectrum for FLAP operation (No.5) /7/

The typical shapes of the spectra named above are shown in Fig. 3.

For spectra No. 1, No. 2 and No. 3, the influence of overloads was also examined.

It should be noted that, because CFRP composites are so sensitive to compressive stresses, all loads derived from the spectrum were applied with the reverse signs, i.e. tensile load cycles became compressive load cycles and vice versa. This was duly taken into account when placing the plus and minus signs on the ordinate in Fig. 3.

2.3.1 Horizontal Tail/Fighter Aircraft Load Spectrum No. 1

The load cycle which was applied (see Fig. 4) was made up of partial spectra with various mean stresses. Both the sequence of load cycles within one flight, and the sequence of flights, were determined using a law of randoms.

The stress ratio $\bar{R} = \frac{\sigma_u}{\sigma_o}$ is in this case $\bar{R} = -0.75$. Each part of the programme comprised 400 flights, with 26 different types of flights and about 65 load cycles per flight. In the tests with interspersed overloads, an additional load cycle of $\sigma_{\ddot{u}} = 1.25\ \sigma_u$ was applied after each subsequence (400 flights).

Further details of the spectrum may be seen from /3/.

2.3.2 Transport Aircraft Sequence of No. 2

The load sequence in this case is the shortened standardized transport load sequence "Mini-Twist" /4/. A subsequence comprises 4000 flights with 10 different types of flight. For the tests using an overload, the maximum load occurring once in each subsequence was increased by 22 %.

2.3.3 n_z Fighter Aircraft Load Sequence No. 3 (g-Spectrum)

This load sequence /5/ (see Fig. 5) was developed from a typical combat aircraft n_z spectrum and combined to form a subsequence of 200 flying hours or 171 flights. The number of load cycles during one flight averages 75. There are 18 different types of flight in the load sequence.

When simulating overloads, the load cycle number of one subsequence was retained. Only the maximum load level was increased by 25 % and graduated as shown in the sketch of Fig. 5.

2.3.4 Combat Aircraft SLAT Load Sequence No. 4

This load sequence /6/ (see Fig. 6) was made up of sub-spectra from different slat positions combined in a subsequence of 160 flights. Seven different flights with about 38 load cycles per flight were arranged.

2.3.5 Combat Aircraft FLAP Load Sequence No. 5

The load sequence /7/ (see Fig. 6) was made up of sub-spectra from different flap positions combined in a subsequence of 200 flights, comprising five different flights with 26 load cycles each.

THIS DOCUMENT PROVIDED BY THE ABBOTT AEROSPACE
TECHNICAL LIBRARY
ABBOTTAEROSPACE.COM

2.4 Method of Test

The tests in part A of the programme, constant-amplitude and flight-by-flight tests, were performed at the Fraunhofer Institut für Betriebsfestigkeit on a Schenck processor-load-controlled hydropulse machine (1.6 kN). The test frequency was between 1 and 35 Hz for the constant-amplitude tests, and 30 Hz for the flight-by-flight tests.

All tests were conducted at RT. The test specimens were protected against buckling by a teflon-coated support.

The tests in part B of the programme were conducted at DFVLR in Köln-Porz, also on a Schenck processor-load-controlled hydropulse machine (2.5 kN).

2.5 Test Results

2.5.1 Static Tests

The results of the static tensile and compressive tests for parts A and B of the programme are shown in Fig. 7.

The static evaluation does not reveal any major differences as to standard deviation between the specimens tested in parts A and B of programme, i.e. the various batches do not have a negative effect on the scatter of the static strength values. The mean values for tensile and compressive strength were actually slightly higher in the subsequently tested specimens.

2.5.2 Fatigue Tests

2.5.2.1 Results of Constant-Amplitude Load Tests

The S/N curves were each determined on 12 specimens. This involved distributing the tests over a range up to 10^7 load cycles, with different stress levels in each case, and evaluating them with a regression equation according Weibul /8/.

Before the flight-by-flight results could be checked using the Miner rule, S/N curves were determined for the stress ratios R = -1, -5 and +5. Intermediate values needed for the assessment of the service life were interpolated from these and other test results, e.g. from /9/.

Fig. 8 gives the results for the constant-amplitude load tests, a sketch for regressive evaluation, and a table showing the relevant constants or boundary conditions.

2.5.2.2 Flight-by-Flight Test Results

The individual results of the flight-by-flight fatigue tests can be seen from Figs. 9, 10, 11.

The scatter $T = 1 \; / \; \frac{N_{F,\ P\ddot{u} = 10\ \%}}{N_{F,\ P\ddot{u} = 90\ \%}}$

relating to the service life proved to vary considerably from one load sequence to another, and was particularly high at T = 1 : 16.4 in the case of the n_z spectrum tests (No. 3).

Figs. 9 and 10 also clearly show the influence of overloads. In Fig. 12 the results are shown more clearly. In the horizontal tail load sequence, the overload $\sigma_{\ddot{u}} = 1.25\ \sigma_u$, which was interspersed once in every subsequence, has the effect of reducing the service life relative to the value Pü = 50 % by the factor 3.0. In the TWIST sequence, the influence of an overload $\sigma_{\ddot{u}} = 1.22\ \sigma_u$ was approximately the factor 1.95. In the n_z sequence No. 3, overloads $\sigma_{\ddot{u}} = 1{,}25\ \sigma_u$ see also para 2.3.3) caused a reduction in the service life by the factor of 1.83.

The wide scatter of results which became evident for load sequence No. 3 was what gave rise to supplementing the programme by part B. Several of the subsequently tested specimens were subjected to an ultrasonic test before the beginning of testing and after about 50 % of the expected service life. One of these specimens, which displayed an obvious ultrasonic failure reading before the start of testing, failed after only 91 flights. The ultrasonic readings for the other specimens were found not to indicate any obvious faults even after half the expected service life.

The results are shown on a probability plot in Fig. 13. As is evident, the values shown as points cannot be joined with a straight line, which means that they do not have a normal logarithmic distribution. When the distribution was examined for unacceptable values /10/, it was found that three values failed to meet the assumed confidence interval of 95 % of the normal logarithmic distribution. The omission of these coordinate values yielded the distribution resulting from the cross-shaped points, and from this a scatter value of T = 1 : 4.9 could be derived. This scatter is of approximately the same order as the scatter occurring in the tests with other load sequences.

THIS DOCUMENT PROVIDED BY THE ABBOTT AEROSPACE
TECHNICAL LIBRARY
ABBOTTAEROSPACE.COM

3. ASSESSMENT OF SERVICE LIFE USING THE PALMGREN/MINER DAMAGE ACCUMULATION HYPOTHESIS

When assessing the service life with the aid of the Palmgren/Miner rule, the following variants were examined:

- Assessment of service life based on spectra obtained from load sequences No. 1 - 5 by the modified level crossing count method (see Fig. 3).
- Assessment of service life based on a rainflow evaluation of load sequences No. 1 - 5 and a damage calculation using the resulting load cycles.
- Assessment of service life using S/N curves and taking into account the endurance limit.
- Assessment of service life using S/N curves with the fatigue strength lines extended from the low cycle range into the endurance limit range on log-log paper in a straight line.
- Assessment of service life by the relative Miner calculation, with the result of load sequence No. 3 being selected as the reference value for the case shown.

In damage calculations using spectra like those yielded by the load sequences after evaluation by the modified level crossing count method, the steps of the spectrum were selected as shown in Fig. 3. In the Miner calculation, the total amplitudes between the step limits in the positive an negative ranges were always taken into account.

Fig. 14 shows the relationship between the test result and the calculation for the above variants (except the relative Miner calculation) on a probability paper for spectra No. 1 - 5. For spectra 1, 2 and 3, calculations were also made for overload cases.

On looking at the results of the service life assessment, it is evident that considering the scatter none of the variants examined has been able to provide a satisfactory life prediction. All the results of the service life assessment, except those of slat load sequence No. 4, are on the unsafe side, some of them as far as factor 14.

Also the extent of scatter T $\left(T = 1/\frac{N_{F_{P\ddot{u}} = 10\ \%}}{N_{F_{P\ddot{u}} = 90\ \%}}\right)$

of the ratios C $\left(C = \frac{\text{life obtained in test, P\"u 50 \%}}{\text{life calculated from spectrum with S/N curves, P\"u 50 \%}}\right)$ is, at 1 : 11 to 1 : 13, very

wide by comparison with metallic materials. There seemed to be no regular pattern as to how far the type or extent of the load spectrum or the load sequence cause the results to tend one way or the other. The ratios C for spectra No. 3 and 5 were, for instance, apart at 0.07 and 0.27 respectively, although these two spectra are similar, at least in their relative quotas of tensile and compressive loads. The discrepancy is evidently due to the higher number of low load cycles which distinguishes spectrum No. 3 from No. 5. As found in LBF tests /9/ as well, this omission effect can be significant and is apparently not sufficiently weighted in the Miner calculation.

Because of the similarity originally presumed to exist between spectra 3 and 5, the tests with spectrum No. 3 were taken as reference values for checking the relative Miner calculation. As will be seen from Fig. 15, the resulting value C differs by a factor of 3.7, the prediction now being on the safe side. This result is not surprising when the positions of the C values for both spectra in Fig. 14 are compared.

In the case of the n_z spectrum, a relative Miner calculation for assessing the influence of overloads yields a prediction slightly on the safe side, equivalent to a displacement of the C value from 0.072 to 0.088. Taking the original spectrum as the reference, the same tendency should be found when assessing the influence of overloads on the Mini-Twist load sequence by means of the relative Miner rule. Here too, as can derived from Fig. 16, the value increases from approximately 0.158 to 0.26 in the case of overload by contrast to the value without overload. The opposite behaviour - in the case of interspersed overloads a relative Miner calculation of service life would yield a result on the unsafe side - can be expected in the case of the horizontal tail load sequence, because the C values for cases with and without overloads are 0.336 and 0.408 respectively thus showing the opposite tendency to that of the Mini-Twist and n_z load sequence.

This means that, although interspersed overloads significantly reduce the service life, the result of the relative Miner calculation does not always tend in the same direction when the original spectrum in question is taken as a reference.

THIS DOCUMENT PROVIDED BY THE TECHNICAL LIBRARY
ABBOTTAEROSPACE.COM

4. CONCLUSION

The investigation revealed that the "Miner Rule" does not yield satisfactory results for dimensioning carbon fibre reinforced composite materials which will be subject to dynamic stresses in fighter and transport aircraft load sequences. With the exception of the relative Miner calculation, none of the variants examined was able to improve the accuracy of prediction to such an extent that variations up to a factor of about 14 were not still likely. Other investigations conducted by MBB /12/, investigations as described in the fibres manual /9/ and those conducted by NASA /13/ all showed that results obtained from the Miner calculation are on the unsafe side.

As expected, a certain improvement in the assessment of service life was obtained with the relative Miner calculation. However, CFRP seems to be much more sensitive to differences in load spectra than are metallic materials. Nevertheless, provided that similar test results are available, this method is at present the best available for assessing the service life.

However, it must be stated that there is no procedure for predicting the fatigue life of CFRP components at the moment which is applicable for a designer and proved by tests. The question if the "Fatigue Residual Strength Degradation Model" by J.N. Yang has the capability to predict the fatigue life of a component under flight-by-flight loading deserves further studies. At that time the prediction of fatigue life of CFRP components must be based on relevant flight-by-flight tests. In Fig. 17 a fatigue life curve based on the spectrum No. 1 is given. It shows the relative steep slope, which is typical for compression-loaded CFRP material.

5. REFERENCES

/1/ A. Palmgren — Die Lebensdauer von Kugellagern; Z.V.D.J.68(1924) S.339-341

/2/ M.A. Miner — Cumulative Damage in Fatigue; J.Appl.Mech., 12(1945) pp. A 159-164

/3/ P. Keerl, D.Weisgerber — Flight-by-Flight Belastungsablauf für ein Kampfflugzeug-Höhenleitwerk, MBB-Bericht Nr. TN-FE 214/3/76

/4/ H. Nowak, J. Franz, D. Schütz (LBF), J.B.des Jonge (NLR) — "Mini Twist - a shortened Version of Twist"; Minutes of the 15th ICAF Conf., May 1977, ICAF Doc. No. 959

/5/ P. Hahn, D. Weisgerber — n_z-Kampfflugzeug-Lastablauf; MBB-interner Bericht

/6/ P. Hahn, D. Weisgerber — Kampfflugzeug-Lastablauf für SLAT's; MBB-interner Bericht

/7/ D. Weisgerber, P. Hahn — Kampfflugzeug-Lastablauf für FLAP's; MBB-interner Bericht

/8/ W. Weibul — Fatigue Testing and Analysis of Results; Pergamon Press, Oxford, London, N.York, Paris, 1961, page 170

/9/ J.J. Gerharz, B. Rott, D. Schütz — Schwingfestigkeitsuntersuchungen an ungekerbten und gekerbten Faserverbundwerkstoffen aus multidirektionalem Laminat; LBF-Bericht Nr. 3396

/10/ Handbuch Struktur-Berechnung, Blatt 04200-01

/11/ D. Schütz, J.J. Gerharz, E. Alschweig — DGLR-Symposium 1978 in Darmstadt; Vortrags-Nr. 78-188

/12/ D. Weisgerber — Einstufen- und Einzelflugschwingfestigkeitsversuche an gekerbten und ungekerbten CFK-Proben; MBB-TN-FE214/5/76

/13/ E.P. Phillips — Effects of Truncation of a Predominantly Compression Load Spectrum on the Life of a Notched Graphite/Epoxy Laminate; NASA Techn. Memorandum 80114, June 1979

/14/ J.N. Yang — Journal of Composite Materials, Vol. 12/1978

Acknowledgement: This paper is an excerpt from MBB-Report No. UFE 1461 which as part of the ZTL-program was funded by the FRG Ministry of Defence.

TECHNICAL LIBRARY
ABBOTTAEROSPACE.COM

LIST OF SYMBOLS

σ	(N/mm²)	Applied Stress
σ_u	(N/mm²)	Lower Stress
σ_o	(N/mm²)	Upper Stress
$R = \sigma_u / \sigma_o$	(N/mm²)	Stress Ratio
$\bar{\sigma}_u$	(N/mm²)	Minimum Spectrum Stress
$\bar{\sigma}_o$	(N/mm²)	Maximum Spectrum Stress
$\bar{R} = \bar{\sigma}_u / \bar{\sigma}_o$	(N/mm²)	Stress Ratio
$\sigma_{\ddot{u}}$	(N/mm²)	Stress induced by an Overload
n_z	(-)	Load Factor of g-Loading
N	(-)	Number of Load Cycles to Failure
N_F	(-)	Number of Flights to Failure
C	(-)	Ratio of Tested Fatigue Life to Calculated Fatigue Life in Flights
Pü	(%)	Probability of Nerveillance
$T = \frac{N_{F,P\ddot{u}\ 90\ \%}}{N_{F,P\ddot{u}\ 10\ \%}}$		Scatter Factor

---

F I G U R E S

Programme	Type of Test	Material	Type of Specimen	Load Sequence/Load Spectrum	Amount of Specimen	Test Institute
A	Static and dynamic tests with specimen from one CFC plate, for checking Miner's Rule					
	Static tests	CFRP (914C, T300, 6K)	Fig.: 2 (unnotched)	Tension, Compression	5 5	LBF Darmstadt
	Constant amplitude tests	CFRP (914C, T300, 6K)	Fig.: 2 (unnotched)	S/N curves for R = -1, R = -5, R = +5	36	LBF Darmstadt
	Flight-by-Flight tests	CFRP (914C, T300, 6K)	Fig.: 2 (unnotched)	$\bar{\sigma}_u$ = -620 N/mm², Loadseq. No. 1; 4 5; $\bar{\sigma}_u$ = -650 N/mm², Loadseq. No. 2 $\bar{\sigma}_u$ = -600 N/mm², Loadseq. No. 3; 4	13 6 4	LBF Darmstadt
	Flight-by-Flight test including overloads	CFRP (914C, T300, 6K)	Fig.: 2 (unnotched)	$\bar{\sigma}_u$ = -775 N/mm², Loadseq.No.1 $\bar{\sigma}_u$ = -793 N/mm², Loadseq.No.2 $\bar{\sigma}_u$ = -750 N/mm², Loadseq.No.3	5 5 4	LBF Darmstadt
B	Tests with CFRP Specimen for evaluating batch influences on the static and dynamic strength					
	Static tests	CFRP (914C, T300 B)	Fig.: 2 (unnotched)	Tension, Compression	14 14	DFVLR - Köln-Porz
	Flight-by-Flight fatigue tests	CFRP (914C, T300 B)	Fig.: 2 (unnotched)	$\bar{\sigma}_u$ = -600 N/mm², Loadseq.No.3	24	DFVLR - Köln-Porz

FIG. 1 TEST PROGRAMME

TECHNICAL LIBRARY
ABBOTTAEROSPACE.COM

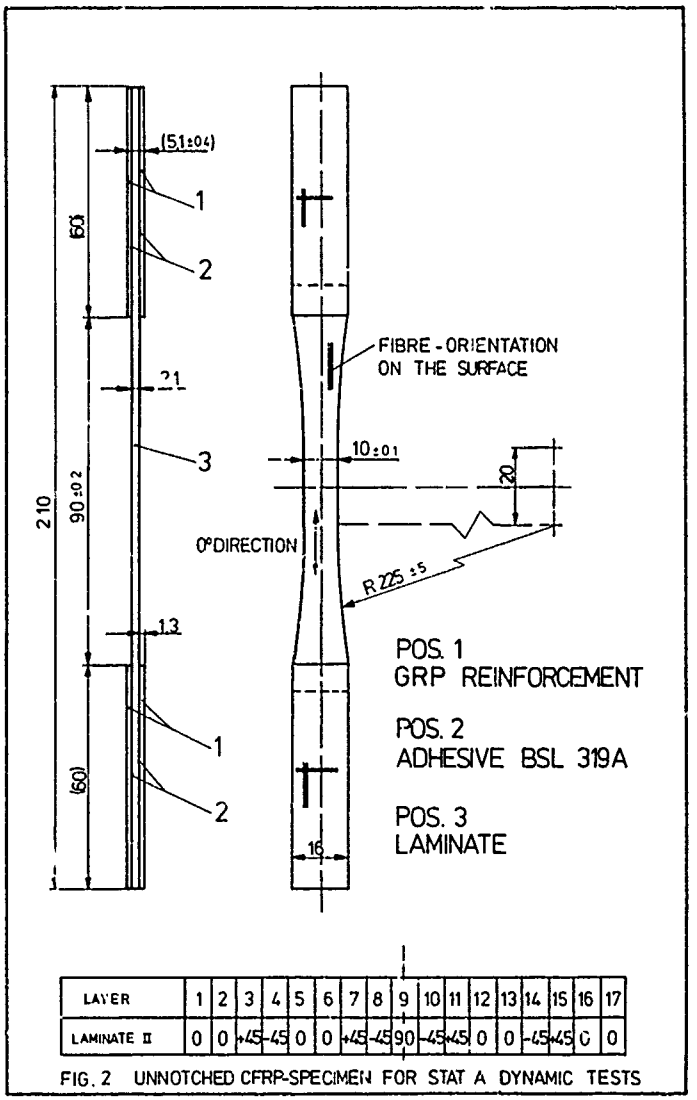

LAYER	1	2	3	4	5	6	7	8	9	10	11	12	13	14	15	16	17
LAMINATE II	0	0	+45	-45	0	0	+45	-45	90	-45	+45	0	0	-45	+45	0	0

FIG. 2 UNNOTCHED CFRP-SPECIMEN FOR STAT A DYNAMIC TESTS

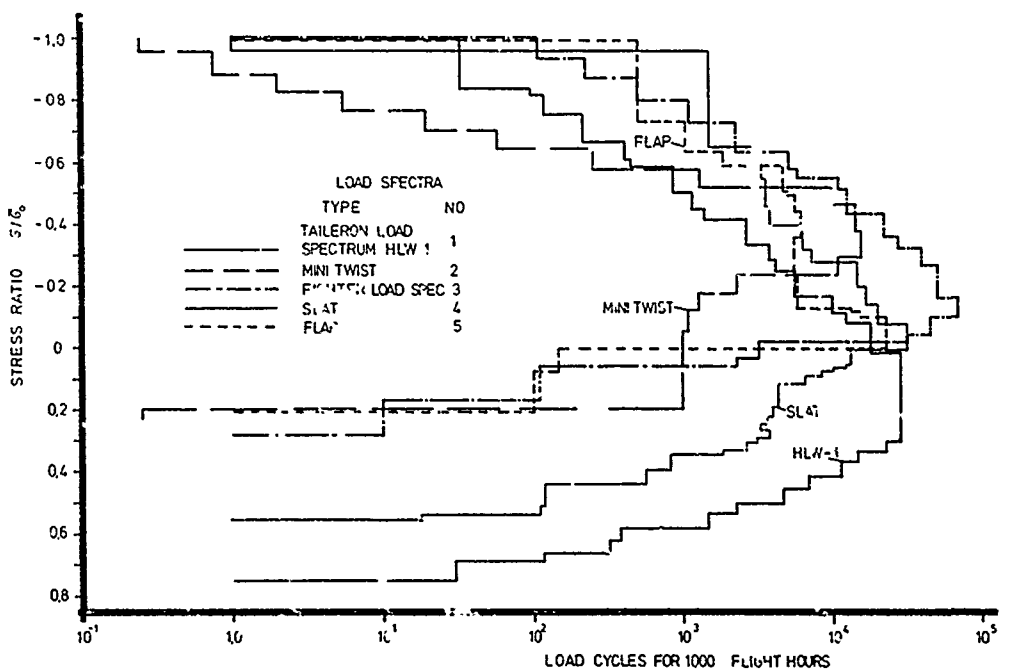

FIG 3 LOAD SPECTRA USED FOR THE INVESTIGATION (EVALUATED ACCORDING TO THE MODIFIED LEVEL CROSSING COUNT METHOD)

THIS DOCUMENT PROVIDED BY THE ABBOTT AEROSPACE
TECHNICAL LIBRARY
ABBOTTAEROSPACE.COM

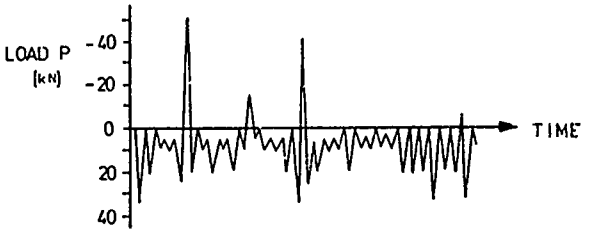

FIG. 4 INVERTED TYPICAL FIGHTER TAILERON LOAD SEQUENCE

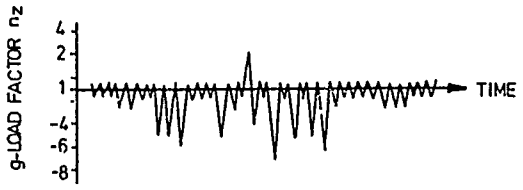

INVERTED TYPICAL FIGHTER LOAD SEQUENCE

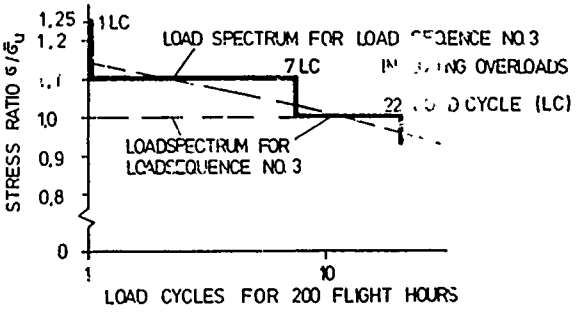

FIG 5 MODIFIED FIGHTER LOAD SPECTRUM WITH INTRODUCED OVERLOADS

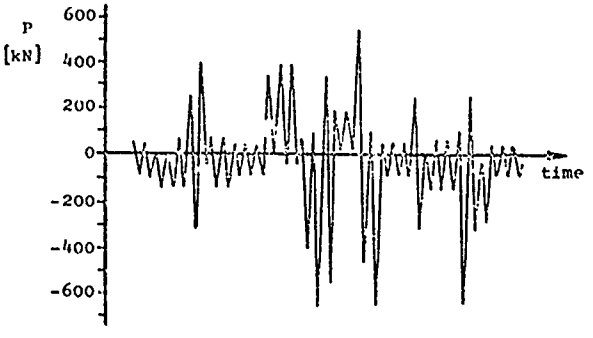

SLAT LOAD SEQUENCE

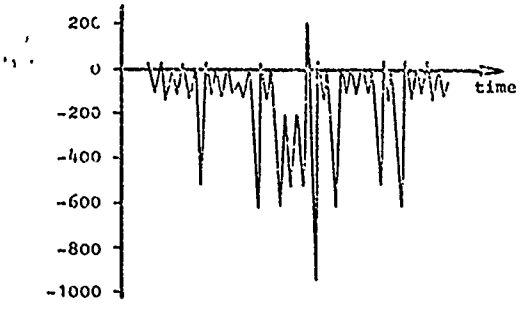

FLAP LOAD SEQUENCE

FIG. 6 TYPICAL LOAD SEQUENCE FOR FLAP AND SLAT LOADING

TECHNICAL LIBRARY
ABBOTTAEROSPACE.COM

	Type of Loading	Failure Stress (N/mm²)	Mean Value and Standard Deviation (N/mm²)
Programme A	Tension	802,90 870,90 792,30 873,50 802,00	$\bar{X}$ = 828,32 S = 40,3
	Compression	- 865,80 - 729,89 - 776,38 - 872,23 - 886,43	$\bar{X}$ = -826,14 S = - 69,05
Programme B	Tension	803,3 905,2 928,6 838,1 833,3 878,6 867,3 943,1 921,1 916,3 908,5 873,2 887,7	$\bar{X}$ = 884,98 S = 41,10
	Compression	- 771,9 - 797,7 - 840,5 - 854,8 - 802,4 - 871,4 - 732,2 - 789,1 - 942,6 - 923,7 - 842,4 - 870,7 - 880,4 - 932,9	$\bar{X}$ = -846,62 S = 41,40

FIG. 7 RESULTS OF STATIC TENSION AND COMPRESSION STRENGTH TEST

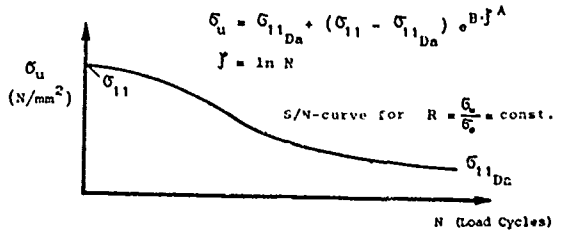

R	A	B	σ_{11Da}*	σ_{11}*
-1	1,8	$-1,1986 \cdot 10^{-2}$	145,6	822,2
-5	2,935	$-7,0365 \cdot 10^{-4}$	262,5	812,6
+5	2,66	$-9,6 \cdot 10^{-4}$	287,3	824,3

* Stress values in N/mm² derived by regression calculation

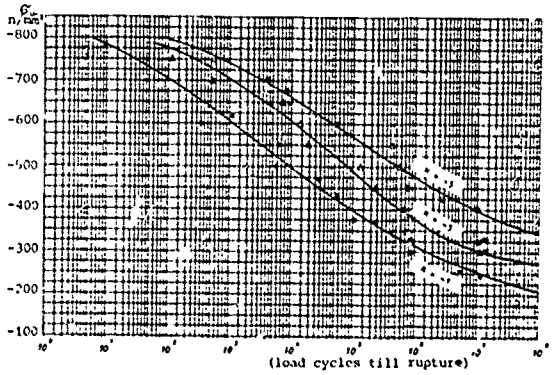

Fig. 8 Results of the Constant Amplitude Fatigue Tests with Unnotched CFC specimen (tested to rupture), evaluated by the above shown regression equation

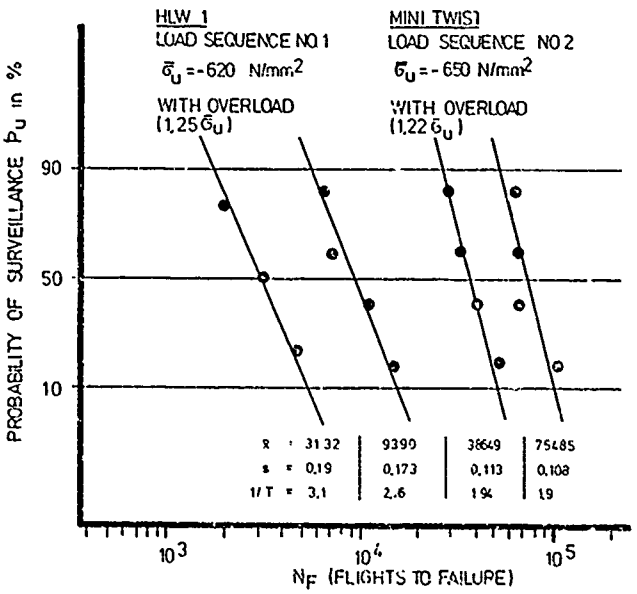

FIG 9. RESULTS OF THE FLIGHT BY FLIGHT FATIGUE TESTS FOR THE LOAD SEQUENCES NO 1 AND NO2 WITH AND WIHTOUT OVERLOADS

TECHNICAL LIBRARY
ABBOTTAEROSPACE.COM

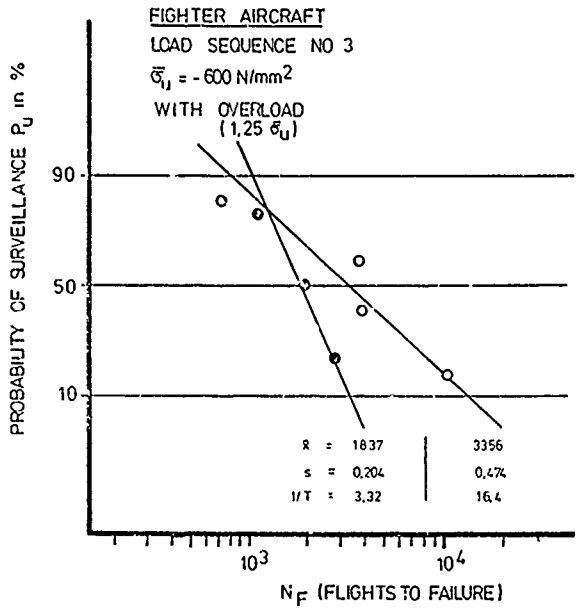

FIG 10 RESULTS OF THE FLIGHT BY FLIGHT FATIGUE TESTS FOR THE LOAD SEQUENCES NO 3 WITH AND WITHOUT OVERLOADS.

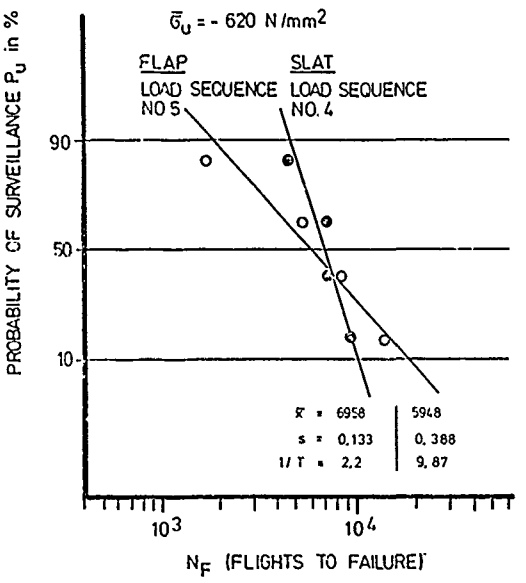

FIG 11 RESULTS OF THE FLIGHT BY FLIGHT FATIGUE TESTS FOR THE LOAD SEQUENCES NO 4 AND NO.5.

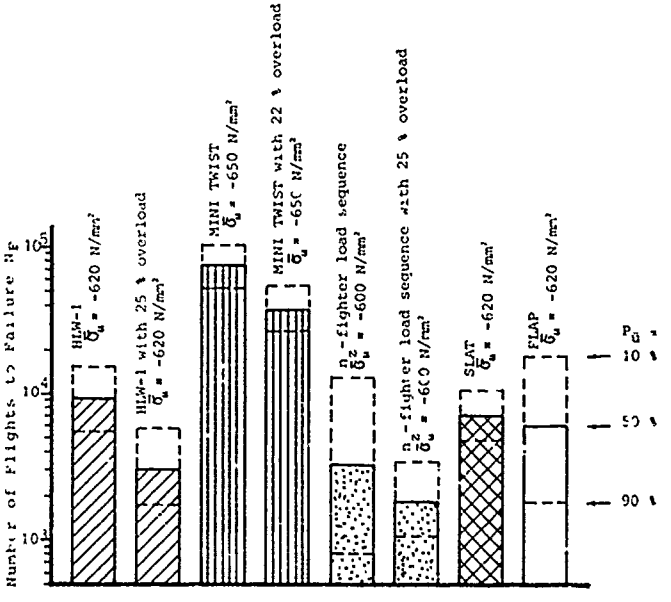

FIG. 12 RESULTS OF FLIGHT-BY-FLIGHT FATIGUE TESTS

TECHNICAL LIBRARY
ABBOTTAEROSPACE.COM

FIG 13 RESULTS OF THE FLIGHT BY FLIGHT FATIGUE TESTS WITH THE n_z-LOAD SEQUENCE NO.3 DERIVED WITH SPECIMEN MANUFACTURED FROM DIFFERENT BATCHES

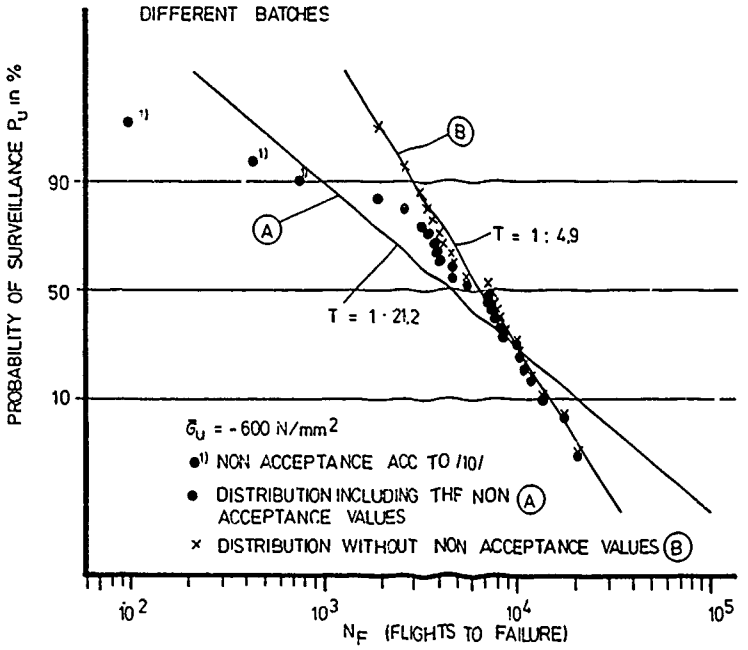

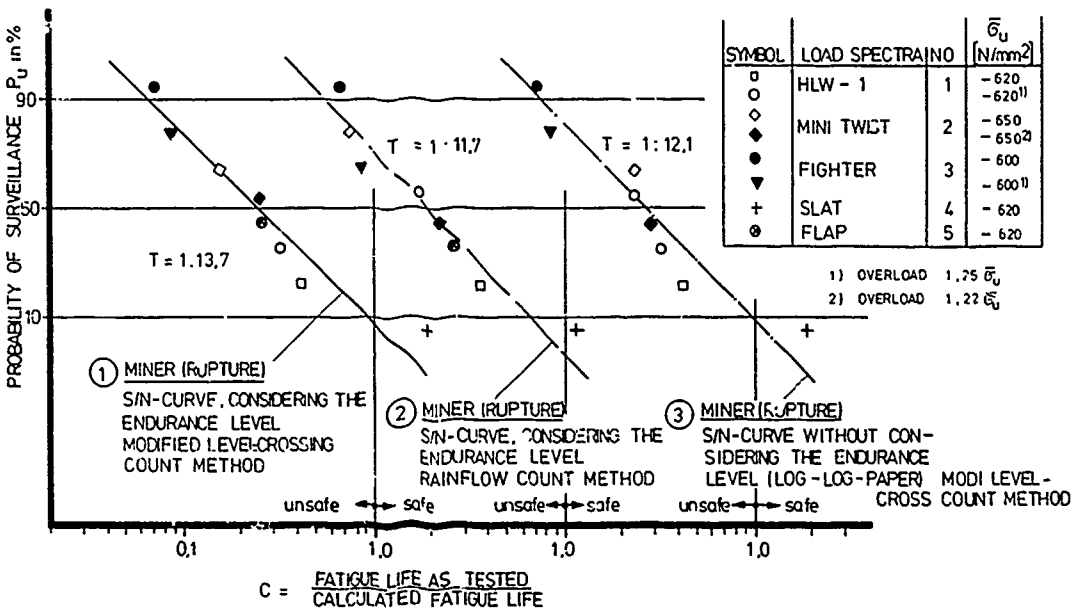

FIG 14 RESULTS OF THE FATIGUE LIFE CALCULATION

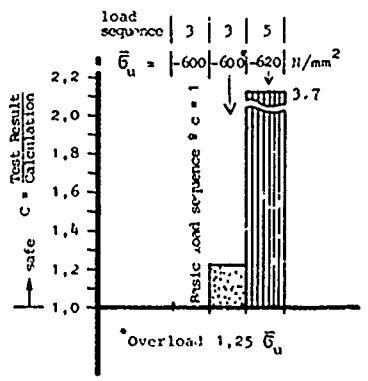

FIG. 15 RESULTS OF THE FATIGUE LIFE CALCULATION ACCORDING TO THE RELATIVE MINER CALCULATION

TECHNICAL LIBRARY
ABBOTTAEROSPACE.COM

Load Spectrum respectively Load Sequence		$\bar{\sigma}_u$	Test Result in Flights	Calculated Fatigue Life in Flights Modified Level Crossing Count Method		Rainflow Count Method
Type	No.	(N/mm²)	Rupture	Rupture I	Rupture II	Rupture I
HLW-1	1	-620	9390	22988	22472	24600
		-620[1)]	3132	9324	9546	17241
MINI TWIST	2	-650	75495	476190	320000	1034928
		-650[2)]	38649	148699	128617	178253
FIGHTER n_z-LOAD SEQ.	3	-600	3356	46512	42553	49850
		-600[1)]	1837	20833	21053	21763
SLAT	4	-620	6958	3604	3902	6110
FLAP	5	-620	5948	22222	24096	22663

I S/N curve, endurance limit considered

II S/N curve, having extended the straight line in the low cycle range in a log-log plot extended into the endurance limit range

1) Overload $1{,}25\,\bar{\sigma}_u$

2) Overload $1{,}22\,\bar{\sigma}_u$

FIG. 16 RESULTS OF THE FATIGUE LIFE CALCULATION ACCORDING TO "MINER'S RULE" FOR UNNOTCHED CFRP SPECIMEN

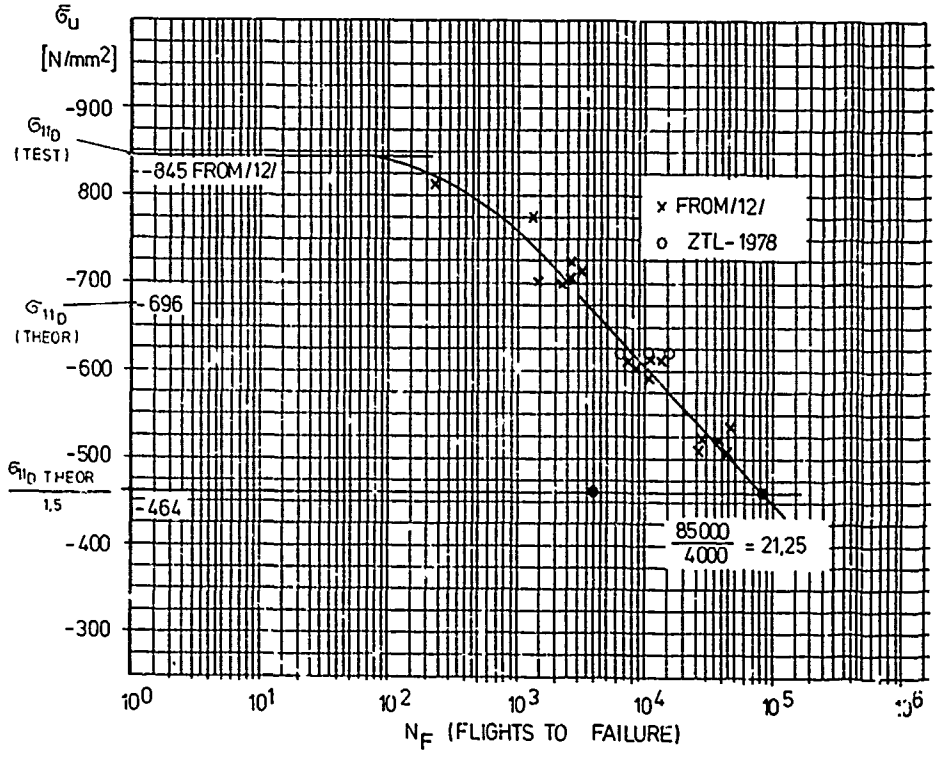

FIG. 17 FATIGUE LIFE CURVE FOR THE LOAD SEQUENCE HLW-1

TECHNICAL LIBRARY
ABBOTTAEROSPACE.COM

FATIGUE STRENGTH OF CFRP UNDER COMBINED FLIGHT-BY-FLIGHT LOADING AND FLIGHT-BY-FLIGHT TEMPERATURE CHANGES

by
J. J. Gerharz and D. Schütz
Fraunhofer-Institut für Betriebsfestigkeit (LBF)
Bartningstraße 47
6100 Darmstadt
Germany (FRG)

SUMMARY

This paper documents a research program on the influence of environment on the fatigue of CFRP unnotched, notched and bolted specimens. Included are program, details, facility set up, test results, and relevant information found in the literature. The specimens are simultaneously subjected to load and environmental histories. A flight-by-flight load and environment sequence typical for the wing-root of a flighter airplane is applied. Test with simplified simulation of environment, allowing high loading frequencies, are run. The admissibility of the simplifications is evaluated by comparing the results of each simplified test with the results from long time "quasi real time" test with temperatures accompanying the loads in each flight. The "quasi real time" flight-by-flight program includes temperature cycles and a humidity cycle. The specimens are heated and cooled by preconditioned air forced through the test chamber. The results of room temperature fatigue tests (base line data) and of static tests at various environmental conditions are presently available. For a constant fatigue-stress level residual strength and stiffness data demonstrate the damage growth made apparent by ultrasonic scan records.

PROGRAM DESCRIPTION

The use of resin matrix composites in primary aircraft structure intoduces a new range of problems. As shown in the chapter "Literature Survey" many experiments reveal a sensitivity of resin matrix and fibre-matrix interface to both environmental degradation and fatigue loading, with interactions between various mechanisms beeing possible. Assurance is therefore needed that any environmental and fatigue damage accumulated during a typical aircraft life will not compromise structural integrity. The research program described herein contributes to a base of design data containing the environmental effect on the design properties of the graphite/epoxy composite material.
The application of composites in Europe is presently beeing developed through advanced fighter aircraft. Considering the aircraft wing as a primary structure candidate for a graphite/epoxy composite design, the loading and environmental conditions of the upper surface structure were chosen for flight simulation testing. Besides beeing subjected especially to solar radiation and rain soak, the loading of the upper surface structure is predominantly compressive and graphite/epoxy composites show a higher sensitivity to cyclic loading in the compression region [1]. A few tests are also planned with lower surface loading and constant amplitude loading with critical stress ratios. Plain specimens of various laminate lay-up and jointed specimens with a specific lay-up are used. The wing loading sequence chosen is The FAtigue Loading STAndard For Fighter Aircraft (FALSTAFF) which is described in detail in [2]. It is based on actual operating experience of fighter aircraft. The average peace time usage for this type of aircraft will be 4 flights per week, summing up to 5,33 flight hours/week; thus 1000 flights will be made in 4.8 years, totalling 1333 flight hours [3]. Clearly a real time replication of environment history in the laboratory to a factored life is not practical, therefore a so-called "Quasi Realtime" test program was developed through acceleration of the actual temperature/moisture/loading history. The development was jointly conducted with the R. E, Structures Department to receive comparable test results from similar RAE and LBF research programs. The objective of an accelerated test spectrum should be to develop the same damage growth and residual strength in the structure as the real time loading spectrum but in such a manner that testing time and cost are minimized. By this criterion a major acceleration in real time environmental effects can be achieved by shortening the ground dwell period, the time the aircraft spends standing on the ground where composites absorb the most moisture. The average moisture content and the distribution of moisture over the laminate thickness developing during service life have specific implications to damage growth and residual strength. This wet condition can be generated and maintained by periodic fast moisture absorption at higher temperatures and humidities [4], for example 95 % relative humidity at 70 ° C see temperature profile "C" in Fig. 1 resembling the actual conditions in a tropic climate. Thereby, ground dwell periods may be shortened drastically by a factor of 400 [3] reducing total test time from 4.8 years to 8.5 weeks for simulation of 1000 flights. This is still to long and therefore reduction of the flight phases is necessary. Here fatigue loading at extreme temperatures, the time for the decay of thermal gradients across the specimen, the heating and cooling rates, the number of flights with changing extreme temperatures and moisture content have specific implications to damage growth and residual strength. Thus, moderate temperature changes can be neglected and more important, constant temperature periods need not to be longer than the time for the load cycles occurring. The FALSTAFF load spectrum applied constists of a repeating sequence of 200 flights of varying severity. Choosing a realistic frequency of 5 Hz [5] for the fatigue loading the most severe flight will last 56 seconds. With regard to decay of temperature gradients, the period where the extreme temperature is constant will last 2 minutes. Keeping the actual temperature change rates of 60 ° C/min, and assuming a mission mix [1] of 1/3 of flights with temperature profile "A" in Fig. 1 and 2/3 of flights with temperature profile "B" in Fig. 1 the test time for 1000 accelerated flights including ground dwell becomes ≈ 12 days. The derived test spectrum was assumed to meet the acceleration criterion. The test program using this spectrum is called "Quasi-Realtime" program. This program utilizes both the flight temperature profiles "A" and "B" as well as the ground dwell temperature profile "C" as noted in Fig. 1. Whereas the flight profiles occur corresponding to the mission mix, the ground moisture dwell periods (profile "C") occurs once every 100 flights in the accelerated test spectrum.

TECHNICAL LIBRARY
ABBOTTAEROSPACE.COM

As shown in Fig. 1 additional testing programs are intended to check-out further allowable simplifications reducing testing time by factors up to 6. The acceptance of these programs is jugded by comparison of their results with those of the "Quasi-Realtime" tests. The simplifications involve an increase of loading frequency to 15 Hz, omission of a complete temperature profile and of a temperature condition within a profile leading eventually to a shorter moisture recovery period as pointed out in Fig. 1. For example in the test program called "Fast" the loading frequency is increased to 15 Hz, the temperature profile "B" is omitted and because of that less time is required for moisture recovery.

In any of these testing programs the same loads occur always at the same temperature; if a temperature is omitted the affected loads will join the room temperature (25 $^{\circ}$ C) periods. The comparison of test results will then show, which of the environment cycles or environment conditions did not contribute to damage. Fig. 2 gives an example, how the loads of the FALSTAFF spectrum are programed to join the temperature cycle. The sequence of temperature and humidity shown, consist of flight temperature profile "A" followed by the ground dwell temperature profile "C". The sequence of loads represents the loading for one flight beginning and ending with the ground loads in tension and with the flight load cycles in compression between them. Specific rules were obeyed in joining the loading to the temperature/humidity cycling:

- Cyclic loading occurs after the appropriate steady state temperature has been achieved; thus temperature and load does not vary simultaneously. This will ease cumulative damage calculations.
- Ground loading is combined with the room temperature periods of the temperature profiles.
- Constant loads during flight loading, ground loading, and ground dwell periods are close to the mean loads of these periods.

So far in the test programs mentioned above simultaneous occurence of environment and load has been looked at. But also testing with flight-by-flight loading separated from flight-by-flight temperature/humidity cycling may lower the costs. Such testing is part of our investigation accomplished by extensive use of virgin and preloaded "traveller specimens". The outcome of these experiments will give some answers to the question whether or not the cyclic loading correlates with environment cycling in their effect on damage development.

In summary the experimental work of our research program can be grouped as follows:

- flight-by-flight loading at room temperature, baseline testing,
- accelerated flight-by-flight temperature/humidity cycling simultaneous with flight-by-flight loading ("Quasi Realtime" testing, baseline to simplified programs),
- simultaneous temperature/humidity and load cycling omitting flight temperature profiles and temperature conditions (simplified progroms),
- flight-by-flight loading seperated from flight-by-flight temperature/humidity cycling (applies to "Quasi-Realtime" and simplified programs) and
- flight-by-flight temperature/humidity cycling only.

TEST SET-UP

All the fatigue tests and the static and residual strength tests at high and low temperatures are conducted in eight load frames. In each load frame two specimens are loaded in parallel by one 20 kN-capacity hydraulic cylinder. Four load frames are blocked together. The test sections of the eight specimens of each block are sitting in a channel through which the preconditioned air is blown with about 10 m/s. Thus 16 specimens can simultaneously be subjected to temperature/moisture/loading. A general view of the test set-up is shown in Fig. 3. The two blocks of load frames are central in the picture. A walkway between the blocks gives ready access to specimens on both sides of the blocks. On the left side some of the specimen-temperature control and recording equipment can be seen. Behind this the tower of cold and hot chambers (designed by Weiss Technik GmbH) shows in which the air is preconditioned to selected temperature and humidity levels. The preconditioned air is circulated through the insulated ducts over the test sections of the specimens.

A close-up view of four blocked load frames is shown in Fig. 4. From the channel guiding the preconditioned air one-half is removed to exhibit the specimens, clamped between antibuckling guides. In the background part of the Schenck analog-load control equipment shows, seen completely on Fig. 5. On top of the central rack is the control equipment for the rate of temperature change. The visual display and typewriter terminals in front are used to put in the environment programs and test parameters, to start the test and to report specimen failure respectively. The twelve channels of the x-t recorders are used to continuously document the measured deformations and the corresponding load signals from eight load cells.

Loading Equipment

A 32 K words memory process computer was programed to read the flight-by-flight loading sequence as command signals into the system shown schematically on Fig. 6 (Load and Environment Programmer). The loads are controlled by Schenck analog load controller. Calibrated strain gages on the piston (load cell) in the hydraulic cylinder provide a feed back signal to the analog load controller to produce an error signal for correction.

One of the eight load frames is also shown schematically in Fig. 6. The load is carried over from the hydraulic cylinder

THIS DOCUMENT PROVIDED BY THE AGARD
TECHNICAL LIBRARY
ABBOTTAEROSPACE.COM

to a stiff beam linked on both ends to the lower fixtures of the specimen, and to the hydraulic brakes. The lower specimen fixtures are connected to a calibrated linear transducer by which the specimen deformations are measured. When the specimen deformations exceeds a present value, for example at specimen failure, a signal from the system controller activates the hydraulic brake linking that end of the beam where the specimen failed rigidly to the load frame. Simultaneously the specimen failure signal is given to the process computer causing the teletyp to report the failure data. Loading automatically continues to failure of the unbroken specimen; when this fails, a signal shuts off the pilot valve, depressurizing the hydraulic load system.

Heating and Moisturizing Equipment

The same process computer providing the load command signal was programed to supply the signals to the temperature/humidity control system shown schematically in Fig. 7. The signals change temperature and humidity by a preset rate at a defined load cycle within the load sequence of the flights, see Program Description. The timing of the temperature cycling andthe loads is realized by a special command.

Thermocouples in the specimen test chamber feed a Temperature Controller from where the process computer expects a signal to continue loading, when the temperature levels of the environment program are reached and a WAIT command was used to interrupt cycling loading during temperature changes. Cooled (- 80 ° C), heated (+ 130 ° C) and moisturized air (95 % r. h. at 70 ° C) are generated in two chambers. Temperature cycling of the chamber enclosed specimens is realized by changing the voltage of the heater and by opening and closing flaps in the ducts connected with the specimen chambers through which the preconditioned air is forced by blowers. The voltage change for the heater and the blower speeds are controlled to meet preset temperature change rates.

TEST RESULTS

Of the research program presented above we have so far carried out some baseline testing with plane specimens from a graphite/epoxy laminate with a $[\pm 45]_{5S}$ lay-up These experiments include static tests at various environmental conditions, FALSTAFF flight-by-flight, and residual strength testing at room temperature. The ± 45 ° -laminate was chosen to start with because the influence of temperature and humidity will show up very clearly as the affected matrix and interface is highly stressed throughout the total specimen cross section. Those of the environmental testing programs mentioned before which will not influence damage growth and residual strength of this laminate, may be excluded from the investigation of 0 ° / ± 45 ° laminates where the portion of highly stressed matrix and interface is less.

The program is behind schedule due to difficulties with the environment testing equipment which is still worked on.

Material Specimen and Testing Procedure

All specimens are made from the same prepreg system, consisting of 60 percent vol. of HT fiber T 300 from Toray and epoxy resin 914 C from Ciba. This material was selected, because preceding investigations have already provided a large amount of experimental fatigue data on plain, notched and jointed specimens fabricated from this material [37, 38]. Furthermore the RAE * , Structures Department, the DFVLR **, Braunschweig are using this prepreg system in their investigationsinto the effect of environment.

From the T 300 / 914 C Tape prepreg material the LBF manufactured, in an autoclave (curing temperature 170 ° C), uniform plates of the 18 layer angle ply composite ($[\pm 45]_{8S}$) from which specimens were cut immediatly after the curing process. As the cut was wet, the specimen were dried in an oven at 50 ° C for half an hour before they were numbered and weighed and then sealed in a plastic bag and stored in a freezer.

The specimen have a constant cross section and unreinforced gripped areas, Fig. 8. An anti-buckling guide prevents compressive buckling by supporting a 4 mm wide area, central to the longitudinal axis of the specimen, as shown in Fig. 8. This design does not influence the development of damage which starts at the free edges of the specimen and keeps the specimen surface accessible to the environment. The clamped-on anti-buckling guides allow a specimen deformation of 4 mm during compressive loading. This type of specimen and anti-buckling guide were applied in static and fatigue testing.

The linear transducers fixed to the lower-grips of the testing machine measure the longitudinal extension of the specimens as mentioned before. These devices were calibrated by simultaneous measurements with strain gauged extensometers installed on the specimen. Deformation was continuously recorded during monotonic and cycling loading; the loading rate were 50 N/s and 15 Hz, respectively. During static tests at + 110 ° C and - 50 ° C the temperature was controlled by a traveller specimen with embedded thermocouples showing that the specimen pick up the temperature within a few seconds. All specimens for residual strength testing were C-scanned before and after fatigue loading. The specimen were gripped between smooth jaws, clamped on by controlled torquing of the screws, to provide a gradual load transfer to the specimen.

* Royal Aircraft Establishment;

** Deutsche Forschungs- und Versuchsanstalt für Luft- und Raumfahrt

THIS DOCUMENT IS FROM THE
TECHNICAL LIBRARY
ABBOTTAEROSPACE.COM

Static Test Results

Experience in composite fatigue data analyses has shown that static test results were a needed part of this information. Static test data are assembled in Table 1. It summarizes test results of wet and dry specimens loaded at R.T., + 110 to 115 ° C and - 50 to - 55 ° C.

As fatigue loading with FALSTAFF flight-by-flight loaded sequence for wing upper surfaces causes damage growth and total failures to occur at compression, static testing was done in compression, too. Plastic shortening of the specimens to the limit of the test fixtures terminated the compression test. The average corresponding strain was three percent. Because no fracture but lateral bending occured at large strains, the stress measured at half the limit strain was chosen to represent compressive strength and stiffness. The rationale for this choice is the occurence of fatigue fracture when increasing deformation approaches 1.5 % strain, as demonstrated in the following chapter, and in ± 45 ° graphite/epoxy laminates, the same modes of failure occur in static compression an in compression-compression fatigue loading as elaborate scanning electron microscope observations by G. C. Grimes [39] have shown.

Fig. 9 shows the stress-strain behaviour at various environmental conditions. The influence of humidity is, for reasons of clarity, separately illustrated in Fig. 10. Generally all stress-strain curves have a non-linear pattern with a relatively small, not well defined linear portion at the origin. Therefore the compressive modulus E_c is determined from the secant line drawn between the origin and the load deformation point at 0.1 % strain [40].

A striking feature is the considerable influence of temperature and moisture that shows up. Wheras at + 115 ° C and in the wet condition (at + 115 ° C and room temperature) strength and stiffness has drastically reduced, at - 50 ° C the opposite is observed; stiffness and strength have become larger and moisture content seems to inerease stiffness even further. Fig. 10 shows that the detrimental influence of moisture content is largest at + 115 ° C and much smaller but still significant at room temperature.

Fatigue Test Results

From the static test results and results of fatigue test with the FALSTAFF load spectrum [1] a stress level was estimated which would result in fatigue lifes ranging from 10^4 to 2×10^4 flights. At the stress level, $\bar{S} = -137.5$ N/mm^2, specimens failed in the average at $L = 1.3 \times 10^4$ flights. Therefore this stress level was chosen to be used for further testing. Accordingly the specimens for the residual strength tests were preloaded on this stress level, too.

Lifes to failure and lifes to the end of test without failure are summarized in Table 2. Failure as well as non-failure data were utilized in the statistical analysis. For the high censored samples point estimates of the Weibull parameters α and β were determined by the maximum likelihood estimation. The mean life E (L) and the standard deviations listed also in Table 2 were calculated through analysis of log. life values. The listet test results are also plotted in an SN-diagramm, Fig. 11. The SN-curve is fitted to the mean values of log. fatigue life at the two stress levels. This is the SN-curve for 50 percent survival if log.-normal distribution is assumed to fit the data.

All specimens failed within the gauge length, as shown in Fig. 12. As mentioned in the description of the loading facility, the fatigue loading of specimen is stopped when it's deformation overshoots a preset value. For two specimens this happend before fracture occured. Both specimens showed local debonding and delamination at their edges and it is assumed that continued fatigue loading would lead to total failure within a negligible fraction of total life, as experienced many times before. As already mentioned the deformation produced during fatigue loading of specimens was registered continuously by linear transducers. From the recorded specimen deformation the values of the ratio $\varepsilon_a / \varepsilon_{ao}$ were determined, where ε_a is the strain range at any flight and $\varepsilon_{a,o}$ is the strain range at the first flights. By a procedure roughly outlined in Fig. 13 the corresponding ratio of compressive secant moduli $E_s / E_{s,o}$ at the largest compressive loads were calculated. In Fig. 14 this stiffness ratio is plotted against the percentage of number of flights relative to number of flights at failure. All data lie within a narrow scatterband demonstrating that stiffness decreases sharply towards the end of life. Just before fracture the remaining stiffness is 70 percent of the initial stiffness at the beginning of fatigue loading. At the stiffness ratio $E_s / E_{s,o} = .66$ a horizontal line is drawn to indicate the compressive strength criterion. It was assumed that the specimens actually failed when stiffness had dropped to 2/3 of the initial stiffness. With the maximum initial compressive strain $\varepsilon_{c,o} = -1.0$ % the corresponding strain at fracture is $\varepsilon_c = -1.5$ %.

Investigations of stiffness or deformation of composites behavior under fatigue loading have shown that the appearing stiffness decrease apparently corresponds to damage development. The residual strength was investigated after preloading to 6 400 and 9 600 flights. 6 400 flights where chosen because from this number of flights on the decrease of stiffness had become discernible. The 6 400 and 9 600 flights correspond to 50 and 75 percent of the mean life to fracture, respectively.

Residual Strength Test Results

The "compressive strength criterion" was also used to determine residual strength values from stress-strain curves of the preloaded specimens. Table 3 summarizes the results of residual strength test. Besides the data of specimens preloaded to 9 400 and 6 400 flights on the selected stress level $\bar{S} = -137.5$ N/mm^2, other residual strength data for various lifes and stress levels were listed. For the preload stress level $\bar{S} = -137.5$ N/mm^2 the residual strength values were plotted in Fig. 15 versus number of flights of the preloading. The corresponding lifes to fracture and the compressive static strength show also on this diagram. The static strength values were plotted on a vertical line at $N = 10^0$ and the lifes to fracture on a

THIS DOCUMENT PROVIDED BY THE ABBOTT AEROSPACE
TECHNICAL LIBRARY
ABBOTTAEROSPACE.COM

horizontal line at $S_c = \bar{S}$.

Curves of constant probability of survival are drawn combining the mean values, the 10 percent survival, and the 90 percent survival data calculated at constant lifes for the static and residual strength data and at constant stress for the life to fracture data. The residual strength for 10 and 90 percent survival and for the mean (E (S)) were computed using the equations in Fig. 15. The statistical analysis applies the two parameter Weibull distribution and considers the facts that specimens fail in fatigue when their residual strength is reduced to the fatigue stress level and that the residual strength data stem from surviving specimens. The same analysis method has been used by J. Awerbuch in [41].

The residual strength curves show that the strength of $\pm$ 45 ° -laminates decrease long before fatigue failure occures. In contrast to this behaviour the strength of unidirectional laminates loaded in the direction of fibers decreases rapidly immediatly before fatigue failure [41]. The shape of the curves resembles that of the stiffness decrease curves. C-scan records of the preloaded specimens shown in Fig. 16 reveal discernable delaminations. Specimens loaded monotonically to tensile fracture actually broke at locations where ultrasonic C-scanning exhibited this damage, see Fig. 17. In Fig. 18 and 19 the stress-strain curves and C-scan records of preloaded specimens show how the damage, identified by ultrasonic C-scanning, correlates with the degradation of strength and stiffness at static tensile and compressive loading, respectively. The influence of preloading is apparently the same in tension and compression. However, the shape of the stress-strain curve of the specimen without any delamination, as indicated by the corresponding C-scan record, suggests that another mode of failure preceds delamination. This has been observed by J. Grimes [39] with a scanning electron microscope in $\pm$ 45 ° graphite/epoxy laminates which had also been fatigue loaded in compression - compression. He concluded that the modes of failures which occured were debonding of fibers at ply interfaces followed by ply delamination and occasional fiber microbuckling. Thus debonding not detectable by the ultrasonic technic seems to be responsible for degradation when loading in compression has not yet caused delamination.

MOISTURE CONDITIONING

Moisture content as well as moisture distribution through the thickness of the specimen affects the hygrothermal state of stress in the composite laminate. Therefore it is desirable to not only keep the moisture content on a realistic level but also to have realistic moisture distribution during flight-by-flight loading. To be on the safe side it was assumed that the home-base of the aircrafts is located in very moist area; then the moisture content in the composite wing structure will level at one percent [8 , 9 , 18]. Except in room temperature base-line testing all specimens will have been preconditioned to at least 1 % moisture content. The distribution of moisture corresponding to real time exposure will be predicted using the computer program W8GAIN developed by G. S. Springer [4]. Therefore about 50 specimens have been placed in an environmental chamber to pick up moisture. Five groups of 10 specimens cut from 5 different plates were put in the chamber at different times. After different periods of steady state conditioning at + 65 ° C and $\approx$ 98 % r. h. the groups were taken out and each specimen of the group was weighed. There was only a negligible small scatter in the data of weight increase within the groups of specimens. The average weight increase of the ten specimens from one plate were plotted in Fig. 20 against the square root of exposure time. By fitting the weight increase function derived from Fick's law to the measured data, the diffusivity and maximum moisture content presented in Fig. 20 were established.

The moisture recovery times needed during flight-by-flight testing to keep the moisture content on the required level will be estimated by the program W8GAIN using these and additional data from the analysis of experimental moisture absorption presented in [42]. Whereas the moisture content of the specimens during environmental fatigue testing will be controlled by measurements on traveller coupons accompanying the test specimens, a computational method is applied to monitor the distribution of moisture.

LITERATURE SURVEY

In the literature on mechanical behaviour of graphite/epoxy composites only few information was found which is related to testing with flight-by-flight temperature / moisture changes applied simultaneously with flight-by-flight loading [6], [7], [8], [9], [10], [11]. Some fatigue and residual strength data from flight-by-flight load/environment fatigue testing are reported in [7], [8] and [11]. Besides providing design data, the investigations referred to in [11] are part of the AFML's "Advanced Composites Serviceability Program" using an accelerated test spectrum related to the temperature/moisture/loading history of the B-1 Vertical Stabilizer. No such testing is known which simulates the temperature/humidity/loading history of a wing upper surface structure. Table 4 summarizes briefly some of the research work on the influence of temperature and humidity (combined with cyclic loading) on residual and fatigue strength of graphite/epoxy laminates.

- The test results indicate only minor influences of environment when stressing is predominantly tension but larger influence when stressing is predominantly compression, shear or bearing.
- However, the vast amount of literature, reporting on effects of temperature and humidity on static and fatigue strength, show that at least temperature cycling, specifically in the low temperature range, [12], [13], [14], [15] as well as high temperatures during loading and moisture contents larger than 1,0 % degradate mechanical properties [16], [17], [18], [19].
- A general conclusion is, that degradation is largest for lay-ups and loadings with inherent high stressing of the matrix and/or the fibre matrix interface [12], [20], [21].

Physical approaches to understanding of these phenomenons have shown that they are related to:

TECHNICAL LIBRARY
ABBOTTAEROSPACE.COM

- residual stresses due to thermal anisotropy [13], [15], [22], [23], [24], [25],
- residual stresses due to swelling with moisture pick-up [23], [26], [27],
- decrease in glas-transition temperature with increasing moisture content [92], [343], [528], [670], and
- matrix crazing [18], [31].

CLOSING

With the wing upper surface load/environment history accelerated for experimental simulation, still missing design data will be established. Initial test results of this research program show that:

- stress-strain behaviour of $[\pm 45]_{8s}$ -graphite/epoxy laminate at compression is strongly influenced by temperature and moisture content;
- heating to + 110 ° C and / or moisture content of about 1.5 % weaken the composite laminate whereas at the freezing temperature of - 55 ° C the laminate had stiffened.

The results of room temperature fatigue and residual strength testing with the FALSTAFF flight-by-flight load sequence indicate that decrease of stiffness and strength correspond to damage growth as made apparent by ultrasonic scanning.

The most essential facts pertinent to the mechanical behaviour of composite material under temperature/humidity/loading conditions were extracted from the literature; they are:

- Generally, degradation is largest for lay-ups and loadings with inherent high stressing of the matrix and/or fibre-matrix interface.
- With cyclic loading predominantly in compression the influence of environment is larger than with cyclic loading predominantly in tension.
- Temperature cycling, specifically in the low temperature range, high temperatures during loading and moisture content above 1.0 % degradate mechanical properties of graphite/epoxy composites significantly.

ACKNOWLEDGMENTS

The research program on the "Fatigue strength of graphite/epoxy composite material" was sponsored by the German Ministry of Defence Research Branch RU Fo IV. The "Fatigue strength of graphite/epoxy composite material" working party was entrusted with planning and monitoring the program; the working party was brought into being by the German Defence Ministry and consists of members of Dornier, MBB, VFW-Fokker, DFVLR-Stuttgart, BWB-ML and LBF.

REFERENCES

[1] Schütz, D. and Gerharz, J.J.: Fatigue Strength of a Fibre-Reinforced Material, Composites, October 1977.

[2] Laboratorium für Betriebsfestigkeit, Darmstadt, Ed., March 1976: Description of a Fighter Aircraft Loading STAndard For Fatigue Evaluation - FALSTAFF - Flugzeugwerke Emmen (F+W), Switzerland, Laboratorium für Betriebsfestigkeit (LBF), Darmstadt, Germany, Nationaal Aerospace Laboratory (NLR), Amsterdam, Netherlands, Industrieanlagen-Betriebsgesellschaft mbH (IABG) Ottobrunn, Germany.

[3] Webb, J.N.: Environmental Fatigue Testing of Composite Structural Elements, RAE, Structures Department, 30. Nov. 1978.

[4] Springer, George, S.: Moisture Content of Composites Under Transient Conditions, J. Composite Materials, Vol. 11, Jan. 1977, p. 107.

[5] Cardrick, A.W. and Smith, M.A.: An Approach to the Development of Meaningful Design Rules for Fatigue-Loaded CFRP-Components, Composites, May 1974.

[6] Waggoner, G.; Erbacher, H.: Damage Tolerance Program for the B-1 Composite Stabilizer, AIAA Paper, No. 77-464, March 1977.

[7] Haskings, J.F.; Wilkins, D.J. and Stein, B.A.: Flight Simulation Testing Equipment for Composite Material Systems. In: Environmental Effects on Advanced Composite Materials, ASTM STP 602, 1976, pp. 23-36.

[8] Wilkins. D.J.; Wolff, R.V.; Shinozuka, M. and Cox, E.F.: Realism in Fatigue Testing: The Effect of Flight-by-Flight Thermal and Random Load Histories on Composite Bonded Joints. In: ASTM STP 569, 1975, pp. 307-322.

[9] Lundemo, Chr. Y. and Thor, S.E.: Influence of Environmental Cycling on the Mechanical Properties of Composite Materials. J. Composite Materials, Vol. 11, July 1977.

TECHNICAL LIBRARY
ABBOTTAEROSPACE.COM

[10] Konishi, D.Y. and Johnson, W.R.: Fatigue Effects on Delaminations and Strength Degradation in Graphite/Epoxy Laminates. NA-78-380, 1978.

[11] Altman, J.M.: Advanced Composites Serviceability Program Status Review. North American Aircraft Div. Rockwell Internation, Los Angeles, 1979.

[12] Hofer, K.E.; Larsen, D.; Humpreys, V.E.: Development of Engineering Data on the Mechanical and Physical Properties of Advanced Composite Materials. III Research Institute, AFML-TR-74-266, Febr. 1975.

[13] Mazzio, V.F. and Mehan, R.L.: Effects of Thermal Cycling on the Properties of Graphite-Epoxy Composites. In: Composite Materials: Testing and Design (Fourth Conference), ASTM STP 617, 1977, pp. 466-480.

[14] Camahort, J.L.; Rennhack, E.H. and Coons, W.C.: Effects of Thermal Cycling Environment on Graphite/Epoxy Composites. In: Environmental Effects on Advanced Composite Materials, ASTM STP 602, American Society for Testing and Materials, 1976, pp. 37-49.

[15] Daniel, I.M. et.al.: Lamination Residual Stresses in Fiber Composites. III Research Institute, Chicago, Illinois, March 1975, N 75-30264.

[16] Chi-Hung Shen and George S. Springer: Effect of Moisture and Temperature on the Strength of Composite Materials. J. Composite Materials, Vol. 11, Jan. 1977, p. 1.

[17] Chi-Hung Shen and Springer, G.S.: Environmental Effects on the Elastic Moduli of Composite Materials. J. Composite Materials, Vol. 11 (July 1977), p. 250.

[18] Hedrick, J.G. and Whiteside, J.B.: Effects of Environment on Advanced Composite Structures. AIAA Paper 77-463, AIAA Conference on Aircraft Composites: The Emerging Methodology for Structural Assurance, San Diego, Calif./ March 24-25, 1977.

[19] Weinberger, R.A.; Somoroff, A.R. and Riley, B.L.: US Navy Certification of Composite Wings for the F-18 and Advanced Harrier Aircraft. AIAA Paper, No. 77-466, March 1977.

[20] Kalble, D.H.; Dynes, P.J.; Crane, L.W. and Maus, L.: Kinetics of Environmental Degradation in Graphite-Epoxy Composites. In: ASTM STP 580, 1975, pp. 247-262.

[21] Judd, Nigel C.W.: The Effect of Wateron Carbon Fibre Composites. In: Reinforced Plastics-Milestone 30, Proceedings of the 13 th Anniversary Techn. and Management Conf., Section 18 A, 1975.

[22] Trabocco, R.E. and Stander, M.: Effect of Natural Weathering on the Mechanical Properties of Graphite/Epoxy Composite Materials. In: Environment Effects on Advanced Composite Materials, ASTM STP 602, American Society for Testing and Materials, 1976, pp. 67-84.

[23] Hahn, H.T.: Residual Stresses in Polymer Matrix Composite Laminates. J. Composite Materials, Vol. 10 (Oct. 1976), p. 266-278.

[24] Kaelble, D.H. and Dynes, P.J.: Nondestructive Test for Shear Strength Degradation of a Graphite-Epoxy Composite. In: Composite Materials: Testing and Design (Fourth Conference), ASTM STP 617, 1977, pp.190.

[25] Daniel, I M. and Liber, T.: Lamination Residual Strains and Stresses in Hybrid Laminates. In: Composite Materials: Testing and Design (Fourth Conference) ASTM STP 617, 1977, pp. 331-343.

[26] Halpin, John C.: An Assessment of Life Assurance Methodology for Advanced Composite Structures Unpublished Paper (AFFDL, Wright Patterson AFB, Ohio).

[27] Pipes, R.B.; Vinson, J.R. and Chou, T.W.: Ohn the Hydrothermal Response of Laminated Composite Systems J. Composite Materials, Vol. 10. April 1976, p. 129-148.

[28] Browning, C.E. and Hartness, J.T.: Effects of Moisture on Properties of High-Performance Structural Resins and Composites. In: ASTM STP 546, 1974, pp. 284-302.

[29] August, A.; Hadcock, R., and Dastin, S.: Composite Materials Design from a Materials and Design Perspective Grumman Aerospace Corporation, Bethpage, New York Presented at the AGARD Fall Meeting, 1975, Ankara,

[30] Roylancee, D. and Roylance, M.: Influence of Outdoor Weathering on Dynamic Mechanical Properties of Glas/Epoxy Laminate. In: Environmental Effects on Advanced Composite Materials, ASTM STP 602, 1976, pp. 85-94.

[31] Browning, C.E.; Husman, G.E. and Whitney, J.M.: Moisture Effects in Epoxy Matric Composites. In: Composite Materials: Testing and Design (Fourth Conference), ASTM STP 617, 1977, pp. 481-496.

[32] Sumsion, H.T. and Williams, D.P.: Effects of Environment on the Fatigue of Graphite-Epoxy Composites. In: ASTM STP 569, 1975, pp. 251-261.

[33] Hofer, K.E. Jr.; Bennett, L.C. and Stander, M.: Effect of Moisture and Fatigue on the Residual Mechanical Properties of S-Glas/Graphite/Epoxy Hybrid Composite. IIT Research Institute, Chicago Illin., Naval Air Systems Command, Washington D.C., 1976.

[34] Bevan, L.G. and Sturgeon, J.B.: Fatigue Limits in CFRP. International Conference on Carbon Fibres, their Place in Modern Technology, London, February 1974, The Plastics Institute, Paper No. 32.

[35] Bevan, L.G.: Axial and Short Beam Shear Fatigue Properties of CFRP Laminates. Composites, Vol. 8, Number 4, Oct. 1977, pp. 227-232.

TECHNICAL LIBRARY
ABBOTTAEROSPACE.COM

[36] Sendeckyi, G.P.; Stalnaker, H.D. and Kleismit, R.A.: Effect of Temperature on Fatigue Response of Surface Notched $/(0/\pm 45/o)_{S/3}$ Graphite-Epoxy Laminate. Paper presented at the ASTM-Symposium on Fatigue of Filamentary Composite Materials, Denver.

[37] Gerharz, J.J.; Rott, D. and Schütz, D.:Schwingfestigkeitsuntersuchungen an ungekerbten und gekerbten Faserverbundwerkstoffproben aus multidirektionalem Laminat. Forschungsbericht aus der Wehrtechnik BMVg-FBWT 79-25, 1979.

[38] Gerharz, J.J.; Rott, D. and Schütz, D.: Schwingfestigkeitsuntersuchungen an Fügungen in Faserbauweise. Forschungsbericht aus der Wehrtechnik, BMVg-FBWT 79-23, 1979.

[39] Grimes, G.C., and Adams, D.F.: Investigation of Compression Fatigue Properties of Advanced Composites Northrop Technical Report, NOR 79-17, Oct. 1979.

[40] ASTM Committee D-30: Standard Test Method for Compressive Properties of Oriented Fiber Composites. ASTM Designation: D 3410-75.

[41] Awerbuch, Jonathan and Hahn, H.T.: Fatigue and Proof-Testing of Unidirectional Graphite/Epoxy Composite In: Fatigue of Filamentary Composite Materials ASTM STP 636, K.L. Reifsnider and K.N. Lauraitis, Eds., 1977, pp. 248-266.

[42] Loos, Alfred, C. and Springer, George S.: Moisture Absorption of Graphite-Epoxy Composites Immersed in Liquids and Humid Air. J. Composite Material, Vol. 13, (April 1979), p. 131.

Table 1 - Results of Static Strength Test (Compression)

Material: T 300/914 C Graphite/Epoxy Tape Lay-up: $[\pm 45^\circ]_{8\,S}$
Specimen: unnotched

Specimen No.	Moisture content %	Temperature at Test °C	Compressive Modulus E_c N/mm²	Mean $E(E_c)^b$ N/mm²	Strength $S_{.015}{}^a$ N/mm²	Mean $E(S)^b$ N/mm²	Standard-deviation s_S	Parameter of Weibull - Distribution β N/mm²	$1/\alpha$
161	0	≈ 25 (R.T.)	23 390	22 544	168.0	164.3	7.02	167.5	0.0346
169	0	≈ 25	21 460		154.5				
183	0	≈ 25	22 850		172.7				
184	0	≈ 25	22 475		161.9				
186	0	≈ 25	18 426		157.4 241.0 [c]				
119	1.48	≈ 25	20 360	20 168	154.2	155.5	3.97	157.3	0.0205
118	1.48	≈ 25	22 468		160.8				
215	0.97	≈ 25	19 620		157.9				
189	1.62	≈ 25	18 576		152.9				
199	1.55	≈ 25	19 814		152.3				
114	0	+ 114	16 403	17 474	124.0	132.0	4.39	134.0	0.0268
188	0	+ 116	20 045		136.7				
137	0	+ 114	15 473		131.5				
164	0	+ 116	17 915		135.0				
127	0	- 51	22 662	22 910	201.8	200.2	2.83	201.4	0.0113
163	0	- 50	21 021		198.0				
193	0	- 51	25 512		203.5				
147	0	- 50	22 686		197.4				
165	1.49	+ 110	15 489	16 022	108.4	110.4			
191	1.58	+ 110	16 554		112.5				
130	1.30	- 50	23 283	24 410	204.2	212.1			
144	1.39	- 50	25 537		219.9				

[a] $S_{.015}$ - stress at 1.5 % strain
[b] $E(\ldots)$ - expected value of ...
[c] tensile strength

TECHNICAL LIBRARY
ABBOTTAEROSPACE.COM

TECHNICAL LIBRARY
ABBOTTAEROSPACE.COM

Table 2 - Results of Fatigue Tests with FALSTAFF Flight-by-Flight Loading at Room Temperature

Material: T 300/914 C Graphite/Epoxy Tape Lay-up: $[\pm 45^\circ]_{8S}$
Specimen: unnotched

Specimen No.	Stress Level, $\bar{S}$ [a] N/mm^2	No. of Flights, L	Fracture	Mean E (log L) [b]	Standard Deviation s	Parameter of Weibull-Distribution $\hat{\beta}_L$	Parameter of Weibull-Distribution $1/\hat{\alpha}_L$
115	- 130	18 350	yes				
141	- 130	18 350	no				
146	- 130	15 000	yes				
174	- 130	15 100	yes				
195	- 130	15 100	no	21 077	0.13	24 145	0.242
209	- 130	23 500	no				
216	- 130	23 500	no				
220	- 130	15 000	no				
124	- 137.5	12 600	no				
126	- 137.5	12 600	yes				
170	- 137.5	10 790	no				
171	- 137.5	10 790	yes				
198	- 137.5	15 060	no				
197	- 137.5	15 060	yes				
208	- 137.5	6 330	no				
149	- 137.5	6 330	yes				
212	- 137.5	10 000	no				
221	- 137.5	10 000	yes	12 864	0.10	14 340	0.191
116	- 137.5	9 400	no				
140	- 137.5	9 400	no				
187	- 137.5	9 400	no				
196	- 137.5	9 400	no				
173	- 137.5	6 400	no				
160	- 137.5	6 400	no				
159	- 137.5	6 400	no				
207	- 137.5	6 400	no				
117	- 137.5	6 400	no				
139	- 137.5	6 400	no				
194	- 137.5	6 400	no				
218	- 137.5	6 400	no				

[a] $\bar{S}$ - stress at peak load of FALSTAFF spectrum

[b] E (...) - expected value of ...

Table 3 - Results of Residual Strength Test at Room Temperature after FALSTAFF Loading

Material: T 300/914 C Graphite/Epoxy Tape Lay-up: $[\pm 45^{\circ}]_{8S}$
Specimen: unnotched

Specimen No.	Conditioning	Loading Stress S / Flights L N/mm² / No. Flights	Residual Strength S_R [a] N/mm²	Size of Damage	Mean $E(S_R)$ [b] N/mm²	Standard-Deviation s_S	Parameter of Weibull Distrib. β_S	$1/\alpha_S$
148	baseline testing (dry)	- 125 / 20 145	+ 135	large				
185		- 125 / 20 014	+ 153.3	small				
216		- 130 / 23 500	+ 139.2	large				
141		- 130 / 18 350	- 150.3	large				
195		- 130 / 15 100	- 151.2	large				
209		- 130 / 23 500	- 145.8	large				
208		- 137.5 / 6 330	+ 141.7	large				
212		- 137.5 / 10 000	+ 142.1	large				
124		- 137.5 / 12 600	- 139.2	large				
170		- 137.5 / 10 790	- 146.9	large				
198		- 137.5 / 15 060	- 156.2	small				
116		- 137.5 / 9 400	- 145.6	large				
140		- 137.5 / 9 400	- 153.2	small				
187		- 137.5 / 9 400	- 159.4	small	154.1	4.88	156.3	0.0256
196		- 137.5 / 9 400	- 157.3	small				
159		- 137.5 / 6 400	- 159.4	large				
160		- 137.5 / 6 400	- 162.5	small				
194		- 137.5 / 6 400	- 170.8	small	163.1	5.80	165.7	0.0287
218		- 137.5 / 6 400	- 160.8	small				

[a] S_R - stress at 1.5 % strain
[b] E (...) - expected value of ...

TECHNICAL LIBRARY ABBOTTAEROSPACE.COM

Table 4 - Brief Summary of Experimental Data on the Effects of Temperature, Humidity and Cyclic Loading on the Fatigue and Residual Strength of Graphite/Epoxy Composite Laminates

Reference	Material, Lay-up, Specimen	Environment	Loading	Application of Load- and Environment-Cycle	Goal of Investigation	Testing	Strength Degradation
[6] Waggoner, G., 1977	AS/3501 heavy section structural elements, hybrid subcomponent	temperature cycling wet	Horizontal stabilizer load-spectrum	simultaneously at constant temperature period	proof of structure	residual strength	small
[7] Haskins J.F., 1976	- A-S/3501 - $[0/\pm 45]_s$ - Coupon	temperature cycling	Flight-by-Flight, wing lower surface (tension)	simultaneously	design data	residual and Fatigue strength	
[9] Lundemo, Chr. Y., 1977	T 300/5208 $[\pm 45]_{S\,8}$ coupon	temperature cycling, wet (quasi realtime)	constant amplitude, R = + 0,1	fatigue loading after temperature cycling	design data	residual-fatigue strength	large
[10] Konishi, D.J. and Johnson, W.R., 1979	AS/3501-5 $[90/0/\pm 45]_{3\,S}$	temperature cycling, wet (accelerated spectrum)	vertical stabilizer load spectrum R = - 1,0 (blocked loads)	simultaneously at const. temperature periods	critical effect of defects	residual strength	
[11] Altmann John, M., 1979	A S/3501 5 A T 300 / 5208 $[(0/+45/90)_S]_2$ $[(0/\pm 45/0)_S]_2$ coupons, structural elements	temperature cycling, wet (quasi realtime)	vertical stabilizer load spectrum R = - 1,0 (blocked loads)	simultaneously at. const. temperature periods	critical effect of defects	residual strength	up to 40 % reduction in compression up to 25 % reduction in bearing yield load
[12] Hofer, K.E., 1975	T 300 / 5208 $[0/\pm 45/0/90]_S$; $[0]_6$ coupon	- steady state conditioning - thermo-humidity cycling - accelerated weathering	constant amplitude R = + 0,1	fatigue loading at elevated temp. after conditioning	design data	fatigue strength	small (up to 20 %)

TECHNICAL LIBRARY ABBOTTAEROSPACE.COM

Table 4 - (continued)

Reference	Material, Lay-up, Specimen	Environment	Loading	Application of Load- and Environment-Cycle	Goal of Investigation	Testing	Strength Degradation
[32] Sumsion, H.T., 1975	A S / 3501 $[\pm 45]_{S\ 12}$; $[0]_{24}$ coupon	constant temperature - water presoak	constant amplitude R = - 1 torsion/preloading) bending	simultaneously (torsion) fatigueing after presoak in R.T. water	damage mechanism	residual strength fatigue strength	large
[33] Hofer, K.E.Jr., 1976	T 300 / 5208 $[0/\pm 45/90]_{S}$; $[0]_{6}$ coupon	steady state humidity conditioning	constant amplitude R = + 0,1	fatigue loading after humidity conditioning	design data	residual strength fatigue strength	small
[34] Bevan, L.G., 1974	0° and 0,90 $^{\circ}$ coupon	steady state temperature conditioning at elevated and freezing temperature	constant amplitude R = - 1,0	fatigue loading at preconditioning temperatures	design data endurance limit	fatigue strength	small
[35] Bevan, L.G., 1977	130 S C/Code 69 $[+45_2/0_2]$ S; $[\pm 45_2/90_2]$ S coupon	steady state temperature conditioning	constant amplitude 1 > R = 0 and R > 1	fatigue loading at room temperature after conditioning	design data	fatigue strength	small
[36] Sendeckyi, G. P.,	T 300 / 5208 $[(0/\pm 45/0)_S]_3$ coupon (surface notch)	constant elevated temperature	flight-by-flight wing lower surface	fatigue loading at elevated temperature	damage mechanism	residual strength	increase in residual strength

TECHNICAL LIBRARY ABBOTTAEROSPACE.COM

This Document Provided by the TECHNICAL LIBRARY ABBOTTAEROSPACE.COM

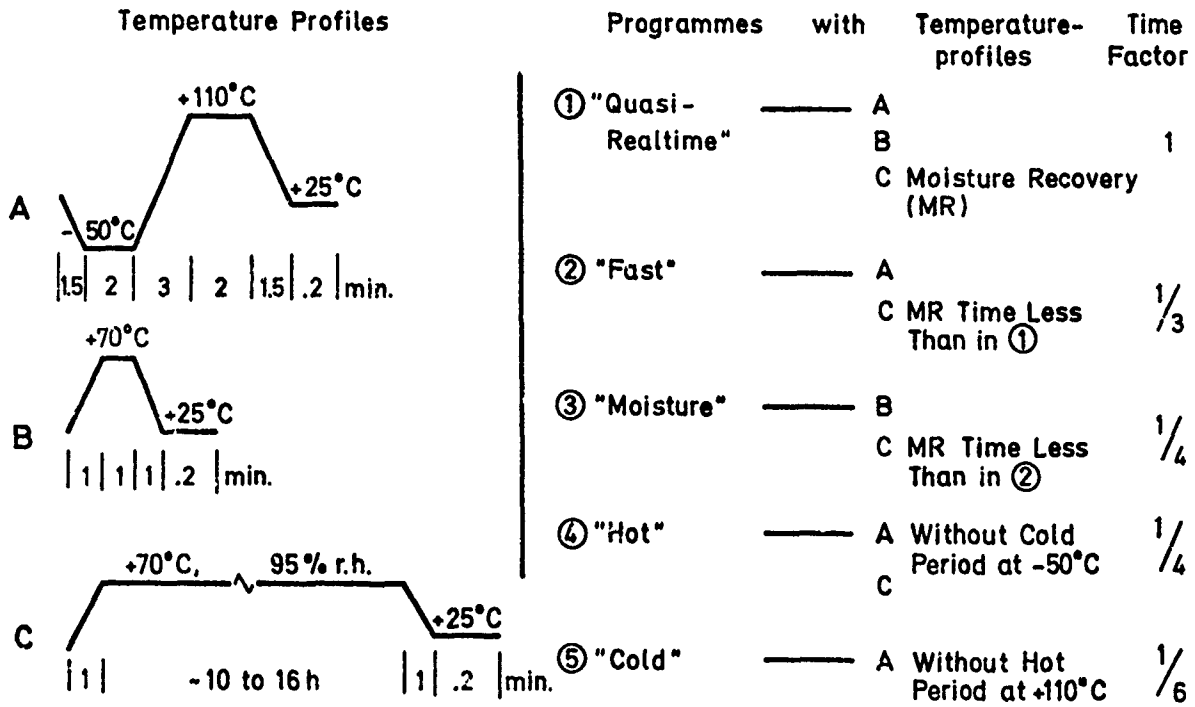

Fig. 1 - Programmes and Temperature Profiles

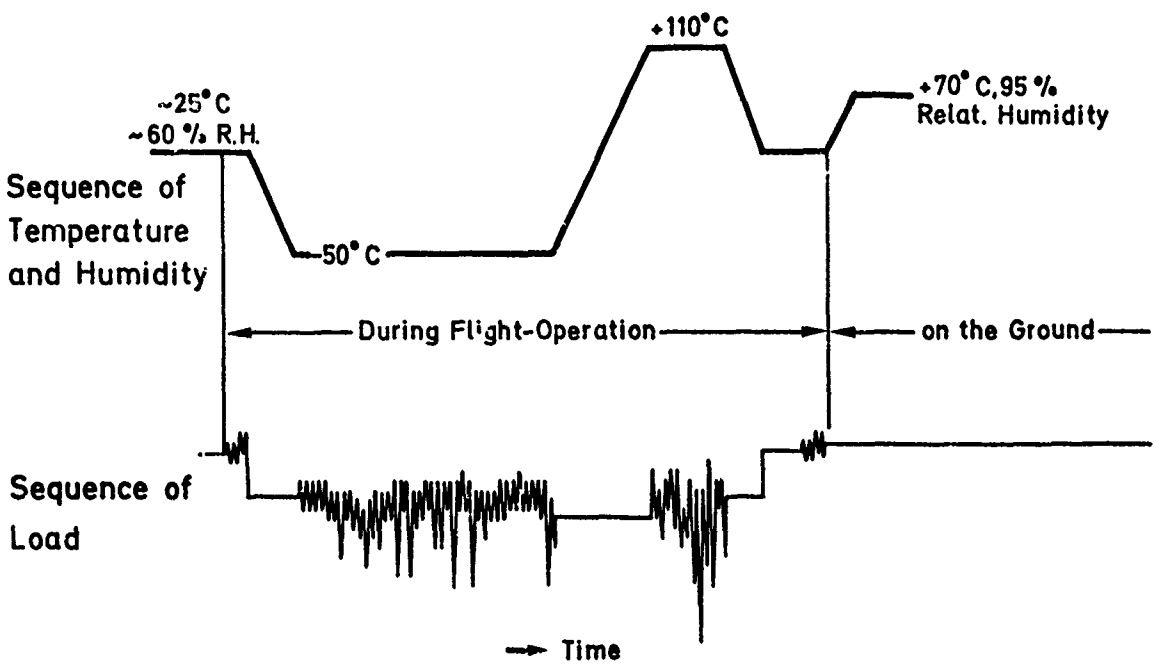

Fig. 2 - Typical Temperature/Humidity and Load Sequence Simulating Wing Upper-Surface Conditions

THIS DOCUMENT PROVIDED BY THE ABBOTT AEROSPACE
TECHNICAL LIBRARY
ABBOTTAEROSPACE.COM

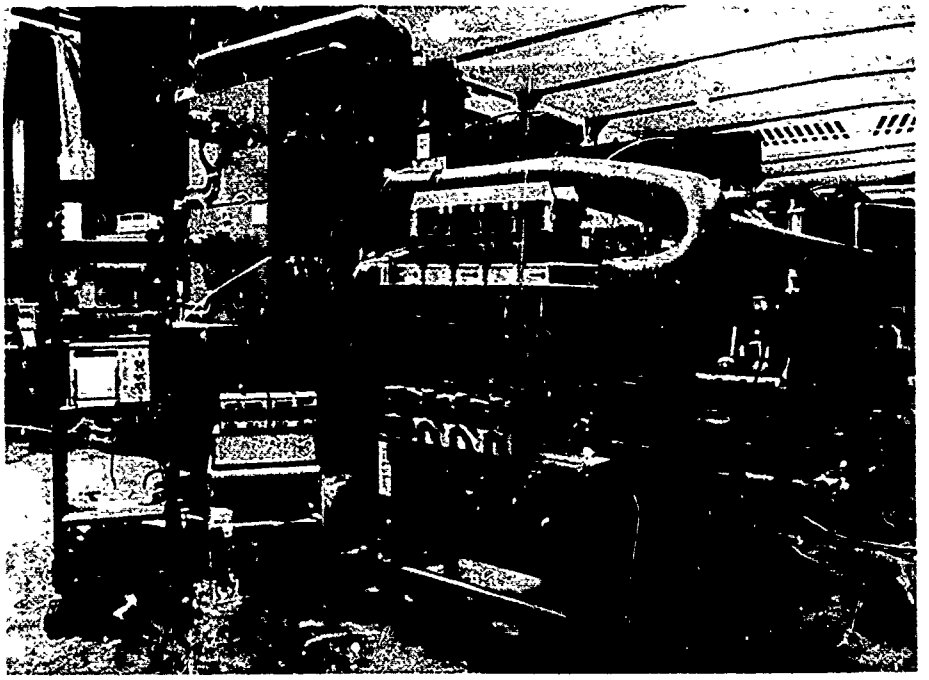

Fig. 3 - Environment and Load Simulation Equipment for Flight-by-Flight Testing

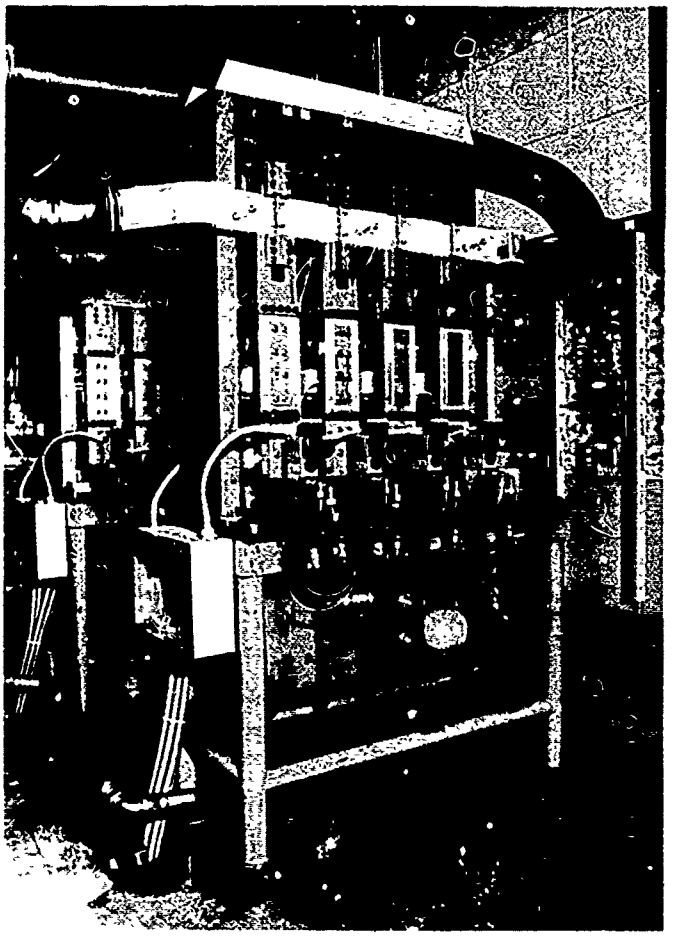

Fig. 4 - Servo-Hydraulic Loading Equipment for Eight Specimens (Two/Hydraulic Cylinder)

THIS DOCUMENT PROVIDED BY THE ABBOTT AEROSPACE
TECHNICAL LIBRARY
ABBOTTAEROSPACE.COM

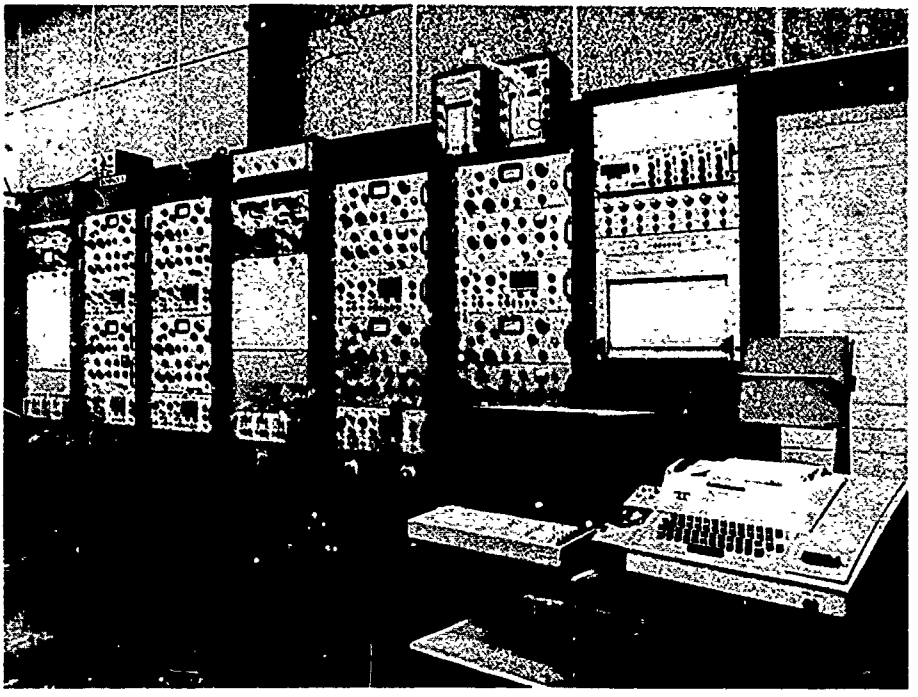

Fig. 5 - Control, Communication and Recording Equipment

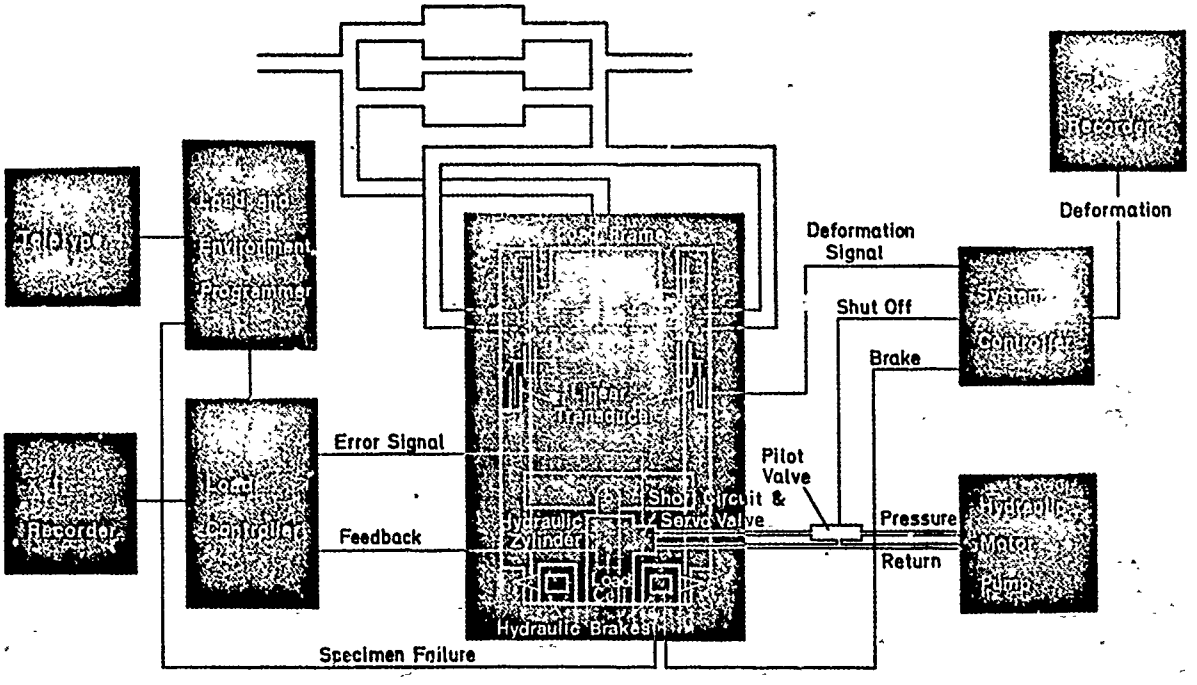

Fig. 6 - Flight-by-Flight Loading Control and Monitoring System

TECHNICAL LIBRARY
ABBOTTAEROSPACE.COM

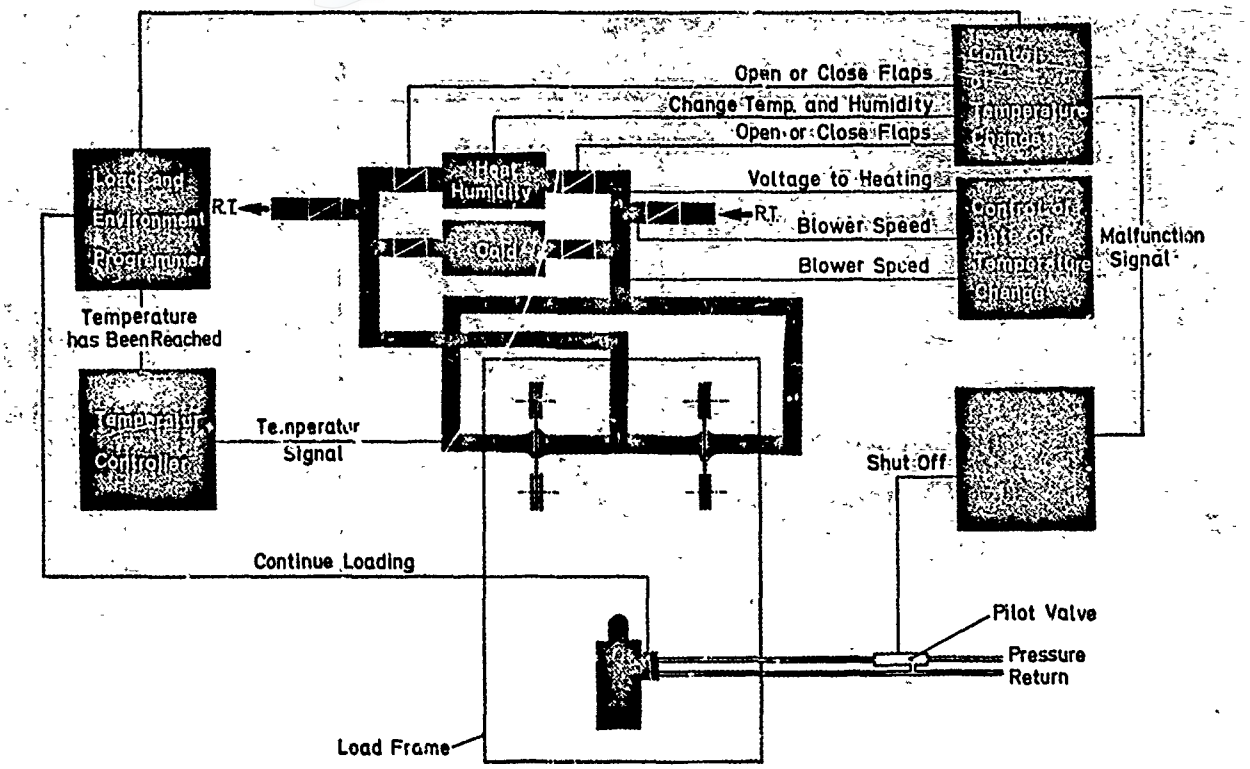

Fig. 7 - Temperature and Humidity Change Control and Monitoring System

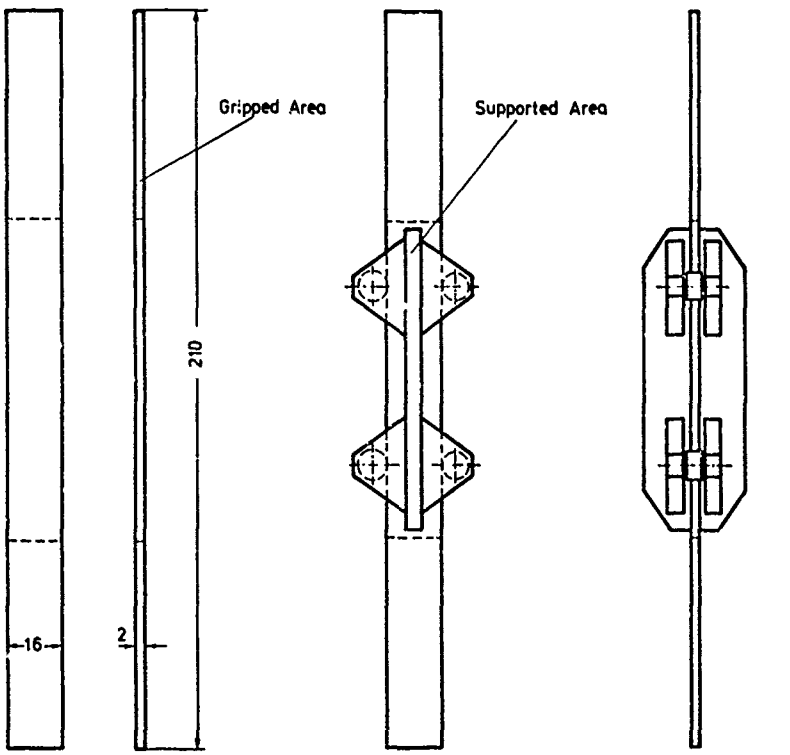

Specimen

Specimen with Anti-Buckling Guide

Material: T 300/914 C Graphite/Epoxy Tape, Lay up: $[\pm 45]_{8s}$

Fibre Content 60 % Vol.

Fig. 8 - Specimen and Anti-Buckling Guide

THIS DOCUMENT PROVIDED BY ABBOTT AEROSPACE
TECHNICAL LIBRARY
ABBOTTAEROSPACE.COM

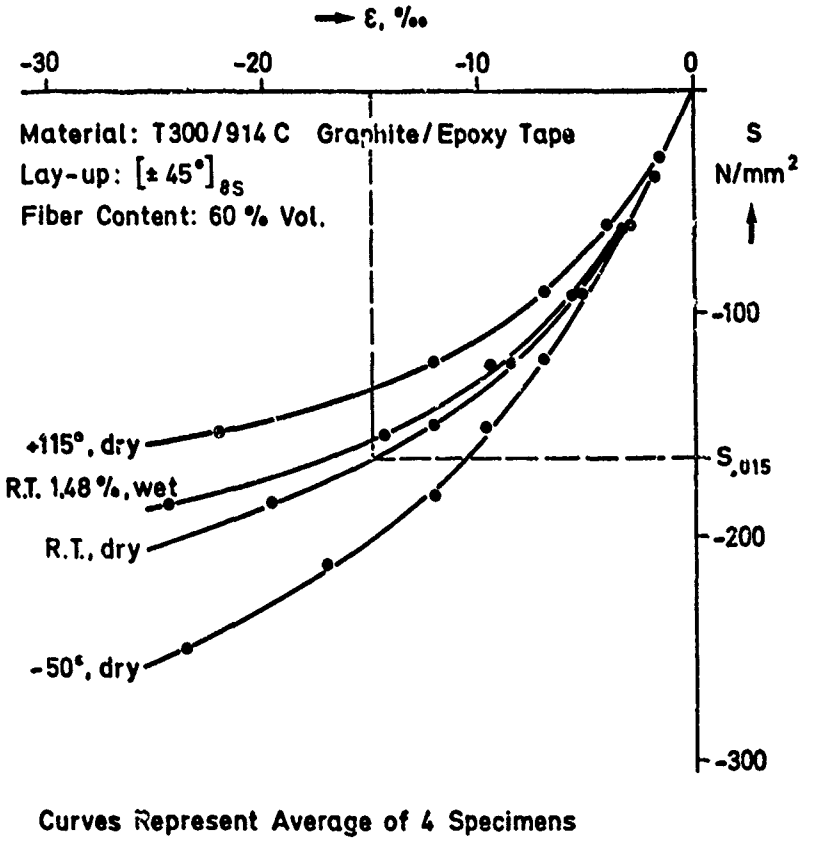

Curves Represent Average of 4 Specimens

Fig. 9 - Influence of Temperature and Humidity on the Stress-Strain Behaviour at Compression

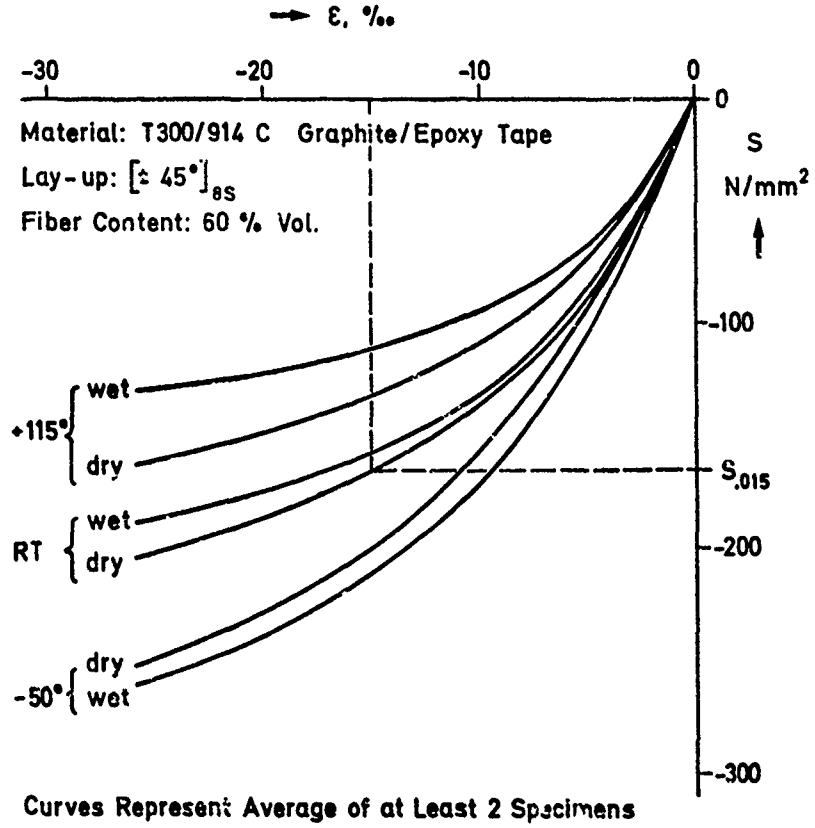

Curves Represent Average of at Least 2 Specimens

Fig. 10 - Influence of Humidity on the Stress-Strain Behaviour at Compression

This Document Provided by the ABBOTT AEROSPACE
TECHNICAL LIBRARY
ABBOTTAEROSPACE.COM

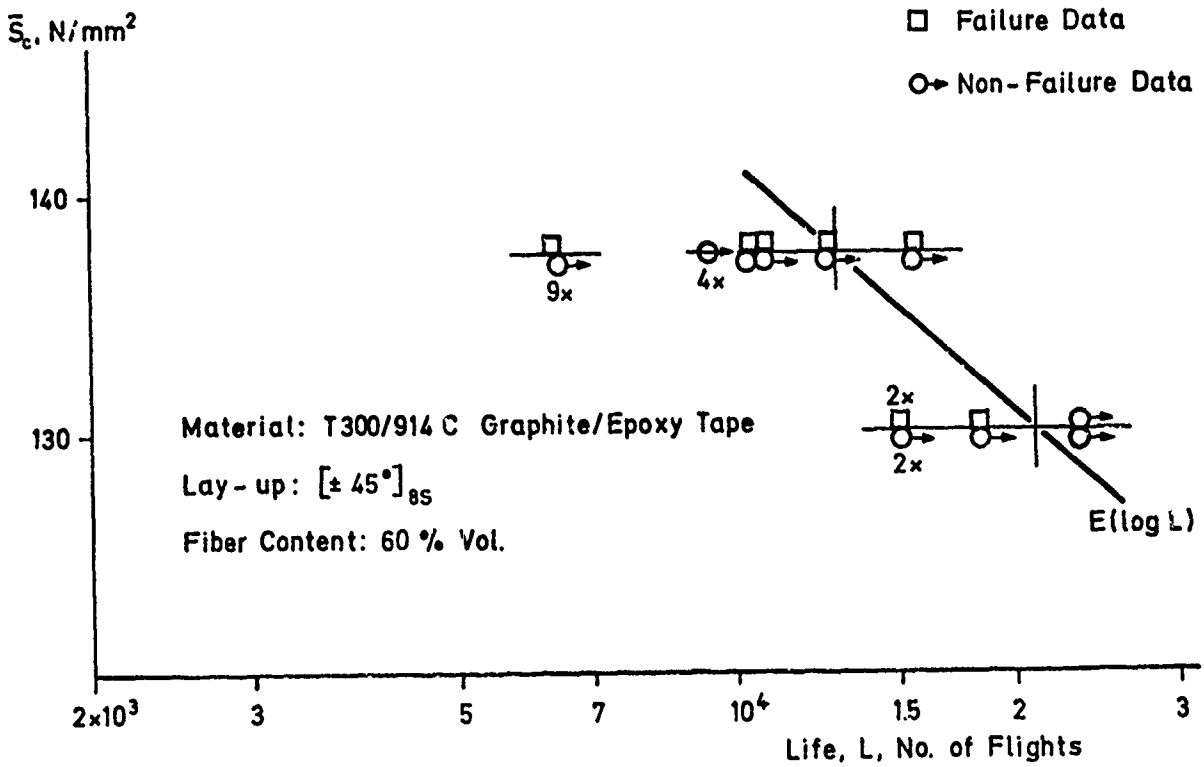

Fig. 11 - Fatigue Test Results with FALSTAFF Loading at Room Temperature

Fig. 12 - Specimens Failed in Fatigue

THIS DOCUMENT PROVIDED BY THE ABBOTT AEROSPACE
TECHNICAL LIBRARY
ABBOTTAEROSPACE.COM

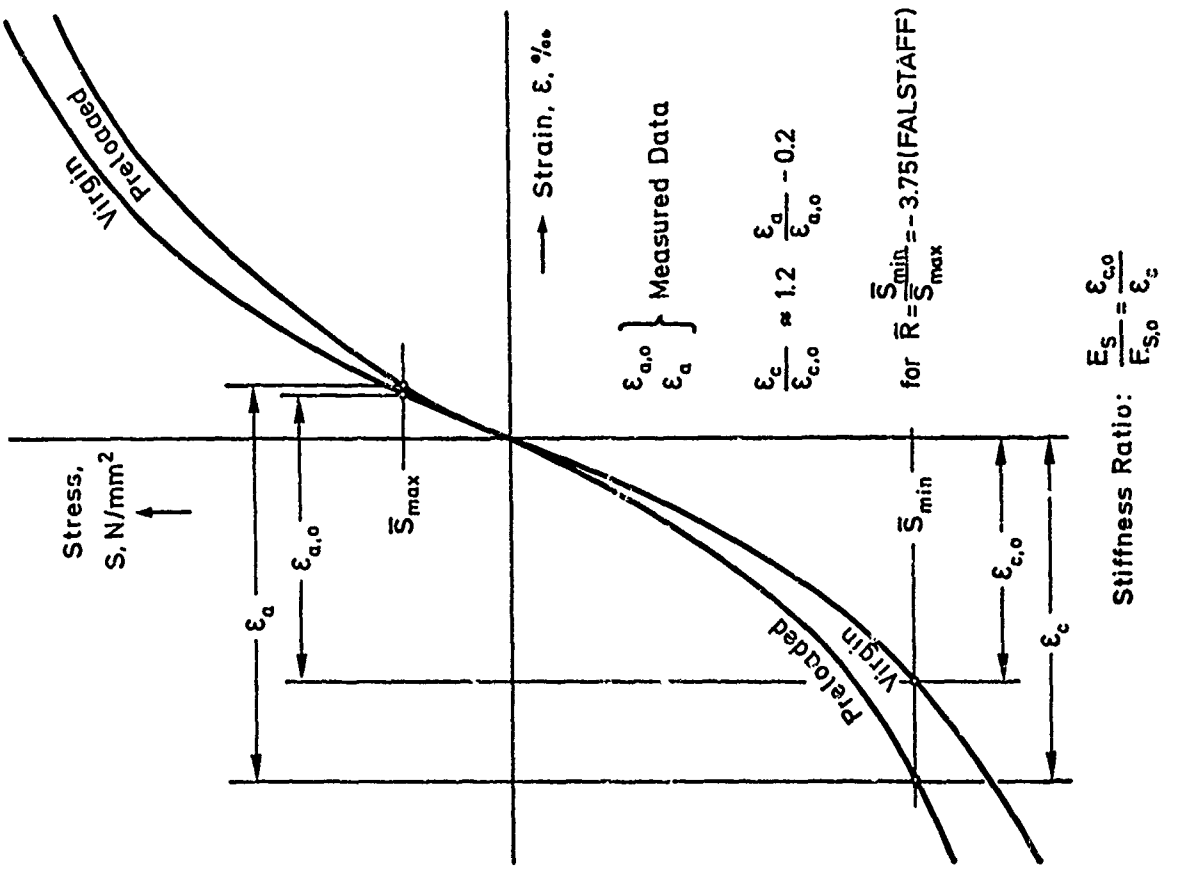

Fig. 13 - Determination of Stiffness Ratio from Measured Strain Data

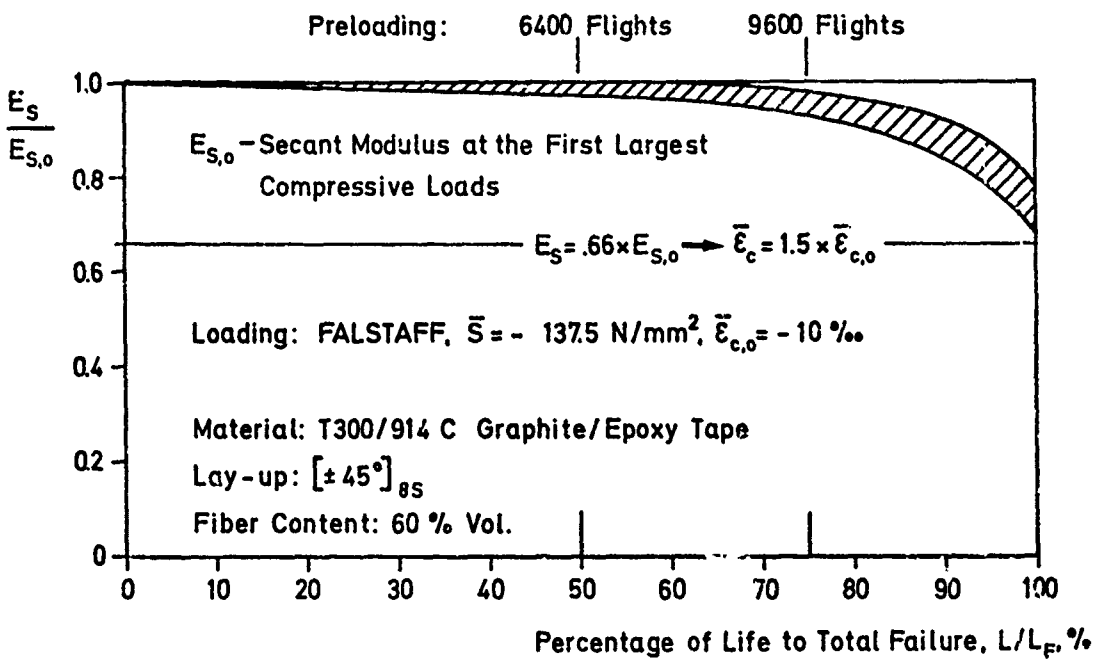

Fig. 14 - Decrease of Stiffness Due to Flight-by-Flight Loading at Room Temperature

THIS DOCUMENT PROVIDED BY THE ABBOTT AEROSPACE
TECHNICAL LIBRARY

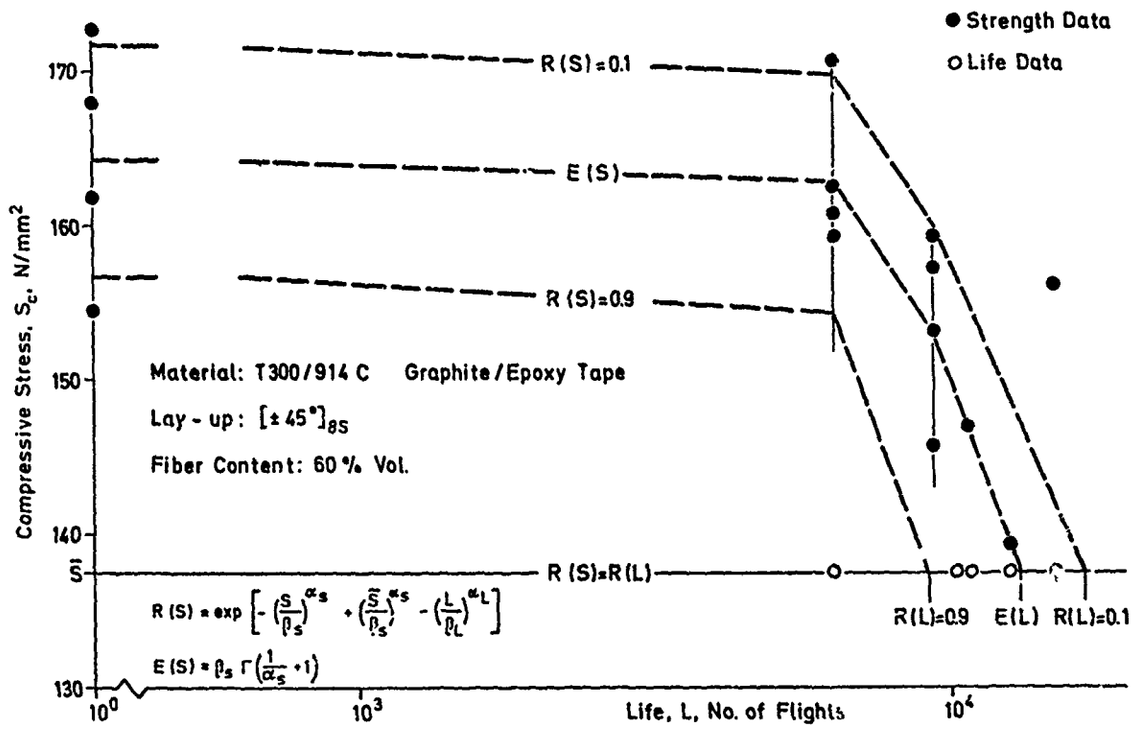

Fig. 15 - Residual Strength vs. Life at Room Temperature

TECHNICAL LIBRARY
ABBOTTAEROSPACE.COM

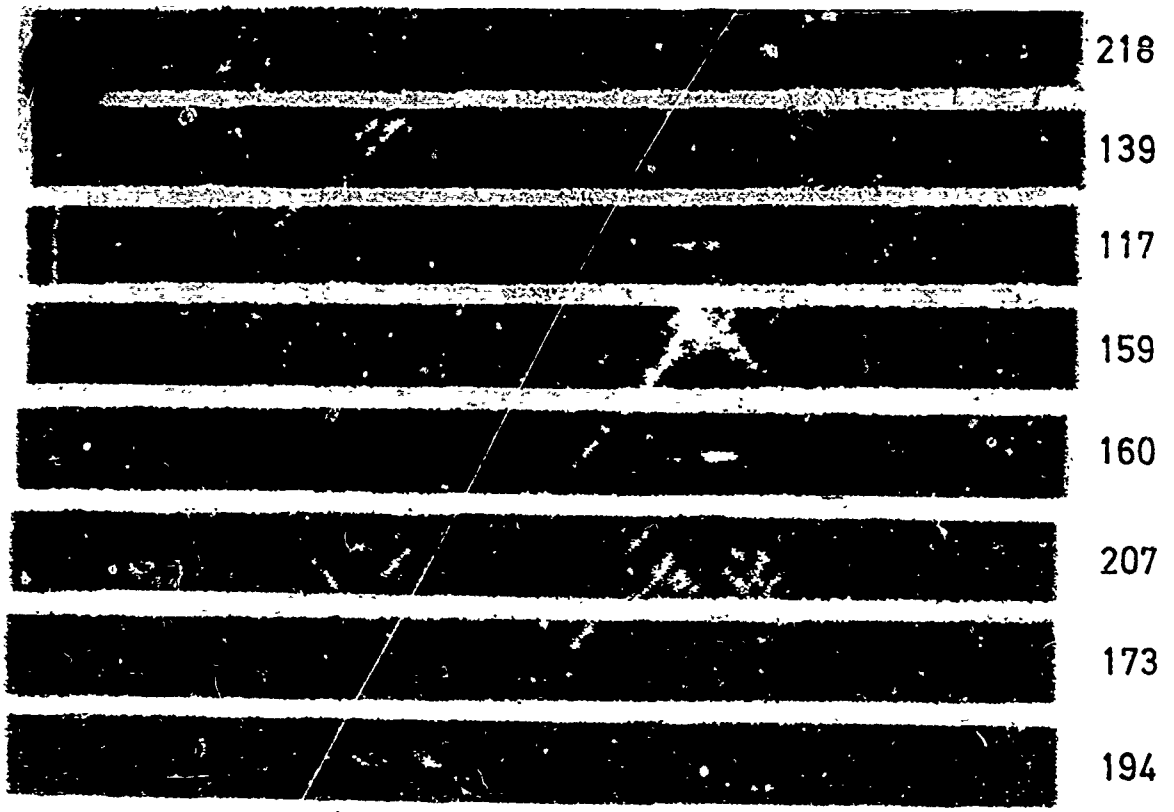

Loaded to 6400 Flights

Loaded to 9400 Flights

Fig. 16 - C-scan Records of Specimens

TECHNICAL LIBRARY
ABBOTTAEROSPACE.COM

Specimen No. 148

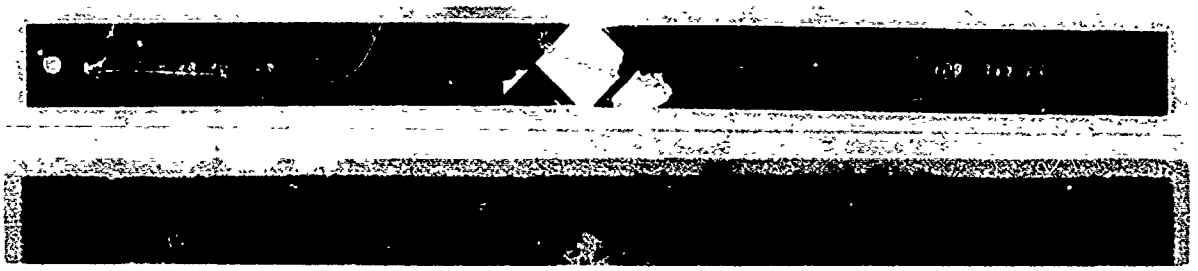

Specimen No. 208

Fig. 17 - Failure and Flaw Location

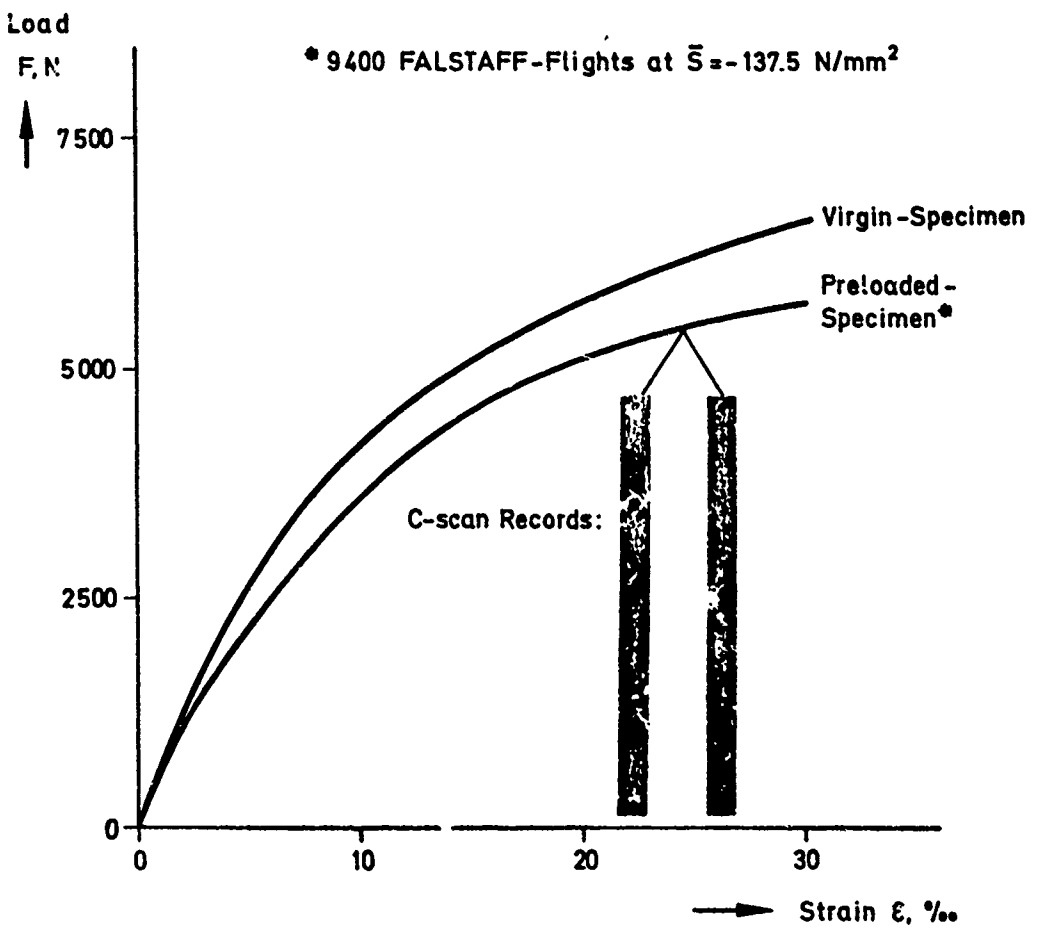

Fig. 18 - Influence of Preloading and Damage Size on Stress-Strain-Behaviour in Tension

THIS DOCUMENT PROVIDED BY THE ABBOTT AEROSPACE
TECHNICAL LIBRARY
ABBOTTAEROSPACE.COM

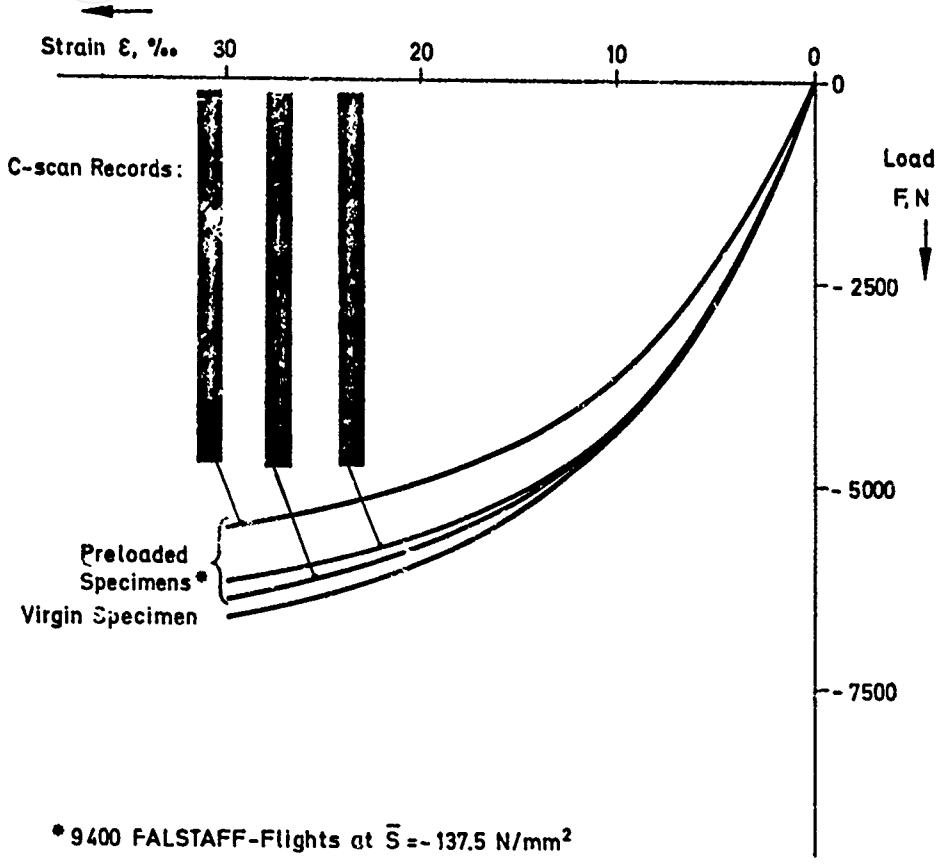

Fig. 19 - Influence of Preloading and Damage Size on Stress-Strain-Behaviour in Compression

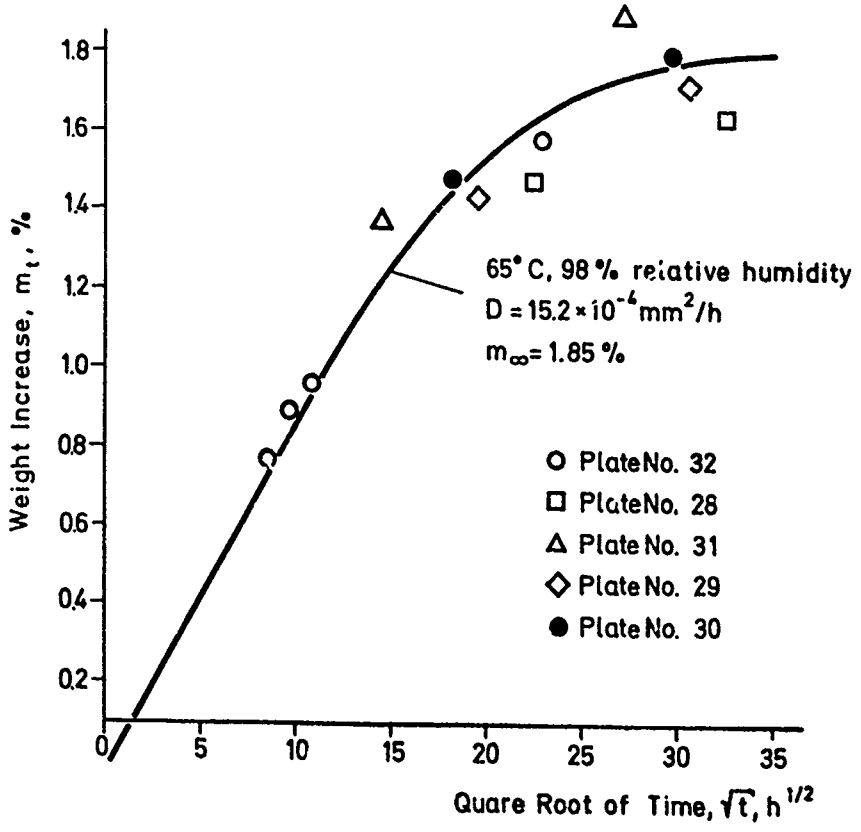

Fig. 20 - Moisture Absorption, Graphite/Epoxy $[\pm 45^\circ]_{8S}$ - Laminate T 300/914 C

TECHNICAL LIBRARY
ABBOTTAEROSPACE.COM

FATIGUE TEST RESULTS OF CARBON FIBRE REINFORCED PLASTIC F 28 AIRCRAFT COMPONENT AND ITS STRUCTURAL DETAILS.

ir. J.A.A.M. Dijns
Fokker VFW
P.O. Box 5952
2280 HZ Rijswijk
Netherlands

SUMMARY.

As a part of the development program on the structural application of carbon fibre reinforced plastic composites in aircraft structures, a speedbrake was designed and built in CFRP and aramide fibre composites for the Fokker F 28 Fellowship. The program was divided into three phases:
- The first phase consisted of a study of different configurations, from which one was selected for a detailed design in the form of a schematic model.
- In the second phase, tests were carried out on structural details and two schematic speedbrake models were fabricated for full scale static and dynamic load tests.
- The third phase contained the production of one speedbrake for flight testing on an operational aircraft.
The tests resulted in a design of the speedbrake in which no metal parts were used and in which all joints were bonded with 120° C and room temperature curing adhesives, without the use of additional fasteners.
The first model speedbrake was successfully tested to ultimate load without failure or any plastic deformation. The second model speedbrake was tested at a maximum fatigue load equal to 65% of the ultimate load.
The full-size CFRP-speedbrake showed a weight saving of 25% when compared with the Al-alloy design. Flight testing under operational conditions with the NLM started in November 1978.

The application of advanced composite materials is considered as an important contribution to the weight saving of future aircraft structures. A large number of investigations has been done to all kinds of parameters such as: material properties, fracture mechanics and durability. This has resulted in a considerable know-how of material behaviour. The developments in the last couple of years make it possible to design and build components with controlled properties and durability.
A number of projects were started at the Technological Centre of Fokker to design, test and manufacture a number of aircraft components with increasing difficulty. The first project concerned an advanced composite nosewheel door of the F 28 Fellowship and two sets of these doors are flying now over three years with more than 7000 flyinghours and 7500 starts and landings with complete satisfaction. The second project was the development of a composite speedbrake for the F 28 and will be reported in this paper. Simultaneously the development of space vehicle components, such as solarcel panels are designed successfully.
The speedbrake as shown in fig. 1 is located on the tail of the fuselage and is used mainly as speed regulator during the landing. This part was chosen for reason of the following characteristics:
- highly loaded hinge arms
- exposed to impact
- sonic fatigue loaded
- interchangeability
- non critical aircraft component

The aim of this project was to gain experience in design, production and flight service with a highly loaded component with the available technology. The following characteristics were known from the existing metal speedbrake design: aerodynamic performance, strength and stiffness requirements, contours and tolerances, configurations of the junctions, quantity of impact damage. The existing Al-alloy speedbrake is based on a multi rib construction with two forged hinge arms and Al-alloy skin sheets.
The project was divided into three phases:
phase 1: Study of different types of structures and selection of the configuration for further design.
phase 2: Design of a schematic model of the speedbrake. Evaluation and tests of structural details. Fabrication of two schematic speedbrakes for static and dynamic load tests.
phase 3: Production of one speedbrake for flight testing on an operational aircraft.

The design chosen after phase 1 is shown in fig. 2. The structure is built up from the following main parts: two hinge arms, constructed as rectangular CFRP beams running from the hinge points to the aft end-rib, two honeycomb sandwich skin panels, two end-ribs, leading edge, trailing edge.
The selection was made with the following criteria: minimum weight, producibility, impact resistance, sonic fatigue resistance, small number of parts. The main materials as used for the speedbrake are listed in tabel I.
The ribs leading and trailing edge consists of solid laminates of aramide fibre composites. The choice was based on low stresses in these parts and the occurence of impact.
The outside skin panel of the speedbrake is mainly loaded with a bending moment and tensile forces, and is exposed to impact. A serie of tests was done on the impact resistance of aramide fibre sandwich honeycomb panels in reference with the impact data of the Al-alloy speedbrake. This resulted in the optimum configuration with a two layer aramide fabric outer face; 7,5 mm Nomex honeycomb core and a 3 layer CFRP innerface. This combination exposed to equivalent impact loading will result in a locally damaged outer skin and honeycomb core and an undestored inner skin. The inside skin panel is loaded in bending and in compression. It is built up from two CFRP skins of 3 layers with a 5 mm Nomex honeycomb core. The Nomex honeycomb was chosen for both skins to avoid corrosion. The edges of both skin panels were partly filled with syntactic foam and partly reinforced with solid aramide fibre laminates.
The hinge arms are constructed as beams, built up out of two U-shaped sections. The laminates consists of 8 to 10 layers U.D. tape with fibre orientations (90°; 0°, $\pm 45^\circ$, 0°)s. The two profiles are connected on the inside with two 4 layers ($\pm 45^\circ$) CFRP laminates bonded with a 120°C curing epoxy adhesive. This design of the hinge arms was mainly chosen to achieve an uniform thickness of the laminates with the available processes at that moment. All profiles were built up and cured on positive moulds with the additional use of pressure plates on all flanges. A disadvantage of this method is that all tolerances appear on the outside.
The load pattern on the hinge arms in the ultimate load condition is shown in fig. 3.

TECHNICAL LIBRARY
ABBOTTAEROSPACE.COM

The hinge points were extensively tested with different designs in a static and dynamic test program with lug type test specimens (fig. 4). The ultimate load for one lug of the speedbrake arms is 24500N. The maximum dynamic load for one lug is 16340 N for 5.10^5 cycles. The first design consisted of the 8 layer basic arm laminate, reinforced on the ends with Ti.6AL.4V doublers bonded to the laminate with a 120°C curing adhesive (fig. 4a). Ti-alloy doublers were chosen to avoid corrosion which likely will occure when Al-alloy is used in combination with CFRP due to electro chemical contact. Also the smaller coefficient of thermal expansion makes the use of Ti more attractive than Al-alloys when high temperature curing adhesive are used. The static strength and stiffness were very near the calculated values and fracture occurred in the middle of the CFRP laminate. The strength P=70550N is nearly three times the required ultimate load. The dynamic load program was carried out with constant amplitude at a frequency of 10 Hz.
The applied load range was: 2950 N - 35300 N (20% - 200% daily load), 2950 N - 26450 N (20% - 160% daily load), 2950 N - 17650 N (20% - 110% daily load). At all load levels delamination occurred in the adhesive layers starting at the ends of the Ti doublers and fatigue cracks started in the Ti doublers aside of the holes. In most cases the final fracture of the test specimens was caused by the fatigue cracks in the Ti doublers and the accompaning delaminations aside of the hole. The test specimens loaded on the lowest load level withstood more than 2.10^6 cycles without fracture and fatigue crack and delamination propagation was very low. However the results were disappointing compared to the static test results.
In order to improve the stiffness transition at the ends of the doublers and to reduce the peak shear stresses a serie of test specimens with tapered Ti.6AL.4V doublers were manufactured and tested with the same load pattern. The thickness of the Ti doublers was increased with 15% and the tapering was machined with standard milling equipment. (fig. 4b). The results of the tests showed an improved resistance at all load levels. Especially the initiations of the delaminations were delayed and the propagation was much lower. Fatigue cracks in the Ti doublers aside of the hole again caused the final breakdown of the test specimens. The test specimens at the lowest load level were not damaged in any way after 10^6 cycles at which the tests were stopped. All test specimens were regularly inspected with the Fokker bondtester.
In comparison with the Ti reinforced lugs a test specimen was designed with CFRP doublers as shown in fig. 4c. The doublers were also laminated of U.D. tape with a fibre orientation calculated for minimum stiffness increase in the tapered part. The tapered ends were machined with diamond tipped tools. The test specimens were static and dynamic tested with the same load pattern as the previous lugs. The test results were more or less equivalent with the results of the specimens with tapered Ti doublers. Damage of the test specimens occurred both static and dynamic through delamination of the layers of the tabs near the bond layer, starting from the machined edges. At the lowest load level no damage was detected after 10^6 cycles.
Although it is likely that improvements can be made with other configurations of the CFRP tabs such as, laminated tapers, other fibre orientations or laplengths, this design was adopted for the hinge points of the speedbrake. The main advantages of this design are: low weight, lack of thermal stresses and elamination of corrosion problems. Also it was a challenge to test such a configuration in service.

After the evaluation of the results of the lug type specimens it was decided to design two different configurations for the actuator attachment point. One with Ti side plates (type I) and one with CFRP side plates. (type II). The test specimens are shown in fig. 5. The configuration chosen for the tests makes it possible to test two actuating points at the same time and is also a try-out for the production process. The configuration with Ti plates differ in the way, that no U section was used between the Ti plates, in which the forces were introduced. All other joints were bonded with a 120° C curing adhesive without the assistance of mechanical fasteners. Both the Ti-6Al-4V and CFRP plates were tapered along the edges to achieve a uniform shear stress in the bondlayers.
One test specimen of each type was loaded until fracture which occurred for the type I specimen at 81910 N and was caused by shear failure in the bond layer and in the outer layer of the CFRP beam laminate. The type II test specimen failed at 84860 N due to shear in the layers of the CFRP plates near the adhesive layer. The requested ultimate load for the speedbrake actuator point is 39600 N which is far below the tested strength. The dynamic load for the speedbrake is equal to limit load (26400 N). The type I test specimen was loaded between 490-29430 N with a frequency of 2 Hz. After 3.10^5 cycles some small delaminations were found in the bond layer between the tapered edges of the Ti-plates and the CFRP beam. During the rest of the test no crack propagation was found. The test specimens were regularly inspected with different non destructive inspection techniques, such as: the Fokker Bondtester, Ultrasonic inspection, X-ray and one time with neutrography. After 5.10^5 cycles a change of response with the bondtester was found in the middle of the bonded area of the Ti plates. This area grew very slowly during the test and is expected to be a degradation of the adhesive layer or the CFRP laminate due to small delaminations. The dynamic load test was stopped after $2.5.10^6$ cycles and a residual strength test was carried out. This resulted in fracture at 70630 N about 15% lower than the initial static strength.
The type II test specimens with CFRP plates were cycled on the same load levels as the type I specimens. After 5.10^5 cycles no damage was found. Therefore it was decided to increase the load level to 490-39240 N. At 10^6 cycles some small delaminations were found in the bond layer between the CFRP plates and the beam near the lug. The different indication with the Fokker bondtester in the middle of the bonded area occurred similar to the type I specimen. The test was continued with a further increased load level of 490-49000 N. This resulted in a fast propagation of the delaminations and no measurable enlargment of the questionable area. After $1.05.10^6$ cycles the test was stopped just before total fracture.
Although both configurations were effective for the speedbrake the design with CFRP plates was chosen for the actuating points for the same reason as the hinge points. (fig. 6).
The main assembly of the speedbrake structure is bonded with a roomtemperature curing adhesive without the use of additional fasteners. The critical joint between the arms and the skin panel is loaded in flatwise tensile. A test program was carried out with different adhesives and configurations to prove the durability of this joint. The test results indicated a sufficient strength of the arm to skin joint for the speedbrake design.

After completing the details tests, two schematic models of the speedbrake were built. (fig. 7). From the point of view of strength, dimensions and production this model is equal to the real speedbrake. The main problem during the assembly was to achieve an uniform thickness of the bond layers between the arms and the skin panels. The mismatches results from the use of positive laminating moulds for the beams and negative moulds for the skins. The models were mounted in a test rig representing the fixation to the aircraft and the aerodynamic forces on the outside skin. The first model was loaded until fracture and broke down at 1.75 times ultimate load. Fracture was initiated through bending of the arms. The second model was dynamic loaded between 1,5% - 65% ultimate load at a frequency of 0,5 Hz. The test was stopped after 10^6 cycles without any significant damage. A very small delamination was found in the adhesive between the arms

TECHNICAL LIBRARY
ABBOTTAEROSPACE.COM

and the outer skins near the front rib. The design of the speedbrake is adapted by the extension of the outer skin panel with two tapered lips in order to decrease the high shear stresses in the adhesive layers. The good results of the tests on the model speedbrakes made it possible to copy the design with only small improvements for the operational speedbrake. Most of the difficulties when building this part, originated in the complicated three dimensional curves and in the control of the processes and tolerances.

In October 1978 the third phase was finished with the installation of a composite speedbrake to the Fokker F 28 Fellowship of the NLM. It is flying now over a year to the complete satisfaction of the operator, with 1500 flying hours and 2000 starts and landings. Apart from the normal schedule the speedbrake is checked regularly following a special inspection scheme on the aircraft and in our inspection laboratory. No damage due to normal service has been found until now after 1500 flying hours. The weight saving for this part was about 25% compared with the Al-alloy speedbrake.

CFRP : F & H CARBOFORM CODE 92; UNDIRECTIONAL PREPREG TAPE 120°C CURING EPOXY;
AFRP : NARMCO 550; 181 SATIN HARNESS; 120°C CURING EPOXY
ADHESIVES : BSL FM 123-5; 120°C CURING EPOXY 3M EC 2216A/B; ROOM TEMPERATURE CURING EPOXY
HONEYCOMB : NOMEX

TECHNICAL LIBRARY
ABBOTTAEROSPACE.COM

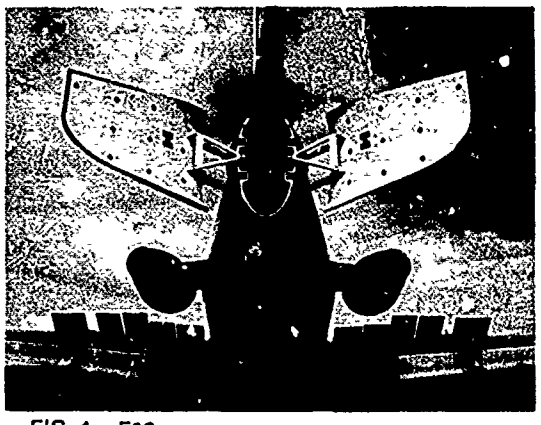

FIG. 1 F28

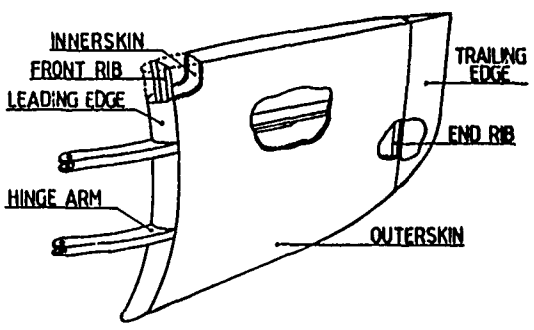

FIG 2: F28 SPEEDBRAKE

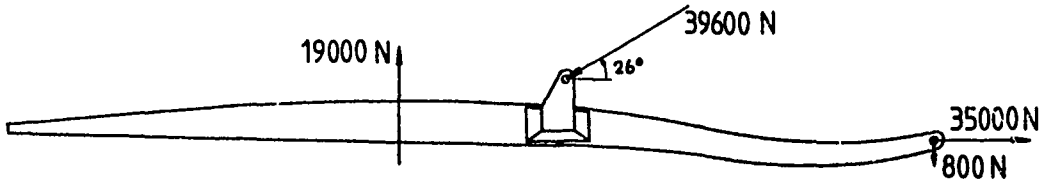

FIG 3 ULTIMATE LOADCASE SPEEDBRAKE HINGE ARM

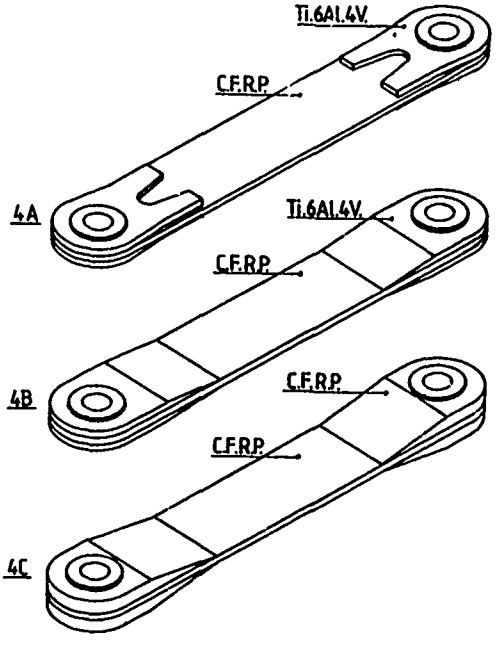

FIG. 4 LUG TYPE TEST SPECIMENS

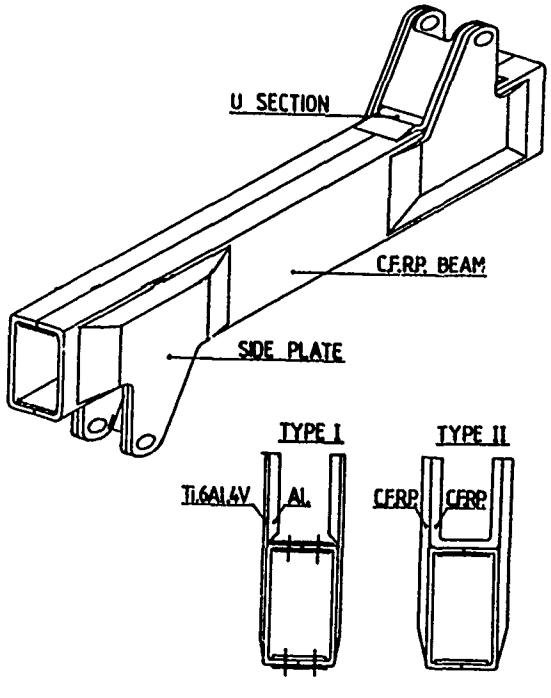

FIG. 5 TEST SPECIMENS ACTUATOR ATTACHMENT POINTS

THIS DOCUMENT PROVIDED BY THE ABBOTT AEROSPACE
TECHNICAL LIBRARY
ABBOTTAEROSPACE.COM

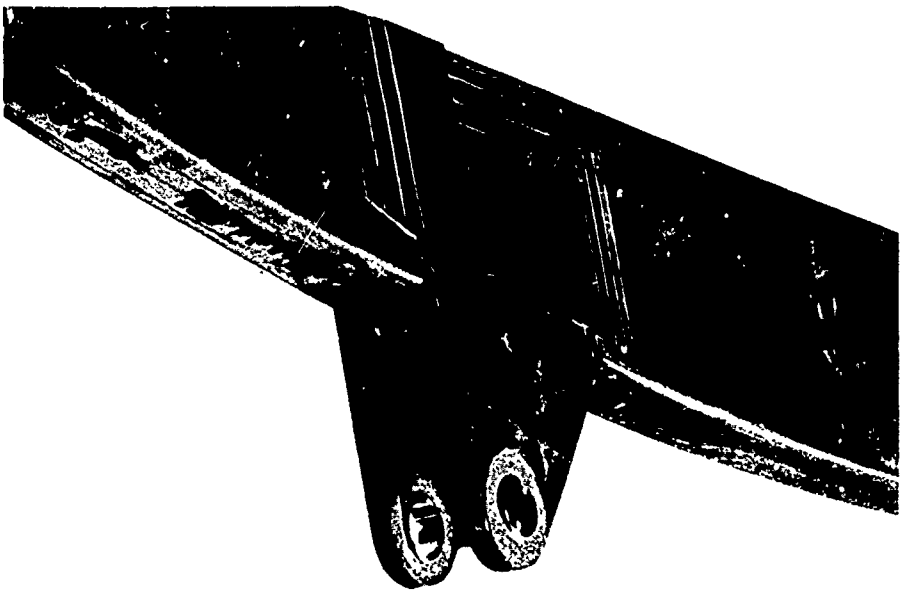

FIG.6 ACTUATOR ATTACHMENT POINT

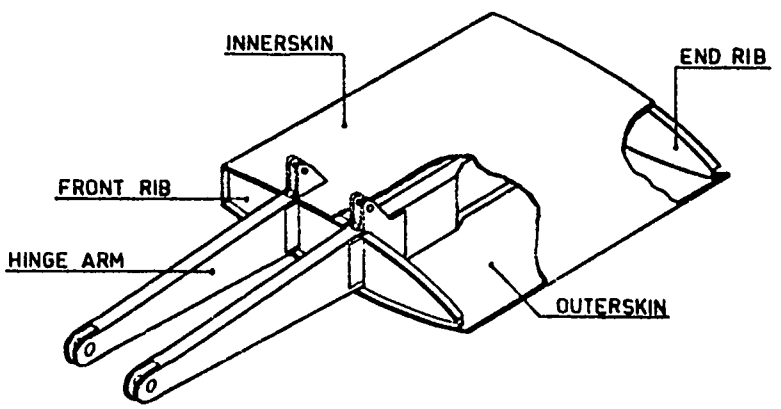

FIG 7 SIMPLIFIED MODEL F28 SPEEDBRAKE IN F.R.P.

THIS DOCUMENT PROVIDED BY THE AEROSPACE INDUSTRIES
TECHNICAL LIBRARY
ABBOTTAEROSPACE.COM

EFFECTS OF TEMPERATURE AND MOISTURE ON THE CREEP COMPLIANCE OF GRAPHITE-EPOXY COMPOSITES

K. G. Kibler
Senior Engineering Specialist
Materials Research Laboratory
General Dynamics
Fort Worth, Texas 76101

SUMMARY

The present work describes investigations to obtain generic information on the time-dependent environmental behavior of graphite-epoxy composites used in aerospace structural applications. Experimental and analytical results are presented for the individual and coupled effects of temperature and absorbed moisture on the creep compliance of unidirectional and cross-plied composites. The scope of the investigation includes measurement of tensile creep response at room temperature and four elevated temperatures (up to the glass transition region of the materials) for dry specimens and for specimens moisture-saturated at 75% and 95% relative humidity. Data are presented for two material systems: Narmco T300/5208 and Hercules AS/3502. The stress levels used are demonstrated to be within the range of linearly viscoelastic response. Superposition techniques are used to determine compliance master curves from the results for individual temperature and moisture conditions.

INTRODUCTION

The use of graphite-epoxy composites for aerospace structural applications has evolved as a result of their mechanical properties, such as high strength-to-weight ratio, and their tailorability of design, relative to conventional materials. The composite constituent materials are usually assumed to respond to external inputs in a linearly elastic manner, and this feature is reflected in the common analytical methodologies used. It must be recognized, however, that composites do exhibit a significant amount of time, temperature, and moisture dependent behavior, particularly in service-type environments. In fact, the problem of time influences the behavior of these materials in several ways; e.g., the time of exposure to environment, the age of the material, and the time (duration) of a particular loading condition.

Although much research has been conducted on the viscoelastic behavior of polymers and particulate-filled composites, only limited investigations on the time-dependence of fibrous composites had been accomplished through 1975 (Ref. 1-7, e.g.). Recent years have witnessed rapidly expanding activities directed more specifically at time-dependent behavior of advanced composite materials systems of particular interest for aerospace applications (Ref. 8-11). These works have established that although the behavior of fibrous composites is in general not linearly viscoelastic, there is often a considerable range of input (temperature, humidity, load) where linear response may at least be a very appropriate approximation.

In the present program, we have undertaken a rather basic attempt to obtain generic information on the time-dependent mechanical response of commonly-used graphite-epoxy materials and to analyze what that time-dependence means within the framework of existing methodologies. We have obtained a fairly complete linearly viscoelastic characterization of the principal properties for two material systems over a range of temperature and humidity conditions representative of (or exceeding) service conditions. We have then used this experimental characterization with conventional analytical techniques to predict time-dependent laminate response, in order to ascertain the magnitude and importance of time, temperature and humidity effects on structural composites.

The overall features of the test/prediction scheme are indicated in Fig. 1. The six types of coupons shown were tested for tensile creep as a function of time (t), temperature (T), and humidity (H). From the $(0)_6$, $(90)_{15}$, and $(\pm 45)_{2S}$ results, the principal moduli were extracted. These moduli were then used to predict the measured longitudinal stiffness strength (σ_R), and creep tests for specimens with non-uniform moisture distribution (M(z)) are also included in our test program, but are beyond the scope of the present discussion.

EXPERIMENTAL CONDITIONS

The present program has included tests on two material systems, Narmco T300/5208 and Hercules AS/3502. Although the fibers are different, the matrix materials for these 450°K (350°F) curing materials are quite similar, consisting in each case of a major and minor

TECHNICAL LIBRARY
ABBOTTAEROSPACE.COM

epoxy and the curing agent.

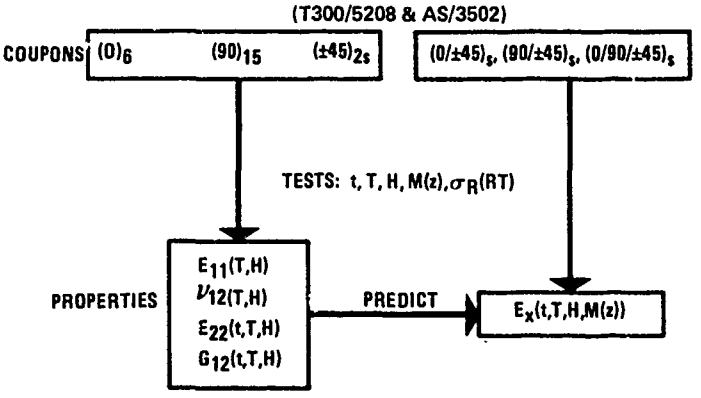

Figure 1 Time-Dependent Tests/Predictions

Longitudinal and transverse expansional strains due to temperature and moisture were measured under various coupled and uncoupled conditions of temperature and humidity. Thermal expansion measurements on both dry and wet specimens were conducted with a Perkin-Elmer TMS-1 Thermomechanical Analyzer (TMA), with temperature and sample dilation monitored and recorded with a Hewlett-Packard 3050B data acquisition system. Moisture-induced swelling measurements were accomplished with four-place micrometers, using alignment fixtures to insure repeatability of specimen alignment and reference point position. Typical transverse expansion values on unidirectional specimens (both materials) with respect to temperature and percent moisture content by weight were $\alpha_{22} = 25\ \mu\epsilon/^{o}K$ and $\beta_{22} = 3000\ \mu\epsilon/\%M$.

Figure 2 shows representative swelling data represented by percent change in width (transverse to fibers) as a function of moisture content. We note the usual threshold value of moisture required before swelling begins (0.1% in this case), the similarity of behavior for the two materials, and the apparent temperature/moisture coupling caused by elevated temperature (ET) conditioning (322 and 339°K) as opposed to room temperature (RT) conditions.

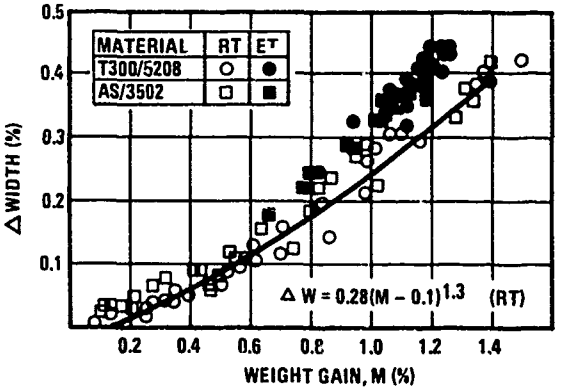

Figure 2 Moisture-Induced Swelling

The test matrix for mechanical testing used in these investigations is indicated in Figure 3. The dashed curve in the figure shows our measured dependence of the glass transition temperature (T_g) on moisture content. Using room temperature and the T_g as the temperature range of our studies, we conducted time-dependent (primarily tensile creep) tests under the conditions indicated by the squares, and baseline stress-strain tests where the X's appear in the figure. The baseline stress-strain to failure tests were conducted prior to any time-dependent tests in order to assess the trends of mechanical response changes to be expected and to aid in selecting stress (strain) levels for creep (stress relaxation) tests.

All creep tests were conducted on sets of three replicate specimens in deadweight creep machines. Several rapid load-unload cycles were used for mechanical "break-in" of the coupons prior to the first creep cycle. In general, the same set of specimens was used for all five test temperatures at each dry or wet test condition.

TECHNICAL LIBRARY
ABBOTTAEROSPACE.COM

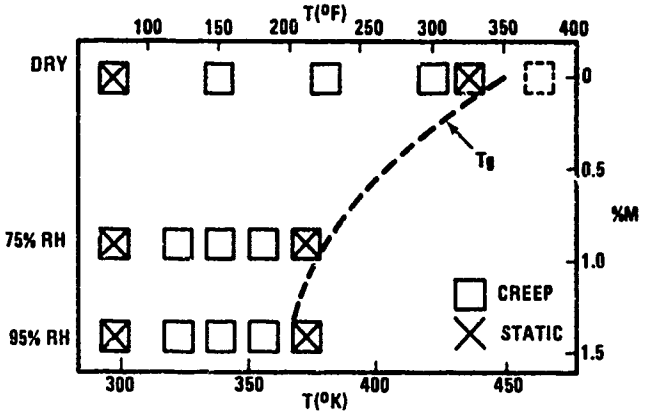

Figure 3 Test Matrix

Dry specimens were desiccated under vacuum/temperature (339°K) for at least seven days prior to test, and desiccant was maintained in the oven during dry creep tests. "Wet" specimens were preconditioned to uniform moisture content at either 75% or 95% relative humidity (and 339°K) prior to test. During the creep testing, the wet specimens were immersed in appropriate mixtures of ethylene glycol and water to maintain the moisture content attained during their prior conditioning. For these wet tests, the strain gages were coated with Micromeasurements M-Coat to retard (but of course not prevent) moisture effects on the gage adhesives. Strain gages would typically function without problems for about five days, which was more than adequate for testing at 5 temperatures.

Essentially all creep runs were 100 minutes in duration, followed by a recovery (no load) period of 100-300 minutes, depending on the next test temperature. Stress levels for creep testing were set at typically 25-35% of ultimate values for each temperature/moisture condition. Verification of linear response was obtained by superposition of creep-recovery results, as shown for a typical case in Figure 4.

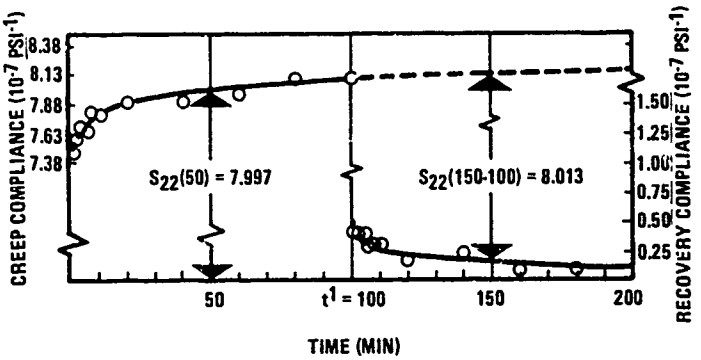

Figure 4 Linear Viscoelasticity of T300/5208 $(90)_{15}$: 95% RH, 150°F

Stress relaxation experiments were conducted on selected coupons by holding constant cross head displacement in an Instron tester and monitoring stress/strain vs. time. As expected for the range of stress/strain values used here, the creep and stress relaxation results agreed very well, in that derived modulus $\propto$ (compliance)$^{-1}$.

EXPERIMENTAL RESULTS

The overall plan of testing and analysis has stressed (1) time-dependent measurements (primarily 100-minute creep) in the region of linear response; (2) generation of compliance master curves by simple horizontal shifting of data (time/temperature/humidity superposition); (3) extraction of moduli using quasi-elastic conversion; (4) prediction of laminate response using principal moduli master curve data points to compute average laminate stiffnesses. We will discuss specific results related to the first three items above in this section, and example predictions will be presented in the following section.

TECHNICAL LIBRARY
ABBOTTAEROSPACE.COM

Figure 5 indicates the superposition technique used to form master compliance curves from short-term creep runs at constant (T,H). We have assumed that the effects of temperature and moisture are uncoupled, in the sense that log a_{TH} = log a_T + log a_H. Although other work (e.g., Ref. 9) suggests coupling is present between moisture and temperature effects, the product form of shift factor appears to describe our results quite adequately and thus presents a practical method for our data analyses. Except where otherwise noted, our master curves are referenced to (T = 297°K, H = 0%) conditions.

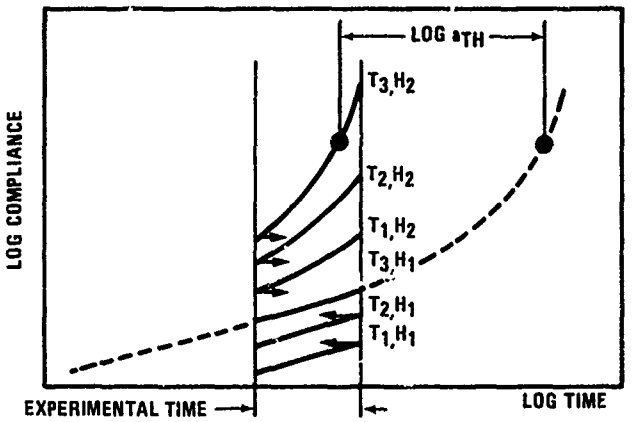

Figure 5 Superposition Procedure

For reference purposes, Figure 6 presents typical stress-relaxation results at room temperature (RT) wet conditions for E_{11} and ν_{12}. The results for these moduli are similar for all test conditions. For both materials E_{11} tends to range between 124 and 138 N/m^2, while ν_{12} falls in the 0.28-0.33 range. There is no apparent regular dependence on either temperature or moisture content, and no sensitivity to time. We therefore treat these moduli as time-independent. A recent paper (Ref. 12) on the time-insensitivity of Poisson's ratio in an unfilled adhesive lends considerable support to this viewpoint.

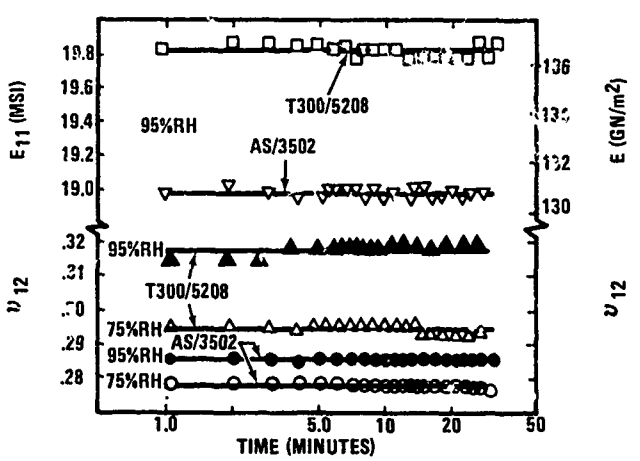

Figure 6 Typical E_{11} and ν_{12} For RT Wet $(0)_6$ Coupons

In Figure 7 are summarized our data for tensile creep compliance of dry (±45) coupons. The data points for the T300/5208 system are horizontally shifted log-log results (referenced to RT) from 100 minute creep tests at 6 temperatures (an extra test was performed in this case at 464°K (375°F) somewhat above the dry T_g). Several features are noteworthy in this figure. (1) A smooth time-temperature curve may be derived from simple horizontal shifting. (2) The two materials have similar mechanical behavior, as evidenced by the dashed AS/3502 master curve compared to the T300/5208 data points. (3) Longer-term tests agree rather well with short-time tests, as indicated by the elevated temperature 5000 and 7000 minute results. (4) The shift factors, a_T, shown in the inset are essentially identical for the two materials.

Using this compliance master curve, we have produced the $G_{12}(t)$ curves shown in Figure 8. The tensile modulus E_R has been taken equal to $(S_{xx})^{-1}$, and the shear modulus is obtained from $E_R(t)$ and the measured (time-insensitive) Poisson ratio ν_{xy} for this coupon. The $G_{12}(t)$ curves are given in Figure 8 for various reference conditions as indicated. With respect to RT dry conditions, time scales of 15 years present minimal

TECHNICAL LIBRARY
ABBOTTAEROSPACE.COM

concern, for the modulus changes by only about 20%. As the material becomes warm and wet, however, comparable decreases in modulus may be expected in times of the order of weeks.

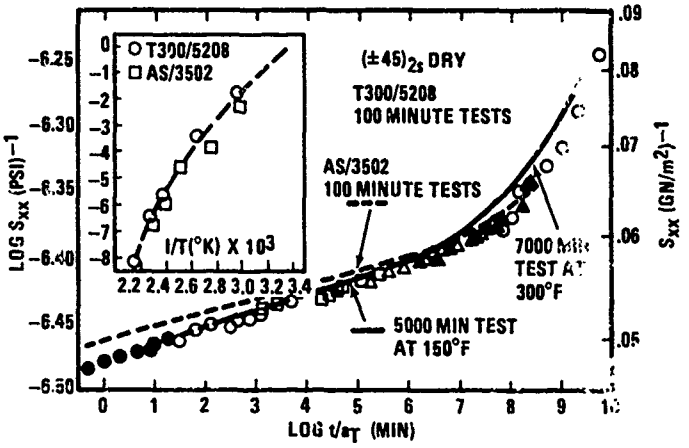

Figure 7 Creep Compliance Master Curve for Dry (+45)

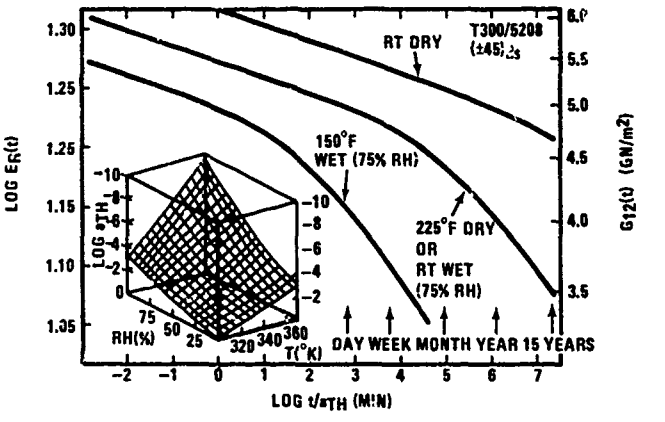

Figure 8 Relaxation Moduli for Dry (+45)

The inset to Fig. 8 presents the log a_{TH} shift surface for a range of temperature and humidity conditions. We note that similar shifts accure for RT/95% RH and for 370°K/ dry conditions. When both moisture and elevated temperature are present, however, the shifts are considerably greater.

Our results for the time-dependence of E_{22} are generally similar to those presented here for G_{12}, although the transverse modulus exhibits slightly less relaxation than does G_{12}, a result similar to that of Ref. 8. We have also generally noted considerably more scatter in our measurements on 90° coupons than is the case for the (±45) specimens. We investigated the possibility of damage in the 90° coupons by using replicate techniques to search for edge cracks. No evidence of damage was found for any of the specimens examined.

Figure 9 demonstrates our results for the 90° coupon compliance, S_{22}, for several possible cases. The shaded curve represents our derived master curve for dry T300/5208 coupons, all of which were approximately one-year old (time since cure). If we superpose our "wet" results, using our previously-derived shift factors from the G_{12} case (assuming all time-dependence is due to the matrix material), then the solid curve results.

The apparent discrepancy between wet and dry results at long-reduced time is obvious. Two possibilities immediately arise. (1) The effects due to temperature and moisture are not superposable in the same manner, although this assumption yielded reasonable results in the G_{12} case. (2) The dry specimens have "aged" (see e.g., Ref. 13) to a greater extent, yielding a lower compliance at long times.

To briefly examine this second possibility, we "unaged" a dry specimen by conditioning it at 464°K (375°F), i.e., somewhat above its glass transition range, for 15 minutes. A long-term creep run (7000 minutes) at 422°K (300°F) was then conducted. The results

TECHNICAL LIBRARY
ABBOTTAEROSPACE.COM

were then shifted by a log a_T previously derived from G_{12} data at that temperature. The results are indicated by the data points in Figure 9.

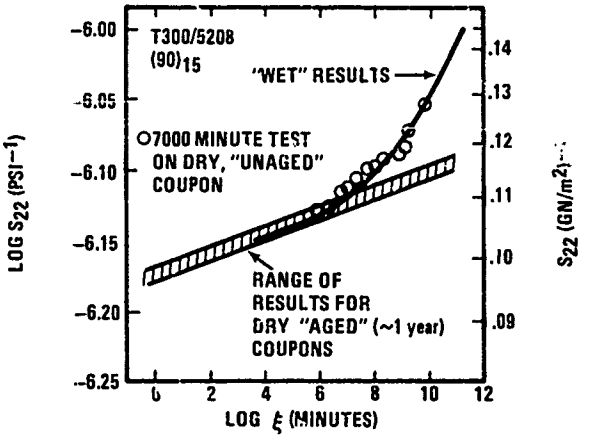

Figure 9 S_{22} Master Curves for T300/5208

Although these latter results must still be regarded as preliminary at this time, the agreement between the wet results and the dry results for "fresh" specimens is striking.

PREDICTIONS

Using principal moduli derived from our compliance curves using quasi-elastic conversion, we have performed some preliminary predictions of expected laminate behavior. The thrust of our work to date has been to see how well we can do using familiar analytical techniques, so our first predictive attempts have concentrated on using time-dependent data in conventional elastic analyses.

As an example, Figure 10 shows Halpin-Tsai predictions for E_m, the effective matrix modulus, and for E_{22}, based on our experimentally derived G_{12} master curve (wet and dry results). We have used fiber properties essentially the same as those given in Ref. 14. The data points (o) are our experimental data from this program while the solid curves are Halpin-Tsai results. The vertical bars on the E_{22} data represent typical scatter in our 90° coupon results. The data points (x) are results from Ref. 15 on neat 3502 resin, which is similar to 5208, as we have noted. The data points (▲) are derived from results in Ref. 16 for 5208 resin.

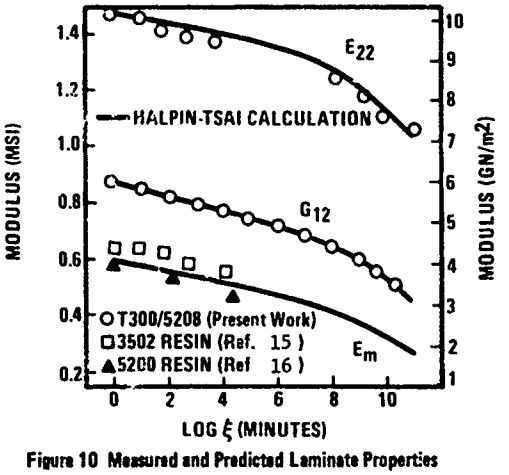

Figure 10 Measured and Predicted Laminate Properties

Several features are worth noting from Figure 10. If we base all calculations on G_{12} results, i.e., if we assume all time dependence is due to the resin material and is properly described by our measurements on (±45)$_s$ tensile coupons, then using reasonable values for fiber properties and geometrical parameters, with no unusual adjustments of parameters, we obtain a very reasonable description of E_{22} results. Additionally, the predicted matrix modulus agrees very well with independent measurements on the cured resin material.

THIS DOCUMENT PROVIDED BY THE ABBOTT AEROSPACE
TECHNICAL LIBRARY
ABBOTTAEROSPACE.COM

Given then the time-dependence for G_{12} and E_{22} shown in Figure 10, we have used an available elastic code to calculate the average stiffness, as a function of time, of a $(90/\pm45)_s$ laminate. For these calculations we used E_{11} = 131 GN/m^2(19 MSI), and ν_{12} = 0.31, which are "average" results from our measurements. Both of these latter moduli are assumed insensitive to time.

Figure 11 presents the prediction obtained on this basis, along with the experimentally-obtained master-curve data for the $(90/\pm45)_s$ T300/5208 laminate. The agreement between measurement and prediction is within about 4% over the entire range of reduced time.

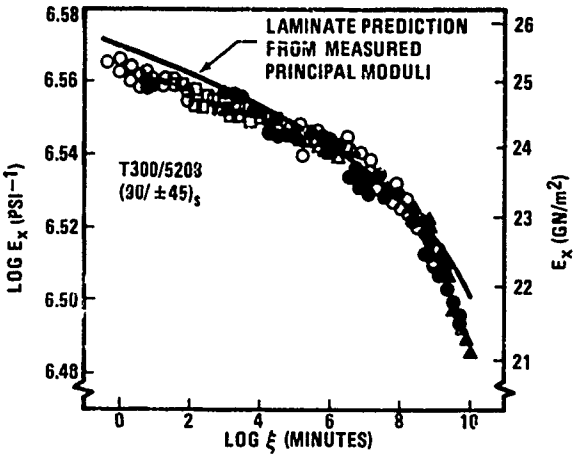

Figure 11 Measured and Predicted Laminate Response

CONCLUSIONS

We have obtained a reasonably complete linearly viscoelastic characterization of two commonly used graphite-epoxy material systems by measuring the principal properties as a function of time, temperature and humidity. We have used this experimental characterization, along with rather conventional analysis techniques, to predict time-dependent laminate response. We believe the results are of general applicability for ascertaining the magnitude and importance of time, temperature and humidity effects on structural composites.

The following statements summarize the main conclusions from our work thus far:

1. Immersion testing is a viable procedure for short-term experiments on "wet" specimens.
2. E_{11} and ν_{12} are not sensitive to time, temperature and moisture.
3. Long-term results are predictable from short-term tests by simple horizontal superposition.
4. Prediction of laminate master curves is possible using conventional analysis procedures.
5. Time-dependent tests on ±45 coupons, along with the Halpin-Tsai equations, provide a good assessment of the expected material response to environment.

REFERENCES

1. J. C. Halpin, "Introduction to Viscoelasticity," Composite Materials Workshop, S. W. Tsai, J. C. Halpin, and N. J. Pagano, eds., Technomic Publishing Co., 1976.
2. J. E. Ashton, "Non-Linear Viscoelastic Response of Fibrous Composites," J. Composite Materials, Vol. 2, 1968, p. 116.
3. Y. C. Lou and R. A. Schapery, "Viscoelastic Characterization of a Non-Linear Fiber-Reinforced Plastic," J. Composite Materials, Vol. 5, 1971, p. 208.
4. R. A. Schapery, S. W. Beckwith, and N. Conrad, "Studies on the Viscoelastic Behavior of Fiber-Reinforced Plastic," AFML-TR-73-179, Wright-Patterson AFB, OH, 1973.
5. A. S. D. Wang and P. K. Lin, "Humidity Effects on the Creep Behavior of an Epoxy-Graphite Material," AIAA/SAE 11th Propulsion Conference, Anaheim, CA, AIAA Paper No. 75-1341, 1975.

TECHNICAL LIBRARY
ABBOTTAEROSPACE.COM

6. A. S. D. Wang, E. J. McQuillen, and A. S. Ahmadi, "Analytical and Experimental Investigation of Time-Temperature Creep of Graphite-Epoxy Composite Laminates," Mechanical Behavior of Materials, Vol. II, Soc. Mat. Sci., Japan, 1974.

7. S. W. Beckwith, "Viscoelastic Characterization of a Non-Linear, Glass/Epoxy Composite Including the Effects of Damage," Texas A&M University Report MM2895-74-8, 1974.

8. Y. T. Yeow, D. H. Morris, and H. F. Brinson, "Time-Temperature Behavior of a Unidirectional Graphite/Epoxy Composite," Composite Materials: Testing and Design (5th Conference), ASTM STP 674, S. W. Tsai, ed., American Society for Testing and Materials, 1979, pp. 263-281.

9. F. W. Crossman and D. L. Flaggs, "Dimensional Stability of Composite Laminates during Environmental Exposure," SAMPE Journal, July/August, 1979, pp. 15-20.

10. W. J. Renton and T. Ho, "The Effect of Environment on the Mechanical Behavior of AS/3501-6 Graphite/Epoxy Material," ATC Report No. B-92100/8CR-105, Vought Corporation, Dallas, TX, August 1978.

11. K. G. Kibler, "Time-Dependent Environmental Behavior of Epoxy Matrix Composites," Mechanics of Composites Review, AFML/MBM, Wright-Patterson AFB, OH, 30 Oct.- Nov., 1979, pp. 57-61.

12. J. Romanko and W. G. Knauss, "On the Time Dependence of the Poisson's Ratio of a Commercial Adhesive Material," J. Adhesion, 10 (to be published), 1979.

13. L. C. E. Struik, Physical Aging in Amorphous Polymers and Other Materials, Elsevier Publishing Co., New York, 1978.

14. R. D. Kriz and W. W. Stinchcomb, "Elastic Moduli of Transversely Isotropic Fibers and Their Composities," Experimental Mechanics, Feb. 1979, p. 41.

15. K. M. Liechti, V. H. Kenner, and W. G. Knauss, "Time Dependent Fracture Processes Relating to Service Life Prediction of Adhesive Joints and Advanced Composites, Progress Report No. 4," GALCIT SM 79-10, California Institute of Technology, Pasadena, CA, Oct. 1979.

16. K. G. Kibler and H. G. Carter, "Viscoelastic Parameters of Epoxy Resin from Thermomechanical and Electrical Conductivity Measurements," Composite Materials: Testing and Design (5th Conference), ASTM STP 674, S. W. Tsai, ed., American Society for Testing and Materials, 1979, pp. 282-288.

ACKNOWLEDGEMENTS

This work was accomplished under Contract F33615-77-C-5109, sponsored by the Air Force Materials Laboratory (AFSC), Wright-Patterson AFB, OH 45433. Dr. J. M. Whitney (AFML/MBM) is the Air Force Project Engineer. Drs. R. A. Schapery and Y. Weitsman, of Texas A&M University, and Dr. W. G. Knauss, of California Institute of Technology, are program associates. Other participants at General Dynamics deserving special acknowledgement include T. Creasy, J. Fruit, J. Reynolds, W. Robinson and J. Halkias.

TECHNICAL LIBRARY
ABBOTTAEROSPACE.COM

RECORDER'S REPORT

SESSION II – ENVIRONMENT SUPERIMPOSED ON STRESSING

by

Dr G.Dorey
Materials Department
Royal Aircraft Establishment
Farnborough, Hampshire GU14 6TD
England

Information is needed on the effects of simultaneous application of load, temperature and humidity on composite materials, to generate confidence that they will perform adequately in the service environment. Reliable analytical methods of predicting performance will obviate much tedious testing. These four papers provided useful additional data. Three of the papers were on fatigue, one on creep compliance; three were on coupon testing, one on an aircraft component.

The paper by Arendts et al on the fatigue of (0, ±45, 90) laminates concentrated on compression, to load the matrix, in flight-by-flight testing at room temperature, with five different loading spectra to represent different aircraft components. Miner's rule was found to be unsatisfactory because composites appear to be particularly sensitive to peak loads, overloads causing a significant decrease in fatigue life.

Gerharz and Schütz tested (±45) laminates, again to load the matrix. Flight-by-flight fatigue tests, so far only at room temperature, showed that degradation in mechanical properties could be related to increased damage shown by ultrasonic C-scan. Static tests showed that elevated temperature and moisture significantly reduced strength and modulus, and this could well affect the fatigue results when environmental fatigue testing is done. The paper contained a useful literature survey.

Kibler's paper also showed that temperature and moisture has a marked effect on the mechanical response of matrix dominated properties. Measurements on simple (0), (0, 90) and (±45) laminates can be used to predict the behaviour of more complex combinations of these orientations, and 100 minute creep tests can be used to produce master creep curves by a simple superposition procedure.

Dijns gave useful information on an actual component, an F28 speed brake. Careful testing of structural elements and load attachment points showed the superior fatigue properties of CFRP compared with titanium and aluminium alloys, and led to an all-composite construction incorporating aramid fibres for impact resistance. In service, the component showed no detectable damage after 2000 landings.

The discussion concentrated on whether laboratory testing could adequately represent the service conditions. There was concern about the different specimen designs used by different organizations, and about problems with moisture gradients produced by accelerated testing.

The session emphasized that effects of load, temperature and humidity have a most significant effect on fatigue and creep when the loading is such as to produce high stresses in the matrix, such as compression, shear and out-of-plane stresses. Combined effects of moisture and temperature are significantly worse than either alone. But if fibres are aligned in the direction of the stresses the effects are much smaller. There seems to be no acceptable way at present of predicting fatigue lives and representative flight-by-flight testing is necessary, but more data will help in producing analytical models.

Although degradation due to fatigue, temperature and moisture can be demonstrated in the laboratory, the data available suggest that, with present design limits, safety factors are adequate and there is no significant fatigue problem. Indeed the practical component described in this session has performed well in service and this was confirmed by experience with other components in service described in Session V.

TECHNICAL LIBRARY
ABBOTTAEROSPACE.COM

RELATIONSHIPS BETWEEN IMPACT RESISTANCE AND FRACTURE TOUGHNESS IN ADVANCED COMPOSITE MATERIALS

by
G Dorey

Materials Department
Royal Aircraft Establishment
Farnborough, Hampshire, GU14 6TD, England

SUMMARY

A variety of CFRP laminates and one GRP laminate were subjected to impact by steel balls, over a range of incident energies, and residual strengths were measured; superimposed static load during impact substantially altered the residual strength curves. The laminates were also tested with machined notches and analysed in terms of fracture toughness; results were compared with impact performance both during impact and in subsequent residual strength tests, with the aim of correlating service performance with laboratory toughness tests. Effects of materials and geometric variables are discussed together with possibilities for improvements.

1 INTRODUCTION

Advanced composite materials, being introduced into aircraft structures because of their high specific strength and stiffness, must perform adequately in the service environment. One possible threat to their performance is that of damage from rough handling or from impact by foreign objects. At low energies this can result in surface damage and delamination and, at higher energies can produce through-thickness cracks and holes[1]. The damaged area may be further affected by temperature, humidity and fatigue loading, but one of the most damaging effects is that of broken fibres reducing the static tensile and compressive strengths.

Full-scale testing of composite components is expensive and time consuming and has to be kept to a minimum. Useful indications of the impact performance of composites can be obtained from coupon tests which simulate service threats. However, this still involves relatively large numbers of specimens, to allow for a range of incident energies, various geometries and different residual mechanical properties. Simple mechanical tests are required that correlate with impact performance so that materials parameters can be modified, improvements made and the most promising materials selected for more searching investigations. This paper describes tests on a variety of CFRP laminates made from several fibre-resin systems using several different lay-ups. Foreign object impact was simulated using dropped weights and steel balls fired from an airgun, some of the coupons being stressed to simulate impact of loaded panels. Residual strengths were measured in flexure or tension and the results compared with those from notched tensile tests.

2 THEORETICAL CONSIDERATIONS

In assessing the impact performance of composite laminates consideration has to be given to both the processes occurring during impact to produce damage and the effect of this damage on residual strengths.

2.1 Impact

The damage done during impact depends on how the stresses build up, on how they compare with the various materials strengths, on how they are redistributed as the fracture progresses, on the fracture energies and on the energy available to drive the fracture processes. These in turn depend on the material properties and geometry of the test specimen and on the energy and momentum of the projectile. No damage need be done if the energy of the projectile can be accommodated by elastic strain energy in the specimen. Simple calculations have been made[1] of energies necessary to cause:

a. shear fracture $(2/9)(\tau^2/E)(wl^3/t)$

b. flexural fracture $(1/18)(\sigma^2/E)(wlt)$

c. penetration $\pi \gamma td$

where τ is the interlaminar shear strength, σ the flexural strength, E the Young's modulus, γ the through-thickness fracture energy, d the diameter of the projectile, and w, l and t the width, length and thickness of the flexed part of the test specimen. Comparison of a and b shows that shear fractures should result for $l/t < \sigma/2\tau$ and flexural fractures for $l/t > \sigma/2\tau$. Small projectiles with sufficient energy but with relatively low momenta are more likely to cause penetration or erosion. It should be noted that these expressions contain critical energy density terms, such as σ^2/E. In addition the extent of the damage will depend on fracture energies, such as γ, to fail fibres, resin and fibre-resin interfaces, expressions for which will also contain critical energy density terms. Thus, both the energy needed to cause damage and the extent of the damage will depend both on the relevant strengths and on the relevant moduli.

TECHNICAL LIBRARY
ABBOTTAEROSPACE.COM

2.2 Residual Strength

Laminates containing impact damage and those with machined notches behave similarly in tension[2,3]. Several models have been proposed to predict the tensile strengths of notched or damaged laminates.

When the local stress at the tip of a notch reaches the strength of the laminate, either the laminate fails or local crack blunting processes occur, such as shear cracking, which reduce the stress concentration. In some laminates such as (0) or (±45), these shear cracks can remove the stress concentrating action of the notch and failure does not occur until the net section stress equals the unnotched failure stress. But in (0,90), (0, 90 ± 45) and (0, ±45) CFRP laminates, failure can occur when relatively small volumes of material at the notch tip are at or near the failure stress, while the average net section stress is still significantly less than the failure stress.

Bishop and McLaughlin[4] used a notch blunting mechanism to explain their results on (0 ± 45) CFRP laminates; with increasing stress, shear cracks at the notch tip increase its effective radius of curvature until a critical radius of curvature is reached, characteristic of the laminate, when failure occurs. The critical applied stress σ_c is given by:

$$\sigma_c = \sigma_o/(1 + q\,(a/\rho_o)^{\frac{1}{2}}) \qquad (1)$$

where σ_o is the strength of the unnotched laminate, 2a is the notch length, q depends on the elastic anisotropy and ρ_o is the characteristic radius of curvature; typical values for ρ_o for CFRP laminates were about 10 mm for a tough laminate and about 5 mm for a brittle laminate.

Potter[5] invoked a similar crack blunting mechanism but he argued that, as the stress and hence the notch tip radius both increased, the stress gradient would decrease, and failure would occur when the stress gradient was reduced to a critical value characteristic of the material. Simplifying the mathematics for relatively sharp notches, the critical applied stress is given by:

$$\sigma_c = \sigma_o/(1 + C\,(a/S_o)^{\frac{1}{2}}) \qquad (2)$$

where C depends on the elastic anisotropy and S_o has the dimensions of length and contains terms that depend on material and laminate properties.

Nuismer and Whitney[6] used an "average stress criterion" in which they did not specify the damage at the notch tip but considered that failure occurs when the elastic stress, averaged over a characteristic distance a_o ahead of the notch, reaches the unnotched laminate strength. This gives:

$$\sigma_c = \sigma_o/(1 + 2\,(a/a_o))^{\frac{1}{2}} \qquad (3)$$

For multidirectional CFRP laminates a_o is typically 2 to 4 mm; the model has also been fitted to notched compression data and a larger value of a_o was found, namely 6.2 mm.

Fracture mechanics has been applied with reasonable success to notched multidirectional laminates[2,3,6]. In this case the shear cracks at the notch tip are considered not so much to blunt the notch but rather to form a damage zone, similar to the plastic zone in a metal, that effectively lengthens the notch and increases the release of strain energy. Thus the fracture toughness K_c becomes $\sigma_c\,(\pi(a + r_p))^{\frac{1}{2}}$ and

$$\sigma_c = K'/(1 + a/r_p)^{\frac{1}{2}} \qquad (4)$$

where K' is $K_c/(\pi r_p)^{\frac{1}{2}}$ and r_p is the effective increase in notch length which is taken to be characteristic of the laminate: typical values for r_p were 1.5 mm for a tough laminate (K_c 50 $MNm^{-3/2}$), 0.3 mm for a brittle laminate (K_c 20 $MNm^{-3/2}$).

Comparisons of equations 1 to 4 reveal strong similarities especially between the notch blunting models of equations 1 and 2 and between the stress-integrating models of equations 3 and 4. Although all four models use different physical mechanisms, they all depend on the form of the stress distribution ahead of the notch and it is not surprising therefore that they all have a $1/\sqrt{a}$ dependency. All four equations can be fitted to most notched tensile strength data on multidirectional CFRP laminates, if the two materials constants in each equation are suitably adjusted. The models associated with equations 1 to 3 have the advantage of being applicable to notches of various shapes, whereas equation 4 depends on laminate toughness and is not related to the unnotched laminate strength. Although equation 4 applies strictly only to sharp notches, Avery and Porter[3] have found that it can be used to predict residual strengths of multidirectional CFRP laminates with irregular impact damage if 2a is put equal to the "transverse lateral damage" (TLD) and a larger value of K' is used than that for sharp notches. All four models assume some form of stress redistribution by the formation of a damage zone at the notch tip and it is not unreasonable to assume that the size of the damage zone will depend on material and laminate properties, especially on shear strengths and shear fracture energies, that control shear cracking. Increased damage zone size increases the amount of work G_c needed to propagate the crack and therefore, since $K_c^2 = G_c E$, larger damage zones tend to be associated with tougher laminates, although if the energy density within the damage zone could be increased, toughness could be increased with less associated damage. The formation of the damage zone also

TECHNICAL LIBRARY
ABBOTTAEROSPACE.COM

increases the volume of highly stressed material at the notch tip and therefore local variations in material strength, such as variations in fibre strength, become important in considerations of the statistics of failure probability.

3 EXPERIMENTAL DETAILS

All the laminates were made from preimpregnated warp sheet, layed up in the required orientations and moulded in an autoclave to give balanced symmetrical laminates with 60% by volume of fibres; a summary of the laminates is given in Table 1. Specimens were cut from the laminates using a diamond slitting wheel, and for tensile specimens aluminium alloy end tabs were glued on with an epoxy adhesive. For notched specimens, saw cuts were made witha 0.25 mm jewellers' saw, or circular holes were drilled with diamond-tipped drills.

Charpy impact specimens, 50 mm x 10 mm and unnotched, were cut from the multidirectional laminates and tested in a pendulum impact machine fitted with a pendulum of capacity 7.5 J; the span was 40 mm and the specimens were mounted so that the deflection was out of plane.

For drop-weight impact, a 12.7 mm diameter steel ball was loaded with weights to adjust the incident energy and dropped through 1 m on to plain rectangular specimens, simply supported over a span of 20 mm for subsequent interlaminar shear testing or a span of 50 mm for subsequent flexural or tensile testing. Ballistic impact was by 6 mm diameter steel balls fired from an airgun, the air pressure in the cylinder being used to control the ball velocity and hence the incident energy; again the specimens were plain rectangular and simply supported on parallel supports 50 mm apart. Specimens were 25 mm wide for laminates 4–6 and 50 mm wide for laminates 7–13 and the GRP. For ballgun impact on loaded laminates, plain rectangular specimens 30 mm wide were mounted in a simple screw-loading frame and the load was measured by calibrated strain gauges on the frame arms.

Residual strengths after impact were measured in a screw driven machine.

4 RESULTS

4.1 Machined Notches

Fig 1 shows the effect of machined centre notches on the tensile strength of laminate 1. It can be seen that the notches reduced the tensile strength by more than the loss in cross sectional area; ie the laminate was notch sensitive. The tensile strength was reduced more by the sharp notches than by the circular holes. The data for the sharp notches are replotted in Fig 2 as fracture toughness, $K_c = \alpha \sigma_c (\pi(a + r_p))^{\frac{1}{2}}$, together with data for laminates 2 and 3, where α is a finite width correction and r_p is the damage zone correction mentioned in section 2. The values of r_p, chosen to give the best fit for the data, were 0.2 mm for laminate 1, 1.2 mm for laminate 2 and 1.6 mm for laminate 3. Observations in a scanning electron microscope of the fracture surfaces near the notch tip showed a surface roughness of 2–3 mm for laminate 3 and 0.4–0.5 mm for laminate 1. Thus fracture toughness was found to predict reasonably well the residual strength of notched laminates with K_c between 20 and 50 $MNm^{-3/2}$, for notches from 2 mm to over 40 mm in length. For notches longer than about ten times the damage zone size ($a > 5\ r_p$), the correction became insignificant compared with the experimental variation in σ_c.

4.2 Impact Damage in the (0 ± 45) Laminates

Laminates 4 to 6 were made from a single batch of type 2 carbon fibres in three different resins, with two lay-ups. The strengths and toughness of the laminates are given in Table 2. The values σ_n/σ_o were the normalized net section stresses for a 8 mm centre notch in a 25 mm wide specimen, and this data was used to calculate the fracture toughness shown. It can be seen that although the unnotched strengths were similar (variations of 30% for flexural strength and 25% for tensile strength) the notched strengths varied by a factor of 4.5 and the Charpy impact energies by a factor of 7.5. In Fig 3 the Charpy impact energy is plotted against the fracture toughness for laminates 4 to 6 and for six other laminates (three other fibre/resin systems with the same a and b lay-ups), showing a good correlation. If the Charpy impact energy is related to the fracture energy G_c then, because $K_c^2 = G_c E$, one would expect a curve of this form. This would only be true if the stored energy at the point of failure in the Charpy test, given in section 2.1 and in this case about 0.3 J, is less than the total fracture energy γ_{wt}, in this case about 1.2 J. For all cases except laminates 6a and 6b, lay-up a, with the 45° layers on the outside, was both tougher than lay-up b and gave greater impact energies. The types of fracture seen in the Charpy impact test are indicated in Fig 3; the tougher laminates showed a fibrous fracture whereas the brittle laminates 6a and 6b showed relatively clean fractures. Fig 4 shows the decrease in interlaminar shear strength caused by drop-weight impact using a small span/depth ratio that resulted in delamination. Figs 5 and 6 show the reductions in flexural strength caused by flexural failures in the drop-weight and ballgun tests. In all these tests resin C (laminates 4a and 4b) gave tougher laminates than resin B (5a and 5b) and resin D gave particularly brittle laminates. Resin D had a large relative density, 1.48 compared with typical values of 1.25, and a large Young's modulus, that gave laminates with good compressive properties but poor notched tensile properties. Lay-up (a) was generally superior to lay-up (b); reference to section 2.1 shows that this was because, although the strengths were similar, having the low modulus 45° layers on the outside caused a lower value of flexural modulus, a lower effective E and therefore a greater value of σ^2/E. It is also worth noting that in the case of ballgun impact, having 0° layers on the outside caused a marked minimum in the residual strength curve and this coincided with the maximum amount of transverse cracking and occurred approximately at the incident energy needed to cause penetration of the laminate.

THIS DOCUMENT PROVIDED BY THE ABBOTT AEROSPACE
TECHNICAL LIBRARY
ABBOTTAEROSPACE.COM

4.3 Impact Damage in the (0, 90 ± 45) Laminates

Laminates 7 to 13 did not cover such a wide range in toughness as laminates 4 to 6, but were more recent materials with greater strengths and greater toughnesses as can be seen from Table 3. For comparison an E-glass laminate was included. The values of σ_n/σ_o and fracture toughness were calculated from tensile specimens 50 mm wide with centre notches 15 mm long (for tougher laminates, larger values of w are needed so as to keep σ_n/σ_o well below unity and hence give a meaningful K_c). It can be seen that, although the value of fracture toughness of the E-glass laminate was similar to those of the carbon fibre laminates, the Charpy impact energy was considerably greater. This was because the E-glass fibres have a Young's modulus only a third that of the carbon fibres; dividing the Charpy impact energy for GRP by three makes the value for GRP similar to those for CFRP Fig 7 shows that there was an increase in Charpy impact energy with increase in K_c, similar to that shown for the (0 ± 45) laminates. Figs 8 and 9 show residual strength curves for drop-weight and ballgun impact. There was not much difference between the laminates made from the two resins, resin E being only slightly better than resin B. There was more effect from the fibres. The type 3 fibre laminates (fibre 2) were weaker in the unnotched strength tests, had lower values of fracture toughness and were generally worse in the impact tests. Laminates made from fibres 1 and 3 were the toughest and performed best in the impact tests. Laminates made from fibre 4, although no weaker in the unnotched strength tests were significantly less tough than those made from fibres 1 and 3. In particular laminate 9 had a large flexural strength undamaged but showed a marked reduction in flexural strength for drop-weight incident energies greater than 2.5 J. There was no significant decrease in the strength of the GRP over the range of incident energies studied; the only damage in the GRP was delamination.

4.4 Superimposed Static Load

Figs 10 and 11 show the effect of superimposed static load during ballgun impact on the residual tensile strength after impact. For static loads up to 35% of the ultimate tensile strength (UTS), the impact of the ball produced damage, and hence reduction in strength, similar to that for unloaded specimens. For static loads of 40% UTS the specimen failed on impact; similar effects have been observed in compression[7]. In Fig 11 the dashed line is for residual tensile strengths equal to the applied stress; one would therefore not expect experimental non-zero points below this line (tensile stress greater than residual strength). The three points just below the line resulted because of the slight relaxation of static stress in the loading frame on impact. If there had been no effect of static stress up to the residual strength one would have expected the sudden drop in residual strength for static stresses of approximately 50% UTS; but the drop in residual strength for applied stresses of 30-38% UTS indicated that the applied static stress caused a slight increase in the extent of the impact damage, that is an increase in the number of 0° load carrying fibres broken.

5 DISCUSSION

The residual strength of a notched or damaged laminate can be predicted from the laminate fracture toughness. The fracture toughness K_c depends on the fracture energy G_c and the effective Young's modulus E, $K_c^2 = G_c E$. Thus for CFRP laminates with similar values of E, the toughness depends on the fracture energy and hence the size and energy density of the damage zone. The toughness can be increased by reducing the fibre-resin bond strength to encourage shear cracking[4] and by increasing the thickness of the layers to promote longer shear cracks in each layer[4,8]. For the GRP laminate the value of K_c, and hence the failure stress σ_c for a given crack length, was similar to that of the CFRP laminates. Because of the lower value of E, σ^2/E would have been greater for GRP and hence the strain energy release rate must have been greater as the fracture progressed, but this must have been counteracted by the increased energy needed to produce a larger damage zone and to break the glass fibres within the damage zone. To increase further the fracture toughness of CFRP laminates either G_c must be increased or the failure mode must be changed, as in the case of 0° composites and $+45^\circ$ laminates, where extensive shear cracking can effectively remove the stress concentration. But such shear cracking may be undesirable because of its effect on other properties such as fatigue strength or environmental degradation.

Although the toughness of the composite laminates was not very sensitive to E, the impact properties were very dependent on E. The threshold energy needed to cause damage depends on the amount of energy that can be stored elastically and therefore on σ^2/E. Thus using glass fibres with lower E or using 45° layers on the outside of a laminate to lower the flexural modulus caused a marked increase in threshold energies. The fracture energy G_c depends on K_c^2/E so the extent of the damage for a given absorbed incident energy will be less for a smaller value of E. GRP and aramid fibre reinforced laminates have better impact properties than CFRP although they may not necessarily be tougher. Thus surface layers of GRP or aramid fibres should produce greater increases in impact resistance than in laminate fracture toughness.

For laminates with similar values of E, $G_c \propto K_c^2$ so that the tougher laminates had superior impact properties, giving greater values of Charpy impact energy, greater threshold energies for damage and greater residual strengths. This was true for laminates 4 to 6, where resin properties were important, and for laminates 7 to 13, where the fibre properties were more important.

TECHNICAL LIBRARY
ABBOTTAEROSPACE.COM

CONCLUSIONS

Fracture mechanics gave reasonably good predictions of the residual strengths of CFRP laminates, with fracture toughness between 20 and 50 $MNm^{-3/2}$, for notch lengths from 2 mm to over 40 mm, if allowance was made for the size of the damage zone at the tip of the notch.

The fracture toughness of CFRP and GRP laminates depended on the details of the fracture processes and hence on the fibre, resin and interface properties, particularly those promoting shear cracking, but it was relatively insensitive to laminate modulus.

The impact properties were significantly dependent on laminate modulus, the use of GRP or surface layers of low modulus 45° layers increasing threshold energies for damage, decreasing the extent of damage and hence giving greater residual strengths.

For laminates with similar values of modulus, the toughness increased with increasing impact resistance and therefore provided a good indication of impact performance.

REFERENCES

1	G Dorey	Fracture behaviour and residual strength of carbon fibre composites subjected to impact loads AGARD Conference Proceedings No 163, Failure modes of composite materials with organic matrices and their consequence on design, paper 8 (1975).
2	G Dorey	Damage tolerance in advanced composite materials AHS/NASA - Ames Conference on Helicopter Structures Technology, Moffett Field, paper 13 (1977) and RAE Technical Report 77172 (1977).
3	J G Avery T R Porter	Comparisons of the ballistic impact response of metals and composites for military aircraft applications. In foreign object impact damage to composites ASTM STP 568, pp3-29, (1975).
4	S M Bishop K S McLaughlin	Thickness effects and fracture mechanisms in notched carbon fibre composites RAE Technical Report 79051 (1979).
5	R T Potter	On the mechanism of tensile fracture in notched fibre reinforced plastics Proceedings of the Royal Society London, A361, 325-341 (1978) and RAE Technical Report 77023 (1977).
6	R J Nuismer J M Whitney	Uniaxial failure of composite laminates containing stress concentrations. In Fracture Mechanics of Composites ASTM STP 593 pp117-142, (1975).
7	R Garcia N D Rhodes	Effects of low-velocity impact on graphite/polyimide compression laminates Proceedings of NASA Symposium on Graphite/polyimide composites, Langley Research Center (1979).
8	P T Curtis G Dorey	Hole interactions in CFRP and aluminium alloys. RAE Technical Report 79138 (1979).

TECHNICAL LIBRARY
ABBOTTAEROSPACE.COM

TABLE 1

SUMMARY OF THE COMPOSITE LAMINATES REFERRED TO

Laminate	Fibre	Resin	Lay-up	Thickness mm	Figures
1	1	A	$[0, 90, 0, +45, -45, 0]_s$	1.5	1-2
2	2	B	$[0, 90, 0, +45, -45, 0]_s$	1.8	2
3	3	B	$[0, 90, 0, +45, -45, 0]_s$	1.8	2
4a	1	C	$[(+45, -45)_2\ 0_4]_s$	2.0	3-6
4b	1	C	$[0_2, +45_2, -45_2\ 0_2]_s$	2.0	3-6
5a	1	B	$[(+45. -45)_2\ 0_4]_s$	2.0	3-6
5b	1	B	$[0_2, +45_2, -45_2\ 0_2]_s$	2.0	3-6
6a	1	D	$[(+45, -45)_2\ 0_4]_s$	2.0	3-6
6b	1	D	$[0_2, +45_2, -45_2\ 0_2]_s$	2.0	3-6
7	1	B	$[0, 90, 0, +45, -45, 0]_s$	1.5	7-9
8	1	E	$[0, 90, 0, +45, -45, 0]_s$	1.5	7-9
9	4	B	$[0, 90, 0, +45, -45, 0]_s$	1.5	7-9
10	4	E	$[0, 90, 0, +45, -45, 0]_s$	1.5	7-9
11	2	B	$[0, 90, 0, +45, -45, 0]_s$	1.5	7-9
12	2	E	$[0, 90, 0, +45, -45, 0]_s$	1.5	7-9
13	3	B	$[0, 90, 0, +45, -45, 0]_s$	1.5	7-9
14	3	B	$[0, 90, 0, +45, -45, 0]_s$	1.5	10-11

Fibre 1 was a type 2, intermediate modulus carbon fibre.

Fibre 2 was a type 3, low modulus carbon fibre.

Fibres 3 and 4 were carbon fibre with modulus between those of types 2 and 3.

All the resins were epoxy resins.

TECHNICAL LIBRARY
ABBOTTAEROSPACE.COM

TABLE 2

STRENGTH AND TOUGHNESS OF (0, ±45) LAMINATES

Laminate	Fibre/Resin	Flexural strength GN/m^2	Tensile strength GN/m^2	σ_n/σ_o	Fracture toughness $MN\,m^{-3/2}$	Charpy impact energy kJ/m^2
4a	1C	0.89	0.80	0.70	42.5	135
4b	1C	1.07	0.71	0.65	34	120
5a	1B	0.78	0.75	0.54	29	83
5b	1B	1.08	0.72	0.42	22	54
6a	1D	0.67	0.65	0.20	9.5	29
6b	1D	0.83	0.52	0.28	11.5	18

TABLE 3

STRENGTHS AND TOUGHNESS OF (0, 90, ±45) LAMINATES

Laminate	Fibre/Resin	Flexural strength GN/m^2	Tensile strength GN/m^2	σ_n/σ_o	Fracture toughness $MN\,m^{-3/2}$	Charpy impact energy kJ/m^2
7	1B	1.16	0.98	0.45	50	85
8	1E	1.16	0.83	0.51	46	85
9	4B	1.26	0.92	0.34	34	77
10	4E	1.17	0.88	0.44	43	82
11	2B	1.00	0.78	0.38	32	81
12	2E	0.87	0.62	0.52	37	71
13	3B	1.23	1.01	0.47	52	94
E-glass/resin B		0.97	0.59	0.68	46	295

THIS DOCUMENT PROVIDED BY THE ABBOTT AEROSPACE
TECHNICAL LIBRARY
ABBOTTAEROSPACE.COM

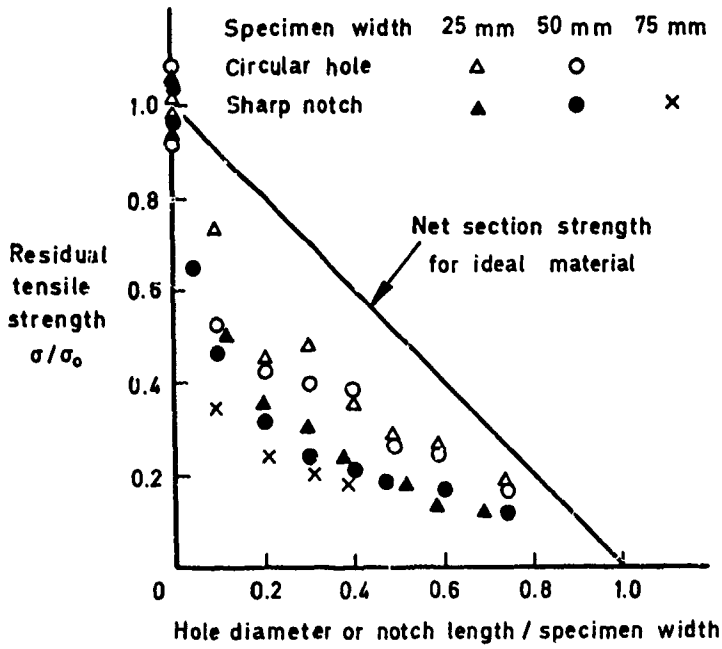

Fig 1 The effect of the size of a machined centre notch on the tensile strength of a CFRP laminate (laminate 1, $[0, 90, 0, \pm 45, 0]_s$).

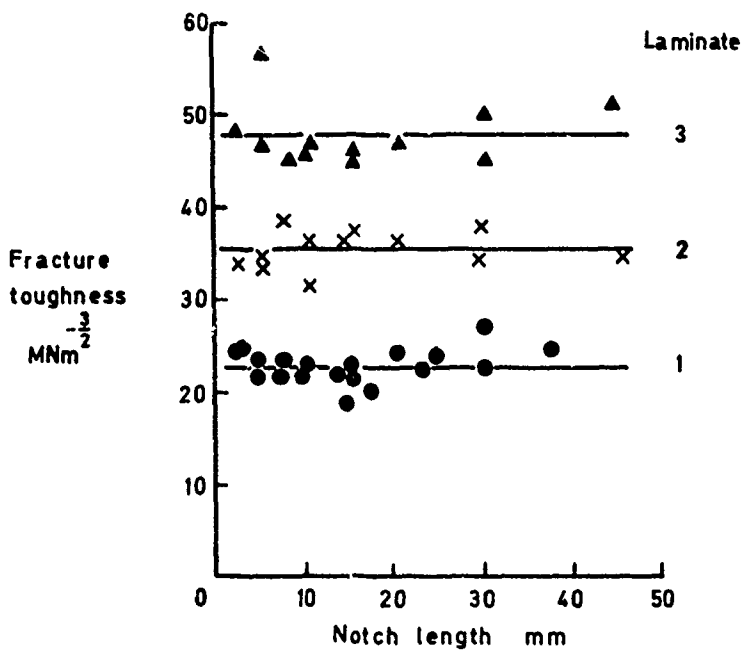

Fig 2 The effect of notch length on the fracture toughness of three CFRP laminates (lay-up $[0, 90, 0, \pm 45, 0]_s$).

TECHNICAL LIBRARY
ABBOTTAEROSPACE.COM

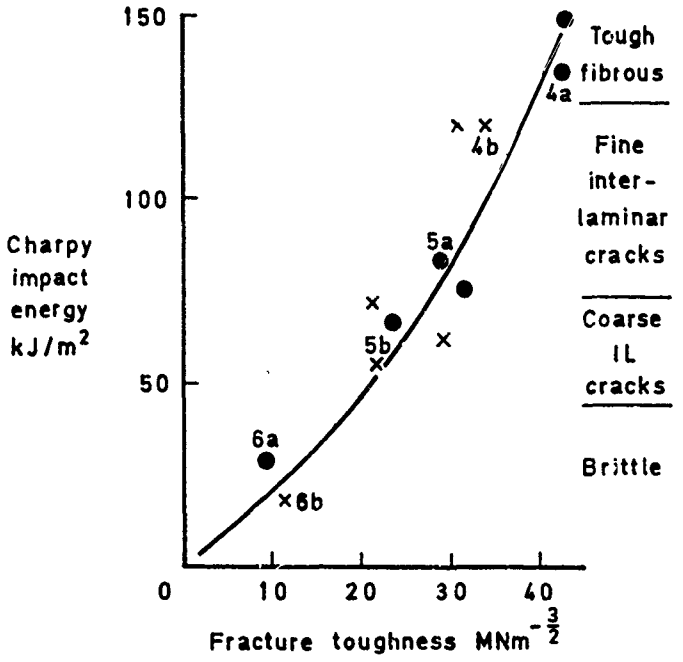

Fig 3 The Charpy impact energies of some CFRP laminates of various fracture toughnesses (lay-ups (a) $[(+45)_2 0_4]_s$, (b) $[0_2, +45_2, -45_2, 0_2]_s$).

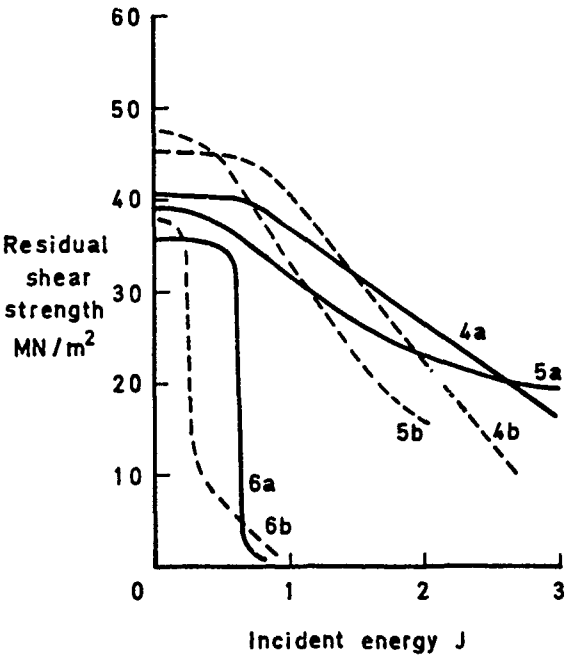

Fig 4 The effect of drop-weight impact on the residual interlaminar shear strength of some CFRP laminates.

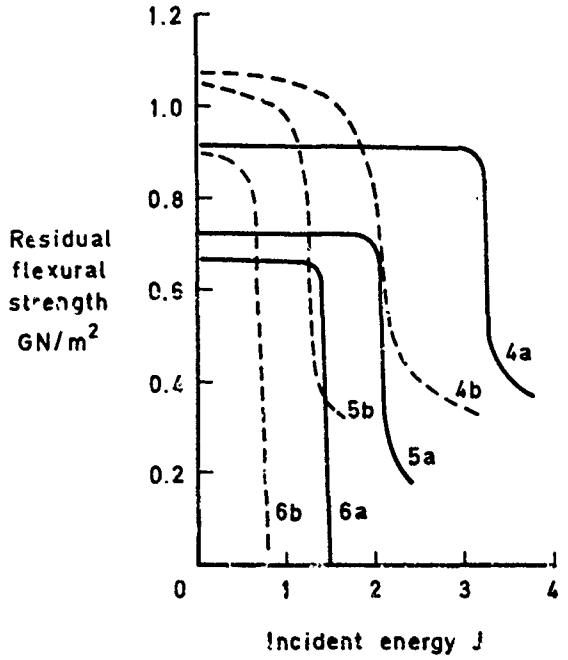

Fig 5 The effect of drop-weight impact on the residual flexural strength of some CFRP laminates.

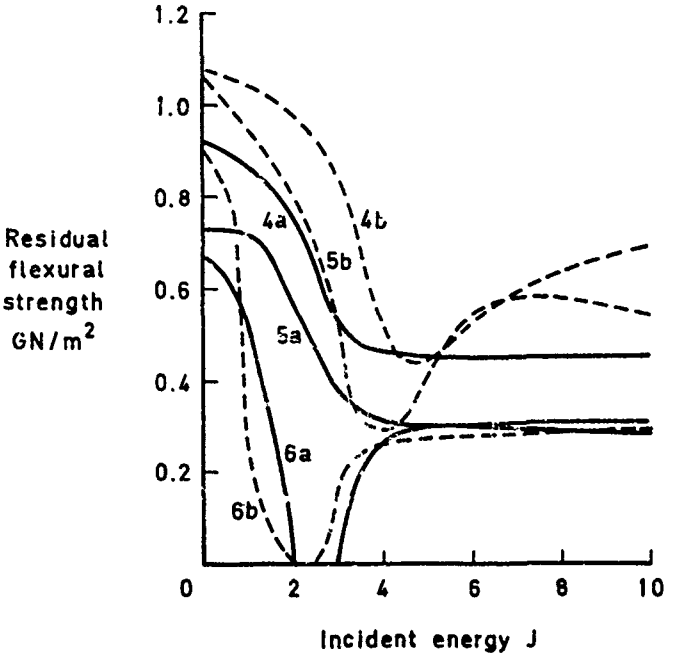

Fig 6 The effect of impact by a 6 mm diameter steel ball from an airgun on the residual flexural strength of some CFRP laminates.

TECHNICAL LIBRARY
ABBOTTAEROSPACE.COM

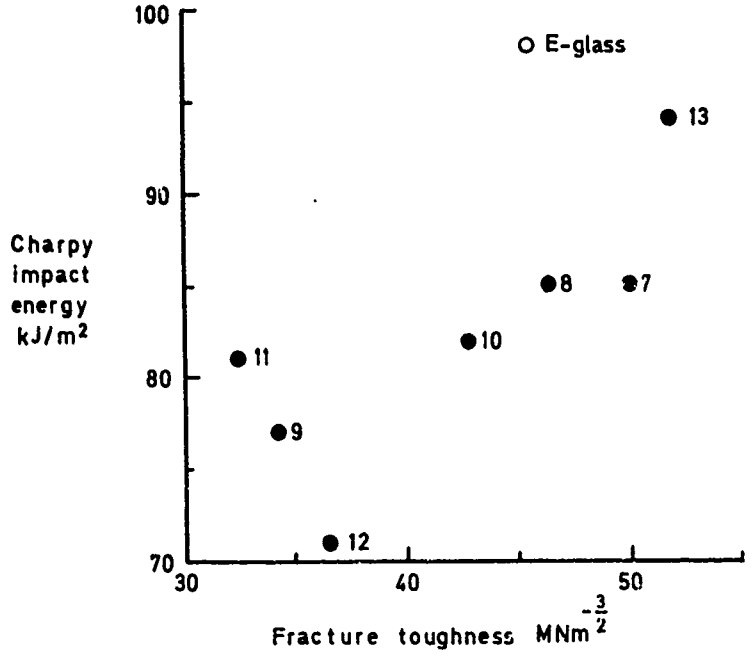

Fig 7 The Charpy impact energies of some CFRP laminates of various fracture toughnesses, and for a GRP laminate whose Charpy impact energy has been factored to allow for the difference in Young's modulus (lay-up $[0, 90, 0, \pm 45, 0]_s$).

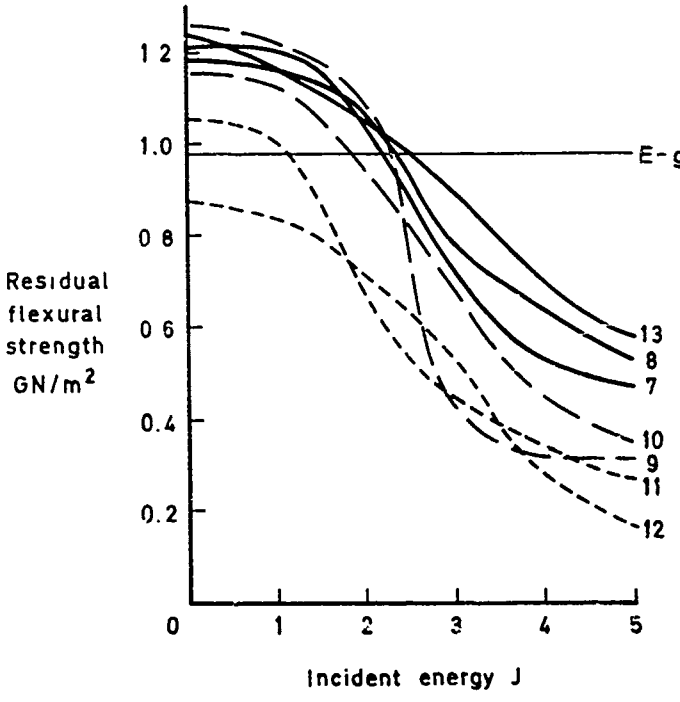

Fig 8 The effect of drop-weight impact on the residual flexural strength of some composite laminates.

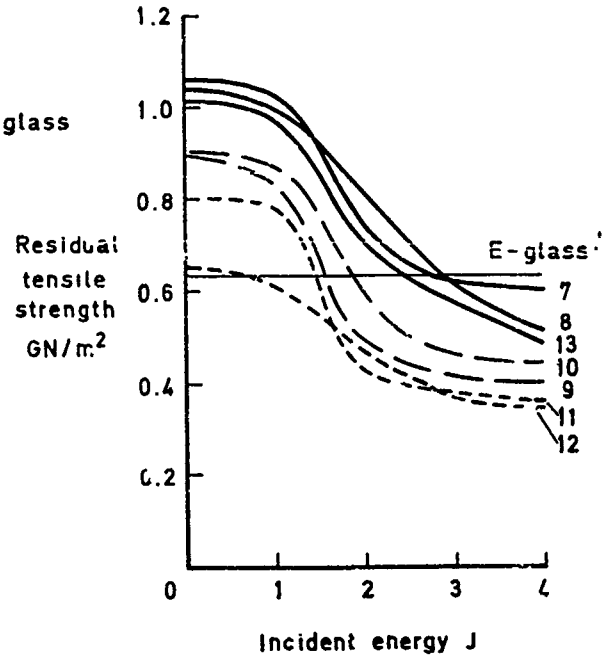

Fig 9 The effect of ballgun impact on the residual tensile strength of some composite laminates.

TECHNICAL LIBRARY
ABBOTTAEROSPACE.COM

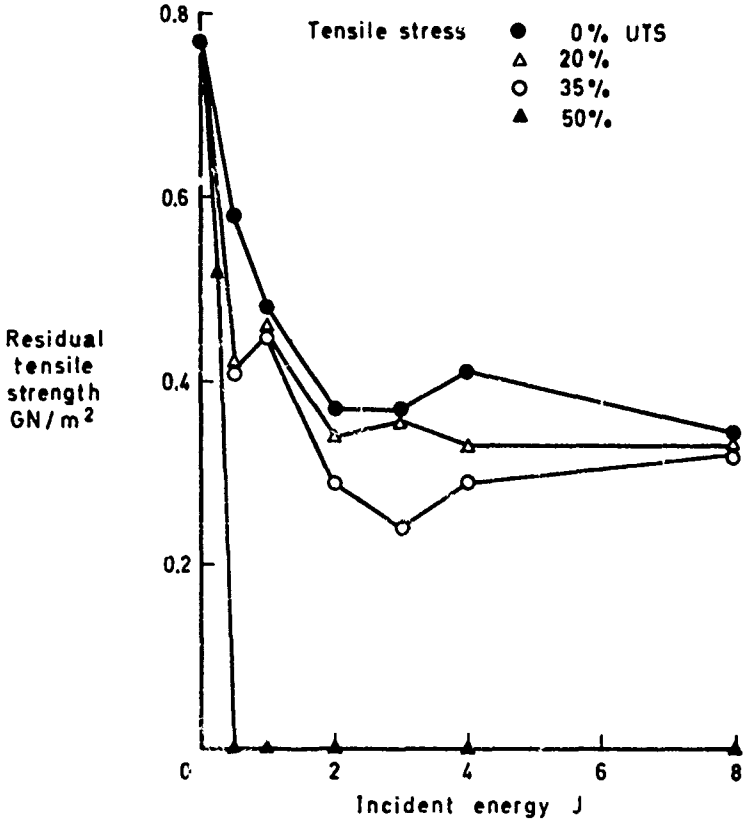

Fig 10 The effect of ballgun impact on the residual tensile strength of a CFRP laminate (laminate 14) that carried a static tensile stress during impact.

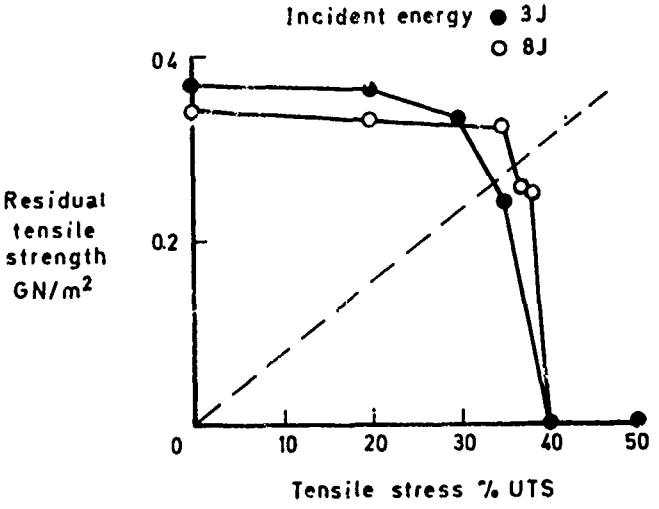

Fig 11 The effect of static tensile stress, during ballgun impact, on the residual tensile strength of a CFRP laminate (laminate 14).

TECHNICAL LIBRARY
ABBOTTAEROSPACE.COM

EROSION ET IMPACTS SUR LES PALES D'HELICOPTERES EN COMPOSITES

par M. TORRES
Département Recherches
SNIAS Division Hélicoptères
13722 - MARIGNANE

RESUME

Les rotors d'hélicoptères sont soumis à un certain nombre d'agressions, liées à l'environnement dans lequel ils doivent évoluer. L'utilisation de matériaux nouveaux tels que les composites verre/époxy et carbone/époxy impose au constructeur des programmes d'essais de qualification spécifiques à chacune de ces agressions.

Cet exposé présente les modes de dégradation du type érosion (à la pluie et au sable) et impacts (civils et militaires) sur les pales en matériaux composites.

Les essais réalisés à la tour d'érosion ont permis de sélectionner les matériaux de protection les plus efficaces.

L'expérience en utilisation ainsi que les essais de tirs et d'impacts réalisés sur pales ont montré un excellent comportement en fatigue après les chocs ou impacts, dû en grande partie au caractère fail safe des matériaux composites. Ce bon comportement, associé à des possibilités de réparation très étendues, est un facteur important contribuant à la supériorité des pales en composites sur les pales métalliques.

Les premières pales d'hélicoptères en matériaux composites produites en série furent celles du SA 341 Gazelle, dès 1971. La fibre de verre fut choisie sous forme de rubans pour constituer le longeron, et sous forme de tissu pour les revêtements et renforts. Puis apportant un allègement notable, le carbone à haut module fut introduit sur les revêtements des pales du SA 360 Dauphin en 1974 et du SA 330 Puma en 1975.

L'utilisation de ces matériaux permit d'étendre la durée de vie des pales jusqu'à une valeur infinie pratique, et d'accroître les performances des hélicoptères grâce aux possibilités de réalisation de formes évolutives et de profils performants.

Les rotors d'hélicoptères sont soumis à un certain nombre d'agressions, liées à l'environnement dans lequel ils doivent évoluer :

- Des conditions climatiques très variables : domaine de température s'étendant de -54° à +70°, degré hygrométrique allant jusqu'à 100 %, conditions givrantes pouvant entraîner des accumulations au bord d'attaque, possibilités de foudroiement, pluie et grêle engendrant une érosion et des impacts dans la zone du bord d'attaque.

- Des impacts, chocs ou érosions, liés à l'utilisation : chocs en manutention, collisions, impacts divers (cailloux, arbres, oiseaux, etc...), érosion au sable, impacts militaires.

L'utilisation de matériaux nouveaux tels que les composites verre/époxy et carbone/époxy impose au constructeur des programmes d'essais de qualification spécifiques à chacune de ces agressions.

Nous présentons dans cet exposé les modes de dégradation du type érosion (à la pluie et au sable) et impacts (civils et militaires), l'expérience et les essais réalisés dans ces domaines, et les choix technologiques effectués pour les protections et les réparations.

1. EROSION

Les vitesses en extrémité de pales sont élevées : 200 à 220 m/s en stationnaire et 280 m/s en croisière rapide. Les effets de l'érosion sont donc importants et les répercussions sur le fonctionnement de l'appareil peuvent être extrêmement néfastes :

- Diminution des performances par perte des caractéristiques aérodynamiques des profils,
- Augmentation des contraintes, des efforts de commande,
- Vieillissement accéléré des résines par l'eau et les rayons ultra violets, dont la pénétration se trouve facilitée par les piqûres dû à l'érosion.

L'érosion sur les pales d'hélicoptères peut être causée par deux facteurs : le sable et la pluie.

Pour étudier les mécanismes de l'érosion et évaluer les différentes protections, un moyen d'essai particulier a été mis en place :

This Document Provided by the ABBOTT AEROSPACE
TECHNICAL LIBRARY
ABBOTTAEROSPACE.COM

1.1. La tour d'érosion (figures 1 et 2)

D'un diamètre de 4,5 m et d'une hauteur de 4,2 m, elle enferme un rotor bipale de 2,9 m de diamètre.

La vitesse en bout de pale est de 225 m/s, et l'incidence peut être réglée entre -6 et +6°.

Un premier dispositif constitué d'une moto-pompe et d'une buse à grand diamètre simule une pluie avec un débit de 4 litres/minute, correspondant à un taux de précipitation de 20 mm/heure. Le diamètre des gouttes rotor arrêté est de 1,9 à 2 mm.

Un deuxième dispositif utilisant un pistolet à dépression d'air projette du sable de bas en haut, avec un débit de 180 grammes/minute. Les particules ont un diamètre compris entre 0,04 et 0,17 mm.

Les essais préliminaires ont montré que les incidences correspondant au maximum d'érosion étaient de 4° pour les essais au sable et 0° pour les essais à la pluie.

La corrélation entre les essais à la tour et les processus naturels d'érosion chez les clients est très difficile à établir. Ce moyen d'essai permet toutefois d'effectuer des comparaisons entre les différents types de protections.

Quelques résultats d'essais sur hélicoptère en environnement naturel nous ont permis de fixer une durée d'essai à la tour, devant couvrir en moyenne 2000 heures de fonctionnement chez l'utilisateur :

- 30 heures pour les essais à la pluie
- 20 heures pour les essais au sable.

Ces chiffres sont basés sur les hypothèses suivantes :

- Temps de fonctionnement sous la pluie égal à 20 % du temps de vol en pays humide
- Temps de rotation avec environnement de sable égal à 2 % du temps de vol total.

1.2. Les mécanismes de l'érosion

A cause des différences de masse et de constitution entre les gouttes d'eau et les grains de sable, on constate des processus d'érosion très différents :

- Les particules de sable susceptibles d'être soulevées par le rotor ont une faible masse : moins de 15 milligrammes, ce qui correspond à des diamètres inférieurs à 100 microns.

  Leur trajectoire au niveau du bord d'attaque suit donc partiellement les lignes de courant, et la zone érodée peut s'étendre vers le bord de fuite.

  Les essais à la tour ont montré que le long d'un profil, l'intensité de l'érosion était fonction de l'angle d'incidence, le maximum se situant dans deux zones situées de part et d'autre de la zone frontale (figures 3, 5 et 6).

  Par ailleurs, on a pu constater sur les rotors en utilisation chez les clients qu'il existe une zone d'érosion d'intensité modérée, de forme triangulaire à l'intrados, en extrémité, suivant une répartition illustrée sur la figure 7.
  Le mécanisme de l'érosion par le sable est tel que, pour chaque point de la surface érodée, le taux d'érosion est constant du début à la fin de l'essai, ce taux variant comme le cube de la vitesse locale.

- A la pluie, les détériorations localisées sur la zone frontale du bord d'attaque sont dues au martelage des gouttes d'eau ; elles sont constituées par des piqûres ou des micro-cratères rapprochés (figures 4, 5 et 6).

  Compte tenu de la grosseur des gouttes d'eau, les effets mécaniques ou aérodynamiques de ces dégradations seront d'autant plus importants que les dimensions de la pale seront faibles.

  Les énergies d'impact développent dans les revêtements des champs de contraintes modulées de compression et de cisaillement. Ainsi apparaissent après une période plus ou moins importante, dite période d'incubation, soit des décollements, soit des micro-fissures de fatigue puis des arrachements de matière, soit des ondulations dues à des allongements locaux du revêtement.

La figure n° 5 montre la répartition en corde des zones d'érosion, pour un profil NACA 0012 aux incidences de -6, 0 et +6°.

On peut constater que, dans certains cas, il peut y avoir un chevauchement des zones d'érosion maximale à la pluie et au sable.

TECHNICAL LIBRARY
ABBOTTAEROSPACE.COM

1.3. Matériaux de protection

Les composites verre/époxy et carbone/époxy, particulièrement sensibles à l'érosion, doivent donc être protégés.

Cette protection doit satisfaire les impératifs suivants :

- Bonne résistance à l'érosion, à la pluie et au sable
- Bonne tenue à la fatigue aux allongements imposés par les déformations de la pale
- Collage efficace, résistant aux sollicitations provoquées par les mouvements de la pale, et à des accélérations centrifuges voisines de 1000 g.
- Remplacement aisé chez le client.
- Prix de revient modéré.

De nombreux matériaux ont été comparés au travers d'essais à la tour d'érosion ; le tableau en annexe présente une sélection de résultats d'essais.

A l'analyse de ce tableau, on peut distinguer deux grandes catégories de matériaux : les métalliques, et les thermoplastiques polyuréthanes.

Les métalliques se caractérisent par une bonne tenue à la pluie et une tenue au sable médiocre.

Avec ce type de matériaux, une épaisseur minimale doit être respectée pour éviter les risques de "martelage" par les gouttes d'eau.

L'acier inox à 90 hectobars réalise un des meilleurs compromis, avec une vitesse d'érosion au sable à la tour de 0,2 mm/heure.

Mais les difficultés de formage de ce matériau sont telles qu'il ne peut être utilisé en une seule pièce, la protection étant alors constituée de plusieurs segments reliés par des cavaliers de jonction.

Cette solution, satisfaisante dans des conditions de fonctionnement normales, ne peut être retenue pour des pales devant voler en conditions givrantes : en effet, les bordures des cavaliers sont des zones préférentielles d'accumulation du givre.

Dans ce cas, la coiffe de protection ne doit former qu'une pièce, ce que permettent de réaliser le titane ou le nickel.

Parmi les alliages de titane, le TA6V présente de bonnes performances à la pluie, mais le taux d'érosion au sable est prohibitif.

Les performances des T40 et T60 sont moyennes.
Le traitement du T40 par nitruration ionique améliore sa tenue à la pluie, lui permettant de franchir le cap des 30 heures ; au sable, aucune amélioration notable n'est constatée.

Le T40 nitruré est donc, parmi les alliages de titane, celui qui présente les meilleures caractéristiques.

Le Nickel, obtenu par électroformage, se présente comme le meilleur de tous les matériaux métalliques ; sa tenue à la pluie est excellente, et son taux d'érosion au sable est de l'ordre de 0,15 mm/heure à la tour d'érosion.

Un dépôt électrolytique de nickel sur une coiffe en inox ou en titane présente les caractéristiques du nickel jusqu'à dégradation de celui-ci, puis celles de la coiffe support.

Les thermoplastiques polyuréthanes se caractérisent par une tenue au sable acceptable et une mauvaise tenue à la pluie.

De nombreuses expérimentations effectuées sur ces produits ont fait apparaître une dispersion importante dans les résultats, due en particulier :

- au mode de fabrication
- à la dureté
- à l'épaisseur
- à l'état de vieillissement du revêtement
- aux contraintes internes résultant de l'emploi de revêtements plans pour l'habillage de formes convexes.

Ces matériaux sont utilisés aujourd'hui sous deux formes :

- bandes de 0,65 mm d'épaisseur, pour des zones à faible vitesse (jusqu'à 0,8 R), ou pour les protections d'intrados en extrémité.
- bandes autocollantes de 0,4 mm d'épaisseur, collées sur les coiffes métalliques ou à l'intrados en extrémité lorsque l'érosion au sable est à craindre.

TECHNICAL LIBRARY
ABBOTTAEROSPACE.COM

1.4. Solutions retenues

Aucun matériau n'offre donc de protection efficace à la fois contre la pluie et le sable.

Les solutions retenues aujourd'hui réalisent un compromis acceptable, mais susceptible d'être encore amélioré :

Pour les pales non dégivrées, le bord d'attaque est protégé dans la zone d'extrémité (après 0,8 R environ) par une coiffe en acier inoxydable épais. De l'attache à 0,8 R, la coiffe de bord d'attaque peut être réalisée en inox plus mince ou en polyuréthane.

La zone triangulaire à l'intrados en extrémité, exposée à l'érosion au sable, est recouverte de polyuréthane. En cas d'utilisation intensive en zone désertique, l'application de bandes auto-adhésives de polyuréthane, renouvelées périodiquement, permet de protéger les coiffes en inox.

Pour les pales dégivrées, la coiffe de protection, nécessairement continue, est réalisée en titane embouti.

1.5. Maintenance

Sur les coiffes métalliques, les rayures, chocs, criques, ou décollements partiels sont admis. Par contre, le remplacement de la coiffe est impératif en cas de perforation due à l'érosion ou à des impacts, ou en cas de décollements importants.

Les protections en polyuréthane, sous l'effet de l'érosion ou du vieillissement, peuvent se dégrader rapidement ; en cas de perforation, cloquage ou décollement, le client doit alors réparer ou remplacer la protection.

2. CHOCS-IMPACTS

Les pales d'hélicoptères peuvent subir au cours de leur vie différents types de dommages :

- chocs, rayures, au cours des opérations de manutention,
- chocs et impacts en exploitation : heurts d'arbres, impacts de cailloux ou d'oiseaux, collisions,
- impacts militaires.

Les matériaux composites ont permis d'améliorer considérablement le comportement des pales d'hélicoptères dans ce domaine : grâce à leur caractère fail safe, les dégradations restent limitées et se propagent lentement ; par ailleurs, grâce à leur faible densité, les épaisseurs de matériaux mises en jeu dans la zone du bord d'attaque sont souvent plus élevées que celles des matériaux métalliques, ce qui a pour effet d'accroître la tenue à la compression, donc la tenue aux chocs frontaux par exemple. Ces propriétés peuvent être illustrées par un certain nombre d'exemples :

2.1. Chocs et impacts en exploitation

Le travail en moyenne montagne, l'exploitation forestière, le transport de commandos, ou le vol tactique, imposent quelquefois de voler à proximité des arbres, et les cas d'interférences sont nombreux.

Pour vérifier le comportement des pales principales dans cette situation, des essais spécifiques ont été réalisés. Ces essais, réalisés sur un rotor de SA 341 Gazelle, ont consisté à introduire des branches d'un diamètre croissant dans le rotor.

Les principaux résultats ont été les suivants :

- jusqu'à un diamètre de 70 mm, les dégâts sont très faibles et on ne constate pas d'augmentation des contraintes ou des efforts de commande.
- Des branches de bois vert de diamètre 120 mm puis de bois sec de 200 mm ont été introduites (figure 8) : on observe alors des dégradations sur le saumon d'extrémité et des décollements de revêtement au bord de fuite. Ces dégradations n'ont pas d'influence sensible sur les performances, c'est-à-dire que la sustentation et le contrôle de l'appareil restent assurés après l'impact ; bien entendu, le niveau vibratoire se dégrade, mais ce type d'impact survient nécessairement au voisinage du sol et peut donc être suivi d'un atterrissage immédiat.

TECHNICAL LIBRARY
ABBOTTAEROSPACE.COM

Un client, lors d'un atterrissage de nuit en brousse avec le SA 330 Puma, a heurté avec ses pales principales en composites (verre et carbone/époxy) des arbres dont le diamètre était d'environ 200 à 400 mm. Malgré cet incident, l'appareil a poursuivi sa mission pendant 45 minutes. Au retour à la base, on observait sur trois pales des dégradations traversant le revêtement et le remplissage nid d'abeille de l'intrados à l'extrados, sur des surfaces de 300 x 300 mm environ ; sur la quatrième pale, on notait des dégradations plus importantes en surface avec rupture de l'arêtier de bord de fuite.

Après l'expertise, seule la quatrième pale a été rebutée, et les trois autres ont pu être réparées (figure 9).

Dans des circonstances plus malheureuses, en Novembre 1975, un hélicoptère SA 341 Gazelle entra en collision avec un avion du type BONANZA. Malgré des dégradations importantes sur le rotor, l'hélicoptère put atterrir et l'équipage sortit indemne de cet accident (figure 10).

2.2. Impacts militaires

Afin de vérifier le comportement des pales en composites à ce type d'impacts, des essais ont été menés pour :

- observer et analyser les dégradations causées par les projectiles
- apprécier la résistance résiduelle, en statique et en fatigue, après impact.

Les essais de fatigue sont effectués sur des bancs (figure 11) capables de simuler, avec la force centrifuge, des charges de battement et de trainée de 3 à 4 fois les charges maximales de vol. Ces installations, propres à chaque type de pale, permettent de tester séparément la zone d'attache ou la zone de partie courante.

Sur SA 341 Gazelle, des tirs ont été effectués aux calibres 20 mm explosif, 12,7 mm normal, et 7,62 mm NATO non perforant.

Le tir au calibre 20 mm était dirigé perpendiculairement au plan de la pale, à 90 mm du bord d'attaque. Les dégâts constatés sont très importants : l'onde de choc a détruit le nid d'abeille en envergure à l'intérieur du bord de fuite sur une longeur de 430 mm de part et d'autre de l'impact. Les ailes du longeron et le revêtement sont délaminés sur une grande longeur.

Bien qu'aucun essai de fatigue n'ait suivi ce tir, il paraît peu probable qu'un appareil ayant subi de tels dégâts sur une pale puisse se poser sans dommage.

Les tirs au calibre 12,7 mm ont donné les résultats suivants : le premier, perpendiculaire au plan de la pale à 90 mm du bord d'attaque, n'entraîne pas de dommages importants ; le deuxième, dans le plan de la pale et face au bord d'attaque, a dégradé une partie du longeron ainsi que le bord de fuite. Un essai statique a montré que la tenue de la pale était encore supérieure aux efforts centrifuges.

Les tirs au calibre 7,62 mm (figures 12 et 13) ont été effectués sur deux tronçons de pales destinés à être testés ensuite en fatigue : le tir sur le tronçon de partie courante était perpendiculaire au plan de la pale, en plein longeron, dans la zone la plus chargée en contraintes ; le tir sur le tronçon d'attache était dirigé perpendiculairement à l'axe de la pale, a proximité des douilles d'attache.

Les essais de fatigue, effectués aux charges maximales de vol, ont été conduits jusqu'à l'équivalent de 3 heures de vol pour le tronçon d'attache, et 10 heures pour celui de partie courante, sans évolution des dégradations autour des impacts.

Ces essais ont donc permis de démontrer qu'un appareil ayant une ou plusieurs pales endommagées, même dans les zones critiques, peut regagner sa base.

Sur SA 330 Puma, les tirs au calibre 12,7 mm perforant ont été effectués sur trois tronçons de fatigue :

- le premier tir traversait perpendiculairement le tronçon de partie courante, en arrière du longeron ; l'essai de fatigue, conduit en battement pur, a été arrêté à l'équivalent de 23 heures de vol.
- le second, tiré sur tronçon de partie courante, traversait la pale dans le sens de la corde, du bord de fuite au bord d'attaque ; l'essai de fatigue, conduit en battement et trainée avec force centrifuge, a été arrêté à l'équivalent de 66 heures de vol.
- le troisième tir était dirigé sur les douilles d'attache ; l'essai de fatigue, conduit en battement et trainée avec force centrifuge, a été arrêté à l'équivalent de 6 heures de vol.

A l'arrêt des trois essais, aucune évolution notable des endommagements n'a été constatée.

THIS DOCUMENT PROVIDED BY THE ABBOTT AEROSPACE
TECHNICAL LIBRARY
ABBOTTAEROSPACE.COM

La fin d'une mission est donc garantie dans tous les cas de vol, au même risque que celui autorisé pour la certification de pales principales, qui est de 10^{-6}.

3. MAINTENANCE - REPARATIONS

Outre l'inspection quotidienne ou à chaque vol, une dépose des pales est prescrite toutes les 100 ou 300 heures suivant les appareils. Au cours de ces déposes, les pales subissent deux contrôles: contrôle visuel de détail et contrôle acoustique ("taping"), permettant de mettre en évidence les décollements et les délaminages.

Un certain nombre de défauts ou dégradations peuvent être admis sans réparation : rayures ou chocs sur le revêtement en composite présentant des endommagements de faibles dimensions (0,1 à 0,3 mm de profondeur, 20 mm de longueur), criques, rayures, ou impacts sur les coiffes métalliques, décollements du revêtement limités en nombre et en surface, etc...

Les dégradations plus importantes nécessitent une réparation. Les limites des défauts admissibles et les réparations sont parfaitement définis et son justifiés par le constructeur grâce à des essais en fatigue sur des tronçons de pales spéciaux.

Deux niveaux sont alors distingués ; les réparations exécutables chez le client, et celles nécessitant un retour en usine ou chez un réparateur agréé.

Chez le client, la réparation de chocs, d'impacts ou de perforations de dimensions limitées peut être réalisée, par empiècement d'une ou deux couches de tissu de verre enduit de résine époxy. Il peut aussi remplacer les protections de bord d'attaque ou d'intrados en polyuréthane.

Les réparations importantes doivent être effectuées en usine ou, pour certaines, chez un réparateur agréé : remplacement des coiffes métalliques, reconstitution du revêtement par empiècement ou éclissage, remplacement d'une zone de remplissage (mousse ou nid d'abeille), réparation de la languette de bord de fuite par addition de cavaliers en tissu de verre/époxy, reconstitution d'une partie du longeron , etc...

Les possibilités de réparation des pales en composites sont très grandes, et souvent seules des considérations de prix de revient limitent l'importance des réparations effectuées en usine.

4. CONCLUSION

Dans le domaine des pales en composites, l'expérience de 15 ans d'essais de laboratoire et de 10 ans d'utilisation opérationnelle dans 50 pays du monde a permis d'obtenir de nombreuses informations sur leur résistance à l'érosion et aux impacts civils ou militaires.

Les essais réalisés à la tour d'érosion ont mis en évidence les bonnes performances à la pluie de l'acier inoxydable, du nickel, et du titane, ainsi que la supériorité du polyuréthane pour l'érosion au sable.

Des incidents en exploitation et des essais spécifiques ont montré l'excellent comportement au choc des pales en composites, à l'occasion d'impacts d'arbres d'au moins 200 mm de diamètre.

Dans le domaine militaire, les essais de fatigue réalisés après des tirs au calibre 12,7 mm dans les zones critiques de la pale ont montré que l'appareil pouvait dans tous les cas rejoindre sa base.

Ce bon comportement aux chocs et aux impacts dû au caractère fail-safe des matériaux composites, associé à des possibilités de réparation très étendues, est un facteur important contribuant à la supériorité des pales en composites sur les pales métalliques.

TECHNICAL LIBRARY
ABBOTTAEROSPACE.COM

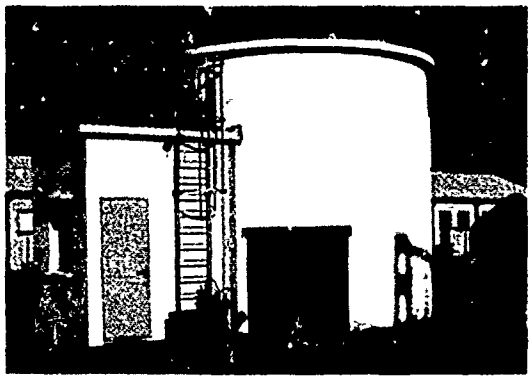

Figure 1 : Tour d'érosion

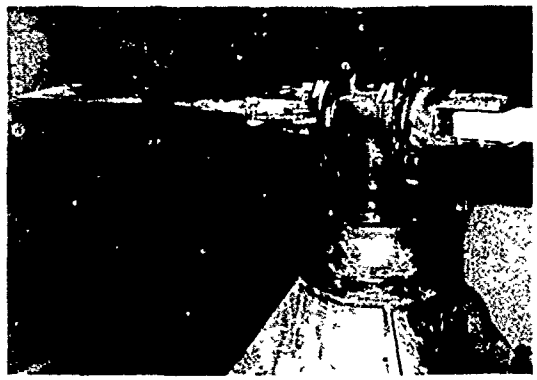

Figure 2 : Rotor pour essais d'érosion

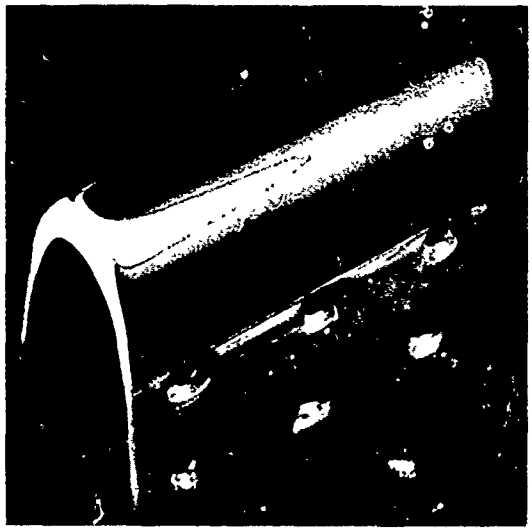

Figure 3 : Eprouvette érodée au sable

Figure 4 : Eprouvette érodée à la pluie

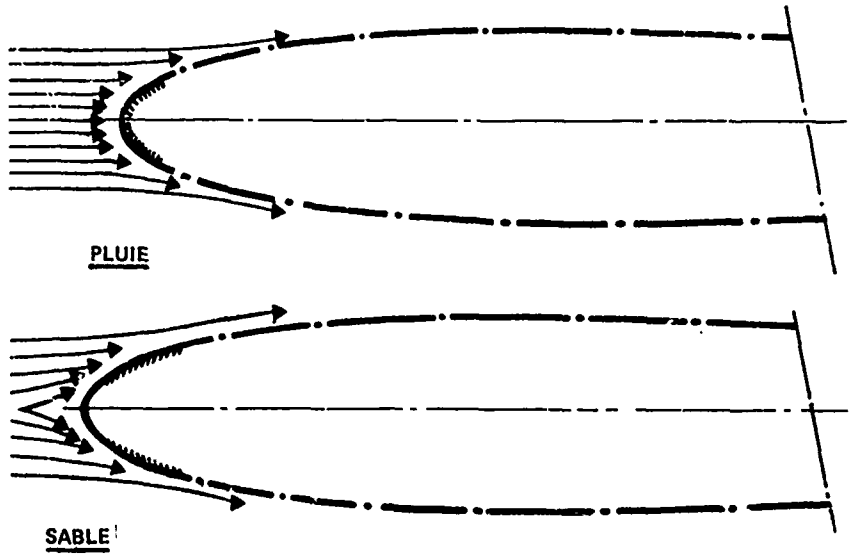

Figure 5 : Processus d'érosion à la pluie et au sable

TECHNICAL LIBRARY
ABBOTTAEROSPACE.COM

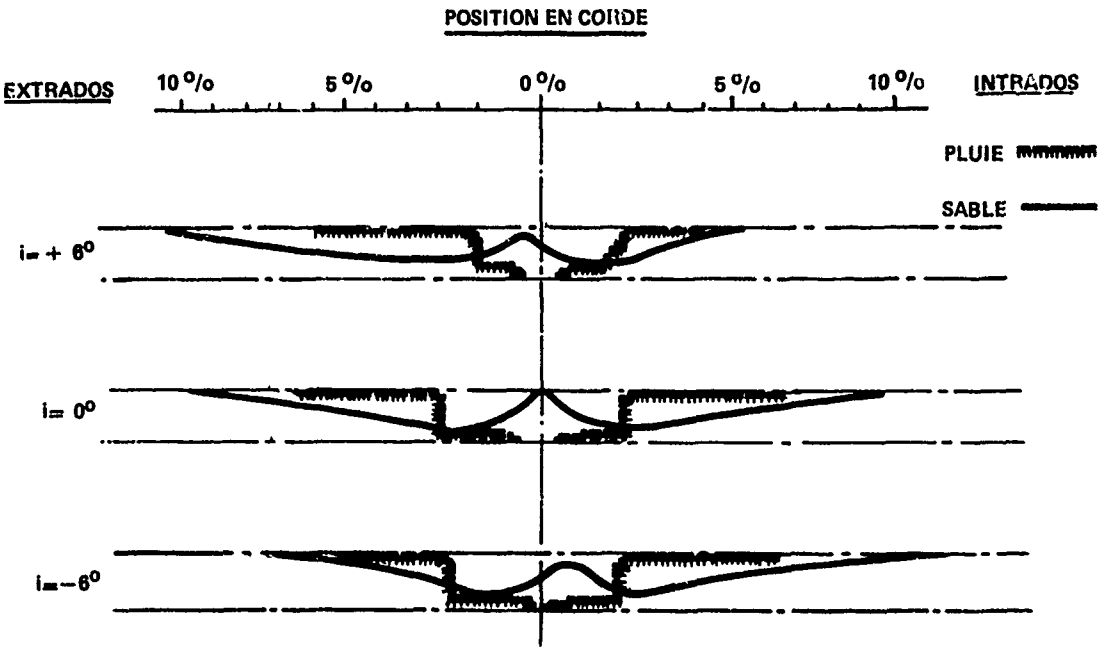

Figure 6 : Zones d'érosion au bord d'attaque

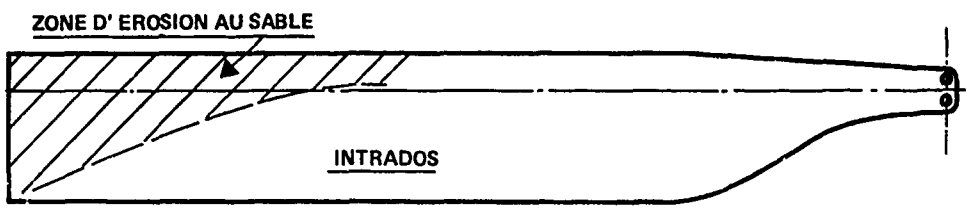

Figure 7 : Profil d'érosion à l'intrados en extrémité

Figure 8 : Rupture d'une perche de bois de 200 mm x 200 mm par des pales Gazelle.

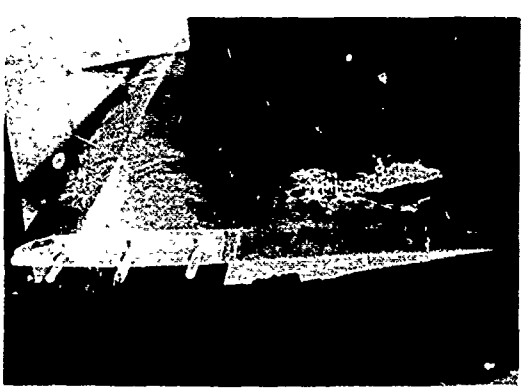

Figure 9 : Pale PUMA détériorée, avant réparation.

THIS DOCUMENT PROVIDED BY THE ABBOTT AEROSPACE
TECHNICAL LIBRARY
ABBOTTAEROSPACE.COM

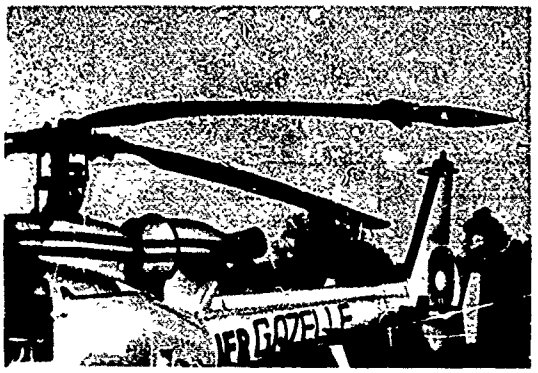

Figure 10 : SA 341 Gazelle après une collision avec un avion léger

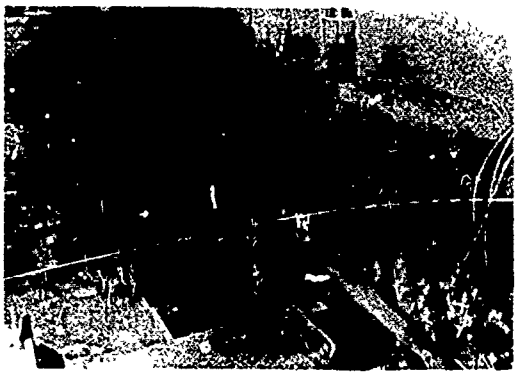

Figure 11 : Essai de fatigue sur pale Puma

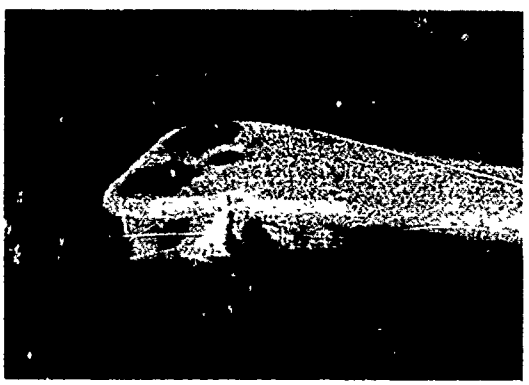

Figure 12 : Tir au calibre 7,62 mm sur attache de pale Gazelle

Figure 13 : Tir au calibre 7,62 sur partie courante de pale Gazelle

THIS DOCUMENT PROVIDED BY THE ABBOTT AEROSPACE
TECHNICAL LIBRARY
ABBOTTAEROSPACE.COM

ANNEXE

ESSAIS D'EROSION

MATERIAUX	EROSION A LA PLUIE Temps d'incubation (heures)	EROSION AU SABLE Vitesse d'érosion (mm/heure)
ACIER INOX 90 hb	20	0,2
TITANE TA6V	> 30	0,5
TITANE T40	> 10	0,2
TITANE TU2, T40 nitruré	> 30	0,2
NICKEL	> 30	0,15
POLYURETHANES	1 à 5	0,05

TECHNICAL LIBRARY
ABBOTTAEROSPACE.COM

GRAPHITE-EPOXY PANEL COMPRESSION STRENGTH REDUCTION DUE TO LOCAL IMPACT

by

Michael F.Card and Marvin D.Rhodes
NASA Langley Research Center
Hampton, Virginia 23665, USA

SUMMARY

A review of results from on-going research to investigate the effects of low-velocity impact on the compressive strength of graphite-epoxy structures is presented. Extensive tests have been conducted on sandwich beams, laminated plates and stiffened panels. Conditions for failures were investigated by impact tests on statically loaded test specimens.

The effects of compression load intensity were such that lightly loaded graphite structures (such as aircraft secondary structure) were insensitive to impact damage. In more heavily loaded structures, (such as wing panels), however, appreciable reductions in compressive strength occurred. The implications of the tests for structural design are discussed by comparing panel masses for designs where ultimate strains have been reduced due to impact considerations with the masses of designs with higher ultimate strains. Finally, preliminary test data is presented to show the possibility of improvements in damage tolerance achievable by using an alternate matrix material.

INTRODUCTION

In the evaluation of filamentary-composite structures for highly stressed aircraft applications, the tolerance of the structure to low-velocity impact damage deserves serious consideration. Unlike metallic structures, composite structures (especially those reinforced with graphite or boron filaments) have exhibited unique failure characteristics in the presence of both high and low velocity impact.

The traditional method of assessing the impact resistance of a material is the notched bar impact test using Charpy and/or Izod impact test apparatus. In this test, a notched specimen in the form of a supported beam is impacted by a pendulum sufficient to fail the specimen in one blow. This test technique has traditionally been used to identify metals that display normal ductility in tension tests but may break in a brittle fashion when tested by a single overload of stress in the notched condition (Ref. 1).

In recent years, the pendulum of the test apparatus has been instrumented to evaluate the load-time material behavior. By applying this test technique to composites, investigators have attempted to determine the energies associated with failure initiation and failure propagation due to impact. However, the impact response of polymer-matrix composite materials is not well defined and many of the existing experimental results appear to be in conflict (Ref. 2).

The purpose of the present report is to summarize the results of an extensive experimental investigation conducted at NASA's Langley Research Center of low-velocity impact damage on composite materials and structural elements (Refs. 3 to 8). In the Langley test program, instead of using the notched bar test, direct measurement of strength reduction was made by impacting the surface of loaded beams, plates and panels with a small projectile and the combined effect of applied in-plane load and surface impact was investigated. The results indicated that notable reductions in strength could be caused by low-velocity impact damage. The tests were conducted primarily on structural specimens loaded in compression; however, some tests were conducted on specimens loaded in tension (Ref. 5).

In the present report, the test specimens and test apparatus used in the investigation are described. Techniques for observing damage during and after impact are reviewed, and the characteristics of damage behavior are discussed. Typical results showing compression strength reductions of sandwich beams, laminated plates, and stiffened panels as functions of impact velocity are presented. The implications of the results for aircraft design are discussed, and preliminary data on the effect of material changes are presented to suggest possible future improvements in damage resistance.

TEST SPECIMENS

Three types of test specimens were used in the investigation: sandwich beams, laminated plates, and stiffened panels. In Figure 1(a) a typical graphite-epoxy sandwich beam is shown. The back face of the specimen is a .32 cm thick steel plate. The sandwich beam specimens were loaded in a four-point beam bending fixture to obtain a

TECHNICAL LIBRARY
ABBOTTAEROSPACE.COM

uniform compressive or tensile loaded test area 7.6 by 7.6 cm in the middle of the specimen.

A typical laminated plate test specimen is shown in Figure 1(b). The plate is simply supported on its sides by two adjustable edge supports and clamped on the top and bottom ends where load is applied.

A typical stiffened panel specimen is shown in Figure 1(c). Panels were either hat-stiffened or blade-stiffened plates that were designed with minimum mass to carry specified compression loads over a specified panel length. The ends of the stiffened panel were potted in a filled epoxy resin while the sides were unsupported.

The epoxy materials used in specimen fabrication were commercially available 450K cure thermosetting systems. The graphite fiber was a high strength continuous filament type and was used in both unidirectional tape and bidirectional balanced weave fabric forms. A test matrix for the test specimens is presented in Table I indicating principal test objectives. Further details can be found in Refs. 3 to 8.

TEST TECHNIQUES

Impact Apparatus

Aluminum spheres, 1.27 cm in diameter with a mass of 3 grams, were used as the impact projectiles. An air gun was used to propel each projectile. As illustrated in Figure 2(a), compressed air is used to pressurize a reservoir, until a thin Mylar diaphragm at one end of the reservoir ruptures. The air in the reservoir is then metered through an orifice plate and subsequently drives the projectile down the barrel. An electronic velocity detector at the end of the barrel is used to measure projectile velocity. The projectile passes through two light beams which trigger electronic timing equipment to record the travel time between beams. The impact conditions were selected to simulate energies from small rock or hailstone damage (such as that occurring during an aircraft take-off or landing) to large hailstones and dropped tools.

The test setup for a typical panel is shown in Figure 2(b). In this case, the panel shown is loaded in compression by the platens of a testing machine. In all tests the impact was normal to the specimen surface. Specimens were damaged by impact at different velocities while subjected to static load to determine the combination of impact and load necessary to cause failure. Specimens which did not fail or which were damaged without load were statically tested to determine the effect of local damage on residual strength.

Failure Observation Techniques

As indicated in Figure 3, several different techniques were used after each test to evaluate damage created by impact. Visual observation was used to detect surface damage on both the front and back sides of the specimens. Many specimens were sectioned and photographed using conventional and electron scanning microscopes (Fig. 3(a)) to observe crack patterns and interface delamination. Ultrasonic C-scan techniques (Fig. 3(b)) were used to determine the size of damaged regions. For some tests, brittle lacquer coatings (Fig. 3(b)) were applied on the side of the specimen opposite the impacted side, and the resulting spallation patterns were found to give good agreement with C-scan damage patterns.

Finally, during residual strength tests, out-of-plane deformations were observed to investigate local damage propagation. The shadow moiré fringe technique was used and a typical example for a panel is shown in Figure 3(c). The out-of-plane deformations were due to loading eccentricities imposed by local impact damage and local buckling of surface plies from impact-induced delamination.

RESULTS AND DISCUSSION

Impact Damage Appearance

Typical local damage in the face sheet of a sandwich beam test specimen is presented in Figure 4(a). The damage shown is typical of the minimum damage that is visually detectable in sandwich structures of this type. The initial damage is a square plug with two sides parallel to the direction of the surface fibers. The plug is divided into approximately equal sections by a cross-shaped crack. The damaged surface area is about the same diameter as the projectile. Damage in the laminate interior was about the same as that observed on the surface. In contrast to laminated plate and stiffened panel specimens, the presence of the sandwich core appeared to confine damage (prior to failure) to this local area.

The appearance of damage in graphite-epoxy plate specimens is shown in Figure 4(b). The first visible evidence of impact damage is a crack on the back surface of the specimen as shown in the lower left photo of Figure 4(b). For the specimen shown that

TECHNICAL LIBRARY
ABBOTTAEROSPACE.COM

was impacted at the lower velocity, there is no visual indication of damage in the contact region. At higher impact velocities, the side opposite the impact location has a large region with surface cracks (right side of Fig. 4(b)) and portions of the surface ply have either delaminated or spalled off. The only evidence of damage in the region of contact was a shallow circular depression about two-thirds of the projectile diameter. Similar observations were made on stiffened panel specimens. All plate and stiffened panel specimens had a larger region of visible damage on the specimen surface opposite the impact location than in the contact region.

Interior Damage

Selected specimens were cross-sectioned to examine the specimen interior after impact. Some typical cross-sections of plate specimens impacted at different velocities are shown in Figure 5. The interior cracking in Figure 5(a) is similar to the fracture [illegible] brittle plate which has been impulsively loaded on one surface. The basic fracture pattern is conically shaped with the apex toward the contact side. This specimen has no visible surface damage. Interior damage of this type is typical of the damage that is first observable in the cross-section of the laminates tested in this investigation. The interior cross-section shown in Figure 5(b) is similar to that shown in Figure 5(a) in that the same basic conical shaped boundary can be seen. In addition, there is considerable intraply cracking and delamination in the conical shaped regions. Although the side of the specimen opposite the impact location did exhibit some surface damage, the interior damage covers a much larger region than visual inspection would indicate.

Examination of the cross-section of laminates indicated that delamination due to impact is more pronounced at interfaces where there is a major change in the angle between plies, e.g., at interfaces between 0° and 45° plies or 0° and 90° plies. Several of these delamination sites were examined with the aid of a scanning electron microscope. Photographs of two typical sites are shown in Figure 3(a). In both cases, there is no splitting of the fibers which suggests that impact-initiated delamination in graphite-epoxy laminates is associated with matrix failures or failures in the fiber to matrix bond.

Damage Sequence

The damage patterns observed suggest a possible sequence for laminate damage to occur due to low-velocity impact. As illustrated in the schematic drawing of Figure 6, local failures are created within the laminate and are probably due to reflection of a stress wave from the back surface. A specimen with such damage would have a reduced local bending stiffness and could deform locally out-of-plane as the projectile decelerates. Such local distortion was observed on several plate specimens. The superimposed compression load could couple with the local out-of-plane deformation to cause the damage to propagate or to cause additional delamination and intraply cracking to develop.

Effect of Impact Damage on Compression Strength

Typical trends of strength reductions plotted as a function of impact kinetic energy are shown in Figure 7(a) and 7(b) for sandwich beams and laminated plates. In Figure 7(a), the solid symbols indicate failure data whereas the open symbols denote conditions where the combination of impact and applied load did not cause failure. A line has been faired through the data to suggest a failure threshold curve. The curve in Figure 7(a) indicates that for the laminate tested, when compressive loading strains are below 50% of the maximum strength of the beam, beams are insensitive to impact damage. However, if the compression strain is higher than 50% of the maximum beam strength, serious reductions of strength occur. The locations of the visible and invisible damage regions shown in Figure 7(a) suggest that surface inspection is inadequate to detect very low-velocity damage. The x-marks on Figure 7(a) indicate the residual strength obtained from the three beams which did not fail on impact. The data shown in Figure 7(a) is for a graphite-epoxy beam made of 181-style cloth with a $[0_2]$ layup. Results obtained for other orientations using graphite tape, Kevlar, and Kevlar-graphite hybrids are similar and can be found in Reference 5. Comparable results were observed for beam laminates loaded in tension, although damage propagation mechanisms are probably different.

In Figure 7(b), typical results for laminated plates are presented. The failure threshold curve shows that plates loaded with compressive strains below about .003 strain are insensitive to impact damage. For higher loads, serious reductions in strength may occur. The data shown in Figure 7(b) is for a 48-ply $(\pm 45/0_2/\pm 45/0_2/\pm 45/0/90)_{2s}$ graphite-epoxy laminate. These trends were found to be typical for several ply orientations, and mixtures of tape and cloth. (See Refs. 6 and 7.)

In Figure 7(c), typical results for graphite-epoxy stiffened panels are shown. For each of three designs, the applied panel compressive strain at failure is compared with the design strain at buckling denoted by the dashed lines. The lightly loaded panels (Design A) achieved their design strength in the presence of impacts of 51-54 m/s on critical stiffener locations, and were insensitive to low-velocity impact damage. The heavily loaded design (Design B) experienced serious strength reductions when impacted on stiffeners at velocities ranging from 51 to 63 m/s, and hence were found to be damage

TECHNICAL LIBRARY
ABBOTTAEROSPACE.COM

sensitive. A similar damage sensitivity was detected in the boron-graphite hybrid panels (Design C). In all three panel designs, impact damage on +45 skins of the panels between stiffeners did not significantly reduce the strength of these panels. Comparable results for blade-stiffened panels can be found in Ref. 8. In Figure 8, a photograph of a hat-stiffened panel is shown after failure has occurred under impact and compression load. In this case, the impacting sphere struck the outermost surface of the third stringer from the left side of the photograph. The appearance is typical of failures observed in beam, plate and stiffened panel specimens.

Aircraft Panel Design Implications

Tests conducted during this investigation indicate that considerable reductions in strength occur due to defects introduced by low-velocity impact. Even damage that is not visually detectable may cause appreciable degradation in compression strength. This situation is of special concern because imposing inspection criteria more severe than the visual procedures currently employed throughout the air transport industry is probably unacceptable to the airlines and may severely restrict the use of composites by the aircraft manufacturers. Although composites have been introduced into commercial service in secondary structural components (such as through NASA's Aircraft Energy Efficiency (ACEE) Program), these articles are designed by stiffness requirements and operate at low design-ultimate-strains where impact damage does not degrade structural performance. Heavily loaded primary structures such as wing or fuselage panels are designed by material strength, and current aluminum components typically have design ultimate strains well above the impact-sensitive strain levels observed for composites in this investigation. For example, a typical distribution of compressive ultimate strains in the wing of current commercial aircraft is presented in Figure 9(a). If, (based on impact considerations), a strain of .0030 is considered as a design ultimate level for composite structures, most of the wing surface operates in an impact-sensitive regime. Thus, heavily loaded composite wing structures deserve careful attention in assessment of damage vulnerability.

To obtain flight experience on composite primary aircraft structures it has been proposed to conduct a flight service program on a transport aircraft with a composite retrofit wing. Preliminary studies have been conducted and the results indicate that using current composite materials and technology the design ultimate strain may be limited by impact damage. An investigation has been conducted to assess the consequence on panel structural efficiency of limiting the design ultimate strain and the results are presented in Reference 8. Selected results are presented in Figure 9(b). The figure displays the mass of optimized compression panels as a function of panel load intensity. The mass parameter $\frac{W}{AL}$ is defined as the mass of the panel divided by the product of the panel cross-sectional area A times the panel length L. The load intensity parameter $\frac{N_x}{L}$ is the compression load per unit panel width N_x divided by panel length L.

In Figure 9(b), curves are presented for graphite-epoxy panels with maximum design strains of .0060 and .0030. The lower strain value corresponds to a safe strain level from an impact damage point of view, whereas the larger strain value is a maximum based on matching the bending and torsional stiffness of an existing aluminum wing. (Matching stiffnesses reduces qualification problems for the retrofitted composite wing). The graphite panel results can be compared with the cross-hatched curves representing the mass requirements for current aluminum commercial aircraft wing panels. For lightly loaded panels ($\frac{N_x}{L}$ ~ .7 Mpa.), a mass-saving of nearly 50 percent is predicted for graphite-epoxy designs versus aluminum designs. For heavily loaded panels, ($\frac{N_x}{L}$ ~ 5 Mpa) savings are about 40 percent for a maximum strain of .0060, and are reduced to about 15 percent when impact sensitivity is accounted for (ε_{max} = .0030).

The calculations presented for graphite panels were obtained from a recently developed structural panel sizing computer code (Ref. 9). The calculations were constrained to match extensional and shear stiffness properties of an equivalent aluminum wing panel structure, and included minimum gage constraints and effects of an overall bow imperfection.

Damage Tolerance Improvements

The preceding results suggest a substantial need for improvements in damage tolerance of heavily loaded composite compression structures. Research on this subject is on-going at the NASA Langley Research Center. Recent preliminary results suggest that matrix material improvements may be feasible.

In Figure 10, a comparison of the impact damage tolerance for two materials is presented. Results are shown for graphite-epoxy material used in the test program summarized in Table I (Material A), and a graphite-epoxy material with a matrix having a much higher elongation to failure (Matrix B). Tensile stress-strain curves for the two matrix materials are presented in the inset in Figure 10.

The data shown in Figure 10 was obtained on 48-ply graphite-epoxy laminated plates. Substantial improvements in impact damage are shown for the material with matrix B. The impact sensitivity threshold strains for the B material are at least .005 for the

THIS DOCUMENT WAS DIGITIZED BY
TECHNICAL LIBRARY
ABBOTTAEROSPACE.COM

preliminary data shown. Thus, it appears that certain matrix materials may be "tougher" in their resistance to impact. In current research, efforts are directed toward understanding what mechanical and chemical properties are critical in enhancing the damage tolerance of compression structures.

Discussion of Impact Test Method

The traditional Charpy and Izod impact tests have been used by a number of investigators to evaluate the impact response of polymer-matrix composite materials. As discussed in Reference 2, however, data from impact tests can provide conflicting results and interpretations. For example, Izod impact tests (Reference 10) conducted on the same material systems as those (Materials A and B) of Figure 10 indicate that Material A exhibited a 45% improvement in impact performance over Material B. By contrast, the low-velocity impact data obtained using ball-type impacts on compression-loaded specimens reported herein, clearly shows the superior impact resistance of Material B over Material A. (See Fig. 10)

It is believed that the type of impact test performed in the present investigation has substantial merit. First, the test method is simple and requires no sophisticated equipment to perform. Second it is more realistic in representing impact effects on in-service structures where in-plane loads and panel response must be considered. Third, the test gives direct information on the reduction in material strength and consequently the data can be used directly in design applications.

CONCLUDING REMARKS

Typical results have been presented from an extensive investigation of the effect of low velocity impact on the compression strength of graphite-epoxy structures. Data were obtained in this investigation on graphite-epoxy sandwich beams with thin facesheets, 48 ply laminated plates and stiffened panels designed for minimum mass to carry specified compression loads. Test results suggest that lightly loaded panels which may be designed by stiffness requirements may achieve their design strength in the presence of impact damage. Heavily loaded, strength-critical panels, however, experienced significant strength reductions due to impact damage that is not visually detectable. Observation of the cross-section of impact-damaged specimens suggests that damage is initiated by stress waves and that local out-of-plane deformation caused by the projectile may propagate the damage or cause additional interior damage to develop. The compression strength of impacted test specimens has been shown to be related to the applied in-plane compression strain when impact occurred.

Current aluminum commercial aircraft wing panels are designed by material strength and have design ultimate strains well above the impact-sensitive strain levels observed for composites in this investigation. Studies indicate that stiffened composite compression panels designed to match extensional and shear stiffness properties of aluminum wing panels with composite strain allowables limited by impact damage offer a potential mass savings of at least 15% when compared to existing aluminum designs. However, savings of up to 40% may be realized if the damage tolerance of graphite-epoxy materials can be improved. Preliminary studies suggest that impact damage tolerance may be enhanced through improvements in the epoxy matrix material. Further research, however, is required to understand the critical chemical and mechanical properties of the matrix necessary to achieve the desired level of damage tolerance in composite compression structures.

REFERENCES

1. Anon: Standard Methods for Notched Bar Impact Testing of Metallic Materials, ASTM E23-72 (Reapproved 1978). 1979 Annual Book of ASTM Standards Part 10, pp. 237-253.

2. Adams, D. F.: Impact Response of Polymer-Matrix Composite Materials. Composite Materials: Testing and Design (Fourth Conference). ASTM STP 617. American Society for Testing and Materials, 1977 pp. 409-426.

3. Rhodes, M. D.; Williams, J. G.; and Starnes, J. H., Jr.: Effect of Low-Velocity Impact Damage on the Compressive Strength of Graphite-Epoxy Hat-Stiffened Panels. NASA TND-8411. April 1977.

4. Rhodes, M. D.; Williams, J. G.; and Starnes, J. H., Jr.: Effect of Impact Damage on the Compression Strength of Filamentary-Composite Hat-Stiffened Panels. Paper presented at the 23rd SAMPE National Symposium and Exhibition. Anaheim, California. May 2-4, 1978.

5. Rhodes, M. D.: Impact Tests on Fibrous Composite Sandwich Structures. NASA TM-78719, 1978.

6. Starnes, J. H., Jr.; Rhodes, M. D.; and Williams, J. G.: The Effect of Impact Damage and Circular Holes on the Compressive Strength of a Graphite-Epoxy Laminate. NASA TM-78796, 1978.

TECHNICAL LIBRARY
ABBOTTAEROSPACE.COM

7. Rhodes, M. D.; Williams, J. G.; and Starnes, J. H., Jr.: Low-Velocity Impact in Graphite-Fiber Reinforced Epoxy Laminates. Paper presented at the 34th Annual Conference Reinforced Plastics/Composite Institute. The Society of the Plastics Industry, Inc. New Orleans, Louisiana. Jan. 29 - Feb. 2, 1979.

8. Williams, J. G.; Anderson, M. S.; Rhodes, M. D.; Starnes, J. H., Jr.; and Stroud, W. J.: Recent Developments in the Design, Testing and Impact-Damage Tolerance of Stiffened Composite Panels. NASA TM 80077. April 1979.

9. Anderson, M. S.; and Stroud, W. J.: A General Panel Sizing Computer Code and Its Application to Composite Structural Panels. AIAA Journal, Vol. 17, Number 8, August 1979. pp. 892-897.

10. Riewald, P. G. and Zweben, C.: Kevlar 49 Hybrid Composites For Commercial and Aerospace Applications. Proceedings 30th Anniversary Conference Reinforced Plastics Composites Institute, The Society of the Plastics Industry, Inc., Feb. 4-7, 1975.

TABLE I.- TEST SPECIMEN MATRIX

SPECIMEN TYPE	SIZE	MATERIALS	NUMBER OF TESTS	IMPACT VELOCITY m/s	PARAMETERS INVESTIGATED
SANDWICH BEAM	55.9 × 7.6cm .056 - .183cm THICK	GRAPHITE-EPOXY KEVLAR-EPOXY	350	5 - 50	•THIN LAMINATE •LAMINATE ORIENTATION •TAPE VS. FABRIC •TENSION VS. COMPRESSION •HYBRIDIZATION
LAMINATED PLATE	11.4 - 38.1 × 24.8 - 25.4cm .56 - .79cm THICK	GRAPHITE-EPOXY	150	50 - 125	•THICK LAMINATES •LAMINATE ORIENTATION •TAPE VS. FABRIC •EFFECT OF INTERMEDIATE SUPPORTS
STIFFENED PANELS	30.5 - 76.2 × 22.1 - 81.3cm DESIGN LOAD: .53 - 5.8MN/m	GRAPHITE-EPOXY BORON-EPOXY	60	50 - 100	•HAT STIFFENERS VS. BLADE STIFFENERS •SKIN VS. STIFFENER IMPACT •WIDTH & LENGTH EFFECTS •DESIGN STRAIN CONDITIONS

TECHNICAL LIBRARY
ABBOTTAEROSPACE.COM

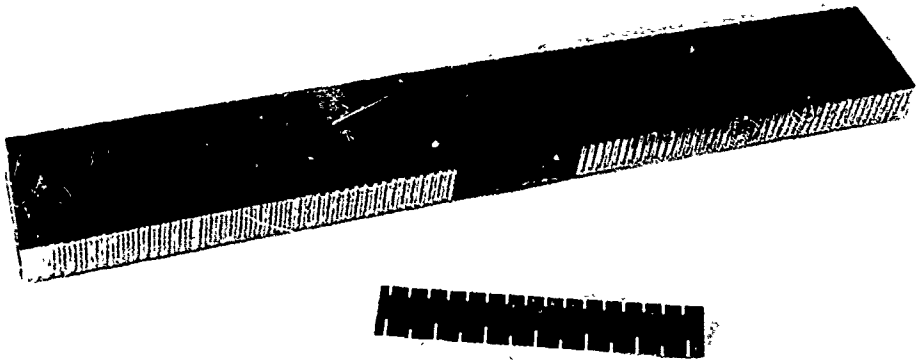

A) Sandwich Beam
Figure 1 - Test Specimens

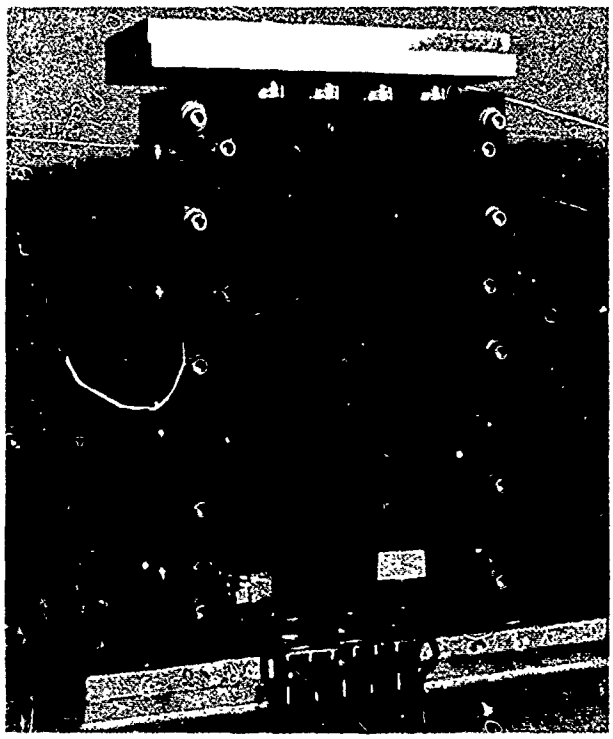

B) Laminated Plate Specimen
Figure 1 - Continued

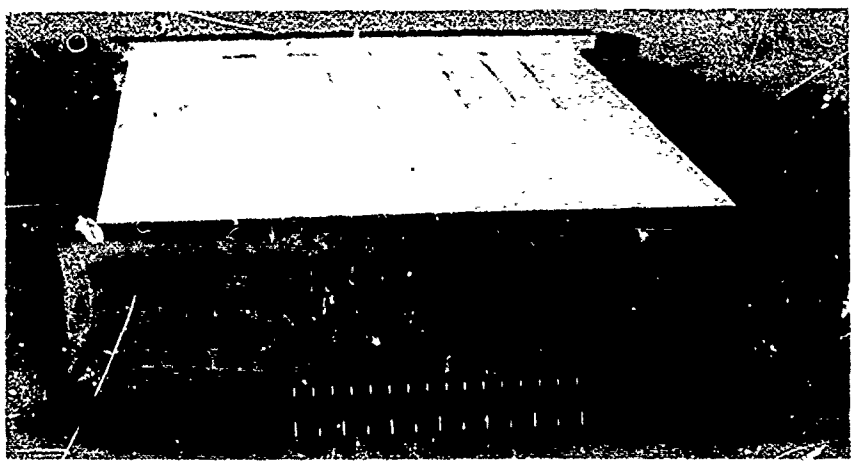

C) Blade-Stiffened Panel
Figure 1 - Concluded

TECHNICAL LIBRARY
ABBOTTAEROSPACE.COM

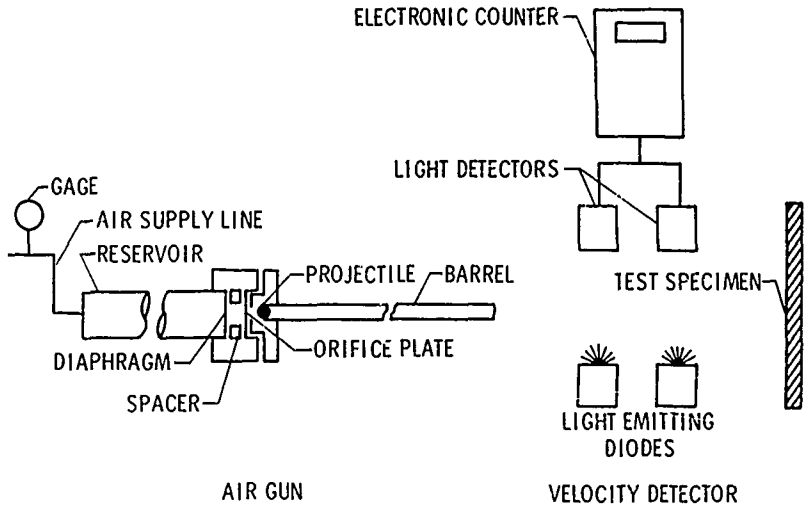

A) Schematic of Air Gun and Velocity Detector

Figure 2 - Test Apparatus

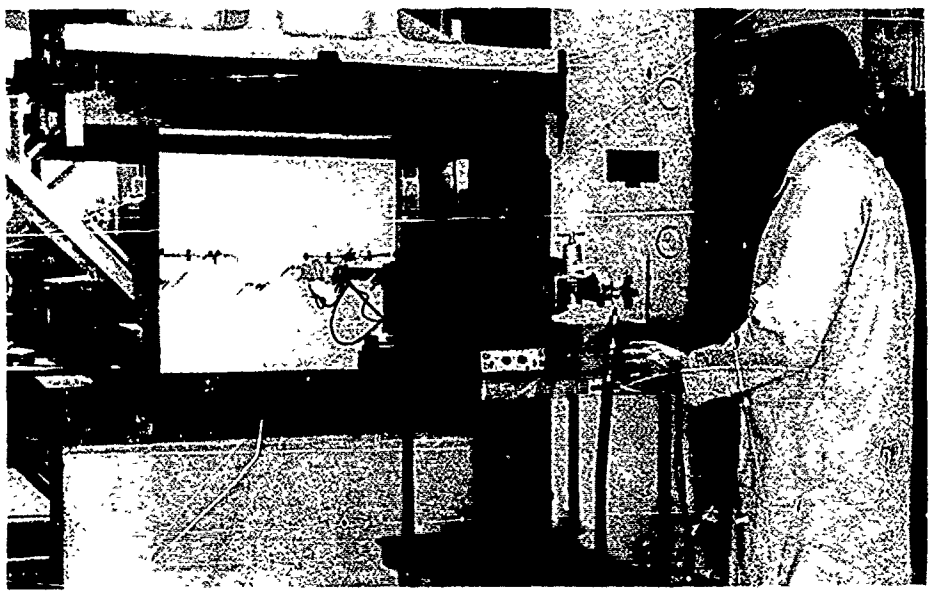

B) Typical Test Setup

Figure 2 - Concluded

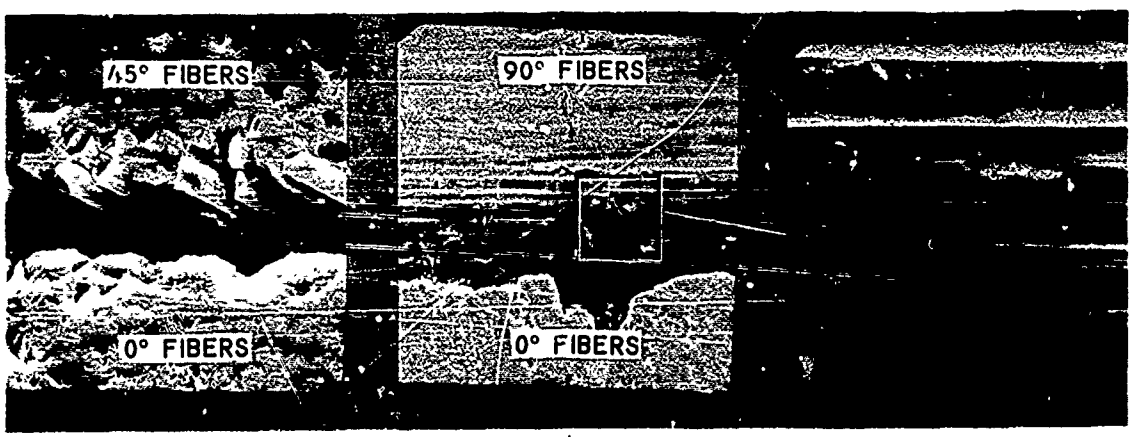

A) Scanning Electron Photomicrographs of Two Delamination Regions

Figure 3 - Damage Measurement Techniques

THIS DOCUMENT IS SCANNED BY THE ABBOTT AEROSPACE
TECHNICAL LIBRARY
ABBOTTAEROSPACE.COM

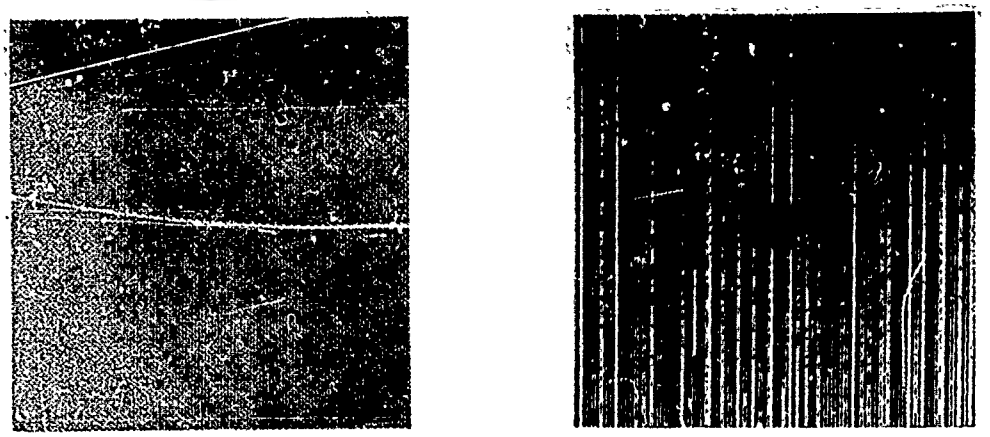

B) Comparison of Results from Brittle Lacquer and C-Scan Techniques

Figure 3 - Continued

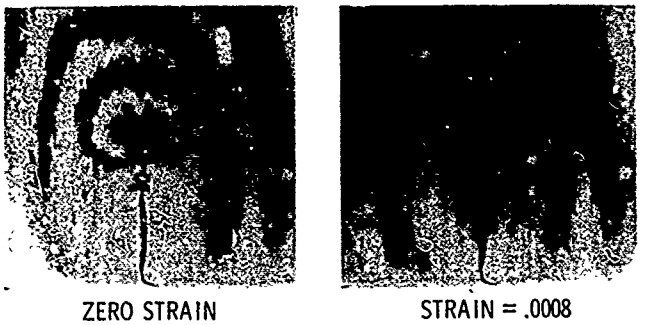

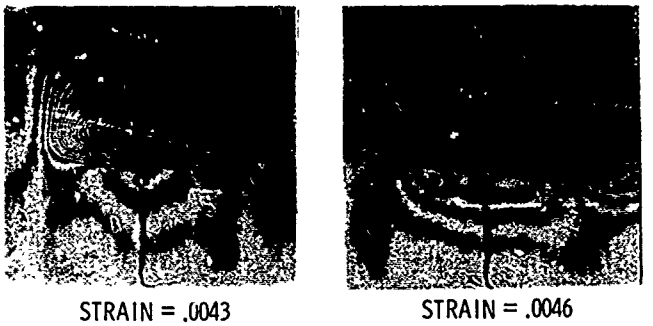

C) Moire Fringe Damage Pattern
(Panel Impacted at Strain .003)

Figure 3 - Concluded

TECHNICAL LIBRARY
ABBOTTAEROSPACE.COM

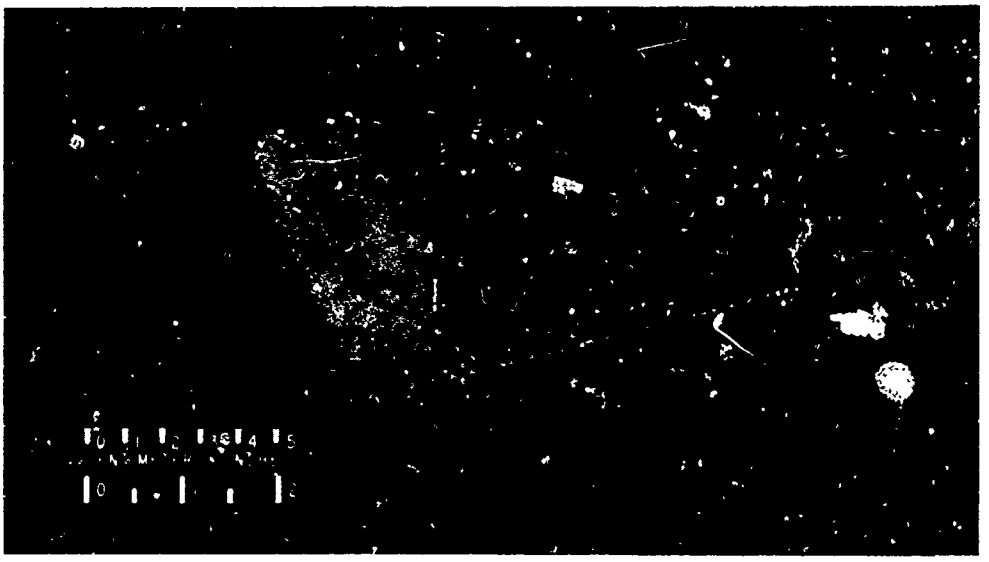

A) Local Damage in Sandwich Beam
Figure 4 - Photographs of Typical Failures of Impact-Damaged Specimens

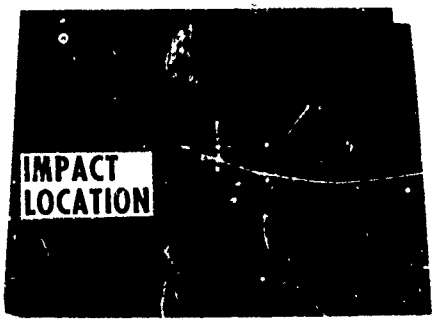

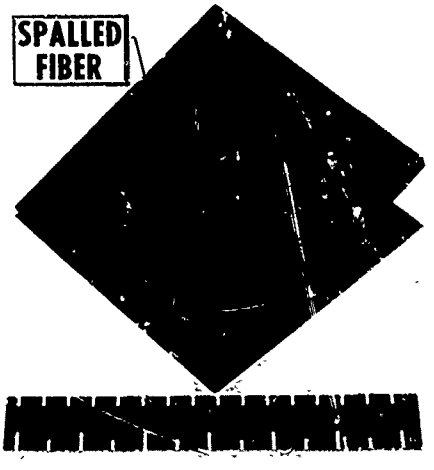

Impact at a Speed of 107.6 M/S

Impact at a Speed of 136.6 M/S

B) Damage Appearance in Plate Specimen

Figure 4 - Continued

TECHNICAL LIBRARY
ABBOTTAEROSPACE.COM

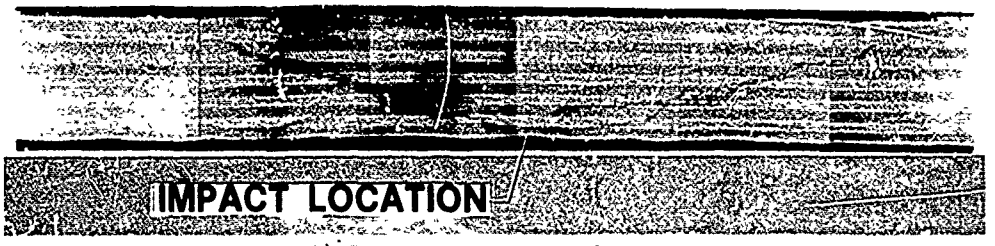

A) Impact Velocity = 62 M/S

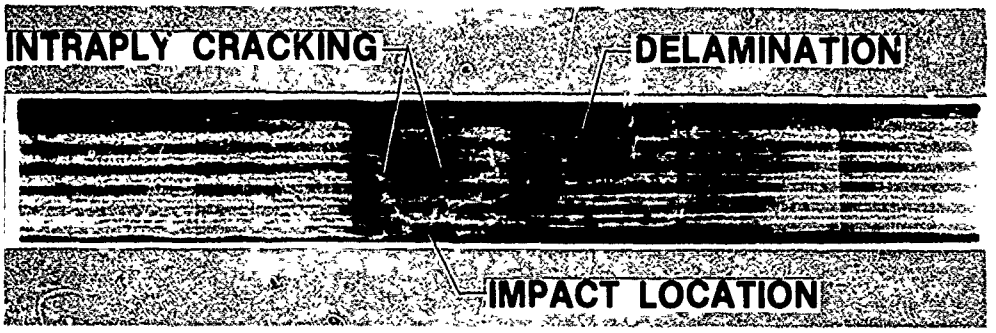

B) Impact Velocity = 123 M/S

Figure 5 - Interior Damage in Cross-Section of Laminated Plate Specimens

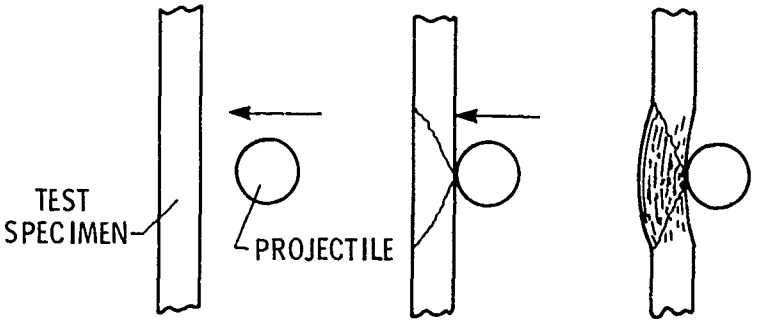

Figure 6 - Possible Damage Sequence

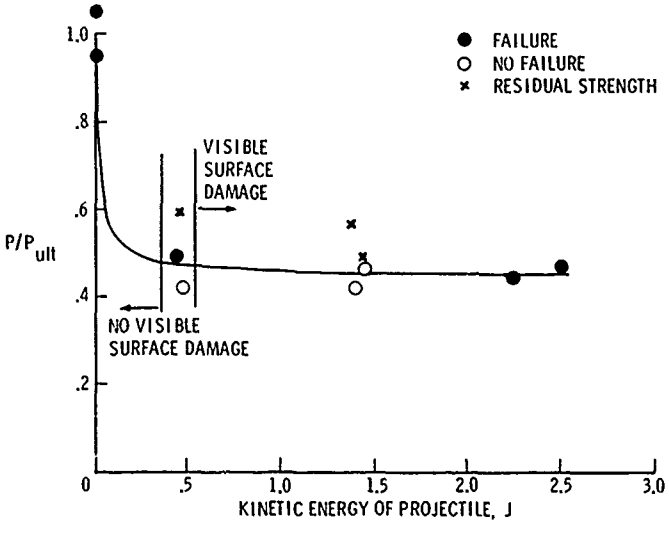

A) Sandwich Beam $(0_2)_T$ 181- Style Graphite Fabric

Figure 7 - Typical Compressive Strength Reductions

THIS DOCUMENT PROVIDED BY THE
TECHNICAL LIBRARY
ABBOTTAEROSPACE.COM

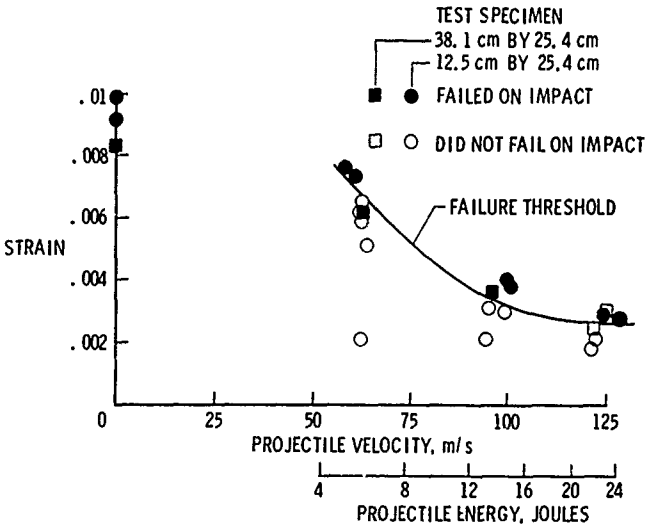

B) Laminated Plate

$(\pm 45/0_2/\pm 45/0_2/\pm 45/0/90)_{2S}$

Graphite tape

Figure 7 - Continued

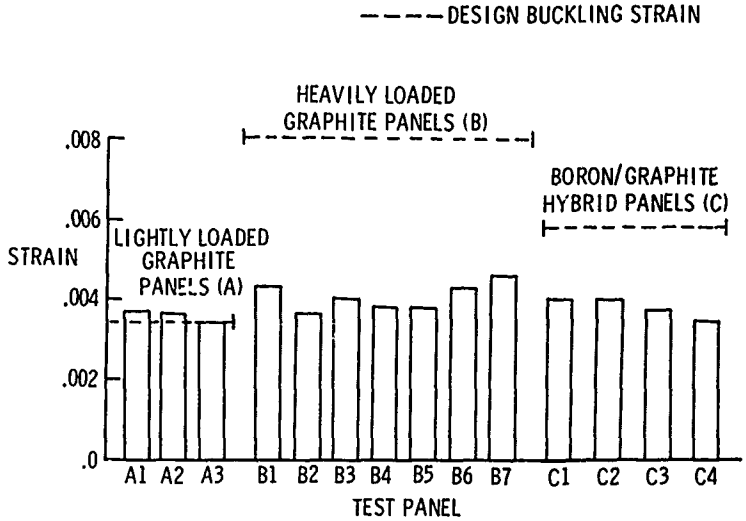

C) Hat-Stiffened Panels

Figure 7 - Concluded

Figure 8 - Hat-Stiffened Panel After Impact Failure

THIS DOCUMENT PROVIDED BY THE
TECHNICAL LIBRARY
ABBOTTAEROSPACE.COM

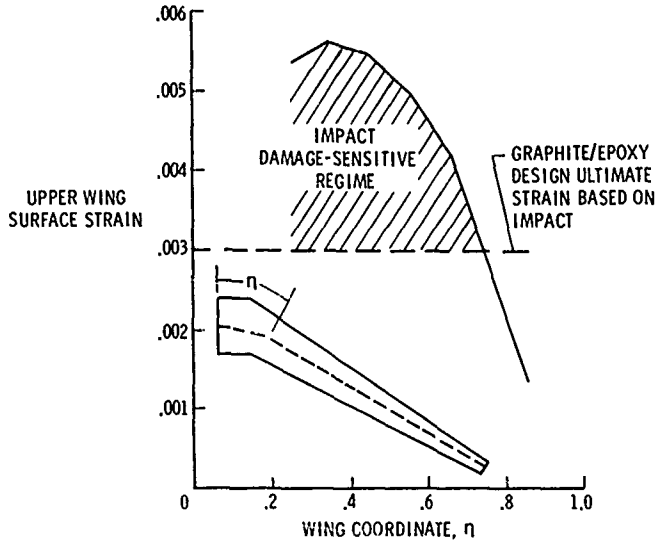

A) Compressive Ultimate Strains for a Commercial Aircraft Wing Structure

Figure 9 - Effect of Strain Limits on Panel Design

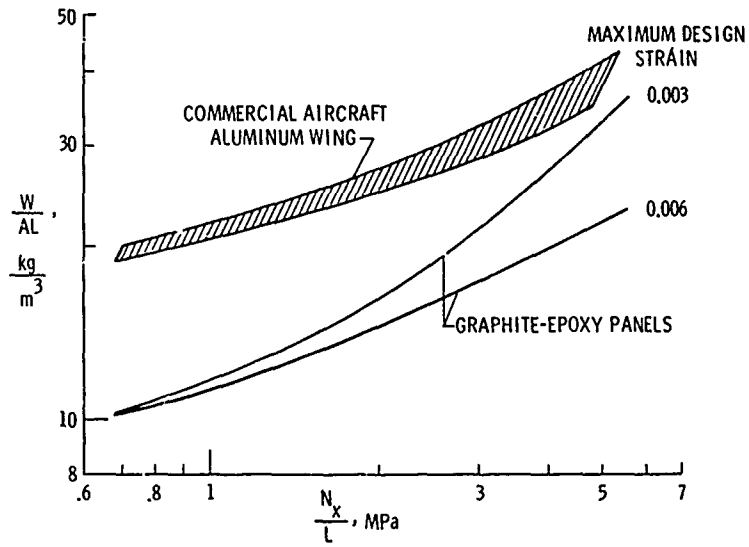

B) Effect of Design Strain on Panel Structural Efficiency

Figure 9 - Concluded

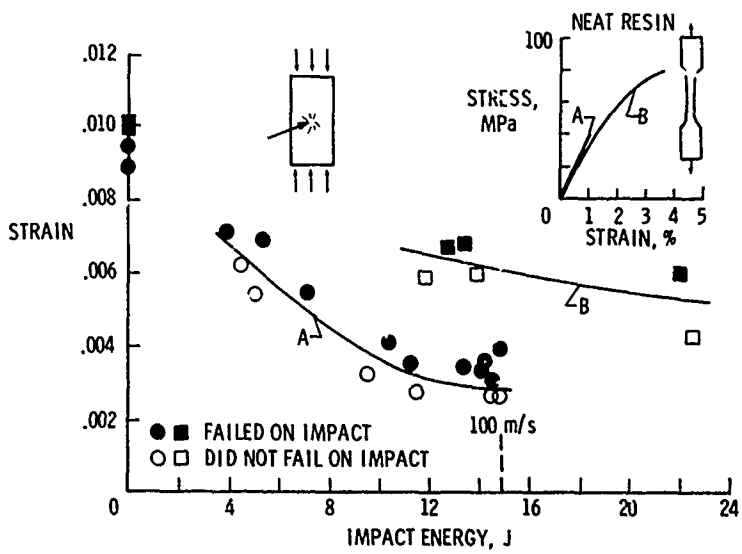

Figure 10 - Damage Tolerance Improvement Using Tougher Matrix

TECHNICAL LIBRARY
ABBOTTAEROSPACE.COM

THE INFLUENCE OF DEFECTS ON THE BEHAVIOUR OF COMPOSITES

by

R. AOKI, K. STELLBRINK

Institut für Bauweisen- und Konstruktionsforschung
Deutsche Forschungs- und Versuchsanstalt
für Luft- und Raumfahrt E.V.
Pfaffenwaldring 38-40, D-7000 Stuttgart 80, Germany

ABSTRACT

The load-carrying capacity of composite structures in aircrafts, spacecrafts etc. is expected to be greatly influenced by inherent defects or damages induced during utilization. This paper reports on the ongoing experimental research in DFVLR WB-BK pertaining to the effect of simulated defects on the fatigue behaviour and residual strength of gfrp and cfrp laminates. Two special kinds of mechanically produced damages in thin laminates caused by dropped tools are the main topics of this paper: a threesquare indentation generated by a tapered triangual tip and a delamination zone produced by a ball-shaped tip. The investigated materials are epoxy resins reinforced with E-glass fabric as well as T300 carbon fibre fabric and unidirectional lay-up with various orientation sequences.

INTRODUCTION

No thing is perfect. For design, quality control and maintenance of an aeroplane the question comes up: which kind and size of deviation is acceptable, which anomaly must be altered so that the structure can do the job it was assigned for. To enable that decision, it is necessary to know something about the behaviour of the observed anomaly, about its influence on the performance of the structure.

The problem of damage tolerance is threefold and consists:

a) of the cause of damage, e.g. during manufacture, by handling or in service,
b) of the effect of a damage, which in general means a local cracked zone, and
c) of the consequence of this damage, which commonly results in a reduction of properties of the affected structural element.

Following this problem classification, we regard as the goal of investigations on damage tolerance of composite material:

1. To minimize the inducements of damages. This is mainly a problem of the manufacturer and the user of a structure.
2. To get informations about the inherent ability of endurance of impact loads without damage as well as the ability to absorb energy by a fracture process. Since these properties sometimes are incompatible, a rank must be settled depending on the purpose of the structure. E.g. for a skin of an outer wing section it seems to be more important to withstand an impact of runway debris without any damage than to stop a high energy object by means of absorbing fracture energy. The opposite might be true for a fuel tank.
3. To get information about the influence of a specific damage on the performance of the structure. Since the considered mechanical damages mostly do not initiate the total breakdown of the structure, we have to find out the damage propagation depending on the service loads. Simplified spoken, this is a fatigue problem.

Minimizing the influence of damage requires consideration of all three items. Of course, the available capacity in the Institut für Bauweisen- und Konstruktionsforschung urged a selection of our activities. At the beginning of our involvement in damage tolerance problems we composed a list of possible inducements of damages in composite materials either by overloading or human error, only as an aid for determination of our future work. On the other hand our first effort was focussed on the damage process in a real

TECHNICAL LIBRARY
ABBOTTAEROSPACE.COM

structural element, the leading edge of the ALPHA-JET horizontal stabilizer, impacted by runway debris or hailstones. After all, we confined us to the investigation of mechanical damages, especially of impact damages, caused by dropped tools, flung runway stones and hailstones.

At present, the effort in our institute is directed towards gaining information about the influence of these mechanical damages on the lifetime of dynamically loaded thin shells made of composite material.

This paper mainly deals with the ongoing experimental investigations in our institute.

ON THE DAMAGE EVENT

A) Impacted Beams

A hard object hitting a composite structure with finite velocity, will induce a visible, non visible or no damage. Earlier efforts were concentrated on the total fracture energy absorption during impact especially in a small three-point-bending beam or cantilever beam. This test procedure was derived from a similar procedure for metallic materials with small changes only. Obviously the aim of earlier investigations mostly was to maximize the total fracture energy. Seldom attention was payed to the elastic, reversible energy absorbed without damage. Both the Izod and Charpy impact tests seem not to be an adequate method to gain beneficial information about the damage in thin plates impacted by dropped tools, stones or hailstones. Stress state, impactor mass and velocity are usually extremely different. As an example Fig. 1 shows the influences of the length-to-thickness ratio and the static versus dynamic loading in three-point-bended beams reinforced with two different fibre types orientated parallel to the main axis. The bending stress and the interlaminar shear stress at failure as well as the fictitious modulus and the elastically endured energy depend strongly on these parameters. The bending stresses shown in the graphs are corrected for large deflections, resp. high length-to-thickness ratios (Fig. 2a). It is easy to explain the shape of the apparent initial modulus of elasticity taking into account the short beam shear deformation (Fig. 2b). But that is not true with respect to the strengths. A failure hypothesis which describes the observed stresses at breakdown of the specimen is not known.
The merit of this test is to give a rough idea of what happens if this material is subjected to tension or compression stresses AND shear stresses AND surface pressure simultaneously for a short time.

The most important experiences delivered from Charpy impact tests which are perhaps transferable to impact loaded plates are the following:

Glass fibres endure more elastic energy and absorb more total fracture energy than carbon fibres, aramid fibres and boron filaments under most load combinations. Unfortunately, one of the most important requirements, stiffness, is not attractive with glass fibres compared to other fibres. The available compromise reached e.g. by mixing glass and carbon fibres is not always a good compromise since in many cases the negative properties (e.g. bending compliances) are more dominant in the mixture. Fair compromises are possible about fracture energies and elastically endured energies as presented in Fig. 3. Those graphs show Charpy impact test data of unnotched specimens composed of different fibres with several stacking sequences.

Charpy tests point out the outstanding role of shear strength for the damage mechanism at impact loads. Even for a length-to-thickness ratio of 40 the beams failed also due to interlaminar shear, not only when statically but also when dynamically loaded even at rather low nominal shear stresses. This is reported by SHLENSKII [10] too. BADER et.al. [2] have shown that the relation between endured elastic energy and total fracture energy depends strongly on the intralaminar shear strength resp. the interfacial bonding.

There are many other features observed on Charpy impact specimens, e.g. the loading rate dependence of interlaminar shear strength pertaining to multidirectional lay-up reported by SAYERS & HARRIS [8] as well as by MALLICK & BROUTMAN [7]. In our opinion, these features are related too strongly to the special

TECHNICAL LIBRARY
ABBOTTAEROSPACE.COM

test conditions, this makes it often very difficult to extend those beam results to impact loaded plates and shells.

B) Impacted Plates and Shells

The significant characteristic of a plate compared to a beam is its two dimensional extension, that means an impact load is parried by primary stresses in three dimensions. This seems to be more complex than in a beam. But in fact it should be easier to understand the stress state in a plate except at the edges than in a beam (a degenerated plate) since the real three-dimensional stress state in a beam is mainly governed by the secondary edge stresses. Nevertheless a theoretical discourse on impact loaded thin orthotropic plates including surface pressure does not exist. Experimental results presented in the literature and achieved by own work - see the scheme of our test equipment Fig. 4 - may allow the following statements, which are of general but of course not absolute validity.

A very important parameter is the lamina or fibre orientation. Unidirectional (UD) lay-up is unacceptable in most cases. One or few very long cracks throughout the laminate would occur even at very small loads. Already shorter cracks form crosswise in a simple $0/90^0$ lay-up or a large zone of sequential delamination will appear as reported e.g. by SIERAKOWSKI [11]. The least extendion of cracks appears generally in a multidirectional lay-up excepting the outmost UD layer. Fig. 5 illustrates some of the statements mentioned above. These long cracks in the outmost UD layer can be impeded by a thin cover of glass or aramid woven fabric. Fig. 6 demonstrates the difference in response of a covered and a non covered laminate to impact by a dropped tool. BEAUMONT, RIEWALD, ZWEBEN [3] and DOREY [4] reported on similar observations.

Concerning the stacking sequence in a $0/90^0$ lay-up SIERAKOWSKI et. al. [11] observed a lower first failure energy and a lower absorbed fracture energy in gfrp composites with alternating stacking sequence containing many sheet boundaries, than in a three-laminae symmetric lay-up. A rough calculation of the stresses could not explain this behaviour. Additionally they reported on a sequential delamination mechanism in $0/90^0$ gfrp, which we observed in $0/90^0$ cfrp laminates at low impact velocities, too.

The most influential impact parameter is the projectile velocity. The damages at different velocities are shown in Fig. 7 for an E-glass laminate with good fibre-to-matrix bonding. With less interface bonding and low velocities the failure mode shifts from fibre crack to interlaminar and intralaminar debonding, nevertheless the dependence of damaged area size on impact velocity is similar. Higher velocities result in larger damage zones up to a velocity where the damage begins to be characterized by a punch-out mechanism. In a limited range the damaged area is linearly related to the kinetic energy as reported e.g. by SIERAKOWSKI [11] and DOREY [4] at their test conditions. Evaluation of Fig. 7 (see the scetch in Fig. 8) confirms this experience. Beside the material parameter this velocity dependence is affected by the support boundary conditions which influence the internal dynamic stress state of the loaded plate (Fig. 8, below). In a sufficiently large plate the deformation mechanism depends on the impact velocity as shown principally in Fig. 8. At low impactor speeds the plate behaves like statically loaded. The energy is stored mainly near the load introduction at the impact locus and the supports, that means in a relatively large material volume. At very high speeds the punching affects an area only slightly larger than the cross section of the projectile. At moderate velocities a mixture of these two mechanisms is evident. At the moment of maximum plate deflection the deformation exists only in a limited area, the extension of which depends on the impactor velocity, mass and stiffness relation between impactor and target and the shell curvature and/or support conditions.

Concerning this punch-out mechanism, we could drasticly prove the outstanding advantage of glass fibre fabric over carbon fibre with a real application. A variant of the leading edge of the ALPHA-JET horizontal stabilizer was made of pure SC 130/Code 69 material in a $0/90^0$ lay-up, 3 mm thick, covered with a 0,2 mm thick aluminum foil. It was impacted with a glass sphere (13g, simulating idealized runway debris) at v = 55 m/s (approx. the landing speed). The response (see Fig. 9) was a penetration. One of the investigated variants, 2,5 mm thick, consists of about 70 % glass cloth style 181 / Code 69 and 30 % sc 130 / Code 69 in the midplane in $0/90^0$ orientation. At the rear side of the impact locus we

THIS DOCUMENT PROVIDED BY THE ABBOTT AEROSPACE
TECHNICAL LIBRARY
ABBOTTAEROSPACE.COM

observe delamination and deformation. The front side shows no visible marks except some whitening which would be invisible under a protective painting [1, 12].

On the whole, the possibilities of designing thin shells for good impact resistance are not very numerous since the most influential parameters are dictated mostly by stiffness, strength, aerodynamics or fabrication requirements. That means, since it is often difficult to optimize a laminate composition with regard to impact resistance, the best we can do seems to gain knowledge about the effect of damages which can not be avoided in commonly used laminate types, and to give recommendations for modest alterations of those laminates to improve damage tolerance without weakening of other specifications significantly.

EFFECT OF DEFECT

In our institute we began to investigate the consequences of an impact damage in composite material especially with respect to the lifetime of the damaged structure. Principally, we try to find the influence of mechanical damage caused by a dropped tool to the resistance of glass and carbon fibre reinforced epoxy on harmonic cyclic loads.

The first preliminary test results are presented below. We started with glass fibre fabric reinforcement. Three kinds of damages were rendered:

a) ball impression onto a rigidly supported laminate with a squeeze force of 5 kN and a ball diameter of 11 mm which results in a visibly damaged area of aboug 30 mm^2,

b) a threesquare indentation into a rigidly supported laminate with a punch force of 5 kN and 6 mm punch diameter which resulted in a visible damage of about 30 mm^2,

c) a ball impact onto a plate clamped in 130 mm diameter with a glass sphere, m = 30 g at v = 45 m/s which resulted in a visibly damaged area of about 50 mm^2 or 500 mm^2 if scattered small interface cracks are taken into account, too.

The pictures in Fig. 10 (middle) illustrate some of these damages in gfrp. The fatigue curve of damaged and undamaged specimens loaded at R = 0.01 (zero-tension) is presented in Fig. 11. The few available test data indicate only a small variation in the behaviour of damaged and undamaged samples. The difference between the two matrix systems results primarily from different fibre volume caused by different fabrication methods (prepreg versus wet lay-up). Glass fibre fabric seems not to be sensitive to those damages we had introduced and tested at harmonic cyclic tension loads. It may be noticeable that the type of failure mode changes from a shear type failure at high loads and a small number of cycles to a tension type failure at low loads and a large number of survived cycles. At high to moderate load levels the defects behave somehow like a drilled hole inspite of remarkable delamination propagation in the course of the loading history (Fig. 12, above). The final break down usually occured all at once without any noticed warning. Two intact specimens were tested for residual quasi-static tension strength after about one million cycles at low cyclic tension stresses. There we observed for the first time a remarkable amount of the residual strength we registered very often later on with cfrp.

Further investigations in our institute were concentrated upon carbon fibre reinforced composites. Up to now we explored T300 in Code 69 from Fothergill & Harvey received as UD prepreg sheets. A small test series was run using balanced T300 cloth in L02/SL from Rütag. These samples consists of 5 layers and were 1,35 mm thick at a fibre content of about 45 vol.%. The corresponding lay-up composed of unidirectional prepreg sheets $(0/90)_{3s}$ was 1,7 mm thick at 54 vol.% fibre content. The most extensively used stacking sequence $(0_2/+/- 45/0_2 /+ /-45/90)_s$ was 2,5 mm thick at 55 vol.% fibre content.

THIS DOCUMENT WAS DIGITIZED BY
TECHNICAL LIBRARY
ABBOTTAEROSPACE.COM

The defects introduced were

1.) the same threesquare indentation as in glass fabric composites mentioned above (Fig. 10) and

2.) an impact damage simulating the defect caused by a dropped tool owning 244 g mass, 10 mm contacting tip diameter and 5 - 7 m/s ultimate speed. The target plates were clamped at 130 mm diameter during the impact event. Thereafter the coupon specimens for fatigue loading were cut from these plates. Since we made the experience that a thin cover of glass cloth (style 120) resulted in a more benign damage (Fig. 6), the plates made from T300/Code 69 and loaded by the "dropped tool" has been covered with it. The fabric was added dry and soaked during the autoclave pressure cycle by the surplus Code 69 resin. The dropped tool damage parameters were chosen in such a manner that the obtained defect could not be detected by glancing at the front of the loaded plate, at least if it would be painted by a tough lacqueur or coating.

The damaged and for comparison undamaged specimens were fatigue loaded or tested for residual strength after dynamic loading according to Tab. 1. The quasi-static strength is included as a special case of fatigue strength.

The results of fatigue strength and residual strength tests with indentation-damaged and intact cfrp samples are presented in Fig. 13. They are not proved very well and consolidated in detail since the available number of specimens and machine time was limited and we preferred to gain a broader overview as a first step than a well founded special information. Nevertheless we believe to have obtained beneficial knowledges.

The fabrik material, just like gfrp, demonstrated only a trifling damage sensitivity if cyclicly tension loaded, although the stated stresses are related to the gross section, since a net section is hard to identify in contrast to the presence of a drilled hole or a saw cut. The two solitary residual strength data of damaged samples rise a little over the estimated fatigue curve.

The corresponding undamaged lay-up made of UD laminae $(0/90)_{3s}$ proved to be rather stronger, even taking into account the different fibre content. Also a remarkable difference in the behaviour of damaged and sound samples was observed. A $0/90^{0}$ lay-up is notch sensitive when tension loaded. The available data are not very easy to interprete, but the estimated fatigue curves of the damaged and intact specimens seem to intersect at about 10 to 100 million cycles. The fatigue strength and the residual strength of the damaged specimens seem not to have been affected significantly by the preceeding dynamic load, whereas the fatigue curve for the undamaged test pieces decreases with increasing number of survived load cycles. Not so the residual strength: again it reaches at least the range of the static strength obviously independent on the preceeding load history.

The multidirectional laminate $(0_2/+/-45/0_2/+/-45/90)_s$ did not show such a substantial variation with damaged and sound samples loaded in cyclic tension. The estimated fatigue curves decrease moderately with increasing lifetime. The difference may be assigned solely to the different effective net section caused by the indentation damages. The residual strengths are obviously independent on the preceeding load history and reach the static strength or even exceed it just like the undamaged specimens.

Loaded in cyclic compression, the multidirectional laminate behaves different. In contrast to the damaged specimens, the undamaged samples demonstrate a remarkable decrease of the fatigue curve with increasing lifetime. Again the residual (compression) strength reaches the corresponding static value or even exceeds it as with the intact test pieces.

The number of specimens damaged by impact ("dropped tool") and tested for fatigue life and residual strength still is very small today. In general they seem to confirm the principal results given above with the indentation damaged samples (Fig. 14). Since the cyclic compression-tension load (R = -1) is one of the most severe harmonic load conditions for the investigated multidirectional laminate both with sound as well as with notched samples as reported by SCHUETZ, GERHARZ et. al. [5, 9], we employed this type of loading with the impact damaged specimens. In contrast to the moderate influence of the impact damage on the static tension strength the quasi-static and dynamic tension-compression strength related to the gross section drops drasticly. Neglecting the compression bearing capacity of the damaged area detected by ultrasonic scan, we may estimate an effective net section of about 40 % of the gross section (Fig. 16).

TECHNICAL LIBRARY
ABBOTTAEROSPACE.COM

That means that the effective net section strength (at R = -1) is placed near the lower bound of the compression fatigue data (R = - ∞) of the undamaged specimens. Concerning the damage propagation during fatigue loading the various composites demonstrated significant differences. The woven fabric laminates usually broke down suddenly by a crack transverse to the load direction crossing the defect, if present. At the $0/90^0$ specimens the edge corners of the upper 0^0 layer split off in the course of the dynamic loading, caused by prevention of the transverse contraction by the 90^0 layer. The abrupt crack perpendicular to the load direction ran through the indent defect. Besides, at damaged specimens a partial delamination and splitting of the damaged outmost sheet with cracks parallel to the fibre direction starting at impact locus was noticed. With the multidirectional laminate $(0_2$ /+/ -45/0_2/+/-45/90$)_s$ this splitting occured earlier and always, even in the static case. Cracks and delamination ran up into the clamping attachments. Often the 45^0 layer beneath the outmost layer was destroyed completely. Also as with the $0/90^0$ laminates the edge corners split off.

The damage propagation in impact damaged samples with multidirectional lay-up was not very pronounced during the tension-compression fatigue loading (R = -1). No damage propagation was noticed visually until quick break-down of the specimens, although an impressive motion of the damaged outmost layers could be seen during load cycling. The ultrasonic scan detects only small changes (Fig. 16). The damages introduced by the "dropped tool" probably are reflected by the fracture feature of the broken test pieces. Sometimes, it is possible to distinguish fibre breaks at centre of impact from the surrounding delamination area. For comparison Fig. 17 shows the fracture of an impact damaged, but staticly tension-loaded specimen and demonstrates the faint detectability of the impact demage in this case, indicating a different fracture mechanism.

Furthermore, the multidirectional lay-up presented a behaviour rather surprising at the first glimpse. All test pieces, except the very short-lived ones, split in the midplane starting from the edges. Fig. 18 evidences midplane delaminations registered by an ultrasonic equipment exploiting the reflected signal intensity in a damaged and in an undamaged specimen. Note that in each left graph the margin of the scan is caused by the sensor size and does not indicate delamination. The upper sketch in Fig. 18 illustrates the remaining thickness which is free of delaminations, detected from the top side of an impact damaged and tension fatigue loaded specimen. This behaviour evinced by the multidirectional orientated laminate, not desirable in our opinien, can be prevented by a 0,1 mm thin glass cloth wrapped around the edges as manifested in Fig. 19. The covered edge exhibited no cracks or only cracks parallel/transverse to the fibre direction in the $+/-45^0$ layers not visible at the flank, whereas the unprotected edge showed midplane delamination up to the centre line when loaded identically. Unfortunately, there has been no possibility till now to investigate the influence of the wrapper upon the lifetime of damaged and intact specimens.

CONCLUSION

HASHIN & ROTEM [6] have shown that in unidirectional cfrp the fatigue tension strength parallel to the fibre direction depends only scantly on the number of cycles, and that the fatigue shear strength transverse to fibre direction and the fatigue shear strength parallel/transverse to the fibres depend strongly on the number of cycles or lifetime. That means, in the course of a load history in an ordinary multidirectionally orientated, cyclicly loaded laminate the shear strength becomes more and more the weakest link. Regarding the damage tolerance of composite materials with respect to fatigue strength, the consequence is manifested in our experimental results. A laminate composition which enables to bypass a damaged region with restricted load-bearing capability by means of longitudinal fibre stressing is superior to any material which has to bear shear stresses principally via matrix or fibre/matrix interface.

Thus, the $0/90^0$ lay-up is notch or damage sensitive when statically or dynamically tension loaded. The material is not capable to by-pass a significant distortion. The destroyed cross section principally expands along the main axis leaving the rest nearly unaffected.

TECHNICAL LIBRARY
ABBOTTAEROSPACE.COM

Obviously, the inherent distortions within the fabric laminate are nearly as efficacious as the artificial indentation defect. The tiny difference in general may be accounted to the different effective cross section at the damage location.

The multidirectionally orientated laminate - considering the tension load case first - is definitely notch insensitive on account of the inherent capability to endure inplane shear stresses by carrying the load with help of fibres. Of course, microscopic shear stresses exist, too, which finally lead together with the decreasing shear strength to the breakage of the specimen. We assume this mechanism to be right with compression loads, too. On the other hand, the microscopic shear stresses are much larger, depending e.g. on the filament alignment which results in a microscopic buckling stress state even in absence of macroscopic buckling. The scanty test data may allow the conclusion that the exhibited reduction of compression strength in sound samples in general is due to this microscopic shear stress which depends substantially on the manufacturing process and perhaps the test method. In a real structure where macroscopic buckling usually is not impeded as with our test pieces, the effective compression strength is expected to be even smaller. Our first results with impact damaged samples - in this case an area of about 10 cm^2 is affected mainly by delamination and partially fibre/matrix debonding but also by fibre fracture - indicate that the damaged area can bear tension loads quite well, but minute compression loads. The influence of the local bending stiffness reduction on panel buckling capacity in a real airframe is expected to be more significant with impact damages than with indentation damages.

For all laminates composed of unidirectional sheets the decreasing fatigue curve in contrast to the residual strength of the not damaged samples indicates that fracture propagates rather quickly after initiation by a small in-built defect.

Summarizing, the existing test results suggest that carbon fibre reinforced plastic generally seems not to be damage sensitive in long-life structures (cyclicly loaded with low load level) since the fatigue curves for damaged and inaffected specimens intersect at high numbers of cycles. An information pertaining to the capability to endure solitary peak loads (in random load history) can not be derived from the given data yet.

They indicate that a damage tolerant design requires a laminate composed of 0^0 layers in the principal load direction, $+/-45^0$ layers achieving shear bearing capability, and 90^0 layers preventing excessive inplane shear deformation by transverse contraction.

Furtheron, the results support the opinion that usual theoretical tools in fracture mechanics are not suitable to treat the time-dependent behaviour of real damages or even geometrically idealized irregularities in many composites since they do not consider single sheets dedicated to different stress states and different time-depending properties.

REFERENCES

[1] AOKI R., WURZEL D.
Composite-Bauteile unter Schlagbelastung und Auswirkung von Defekten auf die Belastbarkeit
DGLR-Symposium, 22. Sept. 1978 in Darmstadt, Vortrag-Nr. 78-190

[2] BADER M.G., BAILEY J.E., BELL I
The effect of fibre-matrix interface strength on the impact and fracture properties of carbon-fibre-reinforced epoxy resin composites
J. Phys. D: Appl. Phys., Vol. 6 (1973) PP. 572 - 586

[3] BEAUMONT P.W.R., RIEWALD P.G., ZWEBEN C.
Methods for Improving the Impact Resistance of Composite Materials
ASTM STP 568 (1974), P. 134 - 158

[4] DOREY G.
Fracture Behaviour and Residual Strength of Carbon Fibre
Composites Subjected to Impact Loads
AGARD-CP-163 (1974)

TECHNICAL LIBRARY
ABBOTTAEROSPACE.COM

(5) GERHARZ J.J., ROTT D., SCHUETZ D.
Schwingfestigkeitsuntersuchungen an ungekerbten und gekerbten Faserverbundwerkstoffproben aus multidirektionalem Laminat
BMVg - FBWT 79-25 (1979)

(6) HASHIN Z., ROTEM A.
A Fatigue Failure Criterion for Fiber Reinforced Materials
J. Comp. Mat., Vol. 7 (1973) PP. 448 - 464

(7) MALLICK P.K., BROUTMAN L.J.
Impact behaviour of hybrid composites
30th SPI (1975) sec. 18f

(8) SAYERS K.H., HARRIS B.
Interlaminar Shear Strength of a Carbon Fibre Reinforced Composite Material Under Impact Conditions
J. Comp. Mat. Vol. 7 (1973) P.129-133

(9) SCHUETZ D., GERGARZ J.J., ALSCHWEIG E.
Zur Schwingfestigkeit von ungekerbten, gekerbten und gefügten Proben aus dem Faserverbundwerkstoff CFK
DGLR-Symposium, 22. Sept. 1978 in Darmstadt, Vortrag-Nr. 78-188

(10) SHLENSKII V.F., FILATOV M.Y.
Fatigue strength of a glass laminate subjected to combined normal and interlaminar shear stresses
Mekhanika Polimerov, No. 2 (1978) PP. 350 - 352

(11) SIERAKOWSKI R.L., ROSS C.A., MALVERN L.E., CRISTESCU N.
Studies on the penetration mechanics of composite plates
U.S. ARMY RESEARCH OFFICE DAAG 29-76-G-0085 (1976)

(12) WURZEL D.,
Schlagtüchtigkeit und Betriebsverhalten von Leitwerksnasen in Hybridbauweise
DFVLR Institutsbericht IB 454 78/15

MATERIAL	LAY-UP	not damaged	DAMAGES		Coupon dimension: width, free length	FATIGUE STRENGTH and RESID. STRENGTH			
			three square indentation on rigid support punch diameter = 6 mm	dropped tool, tip diameter = 10 mm m = 244 g v = 5 - 7 m/s		Zero-tension R = 0.01	Zero-compress. R = -∞	Zero-compress. R = -1	Pure bending (R = -1)
T300 A002 (fabric) L02/SL	$(0/90)_{5x}$ t = 1.35 mm φ = 45 Vol%	X	die force = 2.5 kN		b = 16 mm L = 130 mm	X			
T300 (UD) Code 69	$(0/90)_{3s}$ t = 1.7 mm φ = 54 Vol%	X	die force = 5 kN		b = 16 mm l = 130 mm	X			
	$(0_2/\pm45/0_2/\pm45/90)_s$ t = 2.5 mm φ = 55 Vol%	X	die force = 5 kN		b = 16 mm L = 130 mm	X	X		
	$(0_2/\pm45/0_2/\pm45/90)_s$ covered with E-glass style 120 t = 2.7 mm	(X)		X	b = 40 mm, b = 50 mm L = 80 mm			X	(X)

Table 1: Damage Tolerance Test Parameters with CFRP

THIS DOCUMENT PROVIDED BY THE
TECHNICAL LIBRARY
ABBOTTAEROSPACE.COM

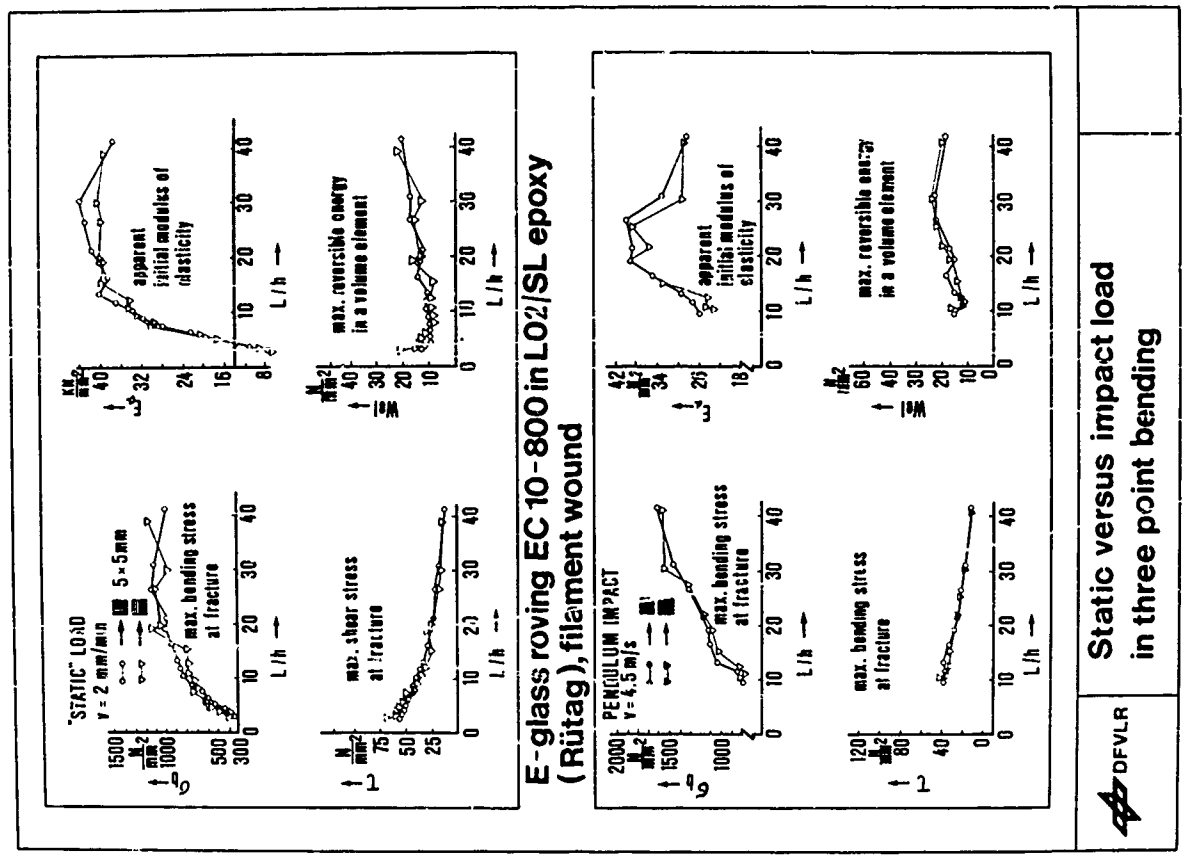

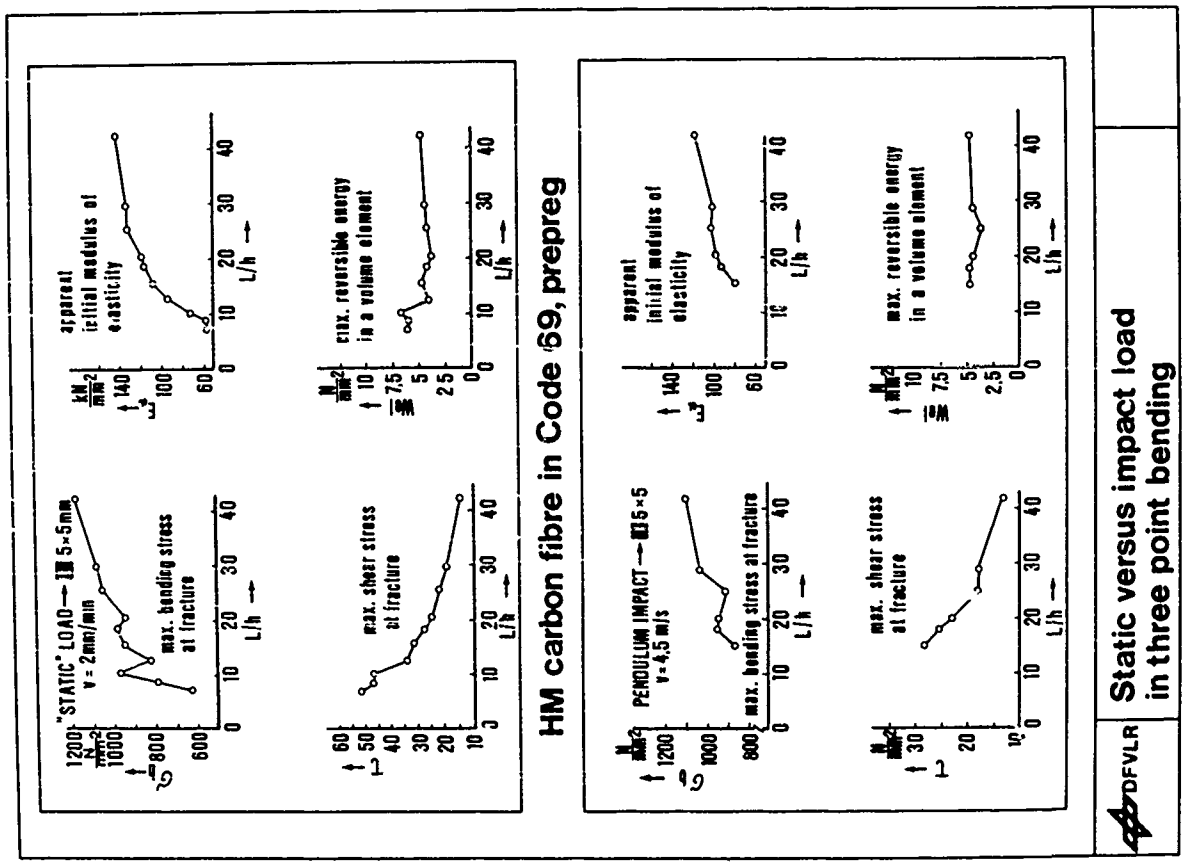

Fig. 1 Charpy Impact Test Results at Different Beam Lengths

TECHNICAL LIBRARY
ABBOTTAEROSPACE.COM

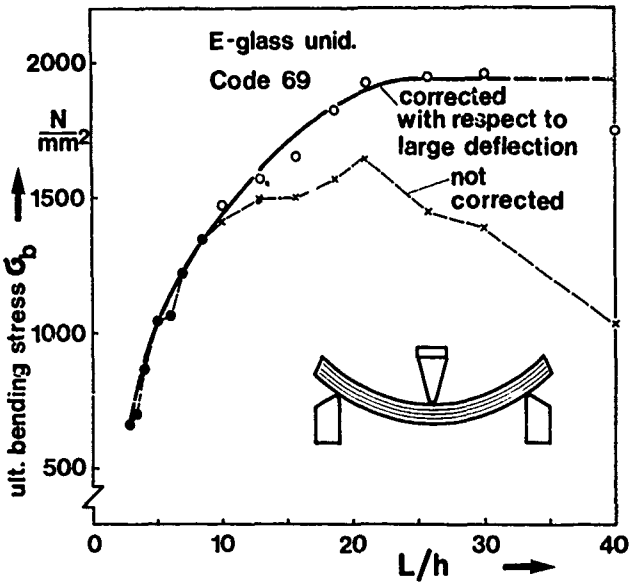

Fig. 2a Long Beam Correction for Ult. Strength

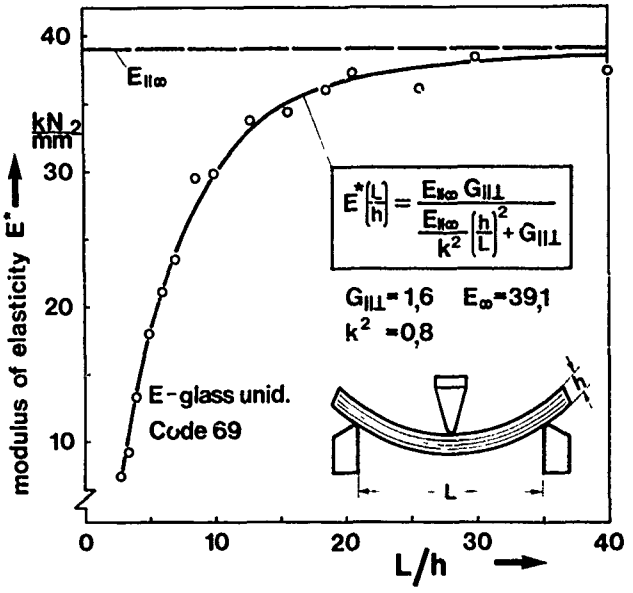

Fig. 2b Apparent Modulus of Elasticity

Fig. 2 Apparent Modulus of Elasticity and Ultimate Bending Strength of Three-Point-Bending Beams

THIS DOCUMENT IS PROVIDED BY THE ABBOTT AEROSPACE
TECHNICAL LIBRARY
ABBOTTAEROSPACE.COM

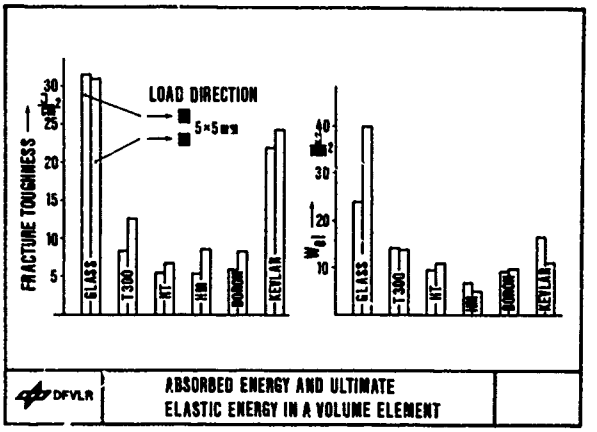

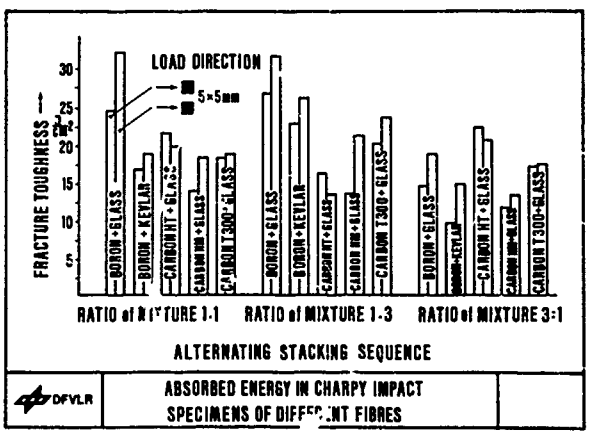

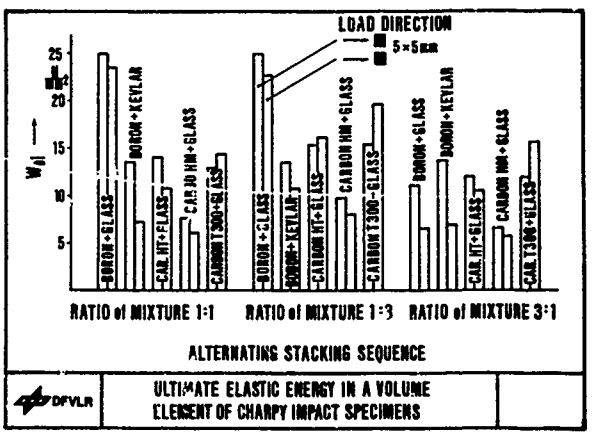

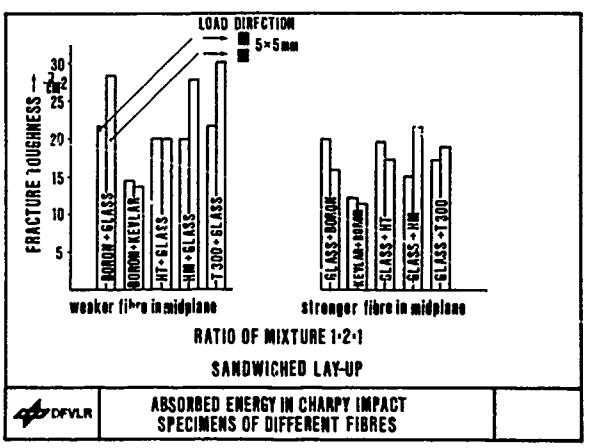

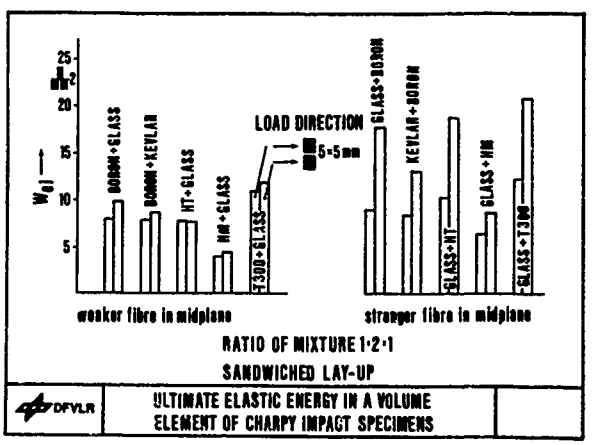

Fig. 3 Totally Absorbed Energy and Elastically Endured Energy in Charpy Impact Beams with Various Unidirectional Reinforced Fibre Compositions

TECHNICAL LIBRARY
ABBOTTAEROSPACE.COM

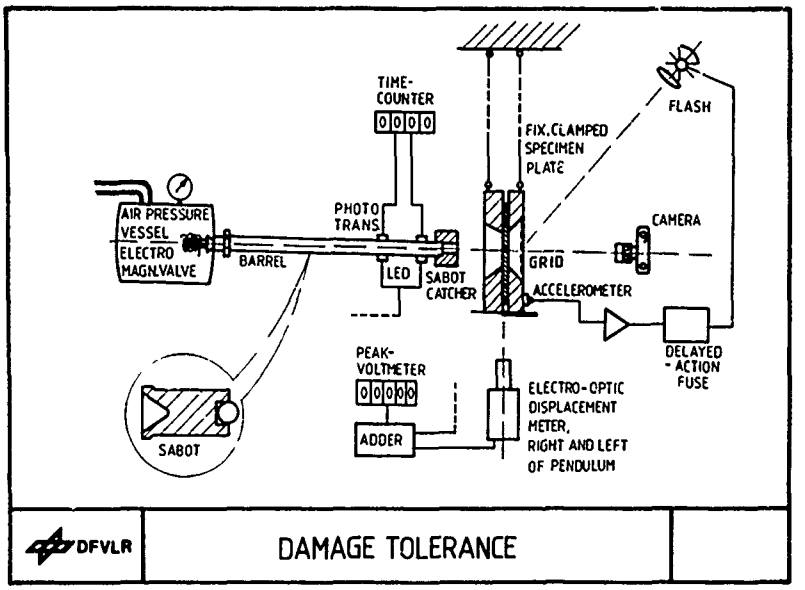

Fig. 4 Test Equipment for Impacting Plates Including Registration of Specimen Deformation and Transmitted Energy

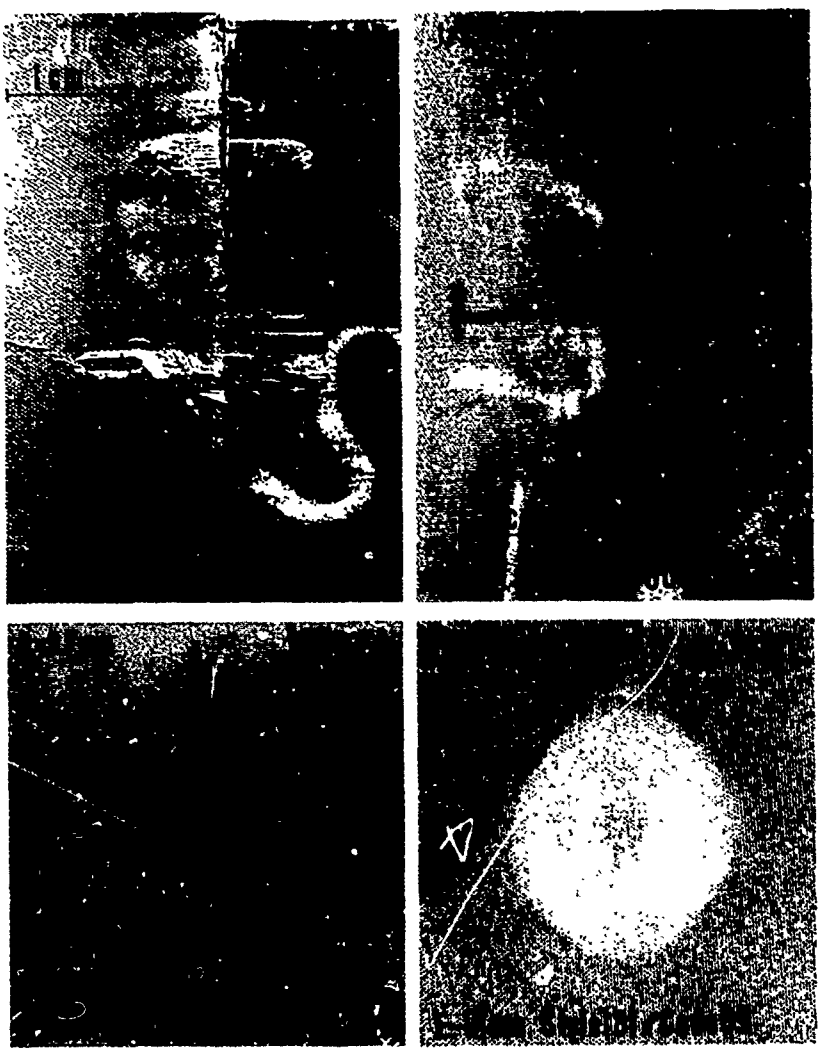

Fig. 5 Response of Various GFRP and CFRP Laminates to Impact by a Glass Sphere, m = 13 g at v = 42 m/s

THIS DOCUMENT PROVIDED BY THE ABBOTT AEROSPACE
TECHNICAL LIBRARY
ABBOTTAEROSPACE.COM

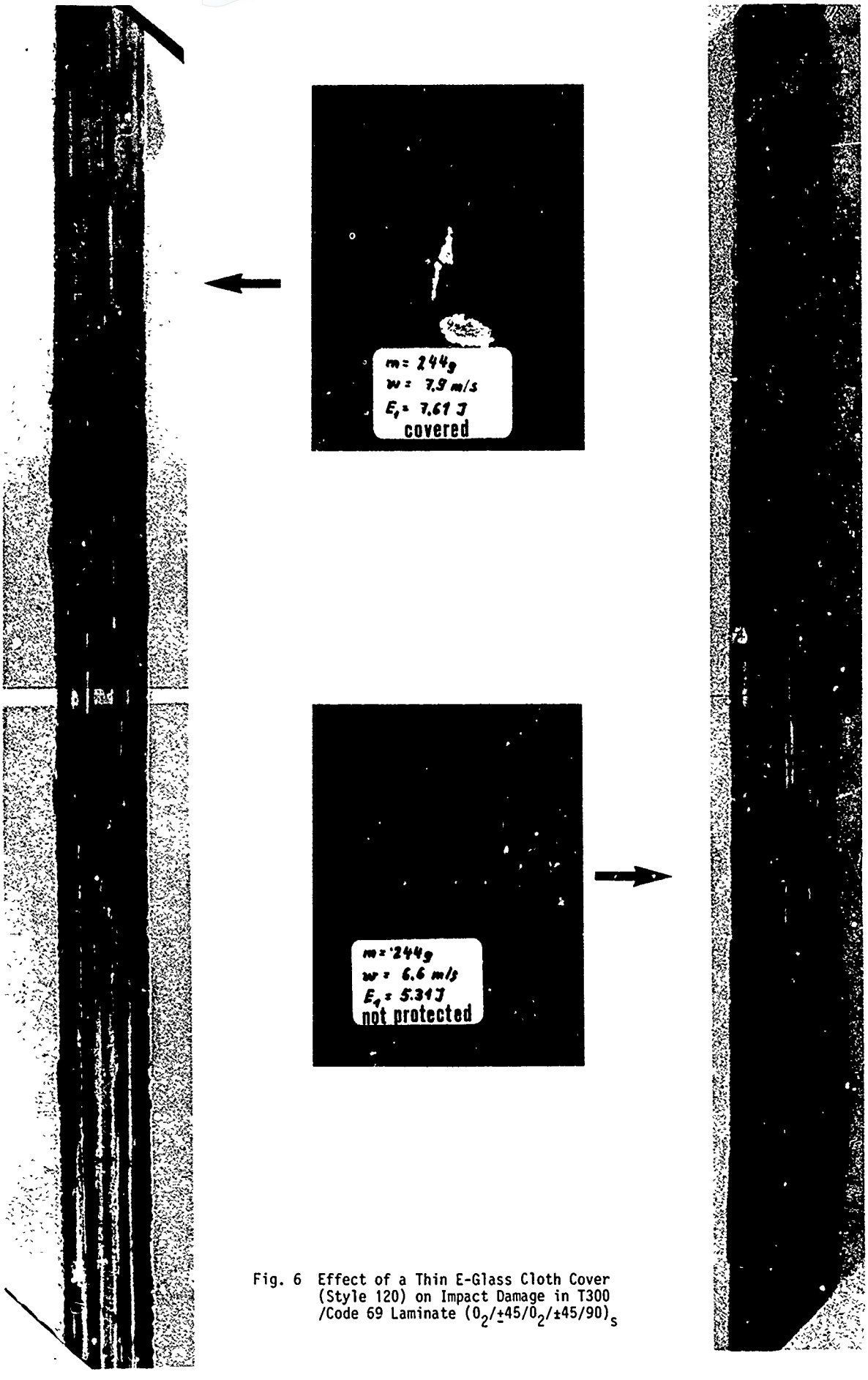

Fig. 6 Effect of a Thin E-Glass Cloth Cover (Style 120) on Impact Damage in T300 /Code 69 Laminate $(0_2/\pm45/0_2/\pm45/90)_s$

TECHNICAL LIBRARY
ABBOTTAEROSPACE.COM

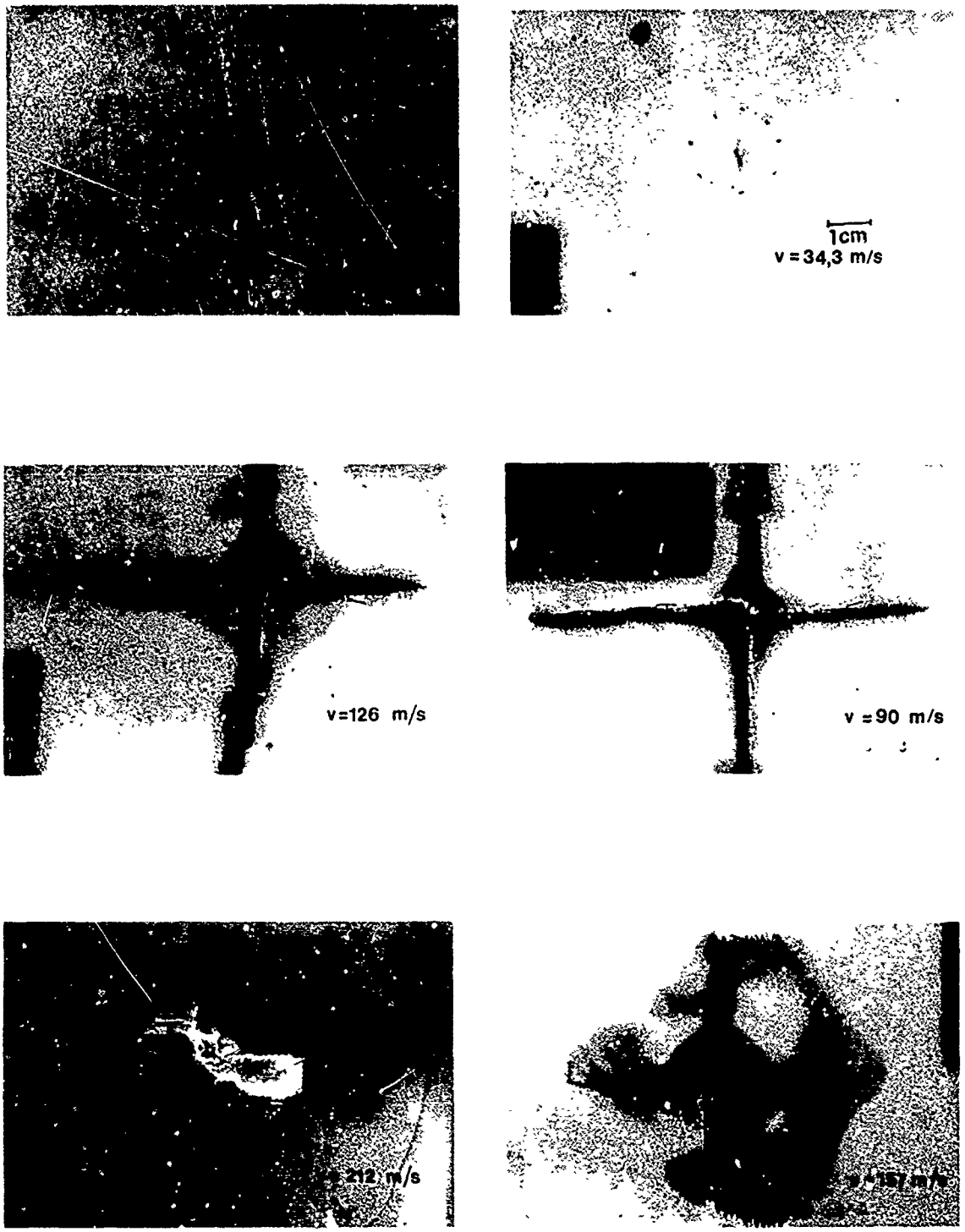

Fig. 7 Damages in E-Glass/Epoxy (R2500-15-181 from BROCHIER) Impacted by a Glass Sphere (m = 13 g) at Various Speeds; The Plate (1.4 mm thick) was Clamped in 130 mm Diameter

TECHNICAL LIBRARY
ABBOTTAEROSPACE.COM

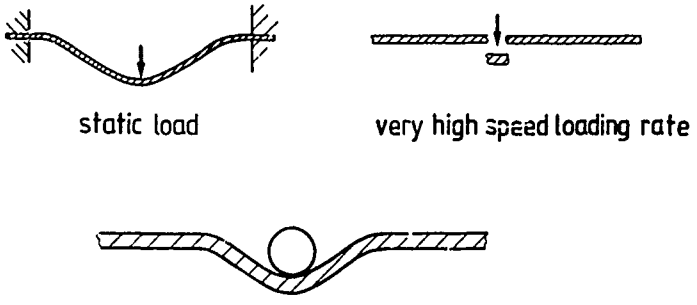

PRINCIPLE OF MAXIMUM DEFORMATIONS IN A THIN PLATE
IN STATIC AND DYNAMIC LOADING

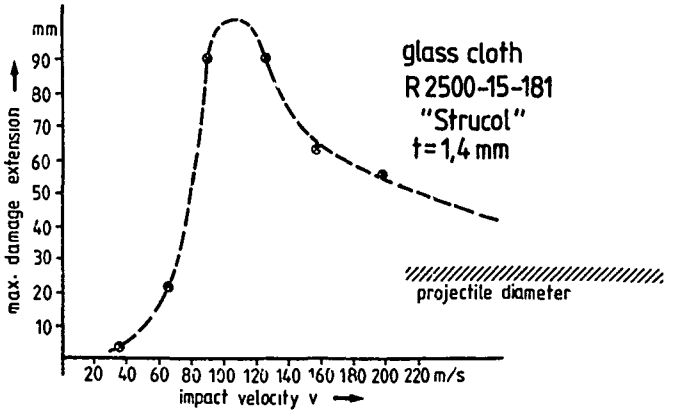

CRACK LENGTHS IN GFRP FABRIC
SHOT WITH A GLASS SPHERE (m=13g)

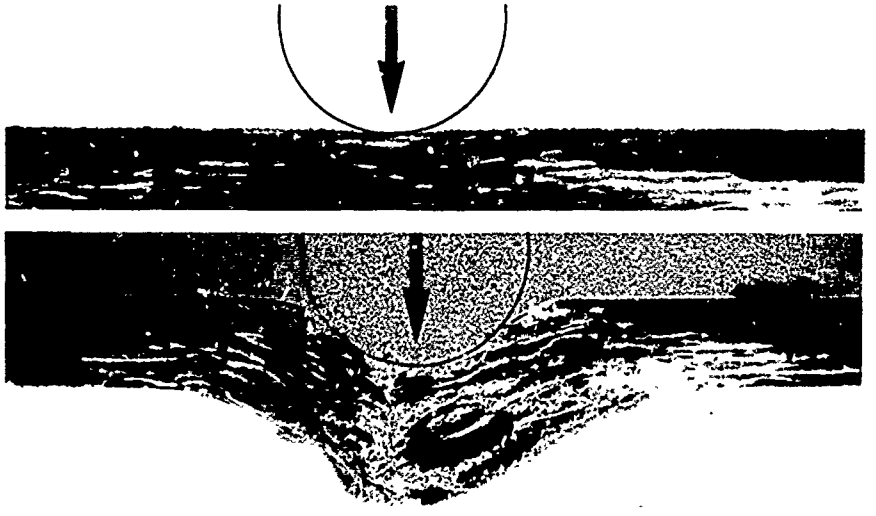

Fig. 8 Principles of Influence of Impactor Velocity and Support Conditions on Specimen Response
Above: Deformation in Large Plates Depending on Impactor Velocity (Evaluation Fig. 7)
Below: Response of GFRP Fabric Laminate on a Dropped Tool (m = 528 g) at Narrow and Wide Support at v = 5.9 m/s

THIS DOCUMENT PROVIDED BY THE ABBOTT AEROSPACE
TECHNICAL LIBRARY
ABBOTTAEROSPACE.COM

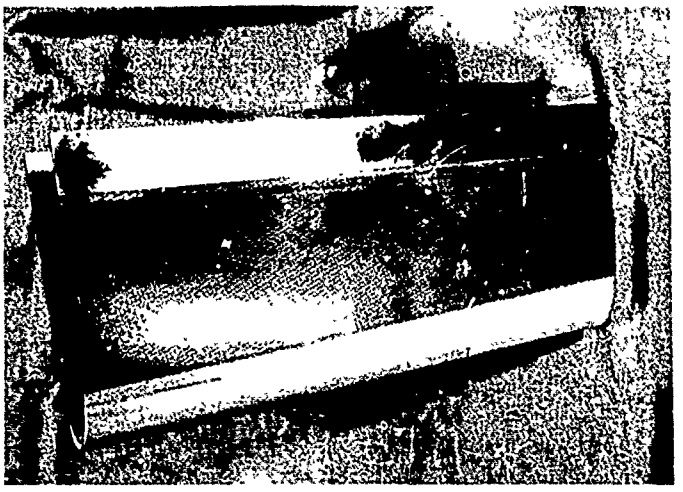

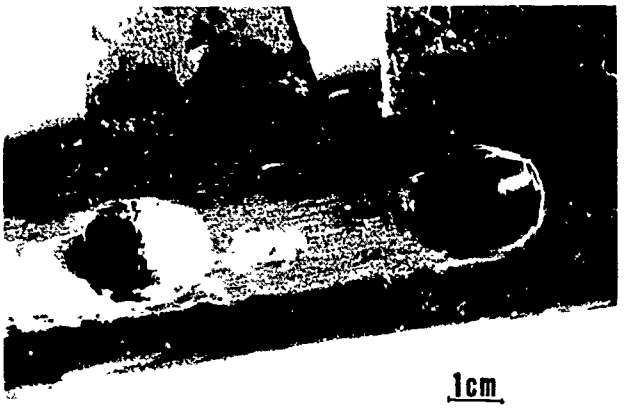

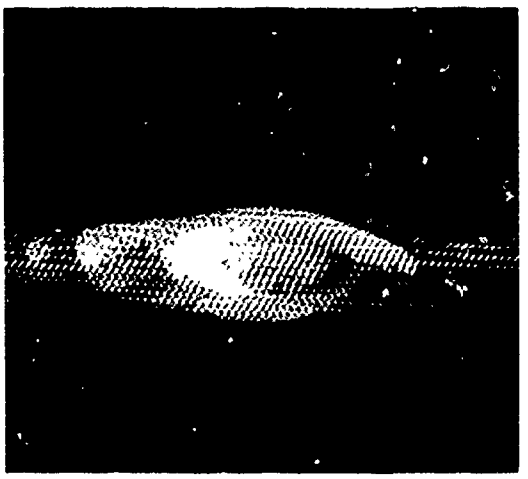

Fig. 9 Demonstration of Impact Resistance of GFRP versus CFRP with the Leading Edge of ALPHA-JET Horizontal Stabilizer (Top)
Load: Impact by a Glass Sphere 21 mm Diameter at v = 54 m/s
Material: 3 mm SC130 / Code69 0/90°, covered with 0.2 mm Aluminium Foil (Middle)
0.8 mm Grade002 / Code 69 Sandwiched by 0.9 mm E-Glass Style 181 (Bottom)

THIS DOCUMENT PROVIDED BY THE ABBOTT AEROSPACE
TECHNICAL LIBRARY
ABBOTTAEROSPACE.COM

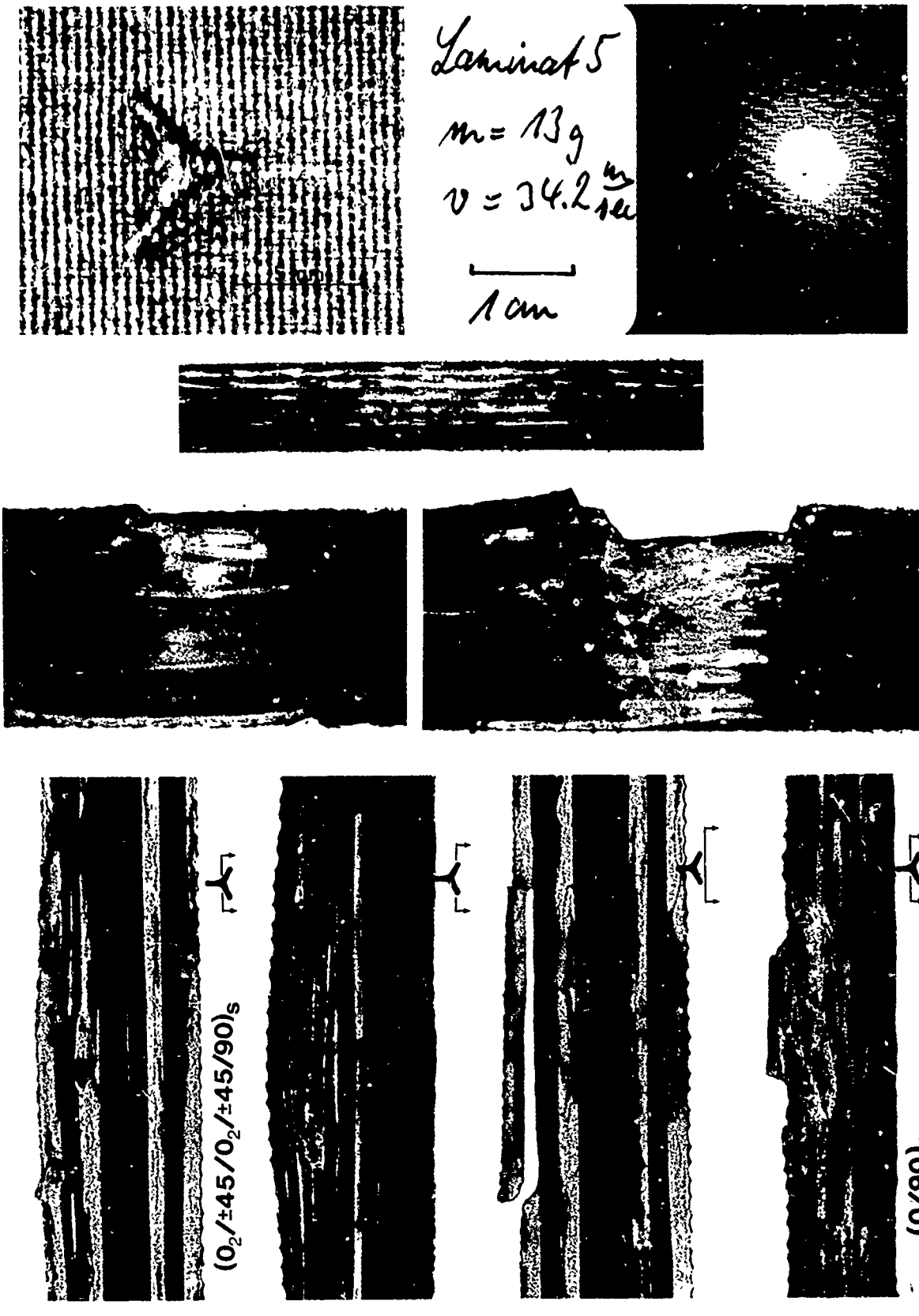

Fig. 10 Defects Introduced in GFRP and CFRP Simulating the Response of Dropped Tools

Above: Threesquare Indent in CFRP, Die Force 5 kN (left)
Glass Sphere Impact on GFRP Fabric 1.7 mm, m = 13 g, v = 45 m/s (right)

Middle: Cross Section of Glass Sphere Impact on GFRP Fabric (above)
Cross Section of Threesquare Indent in GFRP, Die Force 2.F kN (left) 5 kN (right)

Bottom: Cross Section of Threesquare Indents in CFRP T300 / Code69

THIS DOCUMENT PROVIDED BY THE ABBOTT AEROSPACE
TECHNICAL LIBRARY
ABBOTTAEROSPACE.COM

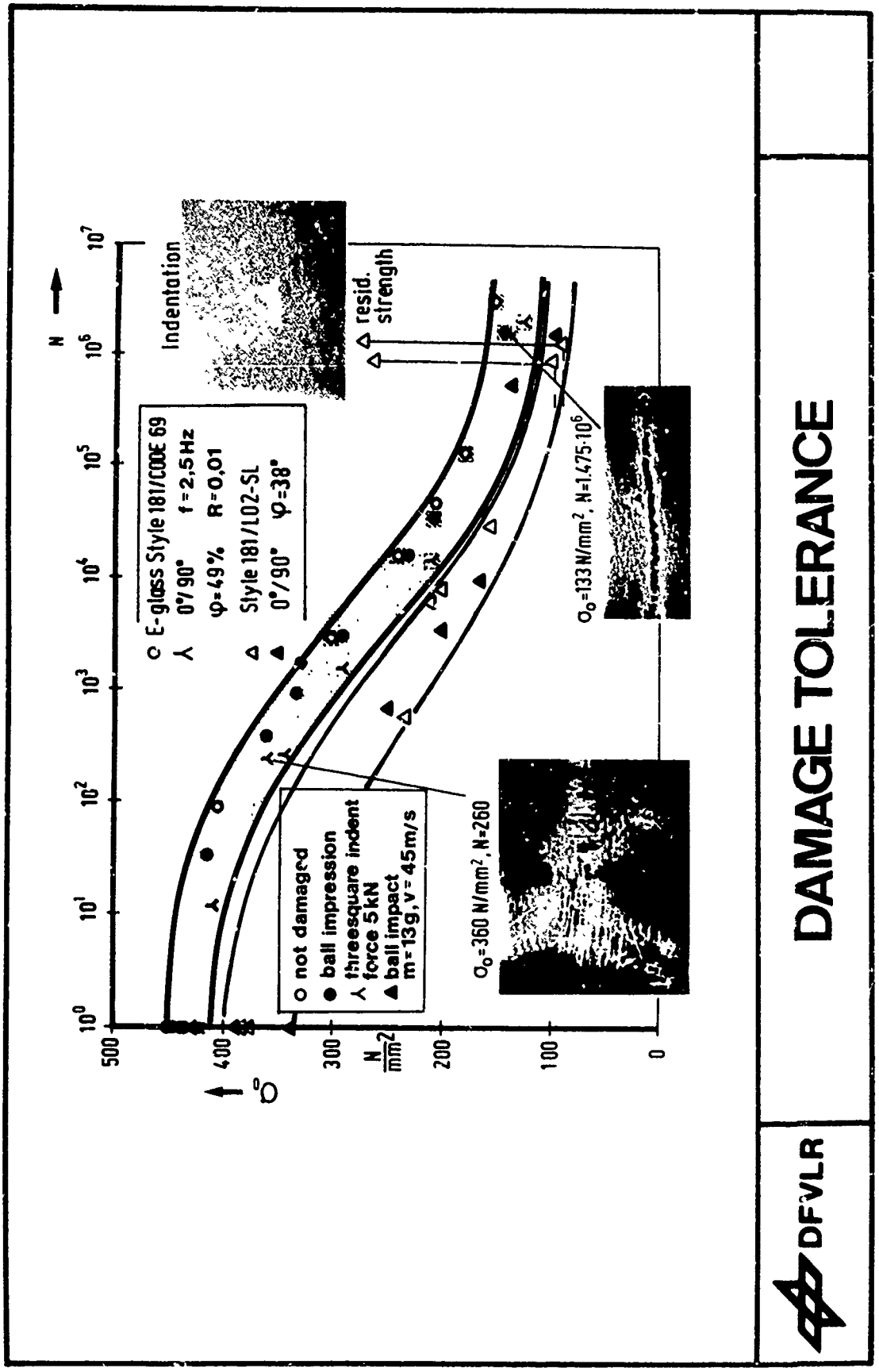

Fig. 11 Fatigue Curves of GFRP Fabric

THIS DOCUMENT IS BASED ON THE BEST COPY AVAILABLE
TECHNICAL LIBRARY
ABBOTTAEROSPACE.COM

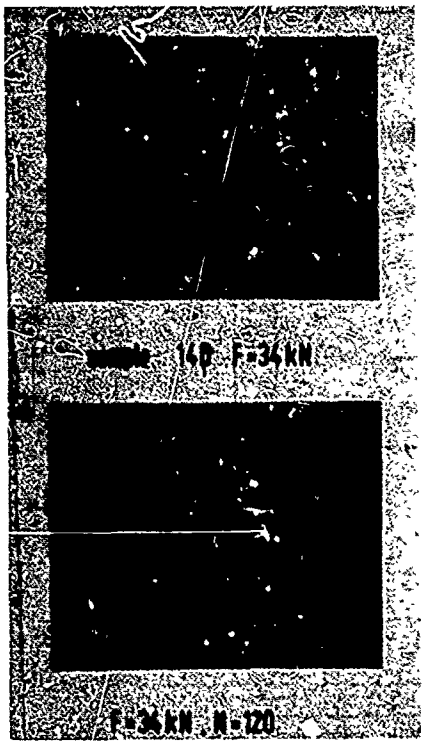

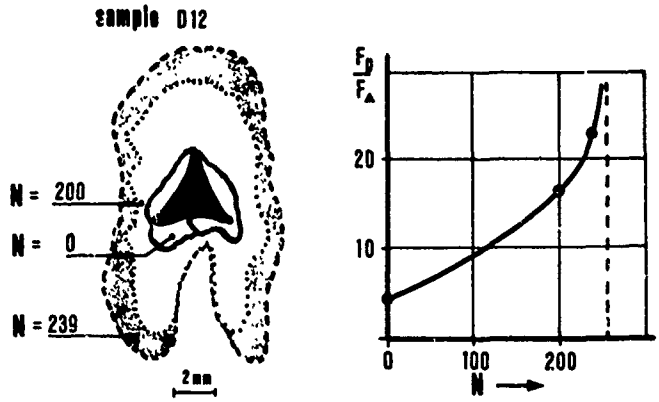

propagation of delamination

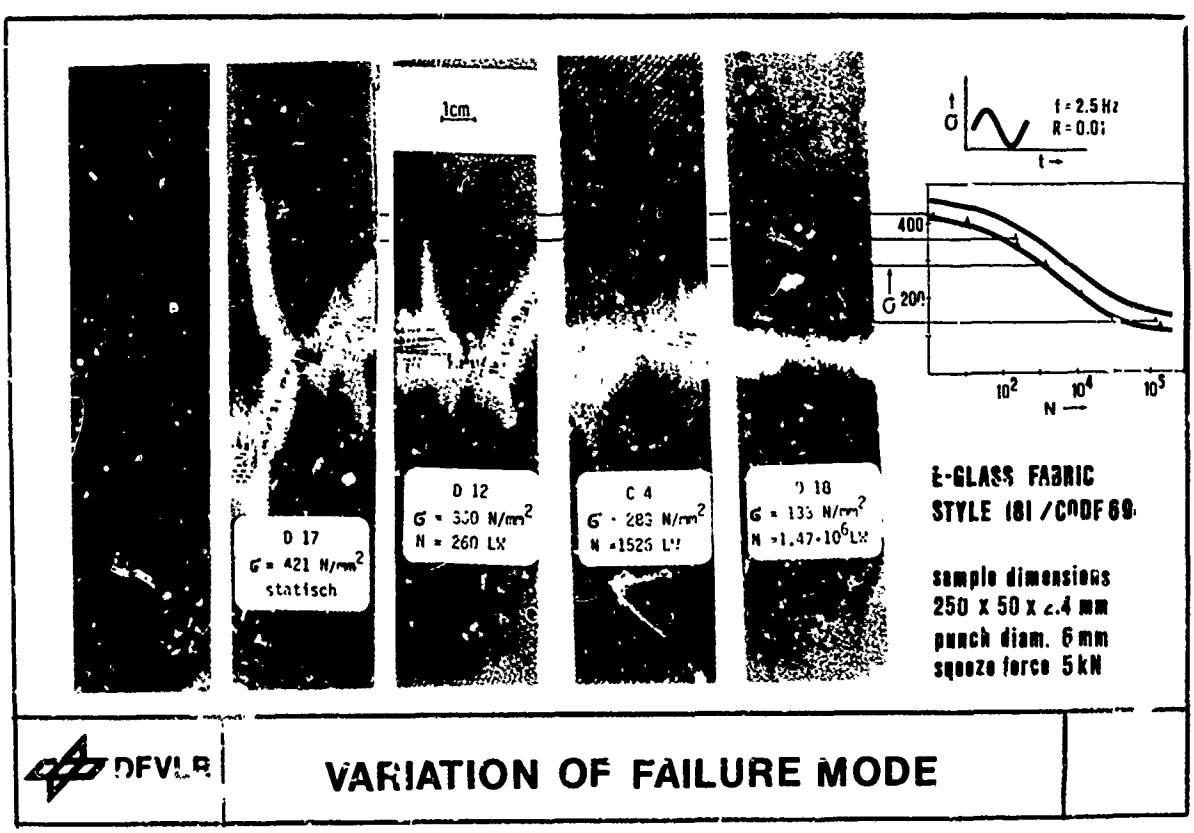

Fig. 12 Types of Failure Mode and Damage Propagation in GFRP Fabric Laminates

TECHNICAL LIBRARY
ABBOTTAEROSPACE.COM

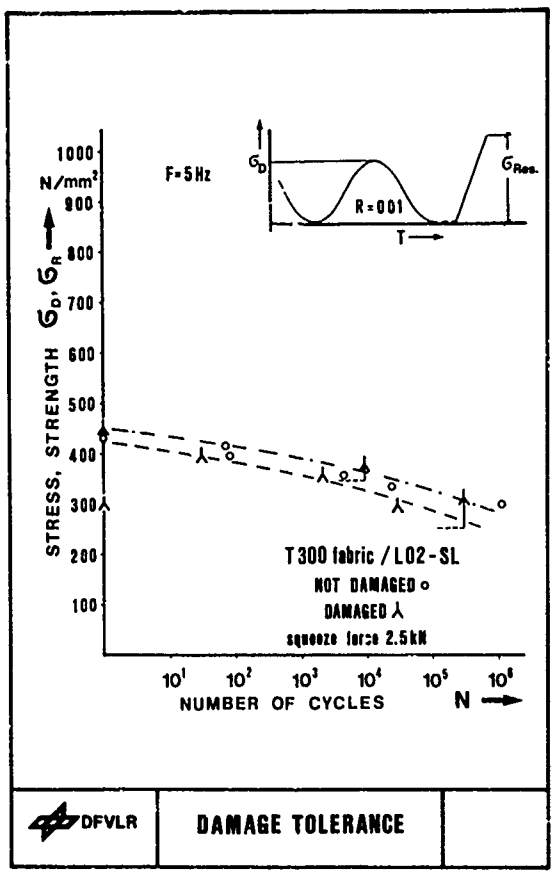

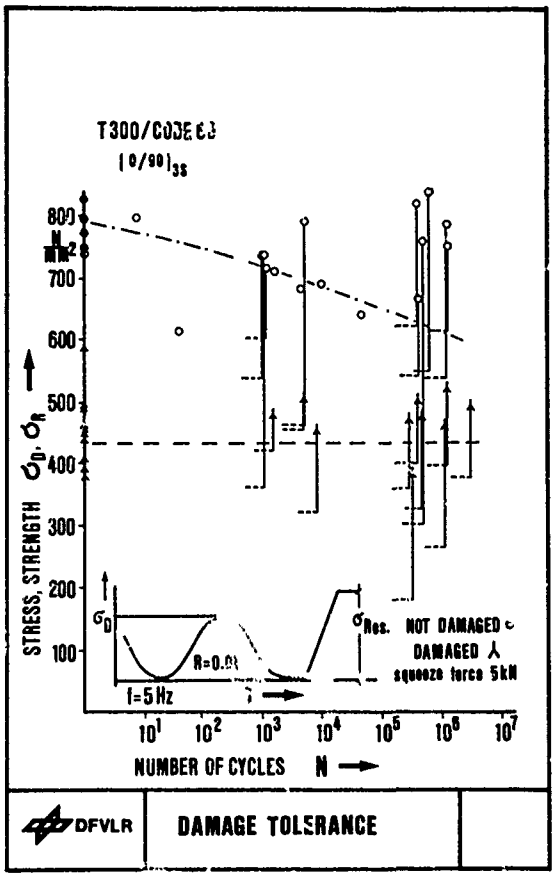

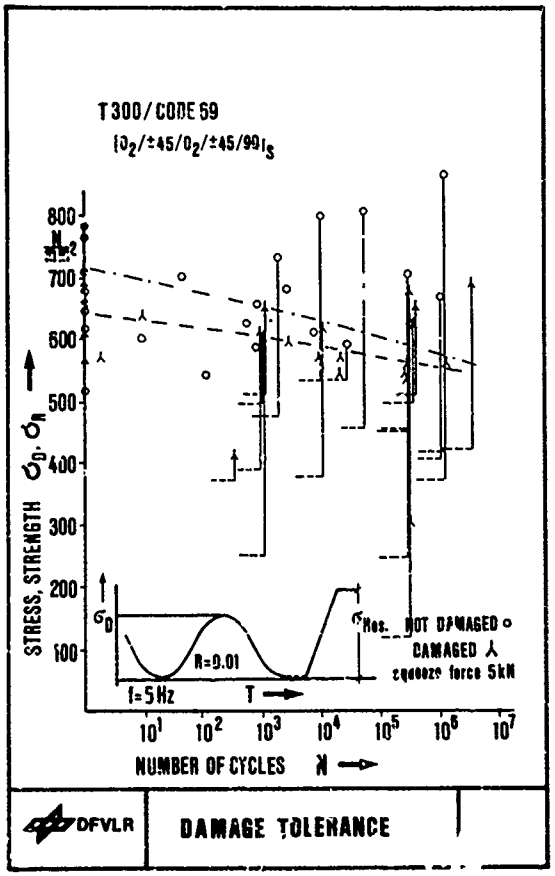

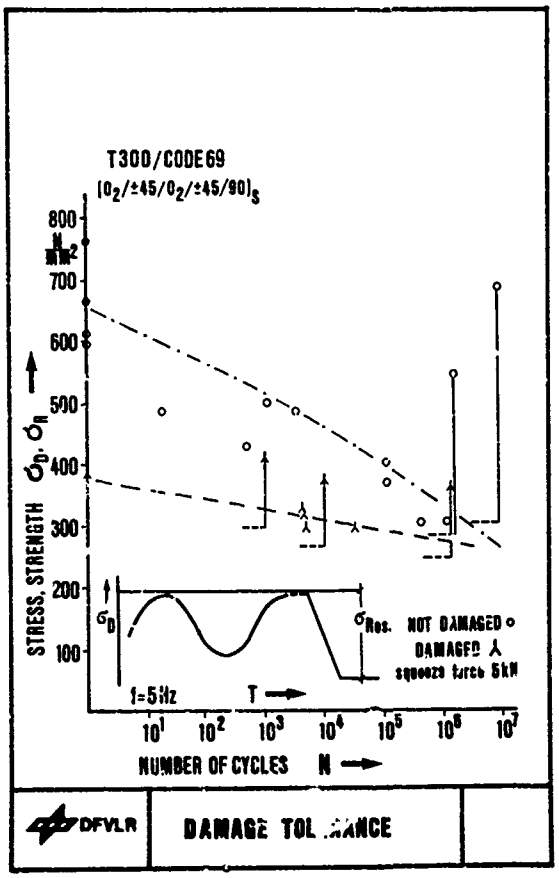

Fig. 13 Fatigue Curves and Residual Strengths (in Tension) of CFRP Specimen with Indentation Damages

TECHNICAL LIBRARY
ABBOTTAEROSPACE.COM

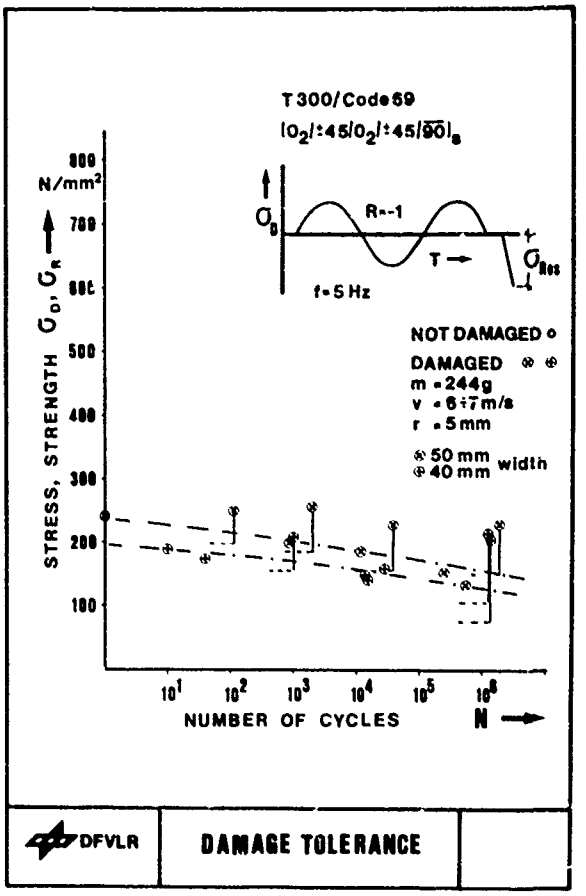

Fig. 14 Fatigue Data of CFRP Specimens with Impact Damages ('Dropped Tool')

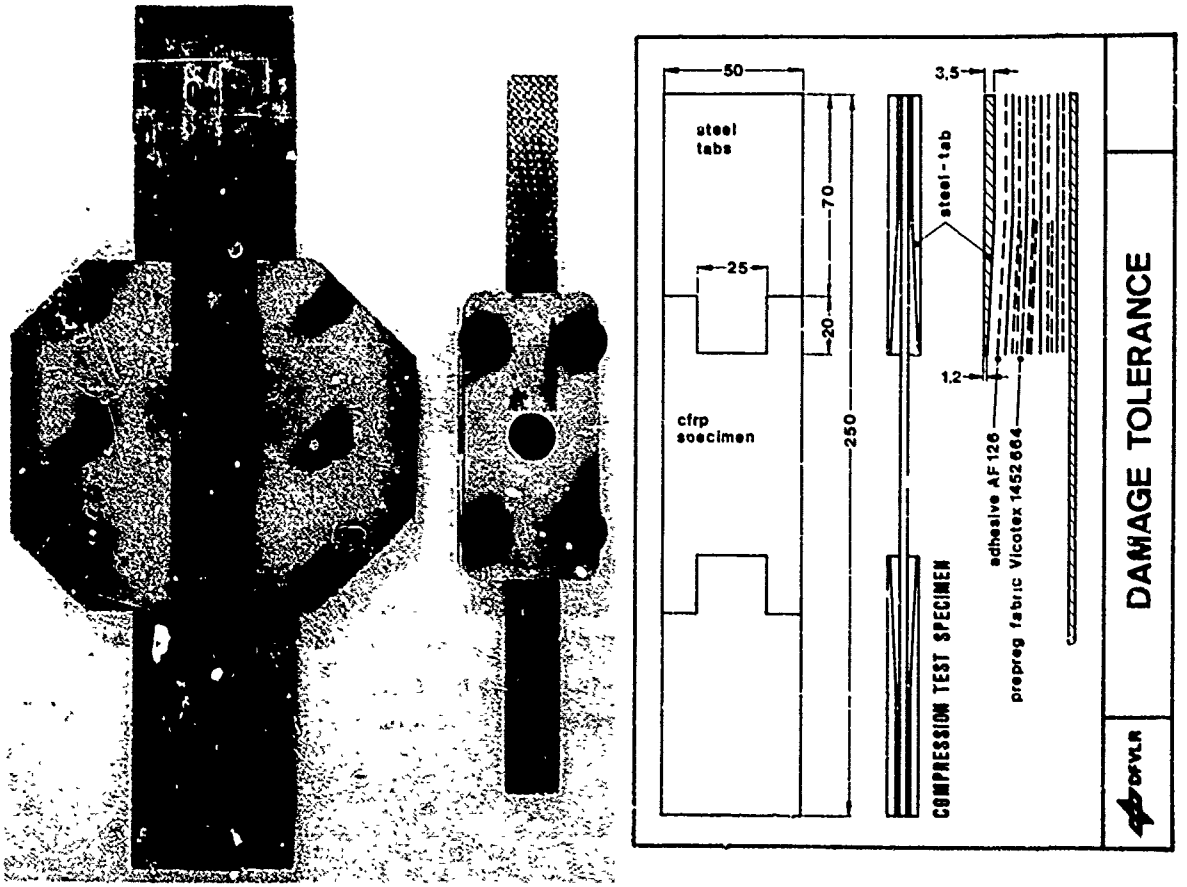

Fig. 15 Antibuckling Devices with Damaged and Fatigue Tested Specimens

THIS DOCUMENT PROVIDED BY AND ACCESSED FROM THE
TECHNICAL LIBRARY
ABBOTTAEROSPACE.COM

Fig. 16 Details of Damaged and Fatigue Tested Specimen Made of T300 / Code 69 $(0_2/\pm45/0_2/\pm45/90)_s$

Impact Parameters: m = 244 g, v = 6.8 m/s, Sontact Tip Radius = 5 mm, E_{kin} = 5.64 J
Plate Clamped in 130 mm Diameter, Irrev. Absorbed .nergy E_{abs} = 3.9 J

Load Parameters: σ_{max} = ±103 n/mm² (R = -1), N = 1.3 Mio Cycles
Residual Compression Strength σ_{re} = 216 N/mm²

TECHNICAL LIBRARY
ABBOTTAEROSPACE.COM

Fig. 17 Fractures of Impact Damaged Specimens after Cyclic Fatigue Loading (R = -1) (above, middle) after Quasi-static Tension Test (bottom); Impact Parameters similar to Fig. 16

THIS DOCUMENT PROVIDED BY THE
TECHNICAL LIBRARY
ABBOTTAEROSPACE.COM

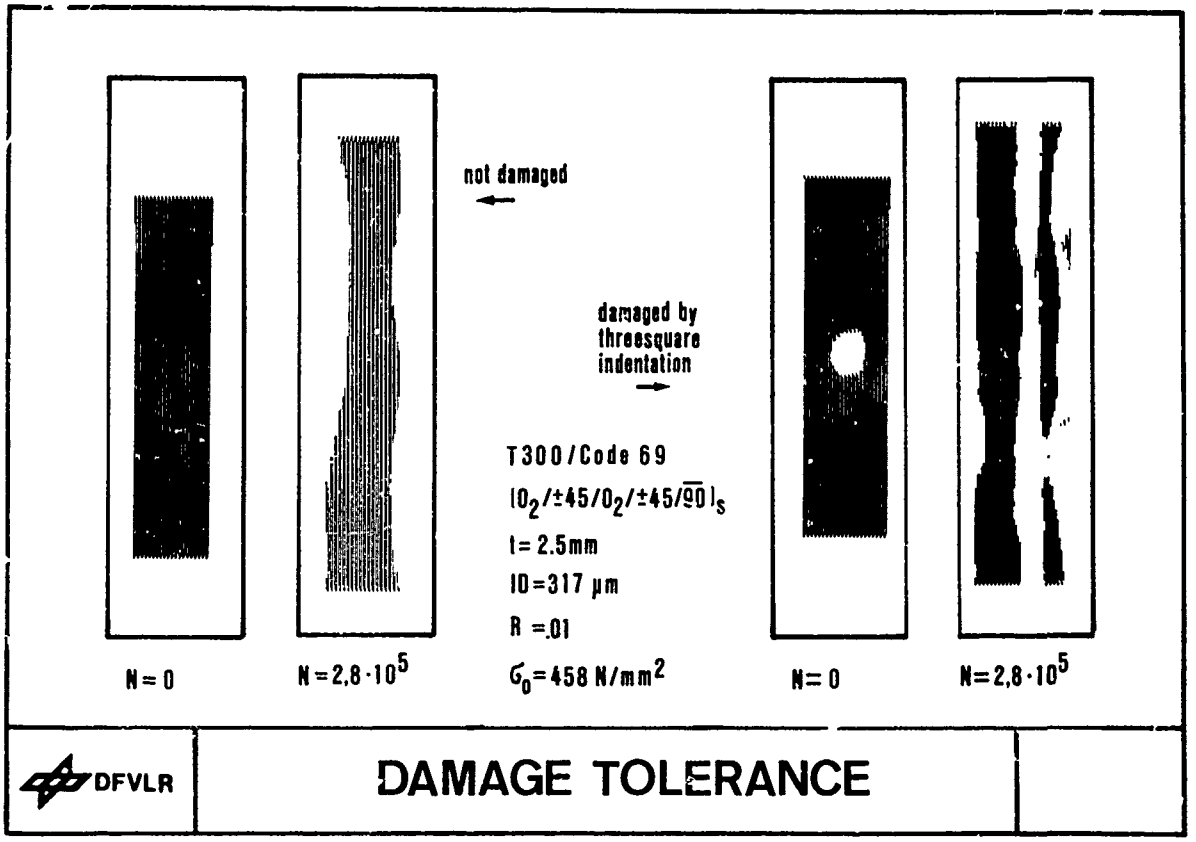

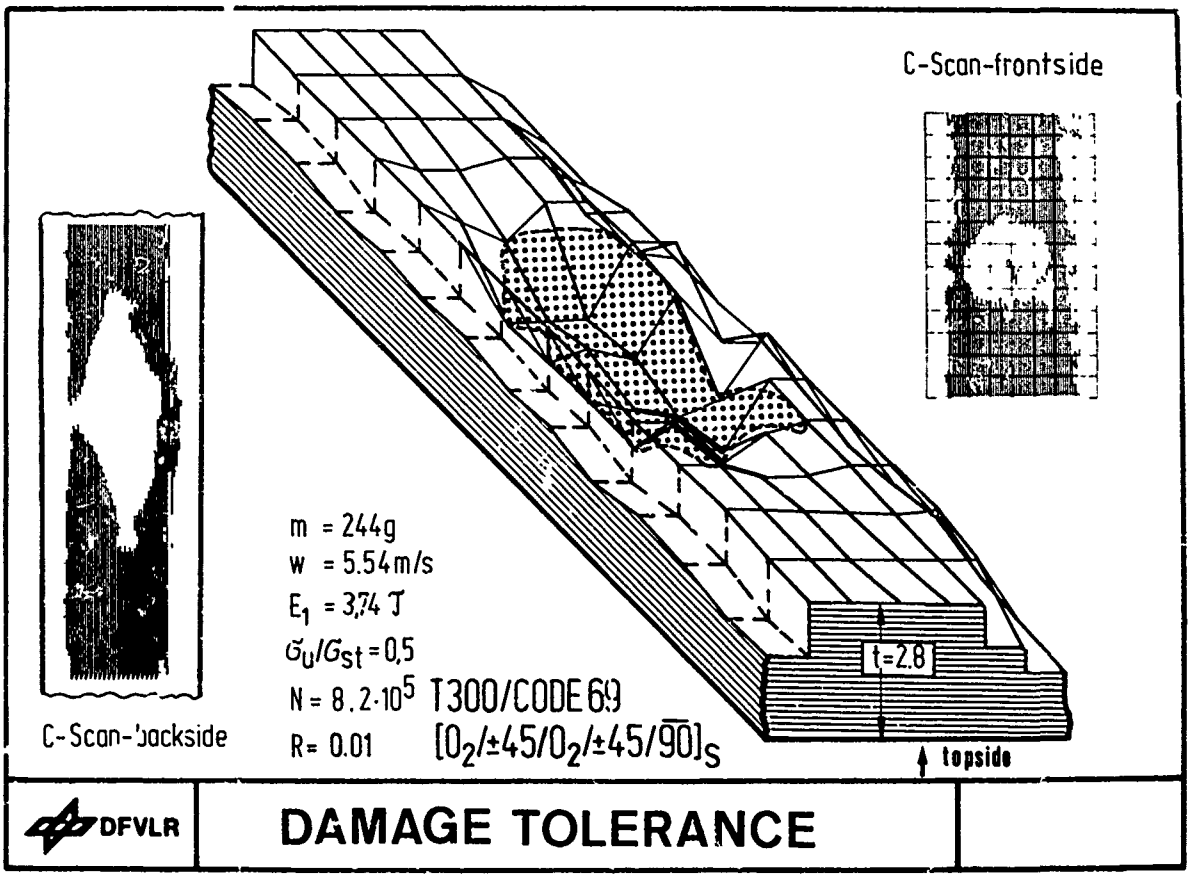

Fig. 18 Ultrasonic Scan of Fatigue Loaded Specimens Indicating Delamination Zones
Impact Damage (above), Indentation Damage (below)

THIS DOCUMENT PROVIDED BY THE ABBOTT AEROSPACE
TECHNICAL LIBRARY
ABBOTTAEROSPACE.COM

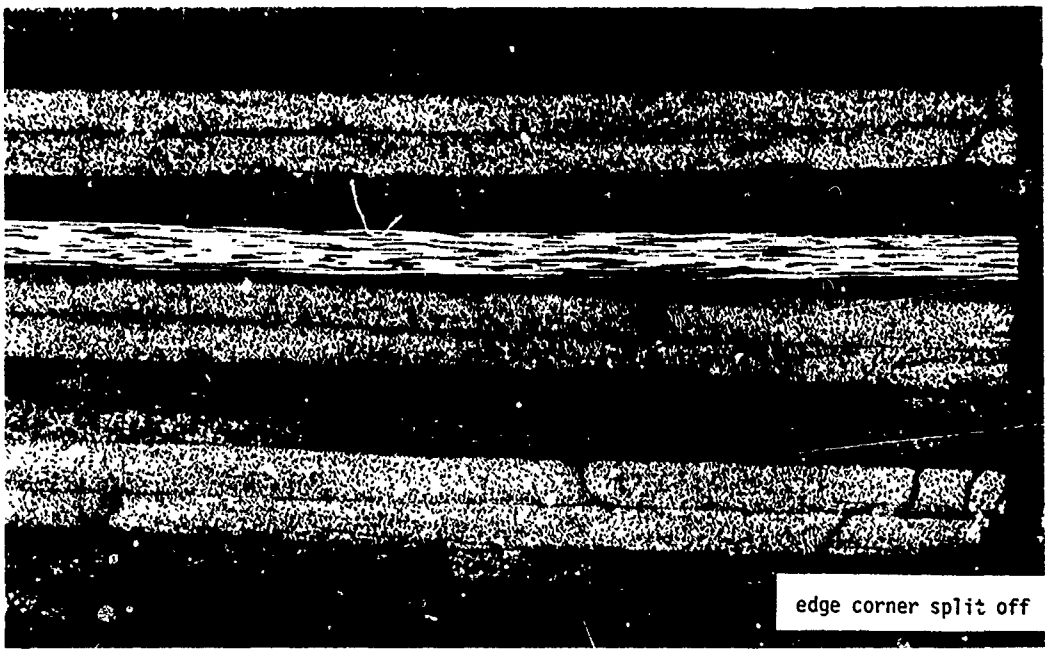

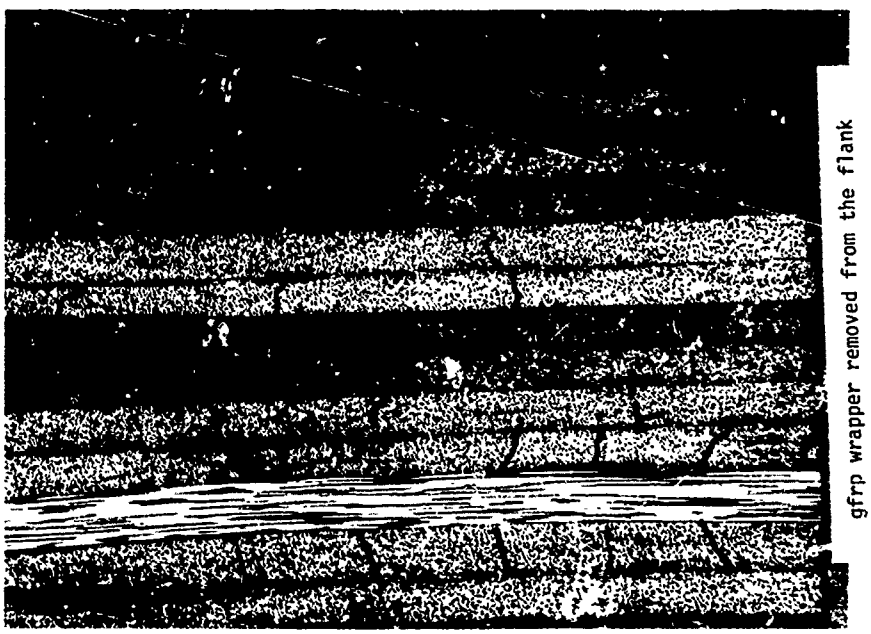

Fig. 19 Prevention of Edge Effect in Tension Loaded Coupon Specimens by Wrapping Around a Thin Glass Cloth; Material: T300 / Code69 $(0_2/\pm45/0_2/\pm45/90)_s$
Load Conditions: σ_u = 600 N/mm², R = =.01, N = $1.1 \cdot 10^5$

THIS DOCUMENT PROVIDED BY THE
TECHNICAL LIBRARY
ABBOTTAEROSPACE.COM

RECORDER'S REPORT

SESSION III -- MECHANICAL EFFECTS AND HAZARDS

by

K.Brunsch
Messerschmitt-Bölkow-Blohm GmbH/UF
Postfach 80 11 60
8000 München 80
West Germany

Four papers were presented as listed below:

"[illegible]ips between Impact Resistance and Fracture Toughness in Advanced Composite Materials" by G.Dorey

"Erosion et Impacts sur les Pales d'Hélicoptères en Composites" par M.G.Torres

"Graphite-Epoxy Panel Compression Strength Reduction due to Local Impact" by M.F.Card and M.D.Rhodes

and

"The Influence of Defects on the Behaviour of Composites" by R.Aoki and K.Stellbrink.

The paper by Torres presented information from service experience and from tests with rotor blades, that is with complete FRC structures. The remaining papers present somewhat more basic research aiming to relate impact defects with residual strength, static and fatigue, and also fracture toughness with residual strength after impact.

Torres very favourably highlighted the excellent structural properties for FRC for rotary wing application. Information on residual strength after extensive damage caused by ballistic impact is given. On the other hand, the need for sufficient erosion protection was also pointed out. The presentation ended with a film of impact tests of SA 340 main rotor blades against wooden rods. Seeing the blades cut a 200 mm thick rod, the recorder was impressed and concerned. The concern is on whether such information might reduce pilots' carefulness.

The paper by Dorey presents the results of impact tests and of tests with machine notched specimens. He corrects for the damage zone (r_p) and by that means achieves reasonably good prediction of the residual strength of notched laminates. K_c is between 20 and 50 MN $m^{-3/2}$, which means that considerable notch sensitivity for some laminates was found. Good correlation was also found between Charpy impact energy and fracture toughness. The reduction of residual strength versus incident energy appears to be more troublesome to predict. The same energy may cause differences in residual strength of up to a factor of 2, depending on impact velocity. The information given is that specimens of one particular laminate failed at incident energy loads of 3 to 8 J when loaded to about 40% of tensile ultimate strength.

The paper by Card and Rhodes presents test results of 560 specimens and components that had been impacted while being compression loaded. The research work reported was done with sandwich beams, laminated plates and top-hat stiffened panels. The most important conclusion from this work is that, with the material investigated, there is a .003 compression strain threshold, i.e. components compression loaded to this strain do not fail when impacted with up to 15 J energy projectiles. This strain threshold was found to be valid when using a resin system with .01 ultimate strain. A tougher matrix system – about .04 ultimate strain – considerably improves damage tolerance. Taking into account the well known rules of stress and strain magnification in transversely loaded composites a .01 ultimate strain matrix system does appear to be too brittle. Even with that matrix system and the low .003 strain threshold, a composite wing is weight effective in comparison to an aluminium alloy wing.

The last paper of the session by Aoki and Stellbrink reported many test results, the most important ones covering the influence of defects on the fatigue strength of CFC specimens. Prior to fatigue testing, the specimen had been damaged by ball impression, three-square indentation and ball impact. Fatigue tests were done with $R = .01$, $R = -0.01$, $R = -1$ and the residual strength after a given number of cycles was determined. Based on a limited number of specimens, the conclusion can be drawn that high-cycle fatigue strength is reduced much less than static strength. Toughness of resins, which contributes to shear strength, again was found to improve damage tolerance.

Generally it must be said that, apart from the excellent papers given, there remains a considerable amount of work to be done with reference to damage tolerance. For example, the influence of moisture and of the load history prior to an impact should also be known.

THIS DOCUMENT PROVIDED BY THE TECHNICAL LIBRARY
ABBOTTAEROSPACE.COM

EVALUATION DU COMPORTEMENT A LA FOUDRE DE STRUCTURES EN MATERIAUX COMPOSITES HAUT MODULE

par
J. ROUCHON, D. GALL
CENTRE D'ESSAIS AERONAUTIQUE DE TOULOUSE
23, avenue Henri Guillaumet
31056 - TOULOUSE CEDEX
France

RESUME

Le foudroiement en vol d'un aéronef est un phénomène relativement fréquent qui se traduit par des endommagements voire des destructions au niveau, d'une part des équipements, d'autre part des structures et en particulier celles en matériaux composites.

Ce document, après quelques généralités sur la foudre, (mesure des caractéristiques de la foudre en vol, procédés de simulation au sol), présente des résultats d'essais effectués en laboratoire sur des échantillons (monolithiques en carbone-époxy, sandwichs avec revêtements bore-époxy), des éléments de structures réels, ainsi que les procédés de contrôle associés.

1 - GENERALITES SUR LE FOUDROIEMENT DES AERONEFS

On estime que globalement, il existe dans le monde à tout instant 2000 à 5000 orages produisant environ une centaine d'éclairs par seconde. Ces orages ne sont pas répartis uniformément autour du globe terrestre. On note en effet environ 200 jours d'orage par an dans les zones équatoriales, alors que dans les zones tempérées on n'en relève seulement que quelques dizaines.

On comprend dès lors que les aéronefs, évoluant à proximité ou dans les masses nuageuses, soient foudroyés en vol.

Les statistiques, à l'échelon mondial montrent qu'à l'heure acutelle, la fréquence des foudroiements est de l'ordre de :

- 1 toutes les 2000 heures de vol pour les courts et moyens courriers.
- 1 toutes les 5000 heures de vol pour les longs courriers

Cette différence est due au fait que les avions courts et moyens courriers ont un temps de vol par mission en basse et moyenne altitude supérieur à celui des longs courriers. Le maximum des foudroiements a lieu à une altitude comprise entre 1000 et 4000 m .

Il importe donc, qu'au cours de la trentaine de coups de foudre que subissent les avions pendant leur vie, il n'encourent non seulement pas de risques catastrophiques, mais encore que les endommagements soient minimes. Les structures composites étant beaucoup plus sensibles aux effets de la foudre que les structures métalliques, des études et essais ont donc été entrepris afin de mesurer les risques et définir des protections spécifiques.

2 - MECANISMES DU FOUDROIEMENT

2.1. Origine de la foudre

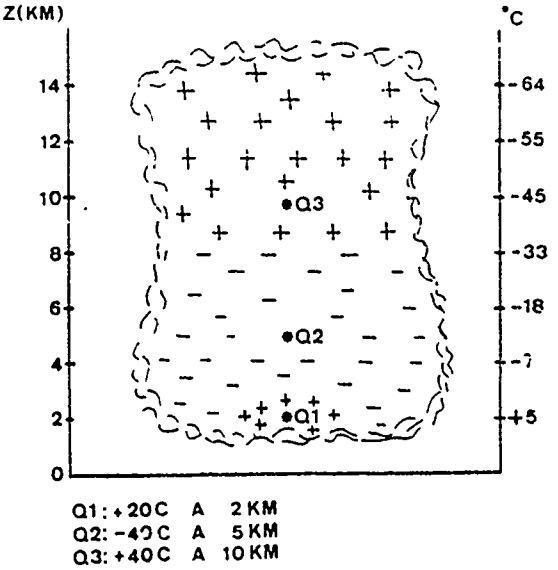

SCHEMA D'UN NUAGE ORAGEUX

- fig. 1 -

This document is provided by the
TECHNICAL LIBRARY
ABBOTTAEROSPACE.COM

L'origine de la foudre se situe généralement au niveau des nuages à développement vertical tels que les cumulo-nimbus (fig. 1). A l'intérieur de ce type de nuages, les violents courants d'air entraînent les gouttelettes d'eau qui par frottement, se chargent en électricité. Ces gouttelettes se répartissent, à l'intérieur du nuage, en îlots de charges électriques plus ou moins nombreux.

Lorsque le champ électrique E = V/d, V différence de potentiel exprimée en volts (plusieurs centaines de millions de volts dans le cas de foudre), d la distance entre les îlots, atteint une valeur suffisante (environ 500 000 V/m) un arc électrique jaillit entre ces charges.

On distingue généralement deux types de coups de foudre :

- ceux entre les nuages et le sol (30 % des cas)
- ceux entre nuages, ou à l'intérieur d'un même nuage (70 % des cas).

Pour les coups de foudre entre nuage et sol, on distingue :

- les coups positifs : amorçage des charges positives du nuage (10 % des cas)
- les coups négatifs : amorçage des charges négatives du nuage (90 % des cas)

2.2. Caractéristiques de la foudre

L'arc électrique qui jaillit entre les charges électriques de signe opposé est constitué de deux types de composantes :

- des composantes impulsionnelles
- des composantes persistantes

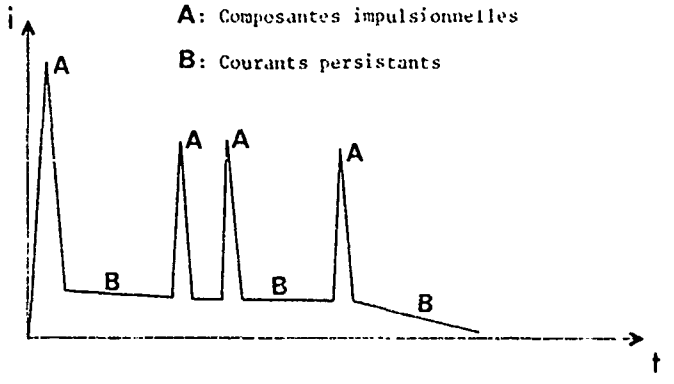

- fig. 2 -

L'ensemble du phénomène a une durée qui peut varier entre quelques dizaines de millisecondes et 1,5 s. La température de l'arc électrique, d'un diamètre de quelques cm à quelques dizaines de cm, est d'environ 20 000 à 30 000° K.

La composante impulsionnelle A (fig.3) est caractérisée par :

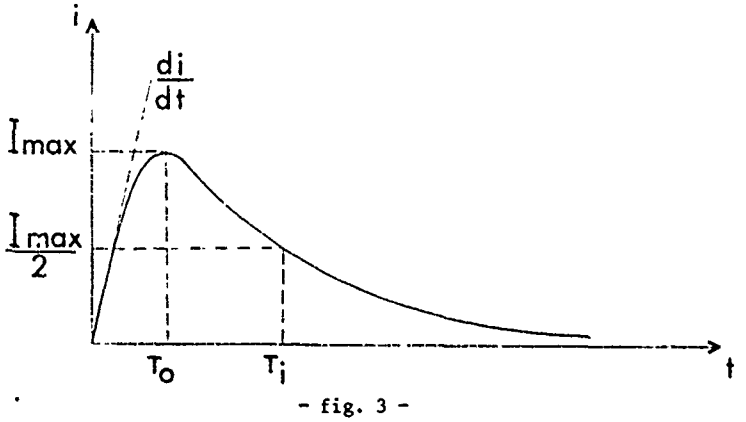

- fig. 3 -

TECHNICAL LIBRARY
ABBOTTAEROSPACE.COM

- le temps To, temps de zéro à I max
- le taux de montée $\frac{di}{dt}$
- le temps Ti, temps à mi-amplitude
- I max
- le transfert de charge $Q = \int idt$
- l'intégrale d'action $\int i^2 dt$

La composante persistante (fig. 4) est caractérisée par :

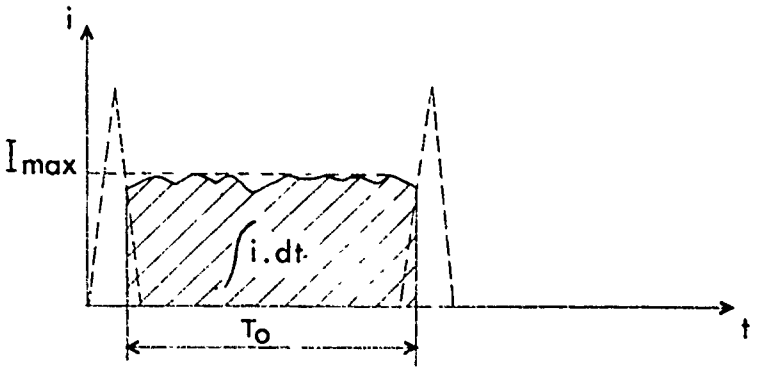

- fig. 4 -

- la durée To
- la valeur max, I max
- le transfert de charge $Q = \int idt$

Le tableau suivant donne à titre indicatif, une valeur moyenne et une valeur maxi de ces différents paramètres pour les coups de foudre entre nuage et sol.

	UNITES	VALEURS MOYENNES	VALEURS MAXIMALES
COMPOSANTES IMPULSIONNELLES			
. Valeur maximale Imax	kA	40	200
. Temps de montée (0 à Imax)	µs	50	⋆ 0,1
. di/dt	kA/µs	10	100
. Temps de décroissance (Imax à Imax/2)	µs	100	1000
. Transfert de charge $\int i\,dt$	C	10	100
. Intégrale d'action $\int i^2\,dt$	10^6 A^2.s	0,1	10
COURANT PERSISTANT			
. Valeur maximale	kA	1	5
. Durée totale	ms	50	800
. Transfert de charge $\int i\,dt$	C	50	250

⋆ Valeur minimale

- fig. 5 -

2.3. Foudroiement d'un avion en vol (fig. 6)

Lorsqu'un avion est foudroyé en vol, sa structure est traversée par le courant dont les caractéristiques ont été définies au § 2.2. Sur certaines parties de l'avion le point d'attachement de l'arc est fixe, alors que sur d'autres il se déplace. Ce phénomène appelé " balayage de foudre" correspond au fait que l'arc est fixe dans l'espace, alors que l'avion, lui est mobile (fig. 7).

THIS DOCUMENT IS BEING PROVIDED BY
TECHNICAL LIBRARY
ABBOTTAEROSPACE.COM

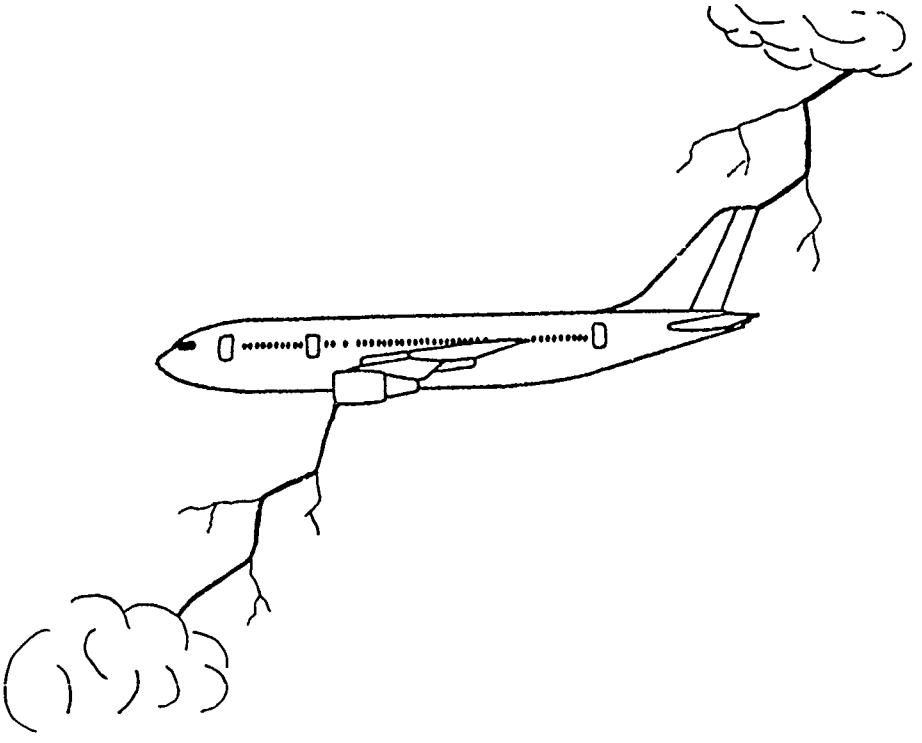

- fig. 6 -

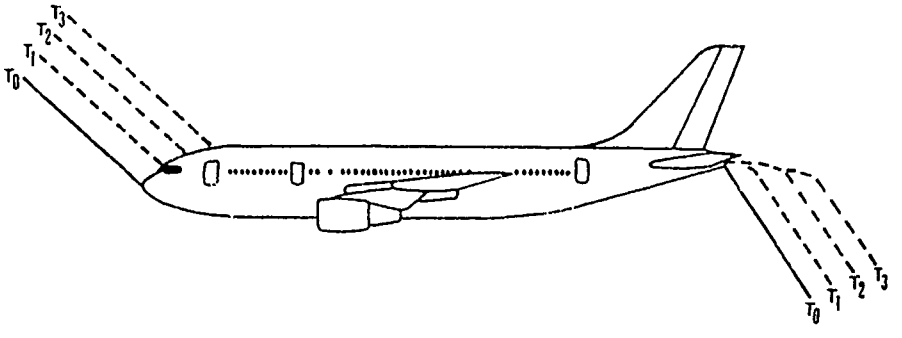

- fig. 7 -

Sur certaines parties de la structure, ce "balayage de foudre" se traduit par une succession de points d'attachement . On définit ainsi 3 zones sur un avion :

- zone 1 : surface pour laquelle il y a une grande probabilité qu'il se produise le premier impact de foudre .
- zone 2 : surface pour laquelle il y a une grande probabilité qu'il y ait "balayage de foudre".
- zone 3 : surfaces autres que celles définies par les zones 1 et 2. Ces surfaces sont cependant susceptibles d'être parcourues par conduction par le courant foudre entre deux points d'attachement.

TECHNICAL LIBRARY
ABBOTTAEROSPACE.COM

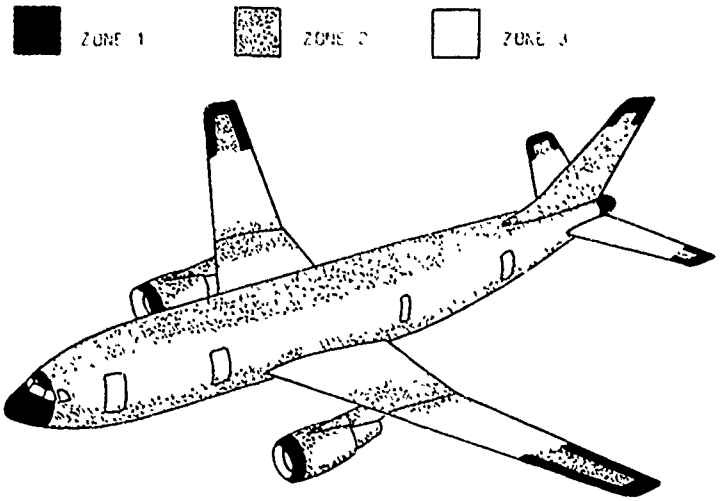

- fig. 8 -

3 - CONSEQUENCES DU FOUDROIEMENT

Les conséquences d'un foudroiement sont de deux types, celles liées aux effets directs et celles liées aux effets indirects.

3.1. Effets directs

Les effets directs sont ceux occasionnés à la structure et qui se traduisent par des dégâts mécaniques : points de fusion, éclatement de carène, etc.

Ces dégâts dépendent bien entendu des caractéristiques électriques du courant foudre, cependant seuls certains paramètres jouent un rôle prépondérant :

- pour la composante impulsionnelle
  . I max
  . Intégrale d'action $\int i^2 dt$
- pour la composante persistante
  . I max
  . durée
  . transfert de charge $\int i dt$

3.2. Effets indirects

Les effets indirects sont ceux induits par le courant foudre au niveau des câblages et équipements de bord (couplage électromagnétique). Les surtensions induites sont fonction non seulement des caractéristiques du courant foudre (I max et $\frac{di}{dt}$ de la composante impulsionnelle) mais aussi de celles de la structure.

L'atténuation des champs électromagnétiques apportée par effet de blindage de la peau de l'avion joue alors un rôle très important.

4 - EXPERIENCE EN VOL - MESURE DES CARACTERISTIQUES DE LA FOUDRE A L'AIDE D'UN AVION TRANSALL

Les caractéristiques de la foudre données au paragraphe 2.2. proviennent de mesures au sol, c'est-à-dire pour les coups de foudre entre nuage et sol. On ne connaît à l'heure actuelle, aucune valeur des caractéristiques des coups de foudre entre nuages ou à l'intérieur d'un nuage, coups de foudre deux fois plus nombreux que ceux impactant le sol.

Afin de connaître les caractéristiques des coups de foudre en altitude, les Services Techniques Aéronautiques français ont décidé de lancer un programme de mesures. Le Centre d'Essais en Vol (CEV) et le Centre d'Essais Aéronautique de Toulouse (CEAT) avec la participation de l'AIA de CLERMONT-FERRAND et de la SEFTIM ont, au cours de l'été 1978 réalisé une campagne de mesures à l'aide d'un avion TRANSALL (fig. 9). L'avion a été équipé de 2 perches de 4 m. de longueur (fig. 10) munies chacune d'un shunt de mesure coaxial.

TECHNICAL LIBRARY
ABBOTTAEROSPACE.COM

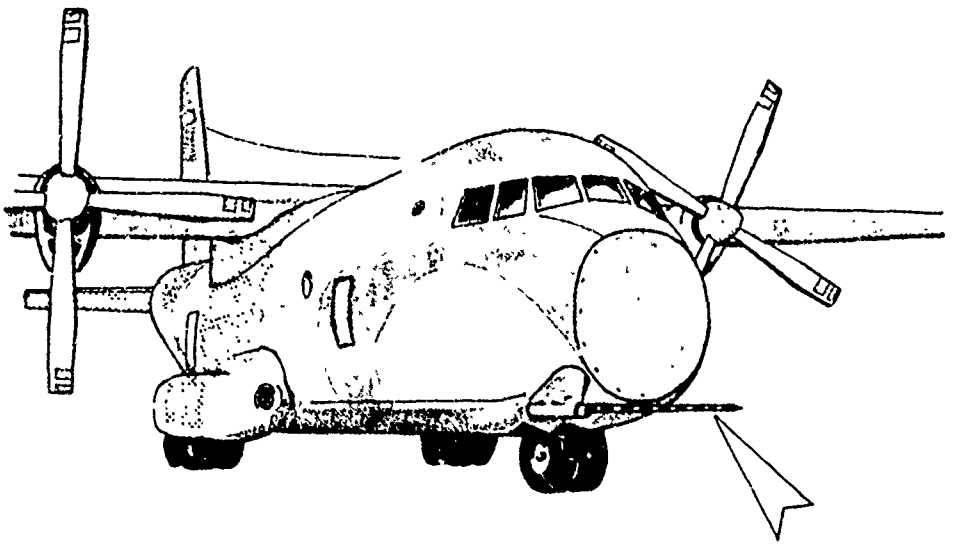

- fig. 9 -

Outre ces mesures spécifiques, d'autres paramètres ont été enregistrés (champ magnétique, courant de peau, surtension dans les réseaux de bord et sur équipements).

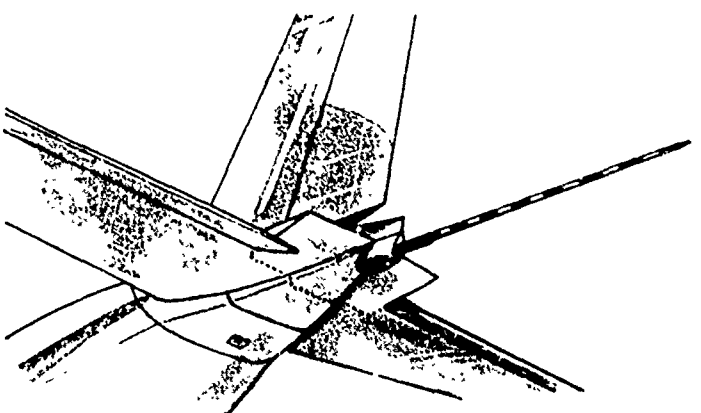

- fig. 10 -

La figure 11 montre le phénomène de balayage de foudre sur la perche avant.

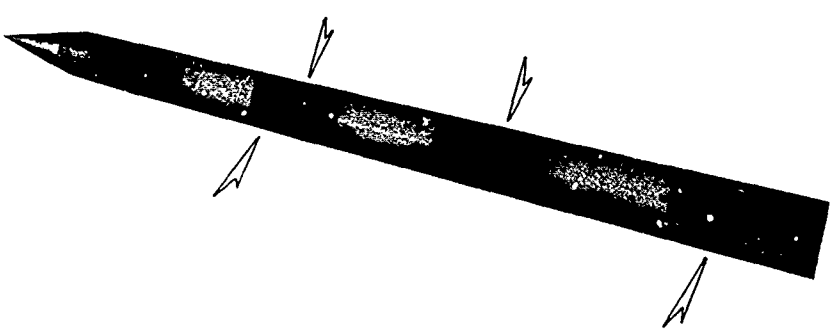

- fig. 11 -

TECHNICAL LIBRARY
ABBOTTAEROSPACE.COM

La figure 12 montre "l'accrochage" de la foudre sur la perche arrière.

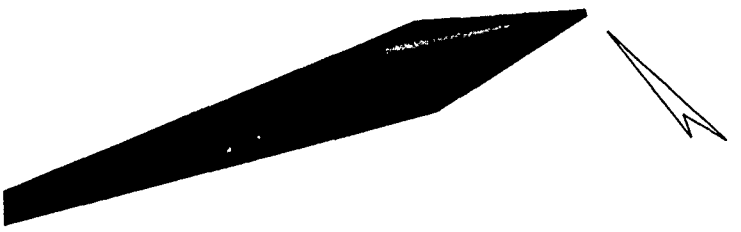

- fig. 12 -

Au cours de 17 vols, 13 enregistrements ont été effectués. Les résultats obtenus montrent que les valeurs du courant mesuré restent à l'intérieur de l'enveloppe des courants mesurés entre nuage et sol.

Une prochaine campagne de mesure est prévue au cours de l'été 1980.

La figure 13 montre un enregistrement d'un coup de foudre typique.

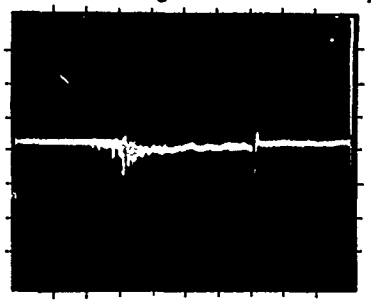

Echelle horizontale : 1 ms par division
Echelle verticale : 20 kA par division

- fig. 13 -

5 - MOYENS DE SIMULATION EN LABORATOIRE

La simulation en laboratoire de la foudre pose un problème technique difficilement concevable à l'heure actuelle : génération simultanée de très haute tension et très fort courant.

Ce problème a été résolu en séparant les deux paramètres.

Un premier simulateur, générateur de choc de tension (fig. 14) permet d'obtenir des impulsions de tension.

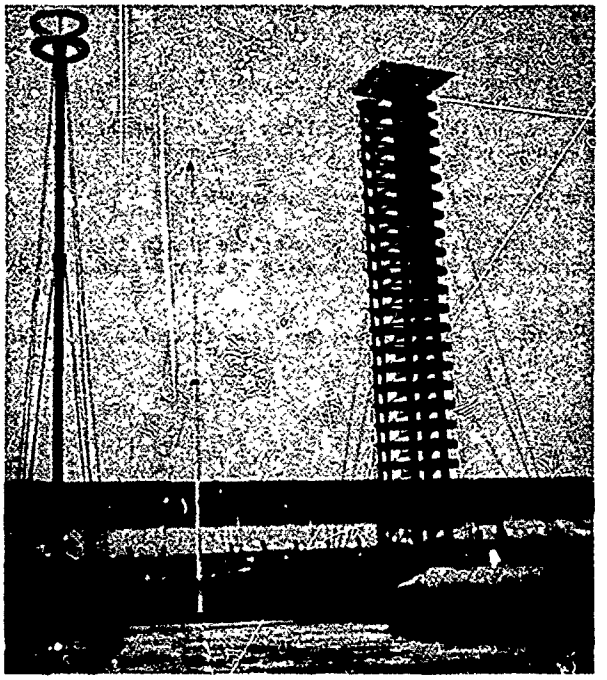

- fig. 14 -

TECHNICAL LIBRARY
ABBOTTAEROSPACE.COM

Installation du CEAT, 5 millions de volts : l'arc électrique obtenu, 6 à 7 m de longueur permet de déterminer les points d'impact et les cheminements.

Un deuxième simulateur (fig. 15) générateur de choc de courant permet d'obtenir des impulsions de courant (installation du CEAT, 200 000A suivis d'une composante continue de 500 Coulomb).

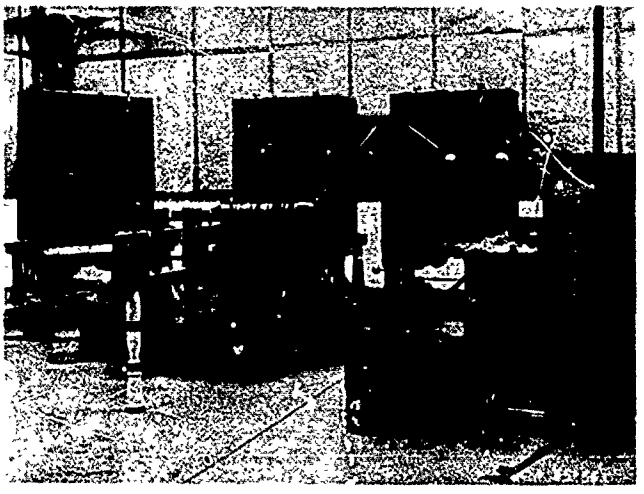

- fig. 15 -

Le courant obtenu, injecté aux points d'impact préalablement déterminés en choc de tension, permet d'évaluer la tenue des structures. C'est en effet le courant qui provoque les endommagements sur les matériaux composites.

Le phénomène de balayage de foudre peut être réalisé, soit par déplacement (linéaire ou circulaire) de l'éprouvette, soit par soufflage de l'arc (soufflage magnétique ou soufflage d'air).

6 - CARACTERISATION DE LA RESISTANCE AU FOUDROIEMENT DES MATERIAUX COMPOSITES

Après une mise en évidence de la vulnérabilité des matériaux composites vis à vis de la foudre, les objectifs des résultats présentés dans cette conférence sont les suivants :

- comparaison de la résistance à la foudre des bore et carbone-époxy
- étude de l'influence du matériau constituant l'âme en nid d'abeille des structures sandwiches (alliage léger ou Nomex).
- étude comparative des systèmes de protection
- évaluation objective des endommagements
- approche expérimentale du phénomène réel : foudroiement avec balayage.

Si dans un premier temps, les essais ont été réalisés sur des composites carbone et bore-époxy, les expérimentations actuelles ne concernent plus que le carbone-époxy.

6.1. Résistance à la foudre comparée des bore et carbone-époxy

La difficulté d'obtenir expérimentalement un transfert de charge électrique avec le bore-époxy (non conducteur), ne permet de comparer les deux matériaux que vis à vis d'un choc de courant seul (composante impulsionnelle).

Les deux photos ci-après montrent les dégâts obtenus sur deux plaques d'épaisseur équivalente (1 mm) après un choc de 200 kA sans transfert de charge.

carbone-époxy

bore-époxy

TECHNICAL LIBRARY
ABBOTTAEROSPACE.COM

6.2. Influence du matériau constituant l'âme en nid d'abeille des structures sandwiches.

Les résultats ci-après ont été obtenus avec des revêtements en composite bore-époxy d'épaisseur 1 mm, et une âme en nid d'abeille métallique ou Nomex.

Montage d'essai :

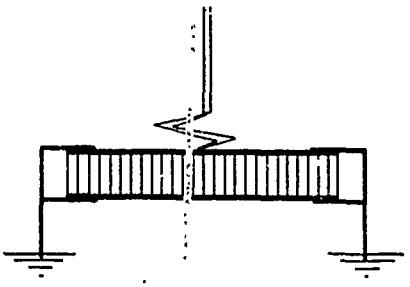

Caractéristiques de l'onde de foudre : choc de 50 kA sans transfert de charge.

Les illustrations ci-après montrent successivement :

- la vue de dessus des dommages
- une radiographie du nid d'abeille
- une coupe transversale de l'éprouvette après essai

Nid d'abeille métallique AG5

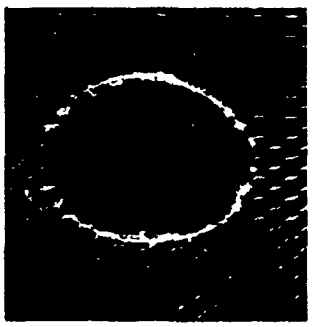

Nid d'abeille NOMEX

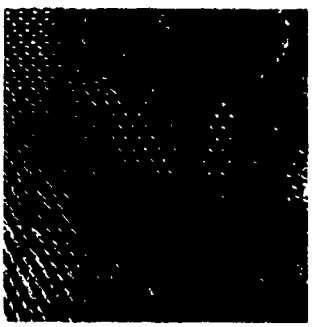

This Document Provided by the Abbott Aerospace
TECHNICAL LIBRARY
ABBOTTAEROSPACE.COM

Avec le nid d'abeille NOMEX non conducteur, l'âme ne paraît que très peu endommagée, la perforation du revêtement est également moins importante.

Ces résultats ont été confirmés avec des peaux en carbone-époxy.

6.3. Etude comparative des systèmes de protection.

Si on considère comme insuffisant l'effet de paratonnerre des encadrements métalliques, la protection des structures en composite ne peut s'obtenir qu'en rendant leur surface conductrice.

A cet effet, plusieurs technologies sont possibles :

- collage de feuillards ou bandes métalliques (alliages d'aluminium acier inox etc.)
- schoopage
- peintures électro-conductrices
- grilles

Après quelques essais préliminaires réalisés en France sur ces différents procédés, le système des grilles de bronze nous est apparu comme ayant le meilleur rapport masse surfacique/efficacité.

Une campagne d'essai réalisée dans le cadre d'un programme de coopération avec la RFA (I.A.B.G.) nous a permis d'étudier plus précisément l'efficacité de ce type de protection vis à vis des différents paramètres de l'onde de foudre (choc de courant et transfert de charge).

- matériau expérimenté : carbone époxy T300-N5208, en plaques monolithiques 8 plis orthogonaux (0,90°)
- montage d'essai:

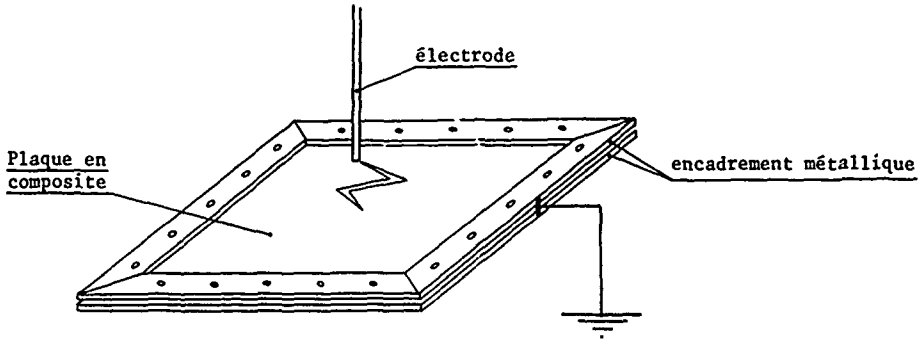

- Protections :
  . grilles de bronze de masses surfaciques 47 g/m^2 - 80 g/m^2 et 250 g/m^2 (placées sur une seule face, côté électrode).

Toutes les éprouvettes ont été peintes.

Les illustrations ci-après permettent de comparer l'efficacité de ces protections vis à vis de trois types de foudroiement.

- choc de 200 kA sans transfert de charge
- choc de 200 kA avec transfert de 210 Coulomb
- Choc de 50 kA avec transfert de 50 Coulomb

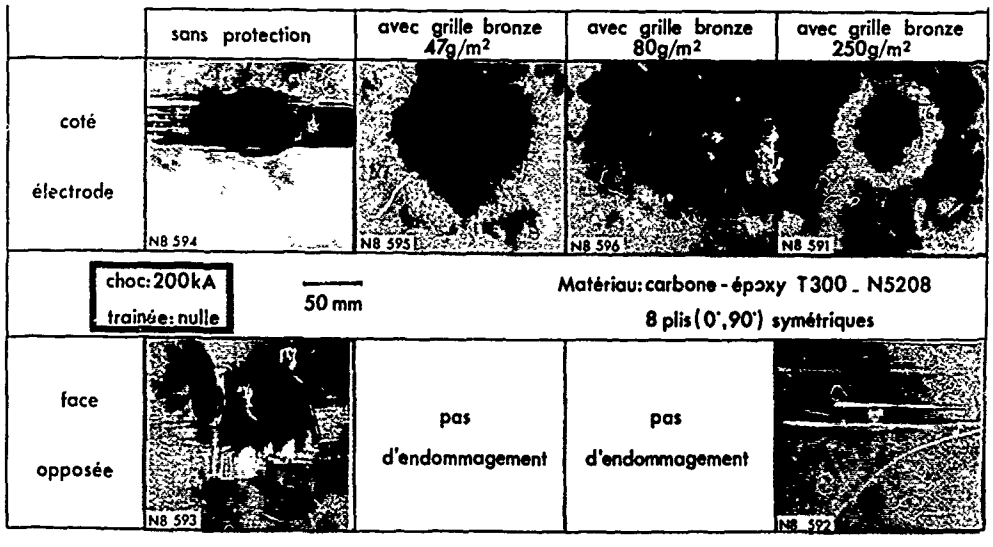

TECHNICAL LIBRARY
ABBOTTAEROSPACE.COM

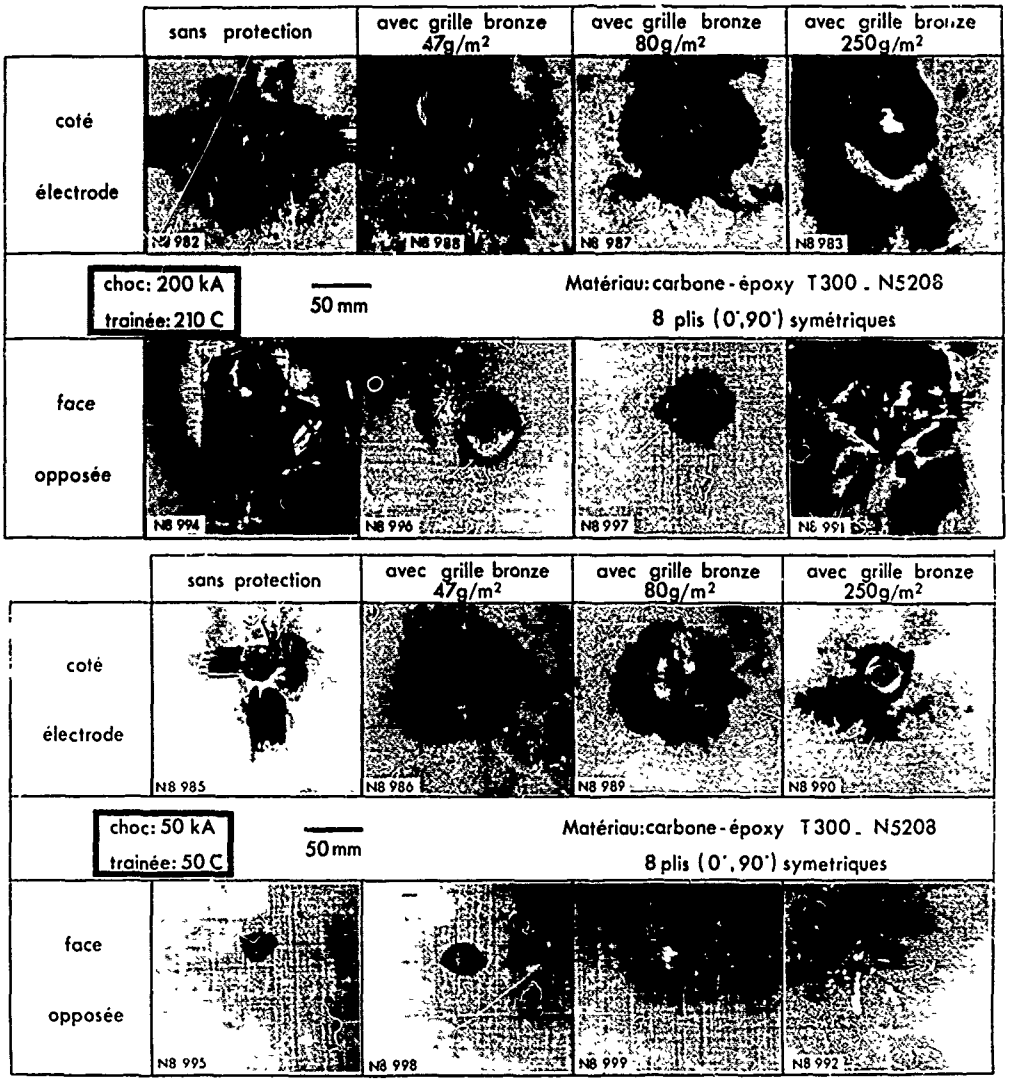

L'observation de ces photos permet de tirer les conclusions suivantes :

- La protection n'apparaît pas proportionnelle à la masse surfacique de la grille, les dommages obtenus avec 250 g/m2 sont supérieurs à ceux constatés avec 47 et 80 g/m2 (en particulier pour l'onde de courant).

- Très efficace contre l'onde de choc de courant, la protection par grille de bronze a peu d'influence sur le transfert d'énergie (voir chocs 50 kA - 50 C)

6.4. Evaluation objective des dommages structuraux provoqués par la foudre.

Les photos ci-dessus ont montré qu'un impact de foudre sur une plaque en matériau composite se traduisait par une perforation plus ou moins importante de cette plaque.

Visuellement, l'aspect de ce dommage est tout à fait comparable à celui qui serait provoqué par le choc à basse vitesse d'un projectile non ogivé.

Pour un carbone-époxy, la perte locale de résistance statique due à l'effet de concentration des contraintes provoqué par un trou lisse est de l'ordre de 30 à 50 % (suivant l'orientation des plis).

De nombreux essais réalisés jusqu'à ce jour ont montré que le délaminage des plis amorcé aux bords libres du trou par des sollicitations de fatigue permettait de récupérer une grande partie de cette perte locale de résistance.

Du point de vue de l'ingénieur structure, le problème est donc de savoir s'il existe un dommage supplémentaire au-delà de celui assimilable à une perforation par impact mécanique, et dont la perte locale de résistance statique serait au pire égale à celle provoquée par un trou lisse.

Afin de lever cette incertitude, des essais de résistance résiduelle ont été réalisés sur des éprouvettes prélevées dans les zones visuellement non endommagées situées au voisinage immédiat des impacts.

Pour pouvoir accéder indépendamment aux propriétés à rupture "commandées" par les fibres ou la matrice, les essais ont été réalisés sur des plaques à arrangement orthogonal (0,90°) avec prélèvement des éprouvettes parallèlement et à 45° par rapport aux directions du renforcement.

TECHNICAL LIBRARY
ABBOTTAEROSPACE.COM

Rupture "commandée" par les fibres

Rupture "commandée" par la matrice

Quatre chocs identiques ont été réalisés sur des plaques monolithiques 8 plis, de 400 x 400 mm, avec le même montage d'essai que ci-dessus (cf. § 6.3.). Deux éprouvettes de traction de 200 x 25 mm ont pu être ainsi prélevées autour de chacun des impacts.

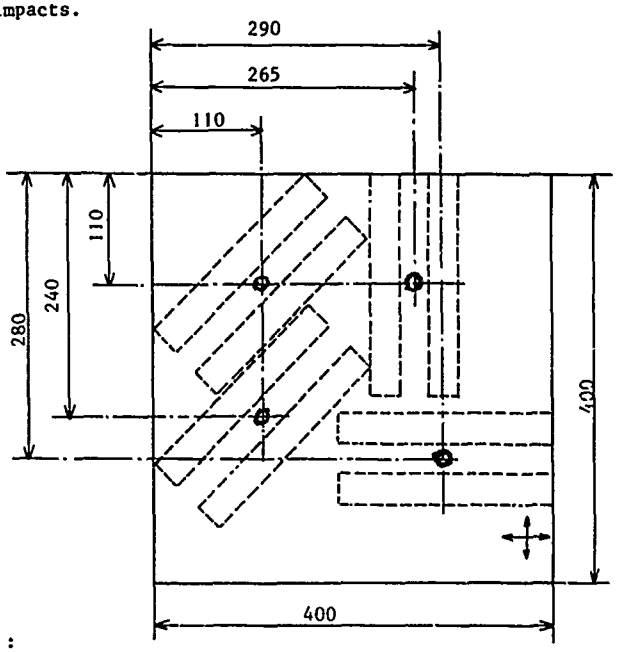

Cas de foudroiement étudiés :

- 50 kA plus 50 C { sans protection { 47 g/m2
  { avec grille de bronze de { 80 g/m2
  { 250 g/m2
- 200 kA plus 210 C, avec grille de bronze de { 47 g/m2
  { 80 g/m2

La photo ci-après illustre le principe du prélèvement des éprouvettes par rapport aux impacts. Soit au voisinage immédiat de la perforation, dans une zone généralement noircie superficiellement mais où n'apparaît en surface ni fibre coupée, ni résine brûlée.

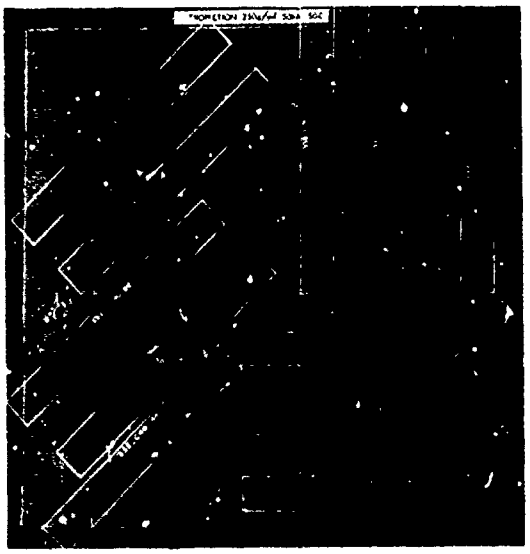

Quelle que soit la configuration du courant de foudre, et le type de protection, les résultats de ces essais mécaniques n'ont pas mis en évidence un endommagement de la résistance autre que celui propre à la perforation.

TECHNICAL LIBRARY
ABBOTTAEROSPACE.COM

6.5. Approche expérimentale du phénomène réel-foudroiement avec balayage.

Les expérimentations en vol effectuées sur TRANSALL ont permis de mettre en évidence le déplacement de l'impact de la foudre sur la structure de l'avion.

Cet effet de balayage impliquant un transfert local d'énergie moindre que dans une expérimentation statique, les dommages provoqués seront de moindre importance.

Dans le but d'une simulation au sol plus fidèle, le C.E.A.T. a donc développé un dispositif expérimental où le balayage est obtenu par rotation, devant l'électrode, d'un disque constituant l'éprouvette à essayer.

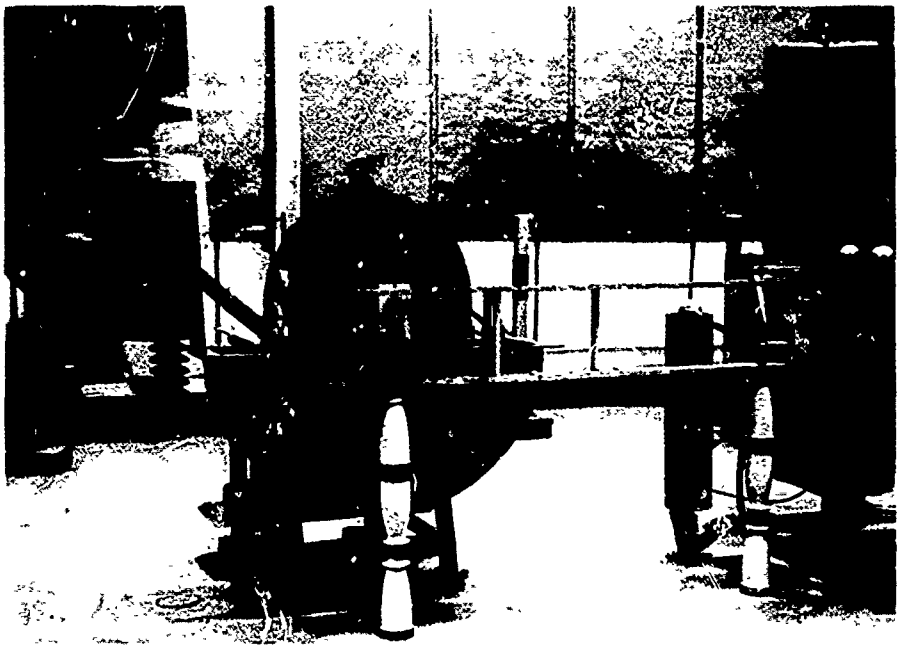

La reprise de l'énergie s'effectue par l'axe du disque.

Dans ce principe, la vitesse de balayage est vite limitée par les forces centrifuges et le diamètre maximum "raisonnable" de l'éprouvette.

Des essais ont pu être réalisés sur des disques en matériau composite de diamètre 600 mm avec une vitesse de 15 km/h au niveau de l'électrode.

Dans ces conditions expérimentales, des résultats obtenus sur disques sandwiches avec âme NOMEX et peaux en carbone-époxy T300-N5208 8 plis, ont démontré l'équivalence des dommages entre les chocs suivants :

- 200 kA - 150 C pendant 0,3 s. de balayage
- 200 kA - 50 C sans balayage (statique)

Ces essais de foudroiement dynamique ont également permis de mettre en évidence l'influence de la couche de peinture protectrice.

Les photos ci-dessous montrent l'effet de concentration des dégâts provoqué par une peinture non conductrice.

Configuration d'essai : 200 kA plus 150 C pendant 0,3 s. avec balayage 15 km/h.

non peinte

peinte

TECHNICAL LIBRARY
ABBOTTAEROSPACE.COM

7 - ESSAIS DE FOUDROIEMENT SUR STRUCTURES REELLES

Leur objectif est la détermination des points d'impact et des cheminements de la foudre sur la structure. Ils permettent donc d'évaluer l'efficacité des paratonnerres "naturels" constitués par les ferrures et encadrements métalliques de la structure, ou artificiels (bandes conductrices disposées spécialement pour capter et écouler le courant de foudre).

Ces essais réalisés sur des installations de choc de tension nécessitent des évaluations complémentaires en choc de courant afin de quantifier les risques de dommage réels dans les zones concernées par l'impact et le cheminement.

Le document ci-après illustre un essai d'efficacité de bande paratonnerre segmentée sur un radôme en verre-époxy.

La bande sur laquelle on distingue très bien l'écoulement de la foudre était constituée de pastilles conductrices de Ø 2,5 mm et distantes de 0,3 mm (fixation sur film de résine époxy suivant principe des circuits imprimés).

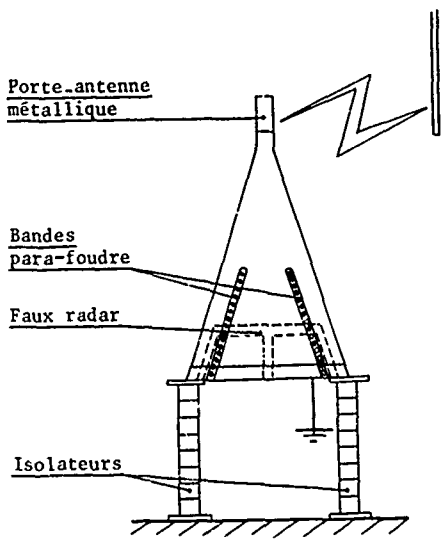

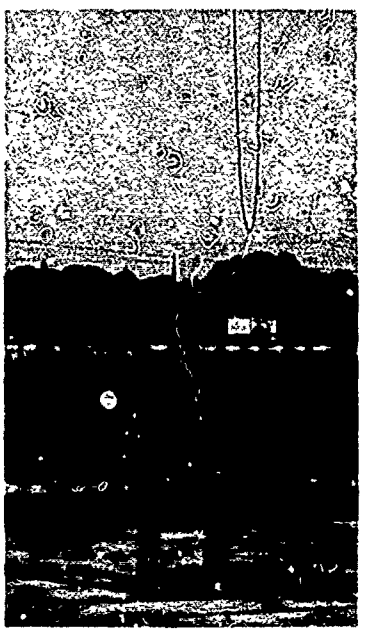

8 - CONCLUSION

Les premiers problèmes de vulnérabilité des matériaux composites à la foudre sont apparus avec les radômes et divers carénages d'antennes en stratifié verre-époxy. Ces problèmes étaient et demeurent d'autant plus complexes à résoudre que leur solution va toujours à l'encontre des impératifs de perméabilité magnétique propres à ce type de structure.

Au début des années 70, pour la première génération de pièces structurales en matériaux composites haut module (gouvernes et caissons d'empennages) sans impératif de perméabilité magnétique, des systèmes de protection simples tels que des bandes conductrices en clinquant ont été systématiquement prévus.

Vu la surface relativement petite de ces structures, leur position sur l'avion et l'importance des encadrements métalliques, la probabilité d'un impact de foudre direct sur le composite est très faible. Ces protections lourdes se sont donc avérées rapidement superflues.

L'évolution actuelle des applications vers des structures beaucoup plus importantes (dérives, voilures) avec beaucoup moins de parties métalliques remet le problème de la sensibilité à la foudre au "goût du jour". Toutefois, aux dommages structuraux directs s'ajoute maintenant le problème de l'ouverture diélectrique créé par ces éléments, et les risques de destruction des circuits électriques situés à l'intérieur qui en découlent. Dans l'avenir, il est même probable que c'est sous ce deuxième aspect que se posera essentiellement le problème du foudroiement des structures en matériaux composites.

Les résultats obtenus en laboratoire sur ces matériaux ont démontré qu'un impact de foudre était assimilable à une légère perforation par choc mécanique, dont l'ampleur pouvait être considérablement réduite par l'utilisations de protections simples et légères. Au niveau de sa conception, la structure devra donc pouvoir tolérer de tels dommages. Cependant, il nous reste encore à acquérir une expérience complémentaire au niveau des liaisons, des peaux monolithiques épaisses susceptibles de contenir du carburant, et du foudroiement des structures sous contrainte mécanique.

TECHNICAL LIBRARY
ABBOTTAEROSPACE.COM

LIGHTNING PROTECTION CONSIDERATIONS FOR GRAPHITE/EPOXY AIRCRAFT STRUCTURE

S. D. Schneider
THE BOEING COMPANY
Mail Stop 47-31
P.O. Box 3707
Seattle, Washington U.S.A. 98124

SUMMARY

When advanced composites such as graphite/epoxy were first being considered for aircraft structure, a common belief was that lightning would heavily damage the structure. This belief has since proven to be false. Advanced composites react to lightning strikes in a manner different from aluminum, but the resultant damage is by no means alarming.

There are two basic types of lightning damage to which aircraft structures are subjected. One type occurs at the arc attachment point, and the other occurs in the intervening structure between lightning attachment points. The effect of graphite/epoxy structure on each of these phenomena is discussed.

Known, documented techniques and design philosophies for protection against lightning-caused structural damage are reviewed for classical aluminum aircraft structure fabricated with metal fasteners, and the impact of graphite/epoxy on these classical approaches is addressed. Detailed lightning test criteria, test techniques, and criteria also are given and related to graphite structures.

INTRODUCTION

The advantages of graphite/epoxy structure are so overwhelming to the structural designer that its widespread use for aircraft structure is inevitable. The graphite/epoxy matrix is roughly 1,000 times less conductive than a comparable aluminum structure. For this reason, use of the material causes some concern to the engineer involved in aircraft structure lightning protection.

Lightning protection of conventional riveted aluminum structure has been straightforward (ref. 1). The conductivity of the basic airframe serves as an adequate current path for lightning discharges. Protection problems created by dielectric sections and access panels were easily corrected by providing conductive paths to the airframe.

Since epoxy matrix is an excellent electrical dielectric, any current flow through the composite must occur in the graphite fibers. Graphite fibers are sufficiently resistive that the localized flow of currents of several amperes can cause localized degradation of the matrix and, in some cases, destroy the structural integrity of the composite.

A number of lightning protection concepts have been developed for graphite (refs. 2, 3, and 4) and can be used effectively where needed. The protection concepts generally involve adding a conductive layer to the outside surface of the graphite/epoxy part in the localized area requiring protection. Many factors must be evaluated, however, before a lightning protection system can be selected. These factors include cost, weight, complexity, criticality of the part, and predicted frequency of lightning strike to the part.

There are two basic types of lightning damage to which aircraft structure may be subjected. One type occurs at the arc attachment point; the other occurs in the intervening structure between lightning attachment points. The effect of these types of damage to graphite/epoxy must be considered when evaluating lightning protection requirements.

Additionally, the protective schemes must be consistent with expected level of lightning threat (which varies with location on the aircraft) and the structural and economic penalty of not providing protection. Protection systems developed must not only prevent degradation of structural integrity, but must also be consistent with the aircraft's total environment and designed in such a manner that damage is detectable and repairable.

This paper only addresses protection against structural damage (i.e., structural degradation) due to lightning. Fuel tank arc and spark protection are not discussed. (See refs. 1 through 4 for more information on these effects.)

LIGHTNING PROTECTION REQUIREMENTS

Lightning strikes to aircraft occur with surprising frequency. The figure commonly used for commercial jet transports is a fleet average of one strike per airplane per year.

Figure 1 illustrates the phenomena of lightning attachment to aircraft structure. First, lightning tends to attach to extremities such as the nose, wingtips, and tail. Lightning does not terminate on the aircraft, but uses the aircraft as part of the discharge path. In effect, each lightning strike has an entrance and exit point on the aircraft. Table 1 lists some of the more important characteristics of lightning.

As shown in the table, a lightning strike is typically 0.2 sec and can be as long as 2 sec. An aircraft can continue to fly through a lightning strike after attachment is made at a forward point, such as the nose. Therefore, aircraft surfaces aft of a forward lightning attachment point must be protected against "swept" lightning strike attachments.

TECHNICAL LIBRARY
ABBOTTAEROSPACE.COM

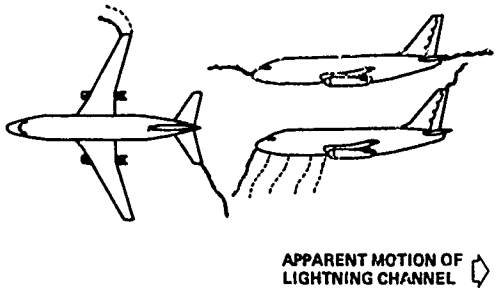

Figure 1. Lightning Attachment Phenomena

Table 1. Lightning Strike Characteristics

CHARACTERISTICS	TYPICAL	PROBABLE WORST CASE
PEAK CURRENT	20,000A	200,000A
CHARGE TRANSFERRED	15C	200C
NUMBER OF HIGH-CURRENT PULSES PER STRIKE	3 OR 4	26
TOTAL DURATION OF STRIKE	0.2 sec	2 sec
LENGTH OF LIGHTNING CHANNEL	5 km	14 km

The classical approach to aircraft protection has been to zone the aircraft according to the probability of lightning strike attachment. The zones are defined below and illustrated in figure 2. Graphite/epoxy is sufficiently conductive that these zones still apply to aircraft with minor or major portions of graphite/epoxy structures.

- Zone 1A: Initial attachment point with low probability of flash hang-on, such as the nose; i.e., the lightning stroke has a high probability of sweeping aft
- Zone 1B: Initial attachment with high probability of flash hang-on, such as a tail cone
- Zone 2A: A swept stroke zone with low probability of flash hang-on, such as a wing midchord
- Zone 2B: A swept stroke zone with high probability of flash hang-on, such as wing trailing edge
- Zone 3: Surfaces other than those covered by zones 1 and 2

Since there is an entrance and exit attachment point for each lightning strike, intervening structure between the attachment points must be designed to sustain the passage of lightning currents.

Structural damage or degradation due to lightning is generally created by two effects. One is thermal; the other is due to high current densities.

Temperature of the channel (arc) of a lightning strike can be as high as 27,000°C, and aircraft surfaces contacted by lightning may be exposed to temperatures that high. Obviously, few materials can withstand these temperatures for very long without thermal effects such as burning, charring, or vaporization. The length of time that lightning can remain attached to an aircraft surface depends on the aircraft lightning zone. Probable worst case dwell times (thermal exposure time) will vary according to the aircraft lightning strike zone. Attachment point times for the various lightning zones are given in table 2.

High current density is also a damage mechanism caused by thermal heating or explosive vaporization of the individual graphite fibers. The tremendous peak current possible in lightning results in high current densities at the arc attachment point. However, the currents tend to diverge rapidly in materials like graphite/epoxy laminates and aluminum, thereby reducing the current densities at short distances from the attachment point.

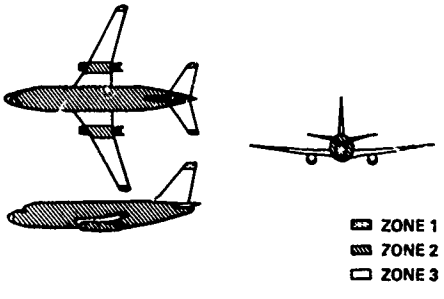

Figure 2. Lightning Strike Zones for a Typical Subsonic Jet Transport

Table 2. Lightning Zone Arc Dwell Times

LIGHTNING ZONE	PROBABLE WORST CASE ATTACHMENT POINT DWELL TIMES
1A	SLIGHTLY GREATER THAN 50 ms
1B	1 sec
2A	50 ms
2B	1 < t < 50 ms*
3	NONE**

*Zone 2B (where lightning sweeps back to a surface and remains) can have a dwell time of from 50 ms to 1 sec.

**Zone 3 encompasses intervening structure between attachment points. This zone is, therefore, not subjected to the hot arc unless the lightning current path is electrically discontinuous. In that case, the lightning currents must arc over the discontinuity, creating an open arc. Arc times then can vary from milliseconds to a second.

LIGHTNING TEST TECHNIQUES

Test waveforms used to test for structural damage are shown in figure 3. Each of the four different discharge waveforms (A, B, C, and D) requires a separate generator. An example of an A component generator is a series parallel bank of capacitors for a total capacitance of 454 μF at 20,000V for the desired energy figure of merit (i.e., action integral).

Various combinations of the four components (fig. 4) are used according to the aircraft lightning zone for which the hardware under test is intended and are structured to be compatible with the dwell times shown in table 2. For example, zone 1B uses all four components, because lightning can attach there and remain attached for the duration of the lightning strike. Zone 1A, however, uses only components A and B, since the strike will sweep aft after attachment.

TECHNICAL LIBRARY
ABBOTTAEROSPACE.COM

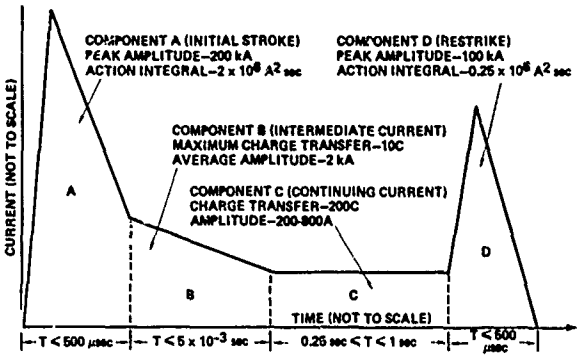

Figure 3. Lightning Test Waveforms for Structural Damage Testing

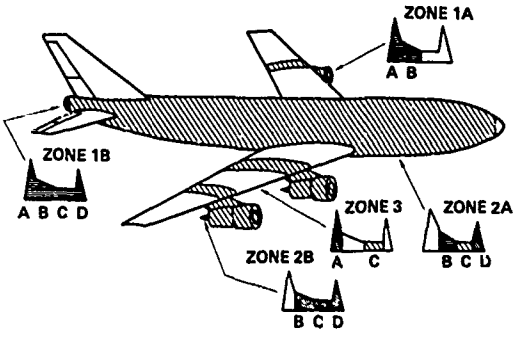

Figure 4. Lightning Strike Zone Testing for Structural Damage

Lightning tests for all waveforms can be conducted by mounting the test specimens on the front panel of a Faraday cage, as shown in figure 5. The Faraday cage, a common test fixture, consists of a 4- x 4- x 6-ft (1.22 x 1.22 x 1.83m) cavity with 1/4-in (6.35 mm)-thick aluminum walls, top and bottom. The front panel is removable to permit replacement, as required, for various lightning tests. Except for the front panel, all other edges are welded for a continuous electrically bonded test cavity. The 4- x 6-ft (1.22 x 1.83m) front panel is held in place by a rigid bolted-on aluminum frame in a manner ensuring that the replaceable front panel does not degrade the electrical continuity of the Faraday cage. Test specimens are rigidly installed in a nonconductive phenolic block, oriented such that lightning currents attached to the upper one-third of the panel are forced down through the lower two-thirds to the electrical ground return on the lower 6-in (152.4 mm) end of the panel.

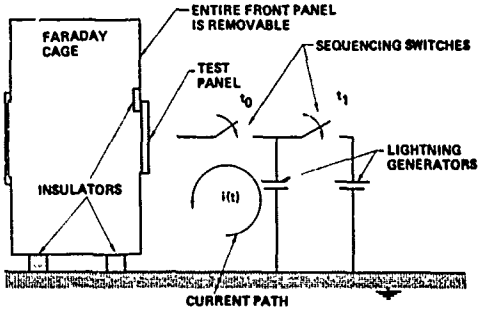

Figure 5. Faraday Cage Setup for Lightning Tests

LIGHTNING PROTECTION CONSIDERATIONS FOR GRAPHITE/EPOXY STRUCTURE

Aluminum appears electrically as a homogeneous material. Graphite/epoxy, on the other hand, consists of conductive fibers matted together by a nonconductive epoxy. Lightning damage appearance is, therefore, different for the two materials. Figure 6 illustrates how 6- x 12-in (152.4 x 304.8 mm) 10-ply graphite/epoxy panels that were subjected to reduced (i.e., not worst case) zone 1A tests of 100,000A and 0.5 x 10^6 A^2sec action integral (energy factor). In the damaged panel area, the epoxy resin is burned away and graphite fibers protrude outward giving it a fuzzy appearance.

In the immediate area of the arc attachment, thermal erosion destroys the epoxy. The high currents through individual fibers rupture the fibers, creating an explosive effect. Both these effects contribute to the typical fuzzy appearance of lightning-damaged graphite/epoxy structure. Fortunately, grapite/epoxy is comparable to aluminum in that lightning damage is generally limited to the visibly damaged area.

A zone 1A test (at a worst case level of 200,000A and 2 x 10^6 A^2sec action integral) to a 6- x 12- x 0.063-in-thick (152.4 x 304.8 x 1.6 mm) aluminum (2024-T3) panel is shown in figure 7. Slight thermal erosion and cooled molten metal are typical of the lightning damage to aluminum. This minor damage is shown as two craters in the upper one-fourth of the panel (the test lightning arc divided to produce two damage sites).

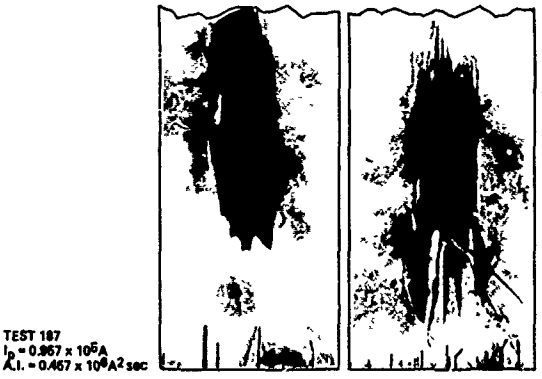

Figure 6. Zone 1A (Reduced Level) Lightning Test to 10-Ply Painted Graphite/Epoxy Test Panel

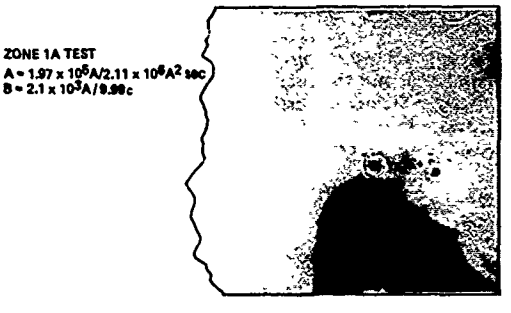

Figure 7. Zone 1A Lightning Test to Painted Aluminum Test Panel

These results suggest that aircraft locations subjected to zone 1 lightning attachments (extremities) will have less nuisance damage if aluminum is used instead of graphite/epoxy. Because areas such as wingtips are usually secondary structure, the benefit of using higher-strength materials like graphite/epoxy is less obvious and aluminum fairings should be considered.

TECHNICAL LIBRARY
ABBOTTAEROSPACE.COM

Fiberglass and Kevlar also are receiving increased interest for structural applications, especially in secondary or lightly loaded structure. Classic protection techniques for fiberglass have included aluminum bus bars, such as for wingtip and radome protection (ref. 1). Fiberglass and Kevlar are nonconductive and, as a result, lightning attaches to the aluminum bus bar (i.e., diverter strip) instead of puncturing the fiberglass or Kevlar part. Graphite/epoxy, however, is so conductive that the diverter strip approach does not work. That is, lightning sees no preference for the aluminum diverter strip and is just as apt to attach to the graphite surface. If protection is considered desirable to reduce damage to a graphite/epoxy part, such as a wingtip, a protective conductive coating should be considered. Candidate coatings are discussed in the next section.

An estimate of the damage to the A component of lightning is illustrated in figure 8, excerpted from reference 1. The data in this figure must be considered approximate because they came from a variety of tests. The data approximate damage as a function of the number of plies and the energy factor. The ordinate value of 2.0 on figure 8 corresponds with a zone 1, or those areas that require 200,000A (see fig. 2). Similarly, the 0.25 level corresponds to the swept stroke zones. As shown, widespread damage does not occur at either test level, except for very thin laminates. Thin laminates typically are used only in noncritical areas (secondary structure). As a result, protection considerations against structural damage caused by lightning are generally economic and not involved in flight safety.

Reference 1 has another clever way to approximate damage. The data used to compile figure 8 also were used to produce table 3, which shows the approximate action integral (energy factor, $\int i^2 dt$) that various cross-sectional areas can sustain with minimal damage.

Total elimination of damage may not always be practical or desirable. Localized heating and thermal erosion will occur on most any material, including aluminum, due to the high temperatures of the lightning arc. It is important, however, to approximate the extent of damage by test or analysis. As detailed in reference 1, the information shown in table 3 will provide an estimation of damage when used with the following equation (see fig. 9).

$$d \geq \frac{A}{\pi r}$$

where d = the necessary skin thickness (cm)
A = cross-sectional area required to conduct the required $\int I^2 dt$, from table 3 (cm^2)
r = radius of permissible damage (cm)

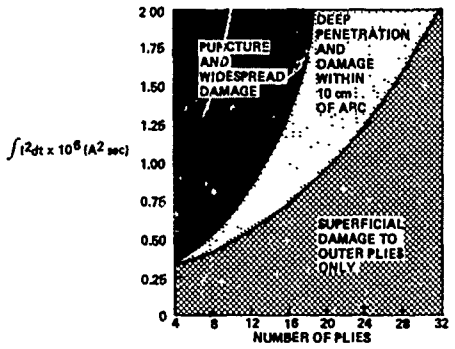

Figure 8. Estimated Visible Damage to Unprotected Graphite Composites

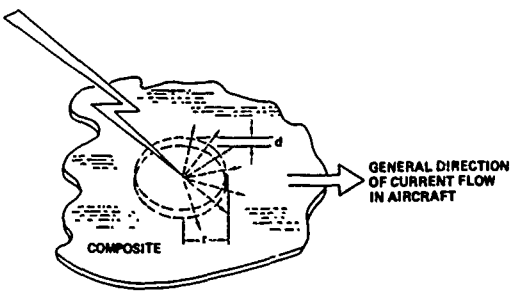

Figure 9. Composite Thickness Versus Area of Damage From Conducted Currents

Consider the following example. A graphite/epoxy laminate is proposed for use in a zone 2A, fuselage section. For structural or repair reasons, it is desirable to limit the damage to an area with an approximate 7-cm radius. From figure 3, we know that the zone 2 action integral is 0.25×10^6 A2 sec. Table 3 indicates that a 1.61 cm^2 cross-section of graphite/epoxy can sustain this level of lightning discharge without significant structural damage. Using the equation above, we find that required laminate thickness would be:

$$d \geq \frac{1.61\ cm^2}{\pi (7\ cm)} = 0.07\ cm$$

Such approaches should be used cautiously, however, since ply orientations, material type, protective paints, curvatures, and the like all have a possible effect on the results. Any safety-of-flight applications of graphite/epoxy structure should be verified by test. Non-flight-safety items may not require tests; past history on comparable hardware may minimize the risk of not testing. Also, the probability of lightning attachment may be low and the cost of repair or replacement may be insignificant.

Table 3. Graphite/Epoxy Lightning Energy Capabilities

CROSS-SECTIONAL AREA		ACTION INTEGRAL
cm^2	in^2	$\int i^2 dt (A^2\ sec)$ LEVEL
0.161	(0.025)	2×10^3
1.61	(0.25)	2×10^5
16.1	(2.50)	2×10^7

TECHNICAL LIBRARY
ABBOTTAEROSPACE.COM

For example, the test levels shown in figures 3 and 4 are for worst case testing, generally reserved for flight-safety items (ref. 5). Commercial aircraft are struck an estimated once per plane per year. This is a coarse fleet-wide average. As shown in table 4 (from ref. 6) the probability of occurrence decreases with threat level. Also, some surfaces are hit more frequently than others; for example, an aileron trailing edge is hit less often than a wingtip. All these factors should be weighted when considering protection for nonsafety-of-flight graphite/epoxy applications.

Table 4. Properties of Statistical Distributions for Lightning Parameters

PARAMETER*	PERCENTAGE OF OCCURRENCE				
	2	10	50	90	98
NUMBER OF RETURN STROKES	10 TO 11	5 TO 6	2 TO 3	–	–
DURATION OF FLASH (ms)	950	480	180	66	36
TIME BETWEEN STROKES (ms)	320	170	60	20	11
RETURN STROKES CURRENT (kA)**	140	65	20	6.2	3.1
CHARGE TRANSFER PER FLASH (C)	200	75	15	2.7	1
TIME TO PEAK CURRENT (μs)	12	5.8	1.8	0.66	0.25
RATES OF CURRENT RISE (kA/μs)	100	58	22	9.5	5.5
CURRENT HALF-VALUE TIME (μs)	170	100	45	17	10.5
DURATION OF CONTINUING CURRENT (ms)	400	260	160	84	58
CONTINUING CURRENT (A)	520	310	140	60	33
CHARGE OF CONTINUING CURRENT (C)	110	64	26	12	7

*Note that not all of the parameters are independent. Some judgment must be made in using the values for consistency.

**Values for first stroke.

LIGHTNING PROTECTION SYSTEMS FOR GRAPHITE/EPOXY

If lightning protection is deemed necessary, there are a number of possible protection systems. During the reference 7 investigation the following systems were evaluated:

- Polyurethane enamel (no protection—as a baseline)
- Aluminum wire screen, 120 x 120 wires/in (25.40 mm)
- Aluminum wire screen, 200 x 200 wires/in (25.40 mm)
- Aluminum metal flame spray
- Aluminum metal foil, 2 mil (0.05 mm)
- Aluminum metal foil, 3 mil (0.08 mm)
- Aluminum metal foil strips, 3 mil (0.08 mm)
- Kapton film dielectric film, 2 mil (0.05 mm), in combination with aluminum metal foil strips, 3 mil (0.08 mm)

Each of the graphite/epoxy tests specimens was painted with polyurethane after the protection system was applied.

Besides lightning testing for all lightning zones, the investigation conducted the following tests on the test specimens:

- Environmental exposure
  - 140°F at 100% relative humidity for 1,000 continuous hr
  - Ground-air-ground flight simulation for 1,000 cycles
  - Temperature = -65°F to 250°F (-53.89°C to 121.11°C)
  - Humidity to 100%
  - Pressure = sea level to 40,000 ft (12.19 km)
  - Cycle time = 1 hr
- Fatigue
  - +9,000 to +20,000 lb (4,082.4 to 9,072 kg) for 1,000,000 cycles (typical)
  - Fatigue rate 1,800 cycles/min

Final candidates were proof-tested on a full-scale section of a graphite/epoxy wing box.

The reference 7 investigation concluded that three systems provided the best lightning protection for graphite/epoxy hardware:

- Aluminum flame spray
- Aluminum flame spray strips
- Aluminum wire screen, 120 x 120 wires/in (25.40 mm)

Test results from this investigation indicated that—

- Environmental exposure did not affect the protection system.
- Fatigue did not affect the protection system.
- Small specimen testing data can be successfully extrapolated to full-scale hardware.

CONCLUSIONS

Lightning damage to graphite/epoxy aircraft structure is not as extensive as once feared. The electrical conductivity qualities of graphite, although less than that of aluminum, normally are adequate to conduct lightning currents except in the immediate area of lightning arc attachment. A formula is given to help estimate the degree of structural damage at this arc attachment point versus threat level and laminate thickness. If safety of flight is involved, estimates of graphite/epoxy structural damage should be verified by testing.

If lightning protection is deemed necessary, a number of conductive protective systems are available and in the literature.

TECHNICAL LIBRARY
ABBOTTAEROSPACE.COM

REFERENCES

1. Fisher, F.A., and Plumer, J.A., "Lightning Protection of Aircraft," October 1977, NASA Reference Publication 1008.

2. 1979 IEEE Symposium on Electromagnetic Compatibility, October 9 to 11, 1979.

3. 1975 Conference on Lightning and Static Electricity, at Culhum Laboratory, England, April 14 to 17, 1975.

4. Conference on Certification of Aircraft to Atmospheric Electricity Hazards, ONERA; Chatillon, France, September 11 to 13, 1978.

5. "Lightning Test Waveforms and Techniques for Aerospace Vehicles and Hardware," Report of SAE Committee AE4L, June 20, 1978.

6. Cianos, N., and Pierce, E.T., Stanford Research Institute, Menlo Park, California, "A Ground-Lightning Environment for Engineering Usage."

7. Hendricks, C.L., Schneider, S.D., and Shumaker, G., "Lightning Protection Techniques for Graphite/Epoxy Aircraft Structures," Third National Symposium, Society for the Advancement of Materials and Process Engineering, Anaheim, California, May 1 to 4, 1978.

TECHNICAL LIBRARY
ABBOTTAEROSPACE.COM

THE POTENTIAL FOR DAMAGE FROM THE ACCIDENTAL RELEASE OF CONDUCTIVE CARBON FIBERS FROM AIRCRAFT COMPOSITES

by
Vernon L. Bell
NASA Langley Research Center
Hampton, Virginia, U. S. A. 23665

SUMMARY

Carbon and graphite fibers are known to be electrically conductive. That property has resulted in damage to electrical equipment from the inadvertent release of virgin fibers into the atmosphere. The rapidly accelerating use of carbon fibers as the reinforcement in filamentary composite materials brought up the possibility of accidental release of carbon fibers from the burning of crashed commercial airliners with carbon composite parts. Such release could conceivably cause widespread damage to electrical and electronic equipment. This paper presents the experimental and analytical results of a comprehensive investigation by the National Aeronautics and Space Administration of the various elements necessary to assess the extent of such potential damage in terms of annual expected costs and maximum losses at low probabilities of occurrence. A review of a NASA materials research program to provide alternate or modified composite materials to overcome any electrical hazards from the use of carbon composites in aircraft structures is described.

INTRODUCTION

The National Aeronautics and Space Administration (NASA) has been deeply committed to the research and development of advanced composites for aerospace applications for more than a dozen years. During the initial years of that research, the NASA followed an evolutionary, rather than revolutionary, approach toward the use of composites on civilian aircraft. Concurrent with several technology programs, NASA-sponsored flight service programs involved the selective reinforcement of conventional metallic structures (1). The modification of the tail cone of a CH-54 helicopter with stringers reinforced with strips of unidirectional boron/epoxy composites served to increase the vertical bending stiffness of the tail cone, while the addition of similar boron/epoxy reinforced stringers and wing planks to the center wing boxes of two C-130 transport airplanes served to reduce the stress levels and increase the fatigue life of the wing boxes. Both modifications were achieved at significant weight savings compared to the comparable metallic fixes.

Following an Air Force/NASA Long Range Planning Study for Composites (RECAST) in 1972 (2), several flight service programs which met the principal objectives of RECAST, to build confidence in the use of composites in aircraft and to point the way to lower costs, were begun. Several Kevlar/epoxy fairings were chosen for flight service evaluation on a number of commercial L-1011 transport aircraft, while aft pylon skins of boron fiber and aluminum were put into service on three DC-10 aircraft to replace production titanium skins. Two flight service programs involving secondary aircraft parts built of carbon/epoxy composites have successfully demonstrated the long term service capability of composite parts. Spoilers with carbon/epoxy skins have flown a cumulative total of more than 1½ million hours in active service on Boeing 737 airliners. DC-10 upper aft rudders built principally of carbon/epoxy materials have also been flown without any major problems in commercial airline service.

In 1975, NASA began a program to accelerate the development of several technologies for improving substantially the fuel efficiency of commercial air transports. A vital part of that Aircraft Energy Efficiency (ACEE) effort (3) is the composite structures development program. That composite program involves the development, under NASA contracts, of six aircraft components (Figure 1) by three major transport manufacturers, Boeing, Douglas, and Lockheed. Carbon fibers are the principal, though not sole, reinforcement material to be used in those composites. This follows the emergence from the early technology and flight service programs of carbon (also referred to in this paper as "graphite") fibers as the filamentary reinforcing material of choice for aircraft composite parts by reason of a combination of desired properties together with low cost, high production, and weight savings potentials.

NASA's accelerated efforts to promote the use of composites as a way to fuel-efficient commercial air transports have been matched not only by the progress achieved in utilization of carbon composites in new U. S. military aircraft, but also by independent programs by major U. S. airframe manufacturers designed to use advanced composites to save weight in their present and future airplanes (4). The concomitant emergence of carbon fibers as a useful material for other industrial production uses, such as in sporting goods manufacture, has led to the realization that this is a material destined for multi-million kilogram quantities within the next decade (Figure 2).

A possible barrier to the optimistic future for carbon fibers appeared with the report (5) that there was an uncertain risk associated with the widespread use of carbon fibers due to their good electrical conductivity. Since they are extremely fine (about 8 microns in diameter) and lightweight (about 1.7 grams per cm^3), they can be transported by the wind for great distances. In contact with electrical devices, they could create

THIS DOCUMENT PROVIDED BY THE ABBOTT AEROSPACE
TECHNICAL LIBRARY
ABBOTTAEROSPACE.COM

a number of adverse electrical effects, including resistive loading, short circuits, and arcing, which could lead to electrical outages or destruction (Table I) (6). Several actual such incidents gave credence to the potential for damage. Several crashes involving U. S. military aircraft with composite parts built of nonconductive boron fibers demonstrated (Figure 3) the likelihood that similar crash and subsequent fire events involving aircraft with carbon fiber composites might release free carbon fibers into the atmosphere after the restraining influence of the resin matrix was removed from the composites through oxidation by the fire. Furthermore, carbon fiber manufacturers and processors have been aware for some time of the electrical problems which could occur from the inadvertent release of carbon fibers during industrial operations, though they soon learned to include simple, yet necessary, preventative steps in their normal manufacturing procedures (7).

The United States Government has an extensive interest in the widespread use of carbon/graphite composite materials and any potential hazards resulting from their use. A number of recent programs have accelerated that interest. Some examples are: NASA's ACEE program to expand the use of composites in civil aviation, federal procurement requirements for lightweight composite materials in high performance military aircraft, and federal automotive fuel consumption standards which require weight reductions that may be met only by the significant utilization of composites. Consequently, the importance of those programs contributed to a decision to conduct a government-wide program to study and quantify any risks which would result from the widespread usage of carbon fibers.

The United States Federal Action Plan to deal with potential carbon fiber problems was begun in early 1978 (8). The overall program, which was coordinated by the Office of Science and Technology Policy (OSTP), involved about ten government departments and agencies shown in Figure 4. Although NASA was to assist other departments in several ways, the main responsibility was to conduct a thorough assessment of the risks of electrical and electronic damage that might result by the inadvertent release of conductive carbon fibers from crashes of civilian aircraft with carbon composite parts. That responsibility also carried an obligation to assess the need for protection of civil aircraft from free carbon fiber. An additional charter for NASA was to take part in, and coordinate, a program of research and development of modified or alternate composite materials which would be harmless from the standpoint of electrical hazards, yet which would satisfy the requirements of advanced composites for aircraft structures. While the R and D program for alternative materials was assigned to all of NASA's research centers, the task of assessing the possible hazards from the use of carbon fibers was assigned to NASA's Langley Research Center.

A Graphite Fiber Risk Analysis Program Office was formed at Langley to conduct the risk analysis. The scenario that was adopted as being of interest for the accidental release of carbon or graphite fibers from civil aircraft is illustrated in Figure 5. This scenario was hypothesized to encompass the consequences of accidents involving civil transport aircraft, usually near major airports, where the efflux from the burning of composite-carrying aircraft has the opportunity to be distributed downwind and thus to contaminate not only the nearby airport environs but also numerous distant facilities as pictured in the illustration. Another dimension of the risk analysis is afforded by the risk analysis flow chart, shown in Figure 6, which includes all of the elements of importance which can lead to damages from the release of conductive carbon fibers. Inasmuch as NASA's risk analysis was organized and conducted according to the elements in the flow chart, this paper will be presented in the same manner.

DISCUSSION OF RESULTS

Sources of Released Carbon Fibers

The Graphite Fiber Risk Analysis scenario assumed carbon fibers to originate principally from fires from crashed commercial aircraft with carbon composite parts, as represented in Figure 7. However, non-crash events such as in-flight or ramp fires were also considered. At the start of this program, there had been no known crashes of commercial aircraft with any carbon composites in their structures. In the absence of actual experience, an investigation of ways to simulate the conditions of commercial aircraft crash fires was deemed essential in order to predict the quantities and forms of carbon fiber residues which might be released.

The earliest experiments in release of carbon fibers from burned composites classified the principal types of fiber residues as shown in Figure 8 (9). Single fibers had the potential for the greatest range of distribution due to their very slow settling rate, while the clustering together of a number of single fibers gave a form of efflux which would fall much faster than individual fibers. A third class of residue consisted of yet faster settling strips of fibers, generally resulting from a single ply of a crossplied composite, with the fibers being bound together either by incompletely burned resin or the char formed by the burned resin. A fourth broad class of fibrous residue was fragments of the composite, widely varied in size and shape. These fragments, which were so dense that they were rarely found beyond the immediate vicinity of the fire, generally resulted only from a substantial impact to the burning or burned composite. Rarely were they formed as the result of a simple fire.

The emphasis of this carbon fiber source study was placed on the generation of single carbon fibers from fire tests. First of all, the spread of single fibers was considered to be the most extensive due to their buoyancy, and damage to electrical and electronic equipment spread over a broad area of population was felt to pose the greatest possible

THIS DOCUMENT CONTAINED ASSOCIATED WITH THE
TECHNICAL LIBRARY
ABBOTTAEROSPACE.COM

economic loss. And secondly, single fibers were considered to be the form of residue which would be most capable of penetrating the filters and cases of equipment to reach the vital interiors. Accordingly, most of the fiber release data was gathered and utilized as the percentage of single fibers released (over one millimeter in length) based on the mass of carbon fiber initially present in the composite test specimens. The initial experiments which defined the broad classes of residues involved the destruction of the burned composites with explosives (10). Obviously, such a procedure lacked credibility for representing the typical commercial aircraft crashes. Furthermore, although the fire plus explosive test showed substantial amounts of the highly buoyant single fibers being released, there was an uncertainty as to both the amounts and the forms of residues which might be generated from the simulated burning of composite aircraft parts without the explosion step.

The testing program was conducted at six locations on contract to NASA-Langley. The majority of the small scale composite burn tests were carried out at the U. S. Navy's Dahlgren (VA) fire test facility, which was a completely enclosed environmental chamber, approximately 100 square meters in area, in which small samples (up to 0.1 square meter in size) were burned with a propane gas burner and a variety of disturbing effects were applied to the fibrous residue after consumption of the matrix resin. The test samples were generally either flat composite plates or small specimens cut from prototype composite aircraft structural components. The principal advantage of this test facility was the complete containment of all the fibers released, which were collected by allowing them to settle onto highly adhesive deposition papers laid out on the floor of the chamber. The fiber output from the tests was then counted, generally by optical microscopic methods, in order to analyze the test results. Additional small scale test support was provided by the AVCO Corporation's fire test facility in Lowell, MA (11) and a NASA-Ames/Scientific Services, Inc. test facility at Redwood City, California (12).

In addition to the small-scale laboratory test, valuable fiber release information was acquired from outdoor composite burn tests conducted by TRW Inc., Redondo Beach, California under U. S. Air Force sponsorship (13), for the purpose of studying not only the nature of fiber release from burning composites, but also to verify predicted dissemination patterns over broad areas. Confirmation of small-scale test data was also obtained from large-scale demonstration testing conducted in the U. S. Navy's Dahlgren, VA tube test facility and at the U. S. Army's Dugway (UT) Proving Ground.

Laboratory testing addressed the effects of the following variables on the amounts and characteristics of carbon fibers from burned composites:

Type of fire fuel (jet fuel, propane, natural gas)
Nature of fire (fuel-rich, fuel-poor)
Duration of fire
Disturbances to residue during and after fire
Composite thickness and configuration (crossply, woven, unidirectional, etc.)
Composite surface and edge effects
Types of composite materials (fibers and resins)
Composite quality

The most important findings of the fiber release investigation were:

1. The type and degree of disturbance to the burning composite or burned fibrous residue is the most critical variable for fiber release, as summarized in Figure 9. The quiescent burning of composites leads to the least amounts of single fibers being released, almost invariably less than 0.1% of the initial mass of fiber present. Internal disturbances to the fire residue, such as the type of flexing, twisting, vibrating, or dropping which could be expected in a burning crashed airplane also released relatively minor amounts of single fibers. While disruption of the fibrous residue applied as a mechanical impact gives off many large fragments but less than one-quarter percent as single fiber, the natural airflow of fires due to wind or fire-induced air currents resulted in amounts of up to 1% single fiber. Although ordnance-type explosives appeared to generate the greatest amounts of single fibers, near sonic airflows up to 250 meters per second, which could simulate the explosion of fuel tanks, released amounts of single carbon fibers almost as great.

2. Fire-generated single fibers were, in general, much shorter than expected. Most tests, both burn and burn plus disturbance, gave fiber length spectra where the great majority (two-thirds or more) were less than one millimeter in length. That length was considered to be the lower limit for fibers of concern from the standpoint of vulnerability of electrical equipment. For those fibers over one millimeter in length, the great majority ranged from one to four millimeters in length, with the observed mean length being between two and three millimeters. Seldom were fibers over ten millimeters long obtained.

3. Despite the oft-quoted "indestructibility" of graphite fiber, substantial masses of carbon fibers from composite aircraft parts were consumed in representative fuel fires considered to be typical of jet aircraft crash fires. This reflects the fact that the carbon/graphite fibers in use today are not graphite to any great extent. However, future use of the more graphitic, high modulus type would undoubtedly lead to less consumption of fibers in fires. The mass loss which was observed was manifested by a reduction in the thickness of the fibers, but there was probably some complete consumption of fibers when released in the hotter regions of the fire as well as from the burning composite itself.

TECHNICAL LIBRARY
ABBOTTAEROSPACE.COM

A major objective of the investigation of the sources of accidentally released fibers was to guide the risk analysis efforts with reliable numbers on the predicted accidental fire-release of fibers. After a thorough analysis of carbon fiber release test results, the following criteria were assigned for use in the risk analyses. For those 85% of aircraft crash fires which accident records disclosed had no explosions, a figure of 1% of the mass of the carbon fibers initially present in those composites burned by the fire was considered to be released as single fibers. For the 15% of crash fires with accompanying explosions, a figure of 3-1/2% single fiber released was used. The fibers released were further defined as having an exponential distribution with a mean length of 2 millimeters for all the lengths, above and below 1 millimeter, resulting in a total of 5×10^9 fibers released per kilogram of carbon fiber. (Actually, the distribution was non-exponential for fibers less than one millimeter in length, which were of little concern from an electrical standpoint, due to the high mean exposures to failure for such short fibers).

Fiber Dissemination

The second of the risk analysis elements is the dissemination, or spread, of the carbon fiber, once it has been released from a burning composite into the environment. Before addressing the subject of dissemination, an explanation of the terms which describe the measure of fiber pollution of the environment is in order (Figure 10). The concentration C of carbon fibers is the number of fibers per cubic meter. Of even greater importance from the standpoint of carbon fiber pollution is the exposure E, which is the concentration times the period of time during which the concentration endures, or the time integral of the concentration. In some cases, the number of fibers that get deposited on the ground, or on some other surface, is a useful measure of pollution. This measure is the deposition D, the number of fibers deposited onto a unit area of surface. Vulnerability of electrical equipment is usually expressed in terms of exposure, as the time consequence of concentration.

The three main parameters which control the dissemination patterns for carbon fibers are the fire, the nature of source of the fibrous materials, and the weather. The fire begins the dissemination problem and it is influenced by such factors as the fire pool size, the amount of fuel, and the burning rate. The source has a great deal to do with the fiber exposure levels, since the source determines how many fibers can be given off, what lengths they are, and what other forms of fibrous debris are released. And of course the weather strongly controls the path and fate of the fibers, since it can determine the height to which the fiber-laden fire plume can rise, how much mixing and dilution of the fire plume can occur, the direction taken by the fall-out, and the settling of the fibers with precipitation such as rain and snow. Much dissemination research has been conducted over the past thirty years or so, including the dissemination of nuclear fall-out and the spread of aerosol pollutants into the environment. Existing Gaussian models for the dissemination of fire effluents, such as the Trethewey-Kramer (14) and EPA-Turner (15) models, were found to be acceptable for the carbon fiber risk analysis. The Gaussian models (Figure 11) provide for dispersion of the cloud in a conical sector downwind from the fire plume, with reflections from both the inversion layer and the ground. The dispersion coefficient, that is, the angles at which the cloud spreads, have been empirically determined for the various Pasquill-Gifford stability classes, ranging from a 10^o cone for stable weather to a 40^o cone for unstable weather.

The fiber materials released from a fire form a cloud which moves with the velocity of the wind and in the same direction as the wind. At a short distance from the fire, the effects of diffusion create Gaussian distributions in the concentrations of fibers along the direction of travel and across the spread of the cloud. The rate of spreading and also the maximum altitude of the fibers within the cloud are determined by the weather conditions. The ground level exposure can be described by a series of contours or "footprints" which link points of equal exposures to either single fibers or lint (clusters of fiber). As Figure 12 shows, overcast or nighttime conditions generally produce longer, narrower contours, with fall-out distances of up to 100 kilometers. Fall velocity has a direct effect on distance, with the heavier lint falling out in proportionately shorter distances. Conditions typical of sunny weather tend to give shorter but broader contours.

The single fiber coverage has been plotted in Figure 13 for a number of quantities of released carbon fibers and for a number of appropriate exposure levels. This exposure analysis allows the rapid determination of just how large a geographical region would be exposed to a certain exposure level of carbon fibers, as the result of the release of a specific weight of single carbon fibers. For example, if 40 kilograms of single carbon fibers with an exponential distribution and a mean length of 2 millimeters were released, an area about the size of the suburb of a city (about 10^7 square meters) would be exposed to 10^6 fiber-seconds per cubic meter. The fiber analyses represented in Figure 13 were developed from dispersion models. They showed that a certain quantity of released carbon fibers would be dispersed over a much broader area than had been estimated initially, but the fiber concentrations would be proportionately lower. The quantity of fiber released in the worst case prediction of this risk analysis is shown by the dotted line. Fiber exposure levels ranging from 10^5 to 10^8 fiber-seconds per cubic meter can be expected to result in some failures of electrical equipment. A more detailed discussion of equipment failures will be given in a later section on Vulnerability.

THIS DOCUMENT PROVIDED BY THE ABBOTT AEROSPACE
TECHNICAL LIBRARY
ABBOTTAEROSPACE.COM

Fiber Life and Redissemination

Some initial thoughts concerning the lifetime of carbon fibers and their possible redissemination after being deposited on the earth's surface were rather uncertain and ominous. Due to the chemical inertness of carbon/graphite fibers, it was easy to imagine that the fiber would live forever and that following the initial dissemination and deposition onto the ground, they would be available to be lofted by winds into the atmosphere where they could continue to wreak havoc on electrical equipment. And each successive release of fiber would build up the pollution to a heavy concentration over huge areas. The subjects of carbon fiber lifetime and redissemination were investigated at the U. S. Army's Dugway Proving Ground, and the findings (16) have helped to alleviate those early fears.

The study involved the monitoring of free single carbon fibers which were spread out from the site of previous tests during which a total of 33 kilograms of virgin carbon fibers had been deposited onto a high desert plateau region with silty clay soil having about a 25% cover of small, high desert scrub vegetation. Fibers were collected by vertical fall-out onto "sticky paper" deposition samplers and also in a horizontal transport mode in mesh screen samplers located 2 feet above the ground. Sampling was conducted for a 24-hour period every two weeks after the initial fiber release for several months followed by less frequent sampling until three years had passed. The fibers which were initially released ranged from 6 to 12 millimeters in length, with a mean length of 8 millimeters.

The data shown in Figure 14 indicates a rapid decrease in the amount of resuspended fiber collected on the vertical mesh screen samplers within a month following the first sampling, after which the collection leveled out to a quantity of fibers numbering only about 5% as many as were found in the initial sampling. A second finding of the surveillance was the drastic change in lengths of the resuspended fiber (Figure 15), which decreased from over 9 millimeters mean length for the initial sampling to less than 1.5 millimeters for fibers collected after 3 years. Combining the decrease in numbers of deposited fibers with their decrease in length leads to the conclusion that after three years, the mass of carbon fibers which had been subjected to resuspension was very low indeed. Examination of the terrain revealed that the fibers were either buried partially or completely in the soil, or entrapped at the ground level by the scrub vegetation. The mechanism for the redissemination process is believed to involve wind-driven particles of soil impacting the entrapped fibers which, because of their inherent brittleness, break off into shorter segments.

The current opinion, and that reflected in the risk analysis, is that redissemination of previously released carbon fibers would be a very small contribution to the entire amount. Certainly vegetated areas, such as grasslands, forests, and cultivated fields would not release any significant amounts of entrapped fibers. The only surface which can be envisioned as leading to a significant amount of redissemination would be hardtop surfaces typical of urban areas, such as paved streets and roads, roofs, parking lots, etc. Even then, precipitation effects could soon wash the fibers from the surfaces, and traffic on roads could also serve to grind many of the fragile fibers into an electrically-harmless powder. Of course, larger forms of carbon fiber debris, such as single-ply strips of burned out carbon composites, which have been shown to be transportable in the air for distances up to one mile from the fire site (13), may have to be cleaned from roadways soon after deposition to prevent the generation of a fresh supply of single fibers by the action of traffic.

Transfer Function

Transfer function is the element of the risk analysis dealing with the penetration of fibers through an interface. As applied to the transport of carbon fibers, the transfer function is the ratio of fibers which pass through an interface to those which encounter the interface. Examples of the interfaces which influence the carbon fiber risks are doors or window screens, filters, and equipment cabinets. The phenomenon of particle transport in air is well understood and a body of data employed for heating and air conditioning purposes was available. In addition, both analytical and experimental studies of the transfer of carbon fibers into buildings through filters, and into equipment boxes were made during this program. Much filter efficiency information was also available from the National Bureau of Standards for widely used types of filters. Typical results of the experimental studies have been shown in Figure 16 (17). The filter factor was determined for a number of different types of filters, such as ordinary household window screen and furnace filters, when exposed to fibers of different lengths. The chart at the right of the figure shows that in addition to the removal by window screen of many of the fibers with a mean length of 2 millimeters, another moderating influence on the potential for electrical damage is afforded by passage of the shorter fibers with a mean length less than 1 millimeter. Carbon fibers so short were considered harmless to virtually all electrical equipment, but that moderating effect was not included in the risk analysis.

In general, intentional or natural filtration of carbon fibers contributes a tremendous reduction in the concentration of fibers actually reaching the critical electrical equipment, with respect to the concentrations which encounter the filter barriers. While such a crude filter as window screen (Figure 16) removed nearly 90% of the 4 millimeter fibers, air conditioning systems for homes and factories give transfer functions of 10^{-3} to 10^{-4} for standard filters. On the other hand, some factors involved in filtration can partially nullify the benefits of filters. For example, filters must be

This Document Provided by the ABBOTT AEROSPACE TECHNICAL LIBRARY
ABBOTTAEROSPACE.COM

properly mounted: even a small gap between the filter and its mounting can reduce the filter efficiency by an order of magnitude or more. Air velocity can also have a substantial effect on the number of fibers passing a filter, with a ten-fold increase in air velocity resulting in a similar increase in passage of fibers. Air filters (or water separators which serve the same purpose) in transport aircraft have extremely small transfer functions ($\sim 2 \times 10^{-5}$). However, as much as three-quarters of the fiber which approaches an open aircraft avionics bay door could pass into that compartment while the plane is on the ground. Entry of carbon fibers could be prevented, in the event of a nearby incident, simply by closing the door. Nevertheless, filtration and natural barriers to the transmission of carbon fibers were shown to provide alleviating effects to the electrical hazards of the fibers.

Vulnerability

The investigation of the elements dealing with the vulnerability, or susceptibility, of electrical and electronic equipment to damage from carbon/graphite fibers was preceded, perhaps, by the most speculation about the seriousness of the problem. While several incidents of damage caused by virgin carbon fibers in or near carbon fiber manufacturing operations were a matter of record at the onset of NASA's study, there was apparently no known instance in which fibers previously incorporated into a composite had been released in an accidental fire and had subsequently caused adverse electrical effects. Consequently, a number of unknowns regarding the non-virgin carbon fibers had to be studied and their effects on damage potential analyzed.

The types of effects that were expected from exposure of equipment to fibers were listed previously in Table I. The categorization shown is very gross, but serves to point out those general regions which were of the most concern. In the low voltage and low power region, a carbon fiber has the capability to maintain a high resistance short without burning out. In that event, the equipment could malfunction although the components incur no local damage. The region of medium voltage and high power causes some concern since the fiber acts as a trigger to potential arcing, and the arcing may be sustained. The result can be blown fuses, stressed components and flashovers at insulators. The third region of most concern is that of both high power and high voltage, where carbon fibers (as is the case for many foreign materials) can lead to corona, and initiate arcing severe enough to disrupt and to damage equipment catastrophically.

The electronic equipment failure model used to describe the vulnerability of electronic equipment to carbon fibers has been shown in Figure 17, where the probability (P) of failure is: $P = 1-\exp\left[-E/\bar{E}\right]$, where $\bar{E}$ is the mean exposure required to fail the equipment during testing and E is the exposure endured by the equipment. At the $\bar{E}$ exposure level, the probability of failure of a piece of equipment is 0.632, while at an exposure of one-tenth the $\bar{E}$, the probability is only .095, meaning about 9 or 10 pieces of equipment of the same type would fail out of 100 exposed.

The NASA Vulnerability Test Program relied principally on two test methods to assess the susceptibility of electrical and electronic equipment to carbon fibers. The simplest technique involved the use of a fiber simulator. This simple device was developed to simulate the electrical characteristics of a carbon fiber. If the electronics or the equipment to be tested had a limited number of nodes, 50 or perhaps no more than 100, it was possible to probe the equipment and so be able to tell if a carbon fiber (as represented by the fiber simulator) could cause the equipment to malfunction or fail. Representative electric appliances which were tested in that manner have been listed in Table II (18).

The most direct method to test electrical equipment for vulnerability to carbon fibers involved direct exposure of the equipment in a controlled chamber. An example of the several chambers used in this program is the one located at NASA's Langley Research Center, pictured in Figure 18. The operations scheme involved placement of the test article in the chamber, while a known quantity (monitored by fiber sensors) of carbon fibers of a desired length were chopped from continuous fiber tow and aspirated into the exposure chamber. The fibers were then kept in suspension until the test article malfunctioned or failed, or until a maximum exposure level (usually 10^8 fiber-seconds per cubic meter) was reached without failure. A number of replicate tests were conducted for each test item, whether it failed or not. A thorough cleaning of the equipment, such as by removal of fibers with a vacuum cleaner, was conducted between tests. A summary of the articles tested in the NASA or other chambers is presented in Table III (19).

Over 150 individual articles were tested for electrical/electronic susceptibility to carbon fibers by the fiber simulator and test chamber methods. The results in Tables II and III indicate that many pieces of equipment were invulnerable to carbon fibers. Most household appliances with 110-volt circuits proved to be unaffected. Enough pieces of consumer equipment were selected to be representative of about 75% of the market value of consumer goods. Very little 220-volt testing was done, but it was expected that 220-volt single-phase circuitry would be about as resistant to carbon fibers as 110-volt, since 440-volt single phase equipment was also proven to be relatively unaffected. (However, arcs could be sustained for 440-volt, 60 hertz industrial power using three phase transformer supplies capable of delivering currents in the range of 400 to 1500 amps, when arcs were initiated. An idea of the exposures leading to failure of some equipment can be seen from Figure 19 (19). Most equipment was vulnerable at 10^5-10^7 fiber-seconds per m^3 for longer fibers, and near 10^8 fiber-seconds per m^3 for very short ones. No equipment failed in the lower left hand region of the figure outlined by shading.

TECHNICAL LIBRARY
ABBOTTAEROSPACE.COM

Figure 20 (19) illustrates an important factor influencing the effect of carbon fibers on electrical circuits. The tests were conducted with three different fiber lengths: short (∿3 mm), medium (∿7 mm), and long (∿12 mm). It is apparent that the longer fibers were much more effective in causing malfunctions than short ones. As was pointed out in the section on Source, most fire-generated carbon fibers are very short, with mean lengths usually between two and three millimeters. Therefore, the exposure levels causing equipment failure are quite high for the fibers released in real-life situations.

Another important relationship which was established by fiber chamber tests was that associated with the resistance of the carbon fibers themselves. Figure 21 (19) shows the effect that the fiber resistance had upon the critical exposure levels for three pieces of equipment. The stereo amplifier was an order of magnitude in exposure less vulnerable to DE 114, a high resistance, low temperature-processed carbon fiber, than it was to the T300 fiber in common use today. Similarly, a color television set and an air traffic control transponder were from 1-1/2 to 2 orders of magnitude of exposure less vulnerable to failure from T300 fiber than they were to two highly conductive, very high modulus fibers GY70 and HMS. Studies also concluded that fibers released from composites by fire had resistivities unchanged from virgin fibers and the damage potential of such fibers was the same as for the raw fibers. Another concern was that of post-exposure vulnerability. Most of the testing of equipment in Table III was done in the "on" condition. There was some concern about whether or not equipment which was exposed while "off" would fail subsequent to turning it "on". A test scheme involving 200 hours of testing of a color television set and a stereo amplifier, including many "on-off" cycles, indicated that post-exposure failure was not a significant problem.

As pointed out in the Introduction, one of NASA's responsibilities in the conduct of its carbon fiber risk analysis was to assess the need for protection of civil aircraft from released carbon fiber as warranted by the vulnerability of those aircraft to carbon fibers. A detailed analysis of the civil transport aircraft built by three domestic U. S. manufacturers was carried out. The analysis included testing of several specific types of avionics equipment typically used in those aircraft and having some expectancy, for various reasons, of being susceptible to damage from carbon fibers. Five pieces of avionics were tested extensively in the Langley test chamber (20): an air traffic control (ATC) transponder, an instrument landing system (ILS) receiver, a very high frequency (VHF) transceiver, distance measuring equipment (DME), and a flight director system. Except for the DME, none of the equipment was conformally coated. The equipment was exposed to fibers with three lengths: 1, 3, and 10 millimeters. All of the values for $\bar{E}$ (mean exposure to failure) were above 4×10^6 fiber-seconds per cubic meter, with the ATC transponder having the lowest value. That represented the oldest electronic design for a piece of equipment tested; it was introduced in the 1960's. It had the greatest open area available for ingesting fibers, with two sides of the dust cover completely perforated with 3.18 millimeter (1/8 inch) holes. Because of the gap sizes in the equipment and the filtering action of the dust covers, 3 millimeter fibers were the most significant in terms of contamination. As a result of detailed analysis based not only on the fiber exposure tests, but also on internal airflow analysis for the aircraft and various operational duty states of the aircraft, it was concluded that ground-exposed aircraft at an airport with a carbon composite crash fire would experience a much lower avionics equipment failure rate from carbon fibers than current normal operational failures. Because of the redundancy required for the current operational failure rate, no further protection for civil aircraft avionics was anticipated to be required.

A final concern in the area of vulnerability was that of carbon fiber-induced shock hazards. Under NASA sponsorship, the National Bureau of Standards examined a large number of household equipment items for susceptibility to failure and/or shock hazard. As mentioned before, 110-volt household appliances were generally invulnerable to carbon fibers. However, at extreme exposure levels some appliances were susceptible to carbon-fiber induced shorts to the external appliance case where potential shock hazard can exist. The most susceptible equipment for the shock potential was found to be the common household toaster (21). An analysis based on the projected carbon fiber usage and accident rates in 1993 (the year for which the risk analysis was performed), indicated less than one potential shock hazard per year would be caused by accidental carbon fiber release. Furthermore, it was predicted that the short current would not be lethal since the fiber would burn out (that is, using the 30 million psi modulus fibers in use in 1980).

Demonstration Testing

A series of tests were conducted (22) in a large, tubular fire facility to demonstrate an agreement between the susceptibility of electronic equipment to carbon fibers generated from burning composites in a jet fuel fire and the vulnerability of the same equipment to clean, virgin fibers in the Langley exposure chamber. The unique fire chamber was a modification of a portion of a long, shock tube located at the Naval Surface Weapons Center, Dahlgren, Virginia. A photograph of the 750-meter long tube is pictured in Figure 22. A 275-meter section of the tube was utilized, with a 1.22-meter square commercial jet A fuel fire being burned at a location where the tube was 4.6 meters in diameter. Composite specimens were burned in the fire and the fire plume was pulled through the last 275 meters of the tube by up to six large fans. A water fog spraying down from the top of the tube served to remove carbon fibers from the smoke plume, which exited from the 7.3-meter (24-foot) diameter end of the tube. During the equipment exposure tests, six identical fan-cooled, unfiltered stereo amplifiers were situated on a target table at 220 meters (700 feet) from the fire. The amplifiers were

TECHNICAL LIBRARY
ABBOTTAEROSPACE.COM

in an operating mode during the fiber release fire test. Strips of carbon fiber/epoxy composites were placed in a wire mesh basket, which was rotated in the middle of the fire during the entire period of the test. The actual failure of the amplifiers have been represented in Figure 23 by the step-wise solid line plot. The first four amplifiers had failed after the first 600 seconds of the test. Those failures have been indicated by the step-up at an exposure of about 6.5×10^5 fiber-seconds per cubic meter, with a fifth failure occurring when an exposure of 2.4×10^6 fiber-seconds per meter^3 had been reached, and the final amplifier failed at a level of about 3.3×10^6 fiber-seconds per meter^3. The experimental failures in the shock tube test matched very well the failures predicted from the Langley chamber-derived exponential probability curve superimposed on the figure.

A series of large scale outdoor demonstration tests was conducted at the U. S. Army's Dugway Proving Ground in Utah (23). The series consisted of two types of tests: source tests designed to measure the extent of fiber release from burning carbon/epoxy composites in a large JP-4 fuel fire and plume tests which were intended to not only capture carbon fibers and so determine the amounts released, but also to disseminate the released fibers over an area so large as to realistically simulate the dispersion expected from the crash and burning of a commercial air transport with carbon composite parts. The tests were carried out using a 10.7-meter diameter fuel pool size and 11.4 cubic meters of JP-4 aviation fuel. Duration of the fires was nominally 1200 seconds. About 45 kilogram quantities of real and test aircraft parts of carbon/epoxy composites were placed on an elevated steel mesh table above the fire pool.

The source tests were conducted during periods of very low wind speeds (less than 0.4 meters per second) in order to allow the fire plume to rise vertically from the fire. A large number of steel mesh sampling devices which captured released carbon fibers on the mesh screen within a cannister were suspended in an array above the fire. The samplers were suspended from cables rigged from four 60-meter high towers, arranged in a 65-meter square around the fire pool.

The dissemination tests were conducted in the same manner except that wind speeds from 2.7 to 5.4 meters per second were desired, and a wind direction of $320^o \pm 35^o$ was required. This permitted the fire plume to pass through a huge "jacobs ladder" (Figure 24). (The 169-meter high Washington Monument has been shown to scope the size of the undertaking). This "jacobs ladder" was constructed from 2.54 mm Kevlar ® rope with horizontal and vertical spacings of 15.25 meters. The 305-meter by 305-meter network was suspended from a catenary which was lofted by two U. S. Air Force 1270 m^3 balloons, with stabilizing tether lines placed out in all directions. The net was placed 153 meters from the fire. Many sampling devices of several types were mounted on the net. These included flat plastic rectangular frames, with their 0.29 m x 0.25 m openings covered with 1 mm mesh fabric coated with a sticky substance to cause fibers to adhere to the mesh when the samplers were placed at the intersections of the rope, normal to the flow of the smoke plume. Other samplers included mesh filters in cardboard cannisters similar to the steel samplers suspended over the fire, eight high voltage electrified grids instrumented to discharge when contacted by fibers, open-ended 0.085 meter diameter cans with adhesive-coated fabric mesh spread over one of the open ends, fiber collection pumps and filters used to monitor the air for excessive concentrations of respirable-sized fibers, and light emitting diode detection devices. As the fire plume passed through the suspended "jacob's ladder", the fibers were detected or collected by the array of monitoring apparatus which was then analyzed subsequent to the test. In addition, the dissemination of fibers was monitored by means of both deposition sticky papers and vertically mounted open-ended mesh can samplers spread out at appropriate intervals for distances of up to 19 kilometers from the fire in the direction of the wind flow.

A summary of the results of both the source and the dissemination tests has been presented in Table IV. Variance from the laboratory tests reported in the Source section of this report was noted only for the average fiber lengths. The average lengths of 5.0, 4.4 and 5.2 millimeters from the three dissemination tests were somewhat higher than the lengths obtained for the laboratory tests. However, the average length (3.2 mm) from the source test was in keeping with the laboratory test findings. The average fiber diameters of 4.1 to 4.7 micrometers indicated a substantial oxidation of the fibers from their normal 6 to 8 micrometers in the virgin state. The weight percent of fiber release was in concert with many of the laboratory results.

Conclusions pertinent to the risk analysis, based on the results of the large scale demonstration tests at Dahlgren and Dugway Proving Ground, are summarized below.

A maximum of 0.5% of carbon fiber, based on the amount initially present in the composite specimens exposed to the fire, was released in the best Dahlgren shock tube fire and equipment exposure test. However, since that was a long duration fire (over 12,000 seconds) and the fiber release was forced, the maximum of 0.19% released from the Dugway demonstration tests was considered more representative of predicted fiber release from commercial air transport fires. Therefore, the figure of 1% carbon fiber release used in the risk calculations was quite conservative. The mean fiber length (2 mm) from the Dahlgren test was in close agreement with the value used in the risk analysis, but some of the mean lengths from the Dugway large scale tests were somewhat longer than the mean length used for the risk analysis. And finally, the Dahlgren demonstration

® Registered trademark for DuPont's Aramid fiber

TECHNICAL LIBRARY
ABBOTTAEROSPACE.COM

tests established that the vulnerability of equipment to fire-released fibers agrees with the vulnerability of the equipment to virgin, unburned carbon fibers, thus justifying the use of fiber chamber test data in the risk calculations.

Facility Surveys

Surveys of 62 public, utility, commercial and industrial installations in the United States were conducted (24) in order to develop a sound foundation for the use of census data generated in the analysis of the overall risk to the community from the use of carbon fibers in civilian aviation. A summary of the number and types of installations of the four major classes has been summarized in Table V. Emphasis was placed on three main elements:

(a) Determination of data for use in modeling the economic impact of fiber-induced failures;

(b) Identification of the sensitivity of life-critical or emergency services to the fiber hazard; and,

(c) Definition of the sensitivity of in-place equipment to airborne fibers.

Analysis of the results of the surveys indicated that life-critical services already have sufficient in-place protection for isolation from the environment so that further protection against airborne carbon fibers was not required. For example, hospital operating rooms and critical care areas use such "absolute" levels of air filtration to guard against airborne infections and contaminations that fibers would not enter those areas. Another finding was that more than half of the 21 industrial installations surveyed had strong in-place barriers against the ingestion of airborne carbon fibers, such as high efficiency filters or coated circuit boards, due to the needs to protect against atmospheric or self-generated contaminants. Assembly lines and other continuous process type operations represent cases where operations could be halted by on-line equipment failures. Quite generally, such operations have preventative or protective in-place measures adequate to resist carbon fiber damage. And finally, many industrial installations have the ability to shift operations or to work around failures in equipment. Where equipment failures caused by other adverse factors are the rule, quickly installed parts are kept in readiness.

Conclusions which resulted from a comprehensive analysis of the survey were, as follows:

o Life critical functions could be excluded from any impact on the risk analysis.

o Emergency services would suffer no interruption. Any economic impact would be limited to specific items of equipment.

o Utilities would suffer no system loss. The economic impact would be confined to local outages and repairs.

o Commercial institutions, such as banks, stores, etc., would incur no interruptions to critical operations. Any adverse impact from carbon fibers would be limited to peripheral equipment.

o Industrial operations: A number of class operations, such as food processors, textile mills, paper mills, printing, chemicals, and others, representing 40% of the national value-of-shipments, would create no adverse impact on the risk analysis because of protection from their present operating environment. Another group (machinery, some transportation) comprising 15% national value-of-shipments would contribute no impact on the carbon fiber risk because their operations require local protection from cutting fluids and contaminants. Other installations representing 10% of value-of-shipments, such as electrical and instrument plants, would create minimal impact on the risk due to their critical need for air conditioning or other control of ambient conditions. And a fourth group of industrial installations, comprising plants having 7% of the national value-of-shipments from their operations, would also contribute a minimal risk impact because their operations are supported by ready spares.

Risk Computations

The primary objective of the risk analysis was to estimate the risk to the nation over the next 15 years (from 1978) resulting from the use of carbon composites in civil aircraft. A secondary purpose was to provide a framework for decision making on composite material usage, material modification, and protection schemes. Two contractors, ORI and Arthur D. Little, Inc. were selected to develop independently methods to numerically evaluate the potential losses due to failures of electrical equipment from airborne carbon fiber contamination originating from civilian aircraft crashes. The risk computations were conducted in two phases. ORI developed a risk model based on the 9 largest hub airports in Phase I (25) and proceeded to translate the risk profiles for a number of individual airports into a national model in Phase II (26). Arthur D. Little, Inc. developed a preliminary national profile from 26 major airports in the first phase (27) and followed up with a number of refinements to the national risk profile in Phase II (28).

THIS DOCUMENT PROVIDED BY THE ABBOTT AEROSPACE
TECHNICAL LIBRARY
ABBOTTAEROSPACE.COM

The available commercial air transport accident records of the National Transportation Safety Board (NTSB) were augmented by information from the three major U. S. airframe manufacturers. They supplied detailed data on accident characteristics, such as fire duration and severity of damage to aircraft, that would affect carbon fiber release conditions. Projections on the extent of carbon fiber usage on U. S. commercial aircraft were also generated by the aircraft manufacturers. Such projections included the numbers of planes expected to be in service in 1993, by three types: small, medium, and large jets, as well as the ranges of quantities of carbon fiber composites which were predicted to be used on those planes. Among the criteria for determining the aircraft crash scenarios were the operational phases during which the accidents occurred. Figure 25 summarizes NTSB data for 1968-1976 (29) indicating that almost half of the severe accidents accompanied by fire occurred during landing, while a quarter of the accidents with fire occurred during takeoff. Furthermore, 60% of the accidents happened at the airport and 80% were within 10 kilometers of airports. Attention was also focused on 26 large hub airports which accounted for nearly 70% of U. S. emplanements. And lastly, 3.8 severe fire accidents were predicted annually in the United States. Based on predictions that 70% of the jet fleet would be using carbon composite parts by 1993, 2.7 fire accidents per year were projected for 1993 for such aircraft.

Figure 26 (27) shows the sequence of events which were modeled in order to describe the carbon fiber risk phenomenon. The simplified event tree logic which was followed to arrive at the local risk profile has been depicted in three sequential figures, Figures 27a, 27b, 27c (30). Random selections are used during many phases of this event tree for selecting the paths. At various points, the random selection leads to inputs from various elements of the entire program. For example, if an accident is randomly selected (Figure 27b) which involved an explosion in addition to a fire, then 3-1/2% single fiber release will be used. If the accident chosen involved fire only, then 1% single fiber release was used in the model of that accident. When the path of the event tree reaches Figure 27c, the areas of the city and/or countryside affected have been defined. Input from the elements of transfer function, vulnerability, and facility surveys then permit the determination of cost impacts from the accident. Examples of costs are repair or replacement of equipment, downtime, product losses, etc. Using a selected historical number of accidents each year (~3 to 6), the random selection of nodes in the event tree and the cost calculations are repeated for each accident and the cost is summed to obtain one estimate of the national cost. One estimate, however, is insufficient to obtain a statistical distribution of estimates, so the national risk calculations must be repeated a large number of times.

The results of the annual risk profiles for economic losses due to commercial air transport fires involving carbon fibers have been given in Figure 28. The Phase I profile was assessed one year earlier than those from Phase II. The markedly lower risks in Phase II were attributable to a number of refinements in single fiber release (5% fire, 25% fire-explosion in Phase I vs. 1% fire, 3-1/2% fire-explosion in Phase II), a ten-fold decrease in infiltration due to use of experimental transfer function data, and extreme diminishments in equipment susceptibility due to shorter fiber lengths and higher mean exposures to failure. An increase in predicted carbon fiber usage in aircraft manufacturing made a slight positive contribution to the risk profile.

As the risk profiles in Figure 28 show, the expected annual risks to the United States due to the predicted use of carbon composites on civil aircraft in 1993 are certainly less than $1000 per year. The chances of national losses reaching significant levels are extremely small. For example, both the ORI and Arthur D. Little (ADL) models indicate (at the crossover for the plots) that an accident resulting in $5000 damage from carbon fibers would only occur every 40 years! Although a trend toward significant use of carbon fiber composites on general aviation aircraft has not yet emerged, separate risk computations dealing with forecasts of up to 55 kilograms of such composite per plane were made. The conclusion from that study was that it was extremely unlikely there would be a substantial dollar loss due to carbon fiber releases in general aviation accidents. Further diminishing the concern for carbon fiber hazards is the fact that loss of life from carbon fiber electrical events is virtually non-existent.

Material Modification

As pointed out in the Introduction, a secondary responsibility assigned to NASA under the Federal Action Plan was to investigate alternative or modified composite materials which would lessen or eliminate electrical hazards as a consequence of the use of composites. This responsibility was assigned to NASA's research centers since new materials research and development fit into the existing charters of the centers' base technology programs. All of the installations (Langley, Ames, and Lewis Research Centers, Marshall Space Flight Center, and the Jet Propulsion Laboratory) had knowledgeable line organizations with composite materials expertise so that a minimal impact on their existing research programs resulted.

The general objective of the resulting program was to develop composites which reduce carbon fiber electrical risks while retaining or improving the structural properties of resin matrix composites which make them desirable for use in aircraft structures. A NASA workshop on modified and alternate materials was held at Langley Research Center (31) in March 1978 as a means of making the composite materials community aware of the carbon fiber hazards program and to solicit the ideas of government, industrial and academic representatives. The cooperative efforts of the workshop resulted in a program with the following elements:

THIS DOCUMENT PROVIDED BY THE ABBOTT AEROSPACE
TECHNICAL LIBRARY
ABBOTTAEROSPACE.COM

Test Methods
Hybrid Composites
Fiber Gasification
Modified Epoxy Resins
Fiber Coatings
Alternate Matrices
High Resistance Fibers
New Fibers

The element of test methods was given the highest priority since it was essential that investigators be able not only to determine the effectiveness of their new or modified materials, but also be able to compare them with other modified materials. However, since research could not be delayed pending the development of standardized test methods, several different tests were developed for determining fiber release at several of the research centers. One rather simple test device was developed at NASA's Ames Research Center (32) and it was utilized to a limited extent for comparing the relative amounts of single fibers which were released from burning composites. The device burned relatively small composite specimens, approximately 25-30 cm^2 in size, with a heat flux fairly realistic for a fuel fire, after which the composite was impacted with a pneumatically driven steel ball. The released fibers could then be collected and measured.

The concept of hybrid composites to minimize the release of conductive fibers was considered to be the most promising approach by the workshop participants. The hope that outer, or alternating, plies of a nonburning fiber reinforcement used together with plies of carbon fiber would help contain free carbon fibers appeared to be valid in preliminary tests, especially for composites which were just burned without any severe disturbance. Although the concept has not been evaluated conclusively, there are indications (33) that the type of disruption applied to the residual post-burned fibrous mass may be critical in determining the validity of the hybrid concept.

Fiber gasification was a novel approach which involved the deposition onto carbon fibers of certain metallic ions which would catalyze the complete consumption of the fibers when exposed to flame. Preliminary results (34) with such contaminants as calcium and barium acetates were promising, although much additional research was required to prove the practicality of this potential solution to the problem.

The modification of the epoxy resins used in composites was attractive from the standpoint of promising a minimum disruption of current applications and the least requalification of the modified composites. It was early recognized in the determination of fiber release from carbon-epoxy composites that epoxies are always converted in fires to a small amount of char which serves to bind individual carbon fibers together, thus preventing their release for some time. Some promising modified epoxies were uncovered by changing the chemistry, catalysts, and blending to give much higher char yields (35). The same thrust toward higher char yield resins was the basis for much of the attention paid to another element in the program, that of alternate matrices.

The general objective of the fiber coatings element of the program was to deposit coatings onto existing carbon fibers and thus to render them nonconducting. Among several coating materials such as silicones, boron nitride, silicates, boron carbide and silicon carbide (36), (37) the latter offered the most promise. A ten-fold increase in resistance of carbon fibers was afforded by a 0.1 micrometer coating, but oxidation of the silicon carbide to silicon dioxide at 1273 K gave six orders of magnitude increase in resistance. However, preliminary tests indicated some undesirable effects on the properties of composites made from the coated fibers.

The last two elements of the materials modification program, nonconductive fibers and new fibers, were considered to be the most long-term in nature and, thus, were relatively low in priority. When the carbon fibers were oxidized to carbon oxide fibers, the resistivities of the resulting fibers were much higher (up to 10^5 ohm/cm). However, the degradation of fiber properties was excessive. As a nonconductive fiber with mechanical properties quite similar to carbon, boron nitride fibers were being studied prior to the emergence of carbon fiber electrical hazards and those early efforts were revived and augmented as a result of this new program. At least one high modulus, nonconductive organic fiber was studied as a hoped-for replacement for carbon fibers.

The materials modification program was undertaken with the full knowledge that the chances of replacing, improving, or even modifying, an existing industrial product such as carbon fiber which had undergone years of industrial development were very remote. It is not possible to claim any positive results from this program at the present time since the program has been underway for less than two years, and some of the leads are still being actively pursued. The findings of extremely low risks as a result of the afore-described carbon fiber risk analysis has certainly diminished the necessity for new materials research. Nevertheless, the incentive which engendered the modified materials research program could well prove to have been the driving force instrumental in the successful development of one or more exciting new composite materials in the future.

Concluding Remarks

A comprehensive assessment of the possible damage to electrical equipment caused by accidental release of carbon fibers from burning civil aircraft with composite parts has been completed. The study concluded that the amounts of fiber expected to be re-

This Document Provided by the ABBOTT AEROSPACE TECHNICAL LIBRARY ABBOTTAEROSPACE.COM

leased were lower than initially supposed: conservative quantities of 1% and 3-1/2% were employed in the risk computations for aircraft crash fires and crash fires plus explosions, respectively. Footprints of carbon fibers determined from dispersion models were found to be much larger in area than originally estimated, but were much lower in fiber concentrations. Redissemination, as a source for fiber, was shown to be insignificant. The susceptibility of electrical equipment to carbon fibers was low for current structural fibers. Consumer appliances, industrial electronics, and aviation instrumentation were relatively invulnerable to carbon fibers. The overall risk costs were shown to be extremely low: the expected annual cost was less than $1000 and it was predicted that there was only one chance in two thousand of exceeding $150,000 equipment loss in 1993. Furthermore, the potential shock hazard from carbon fibers was insignificant, so risk of life from electrical fiber effects was not considered to be a factor in the overall risk associated with the widespread use of carbon fiber composites in commercial aircraft structures.

The results of the NASA risk assessment program are such that the electrical effects of carbon fibers should not be considered an impediment to further development of carbon composites in aircraft use. In addition, a program to develop alternate materials specifically to overcome that perceived hazard is not necessary.

REFERENCES

1. Brooks, W. A., Jr.; Mathauser, E. E.; and Pride, R. A.: Application of Composites to the Selective Reinforcement of Metallic Aerospace Structures. Conference Reprint No. 112, Presented at the AGARD Conference on Impact of Composite Materials on Aerospace Vehicles and Propulsion Systems, Toulouse, France, September 20-22, 1972.

2. Yaffee, M. L.: Use of Composites to Increase. Aviation Week and Space Technology, September 11, 1972, pp. 87-91.

3. Vosteen, L. F.: Composite Structures for Commercial Transport Aircraft. NASA TM 78730, 1978.

4. Card, M. F.: Highlights 1979 - Materials. Astronautics and Aeronautics, Vol. 17, No. 12, 1979, pp. 98-100.

5. A Report of Observed Effects on Electrical Systems of Airborne Carbon/Graphite Fibers. NASA TM 78652, 1978.

6. Taback, I.: Vulnerability. NASA Conference Publication 2074, 1979, pp. 109-123.

7. McFerrin, J. H.; and Trulson, O. C.: Electrical Equipment Protection and Waste Disposal Practices - Carbon Fiber Manufacture. Society of Automotive Engineer Technical Paper 790034, Congress and Exposition, February 26 - March 2, 1979.

8. Carbon Fiber Study. NASA TM 78718, 1978.

9. Bell, V. L.: Source of Released Carbon Fibers. NASA Conference Publication 2074, 1979, pp. 41-71.

10. Babinsky, T. C.; and Musselman, K. A.: Burn/Blast Tests of Aircraft Structural Elements. U. S. Naval Surface Weapons Center, NSWC/DL TR 3897, 1978.

11. Alexander, J. G.: Development of a Fire Test Facility for Graphite Fiber - Reinforced Composites. (AVCO Corporation; NASA Contract NAS1-15511). NASA CR 159193, 1980.

12. Wilton, C.; Kamburnoff, G.; and Boyes, J.: Fire Testing of NASA Samples - Phase I. (Scientific Services, Inc.; NASA Contract NAS2-9945) NASA CR 152339, 1979.

13. Lieberman, P., Chovitt, A. R.; Sussholz, B.; and Korman, H. F.: Data Reduction and Analysis of Graphite Fiber Release Experiments. (TRW Defense and Space Systems Group; NASA Contract NAS1-15465). NASA CR 159032, 1979.

14. Dumbould, R. K.; and Bjorklund, J. R.: NASA/MSFC Multilayer Diffusion Models and Computer Programs--Version 5. (H. E. Cramer Co., Inc.) NASA CR 2631, 1975.

15. Turner, D. B.: Workbook of Atmospheric Dispersion Estimates. Rev. 1970 Environmental Protection Agency, Office of Air Programs Publication AP-26.

16. Trethewey, J. D.; and Whiting, J. H.: Surveillance Sampling of Carbon Fiber Material, June 1975 - August 1976. U. S. Army Dugway Proving Ground, DPG-FR-79-304, 1978.

17. Paszek, J. J.; Davis, D. D. and Patrick, J. H.: Carbon Fiber Transfer Functions Through Filters and Enclosures. U. S. Army Ballistic Research Laboratory Report ARBRL-MR-02946, 1980.

18. Lovett, C. D.; and Wise. R. A.: A Study of the Effects of Carbon Fibers on Home Appliances. National Bureau of Standards Report NBS-IR-79-1952, 1979.

TECHNICAL LIBRARY
ABBOTTAEROSPACE.COM

19. Taback, I.: Evaluation of Equipment Vulnerability and Potential Shock Hazards. NASA Conference Publication 2119, 1980, pp. 73-99.

20. Meyers, J. A.: The Vulnerability of Commercial Aircraft Avionics to Carbon Fibers. (The Bionetics Corporation; NASA Contract NAS1-15238). NASA CR 159213, 1980.

21. Meyers, J. A.: The Potential of Carbon Fiber Induced Hazards in Household Toasters. (The Bionetics Corporation, NASA Contract NAS1-15238). NASA CR 159147, 1979.

22. Musselman, K. R.; Pride, R. A.; and McHatton, A. D.: Electronic Equipment Vulnerability to Fire-Released Fiber Exposures. NASA TM 80219, 1980.

23. Pride, R. A.: Large-Scale Tests. NASA TM 80218, 1980.

24. Butterfield, A. J.: Surveys of Industrial, Business and Public Facilities to Establish Fiber - Induced Failure Consequence. NASA Conference Publication 2119, 1980, pp 137-149.

25. Pocinki, L. S.; Kaplan, L. D.; Cornell, M. E.; and Greenstone, R: Advanced Risk Assessment of the Effects of Graphite Fibers on Electronic and Electrical Equipment. Final Phase I Report (ORI Inc., NASA Contract NAS1-15379). NASA CR 159027, 1979.

26. Pocinki, L. S.; Kaplan, L. D.; and Cornell, M. E.: Advanced Risk Assessment of the Effects of Graphite Fibers on Electronic and Electric Equipment. Final Phase II Report (ORI Inc., NASA Contract NAS1-15379). NASA CR 159210, 1980.

27. Kalelkar, A. S.; Fiksel, J.; Raj, Phani P. K.; and Rosenfield, D. B.: An Assessment of the Risk Presented by the Use of Carbon Fiber Composites in Commercial Aviation. (Arthur D. Little, Inc., NASA Contract NAS1-15380). NASA CR 158989, 1979.

28. Fiksel, J.; Kalelkar, A. S.; and Rosenfield, D. B.: An Assessment of the Risk Arising From Electrical Effects Associated with Carbon Fibers Released From Commercial Aircraft Fires. (Arthur D. Little, Inc., NASA Contract NAS1-15380). NASA CR 159205, 1980.

29. The National Transportation Safety Board Annual Review of Accident Data for U. S. Air Carrier Operations, 1968 - 1976. Department of Transportation.

30. Credeur, K. R.: Risk Methodology Overview. NASA Conference Publication 2074, 1979, pp. 159-171.

31. Dicus, D. L., Compiler: Modified Composite Materials Workshop. NASA TM 78761, 1978.

32. Gilwee, W. J., Jr.; and Fish, R. H.: A Small-Scale Test for Fiber Release From Carbon Composites. Presented at Society of Plastics Engineers Conference on "Advanced Composites - Special Topics", El Segundo, CA, December 4-6, 1979.

33. Tompkins, S. S.; and Brewer, W. D.: Preliminary Burn and Impact Tests of Hybrid Polymeric Composites. NASA TM 78762, 1978.

34. Ramohalli, K.: Novel Approaches for Alleviation of Electrical Hazards of Graphite-Fiber Composites. Jet Propulsion Laboratory Publication 79-63, 1979.

35. Serafini, T. R.; Delvigs, P.; and Vannucci, R. D.: High Char Imide - Modified Epoxy Matrix Resins. NASA TM 79226, 1979.

36. Suplinkas, R. J.; and Henze, T. W.: A Study of the Deposition of Carbide Coatings on Graphite Fibers. (AVCO Corporation, NASA Contract NAS1-15374). NASA CR 159133, 1979.

37. Galasso, F. S.; Veltri, R. D.; and Scola, D. A.: Study of High Resistance Inorganic Coatings on Graphite Fibers. (United Technologies, NASA Contract NAS1-14346). NASA CR 159078, 1979.

ACKNOWLEDGMENTS

This paper summarizes the contributions of the team that performed a comprehensive carbon fiber risk analysis. Overall program manager was Mr. Robert J. Huston. The technical elements of the program were directed by the following team members: Dr. Wolf Elber (Dissemination, Redissemination and Risk Computations), Dr. Vernon L. Bell (Fiber Source), Mr. Richard A. Pride (Demonstration Testing), Mr. Arthur L. Newcomb (Electronic Instrumentation and Testing), Mr. Israel Taback (Vulnerability), and Mr. Ansel J. Butterfield (Industrial Surveys).

TECHNICAL LIBRARY
ABBOTTAEROSPACE.COM

TABLE I.-TYPICAL ELECTRICAL EFFECTS FROM CARBON FIBERS

Voltage Range	Low Power (Up to 100W)	High Power (Above 100W)
Low (0 to 30 Volts)	Sustained shorts Fiber not burned Malfunctions No local damage	Sustained shorts Fiber not burned No equipment damage
Medium (30 to 1000 Volts)	Sparking or shorts Possible fiber burn Transients Blown fuses Stressed components Low damage potential	Some sustained arcs Fiber burns Transients Blown fuses Stressed components Damage usually repairable
High (>1000 Volts)	Sparks, no sustained arcs Low voltage corona Transients Interruptions	Sustained arcs Corona Flashover May be severe damage

TABLE II.-APPLIANCES TESTED WITH FIBER SIMULATOR

With No Significant Failures*

- Refrigerators
- Freezers
- Ranges
- Dishwashers
- Clothes washer
- Clothes dryer
- Vacuum cleaners
- Irons
- Fry pans
- Bed covers
- Coffee makers
- Percolators
- Food mixers
- Can openers
- Portable heaters

With Failures

None

*Significant failures are those resulting in equipment damage or loss of function.

TECHNICAL LIBRARY
ABBOTTAEROSPACE.COM

TABLE III.-EQUIPMENT TESTED IN FIBER TEST CHAMBER

With No Failures

- Telecommunicator
- Black & white television
- Air Surveillance Radar (ASR-3)
- Calculator
- Calculator and printer
- Tape recorder
- Electric motors (6) 110 V.
- Thermostats (2)
- Cash registers
- Portable heater
- AM/FM Radio
- Home music system
- Clock radio
- 10 Band radio
- Car radio
- Toasters
- Instrument Landing System receiver
- Distance Measuring Equipment
- Smoke alarms

With Failures

- Military equipment (70) (High modulus fibers, restricted lengths)
- Computer
- Color television
- Digital voltmeter
- Air Traffic Control transponder
- Very High Frequency transceiver
- Flight director
- Connector blocks
- Quick disconnects
- Relays
- Generic circuits
- Power amplifier
- Microwave oven

TEST IV.-SINGLE CARBON FIBERS RELEASED FROM DUGWAY OUTDOOR FIRE TESTS

Test	Carbon Fiber Mass in Fire, kg	Total Number	Average Length mm	Average Diameter μm	Single Fibers Released g	Single Fibers Released %
D-1	31.8	1.5×10^8	5.0	4.7	50	0.16
D-2	31.8	2.1×10^8	4.4	4.4	62	.19
D-3	52.0	1.1×10^8	5.2	4.1	38	.07
S-1	34.9	2.9×10^8	3.3	4.7	64	.18
S-2	31.8	2.2×10^8	3.2	4.6	47	.15

TECHNICAL LIBRARY
ABBOTTAEROSPACE.COM

TABLE V.-SUMMARY OF FACILITIES SURVEYED

1) Public Support	No.
Hospitals	7
Air traffic controls	6
Airports-Airlines	3
Police headquarters	2
Fire dispatch	2
Post offices	1
Traffic control	1

2) Utilities	
Telephone exchanges	3
Power generation and distribution	3
Refuse incinerators	2
AMTRAK Railway System	1

3) Commercial Installations	No.
Department stores	2
Financial institutions	2
Radio and TV stations	6
Analytical laboratories	1

4) Manufacturing Operations	
Meat packing	1
Textile mill	1
Garments	1
Pulp and paper	1
Publishing	2
Textile fibers	1
Toiletries	1
Steel mills	2
Wire, cable	1
Electrical equip.	6
Automotive fab/assy	4

THIS DOCUMENT PROVIDED BY THE ABBOTT AEROSPACE
TECHNICAL LIBRARY
ABBOTTAEROSPACE.COM

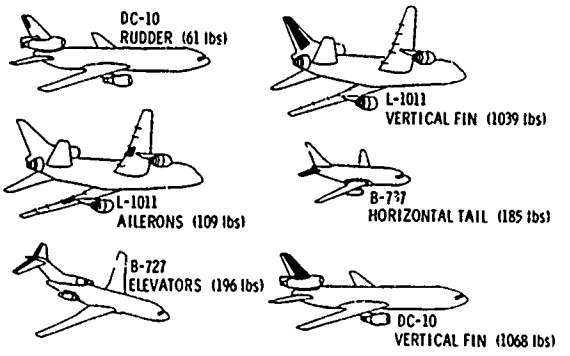

Figure 1. Aircraft Energy Efficient (ACEE) composite components.

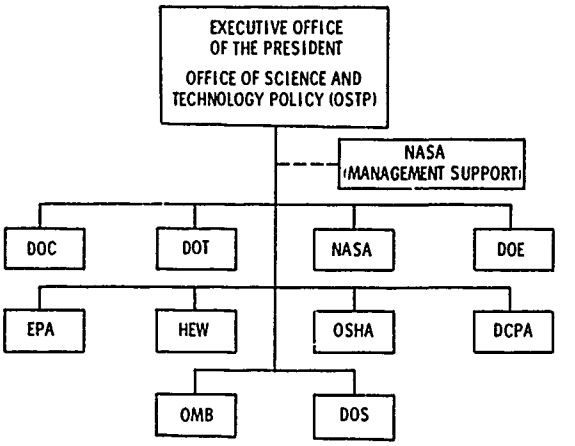

Figure 4. Organization of U. S. Carbon Fiber Study.

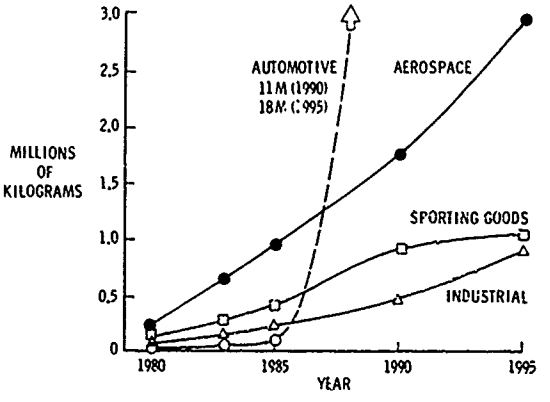

Figure 2. Projected U. S. consumption of carbon fibers.

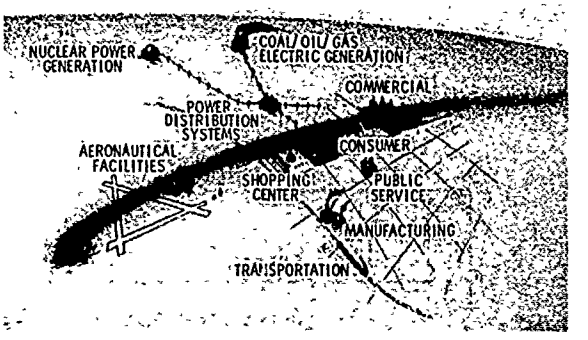

Figure 5. Scenario of the carbon fiber risk analysis.

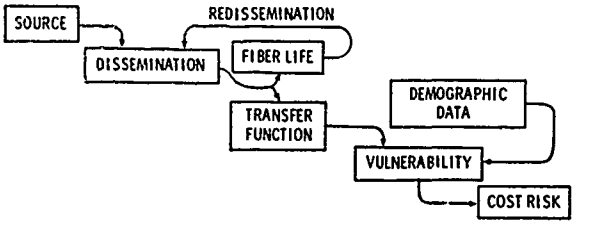

Figure 6. Elements of carbon fiber risk analysis program.

Figure 3. Boron fibers released from aircraft crash.

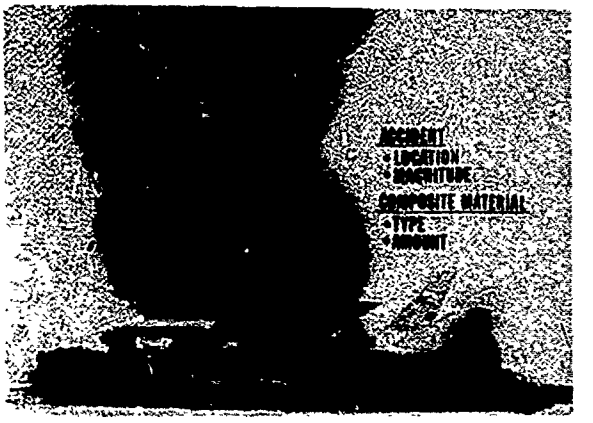

Figure 7. Scenario for crash of civilian airliner.

This document is provided from the TECHNICAL LIBRARY
ABBOTTAEROSPACE.COM

SINGLE FIBERS
SIZE: 3 TO 8μm DIA., 0.1 TO 15mm LONG
FALL RATE: 2cm/sec
DISPERSION RANGE: 0 TO > 100km

CLUSTERS OR LINT
HUNDREDS OF FIBERS
FALL RATE: 10 - 20 cm/sec
DISPERSION RANGE: 0 TO 10km

STRIPS
SINGLE LAMINAE: 0.15mm THICK, VARYING LENGTHS AND WIDTHS
FALL RATES: 1 TO 5m/sec
DISPERSION RANGE: 0 TO 2km

IMPACT FRAGMENTS
MULTIPLE LAMINATE PIECES
OCCURS ONLY IN IMMEDIATE VICINITY OF CRASH/FIRE

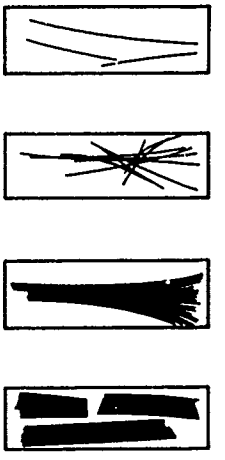

Figure 8. Carbon fiber residues released from fires.

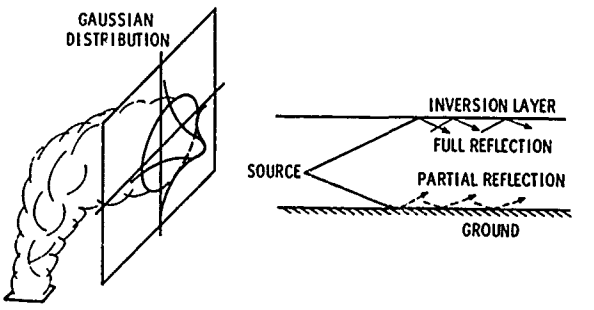

Figure 11. Gaussian distribution of pollutant in drifting cloud, with inversion layer and ground reflections.

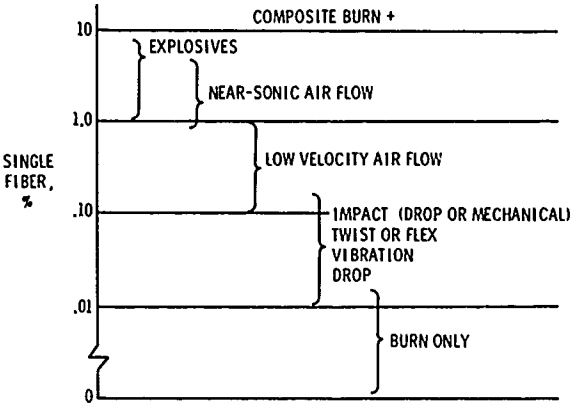

Figure 9. Summary of disturbance effects on single fiber release.

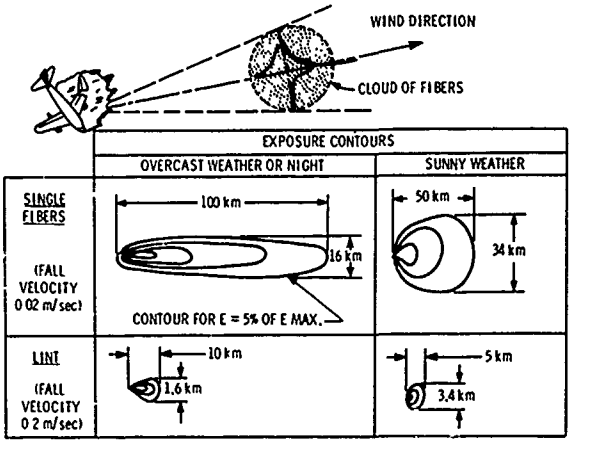

Figure 12. Weather conditions and fiber dispersion.

1. CONCENTRATION, $C = \frac{\text{NUMBER OF PARTICLES}}{\text{VOLUME}}$

2. EXPOSURE OR DOSAGE, $E = \text{CONCENTRATION} \times \text{TIME} = \int C\,dt$

3. DEPOSITION, $D = \frac{\text{NUMBER OF PARTICLES}}{\text{AREA}}$

Figure 10. Measures of carbon fiber pollution.

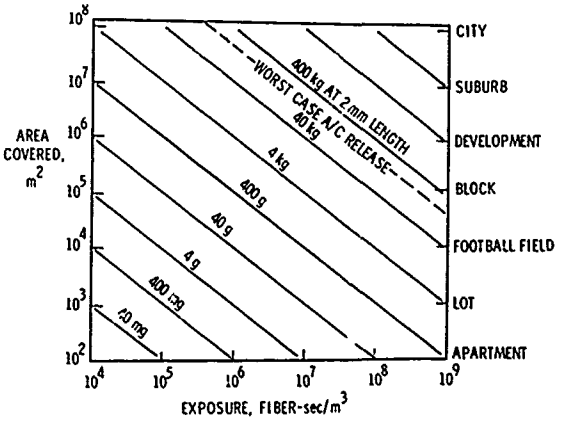

Figure 13. Parametric plot of carbon fiber area coverage.

TECHNICAL LIBRARY
ABBOTTAEROSPACE.COM

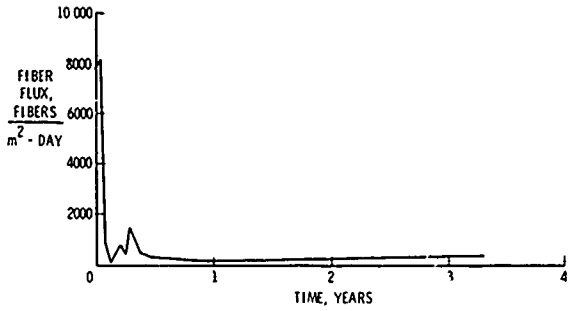

Figure 14. Extent of carbon fiber resuspension with time.

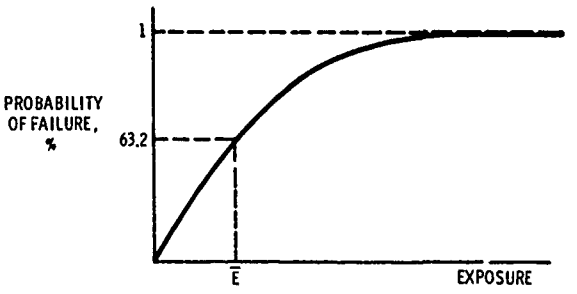

PROBABILITY OF FAILURE $1 - e^{-(E/\bar{E})}$
$\bar{E}$ = AVERAGE EXPOSURE TO FAILURE

EXPOSURE	PERCENT FAILURES
$\bar{E}/100$	1.0%
$\bar{E}/10$	9.5%
$\bar{E}$	63.2%
$10\bar{E}$	99.9%

Figure 17. Electronic equipment failure mode.

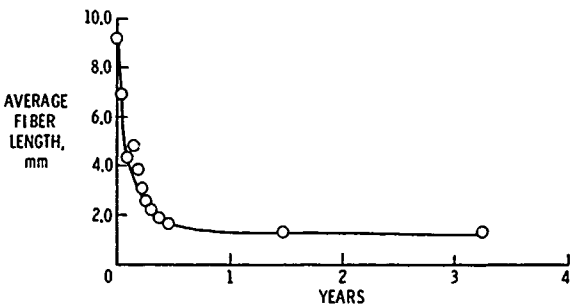

Figure 15. Change in fiber lengths with resuspension.

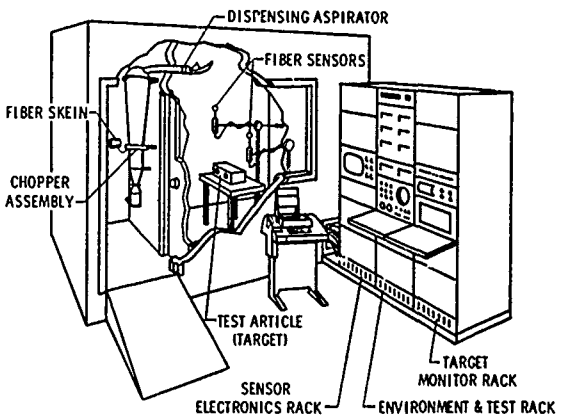

Figure 18. NASA carbon fiber exposure chamber.

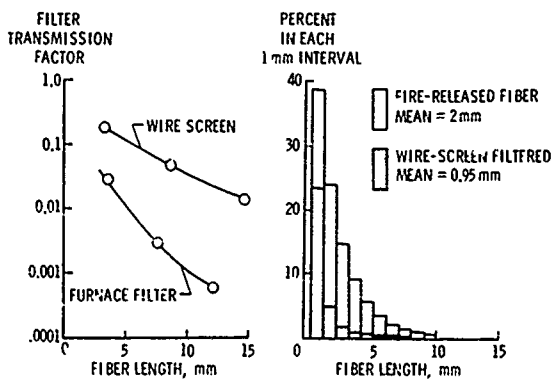

Figure 16. Carbon fiber filtration data.

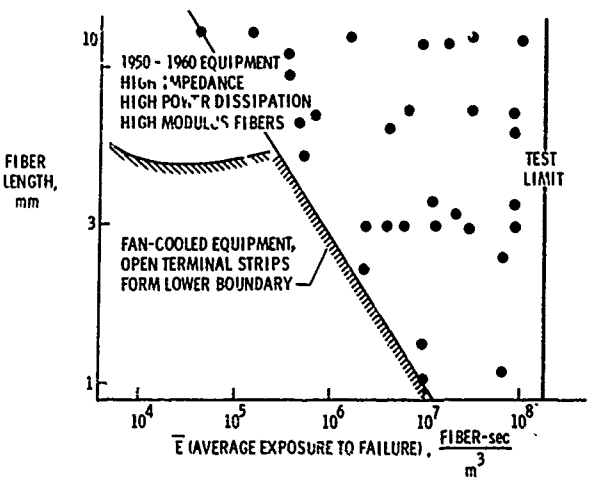

Figure 19. Average exposure to failure for vulnerable equipment.

THIS DOCUMENT ARCHIVED BY THE
TECHNICAL LIBRARY
ABBOTTAEROSPACE.COM

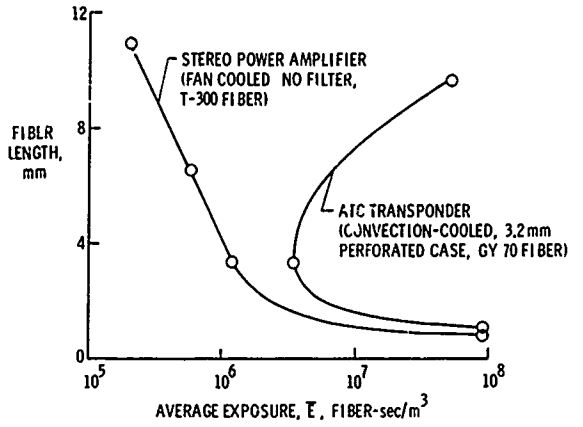

Figure 20. Effect of fiber length on equipment vulnerability.

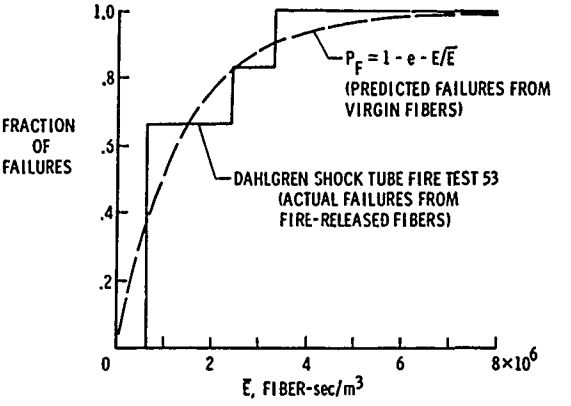

Figure 23. Probability of failure of stereo amplifiers to fire-released fibers in comparison to virgin fibers.

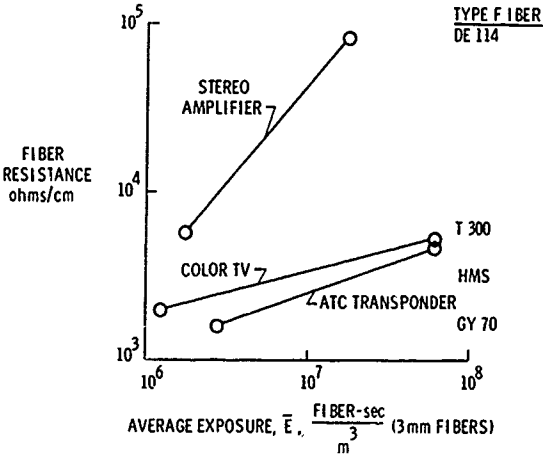

Figure 21. Effect of fiber resistance on equipment vulnerability.

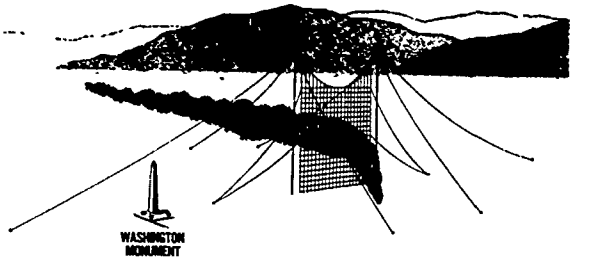

Figure 24. Balloon-supported "jacob's ladder" fire plume sampling net.

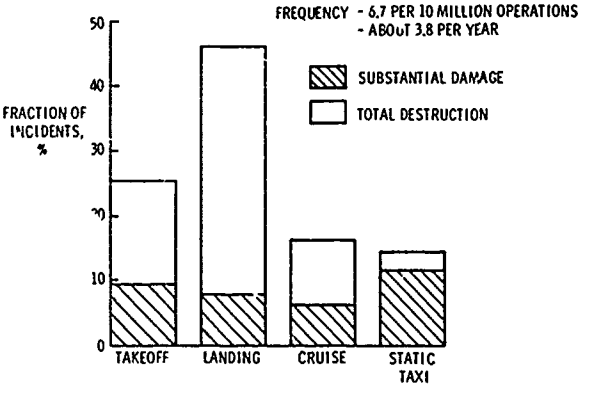

Figure 25. Domestic air carrier incidents with fire and/or explosion, 1968-1976 (Source: NTSB)

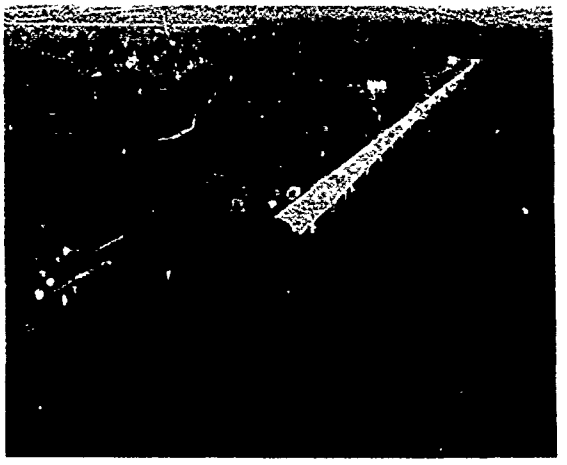

Figure 22. Shock tube fire facility at Dahlgren, Virginia.

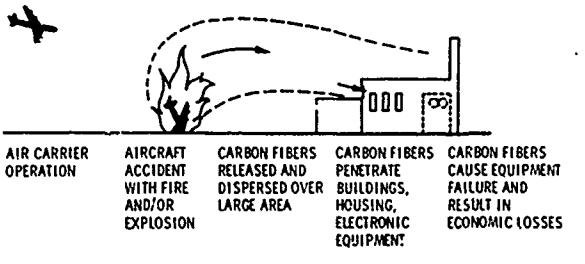

Figure 26. Sequence of events modeled in risk analysis.

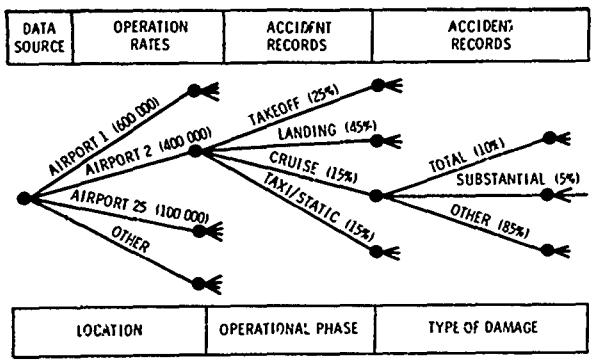

Figure 27a. Simplified event tree logic.

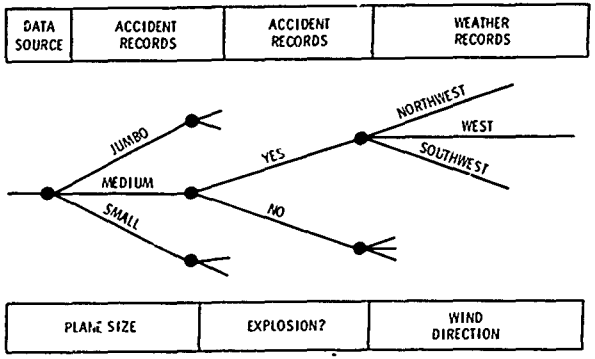

Figure 27b. Simplified event tree logic.

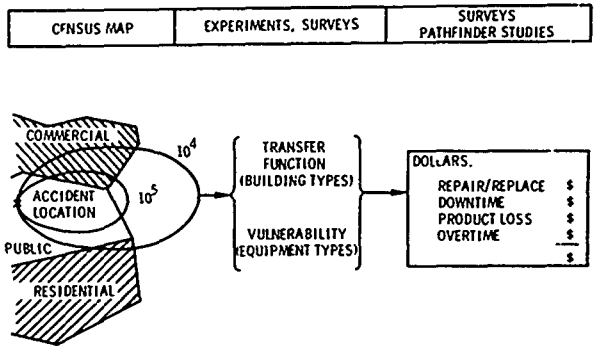

Figure 27c. Simplified event tree logic.

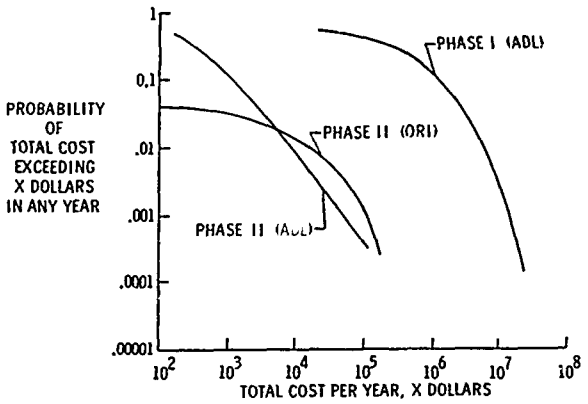

Figure 28. Phase I and Phase II risk profiles.

TECHNICAL LIBRARY
ABBOTTAEROSPACE.COM

THIS DOCUMENT IS PROVIDED BY ABBOTT AEROSPACE
TECHNICAL LIBRARY
ABBOTTAEROSPACE.COM

EROSION OF COMPOSITE MATERIALS

George S. Springer
Department of Mechanical Engineering
The University of Michigan
Ann Arbor, Michigan 48109

SUMMARY

A model is presented which describes the response of uncoated and coated fiber reinforced composites subjected to repeated impingements of liquid (rain) droplets. The model is based on the concept that fatigue is the dominant factor in the erosion process. Algebraic expressions are provided which give the incubation period, the rate of mass loss past the incubation period, and the total mass loss of the material during rain impact. Results are presented which show the influence of material properties on erosion damage and the protection offered by different coatings, and illustrate the use of the model in the design of structures and components.

NOMENCLATURE

a_1-a_7	constants (dimensionless)
b	constant, dimensionless
b_2	knee in fatigue curve, dimensionless
C	speed of sound, m s^{-1}
d	drop diameter, mm
E	Young's modulus, N m^{-2}
E_{11}	Young's modulus in longitudinal direction, N m^{-2} (See Ref. 1)
E_{22}	Young's modulus in transverse direction, N m^{-2} (See Ref. 1)
f	number of stress cycles, dimensionless
F	force on surface of uncoated materials, N
G	shear modulus, N m^{-2}
G_{12}	shear modulus in longitudinal direction, N m^{-2} (See Ref. 1)
G_{23}	shear modulus in transverse direction, N m^{-2} (See Ref. 1)
h_s	thickness of the solid material or the substrate, mm
h_c	thickness of coating, mm
I	rain intensity, mm h^{-1}
K	number of stress wave reflections in the coating during the time of impact, dimensionless
m	mass loss per unit area, kg m^{-2}
m^*	mass loss, dimensionless
n	number of impacts per unit area, number/m^2
n_i	number of impacts per unit area during the incubation period, number/m^2
n_f	number of impacts per unit area prior to the final erosion region, number/m^2
n^*	number of impacts per site, dimensionless
n_a^*	number of impacts per site corresponding to characteristic life, dimensionless
n_i^*	number of impacts per site during the incubation period, dimensionless
N	fatigue life in cycles, dimensionless
p	probability of failure, dimensionless
P	impact pressure, N m^{-2}
r	radial coordinate in plane of surface, m
S	strength parameter, N m^{-2}
S_c	strength parameter for the coating, N m^{-2}
S_{ec}	effective strength parameter for the coating, N m^{-2}
t	exposure time to rain, s
t_i	incubation time, s
t_f	exposure time to rain prior to final erosion region, s
v_f	volume fraction of fiber, dimensionless
v_m	volume fraction of matrix, dimensionless
V	relative velocity between surface and impacting droplet, m s^{-1}
V_t	terminal velocity of rain, m s^{-1}
w	weight loss of material, N
Z	impedance, g $cm^{-2}s^{-1}$
α	rate of mass loss, kg/impacts
α^*	rate of mass loss, dimensionless
β	constant, dimensionless
ϕ	angle relative to fiber direction, radian
γ	parameter related to coating thickness, dimensionless
ν	Poisson's ratio, dimensionless
ν_{12}	Poisson's ratio in the longitudinal direction, dimensionless (See Ref. 1)
ν_{21}	Poisson's ratio in the transverse direction, dimensionless (See Ref. 1)
ν_ϕ	Poisson's ratio of composite materials in the ϕ direction, dimensionless (See Ref. 1)
ρ	density, g cm^{-3}
ρ_s	density of solid, g cm^{-3}
θ	angle of impact, radian or degree
σ	stress, N m^{-2}
σ_a	stress of amplitude σ_a, N m^{-2}
σ_e	equivalent dynamic stress, N m^{-2}
σ_I	endurance limit, N m^{-2}
σ_u	ultimate tensile strength, N m^{-2}
$\overline{\sigma^0}$	average stress on the surface of the coating, N m^{-2}
ψ	impedance ratio, dimensionless

Subscripts

c	coating
f	fiber; or beginning of final erosion region
i	end of incubation period
m	matrix
L	liquid
s	solid
sc	coat-substrate interface
Lc	liquid-coat interface
w	water

INTRODUCTION

When liquid droplets impinge repeatedly upon a solid surface the stresses created by the droplets may damage the material significantly. Fiber reinforced organic matrix composites are particularly susceptible to such "rain erosion" damage. Therefore, in order to utilize the full potential of composite materials, the response of such materials to rain erosion must be known.

TECHNICAL LIBRARY
ABBOTTAEROSPACE.COM

The desired information on erosion damage can be obtained either through testing or through analytical models. Indeed, considerable data have been generated in the past on the erosion of composite materials. These data provide information on the behavior of selected materials under selected conditions but do not describe material behavior beyond the range of the tests in which they were obtained. Alone, the test results neither predict the behavior of materials under untested conditions, nor indicate the behavior of untested materials. These shortcomings of selected testing can be overcome by the use of analytical models. In this paper a model is described which can be used to estimate erosion damage of both coated and uncoated fiber reinforced composites.

THE PROBLEM

The following problem is considered. A body, made of a composite material, moves through a rain (Fig. 1). The impinging droplets damage the material causing pits, cracks, and weight loss. We are concerned with the damage as manifested by the weight loss. Under actual conditions the weight loss generally varies with time as shown in Fig. 2. During the incubation period the weight loss is negligible. For some time after the incubation period the weight loss is nearly constant. Past this region the relationship between the weight loss and the exposure time becomes complex. Here attention is focused only on the incubation period and on the constant weight loss rate past the incubation period.

To facilitate the development of the model, the weight loss is replaced with the mass loss per unit area m, and the time with the number of impacts per unit are n. The data are then approximated by two straight lines (Fig. 3). Accordingly, the mass loss is

$$m = 0 \qquad n < n_i \tag{1}$$

$$m = \alpha(n - n_i) \qquad n_i < n < n_f \tag{2}$$

The material loss m produced by a certain number of impacts n can be calculated once the incubation period n_i and the subsequent mass loss rate α are known. Therefore, the problem is to determine n_i and α.

The rain is considered to have uniform spatial distribution and to be composed of spherical droplets. The drop diameter d, impact velocity V and the impact angle θ for each droplet are taken to be the same. The parameters n and t are then related by the expression

$$n = \frac{6}{\pi} \frac{V \cos\theta}{V_t d^3} It \tag{3}$$

where V_t is the terminal velocity and I is the rain intensity.

The composite material is assumed to contain uniformly distributed, noncontiguous fibers which are parallel to the surface. In addition, it is assumed that a) the composite is macroscopically homogeneous, b) locally both the matrix and the fiber are homogeneous and isotropic, and c) there is a perfect bond between the matrix and fibers and between the coating and the substrate. Wave reflections are neglected in uncoated composites and in the substrate of coated composites. However, wave reflections within the coating are taken into account.

The impact pressure is calculated by the expression

$$P = \frac{\rho_L C_L V \cos\theta}{1 + \rho_L C_L / \rho_s C_s} = \frac{Z_L V \cos\theta}{1 + Z_L / Z_s} \tag{4}$$

ρ and C are the density and the speed of sound. The subscripts L and s refer to the liquid and the surface. For coated composites, ρ_s and C_s are the density and speed of sound of the coating. For uncoated composites ρ_s and C_s are

$$\rho_s = \rho_f v_f + \rho_m v_m \qquad C_s = \left(\frac{E_{22}}{\rho_s}\right)^{1/2} \tag{5}$$

v is the volume fraction and E_{22} is the equivalent Young modulus in the direction normal to the fibers. The subscripts m and f denote the matrix and the fiber.

On the basis of the foregoing simplifications a model is described which provides the incubation period and the subsequent mass loss rate. Details of this model were presented in references 1 and 2 and will not be repeated here. In the following, only the method of approach is emphasized and the results are summarized enabling the interpretation and assessment of the results.

INCUBATION PERIOD

The model to be formulated is based on the idea that fatigue plays an important role in the erosion process. Each droplet which impinges on the surface creates a stress at point B (Fig. 4). The effects of these stresses are taken to be cumulative. The material at point B fails after it underwent a certain number of stress cycles. The number of stress cycles after which failure occurs is calculated by Miner's rule (3)

$$\frac{f_1}{N_1} + \frac{f_2}{N_2} + \ldots + \frac{f_q}{N_q} = a_1 \tag{6}$$

THIS DOCUMENT PROVIDED BY THE ABBOTT AEROSPACE
TECHNICAL LIBRARY
ABBOTTAEROSPACE.COM

where f_1, f_2... represent the number of cycles the specimen is subjected to specified overstress levels σ_1, σ_2..., and N_1, N_2... represent the life (in cycles) at these overstress levels. a_1 is a constant. A droplet impinging on the surface at a distance r from point B creates a stress σ at the point B

$$\sigma(r,\phi) = \frac{F(1 - 2\nu_\phi)}{2\pi r^2} \tag{7}$$

where F is a point force and ν_ϕ is the Poisson ratio (Ref. 1). The stress at point B fluctuates. This time varying stress is generally replaced by an equivalent dynamic stress (4)

$$\sigma_e = \frac{(\sigma/2)(\sigma_u)}{\sigma_u - \sigma/2} \tag{8}$$

The number of cycles for which the material at point B is subjected to a given stress between σ_e and $\sigma_e + d\sigma_e$ is equal to the number of impacts on a surface element of area rdrdϕ

$$f(r,\phi) = n_i r\, dr\, d\phi \tag{9}$$

Thus we express Miner's rule as

$$\int_0^{2\pi}\int_c^{\infty} \frac{n_i r\, dr\, d\phi}{N} = a_1 \tag{10}$$

In order to perform the integration, the fatigue life N must be known as a function of the stress. For N the following approximation is introduced (Fig. 5):

$$N = \left(\frac{\sigma_u}{\sigma_e}\right)^b \qquad b = \frac{b_2}{\log_{10}(\sigma_u/\sigma_I)} \qquad b = \frac{b_2}{\log_{10}(\sigma_{um}/\sigma_{Im})} \tag{11),(12}$$

For fiber reinforced composites the ultimate tensile strength σ_u and the endurance limit σ_I are calculated by the expressions

$$\sigma_u = \sigma_{um}\frac{E_\phi}{E_m} \tag{13}$$

$$\sigma_I = \sigma_{Im}\frac{E_\phi}{E_m} \tag{14}$$

By introducing the dimensionless parameter

$$n_i^* = n_i \frac{\pi d^2}{4} \tag{15}$$

and by integrating Eq. (10), we obtain

$$n_i^* = a_1\left(\frac{S}{P}\right) \tag{16}$$

where

$$S = \frac{4\sigma_{um}(b_m - 1)}{E_m}\left[\frac{3}{8}\left(\frac{1}{E_{11}} + \frac{1}{E_{22}}\right) + \frac{1}{8}\left(\frac{1}{G_{12}} - \frac{2\nu_{12}}{E_{11}}\right) - \frac{2\nu_{12}}{E_{11}} + \frac{1}{4}\left(\frac{1 + 2\nu_{12}}{E_{11}} + \frac{1}{E_{22}} - \frac{1}{G_{12}}\right)\right]^{-1} \tag{17}$$

The parameter S represents the "strength" of the material. Thus, the result shows that the number of impacts needed to initiate damage is proportional to the strength to pressure ratio. In order to extend the range of applicability of Eq. (16) we write arbitrarily

$$n_i^* = a_1\left(\frac{S}{P}\right)^{a_2} \tag{18}$$

The constants a_1 and a_2 were determined by matching Eq. (18) to data generated for homogeneous materials (5). By adopting the same constants for composite materials, we obtain

$$n_i^* = 7\times10^{-6}\left(\frac{S}{P}\right)^{5.7} \tag{19}$$

For coated materials stress waves travel inside the coating as illustrated in Fig. 6. These stress waves were included in the model by assuming that the waves are one-dimensional and propogate normal to the surface, and that there is a perfect bond between the coating and the substrate. It was also assumed that failure occurs first in the coating. The calculations including wave reflections are lengthy and are documented elsewhere (1,2,6). Therefore, only the result is quoted here, which is

$$n_{i_c}^* = 7\times10^{-6}\left(\frac{S_{ec}}{\sigma^0}\right)^{5.7} \tag{20}$$

TECHNICAL LIBRARY
ABBOTTAEROSPACE.COM

The subscript c indicates coating. S_{ec} is the "strength" of the coating

$$S_{ec} = \frac{S_c}{1 + 2\bar{k}|\psi_{sc}|} \tag{21}$$

and $\overline{\sigma^v}$ is the average stress on the surface of the coating. S_c is the "strength" of the coating material as given by Eq. (17). The parameters $\bar{k}$ and ψ_{sc} as well as $\overline{\sigma^v}$ are specified in Table 1.

In Eq. (21) $2\bar{k}|\psi_{sc}|$ represents the reduction in "strength" of the coating due to stress oscillations. Note that if the coating is very thin, the strength S_c may be reduced to the point where the incubation time is actually shorter with the coating than without it.

RATE OF MASS REMOVAL

The erosion rate past the incubation period is also modeled by drawing upon fatigue concepts. The probability that a specimen will fail in fatigue between a minimum life ℓ_i and any arbitrary longer life ℓ may be estimated from the Weibull distribution

$$p = 1 - \exp\left[-\left(\frac{\ell - \ell_i}{\ell_a}\right)^{\beta}\right] \simeq \left(\frac{\ell - \ell_i}{\ell_a}\right)^{\beta} \tag{22}$$

where ℓ_a is the characteristic life corresponding to a 63.2 percent failure point and β is a constant. For erosion, the life may be replaced by the number of impacts n* and the amount of material lost by p. By introducing the dimensionless parameter

$$m^* = \frac{m}{\rho_s d} \tag{23}$$

and by relating m* and p by a power-law-type expression $m^* = a_3 p^{a_4}$, we obtain

$$\frac{m}{\rho_s d} = a_3\left(\frac{n^* - n_i^*}{n_a^*}\right)^{a_4\beta} \tag{24}$$

ρ_s is the density of the material on which the droplets impinge and a_3 and a_4 are constants. Equations (2), (15) and (24) give

$$\frac{\alpha}{\rho_s \pi d^3/4} = a_3 \frac{1}{(n_a^*)^{a_4\beta}} \frac{(n^* - n_i^*)^{a_4\beta}}{n - n_i^*} \tag{25}$$

It was postulated that α is a constant and is independent of n^* and n_i^* (Fig. 3). This condition is met if $a_4\beta = 1$. By setting $a_4\beta$ equal to unity, by relating n_a^* to n_i^* by a power law ($n_a^* = a_5 n_i^{*\,a_6}$), and by introducing the dimensionless parameter

$$\alpha^* = \frac{\alpha}{\rho_s \pi d^3/4} \tag{26}$$

we obtain

$$\alpha^* = a_7 \frac{1}{(n_i^*)^{a_6}} \tag{27}$$

The constants a_6 and a_7 were evaluated by comparing Eq. (27) to data obtained with homogenous materials (5). By adopting the same constants for composite materials, α^* becomes

$$\alpha^* = 0.023 \frac{1}{(n_i^*)^{0.7}} \tag{28}$$

RESULTS

Equation (28) applies both the coated and uncoated composites. The expressions for calculating the incubation period and the rate of mass loss are summarized in Reference 1. The results are compared to data in Figs. 7 and 8. As can be seen, there is excellent agreement between the measured and calculated n_i^* and α^* values over a wide range of conditions. This agreement lends support to the validity of the model and suggests that the model may be used to analyze and predict erosion damage and to guide in material development. The model also provides a means for comparing the response of different materials to erosion as illustrated by the comparisons presented below.

In Figs. 9-11 the incubation period and the rate of mass loss are presented for three metals and for three fiber reinforced composites. The incubation periods of graphite-epoxy and glass-polyester composites are several orders of magnitude lower than for metals. Only the incubation period of boron-epoxy composites is comparable to that of one of the metals (aluminum). However, even boron-epoxy has an incubation period which is about four orders of magnitude lower than steel. The mass loss rates of composites are also lower than those of metals by several orders of magnitude.

The impact velocity affects significantly both the incubation period and the rate of mass loss (Figs. 9, 11). At impact velocities (Vcos θ) below 200 m/s the incubation period for graphite-epoxy composites is about an hour. The incubation period decreases rapidly with impact velocity. At 400 m/s the incubation period of graphite-epoxy is only about one minute. Consequently, the material should be protected, particularly at high impact velocities. One convenient method of protection is by the application of a coating. The appropriate coating material and coating thickness, as well as the protection provided by the coating, may be calculated by the expressions given in Table 2. The results of sample calculations are

TECHNICAL LIBRARY
ABBOTTAEROSPACE.COM

shown in Fig. 12. The results in this figure illustrate that the coating must be selected carefully. Some coatings do not provide protection and may even reduce the incubation time. For example, the many stress oscillations in the teflon coating on graphite-epoxy weaken the coating to such an extent that the incubation period for the coating (teflon) is actually shorter than it is for the substrate (graphite-epoxy).

CONCLUDING REMARKS

The erosion model presented here was developed on the basis of physical concepts and experimental observations. Although there are a number of approximations and simplifications included in this model, the results agree well with existing data. Nevertheless, the limitation introduced by the approximations should always be borne in mind when applying the results to new situations.

REFERENCES

1. Springer, G.S., Erosion by Liquid Impact, New York: J. Wiley and Sons, 1976.

2. Springer, G.S. and Yang, C.I., "A model for the rain erosion of fiber reinforced composites," AIAA Journal, 13, 1975, 877-883.

3. Miner, M.A., "Cumulative damage in fatigue," Journal of Applied Mechanics, Trans. ASME, 12, 1945, A159-A164.

4. Juvinall, R.C., Stress, Strain and Strength, New York: McGraw-Hill Book Company, 1967.

5. Springer, G.S. and Baxi, C.B., "A model for rain erosion of homogeneous materials," in Erosion, Wear and Interfaces with Corrosion, ASTM STP 567, Society for Testing and Materials, 1974, 106-122.

6. Springer, G.S., Yang, C.I., and Larsen, P.S., "Rain erosion of coated materials," Journal of Composite Materials, 8, 1974, 229-250.

7. Lapp, R.R., Stutzman, R.H., and Wahl, N.E., "Summary report on the rain erosion of aircraft materials," 1956, WADC Technical Report 53-18., Part 3.

8. Lapp, R.R., Thorpe, D.H., Stutzman, R.A., and Wahl, N.E., "The study of erosion of aircraft materials at high speeds in rain," 1958, WADC Technical Report 53-185, Part 4.

9. Schmitt, G.F., Jr., and Krabill, A.H., "Velocity erosion relationships of materials in rain at supersonic speeds," AFML-TR-70-44, 1970.

10. Schmitt, G.F., Jr., "Rain erosion behavior of graphite and boron-fiber reinforced epoxy composite materials, AFML-TR-70-316, 1971.

11. Schmitt, G.F., Jr., "Material parameters that govern the rain erosion behavior of polymeric coatings and composties at subsonic velocities," AFML-TR-71-197, 1971.

12. Lapp, R.R., Stutzman, R.H., and Wahl, N.E., "A study of the rain erosion of plastics and metals," 1955, WADC Technical Report 53-185, Part II.

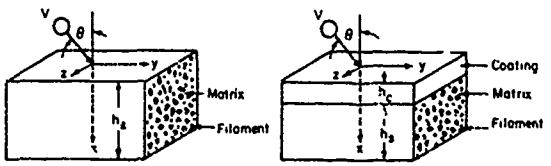

Fig. 1 Droplet impingements on uncoated and coated fiber-reinforced composites

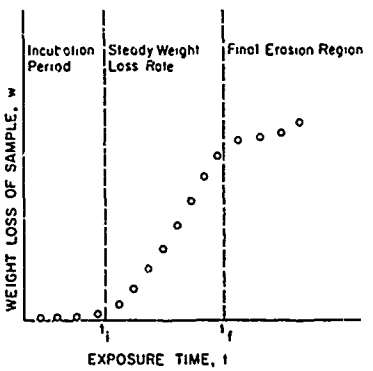

Fig. 2 Schematic of typical test data

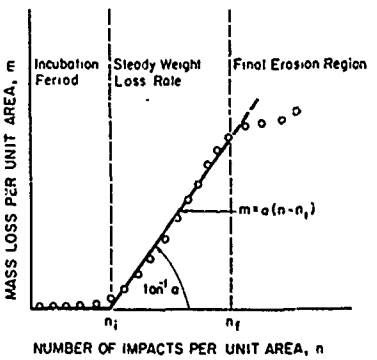

Fig. 3 Representation of the model

THIS DOCUMENT PROVIDED BY THE ABBOTT AEROSPACE
TECHNICAL LIBRARY
ABBOTTAEROSPACE.COM

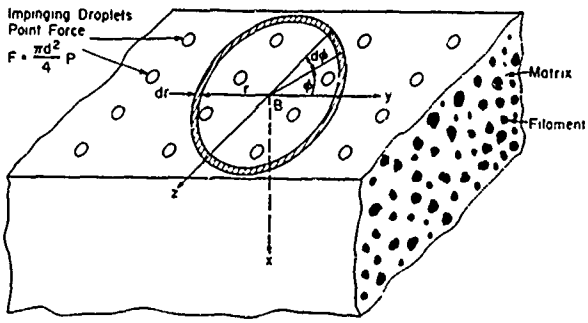

Fig. 4 Force distribution on the surface due to the impinging droplets

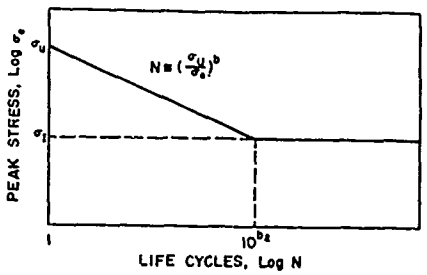

Fig. 5 Schematic of σ_e - N curve used in the model

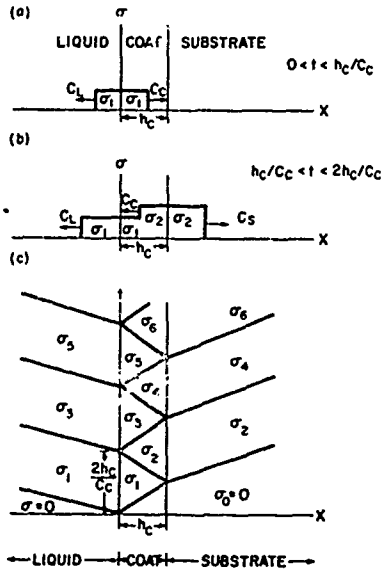

Fig. 6 Stress wave pattern in coated composites

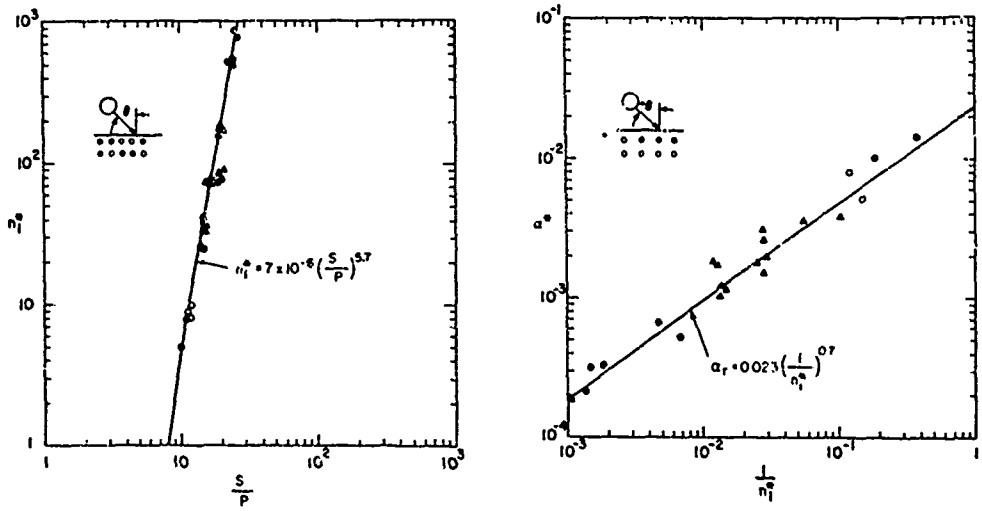

Fig. 7 Comparison between calculated and measured incubation period and rate of mass loss for uncoated composites. Data are from References (7) - (11)

TECHNICAL LIBRARY
ABBOTTAEROSPACE.COM

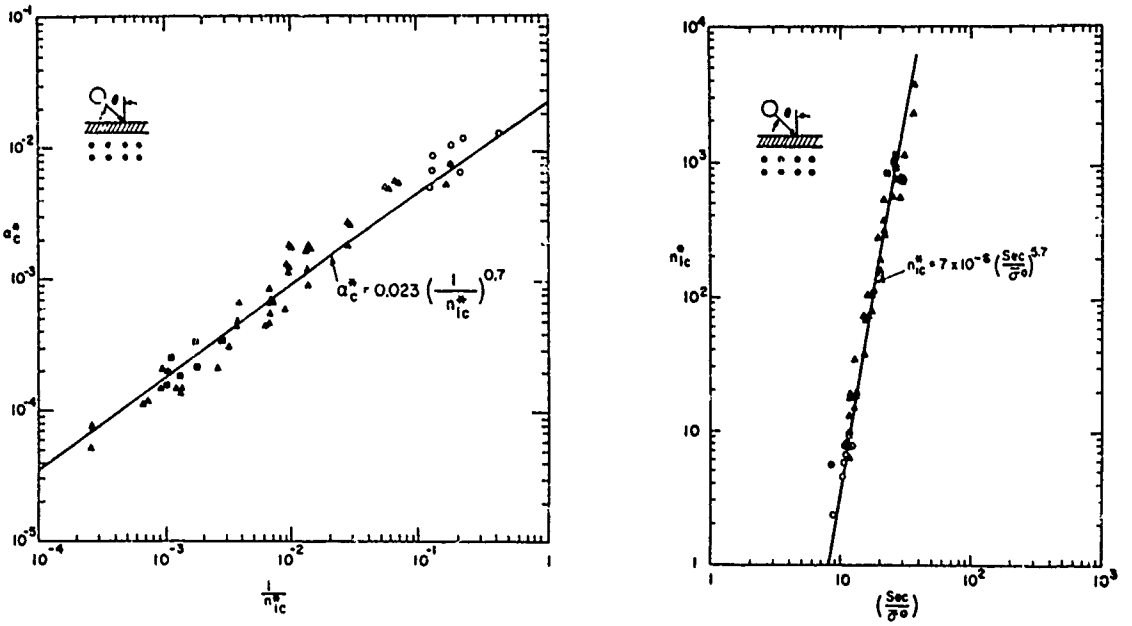

Fig. 8 Comparison between calculated and measured incubation period and rate of mass loss for coated composites. Data are from Referencer (7) - (10), (12)

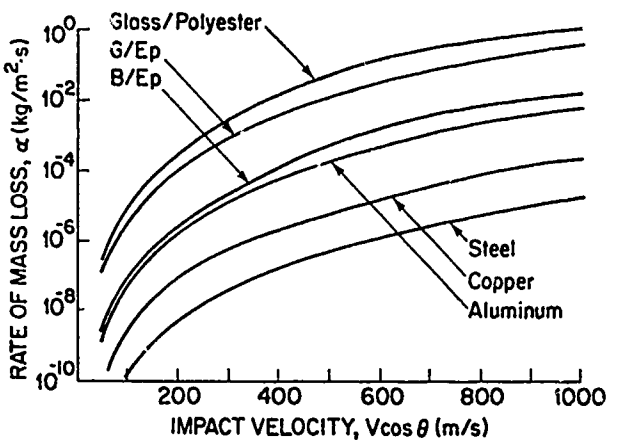

Fig. 9 Incubation times of different uncoated materials calculated by the model. Rain intensity 25 mm/hr, drop diameter 2 mm

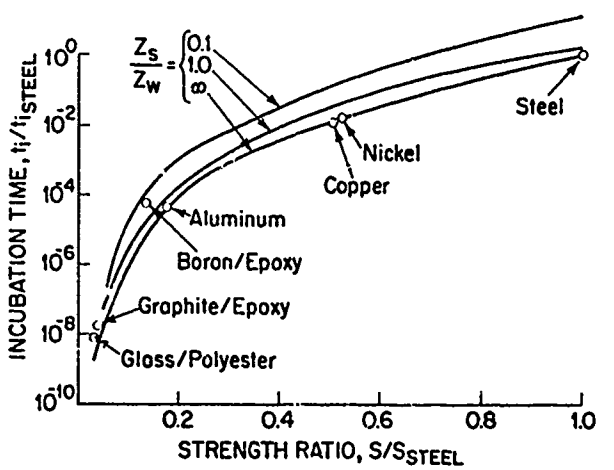

Fig. 10 Incubation times of different uncoated materials compared to incubation time of steel. Results calculated by the model-

TECHNICAL LIBRARY
ABBOTTAEROSPACE.COM

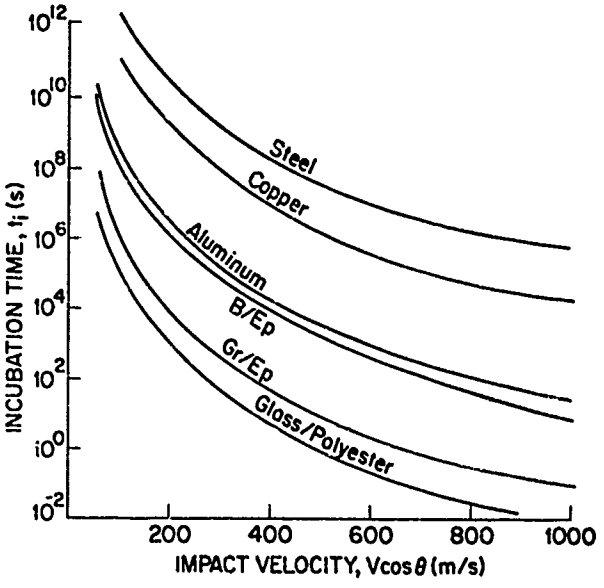

Fig. 11 Rate of mass loss of different uncoated materials calculated by the model. Rain intensity 25 mm/hr, drop diameter 2 mm.

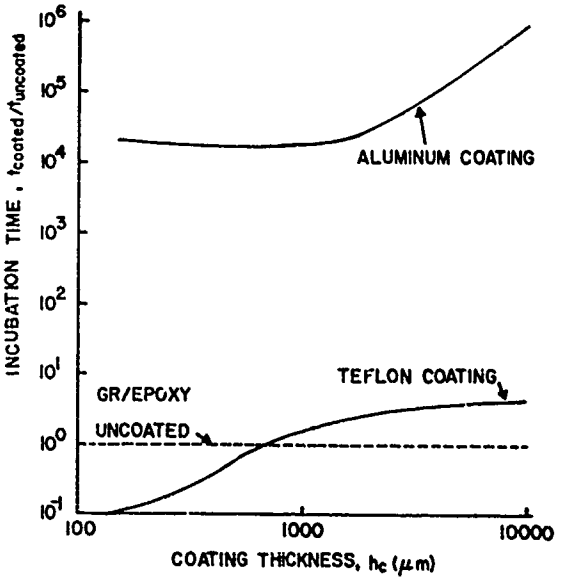

Fig. 12 The effect of coating on the incubation period as calculated by the model. Rain intensity 25 mm/hr, drop diameter 1.5 mm, impact velocity 260 m/s.

THIS DOCUMENT PROVIDED BY THE ABBOTT AEROSPACE
TECHNICAL LIBRARY
ABBOTTAEROSPACE.COM

TABLE 1 Parameters used in the calculation of the strength of coated composites. The units to be used for each parameter are given in the "Nomenclature."

Name	Symbol	Result	Units
Impedance parameters	ψ_{sc}	$\frac{Z_s - Z_c}{Z_s + Z_c}$	Dimensionless
	ψ_{Lc}	$\frac{Z_L - Z_c}{Z_L + Z_c}$	Dimensionless
Parameter related to coating thickness	γ	$\frac{C_c}{C_L}\frac{d}{h_c}\frac{1 + Z_L/Z_s}{1 + (Z_c/Z_s)}\frac{2}{1 + (Z_L/Z_c)}$	Dimensionless
Number of stress wave reflections in coating	$\bar{k}$	$\frac{1}{1 - \psi_{sc}\psi_{Lc}}[1 - \exp(-\gamma)]$	Dimensionless
Average stress at the coat-liquid interface	$\overline{\sigma^0}$	$\Gamma\, i\, \frac{1 + \psi_{sc}}{1 - \psi_{sc}\psi_{Lc}}\left[1 - \psi_{sc}\frac{1 + \psi_{Lc}}{1 + \psi_{sc}}\frac{1 - \exp(-\gamma)}{\gamma}\right]$	$N\ m^{-2}$

TECHNICAL LIBRARY
ABBOTTAEROSPACE.COM

RECORDER'S REPORT

Session IV - Physical Hazards

by

Renato BARBONI
Scuola d'Ingegneria Aerospaziale
dell'Universita di Roma
Istituto di Tecnologia Aerospaziale
Via Eudossiana, 16
00184 Roma - Italy

The aim of Session IV was to examine the physical hazards related to the use of composite materials. Three fundamental aspects were taken into account:

1. Effect of lightning on aircraft and the protection requirements.
2. The risks of accidental release of carbon fibers from burning of crashed commercial airlines.
3. The material damage due to repeated impingements of rain drops.

As far as structural damage due to lightning is concerned, the results of two experimental investigations which pointed out the thermal and the high current density effects were presented. Both papers agree with the basic point of view that, in spite of the reaction of composites to lightning strikes in a manner different from conventional materials, the resultant damage is by no means alarming. Nevertheless, I would note some interesting considerations that appear from the papers presented by Rouchon and Schneider:

i) the importance of honeycomb core material for sandwich structures

ii) the sensitivity of some types of joints to lightning

iii) if lightning protection is deemed necessary, a number of conductive protective systems are available, but the effectiveness of the coatings must be fully evaluated. In fact, even if environmental exposure and fatigue did not affect the protection system, nevertheless the effectiveness is not in proportion to its mass per unit area.

The third paper, by Bell, was concerned with experimental and analytical results on the potential damage to electrical and electronic equipment and the risk to the community due to accidental release of carbon fibers. The graphite fiber risk analysis scenario assumed carbon fibers to originate principally from fires from crashed commercial aircraft with carbon composite parts. The unusual situation for experimental research was the absence of actual experience because fortunately, up to now, crashes of commercial aircraft with any carbon composites in their structure have not occurred. Of course, simulated experiments have been carried out and interesting results on the burning, dissemination and redissemination of graphite fiber obtained. The results indicate that:

1. about the vulnerability or susceptibility of electrical and electron equipment, many of them were invulnerable.
2. no risk to the community is to be expected from the use of carbon fibers in civil aviation.
3. the chances of national losses reaching significant levels are extremely small.
4. furthermore, the potential shock hazard from carbon fibers is insignificant.

In conclusion, no problems are posed to the community by an extensive utilization of carbon fiber and programs to develop alternate materials specifically to overcome that perceived hazard are not necessary.

The response of composite materials to liquid droplets erosion is examined in the last paper of Session IV. Springer proposes an analytical model based on the idea that fatigue plays the dominant role in the erosion process. The incubation period and the subsequent rate of mass loss have been chosen as the fundamental parameters in order to evaluate the real life of the material. Theoretical considerations lead to very simple formulae to predict the number of impacts needed to initiate damage, and the erosion rate. Comparisons between theoretical results and experimental data excerpted from other authors seem to certify the validity of the model. Unfortunately the application of the model to graphite-epoxy composites gives incubation periods of several orders of magnitude lower than for metals. This means, for example, that the real life of CFRP

THIS DOCUMENT PROVIDED BY THE
TECHNICAL LIBRARY
ABBOTTAEROSPACE.COM

utilized in a civil aeroplane exposed to rain is only of the order of several minutes.

The conclusion from the papers presented in Session IV is that the most dangerous physical hazard is for CFRP and is due to the most natural physical phenomenon, rain.

THIS DOCUMENT IS FROM THE HELICOPTER TECHNICAL LIBRARY
ABBOTTAEROSPACE.COM

FATIGUE AND DAMAGE PROPAGATION IN COMPOSITE ROTOR BLADES

Dr. A.J. Barnard
Head of Advanced Technology
Westland Helicopters Limited
Yeovil
Somerset
BA20 2YB
United Kingdom

SUMMARY

This paper describes recent work performed at Westland Helicopters on the development and flight evaluation of carbon/glass fibre-reinforced plastic rotor blades. Results are presented from tests undertaken on tail and main blades. Discussion is centred on the excellent fatigue and damage propagation characteristics of the blades. The work has shown low material scatter factors and has led to the development of blades with unlimited fatigue lives.

1. INTRODUCTION

During its service life the helicopter experiences a severe high-cycle fatigue environment, the total number of cycles being, typically, of the order of 10^9. This condition is particularly demanding for the rotor blades in which stress levels are necessarily high due to the strict constraints which exist on geometry, aeroelasticity and weight. To design a blade which will endure this fatigue environment is an objective which, with metals, is extremely difficult to achieve.

To overcome this problem helicopter rotor blades are now being produced from fibre-reinforced composites. At Westland Helicopters glass fibre in epoxy resin is largely employed with selective use of carbon fibre for additional stiffening where necessary. These materials have the high fatigue strength-to-density ratios which when properly used in rotor blade design allow components with unlimited fatigue life to be produced.

The use of composite materials also permits the advanced blade shapes now being demanded by the rotor system designer to be produced accurately and economically, and hence large improvements in rotor performance can be achieved. Additionally, the use of composite materials allows blades to be designed which exhibit a high level of damage tolerance. Blades manufactured with glass-reinforced epoxy spars show extremely low rates of damage propagation which contributes to improved safety. One of the most exciting potential advantages of composite rotor blades lies in the ability to manipulate, to a high degree, the blades' elastic properties and hence to tailor blade designs for optimum dynamic and aeroelastic performance and minimum vibration levels.

This paper describes recent work performed by Westland Helicopters on composite tail and main rotor blades. The paper concentrates on the performance of blades for the Westland Sea King and WG.30 helicopters under the fatigue environment in both rig and flight tests.

2. BLADE CONSTRUCTION

Blade construction is, typically, of a hollow 'D'-spar composed largely of unidirectional glass-reinforced plastic with internal and external woven wraps. The trailing-edge skins are of spanwise unidirectional and angle plies. In tail rotor blades built to date these trailing-edge skins have been manufactured in carbon fibre/epoxy and supported by a rigid polymethacrylimide foam filling. In main blades, however, the trailing-edge skins may be either carbon or glass fibre/epoxy (or a hybrid of the two) on a 'Nomex' honeycomb core. A bolted joint is used at the root-end in all cases with local reinforcement of the spar. There is provision for the fitting of a heater mat on main blades if this is required for de-icing purposes. A titanium erosion shield provides the necessary leading-edge protection, and tip weights and a tip cap are installed at the outer end of the blades.

The construction of a tail rotor blade is detailed in Fig.1. This blade is designed for the Sea King and is shown in its ready-for-flight state in Fig.2. A cross-sectional view of a Sea King main rotor blade is shown in Fig.3.

TECHNICAL LIBRARY
ABBOTTAEROSPACE.COM

3. TESTING PHILOSOPHY

The approach adopted for the clearance of composite rotor blades for flight incorporates two series of tests. The first series is performed upon what is known as 'Structural Elements'. These tests provide S-N curve shapes and statistical data on the scatter characteristics of the structure/material in various critical areas of the blade. It is therefore important that structural elements are either cut directly from actual blades or manufactured by the means, and from the materials, of the blade itself. It is from this series of tests that the materials scatter factors employed in the design are validated, and therefore representative failure modes must be achieved.

Mean strength values, however, are not sought from these tests. These are derived instead from the second series of tests which are performed on a limited number of full-size blades. The root-end and outboard aerofoil sections of the blade are tested by separate specimens. The fatigue testing involves the application of programmed series of loading blocks designed to correspond closely to actual flight conditions.

In this way the costly and lengthy process of full-size blade testing is minimised. The two series of tests examine both the static and fatigue performance of the specimens. Full-size specimens are also used to assess the damage propagation characteristics and to investigate the effects of extreme conditions of temperature and humidity (both natural and artificial).

4. TESTING OF COMPOSITE ROTOR BLADES

The test work described in this section was performed largely under the Ministry of Defence-supported 'Helicopter Technology Demonstrator Programme' which comprises a number of projects aimed at the demonstration of advanced technology in key areas of the helicopter. The tests performed on the Sea King tail and main rotor blades provide the necessary information for the 50-hour flight clearance required under this programme.

4.1 Structural Element Tests

Structural element tests are performed under static and both constant and variable amplitude fatigue loading. The critical areas of the blades chosen for test were:

i) Spar aerofoil section
ii) Trailing-edge skin section
iii) Root-end attachment
iv) Transition area (between root and aerofoil)

The positions of these areas are shown in Fig.4. In most cases some development work has proved necessary on the design of specimens to ensure that a representative failure takes place in the test section. The lay-up of the Sea King tail rotor blade structural elements is shown in Table 1. A tensile loading was used for these tests. In the fatigue case a $1.1P \pm P$ form was adopted. The failure modes of the different structural elements for this blade are described below:

i) Spar

The failure modes obtained for three of the spar specimens are shown in Fig.5. This type of failure is similar to that obtained in the static case with cracking occurring along and across the 45° cross-plied carbon and woven glass layers, together with pull-out of the unidirectional glass material.

ii) Trailing-Edge Skins

This specimen consisted largely of epoxy/carbon fibre. Specimen development proved more difficult in this case and a more violent tensile failure mode occurred, causing severe damage to the element.

iii) Root-End

In the static tests failure occurred in a lug tension mode with some local pull-out of unidirectional glass. In the fatigue case the failure modes differed from those seen under the static tests in that much less fibre pull-out occurred. Four of these fatigue specimens can be seen in Fig.6. Although a good deal of damage to the flat surfaces around the holes can be seen, there is no evidence of failure origins between the bush and the bore of the holes due to fretting effects.

THIS DOCUMENT IS PROVIDED BY THE ABBOTT AEROSPACE TECHNICAL LIBRARY
ABBOTTAEROSPACE.COM

iv) Transition

These elements gave both static and fatigue failure modes which proved very similar to those of the spar elements.

The results from the above structural element tests performed for the Sea King tail rotor blade are shown in Figs. 7-10. A summary of the values calculated for material scatter factors is given in Table 2. These factors, which are for use when two full-size specimens are tested, are encouragingly low and compare favourably with those assumed in the original design (also given in Table 2). If more than two full-size specimens are tested these will, of course, reduce.

The variable-amplitude structural element fatigue tests for this blade are in progress at present. (The results from these tests were not required for the initial 50-hour demonstrator clearance).

Also in progress at present is the structural element testing for the Sea King main rotor blade Demonstrator. At the time of writing, information is complete for the trailing-edge skin elements only. Again encouraging results have been obtained. A static coefficient of variation for the population (7 specimens) of 0.046 gives a two-specimen material test factor of 1.07. In constant amplitude fatigue a two-specimen material scatter factor of 1.37 has been demonstrated.

4.2 Full-size Strength and Damage Propagation Tests

Static and fatigue tests are performed on two sorts of full-size specimen: one loaded to test the outboard aerofoil section and one to test the root end. For 50-hour clearance two full-size specimens are required for both static and fatigue loading for both outboard and root-end tests, i.e. a total of 8 specimens for each blade.

Fig.11 shows one of the rigs used for the Sea King tail rotor blade tests. The static tests relate to two load cases. One case represents the peak flapping and lag bending moments and torsional loads occurring in the worst flight condition together with centrifugal loads appropriate to normal rotor speed. The other case represents the effect of rotor overspeed and consists of a peak centrifugal force together with nominal values of flap, lag and torsion.

The fatigue tests are carried out under a programme of vibratory flap, lag and torsional loads together with steady C.F. loads in a series of ascending - descending blocks. Between each block is interspersed a programme of once per flight applications and relaxations of centrifugal loads together with a flap and lag moment and torsional load.

For the Sea King tail rotor blade the two static specimens for the outboard case achieved 105% and 110% of design ultimate load, respectively. This load includes a 1.5 aircraft ultimate factor and an assumed 1.5 materials scatter factor. Fig.12 shows that the failure mode is one of wrinkling of the trailing edge skin. This is caused by the lag bending component generated due to the fact that the centrifugal load path is offset from the blade neutral axis at the outer sections of the blade. In the case of the root-end static specimens, failure occurred at 100% and 106% respectively, of the design ultimate load.

Fatigue testing of an early standard of Sea King tail rotor blade root-end specimens indicated a weakness in the blade spar near to the erosion shield termination which limited the life of this standard of blade to about 87 hours. Design and manufacturing changes were made at the root-end and a new standard of blade was produced. After the fatigue testing at fully-factored, programmed loads of two root-end specimens to this standard no failure occurred and hence unlimited fatigue life has been shown.

A photograph of one of these specimens after it had finished its complete, fully factored, fatigue testing programme is shown in Fig.13. A crack of about 20 mm in length can be seen in the adhesive near the erosion shield but this crack does not extend to the load-carrying structure of the blade. At the root end, de-bonding of the bushes had led to slight fretting, and some scorching of the surface in contact with the 'dummy' blade cuff had occurred. Additional fatigue loading of a similar blade specimen (which had already sustained the complete fully-factored fatigue testing programme) at first 120% and then 140% of the fully-factored loads, eventually lead to a wear/bearing failure in the composite material at the bolt holes.

Fatigue testing of the outboard specimens completed 10^7 cycles of fully-factored, programmed loading. The titanium erosion shield failed during this testing but the blade itself has remained unfailed and has demonstrated an unlimited fatigue life.

TECHNICAL LIBRARY
ABBOTTAEROSPACE.COM

Damage propagation testing has been performed on (known) sub-standard blades with initial cracks of approximately 10 mm in the spar at the root-end high bending load position. After being subjected to a full programme of flight loads no damage propagation or loss of stiffness could be detected.

Work on the fatigue testing of full-scale composite main rotor blade specimens is under way at present and results to date have shown that the excellent fatigue and damage propagation properties obtained with tail rotor blades can also be achieved with main rotor blades.

4.3 Tests Under Extremes of Temperature and Humidity

Tests are in progress at present to assess the effects of extremes of temperature and humidity on the strength and stiffness characteristics of composite rotor blades. These tests fall into two catagories:

i) Real-time (Natural) environmental exposure, and
ii) Accelerated (Artificial) ageing.

In the former catagory the approach is to subject a total of 20 complete blades under load to severe natural environments as follows;

Hot/Wet : 8 blades (Innisfail, Australia)
Hot/Dry : 4 blades (Cloncurry, Australia)
Temperate : 8 blades (Yeovil, U.K.)

After exposure of up to 5 years these blades will be returned to W.H.L. and converted into equal numbers of root-end and outboard test specimens. The blade specimens will then be tested under fatigue and static loads in exactly the same manner as described in the previous section. Stiffness and strength results will then be compared with those obtained from unexposed blades.

Artificial ageing work has been in progress for some time on coupon specimens. The objective of this activity is to investigate the temperature -humidity-thickness-time relationships and define the conditions under which full-scale artificial ageing tests should be conducted. Twelve complete composite tail rotor blades are allocated for this full-scale work. After exposure, 6 root-end and 6 outboard test specimens will be made from these blades. Static and fatigue testing will then be performed for direct comparison which tests performed on naturally aged blades. The development of a reliable accelerated ageing technique is clearly essential for the economic and rapid appraisal of environmental effects on composite rotor blades.

5. FLIGHT TRIALS ON SEA KING AND WG.30

Following some 20 hours ground running, flight trials of the Sea King composite tail rotor blades took place during mid-1979 (see Fig.14). A comprehensive set of manoeuvres and conditions were investigated at various weights, centre of gravity positions and altitudes. Loads in the blades were monitored by a telemetry link and proved to be largely as predicted, although a little greater than anticipated in flap. This additional loading is, in fact, more than balanced by, what has proved to be, pessimistic assumptions on materials scatter factors in the original design. The general performance of the aircraft with the composite blades fitted has proved most satisfactory.

Composite tail rotor blades are now also flying on the Westland WG.30 (see Fig.15). A near complete coverage of the flight envelope has been achieved with blade loads proving to be close to those calculated. Blade lives derived from rig tests and flight measurements are again virtually unlimited.

6. CONCLUSIONS

The rig and flight test programmes performed on composite rotor blades have shown that blades of high structural integrity can be designed and manufactured in composite materials. It has been demonstrated that unlimited fatigue lives can be achieved and that advanced aerofoils can be produced accurately and economically thus making possible significant performance improvements.

The structural element tests have shown encouragingly low material scatter in both static and fatigue cases. It seems that static factors of about 1.2 and fatigue factors of about 1.5 could eventually be used to achieve a level of safety comparable with that of metal blades. Indeed, these factors are themselves

TECHNICAL LIBRARY
ABBOTTAEROSPACE.COM

not dissimilar to those used for metallic materials at present.

Damage propagation testing performed on composite blades to date has shown that, under flight load levels, propagation does not occur from significant defects (about 10 mm) in the G.R.P. blade spar. This fact can contribute significantly to improving helicopter safety through the use of composite rotor blades.

Work at Westland Helicopters is now concentrating on the gathering of further test data for the composite tail rotor blades on WG.30 and composite main rotor blades on Sea King and WG.34. This involves, in particular, further rig testing of root-end and outboard specimens and the collation of the information being generated from blades subjected to extremes of temperature and humidity.

ACKNOWLEDGEMENTS

Much of the work reported in this paper was funded by the Ministry of Defence under the Helicopter Technology Demonstrator Programme.

TECHNICAL LIBRARY
ABBOTTAEROSPACE.COM

Table 1 Lay-Up Summary for Sea King Tail Rotor Blade Structural Elements

Structural Element Type	Resin System*	Fibre Type	Woven or Unidirectional	No./Direction of Layers
Spar	916	120 Glass	Woven	3/45° 2/0-90°
	913	XAS Carbon	Uni.	1/+45° 1/-45° 1/0°
	913	E Glass	Uni.	7/0°
Trailing-Edge Skin	916	120 Glass	Woven	1/45°
	913	XAS Carbon	Uni.	1/-45° 1/+45° 1/0°
Root-End	916	120 Glass	Woven	4/45° 4/0-90°
	916	181 Glass	Woven	18/45° 10/0-90°
	913	E Glass	Uni.	24/0°
	913	XAS Carbon	Uni.	3/+45° 3/-45° 2/0°
Transition	916	120 Glass	Woven	1/0-90° 4/45°
	913	E Glass	Uni.	7/0°
	913	XAS Carbon	Uni.	1/0° 1/+45° 1/-45°
	916	181 Glass	Woven	1/45°
(doublers)	916	120 Glass	Woven	2/0-90°
	916	181 Glass	Woven	2/0-90° 4/45°
	913	E Glass	Uni.	6/0°
	913	XAS Carbon	Uni.	2/+45° 2/-45° 1/0°

*CIBA-GEIGY Fibredux

Table 2 Material Scatter Factors Derived from Structural Element Tests
(Sea King Composite Tail Rotor Blade)

Structural Element Type	Coefficient of Variation of Population — Static (No. of Specimens Tested)	Materials Test Factor for Use with Two Full-Size Specimens — Static	Material Scatter Factor for Use with Two Full-Size Specimens — Constant Amplitude Fatigue (No. of Specimens Tested)
Aerofoil Spar	0.076 (6)	1.16	1.45 (20)
Aerofoil Trailing-Edge Skin	0.066 (5)	1.15	1.19 (20)
Root-End Attachment	0.045 (5)	1.07	1.27 (20)
Transition Region	0.032 (5)	1.04	1.38 (20)
Material Scatter Factor Assumed in Design		1.5	1.67

TECHNICAL LIBRARY
ABBOTTAEROSPACE.COM

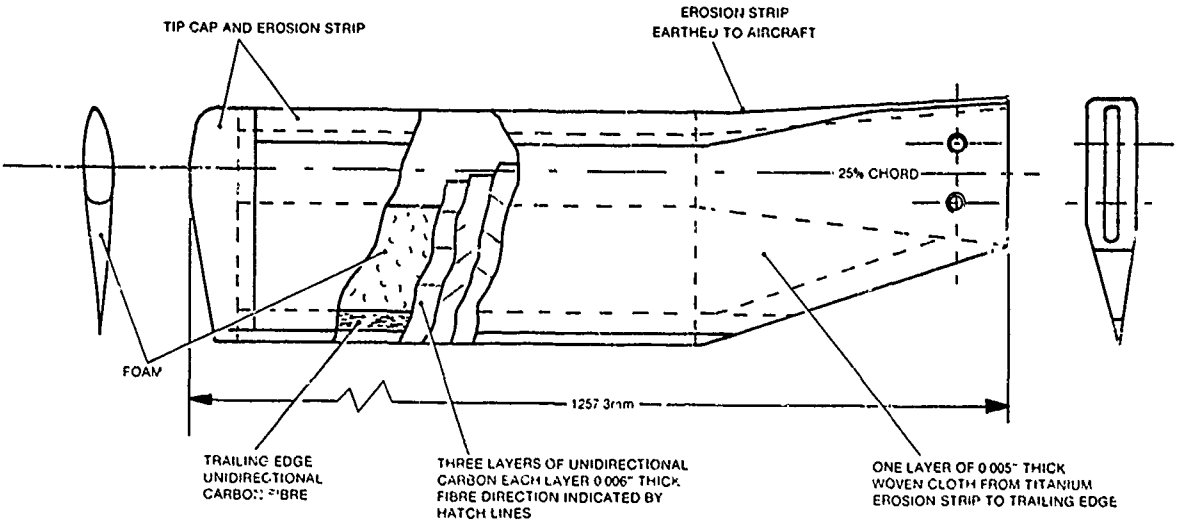

Fig.1 Composite Tail Rotor Blade Construction

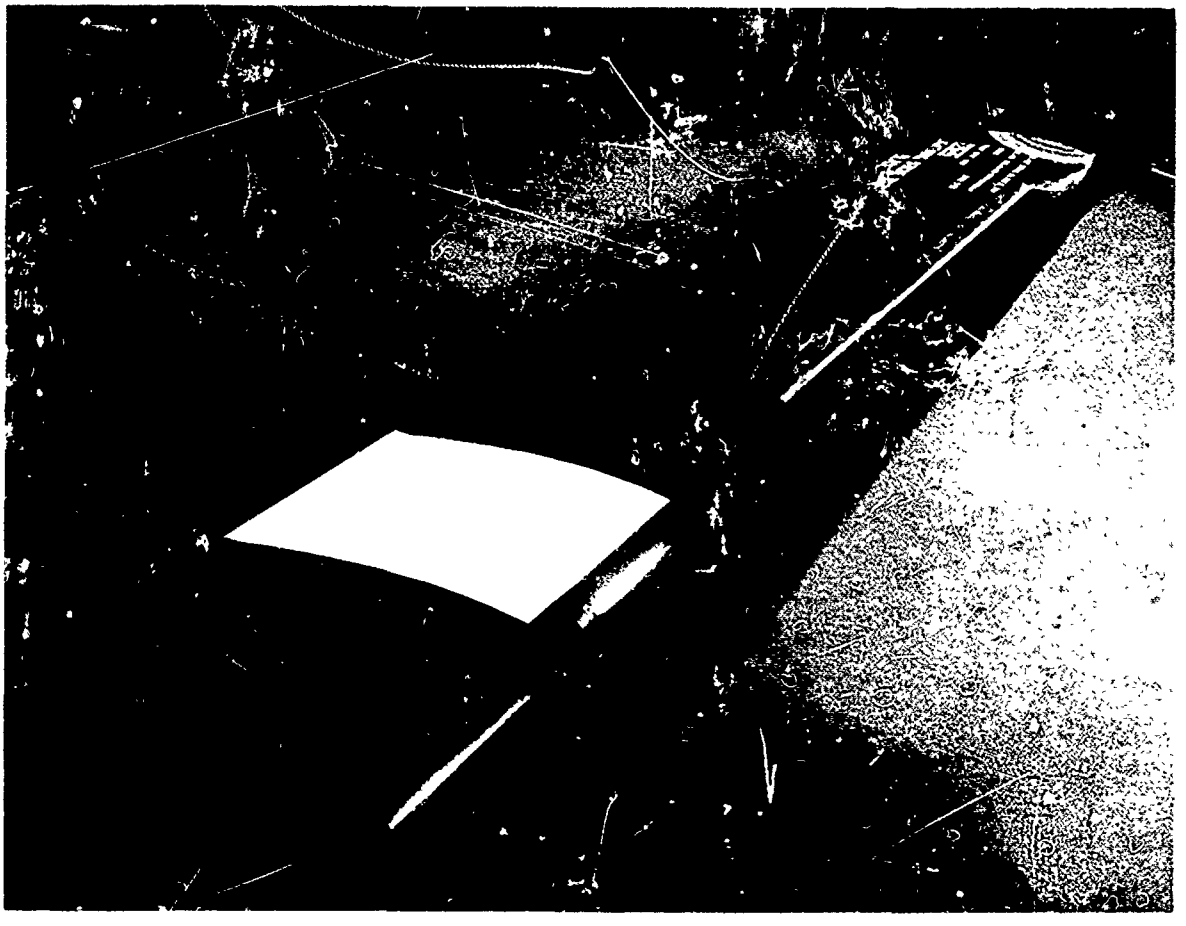

Fig.2 Completed Sea King Composite Tail Rotor Blade

THIS DOCUMENT PROVIDED BY
TECHNICAL LIBRARY
ABBOTTAEROSPACE.COM

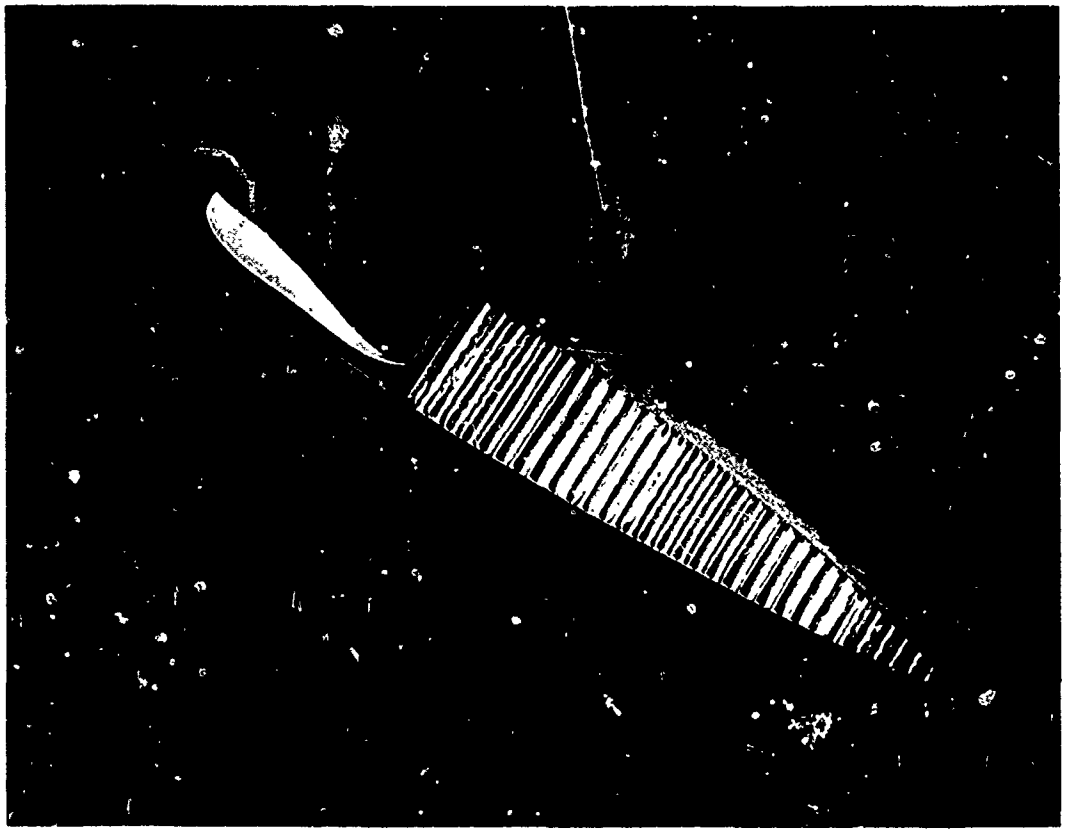

Fig.3 Section of Sea King Composite Main Rotor Blade

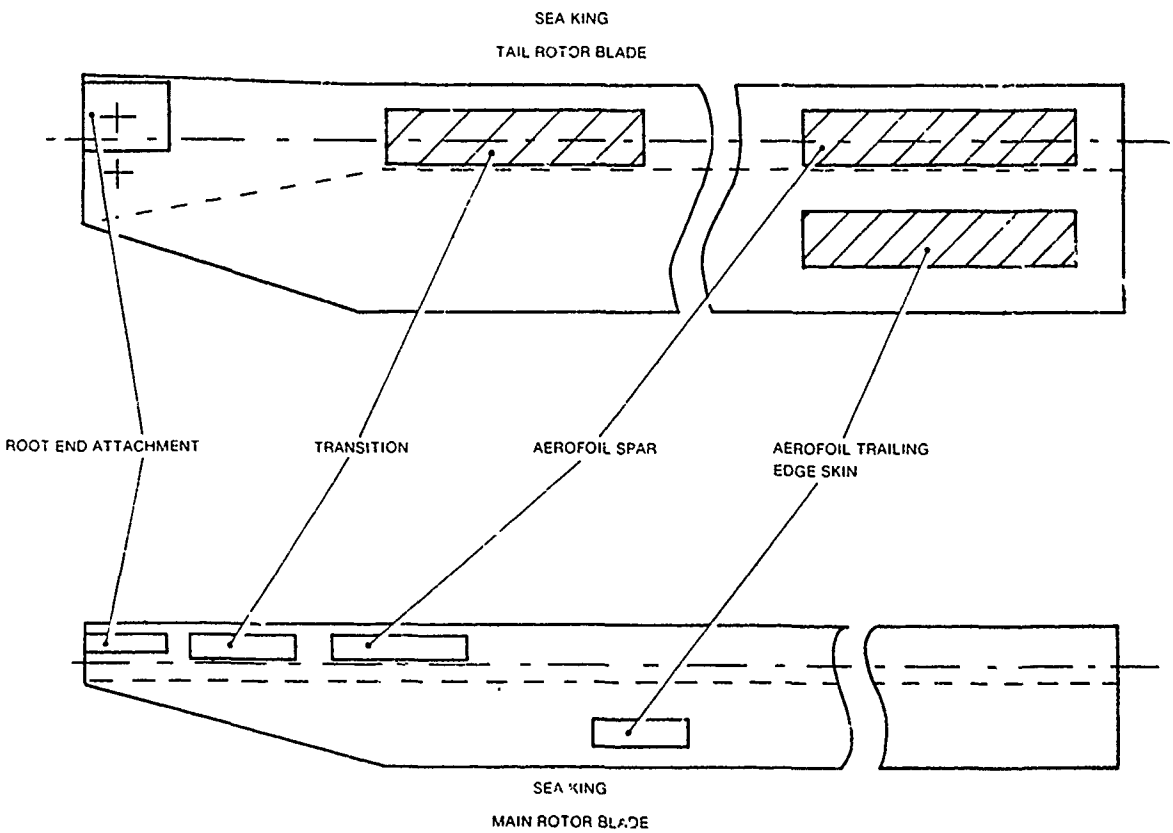

Fig.4 Areas Represented by Structural Elements

TECHNICAL LIBRARY
ABBOTTAEROSPACE.COM

Fig.5 Tail Rotor Blade Spar Constant-Amplitude Fatigue Structural Elements

THIS DOCUMENT PROVIDED BY THE
TECHNICAL LIBRARY
ABBOTTAEROSPACE.COM

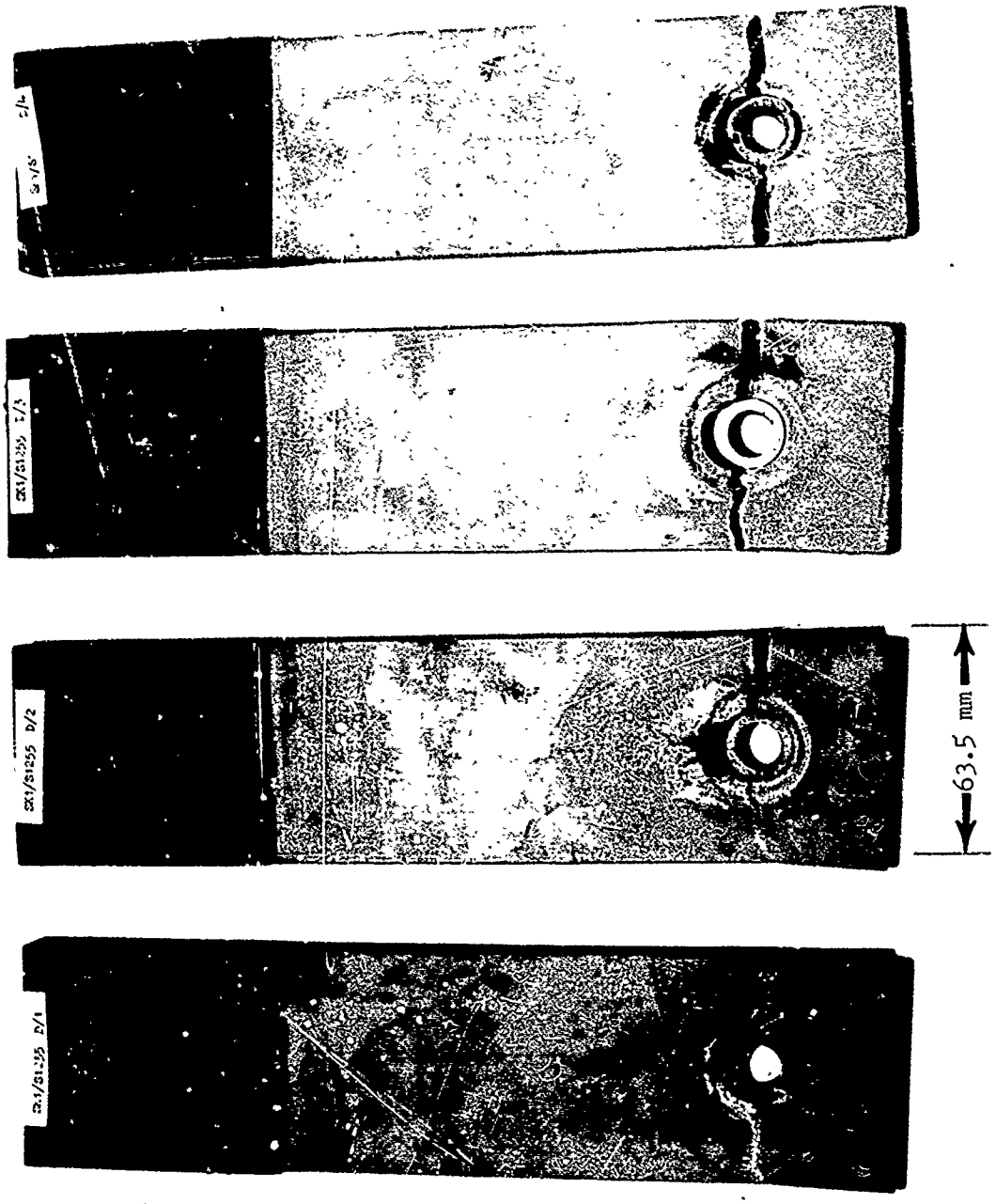

Fig.6 Tail Rotor Blade Root-End Constant-Amplitude Fatigue Structural Elements

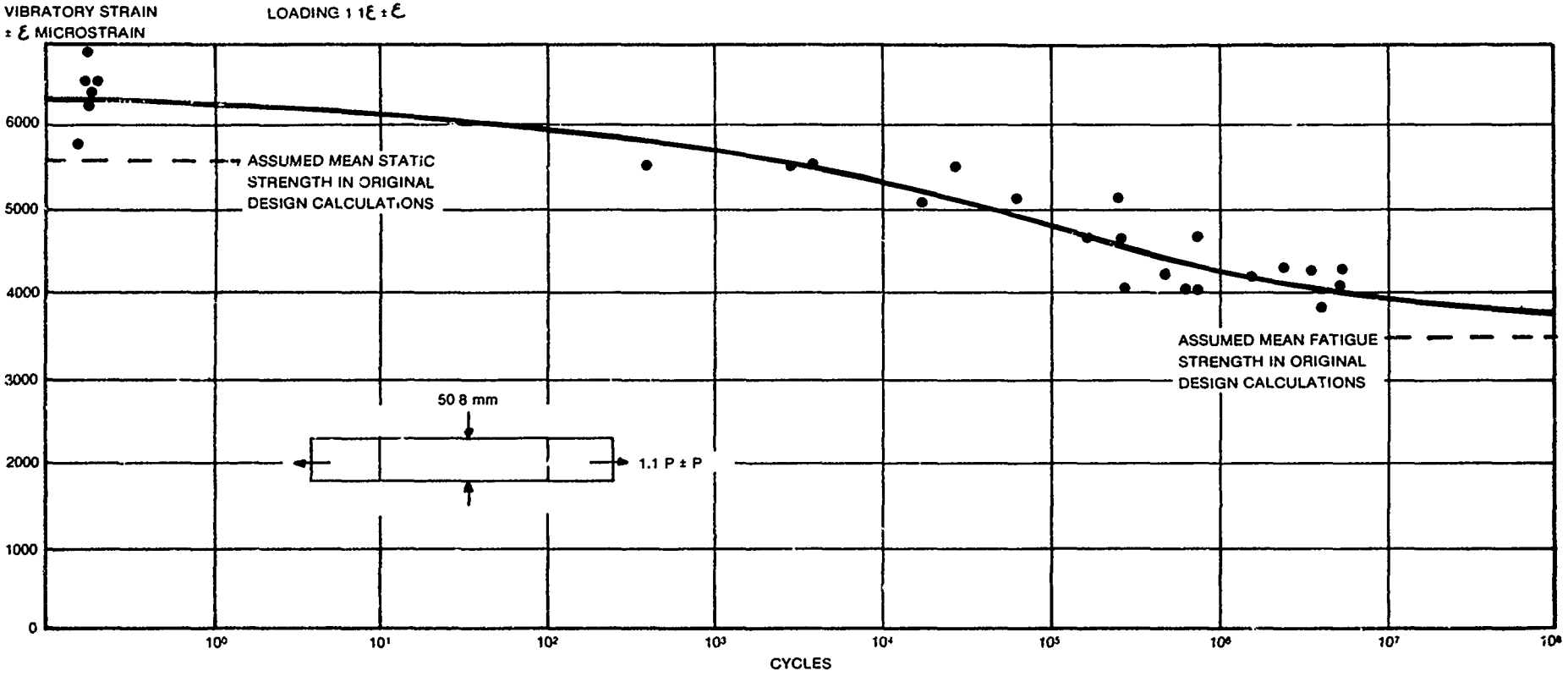

STATIC DATA
6 SPEC. SAMPLE STD. DEVN $S = 686\ \mu\varepsilon$
POPN SAMPLE STD. DEVN. $\sigma = 1022\ \mu\varepsilon$
SAMPLE MEAN $\mu = 13{,}480\ \mu\varepsilon$
POPN. C OF V = 0.076
2 SPEC TEST FACTOR = 1.18

FATIGUE DATA
MEAN STRAIN = 4125 ± 3750 $\mu\varepsilon$
2 SPEC. MATERIAL SCATTER FACTOR (M.S.F.) = 1.45
6 SPEC. M.S.F. = 1.40

Fig.7 Sea King Composite Tail Rotor Blade - Spar Structural Element Test Results

TECHNICAL LIBRARY
ABBOTTAEROSPACE.COM

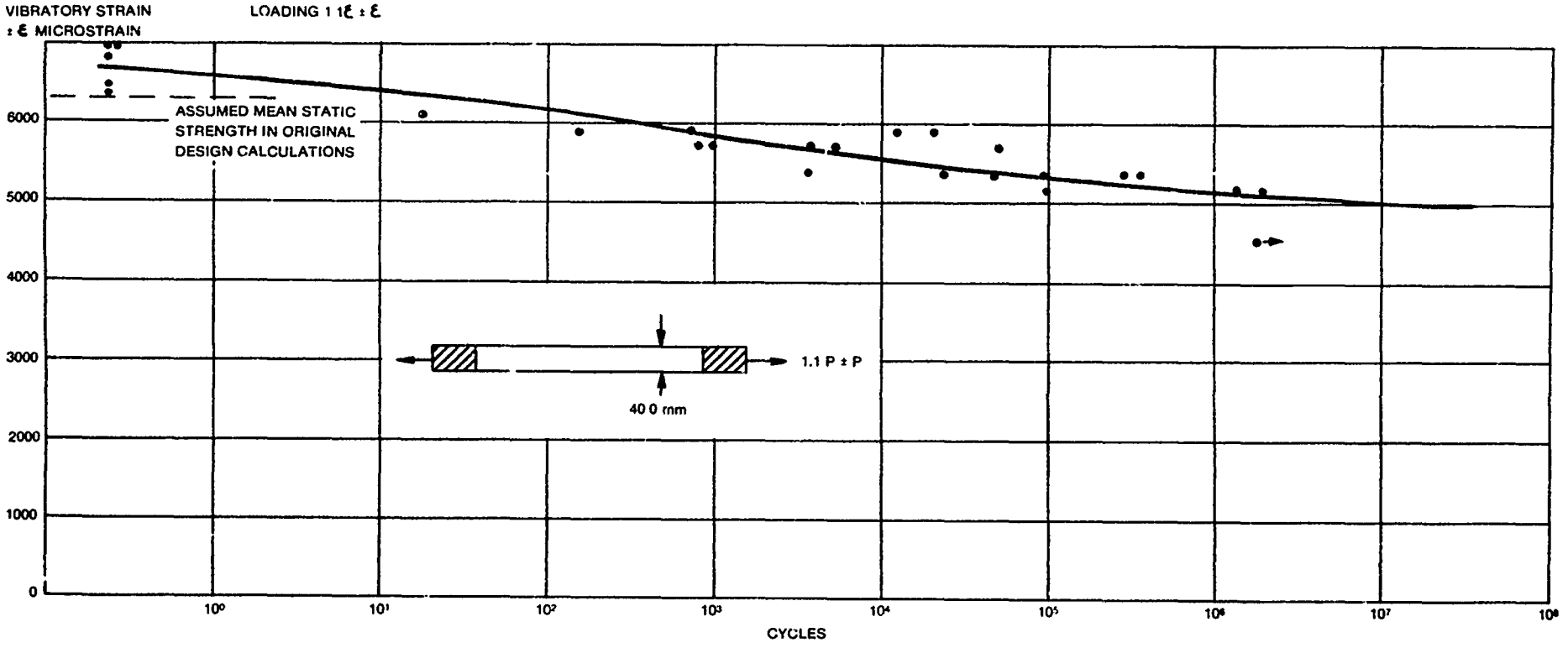

STATIC DATA
5 SPEC. SAMPLE STD DEVN. S = 572 με
POPN SAMPLE STD DEVN. σ = 921 με
SAMPLE MEAN μ = 14,090με
POPN. C OF V = 0.066
2 SPEC. TEST FACTOR = 1.15

FATIGUE DATA
MEAN STRAIN = 5,500 ± 5,000 με
2 SPEC MATERIALS SCATTER FACTOR (M.S F) = 1.19
6 SPEC. M.S.F = 1.17

Fig.8 Sea King Composite Tail Rotor Blade - Aerofoil Trailing-Edge Skin Structural Element Test Results

THIS DOCUMENT HAS BEEN DIGITIZED BY THE TECHNICAL LIBRARY
ABBOTTAEROSPACE.COM

TECHNICAL LIBRARY
ABBOTTAEROSPACE.COM

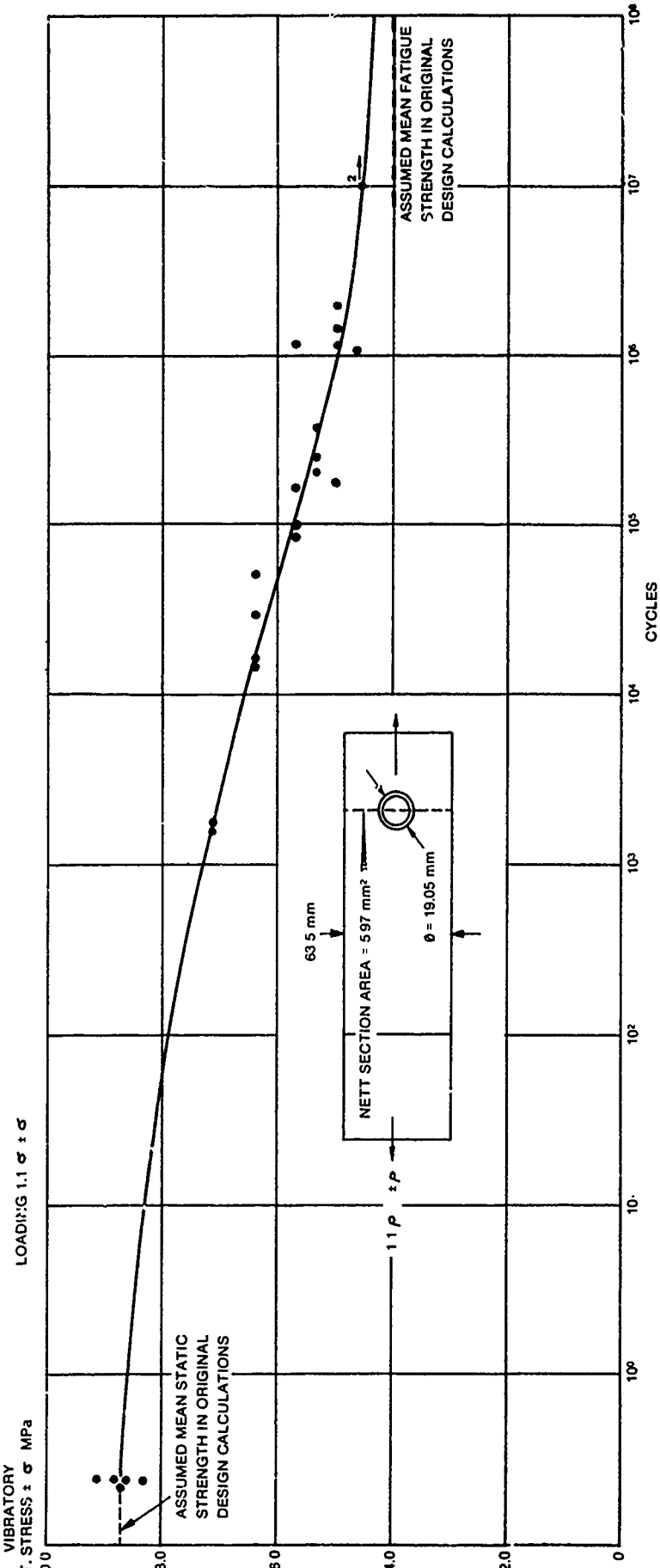

Fig.9 Sea King Composite Tail Rotor Blade - Root-End Structural Element Test Results

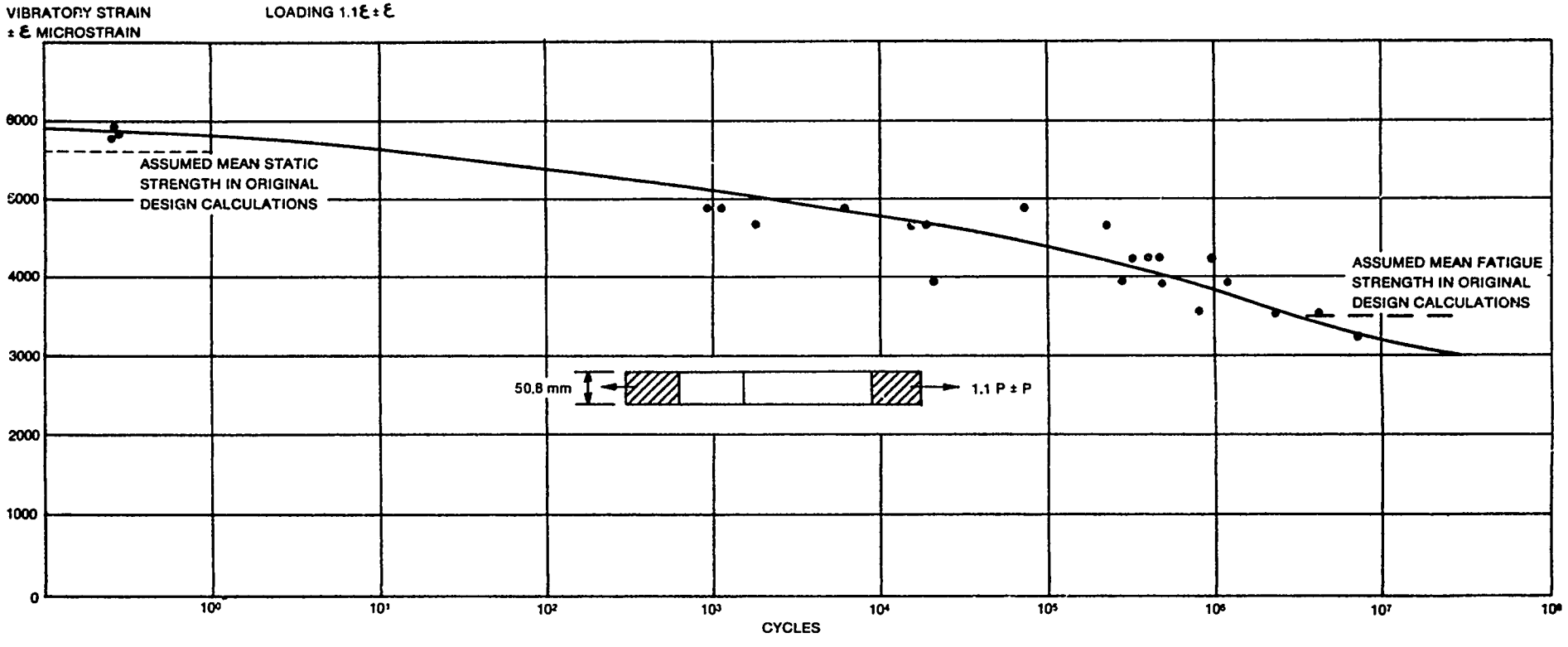

STATIC DATA
5 SPEC. SAMPLE STD. DEVN. S = 242 $\mu\varepsilon$
POPN. SAMPLE STD. DEVN. σ = 390 $\mu\varepsilon$
SAMPLE MEAN μ = 12,128 $\mu\varepsilon$
POPN. C OF V = 0.032
2 SPEC. TEST FACTOR = 1 04

FATIGUE DATA
MEAN STRAIN = 30.0 ± 3,000 $\mu\varepsilon$
2 SPEC. MATERIAL SCATTER FACTOR (M.S.F.) = 1.38
6 SPEC. M.S.F = 1.32

Fig.10 Se· King Composite Tail Rotor Blade - Transition Structural Element Test Results

TECHNICAL LIBRARY
ABBOTTAEROSPACE.COM

THIS DOCUMENT PROVIDED BY THE ABBOTT AEROSPACE
TECHNICAL LIBRARY
ABBOTTAEROSPACE.COM

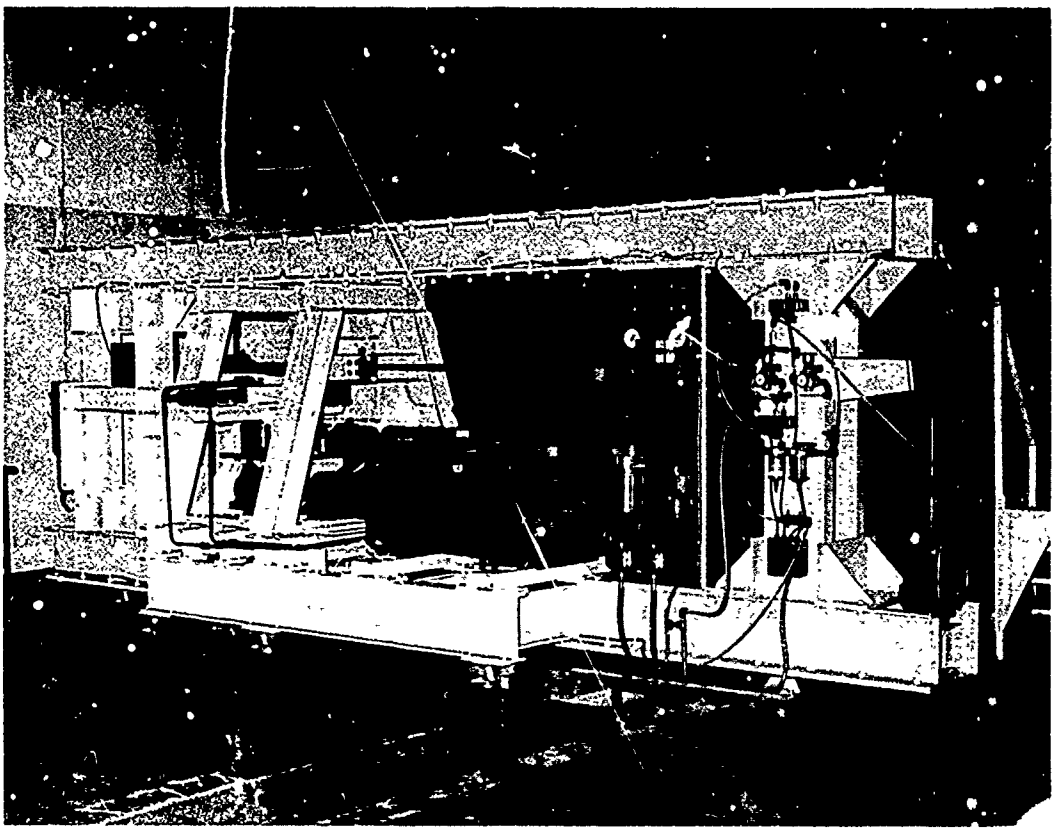

Fig.11 A Composite Tail Rotor Blade Test Rig

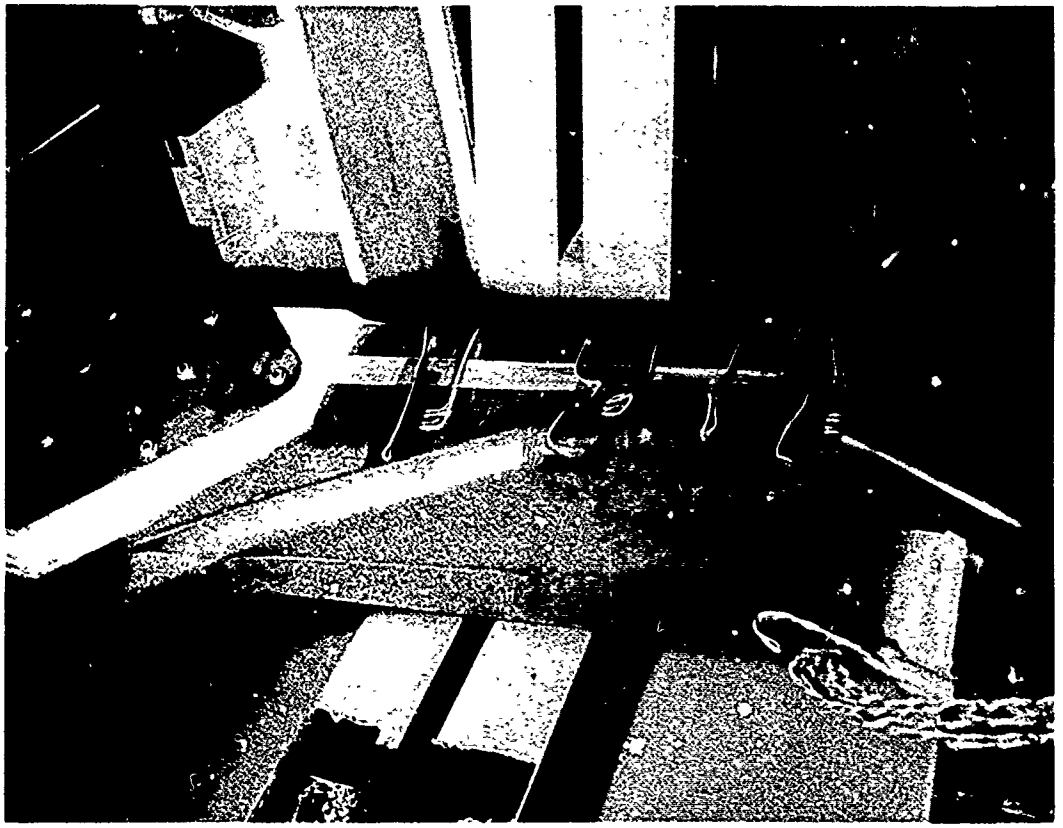

Fig.12 Typical Sea King Tail Rotor Blade Outboard Failure Mode (Static)

THIS DOCUMENT PROVIDED BY THE ABBOTT AEROSPACE
TECHNICAL LIBRARY
ABBOTTAEROSPACE.COM

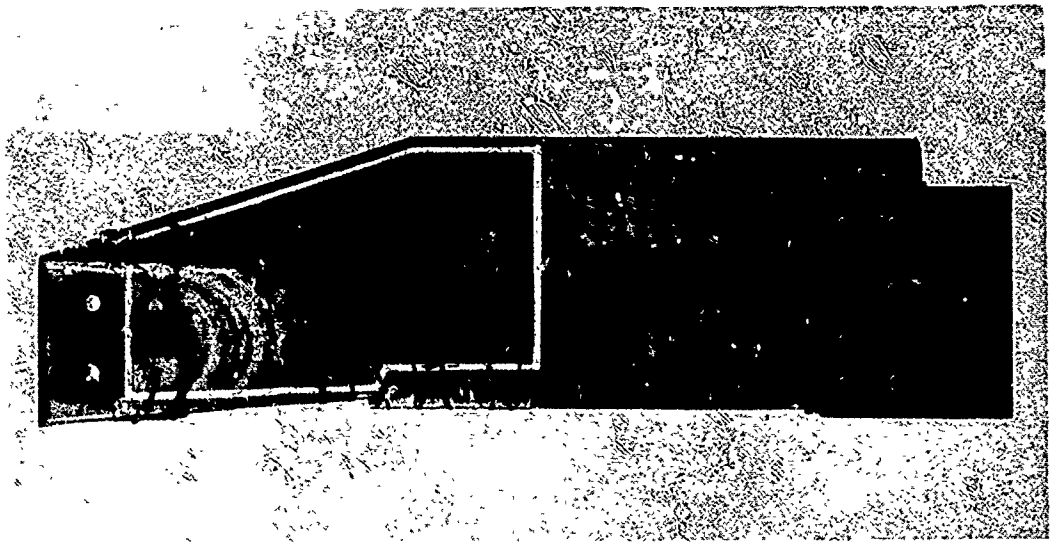

Fig.13 Tail Rotor Blade Root-End Test Specimen After Completion of Fatigue Loading

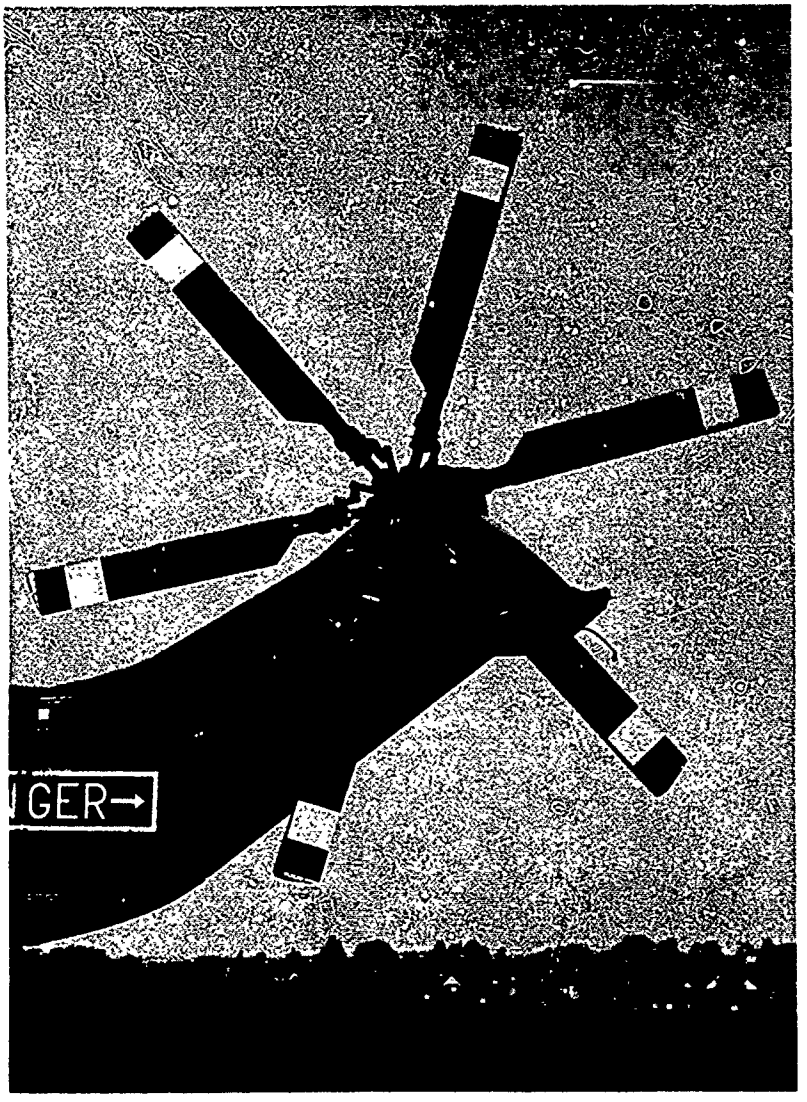

Fig.14 Westland Sea King Composite Tail Rotor Blade Flight Installation

THIS DOCUMENT PROVIDED BY THE
TECHNICAL LIBRARY
ABBOTTAEROSPACE.COM

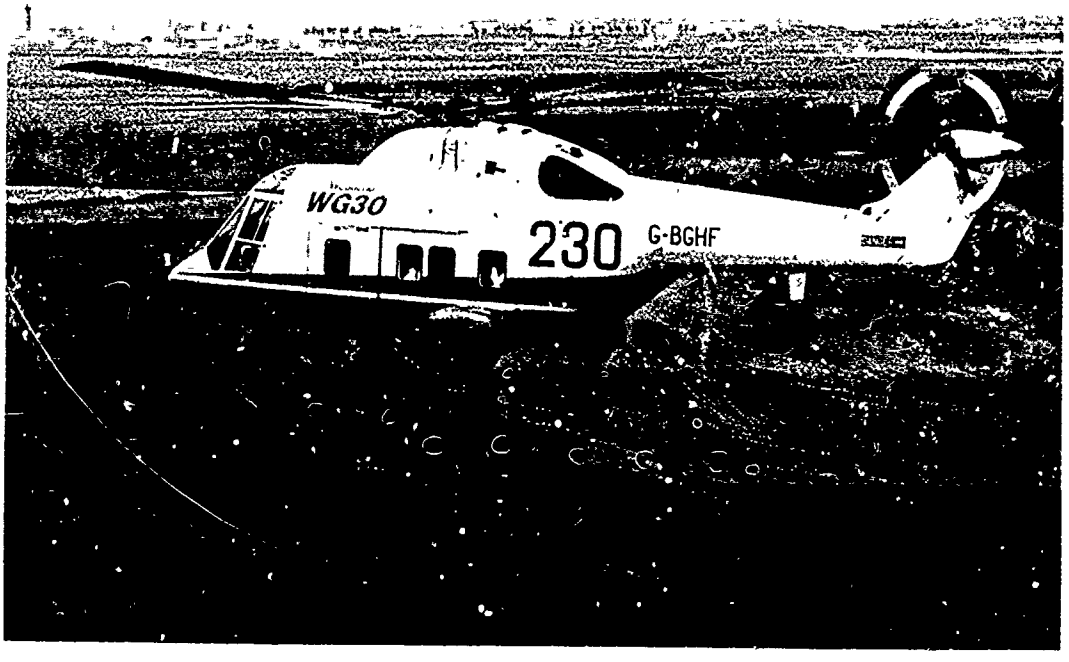

Fig.15 Westland WG.30 in Flight with Composite Tail Rotor Blade

THIS DOCUMENT PROVIDED BY THE ABBOTT AEROSPACE
TECHNICAL LIBRARY
ABBOTTAEROSPACE.COM

SERVICE EXPERIENCE WITH GRC HELICOPTER BLADES (BO-105)

by

K. Brunsch
Messerschmitt-Bölkow- Blohm GmbH
Postfach 801140
8000 München 80, Germany

SUMMARY

By the end of 1979 more than 400 light helicopters BO-105 had been in service both for civil and military operations accumulating approximately 500 000 hours of flight. Some of the helicopters have exceeded 5000 flight hours. The BO-105 being the first production helicopter with a hingeless type main and a teetering type tailrotor with fiberglass rotorblades makes the service experience with the hingeless rotor and the GRC rotorblades unique.

The service experience accumulated with the GRC rotorblades is presented. A comparison of fullscale fatigue test results with new blades and blades after 4000 hours of flight is given, also a comparison of coupon test results, coupons cut out of blades before and after some thousands of service hours.

A general comparison of GRC and metalrotorblades is made. Some recommendations resulting out of the service experience conclude the presentation.

INTRODUCTION

When the BO-105 started operational service nearly ten years ago it was the first production helicopter fitted with composite (GRC) rotorblades both for main- and tailrotor. This pioneering event - use of GRC for the rotorblades of a mass produced helicopter - was result of R + D efforts on composite rotorblades starting as early as 1958, with the first blades flown in 1962. Within that R + D work the unique combinations of low stiffness and excellent fatigue strength owing to glassfibre composite became evident.

Adequate utilization of these mechanical properties resulted in the design of the meanwhile well know hingeless MBB mainrotorsystem. This rotorsystem combines a stiff titanium hub with rotorblades soft in flap- and chordwise bending. Flap- and lagging hinges quasi are replaced by flexible deformation of the GRC-rotorblades. By that, the MBB hingeless rotorsystem was pioneering with respect to structural material not only, it also was pioneering in system simplyfication by the application of new materials - drastically reducing number of parts and maintenance costs (Fig. 1).

Today it can be said, that the enormous courage of the MBB management, when taking the risk to decide for production of the BO-105 has paid off well. More than 400 BO-105 helicopters are in service worldwide.

Most of them fly civil missions, supply to German army started in 1979. The wide field of operation and experience covers missions like off shore, utility, rescue, police, executive, lighthouse supply and scout, antitank and LOH in military operations. The 400 BO-105 flying in 28 countries have accumulated approximately 500 000 hours of flighttime, equivalent to some 2 millions of mainrotorblade hours and 1 million tailrotorblade hours. Blades have been in service since 9 years, the maximum hours of flight blades just approaching the 6000 hours mark, which is half of TBR. Flight environment ranges from -40°C to more than +45°C, from dry desert areas to the 100% humidity, hot climate of Gulf of Mexico.

The experience with the BO-105 GRC-rotorblades is of great interest, because of the many composite rotorblades being developped or starting production just know. Aside of the benefits those projects might draw the excellent structural experience should spur any projects trying to develope bearingless rotorsystems. All well known helicopter companies like AS, Bell, Boeing, MBB, just to name someones make R + D efforts in this field (Fig. 2).

DESIGN OF ROTORBLADES

The design of the mainrotorblade is simple - rectangular plan form (Fig. 3) with an inboard cut out and constant NACA 23012 mod. airfoil. With reference to the experience to be presented later only the bud joints of the erosion protection should be kept in mind. The crossection of the airfoil (Fig. 4) shows the structural and semistructural components. The skin of the blade is built up of fabric with $\pm 45°$ fibre orientation to provide torsional stiffness mainly. To make the torsion box continuous

TECHNICAL LIBRARY
ABBOTTAEROSPACE.COM

all around the airfoil there is a broad bond-line at the trailing edge. The geometry of the transition area airfoil to tab was developped to improve stall characteristics of the airfoil. At the leading edge the lower and the upper skin are connected via the erosion protection strip , joined to the blade by a secondary bond. At the inboard area with its cut out the torsion box is made of GRC only. After curing of the blade two U-shaped shells are bonded to the skin.

The C-spar, made of unidirectional E-glass provides tensile strength and contributes to chord- and flapwise stiffness. The foam core machined out of plates of modified PVC does stabilize the skin and participates in shear load transfer between upper and lower skin. The fabric wrapped around the cg balancing mass made out of lead also improves shear load transfer.

The mainrotorblade is attached to the hub by a titanium fitting. The mainly GRC-uni-structures horse-shoe shape completely is embedded in the fitting. To compensate for manufacturing tolerances the groove in the fitting is slightly oversized with reference to the blade root. The gap between fitting and blade is filled with an adhesive (Fig. 5). Prior to that the fitting is thoroughly sprayed with a release to avoid any bonding blade to fitting. The fitting is attached to the hub by the mainbolt which transfers centrifugal load and flapwise bending and by the secondary bolt contributing to chordwise bending moment transfer only.

The design of the tailrotorblade is like that of the mainrotorblade rather simple. The planform again is rectangular (Fig. 6), the airfoil is NACA 0012 mod. all along the blade span. The blade is attached to the teetering type rotorhub by two bolts. The unidirectional GRC does circumvent the bolts of the tailrotor attachment. The internal structure is like that of the mainrotorblade (Fig. 7).

MANUFACTURING TECHNOLOGY

It is the authors opinion that the usefullness in service of a composite component severely is influenced by manufacturing technology and -quality. Therefore the manufacturing technology of the blades is described briefly. Tools both for main- and tailrotor are female moulds for lower and upper side (Fig. 8). Moulds are NC-milled out of stretched Aluminium. Aluminium was selected for ease of machining, good thermal conductivity and coefficient of thermal expansion being higher than that of GRC.

By the later heating up of the mould tends to improve fibre alignment rather than to buckle the laminate. Blade production starts with a wet hand-lay-up of fabric sheets. The mass of each set of fabric sheets cut for one blade is noticed before. For an exactly specified number of sheets always the same amount of resin is to be used. To control that the total mass of resin to be used for skin impregnation is split into many fractions, eg like tabled below for Main Rotor Blade (MRB).

Layer	Mass (g)
1 Layer part No. 35 (8.4505.6) 2 Layer part No. 36 (8.4548.6)	6 x 190
4 Layer part No. 36 (8.4548.6)	4 x 220 2 x 130
each 1 Layer part No. 37-43	2 x 100
3 Layer part No. 47	1 x 250
6 Layer part No. 48 6 Layer part No. 49 5 Layer part No. 50	1 x 50

Everymix of resin is reported with reference to total mass, mass of resin and mass of hardener although an automated dosing unit is used.

To provide controlability of fibre alignment- the skins fibreorientation is ±45° to blade span- the fabric is fitted with tracer fibres.

To ease impregnation moulds are heated to 43 ± 2°C. As soon as the skin laminate is completed the spars are built up out of roving tapes. A special technology was developed to ensure very high roving tape quality. Each roving tape consists of 18 rovings with 768 tex (Fig. 9). The set of bobbins (Fig. 10) is put together in such a way, that the mass per unit of length of the dry roving tape is always the same.

TECHNICAL LIBRARY
ABBOTTAEROSPACE.COM

Experience is, that the mass per unit of length nearly ever is constant for all the material on one bobbin.

Nevertheless each start of the impregnation unit is preceeded by a test to define the mass of one meter of dry roving tape. The roving tape is pulled over a drum which dives into a resin container to about 40% of its diameter (Fig. 11). The drum picks up a resin film part of which attaches to the roving tape. Then the roving tape goes through an oven 55°C in thermal temperature. Thereby wetting and netting resin to glass is improved considerably (Fig. 12). After that excessive resin - approximately 50% of that picked up - are squeezed out by an adjustable fixture (Fig. 13). The roving tape then is pulled through nozzles intended to form the final geometry of the tape only but not to squeeze out resin. Both tapes for main- and tailrotorblade have the same cross-sectional area but different geometry.

Impregnation is done discontinuously,tapes with slightly more than twice of the length of the MRB are produced. Of any tape a dual knife (Fig. 14) cuts a constant length specimen dropping on a scale without being touched.The scale indicates and records individual tape specimen mass and accumulated tape specimen mass. With the dry roving mass being constant always the scale gives an exact information on resin content.

Fibre content is controlled to 73,8% per weight.
The roving tapes are laminated onto the skin already in the moulds starting from the tip of the blade to the inboard attachment area, around the fitting (MRB) or attachment bushings Tail Rotor Blade (TRB) and back to the tip again.
After deposition of 20, 40, 60 and 76 tapes per female mould (MRB) templates are used to control for proper spar geometry.

60 additional roving tapes are laminated to the MRB spar in the attachment area. When the spar production is completed a core machined out of modified PVC foam is inserted to the lower mould, also a rope of lead for chordwise cg balancing.
The "upper" mould is lifted by crane, rotated for 180° and carefully lowered to the other one. The two half moulds are pressed to one another by large bolts and curing temperature becomes applied. After curing the MRB is hung up at the attachment loop and allowed to relaxe from thermal stresses induced by curing for 6 weeks.

Production is continued with bonding of the erosion protective strip and of the GRC shells in the attachment area to the blade and with mating the fitting (MRB) to the attachment lug. The point applied then particularly is used for spanwise balancing. After final static balancing the blades are ready for dynamic balancing on the whirl tower.

Following this brief description of the B0-105 GRC-rotorblades the service experience gathered with them will be described.

SERVICE INFLUENCE ON STRUCTURAL MATERIAL PROPERTIES

Strength Properties

The application of GRC for a hingeless type rotor was quite innovative when MBB started R + D on this system. Excessive material testing, especially fatigue testing was necessary to evaluate material properties. Specimen testing was done with specimen cut out of blades only. The tooling built up for experimental blade production allowed for manufacturing of better composite material than the equipment available in the laboratories. Some thousands of spar material specimen have been tested to establish tensile, flexural and shear fatigue strength data. With respect to service influence on material strength the best information can be drawn from comparison of those datas with that produced from specimen which have been cut out of blades that had been in service. Specimen have been cut out of blades that had accumulated up to some 3000 hours within 5 years and fatigue tested. Test result indicate a shear strength reduction of 1,8 % at 10^7 cycles (Fig. 15).
Flexural fatigue strength appears to be slightly higher than that evaluated with specimen cut out of new blades (Fig. 16).

As there is no physical explanation the later result is considered to caused by a limited number of specimen. Generally can be concluded, that there is no adverse influence on spar material strength. Taking in account the load cycles the blade has accumulated (Fig. 17) and adding the representative number of cycles to those applied with specimen testing shear fatigue strength also is like that of new blades spar material.

Service influence on blade skin fatigue strength was investigated by component testing only. Therefore the number of test results is very small. The reason for component testing was that all efforts to develope an usefull skin test specimen (to be cut of the blades) had failed due to the curvature of the blade surface and the assymetry of the design of the skin.(Difference of resin content eg because of foam core adjacence at skin at one side and the metal mould at the other). Two types of fatigue tests have been performed - flapwise bending in a resonant beam bending mode (Fig. 18) ie without simulation of CF and a tension torsion test (Fig. 19), where torsional and CF loading was simulated. Test results again indicate, that there is no adverse influence on skin

TECHNICAL LIBRARY
ABBOTTAEROSPACE.COM

fatigue strength.

Finally the most complex components of the mainrotorblade, the attachment areas, were fatigue tested too. Fatigue test results again demonstrated that here is no adverse influence on the fatigue strength of the blade material composed and produced as described before (Fig. 20).
On the other hand there was a significant influence of service environment on material properties with reference to blade skin. In the early days of BO-105 the inboard area (the so called swan neck) was coated with a transparent Pu-paint to allow for visual detection of any deterioration that might show up. Unfortunately deteriorations became evident very soon. The UV part of solar radiation penetrated the Pu coating and severely damaged the epoxy resin at the interface to the Pu-laquer. With some blades excessive peel off of the PU-coating occured (Fig. 21).

ELASTIC PROPERTIES

Aside of strength properties service influence on elastic constants are may be of even greater interest with composit materials used for rotorblades. Rotorblades are designed extremely carefully to avoid any vibration caused by the exciting frequencies (mainrotor, tailrotor, number of blades, tailboom natural frequency and so on).
The manifold of exciting frequencies, -especially higher modes - does incorporate the risk that even minor changes in frequency result in unacceptable vibration of the helicopter caused by (partial) resonance. Determination of changes in elastic properties has been done more or less by three ways - mainrotor blades have been flown in excess of 6000 hours without any adverse influence on vibratory characteristics of the helicopter. That means that non of the "eigen" modes had changed to come close to an exciting frequency. Second a pair of blades that had exceeded 6000 service hours successfully has been mated with a pair of new blades. Again no adverse influence on helicopter vibration showed up.

Finally a lot of frequency testing has been done. In the early production phase every MRB was tested for flap- and chordwise bending frequencies 1st and 2nd mode in a free-free test set up (Fig. 22). Again the best information concerning service influence on dynamic properties can be drawn from comparison of frequency test results of new blades and of blades after service. The results presented in Fig. 22 indicate that there is no adverse influence detectable. An exact number of new blades tested is not given because any 100th new MRB is tested for quality control. Thereby the number of blades tested steadily does increase. Tests in a clamped-free configuration also have been done. Due to the BO-105 specific attachment design these test showed considerable scatter, also major differences in test results were evaluated when changing from a set up with horizontal chordline to a set up with vertical chordline. Therefore this testing is considered not to provide valid information. Aside of problems with testing there is another fact making the type of test suspicious. As described before there is a layer of filler material in between the titanium fitting and the GRC blade. This layer initially was made out of AW 106, a special product of Ciba.
This material performed pretty well in component testing but was not acceptable in service, due to severe deterioration (Fig. 23) caused by hot humid environment. The filler material was replaced by a product with trade name AV 138 M and the problem seems to be overcome. Nevertheless minor abrasion at the outboard position of the attachment lug still does occur. With Centrifugal Force (CF) abrasion does not influence natural frequencies. When fatigue testing blade root components with load well above max. manual load considerable wear of the filler materials was produced. Without repairing the filler material frequency testing with CF was done. Test results were the same with new components and components with the filler material worn off the outboard areas of the attachment lug.
Without CF - as in testing with a complete blade - the influence is remarkable. Therefore a repair of the filler is to be done prior to testing bringing natural frequencies back to the band known from new blades (Fig. 24).

TECHNICAL LIBRARY
ABBOTTAEROSPACE.COM

SERVICE INFLUENCE ON SEMI- AND NONSTRUCTURAL COMPONENTS OF ROTORBLADES

Erosion - Corrosion Problems

Composite structures generally are known to be very susceptible both to rain and sanderosion. The BO-105 rotorblades are protected against rain erosion in the leading edge area by hotformed titanium strips. Two different technologies are used - hotforming in a "Murdoc press at 735°C"and normal atmosphere the surface of the titanium protected against corrosion by a molybdenium compound and a kind of creepforming for the thin tailrotorblade strips at 600°C and Argon atmosphere. Both processes require intensive cleaning of the surface prior the etching to prepare for adhesive bonding. The strips for the MRB are chem milled even to remove any impurity before etching.
Although the processing of adhesive bonding is controlled very intensively some debonding of erosion protective strips from blades in service is reported.

This evidently is caused by some kind of deterioration, that means corrosion of the bondline. A real good understanding of this phenomena does not yet exist. The rotorblades are completely coated with a polyurethane laquer. This partially is eroded away in blade tip area at first. Thereby the end of the bondline becomes improtected but unfortunately debonding is not restricted to this area only. The experience in this field is that only higher reliable adhesive systems - adhesive and primer and surface treatment procedure - shall be used for composite rotorblades.

But there are other problems with erosion protection.
Service experience with the BO-105 demonstrates, that there is no erosion protective paint to withstand the extremely severe erosive environment that helicopters are flying in. With heavy rain or sand erosion the paint is abraded rather soon chordwise all along the metal protective strip. The GRC becoming unprotected thereby will be abraided very badly. 500 hours of flight in a desert area without repainting caused locally up to 60% of thickness abrasion of mainrotorblade skin. Todays experience with BO-105 rotorblades is, that towards blade tip areas metal erosion protection of at least 40% chordwidth will be necessary and also a metal tip cap.

For quite a while it was hoped, that improvements with erosion resistant coatings might solve the problem. Todays impression is that this never will be. BO-105 rotorblades initially were coated with a polyurethane paint part No. N 53634.
With this material repainting to avoid abrasion of the composite material was necessary after about 1000 hours in central Europe and after about 300 Hours in the Gulf of Mexico area (Fig. 25). Improvements were achieved by changing to the "erosion resistant" system part No. N 53631. Time between over roughly were trippled. The problem with this paint is, that after some time of service considerable local abrasion and peel off is created. Again considerable maintenance cost are caused by need of repainting. The latest coating system in service evaluation is the "chemglace" No. V 200 paint.
Whirling arm testing indicated an improvement by the magnitude of more than ten compared to coating systems used before with reference to onset of erosion. Service testing did back those test results, but still there will be considerable of maintenance cost.
The erosion shown in Fig. 26 is caused by 500 flight hours in off shore missions.
With that amount of abrasion MBB does recommend repair of the paint.

Shifting the removal of the PU coating from one shop (well trained with GRC-blades) to another one, experienced with metal blades only resulted in more than a dozen of TRBS made scrap by blade skin abrasion.
Such things of course do not positively influence maintenance cost. But the increase of maintenance cost making abraded blades scrap is the by far minor a problem compared to that an abraded blade might be taken in service again. Especially with the tailrotorblades blade skin abrasion significantly could reduce safety of flight. The operators of the BO-105 evidently do know about that. Up to now no accident/incident is known which was caused by rotorblade failure due to GRC abrasion. On the other hand there have been sent quite a lot of blades to MBB to clearify wether the coating had been removed accurately or what to be done with the blades renew painting only, repair of GRC or scrap. Most of the blades went back to service again.

PROBLEMS DUE TO LACK OF UNDERSTANDING OF GRC FAILURE MECHANICS

A deterioration, that would catastrophically fail a metal rotorblade in very short time may not at all influence the fatigue strength of a glassfibre-composite rotorblade. This phenomena is very well known to people who have participated with the numerous fatigue tests necessary for rotorblade certification.
It is absolutely unknown to people that get their first helicopter with GRC-rotorblades just to operate it and make that maintenance required. Quite a number of mainrotorblades have been removed from service without need. Some of them have been damaged substantially when trying to make a repair not necessary at all. At that station where the GRC MRB comes out of the fitting the maximum wear of the filler material is caused. Sometimes minor delamination of the GRC shells in those areas becomes evident. Delaminations in this area were the reason to remove blades from service. To prevent operators from removing blades from service without need a fatigue test was done and the "delamination phenomena" documented very carefully. With high loads in this test minor delamination became detectable after about half a million of cycles. The best was

THIS DOCUMENT PROVIDED BY AGARD ADVISORY CENTRE
TECHNICAL LIBRARY
ABBOTTAEROSPACE.COM

stopped after simulation of 5 MRB lifes equivalent to 6 x 10^6 cycles. Towards the end of testing the delaminated area had approximately trippled compared to that detectable after 5 million cycles.

IMPACT STRENGTH

The last item of this paper is impact strength of GRC rotorblades. This strength being reasonable good the author wishes to point out that he does not intend to encourage for any in flight inpact test. The service experience in this area is upto today:
Two mainrotors went through oak trees cutting off branches in excess of 50 mm.
The rotorblades were thoroughly inspected and cleared for further service without repair of the GRC.
A hovering BO-105drifted backward and the tailrotor impacted a MRB of an UH 1 D on ground. All rotorblades engaged were severely damaged. The composite tailrotorblades failed at the impact station only (Fig. 27). The remainders of the TRB provided sufficient thrust to allow the pilot for a safe landing.

CONCLUSION

Well designed and produced GRC is the best structural material for rotary wing application known to the author. Todays experience indicates that there is no adverse influence on material properties by service environment.

The pure resistance of GRC against rain- and sanderosion requires very carefully designed erosion protection systems. Also the methods for repairing the protective coating need further improvement.

LITERATURE

1. Weiland, E.F.: "Development and Test of the BO-105 Rigid Rotor Helicopter", J.American Helicopter Soc Vol. 14, No. 1, January 1969

2. Barth, R.: "The Hingeless Rotor - A Concept to Increase Mission Effectiveness at Reduced Costs". AGARD Annual Meeting, September 1973

3. Reichert, G.:" The Impact of Helicopter Mission Spectra on Fatigue" in AGARD Specialists Meeting on Helicopter Design Mission Load Spectra, AGARD-CP-206, 1976

4. Brunsch, K., Wackerle,P.M.: "Ballistic and Impact Resistance of Composite Rotorblades",Second European Rotorcraft and Powered Lift Aircraft Forum,Bückeburg, 20. - 22.9.1976

5. Reichert, G., Weiland E.F.: "Long Term Experience with a Hingeless / Composite Rotor" AGARD Flight Mechanics Panel Symposium on Rotorcraft Design, 16.-19.5.1977

6. Hoffrichter, J.S.:, "Evaluation of the Effect of Usage on Composite Main Rotor Blades", Boeing Vertol Company, Philadelphia, 14.4.1978

This Document Provided by the ABBOTT AEROSPACE
TECHNICAL LIBRARY
ABBOTTAEROSPACE.COM

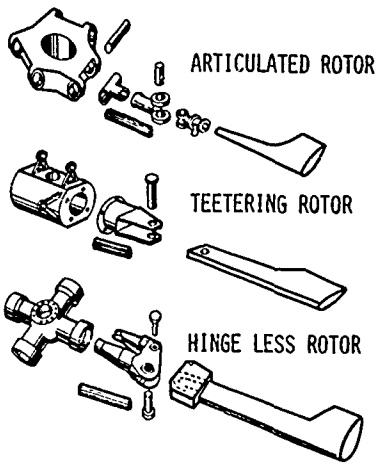

FIG. 1: NUMBER OF PARTS OF DIFF. ROTOR-SYSTEMS

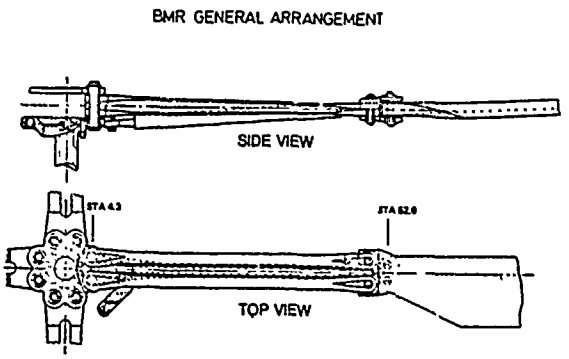

FIG. 2: BEARINGLESS MAINROTOR OF BOEING-VERTOL

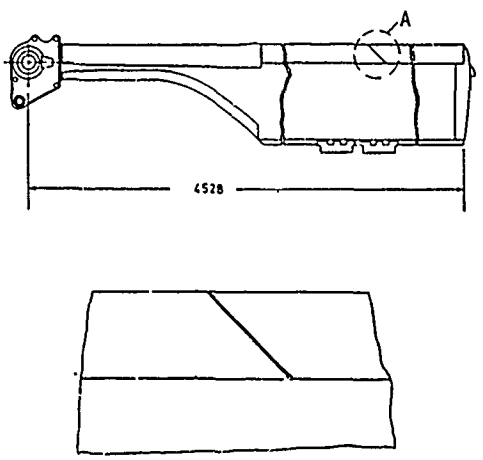

FIG. 3: MAINROTORBLADE, PLANVIEW

THIS DOCUMENT PROVIDED BY THE
TECHNICAL LIBRARY
ABBOTTAEROSPACE.COM

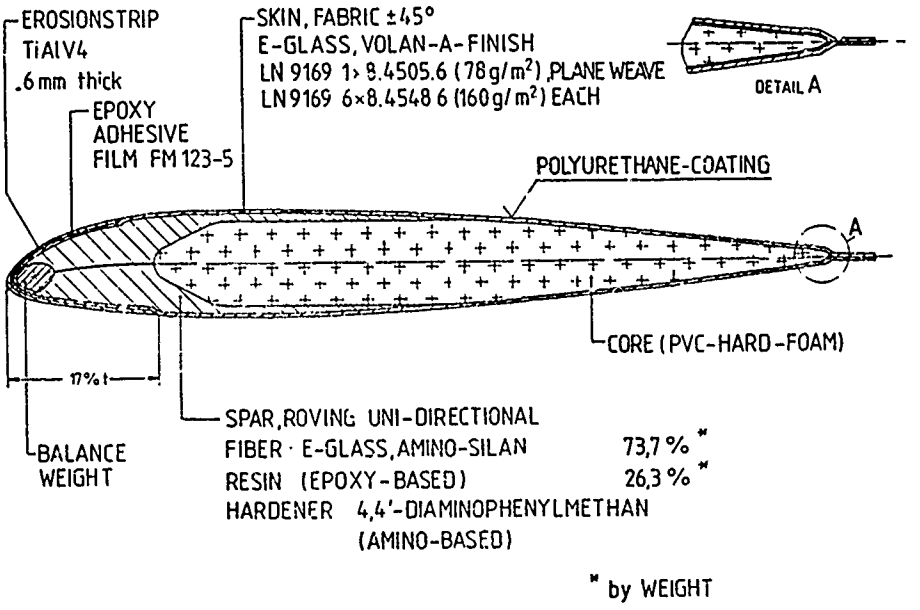

FIG. 4: MAINROTORBLADE, CROSSECTION

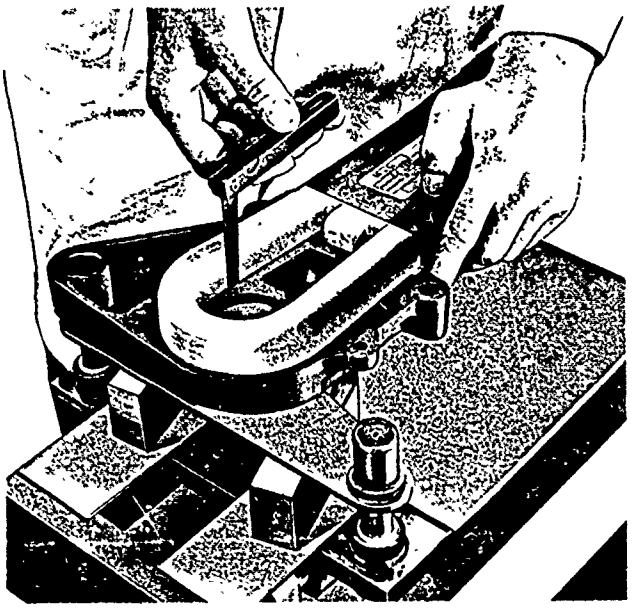

FIG. 5: MAINROTORBLADE ATTACHMENT, GAP FOR FILLER

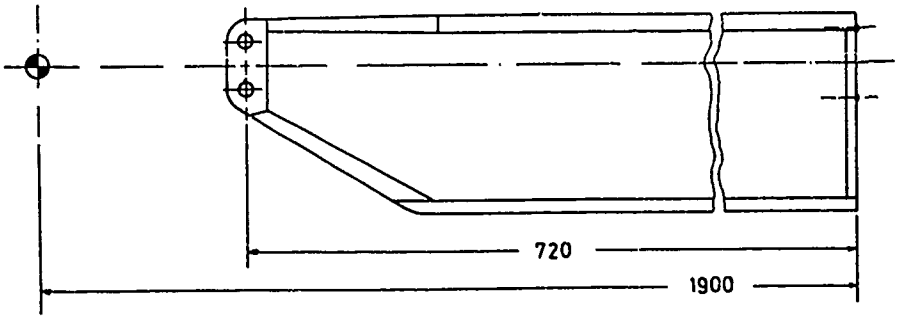

FIG. 6: TAILROTORBLADE, PLANVIEW

THIS DOCUMENT PROVIDED BY THE TECHNICAL LIBRARY
ABBOTTAEROSPACE.COM

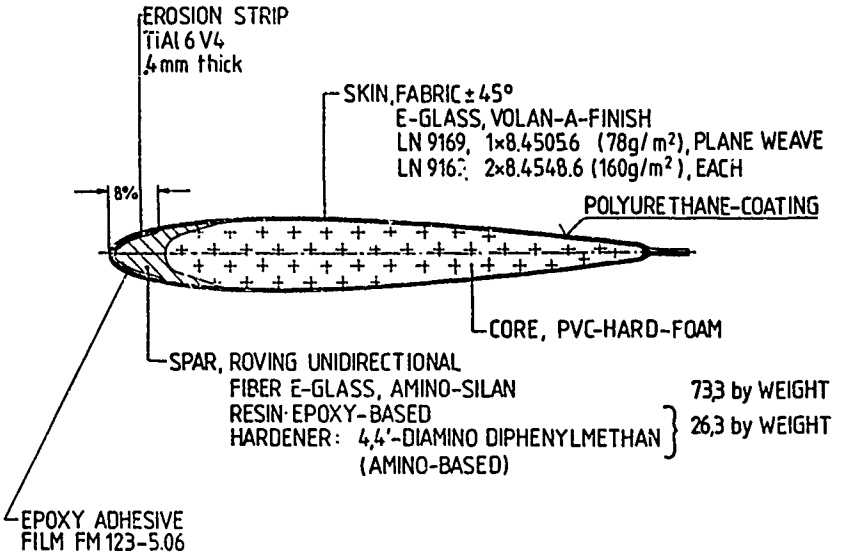

FIG. 7: TAILROTORBLADE, CROSSECTION

FIG. 8: ROTORBLADE PRODUCTION MOULD

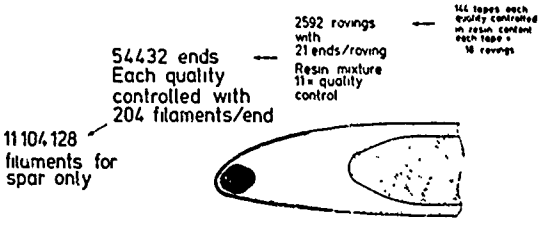

FIG. 9: BO-105 BLADE SPAR BUILD UP

This Document Provided by the
TECHNICAL LIBRARY
ABBOTTAEROSPACE.COM

FIG. 10: SET OF BOBBINS

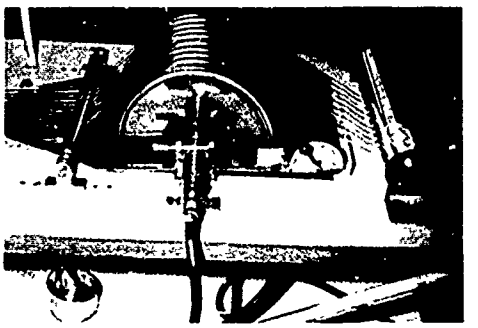

FIG.11: IMPREGNATION DRUM

FIG. 12: IMPREGNATION QUALITY
LOWER PICTURE WITH OVEN

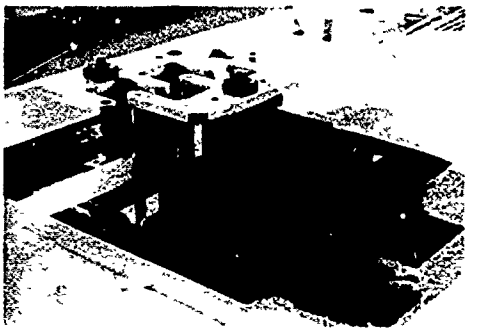

FIG.13: FIXTURE FOR RESIN CONTROL

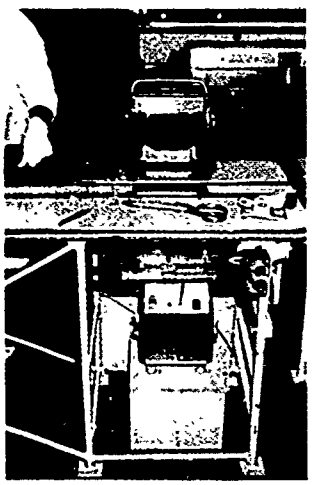

FIG.14: RESIN CONTENT SPECIMEN CUTTER

TECHNICAL LIBRARY
ABBOTTAEROSPACE.COM

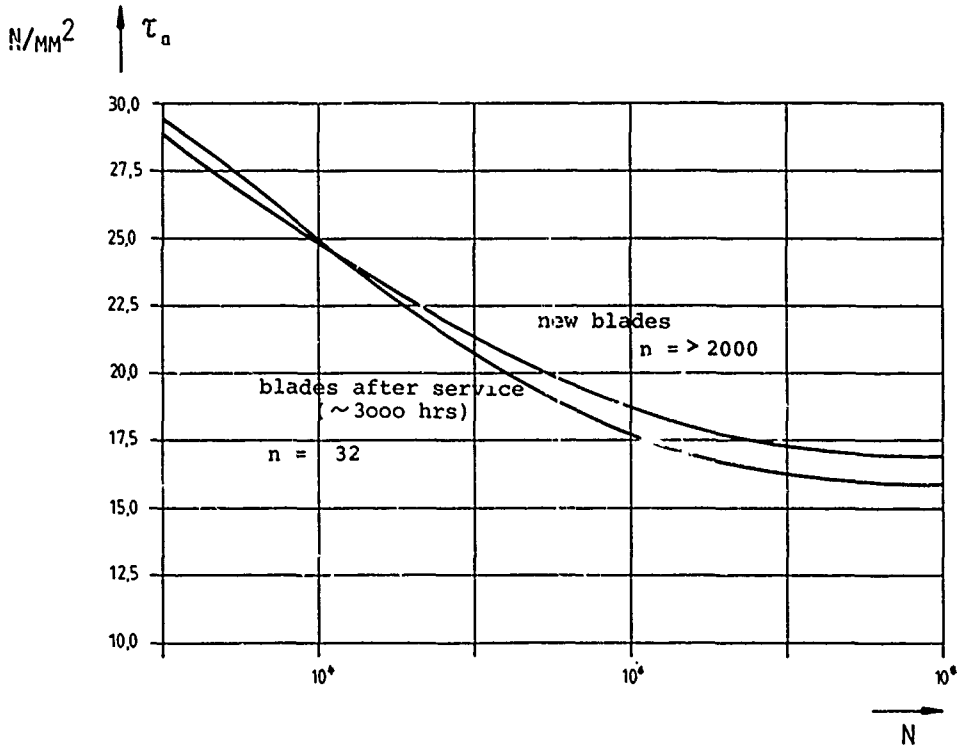

FIG.15: BLADE SPAR SPECIMEN
SHEAR FATIGUE STRENGTH, A = 2/3, S = 50%, P = 50%

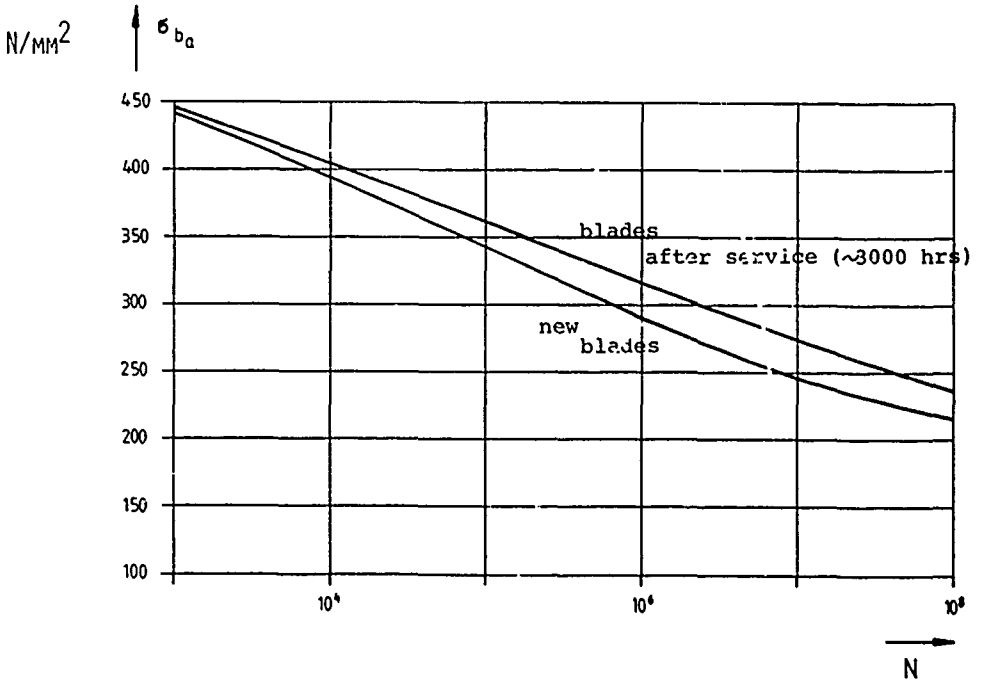

FIG. 16: BLADE SPAR SPECIMEN
FLEXURAL FATIGUE STRENGTH, A = 2/3, S = 50%, P = 50%

TECHNICAL LIBRARY
ABBOTTAEROSPACE.COM

BO-105 MAINROTORBLADE

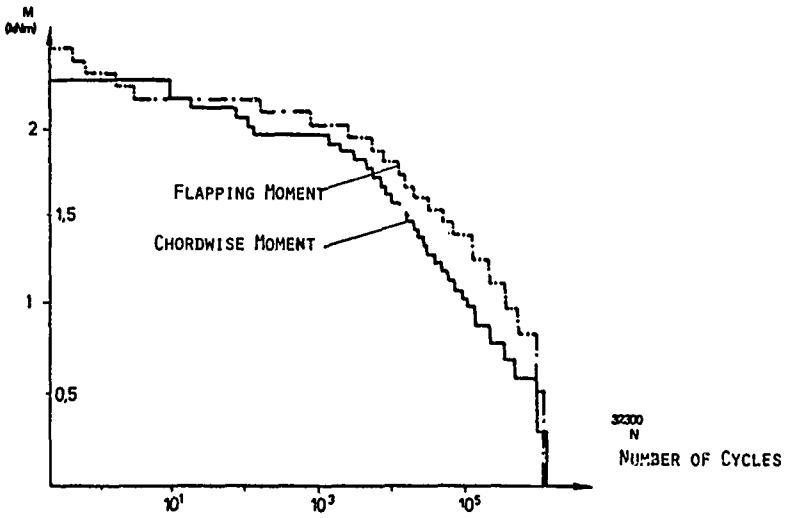

FIG. 17: LOGARITHM. CUMULATIV OF OCCURENCE OF ALTERNATING BENDINGMOMENTS, FLIGHTTIME 100 H

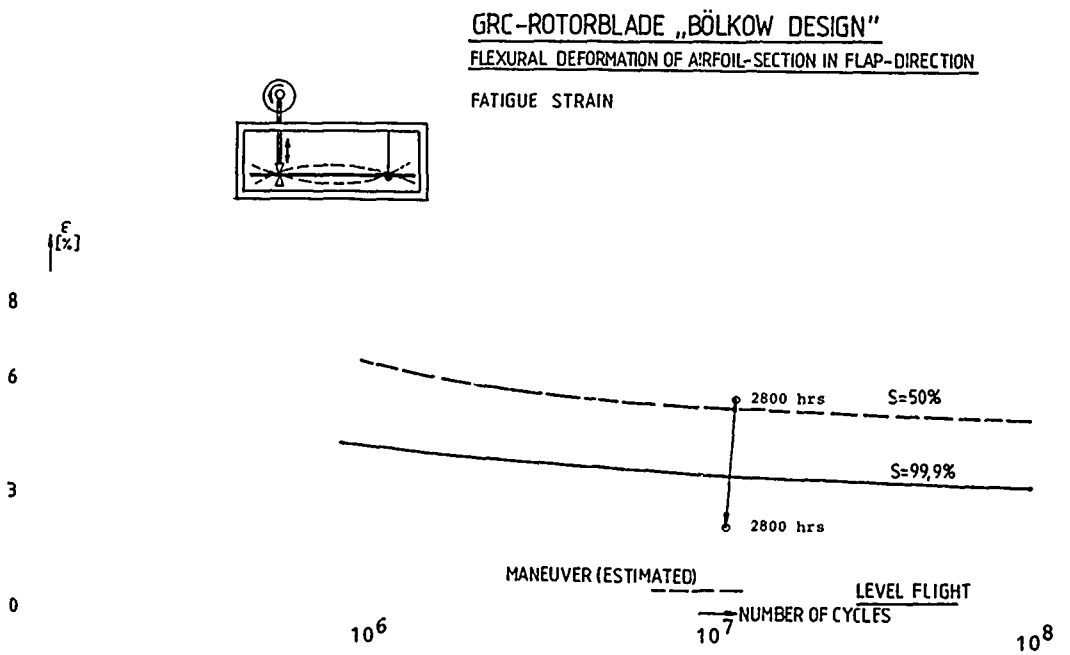

FIG. 18: FLAPWISE BENDING FATIGUE STRENGTH

THIS DOCUMENT PROVIDED BY THE ABBOTT AEROSPACE
TECHNICAL LIBRARY
ABBOTTAEROSPACE.COM

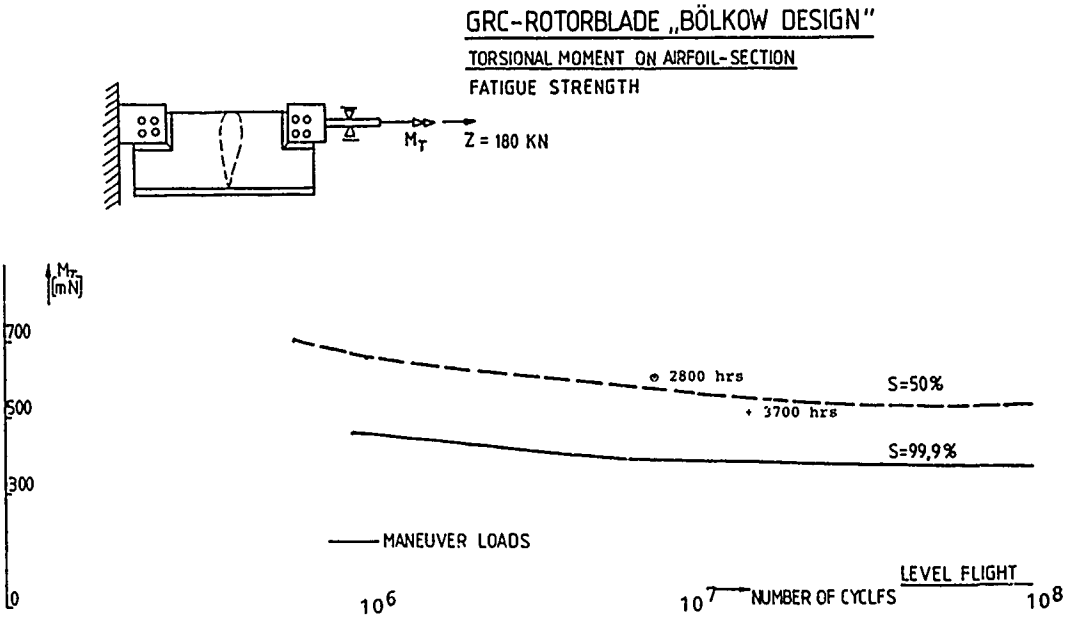

FIG. 19: TENSION-TORSION, FATIGUE STRENGTH

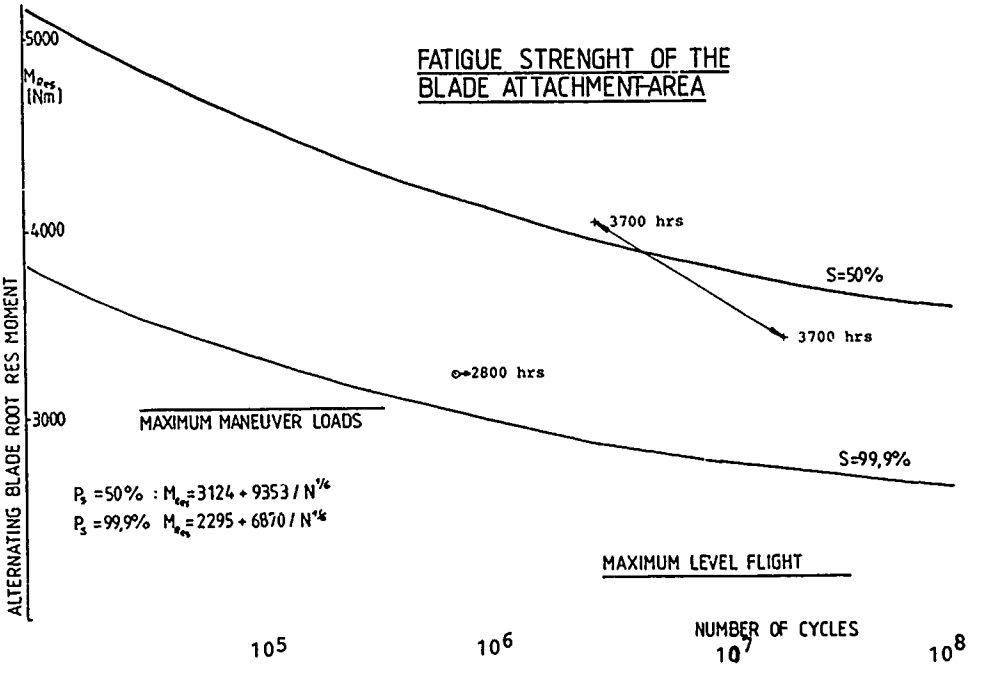

FIG. 20: BLADE-ROOT - FATIGUE STRENGTH

TECHNICAL LIBRARY
ABBOTTAEROSPACE.COM

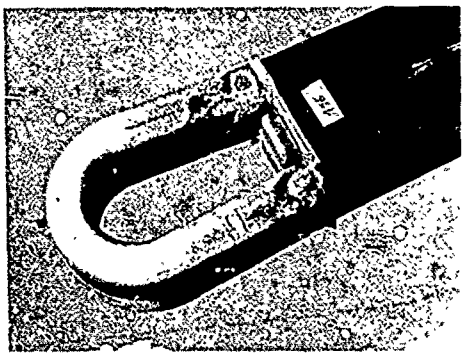

FIG. 21: PAINT ABRASION

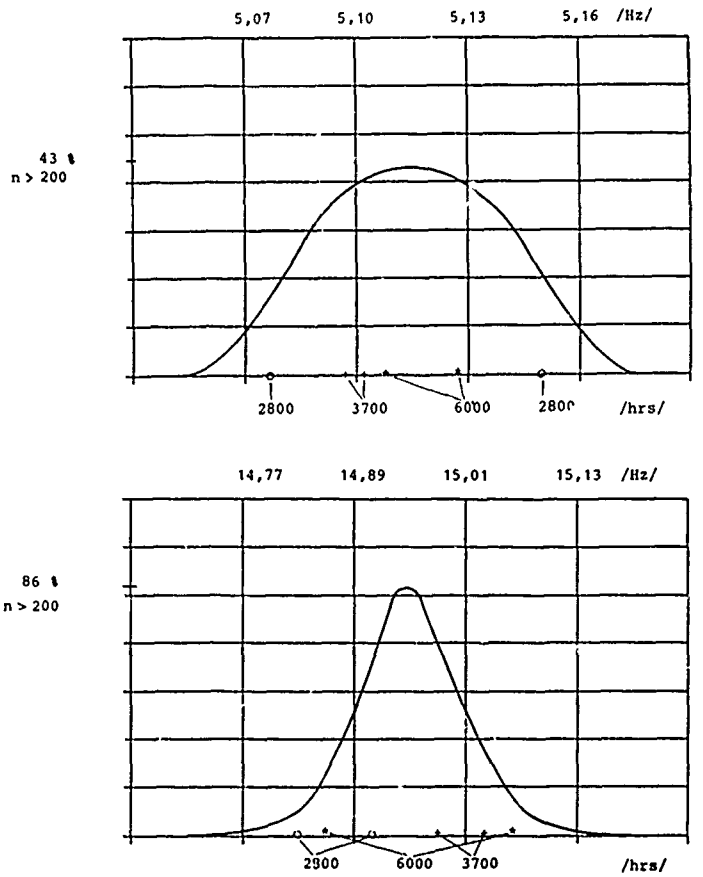

FIG. 22: FLAPWISE FREQUENCY 1ST AND 2ND MODE FREE-FREE

THIS DOCUMENT PROVIDED BY THE ABBOTT AEROSPACE
TECHNICAL LIBRARY
ABBOTTAEROSPACE.COM

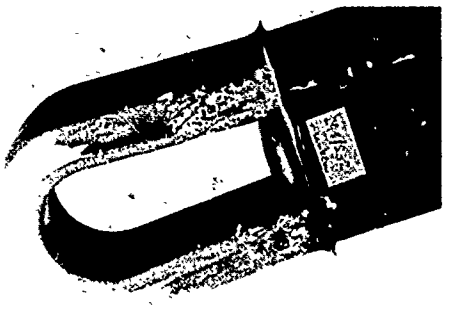

Fig.23: FILLER (AW 106) DETERIORATION

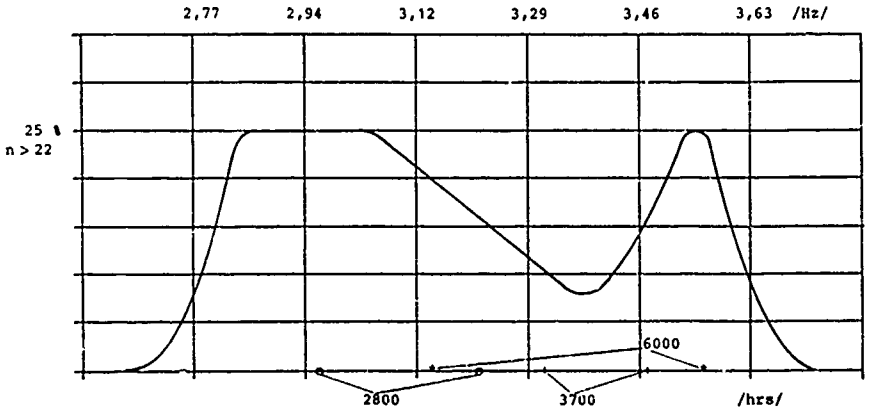

Fig. 24: CHORDWISE FREQUENCY 1st MODE CLAMPED-FREE

TECHNICAL LIBRARY
ABBOTTAEROSPACE.COM

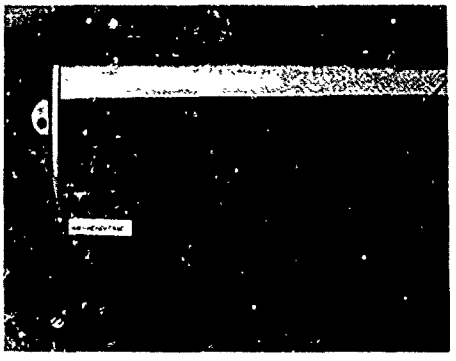

FIG. 25: PAINT ABRASION AFTER 300 HRS GULF OF MEXICO

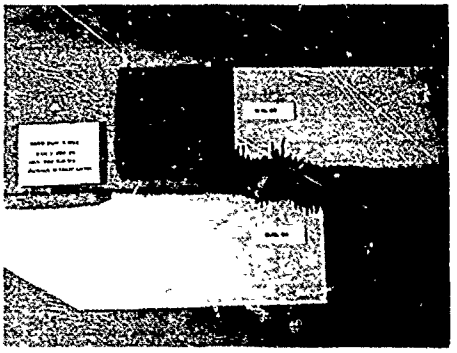

FIG. 26: PAINT ABRASION AFTER 1200 HRS GULF OF MEXICO (IMPROVED COATING)

TECHNICAL LIBRARY
ABBOTTAEROSPACE.COM

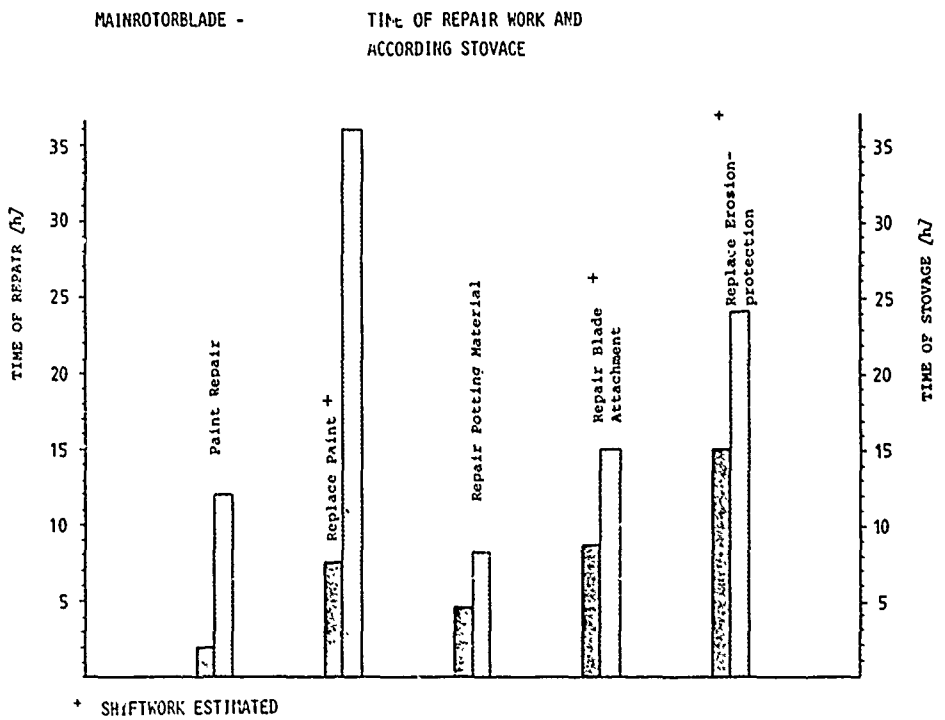

FIG. 27: MAINTENANCE HOURS FOR MAINROTORBLADE-REPAIR

FIG. 28: TAILROTORBLADE AFTER IMPACT

TECHNICAL LIBRARY
ABBOTTAEROSPACE.COM

COMPOSITE COMPONENTS ON COMMERCIAL AIRCRAFT

H. Benson Dexter
NASA Langley Research Center
Hampton, Virginia, U.S.A. 23665

SUMMARY

The technology development of advanced composite structures has progressed to the point where commercial aircraft manufacturers are making production commitments to composite structure for future aircraft and modifications to current production aircraft. NASA has been active in sponsoring flight service programs with advanced composites during the past 10 years. Approximately 2.5 million total composite component flight hours have been accumulated since 1970 on both commercial transports and helicopters. Design concepts with significant mass savings were developed, appropriate inspection and maintenance procedures were established, and satisfactory service was achieved for the various composite components. Also, a major NASA/U.S. industry technology program to reduce fuel consumption of commercial transport aircraft through the use of advanced composites has been undertaken. Ground and flight environmental effects on the composite materials used in the flight service programs supplement the flight service evaluation.

INTRODUCTION

Advanced composite aircraft structures have the potential to reduce airframe structural mass by 20 to 30 percent, reduce fuel consumption by 10 to 15 percent, and thus reduce the direct operating costs to the airline operator. The U.S. Government and industry have been developing advanced composites technology for the past 15 years. This technology has matured to the point where commercial aircraft manufacturers are starting to make production commitments to this new class of materials.

The NASA Langley Research Center has been instrumental in the development of advanced composite structures primarily for commercial aircraft. Flight service evaluation programs were initiated in the early 1970's to develop confidence in the long-term durability of advanced composites in actual aircraft operating environments. Concurrent with the flight evaluation of structural composite components, NASA initiated programs to determine the outdoor environmental effects, the effects of aircraft fuels and fluids, and the effects of sustained stress on several thousand composite test coupons.

In 1975, NASA initiated an extensive aircraft energy efficiency (ACEE) program to improve the efficiency of commercial transport aircraft through the development and application of advanced technologies such as advanced composites. The objective of the ACEE program is to accelerate the development of advanced technologies to the point where U.S. commercial transport manufacturers can economically incorporate the technology into their production aircraft. Six components, three secondary structures, and three primary structures, are presently under development.

The purpose of this paper is to outline some of the NASA/U.S. industry composite programs and report on the service experience gained with numerous composite components during the past decade.

NASA FLIGHT SERVICE PROGRAMS

NASA recognized the need to build confidence in the long-term durability of advanced composites to allow aircraft manufacturers and operators to make future production decisions. NASA initiated a systematic program for the design, fabrication, test, and flight service evaluation of numerous composite components that will provide the necessary confidence. Early applications were for selective reinforcement of military aircraft structures [1 to 6] but major emphasis was placed on evaluating advanced composites on commercial transport aircraft [7 to 13]. Commercial aircraft were chosen because of their high utilization rates, exposure to worldwide environmental conditions, and systematic maintenace procedures.

A typical NASA flight service program takes approximately 3 years for component development, detail design, fabrication, and ground testing and 5 years or more for service evaluation. In some cases, selected components are periodically removed from service for residual strength testing. In addition to component evaluation, environmental tests on small coupons are conducted throughout the flight evaluation program. These tests generally include outdoor and controlled laboratory exposure tests, thermal cycling, and exposure at airline terminals and at Langley Research Center.

This Document Provided by the ABBOTT Aerospace
TECHNICAL LIBRARY
ABBOTTAEROSPACE.COM

Component Description

The composite components currently being evaluated in the NASA flight service programs are shown in Figure 1. All components shown have been in service except for the Bell 206L helicopter doors and fairing which are being fabricated. Details of the current and planned flight service evaluation components are shown in Figure 2. The first flight service program involved reinforcement of a U.S. Army CH-54B helicopter tail cone with unidirectional boron/epoxy [1 and 2]. Boron/epoxy strips bonded to the tail cone stringers increased the tail cone stiffness and reduced the structural mass by 14 percent. Eighteen Kevlar/epoxy fairings are being evaluated on three Lockheed L-1011 aircraft [7 and 8]. Solid laminate and Nomex honeycomb sandwich panels were installed as a direct replacement for production fiberglass parts. An average mass saving of 26.8 percent compared to the fiberglass panels was achieved.

The largest number of components is being evaluated on Boeing 737 aircraft [9 and 10]. One hundred and eight graphite/epoxy spoilers have been installed in sets of four by six different commercial airlines on 27 aircraft for worldwide flight service. The spoilers are constructed with graphite/epoxy upper and lower skins, corrosion resistant aluminum honeycomb core, aluminum spar and hinge assemblies, and fiberglass closure ribs. The finished spoilers are 35 percent composite and are 16.9 percent lighter than the standard production aluminum spoilers. Two boron/epoxy-reinforced aluminum center-wing boxes are in service with the U.S. Air Force on C-130 transport aircraft [3 to 6]. Boron/epoxy bonded to the covers on both the wing planks and hat-section stringers resulted in an increased fatigue life and a 10 percent mass saving. Three boron/aluminum aft pylon skin panels are in service on three DC-10 aircraft [11]. These panels are subjected to elevated temperatures and high-intensity acoustic loading as a result of their proximity to the center engine. A mass saving of 27.3 percent compared to baseline titanium was achieved.

Nine graphite/epoxy DC-10 upper aft rudders are in service on seven commercial airlines [12 and 13]. These multi-rib stiffened rudders weigh 32.9 percent less than standard production aluminum rudders. An important aspect of the DC-10 graphite/epoxy rudder program was the development of a cost competitive manufacturing procedure to allow a single oven cure cycle for the total structural box. The process selected is identified as the "trapped rubber" process and is shown in Figure 3. The process begins with the layup and densification of the right and left side skin panels and preforming the spars and ribs. The front spar web has lightening holes that permit the spar to fit over internal metal mandrels of the tool. The mandrels are centered in the cavity formed by adjacent ribs and the skins. Each mandrel is surrounded by carefully sized blocks of silicone rubber that fill each cavity. Once all the ribs are located, the outer skins are installed and heavy steel plates are attached to the tool to form a closed system. The tool is rolled into an oven where temperature is increased at specified rates and the rubber expands against the graphite/epoxy to develop the desired cure pressures. Once the cure cycle is completed, the tools and silicone rubber are removed and the finished structural box is ready for installation of standard aluminum alloy hinges and actuator fittings and the standard glass/epoxy leading and trailing edge members and tip assembly. Additional details on these NASA flight service components can be found in [14].

The most recent flight service program involves installing 40 shipsets of Kevlar/epoxy doors and fairings on Bell 206L commercial helicopters. The composite components are being fabricated and flight service will begin in late 1980. Three design concepts - stiffened foam sandwich, stiffened skin, and honeycomb sandwich - as shown in Figure 4, will be evaluated. An overall mass saving of 25.9 percent compared to the production components is estimated. The helicopters will operate in diverse environments in Alaska, Canada, and the U.S. Gulf Coast. Coupons exposed to ground and flight environments will be tested at specified intervals to determine effects of the various helicopter operating environments on material strength. Also, selected components will be removed from service and tested to failure to compare residual strength with original strength.

Sikorsky Aircraft has committed to extensive use of secondary and primary Kevlar/epoxy and graphite/epoxy structural composites in their S-76 commercial helicopter. NASA Langley Research Center and Sikorsky are planning a joint program to determine the long-term durability of composite components on the S-76. The objective of the NASA/Sikorsky program is to determine the effects of realistic operational service environments on typical composite helicopter structures. Fourteen tail rotors and four horizontal stabilizers such as those shown in Figure 5 will be removed from helicopters after up to 10 years of operational service. The tail rotor has a laminated graphite/epoxy spar with a glass/epoxy skin. The horizontal stabilizer has a Kevlar/epoxy torque tube with graphite/epoxy spar caps, full-depth honeycomb sandwich core, and Kevlar/epoxy skins. The two composite components have a total mass of 24.7 kg. Static and fatigue tests will be conducted on the components removed from service and the results will be compared with baseline certification test results. In addition, several hundred composite coupons exposed to the outdoor environment will be tested for comparison with the component test results.

THIS DOCUMENT PROVIDED BY THE ABBOTT AEROSPACE
TECHNICAL LIBRARY
ABBOTTAEROSPACE.COM

Flight Service Summary

A total of 142 composite components have been in flight service with 17 different operators, including foreign and domestic airlines, the U.S. Army, and the U.S. Air Force. The NASA flight service program was initiated in 1972 to determine the long-term durability of boron, Kevlar, and graphite composites in realistic flight environments. Nearly two million component flight hours have been accumulated with the high time aircraft having 17,718 hours as shown in Figure 6. The boron/epoxy reinforcement in the CH-54B helicopter has been in service the longest, over 7 years, but it has been flown very little compared to the other types of aircraft. This CH-54B helicopter was removed from flight service in October 1979 when it was damaged by a tornado. The graphite/epoxy in one of the DC-10 upper aft rudders has been acquiring flight service time at the greatest rate of any of the components listed in Figure 6, a rate of over 300 hours per month. The graphite/epoxy in the 108 spoilers on the Boeing 737 airlines has accumulated the greatest total component flight hours, 1,438,000 in 6 1/2 years. The high-time spoiler has 17,500 flight hours and approximately two-thirds of the spoilers have accumulated over 10,000 flight hours.

The large number of spoilers with graphite/epoxy skins allows planned retrievals from flight service without seriously impairing the total exposure. Six spoilers are selected at random for removal from service annually, two of each of three material systems used in fabricating the spoilers. These spoilers are shipped to Boeing for ultrasonic inspection. Three of the spoilers are returned to service after inspection and three are tested to failure to compare residual strengths with the strength of 16 new spoilers that were tested early in the program. Results of these tests are shown in Figure 7. After 5 years of service, the strengths for the individual spoilers generally fall within the same scatter band as was defined by strengths of the new spoilers. These results indicate essentially no degradation in strength after the 5 year period of service.

In addition to structural tests of the spoilers, tests are conducted to determine absorbed moisture content of the graphite/epoxy skins. The moisture content in the graphite/epoxy spoilers is determined from plugs cut near the trailing edge as shown in Figure 8. The plugs consist of aluminum honeycomb core, two graphite/epoxy face sheets, two layers of epoxy film adhesive, and two exterior coats of polyurethane paint. About 90 percent of the plug mass is in the composite faces, including the paint and adhesive. The moisture content is determined by drying the plugs and recording the mass change. The data shown in Figure 8 for plugs removed from three spoilers after 5 years service indicate moisture levels in the graphite/epoxy skins ranging from 0.66 to 0.75 percent for T300/5209, T300/2544, and AS/3501 material systems. Apparently, these moisture levels have not effected the room temperature strengths of the spoilers as shown in Figure 7.

Inspection and Maintenance

The composite components in the NASA flight service evaluation program are being inspected at periodic intervals to check for damage, defects, or repairs that may occur during normal aircraft operation. The maintenance data shown in Figure 9 were reported by the aircraft manufacturers who fabricated the various components. The composite components are being inspected by the aircraft operators and manufacturers and in most cases both visual and ultrasonic inspection methods are being used.

Minor disbonds have been found under small portions of the CH-54B boron/epoxy reinforcement. These disbonds were small and did not require repair. The Kevlar/epoxy fairings on the L-1011 aircraft are visually inspected annually. Minor impact damage from equipment and foreign objects has been noted on the wing-to-body Nomex honeycomb sandwich fairings. Fiber fraying, characteristic of Kevlar, and fastener hole elongations have been noted on all the Kevlar/epoxy fairings but no repair has been required. The 737 graphite/epoxy spoilers are inspected annually by Boeing and any defective spoilers are returned to Boeing for repair. Infrequent minor damage has occurred which included a mechanical interference problem and front spar exfoliation-corrosion damage. The spar exfoliation-corrosion was caused by accidental breaching of the corrosion-inhibiting system prior to final bonding of the graphite/epoxy skins during the fabrication process. Visual, ultrasonic, and destructive testing have found no evidence of moisture migration into the aluminum honeycomb core and no core corrosion.

The boron/epoxy-reinforced C-130 wing boxes are inspected every 6 months and no defects have been detected after more than 5 years of service. The boron/aluminum aft pylon skins on the DC-10 aircraft are inspected annually and minor surface corrosion has been reported on one panel. This corrosion is believed to have been caused by improper surface preparation during fabrication of the panels. The graphite/epoxy rudders on the DC-10 are visually inspected every 3 months and ultrasonically inspected every 12 months. Minor honeycomb-to-skin disbonds have been detected on two rudders but repairs are not required. These minor disbonds may have been caused by thermal stresses during cooldown after the manufacturing cure cycle. Overall, excellent performance has been achieved with the NASA flight service composite components.

This Document Provided by the ABBOTT AEROSPACE
TECHNICAL LIBRARY
ABBOTTAEROSPACE.COM

AIRCRAFT COMPANY FLIGHT SERVICE PROGRAMS

Component Description

The U.S. commercial aircraft manufacturers have installed numerous advanced composite components on aircraft for flight service evaluation. The objective of these programs is to determine the reliability and maintainability of composite components under normal airline fleet conditions. The composite components developed by the U.S. commercial transport manufacturers are indicated in Figure 10. Some of the components were designed as direct replacements for production fiberglass parts while other components were new designs to replace metal production parts.

Boeing has installed about 118 m^2 of graphite/epoxy floor panels on each of 30 B-747 aircraft. These panels have a mass of 312.5 kg which represents a mass saving of 30.8 percent compared to production fiberglass panels. Boeing also has two boron/epoxy foreflaps installed on B-707 aircraft. The foreflap as shown in Figure 11 is an aluminum honeycomb monocoque shell which replaced the rib-and-skin production design. The shell structure is closed out with fiberglass end ribs and titanium plates for attachment to the flap carriage. A mass saving of 25.3 percent was achieved.

The Douglas Aircraft Company has designed and fabricated several graphite and Kevlar composite components for service on DC-9 and DC-10 aircraft. Sketches of some of the components are shown in Figure 12. The types of structures being evaluated include panels, beams, doors, and engine nacelle structures. The largest component is a Kevlar/epoxy nose cowl for the DC-9 which has a mass of 73.9 kg. The cowl has a Kevlar/epoxy outer barrel with an aluminum honeycomb sandwich inner barrel for a mass saving of 26.6 percent.

The Lockheed California Company has made extensive applications of Kevlar/epoxy on their L-1011-500 aircraft. As shown in Figure 13, numerous fiberglass parts have been replaced by 1134 kg of Kevlar/epoxy for an average mass saving of 24.4 percent. Most of the applications are for secondary components such as panels, doors, trailing edge wedges, and fairings. In addition, numerous interior structures such as ceiling panels and stowage compartments are fabricated with Kevlar composites. Lockheed has four large graphite/epoxy cowl doors installed on L-1011 aircraft. These doors, shown in Figure 14, have graphite/epoxy skins with aluminum honeycomb core. These doors were developed by Rolls-Royce for the L-1011 engines and production is planned for early 1980. A set of doors has a mass of 94.3 kg which represents a 22.1 percent mass saving compared to the aluminum production doors. Lockheed also has a small laminated I-beam floor post in service on an L-1011 aircraft which represents a 23.5 percent mass saving.

Flight Service Summary

As indicated in Figure 15, the 56 company-developed composite components currently in service on a variety of commercial transport aircraft have accumulated over 600,000 flight hours. Boeing has accumulated 496,000 successful flight hours during the last 9 years on graphite/epoxy floor panels installed on 30 B-747 aircraft. Similar floor panels are now provided as customer options to save considerable mass compared to the standard fiberglass floor panels. Douglas has accumulated about 45,000 component flight hours on their DC-9 and DC-10 composite components. The high-time component is the Kevlar/epoxy nose cowl on the DC-9 which was installed in 1976 and has 9,000 flight hours. Lockheed started delivery of their L-1011-500 aircraft in April 1979; hence, not many flight hours have been accumulated on their Kevlar/epoxy production components. However, these components are expected to accumulate about 2,500 flight hours per year. Lockheed has accumulated almost 10,000 hours on four graphite/epoxy cowl doors and almost 18,000 hours on a graphite/epoxy floor post.

The aircraft companies have reported excellent service performance with all their composite components. The success of the NASA and industry flight service programs has led to large commitments of secondary composite components on future commercial aircraft. Continued success of these programs will lead to the introduction of primary composite components in the commercial airline fleet which will translate into improved fuel economy.

COMPOSITES ON COMMERCIAL HELICOPTERS

The commercial helicopter industry is starting to make use of advanced composites to save structural mass and thus increase helicopter range and payload. Sikorsky Aircraft has been the major user of advanced composites on both commercial and military helicopters. The most widely used composite material is Kevlar/epoxy, primarily because it costs less than graphite/epoxy. The Sikorsky S-76 commercial helicopter makes extensive use of Kevlar and graphite composite structure as shown in Figure 16. Over 115 kg of Kevlar/epoxy primary structure, secondary structure, and non-structural applications are currently in production on the S-76. Sikorsky chose Kevlar/epoxy because of its combination of mechanical properties, intermediate costs, and formability similar to fiberglass. Also, successful flight service experience of Kevlar/epoxy secondary structures on a Sikorsky CH-53D marine helicopter helped establish the necessary confidence required to enter into commercial production.

TECHNICAL LIBRARY
ABBOTTAEROSPACE.COM

Kevlar/epoxy components account for approximately 45 percent of the wetted external surface of the S-76. Applications include the horizontal stabilizer, main-rotor blade-tip caps, canopy, radome, cabin doors, forward and aft engine fairings above the cabin, landing gear and baggage compartment doors, and internal non-structural items. Graphite/epoxy and Kevlar/epoxy hybrids are used in selected components to improve strength and stiffness. Several of the composite components are shown in Figure 17. In most hybrid applications the graphite carries the primary bending loads and the Kevlar carries the shear loads. An example is shown in Figure 18 for a horizontal stabilizer where uniaxial graphite/epoxy carries bending loads in spar caps and cross-plied Kevlar/epoxy basically carries shear loads. The application of graphite/epoxy in the tail rotor spar takes advantage of the superior fatigue characteristics of this material for a primary, dynamic structural component. The composite components have been flying for over 2 years on three S-76 prototypes with no major malfunctions. The first commercial delivery of the S-76 helicopter was in February 1979. As of December 1979, 27 S-76 helicopters have been delivered and a total of 5450 successful flight hours have been accumulated on the composite components.

Boeing-Vertol has an extensive development program underway to place Kevlar and graphite composite components into production on Boeing 234 commercial helicopters. Primary emphasis is on extending the range of the helicopter through the use of Kevlar-graphite hybrid fuel pods as shown in Figure 19. Other graphite and Kevlar components include doors, fairings, cabin floor, and support beams. The Boeing 234 helicopter is scheduled to enter commercial service in early 1981.

Bell Helicopter is using advanced composites in crew seats on the Bell 222 commercial helicopter. The seat shown in Figure 20 uses Kevlar skins and aluminum honeycomb in sandwich construction for the bucket and a graphite/epoxy energy attenuator tube as part of the seat support structure. Twelve model 222 helicopters have been delivered with two lightweight energy-absorbing crew seats in each aircraft.

NASA AIRCRAFT ENERGY EFFICIENCY PROGRAM (ACEE)

Since 1975, NASA has been sponsoring an extensive program to improve the efficiency of current commercial transport aircraft through the development and application of several technologies that could reduce fuel consumption of new aircraft by up to 50 percent. Advanced composite structures alone have the potential to reduce fuel consumption by 10 to 15 percent. The broad objective of the composites part of this program is to conduct research to provide the technology and confidence so that commercial transport manufacturers can commit to production of composites in their future aircraft. Composites technology is being developed for large secondary structures and medium primary structures. As shown in Figure 21, the technology readiness dates are to make such commitments for secondary structures in the 1980-1985 time frame and for primary structures in 1985-1990. Verification of design methods and cost competitive manufacturing processes are required to determine technology readiness. Confidence in composite structures is being developed through durability tests that lead to warranty of the aircraft, cost verification through manufacture of multiple components in the production mode, FAA certification, and airline acceptance.

Composite Secondary Structures

Each of the three major U.S. commercial transport manufacturers are under contract to NASA to design, fabricate, and test major secondary composite components as shown in Figure 22. Douglas has completed fabrication of additional graphite/epoxy DC-10 upper aft rudders using cost-effective fabrication and tooling methods, Boeing has fabricated graphite/epoxy elevators for the B-727 and Lockheed is fabricating graphite/epoxy ailerons for the L-1011. Several shipsets of these components will be placed into airline service for evaluation.

All of the ACEE composite secondary components are large enough to present manufacturing problems that may be encountered in constructing many other aircraft structures. Details of the three graphite/epoxy secondary components are summarized in Figure 23. The L-1011 aileron is about 1.2 m wide by 2.4 m long and has a mass of 45.4 kg. The composite design features a syntactic-core sandwich with graphite/epoxy face sheets. The total number of ribs has been reduced from 18 for the aluminum aileron to 10 for the composite aileron, the number of parts has been reduced from 398 to 205, and the number of mechanical fasteners has been reduced from 5253 to 2574. A mass saving of 28.5 percent is projected for the composite aileron. Some of the construction details are shown in Figure 24 for an aileron located in the assembly fixture. The upper surface, ribs, and spars are permanently fastened using titanium fasteners, whereas, the lower surface, trailing edge wedge, and end fairings are attached with removable fasteners. Analysis indicates that the composite design is cost competitive with the production aluminum aileron. Twenty-two composite ailerons will be fabricated to establish a good basis for projecting costs. Upon completion of aileron fabrication and detailed manufacturing analysis, a production decision will be made by Lockheed.

The graphite/epoxy upper aft rudder for the DC-10 is 0.8 m wide by 4.0 m long and has a mass of 30.3 kg. The composite design features multi-rib construction with two spars. As discussed previously, the structural box is manufactured as a single cocured unit and represents a 26.8 percent mass saving compared to the production aluminum

TECHNICAL LIBRARY
ABBOTTAEROSPACE.COM

rudders. An additional 11 rudders have been manufactured under the ACEE program to develop more efficient manufacturing methods and to obtain quantitative cost data. The rudders have been FAA certified and Douglas is considering fleet production of the graphite/epoxy rudders for new DC-10 aircraft.

The graphite/epoxy elevator for the B-727 is 0.9 m wide by 5.8 m long and has a mass of 89.4 kg. The elevator design is dictated primarily by stiffness requirements and makes efficient use of graphite/epoxy Nomex honeycomb sandwich skins to carry normal pressure and in-plane shear loads. The upper and lower skins are attached to the substructure with titanium fasteners. With this design, most of the interior ribs used in the production elevators are eliminated and a mass saving of 23.6 percent has been achieved. Since the elevator is mass-balanced, additional mass saving can be effected through the use of graphite/epoxy. Eleven elevators have been fabricated to verify cost projections and FAA certification has been received. Five shipsets of graphite/epoxy elevators will be placed into airline service for evaluation. Four shipsets of assembled graphite/epoxy elevators are shown in Figure 25. Boeing is considering fabrication of up to 25 additional shipsets of elevators to establish manufacturing learning curves.

Composite Primary Structures

Each of the three major U.S. commercial transport manufacturers are also under NASA contract to design, fabricate, and test medium-sized primary composite components as shown in Figure 26. Douglas and Lockheed will fabricate graphite/epoxy vertical fins for the DC-10 and L-1011, respectively, and Boeing will build horizontal stabilizers for the B-737. The ACEE composite primary components are more complex than the secondary components and thus present a greater design and manufacturing challenge. Details of the three graphite/epoxy primary components are summarized in Figure 27.

The composite L-1011 vertical fin is about 2.7 m wide by 7.6 m long and has a mass of 272.2 kg. The structural configuration consists of cocured hat-stiffened skins, cocured I-beam stiffened front and rear spars, and multiple ribs. Using this design approach a mass saving of 30.1 percent is projected. The tooling for the stiffeners consists of inflatable silicone rubber bladders to provide internal pressure, exterior caul plates, and a vacuum bag. The entire skin panel is cured in an autoclave under pressure and elevated temperature. Upon completion of the cure, the inflatable bladders are easily removed from the stiffener cavity as shown in Figure 28. Three L-1011 fins will be fabricated to validate manufacturing cost projections.

The graphite/epoxy vertical stabilizer for the DC-10 is 2.4 m wide by 7.6 m long and has a mass of 350.3 kg. The design configuration selected for the DC-10 vertical fin consists of Nomex honeycomb sandwich skins, four I-beam spars with sine-wave webs, and multiple sine-wave ribs. Titanium lug fittings are cocured into the spar caps to provide root-end attachments. The ribs and spars are joined by adhesive bonded angle clips and the skins are mechanically fastened to the substructure with titanium bolts. A mass saving of 22.8 percent is projected using this design concept. Seven DC-10 vertical stabilizers will be fabricated to obtain manufacturing cost data.

The graphite/epoxy horizontal stabilizer for the Boeing 737 aircraft is 1.2 m wide by 5.2 m long and has a mass of 91.6 kg. The design selected consists of cocured integrally stiffened skins, laminated front and rear spars with titanium lug attachments, seven inboard Nomex honeycomb ribs, two closure ribs, and a laminated trailing-edge beam. The honeycomb ribs have cutouts to allow passage of the continuous skin stiffeners as shown in Figure 29. Assembly of the structural box is accomplished with titanium mechanical fasteners. With this design configuration, a mass saving of 22.9 percent is projected. Eleven B-737 horizontal stabilizers will be fabricated to verify predicted manufacturing learning curves.

Ancillary Test Plan

Numerous ancillary tests are being conducted by the ACEE contractors to verify design procedures, provide design allowables data, and provide data in support of certification requirements. The tests vary in size and difficulty from small static coupons to large combined-load subcomponents. Some of the tests are shown schematically in Figure 30. As indicated, mechanical tests such as panel compression, root-end load transfer, impact damage, rib-to-skin attachments, and lap joints are being conducted. Most of these tests are conducted at room temperature or at elevated temperature with and without moisture conditioning. Additional details of the NASA ACEE composite structures program can be found in [15].

NEAR-TERM PRODUCTION PLANS

Advanced composites technology has been developed to the point where U.S. commercial aircraft manufacturers are starting to make production commitments to these materials. Success of the flight service evaluation programs and technology developments under the NASA ACEE composites program has led Boeing to plan extensive use of advanced composites on their new B-767 aircraft. As shown in Figure 31, most of the control surfaces, including rudders, elevators, spoilers, and ailerons, will be built with graphite/epoxy composites. Graphite-Kevlar hybrids will be used in numerous structures

TECHNICAL LIBRARY
ABBOTTAEROSPACE.COM

such as leading and trailing edge panels, cowl components, landing gear doors, and fairings. Replacement of standard fiberglass parts with Kevlar and graphite composites will result in mass savings of up to 30 percent.

Lockheed has made extensive production commitments to Kevlar/epoxy secondary structures on the L-1011-500 as discussed previously. Design studies are currently underway to investigate potential graphite/epoxy structure applications on the L-1011 aircraft. Components being studied include the vertical fin, rudders, elevators, ailerons, flaps, doors, and floor beams and posts. As shown in Figure 32, graphite/epoxy applications being studied have a mass of 2560 kg which represents a 26 percent mass saving compared to the current production components. At the conclusion of these studies Lockheed will be in a position to make future production decisions provided the composite components are economically feasible.

Douglas is also conducting studies to determine the economic feasibility of committing to production of numerous composite components on their DC-10 aircraft. Some of the potential components as shown in Figure 33 include graphite/epoxy vertical stabilizers, rudders, elevators, spoilers, and ailerons. Other graphite/epoxy components include doors, panels, beams, and nacelle structure. Potential Kevlar/epoxy components include extensive fairings, tail cone, and nose cowl structure.

ENVIRONMENTAL EFFECTS ON COMPOSITES

In conjunction with the flight service evaluation of composite components, approximately 17,000 composite specimens are being tested to determine the long-term environmental effects on composites. Epoxy matrix composites inherently absorb moisture from the surrounding environment and ultraviolet radiation can attack the molecular structure of polymeric materials. This combination of moisture, elevated temperature, and ultraviolet radiation can reduce the mechanical properties of composite materials. Mechanical property tests are being conducted on small specimens to determine the effect of these environments on the strength of several composite material systems. Specimens are being exposed worldwide to outdoor ground environments, to indoor controlled laboratory environments, and real-time flight exposure.

The worldwide ground exposure specimens are mounted in racks which are deployed on roofs of airline buildings at a number of airports around the world to receive maximum exposure to the airport environment. Racks are located in Germany, Brazil, New Zealand, Hawaii, and several locations within the continental United States. The exposure racks contain several different graphite and Kevlar composite material systems. Figure 34 shows a typical exposure rack, the various specimen configurations and the worldwide exposure locations. Tests performed include short beam interlaminar shear, flexure, compression, and tension. Most of the deployed specimens are unstressed. However, three racks have been deployed with tensile specimens under sustained load. Two distinct sets of composite specimens have been deployed. One set is unpainted to provide maximum exposure of the matrix materials and a second set of specimens is painted with standard aircraft polyurethane paint to protect the matrix from direct ultraviolet radiation exposure. Specimens are periodically removed from the racks and shipped to NASA Langley for mechanical property testing. The specimens are weighed to determine mass changes associated with moisture absorption and weathering. The specimens are tested to failure to compare residual strengths with baseline control specimens with no prior environmental exposure. Specimens are removed from the racks for testing after 1, 3, 5, 7, and 10 years exposure.

The moisture contents for four graphite/epoxy material systems and two Kevlar/epoxy material systems have been determined after 3 years outdoor environmental exposure. Data shown in Figure 35 for specimens removed from racks at six different exposure sites indicate moisture contents ranging from about 0.5 percent to 2.0 percent. Additional moisture data will be collected after 5, 7, and 10 years exposure. The effects of absorbed moisture and ultraviolet radiation on composite mechanical properties have been determined after 5 years outdoor exposure at six locations. The room temperature residual flexure strengths for six composite materials are shown in Figure 36. Most of the test data fall within the scatter band for the baseline strength of unexposed specimens. These results indicate essentially no degradation in the flexure strength of the six composite materials after 5 years outdoor exposure. Results from shear and compression tests indicate strength reductions of up to 15 percent after 5 years exposure. Since these properties are more matrix dominated than are the flexure properties, shear and compression properties are normally more sensitive to absorbed moisture.

To consider the possible influence of constant stress during the outdoor exposure, tensile specimens are being exposed at NASA Langley Research Center and San Francisco Airport with a sustained stress of 40 percent of the original ultimate strength. Test results for T300/5208 graphite/epoxy laminates are shown in Figure 37. Quasi-isotropic laminated tensile specimens have been tested after 1, 3, and 5 years exposure for both stressed and unstressed conditions. Essentially no difference between strength of stressed and unstressed specimens and no degradation in tensile strength was found for any condition.

This Document Provided by the ABBOTT AEROSPACE
TECHNICAL LIBRARY
ABBOTTAEROSPACE.COM

Another type of environmental exposure that must be considered is the interaction of composite materials with long-term exposure to aircraft fuels and hydraulic fluids. Under NASA contract, the Boeing Company is conducting a series of exposures of composite materials to JP-4 jet fuel, Skydrol, fuel-and-water mixture, and a fuel-and-air cyclic environment. Results for T300/5209 tensile specimens with [±45°] ply orientations are shown in Figure 38. A maximum degradation of 10 percent in the tensile strength occurred after 5 years exposure to the fuels and fluids indicated. However, Kevlar/2544 exhibited a 40 percent loss in short beam shear strength when exposed to fuel/water immersion.

The most recent NASA Langley Research Center environmental exposure program involves flight exposure of composite specimens on scheduled airlines. Moisture absorption in flight is being determined for composite specimens mounted on the Boeing 737 aircraft. Unstressed exterior exposure is obtained with specimens mounted on the top and bottom surfaces of the flap track fairing cone as shown in Figure 39. Interior stressed and unstressed exposure is obtained with specimens mounted in an aft fuselage vented compartment. The exterior specimens were deployed first and moisture absorption data have been obtained after 18 months of flight exposure. Composite mass change for three graphite/epoxy material systems is shown in Figure 40 for specimens removed from the exterior surface of three commercial airlines which operate in distinct climatic conditions. Specimen mass varied with seasonal weather variations, with mass change being more pronounced in the temperate regions having wide seasonal variations than in the tropical region having a more uniform year-round climate. The T300/5209 system experienced somewhat less mass gain than did the T300/5208 and AS/3501 systems. Maximum mass gain in any climate was only slightly greater than one percent. Mass changes such as these result from moisture absorption, drying, and ultraviolet radiation, all of which could have cumulative damaging effects on composites. These tests will be conducted over a period of several years to determine saturation levels and the repetitive nature of the seasonal variations. The results of these tests will be compared with outdoor ground environmental test results and indoor controlled laboratory results. Methodologies for predicting environmental behavior are being systematically developed during a comprehensive 10-year program. Additional details of the NASA Langley environmental effects programs can be found in [16].

CONCLUDING REMARKS

Excellent experience has been achieved with approximately 200 composite components in flight service for 2.5 million total component hours.

No significant degradation has been observed in residual strength of composite components or environmental exposure specimens after 5 years service or exposure.

Technology is being developed that will lead to extensive production of advanced composites in future aircraft.

Confidence in advanced composites technology is being developed to the extent that commercial transport and helicopter manufacturers have made production commitments to composites for selected components.

REFERENCES

1. Welge, R. T.: Application of Boron/Epoxy Reinforced Aluminum Stringer for the CH-54B Helicopter Tail Cone. Phase I: Design, Analysis, Fabrication, and Test. Sikorsky Aircraft, United Aircraft Corporation, NASA CR-111929, July 1971.

2. Welge, R. T.: Application of Boron/Epoxy Reinforced Aluminum Stringers and Boron/Epoxy Skid Gear for the CH-54B Helicopter Tail Cone. Phase II: Fabrication, Inspection, and Flight Test. Sikorsky Aircraft, United Aircraft Corporation, NASA CR-112101, July 1972.

3. Harvill, W. E.; Kays, A. O.; Young, E. C.; and McGee, W. M.: Program for Establishing Long-Time Flight Service Performance of Composite Materials in the Center Wing Structure of C-130 Aircraft. Phase I - Advanced Development. Lockheed-Georgia Company, NASA CR-112126, September 1972.

4. Harvill, W. E.; Duhig, J. J.; and Spencer, B. R.: Program for Establishing Long-Time Flight Service Performance of Composite Materials in the Center Wing Structure of C-130 Aircraft. Phase II - Detailed Design. Lockheed-Georgia Company, NASA CR-112272, April 1973.

5. Harvill, W. E.; and Kays, A. O.: Program for Establishing Long-Time Flight Service Performance of Composite Materials in the Center Wing Structure of C-130 Aircraft. Phase III - Fabrication. Lockheed-Georgia Company, NASA CR-132495, September 1974.

TECHNICAL LIBRARY
ABBOTTAEROSPACE.COM

6. Harvill, W. E.; and Kizer, J. A.: Program for Establishing Long-Time Flight Service Performance of Composite Materials in the Center Wing Structure of C-130 Aircraft. Phase IV - Ground/Flight Acceptance Tests. Lockheed-Georgia Company, NASA CR-145043, September 1976.

7. Wooley, J. H.; Paschal, D. R.; and Crilly, E. R.: Flight Service Evaluation of PRD-49/Epoxy Composite Panels in Wide-Bodied Commercial Transport Aircraft. Lockheed-California Company, NASA CR-112250, March 1973.

8. Stone, R. H.: Flight Service Evaluation of Kevlar-49/Epoxy Composite Panels in Wide-Bodied Commercial Transport Aircraft. Lockheed-California Company, NASA CR-159071, March 1979.

9. Stoecklin, Robert L.: A Study of the Effects of Long Term Ground and Flight Environment Exposure on the Behavior of Graphite/Epoxy Spoilers - Manufacturing and Test. The Boeing Company, NASA CR-132682, June 1975.

10. Stoecklin, Robert L.: 737 Graphite Composite Flight Spoiler Flight Service Evaluation. Boeing Commercial Airplane Company, Fourth Annual Report, NASA CR-158933, August 1978.

11. Elliot, S. Y.: Boron/Aluminum Skins for the DC-10 Aft Pylon. Douglas Aircraft Corporation, NASA CR-132645, May 1975.

12. Lehman, George M., et al: Advanced Composite Rudders for DC-10 Aircraft - Design, Manufacturing, and Ground Tests. McDonnell Douglas Corporation, NASA CR-145068, November 1976.

13. Lehman, G. M.: Flight-Service Program for Advanced Composite Rudders on Transport Aircraft. First Annual Summary Report, McDonnell Douglas Corporation, NASA CR-145385, July 1977.

14. Heldenfels, R. R.: Recent NASA Progress in Composites. NASA TM X-72713, August 1975.

15. Vosteen, Louis F.: Composite Structures for Commercial Transport Aircraft. NASA Technical Memorandum 78730, June 1978.

16. Pride, Richard A.: Environmental Effects on Composites for Aircraft. NASA Technical Memorandum 78716, May 1978.

ACKNOWLEDGEMENT

Portions of the data reported herein were obtained from U.S. commercial transport aircraft and helicopter manufacturers. Several NASA researchers participated in developing the data reported for the NASA composites program. The author gratefully acknowledges these contributions.

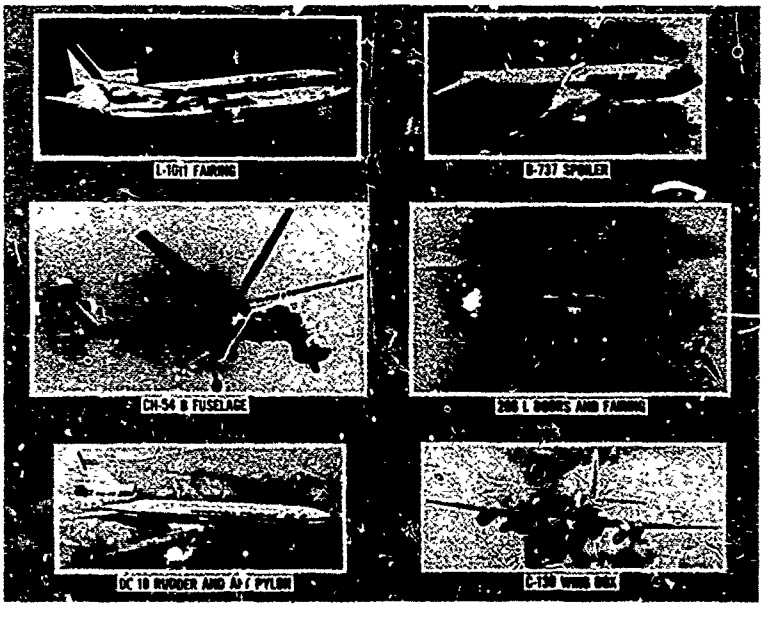

Figure 1. NASA flight service composite components.

TECHNICAL LIBRARY
ABBOTTAEROSPACE.COM

COMPONENT	COMPOSITE MATERIAL	STRUCTURAL CONFIGURATION	BASELINE MASS, kg	COMPOSITE MASS, kg	MASS SAVINGS, %
CH-54B TAIL CONE	BORON/EPOXY	REINF. AL	209.5	180.1	14.0
L-1011 FAIRINGS	KEVLAR/EPOXY	NOMEX H/C AND SOLID LAMINATE	13.8	10.1	26.8
B-737 SPOILER	GRAPHITE/EPOXY AND GLASS/EPOXY	AL H/C SAND.	7.1	5.9	16.9
C-130 CENTER WING BOX	BORON/EPOXY	REINF. AL	2240.0	2017.0	10.0
DC-10 AFT PYLON SKIN	BORON/ALUMINUM	SOLID LAMINATE	2.2	1.6	27.3
DC-10 UPPER AFT RUDDER	GRAPHITE/EPOXY AND GLASS/EPOXY	RIB-STIFFENED SKIN	41.4	27.8	32 9
206L DOORS AND FAIRING	KEVLAR/EPOXY	NOMEX H/C, STIFFENED SKIN, AND FOAM SAND.	10.8	8.0	25.9
S-76 TAIL ROTOR AND HORIZ. STAB.	GRAPHITE/EPOXY, KEVLAR/EPOXY, AND GLASS/EPOXY	SOLID LAMINATE AND NOMEX H/C SAND.	24.7	24.7	N/A

Figure 2. Details of NASA flight service components.

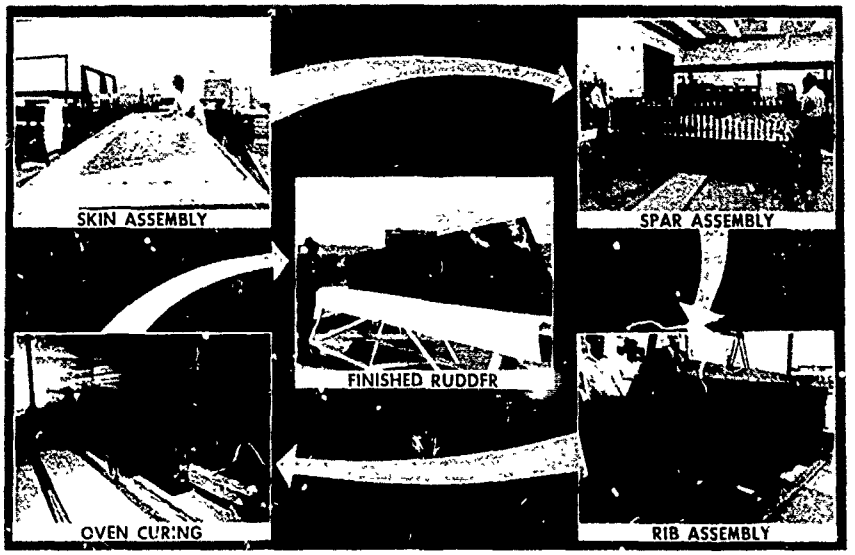

Figure 3. DC-10 upper aft rudder manufacturing sequence.

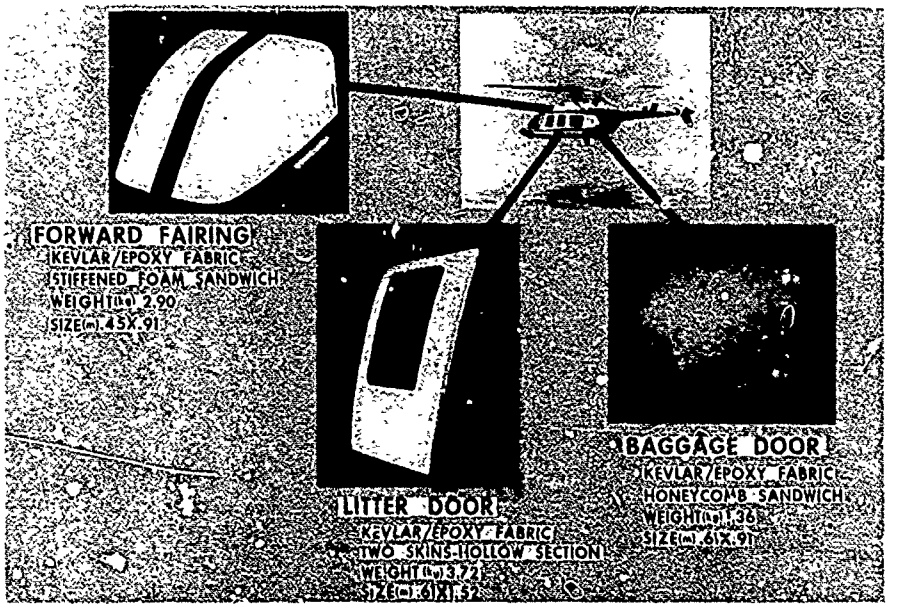

Figure 4. Bell 206L helicopter composite components.

TECHNICAL LIBRARY
ABBOTTAEROSPACE.COM

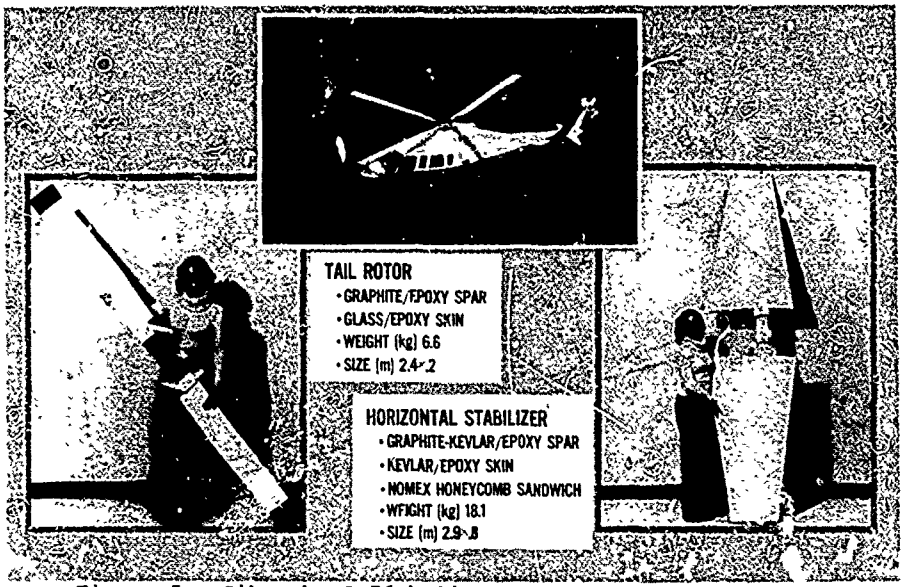

Figure 5. Sikorsky S-76 helicopter composite components.

AIRCRAFT, COMPONENT	TOTAL COMPONENTS	START OF FLIGHT SERVICE	CUMULATIVE FLIGHT HOURS	
			HIGH TIME AIRCRAFT	TOTAL COMPONENT
CH-54B TAIL CONE	1	MARCH 1972	1,140	1,140
L-1011 FAIRING PANELS	18	JANUARY 1973	17,718	282,870
737 SPOILER	108	JULY 1973	17,500	1,438,000
C-130 CENTER WING BOX	2	OCTOBER 1974	3,840	7,650
DC-10 AFT PYLON SKIN	3	AUGUST 1975	11,880	35,300
DC-10 UPPER AFT RUDDER	10	APRIL 1976	14,470	92,800
SPAND TOTAL	142			1,857,760

Figure 6. NASA composite structures flight service summary.

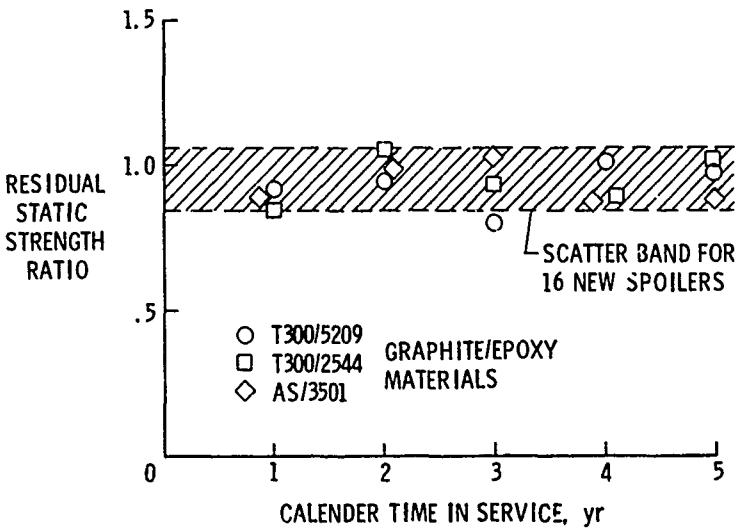

Figure 7. Residual strength of graphite/epoxy spoilers.

TECHNICAL LIBRARY
ABBOTTAEROSPACE.COM

5 YEARS SERVICE

GRAPHITE/EPOXY	MOISTURE CONTENT, PERCENT
T300/5209	0.67
T300/2544	0.66
AS/3501	0.75

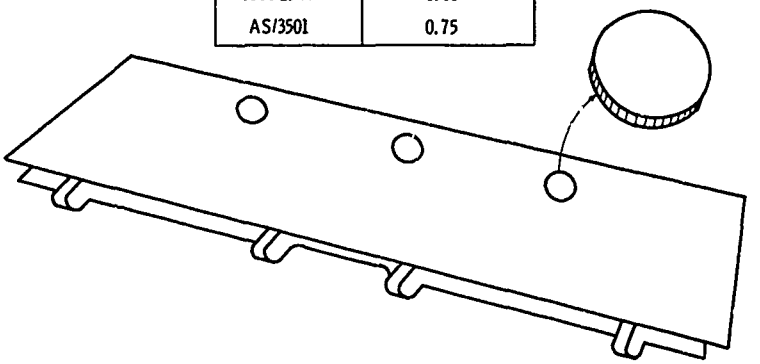

Figure 8. Spoiler moisture levels determined from plugs.

COMPONENT	INSPECTION INTERVAL, months	INSPECTION METHODS	STATUS
CH-54B TAIL CONE	2	VISUAL ULTRASONIC	MINOR DISBONDS NO REPAIR REQUIRED
L-1011 FAIRING PANELS	12	VISUAL	MINOR IMPACT DAMAGE, FIBER FRAYING AND HOLE ELONGATIONS
737 SPOILER	12	VISUAL ULTRASONIC	INFREQUENT MINOR DAMAGE REPAIRED AT BOEING
C-130 CENTER WING BOX	6	VISUAL ULTRASONIC	NO DEFECTS AFTER MORE THAN 5 YEARS SERVICE
DC-10 AFT PYLON SKIN	12	VISUAL	MINOR SURFACE CORROSION ON ONE SKIN
DC-10 UPPER AFT RUDDER	3, 12	VISUAL ULTRASONIC	MINOR RIB-TO-SKIN DISBOND ON TWO RUDDERS

Figure 9. NASA composite component inspection and maintenance results.

COMPONENT	COMPOSITE MATERIAL	STRUCTURAL CONFIGURATION	*BASELINE MASS, kg	*COMPOSITE MASS, kg	MASS SAVINGS, %
B-747 FLOOR PANELS	GRAPHITE/EPOXY	NOMEX H/C SAND.	451.3	312.5	30.8
B-707 FOREFLAP	BORON/EPOXY	AL H/C MONOCOQUE SHELL	9.1	6.8	25.3
DC-10 VERT. STAB. T.E. PANEL	GRAPHITE/EPOXY	HAT-STIFFENED	1.0	0.8	20.0
DC-10 FLOOR BEAM	GRAPHITE/EPOXY	LAMINATED J-SECTION	14.5	10.9	24.8
DC-9 COWL DOOR	KEVLAR/EPOXY & GRAPHITE/EPOXY	AL H/C FRAME STIFFENED	65.3	50.4	22.8
DC-9 NOSE COWL	KEVLAR/EPOXY	AL H/C INNER BARREL	100.7	73.9	26.6
DC-9 TAIL CONE	KEVLAR/EPOXY	NOMEX H/C SAND	34.0	27.7	18.5
L-1011 PANELS, DOORS, T.E. WEDGES & FAIRINGS	KEVLAR/EPOXY	NOMEX H/C SAND. & SOLID LAM.	1500.0	1134.0	24.4
L-1011 COWL DOOR	GRAPHITE/EPOXY	AL H/C SAND.	121.1	94.3	22.1
L-1011 FLOOR POST	GRAPHITE/EPOXY	LAMINATED I-BEAM	1.7	1.3	23.5

*COMPONENT MASS PER AIRCRAFT

Figure 10. Details of aircraft company composite components.

THIS DOCUMENT PROVIDED BY THE ABBOTT AEROSPACE
TECHNICAL LIBRARY
ABBOTTAEROSPACE.COM

Figure 11. Boeing 707 boron/epoxy foreflap.

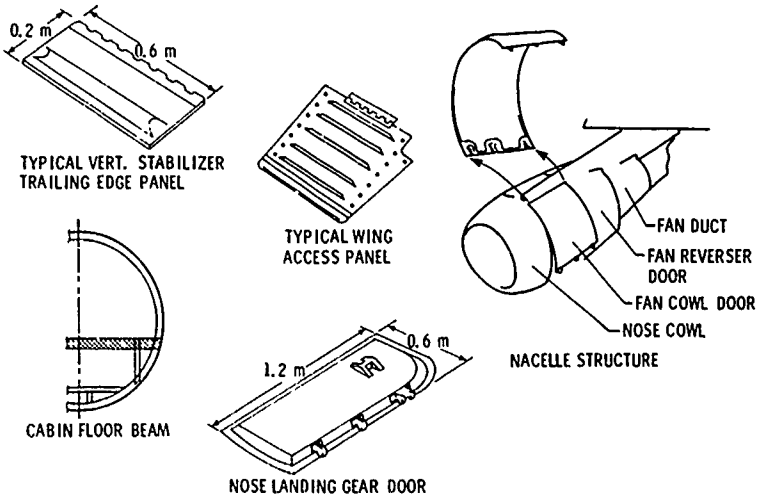

Figure 12. Douglas flight service composite components.

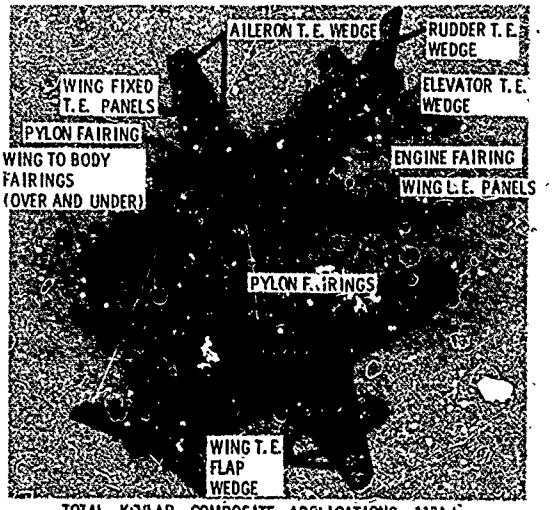

Figure 13. Lockheed L-1011 Kevlar/epoxy composite applications.

TECHNICAL LIBRARY
ABBOTTAEROSPACE.COM

Figure 14. Lockheed L-1011 graphite/epoxy cowl door.

COMPONENT	TOTAL COMPONENTS	START OF FLIGHT SERVICE	CUMULATIVE FLIGHT HOURS	
			HIGH TIME AIRCRAFT	TOTAL COMPONENT
B-747 FLOOR PANELS	30 A/C	APRIL 1970	33,000	496,000
B-707 FOREFLAP	2	MAY 1970	17,500	35,000
DC-10 VERT. STAB. T.E. PANEL	5	JANUARY 1978	5,340	22,400
DC-10 FLOOR BEAM	3	MAY 1979	1,500	2,600
DC-9 COWL DOOR	4	AUGUST 1978	3,500	10,300
DC-9 NOSE COWL	1	MAY 1976	9,000	9,000
L-1011 PANELS, DOORS T.E. WEDGES & FAIRINGS	6 A/C	APRIL 1979	1,890	8,160
L-1011 COWL DOOR	4	DECEMBER 1978	2,600	9,680
L-1011 FLOOR POST	1	JANUARY 1972	17,900	17,900
GRAND TOTAL	56			611,040

Figure 15. Flight service summary of aircraft company composite components.

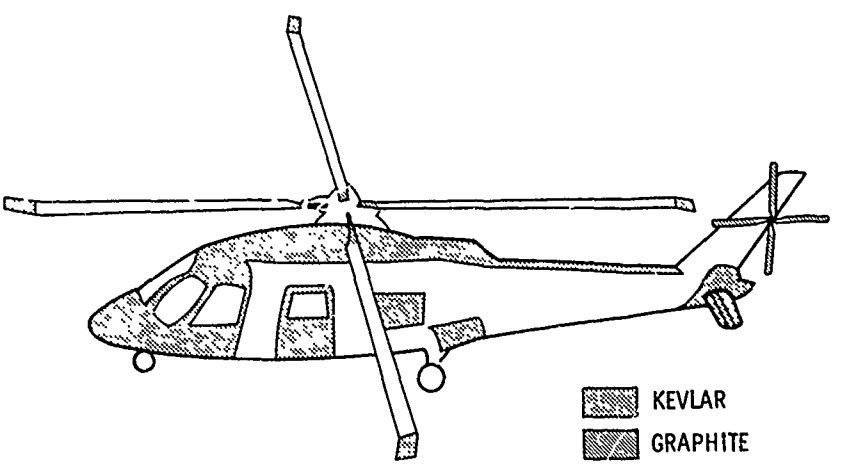

Figure 16. Sikorsky S-76 helicopter composite applications.

TECHNICAL LIBRARY
ABBOTTAEROSPACE.COM

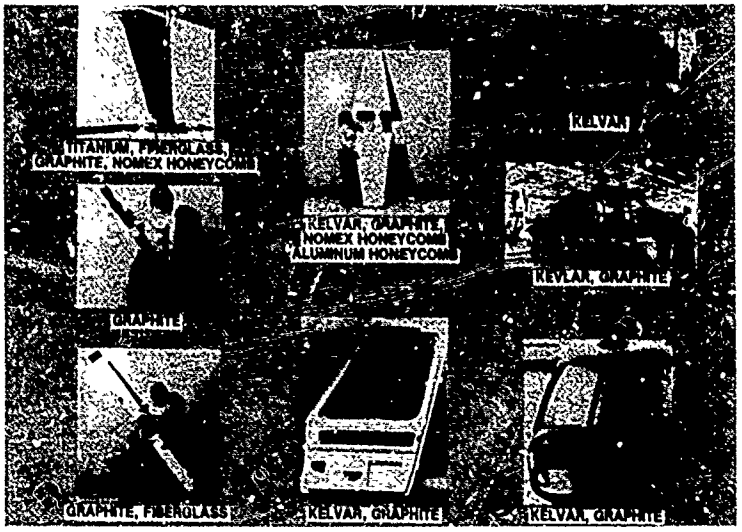

Figure 17. S-76 composite applications.

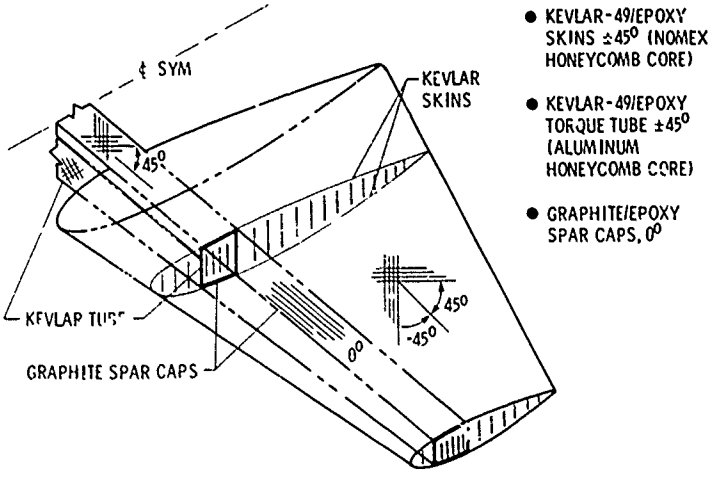

Figure 18. S-76 composite horizontal stabilizer.

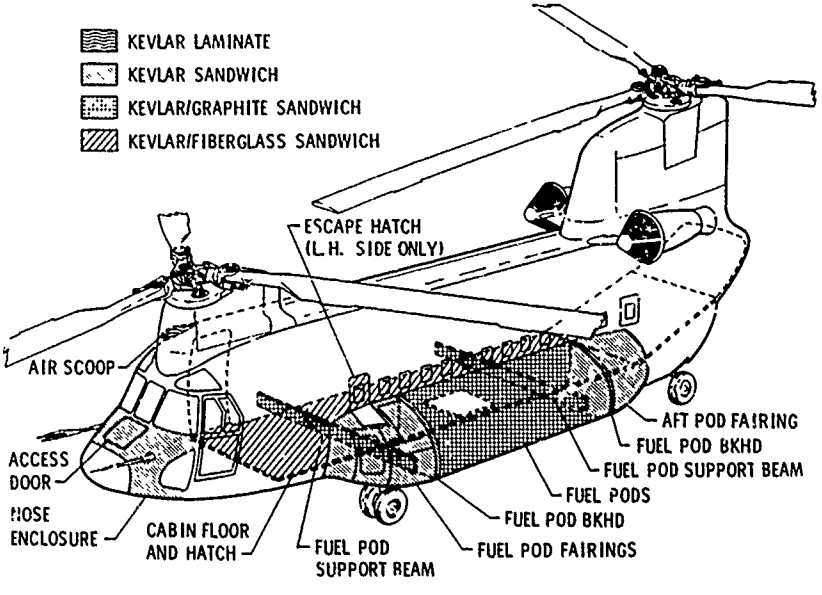

Figure 19. Boeing 234 helicopter composite applications.

THIS DOCUMENT PROVIDED BY THE ABBOTT AEROSPACE
TECHNICAL LIBRARY
ABBOTTAEROSPACE.COM

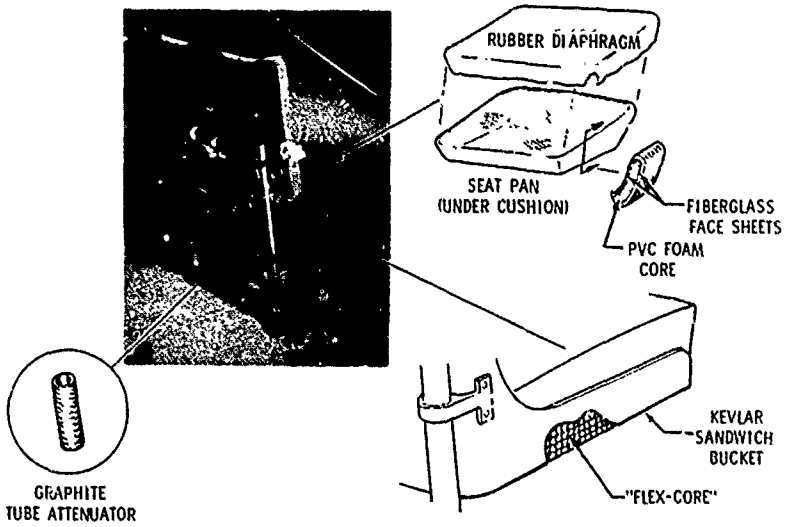

Figure 20. Bell 222 composite crew seat.

OBJECTIVE

PROVIDE THE **TECHNOLOGY** AND **CONFIDENCE** SO THAT COMMERCIAL TRANSPORT MANUFACTURERS CAN COMMIT TO PRODUCTION OF COMPOSITES IN THEIR FUTURE AIRCRAFT:

SECONDARY STRUCTURE - 1980 TO 1985

PRIMARY STRUCTURE - 1985 - 1990

TECHNOLOGY

- DESIGN CRITERIA, METHODS AND DATA
- QUALIFIED DESIGN CONCEPTS
- COST COMPETITIVE MANUFACTURING PROCESSES

CONFIDENCE

- DURABILITY/WARRANTY
- QUANTITY COST VERIFICATION
- FAA CERTIFICATION
- AIRLINE ACCEPTANCE

Figure 21. NASA ACEE composite program.

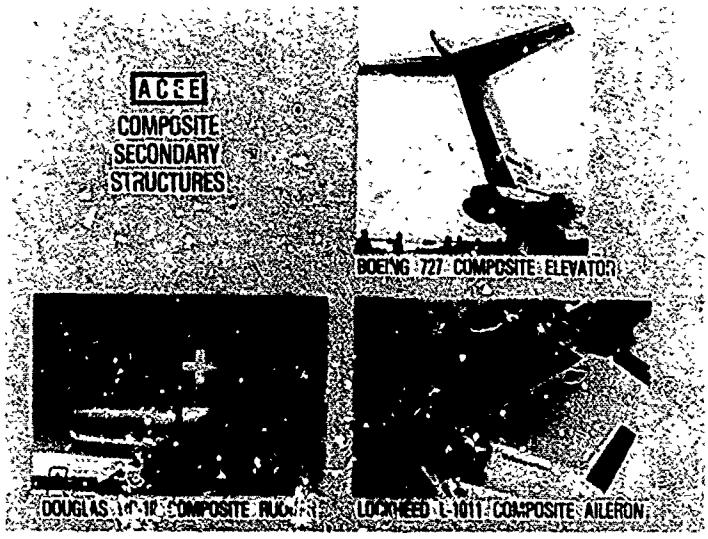

Figure 22. NASA ACEE composite secondary structures.

TECHNICAL LIBRARY
ABBOTTAEROSPACE.COM

COMPONENT	L-1011 AILERON	DC-10 RUDDER	B-727 ELEVATOR
SIZE, m	1.2 × 2.4	0.8 × 4.0	0.9 × 5.8
BASELINE METAL MASS, kg	63.5	41.4	117.0
COMPOSITE MASS, kg	45.4	30.3	89.4
MASS SAVING, %	28.5	26.8	23.6
QUANTITY TO BE FABRICATED	22	11*	11*
CERTIFICATION	MID-1980	YES	YES
PRODUCTION	UNCERTAIN	PENDING	UNCERTAIN

*FABRICATION COMPLETED

Figure 23. Details of NASA ACEE composite secondary components.

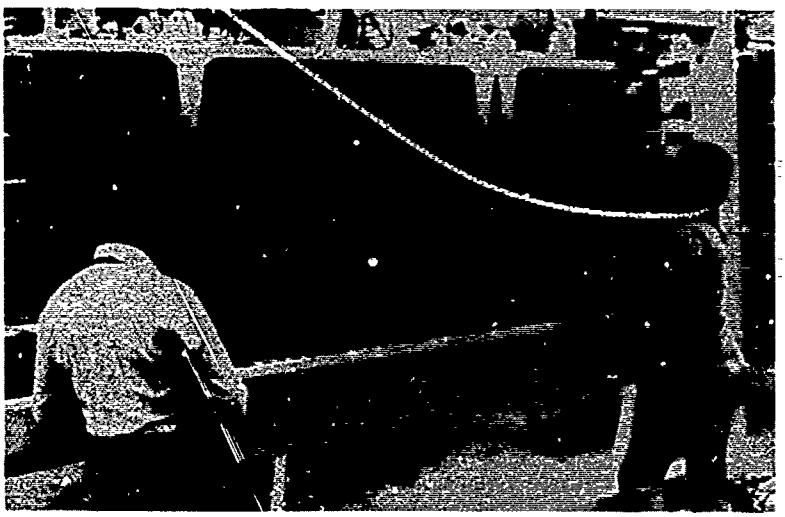

Figure 24. Assembly of Lockheed L-1011 composite aileron.

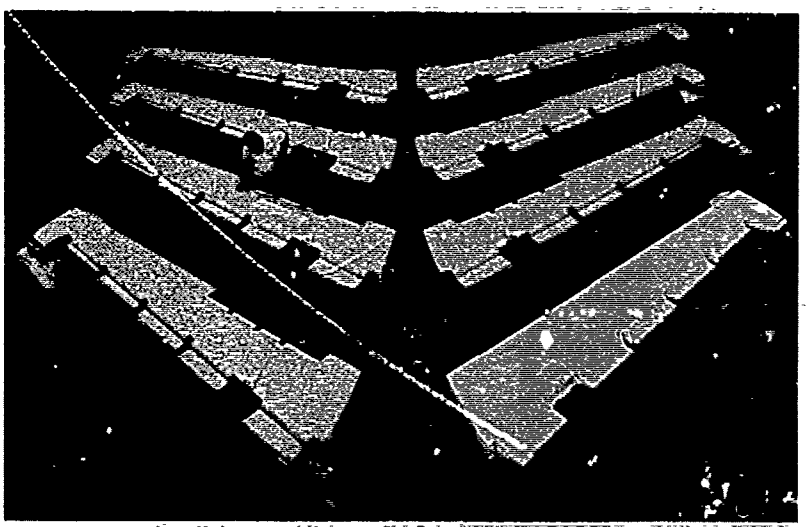

Figure 25. Boeing 727 graphite/epoxy elevators.

TECHNICAL LIBRARY
ABBOTTAEROSPACE.COM

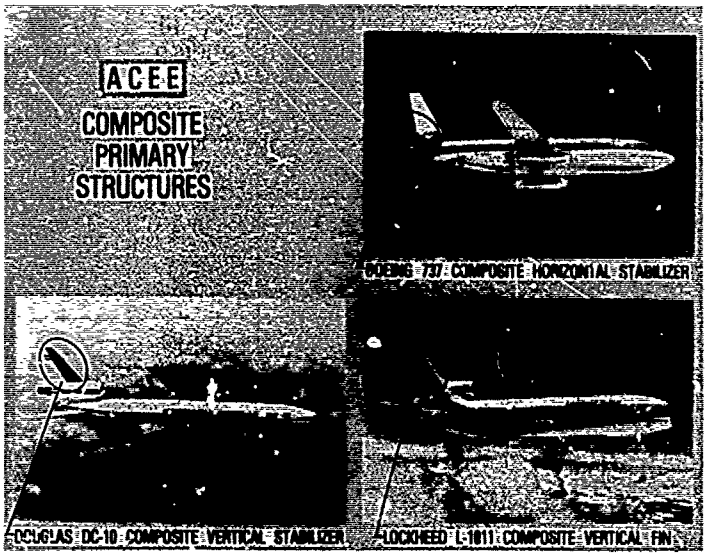

Figure 26. NASA ACEE composite primary structures.

COMPONENT	L-1011 VERT. FIN	DC-10 VERT. STAB.	B-737 HORIZ. STAB.
SIZE, m	2.7 × 7.6	2.4 × 7.6	1.2 × 5.2
BASELINE METAL MASS, kg	389.2	453.6	118.9
COMPOSITE MASS, kg	272.2	350.3	91.6
PROJECTED MASS SAVINGS, %	30.1	22.8	22.9
QUANTITY TO BE FABRICATED	3	7	11

Figure 27. Details of NASA ACEE composite primary components.

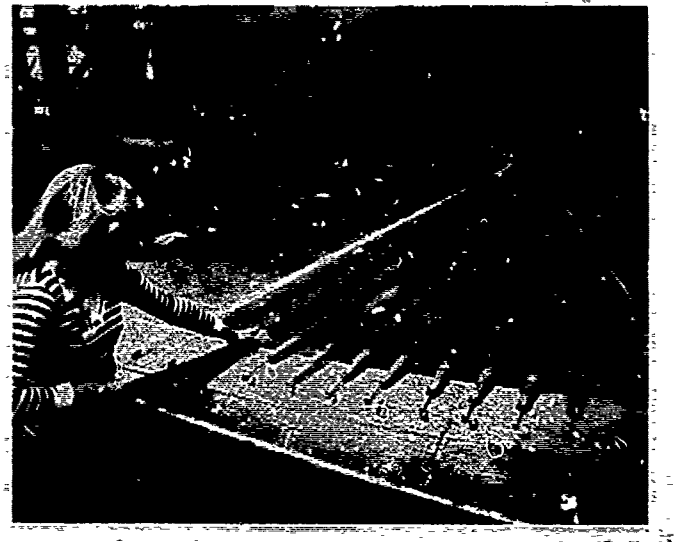

Figure 28. Graphite/epoxy skin panel for Lockheed L-1011 vertical fin.

TECHNICAL LIBRARY
ABBOTTAEROSPACE.COM

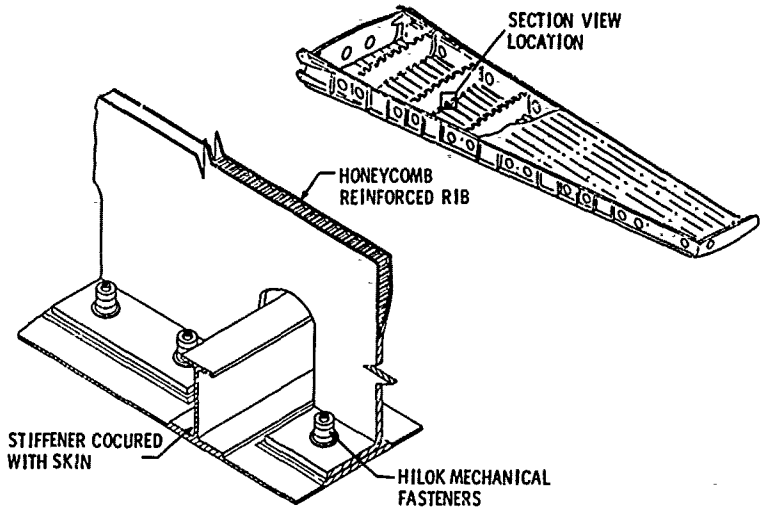

Figure 29. Boeing 737 composite stabilizer assembly.

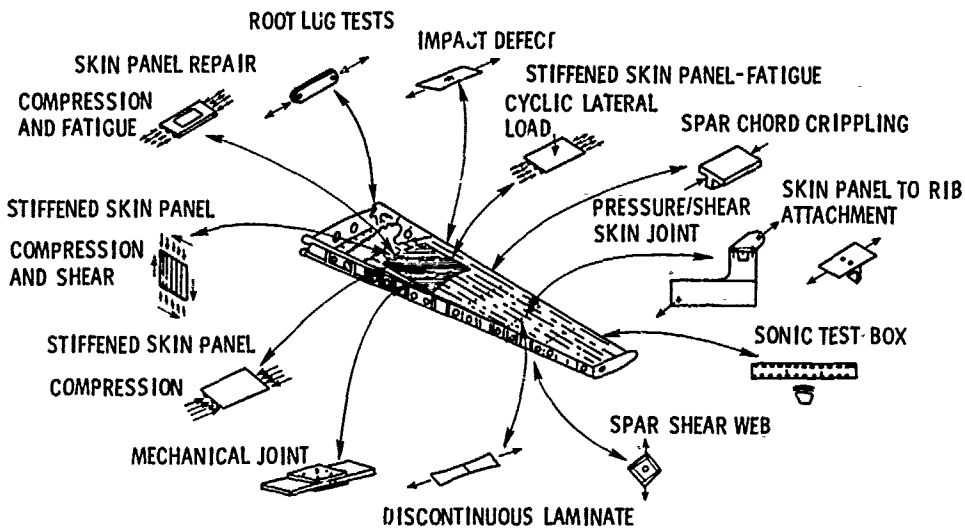

Figure 30. NASA ACEE composites ancillary tests.

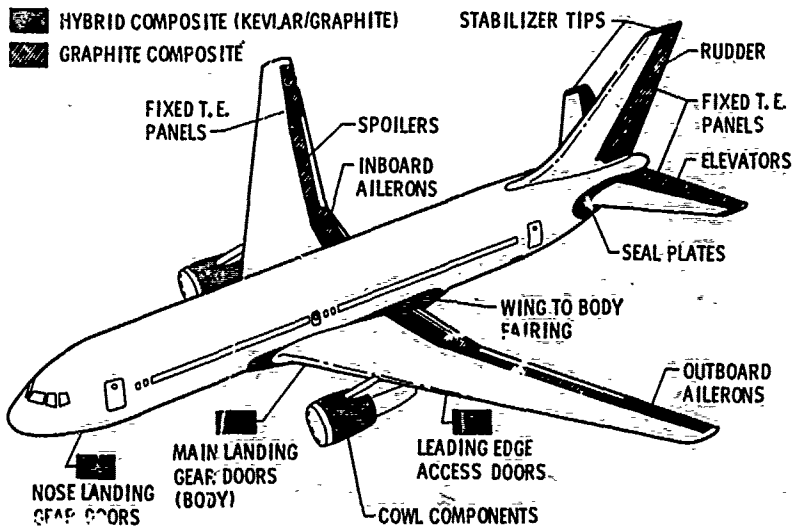

Figure 31. Boeing 767 composite applications.

THIS DOCUMENT PROVIDED BY
TECHNICAL LIBRARY
ABBOTTAEROSPACE.COM

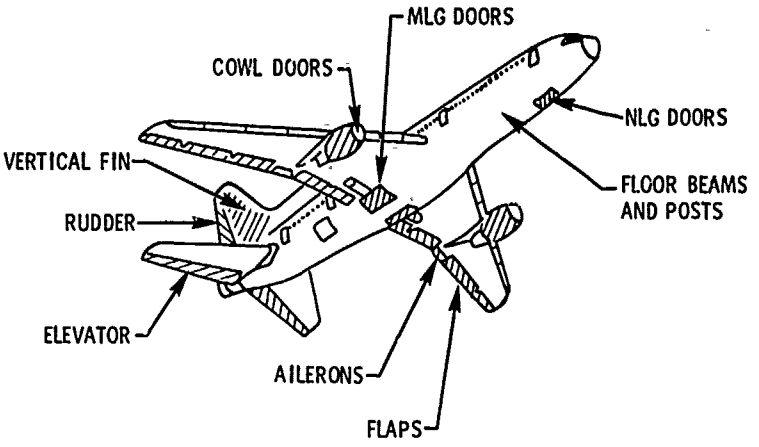

TOTAL GRAPHITE/EPOXY COMPOSITE APPLICATIONS - 2560 kg
MASS SAVED - 915 kg

Figure 32. Potential composite structure applications on Lockheed L-1011.

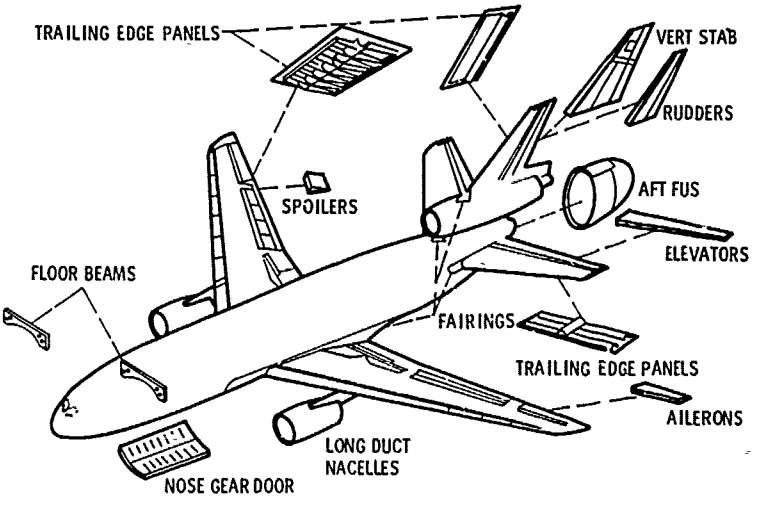

Figure 33. Potential composite structure applications on Douglas DC-10.

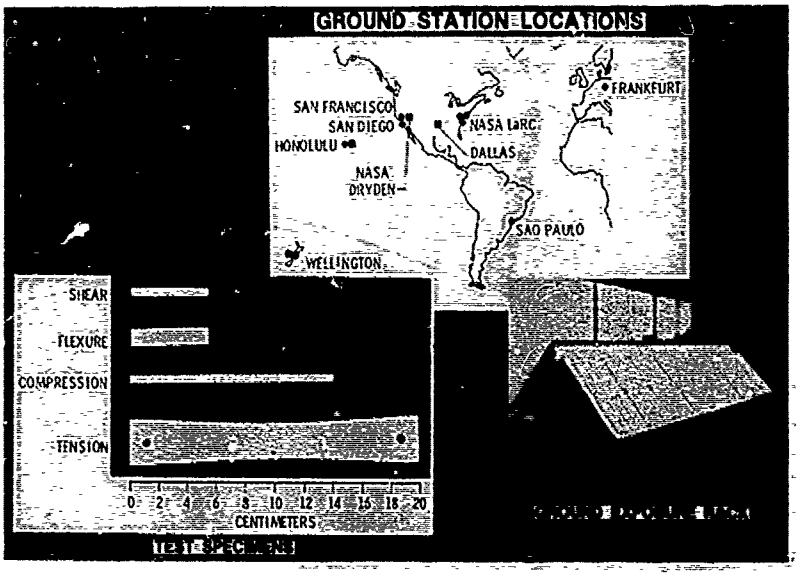

Figure 34. Worldwide environmental exposure of composite materials for commercial aircraft.

THIS DOCUMENT PROVIDED BY THE TECHNICAL LIBRARY
ABBOTTAEROSPACE.COM

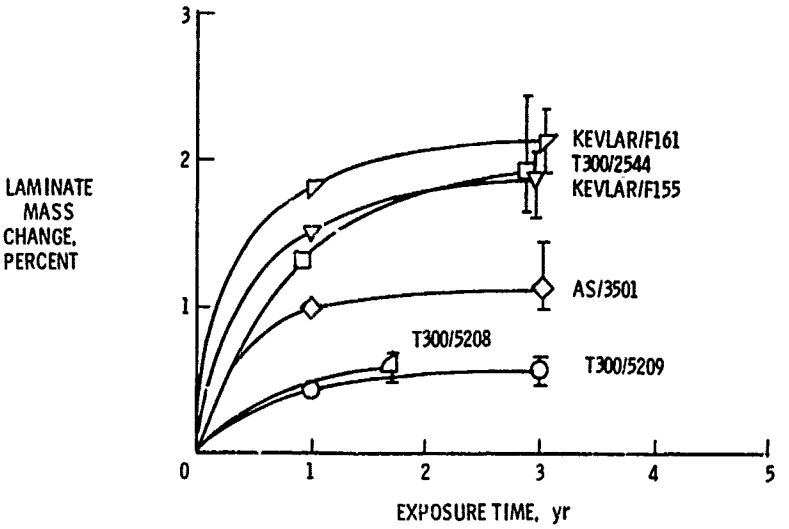

Figure 35. Moisture pickup after worldwide exposures.

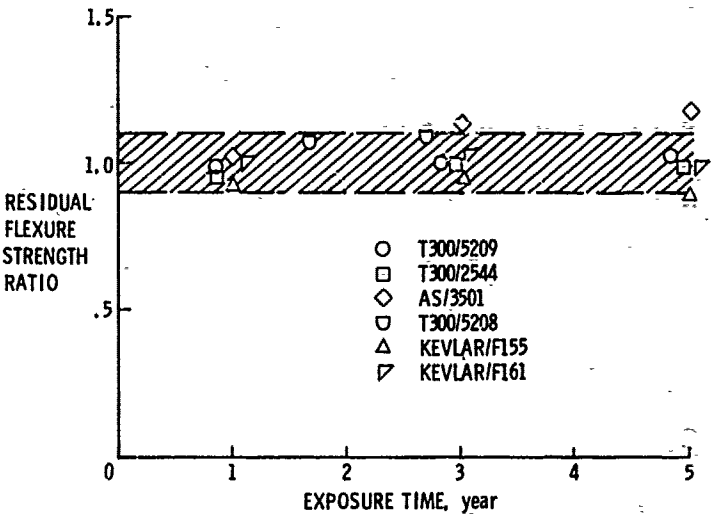

Figure 36. Residual flexure strength after worldwide exposure.

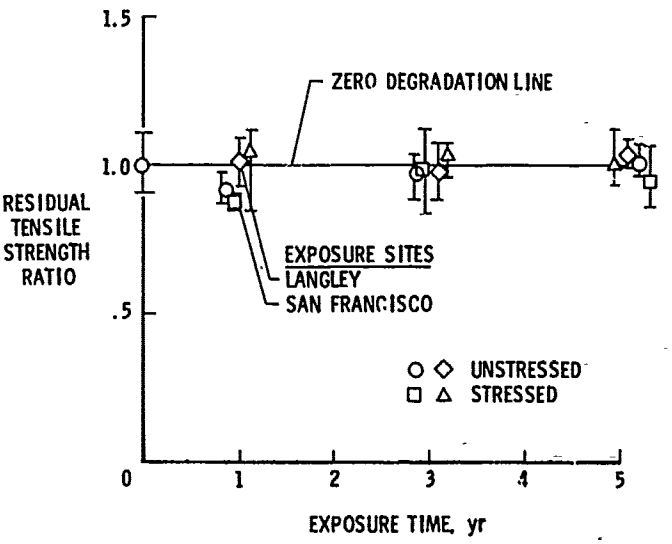

Figure 37. Residual tensile strength after sustained stress outdoor exposures; T300/5208, [0°±45°,90°] laminate stressed at 40 percent ultimate.

TECHNICAL LIBRARY
ABBOTTAEROSPACE.COM

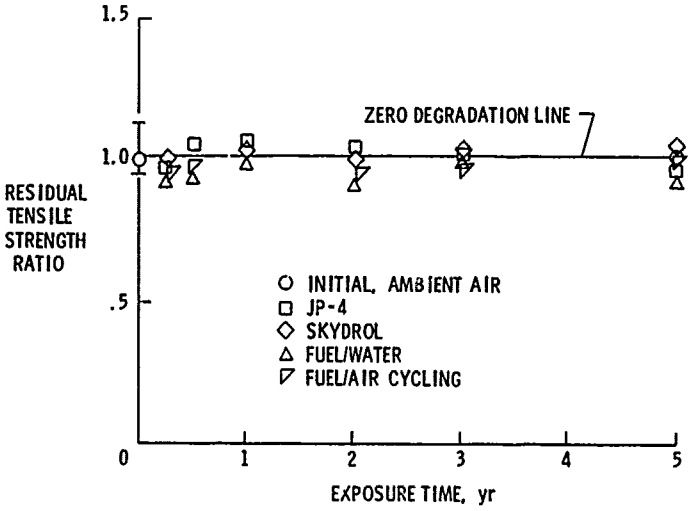

Figure 38. Effect of fuels and fluids on strength; T300/5209, ±45° tensile specimens.

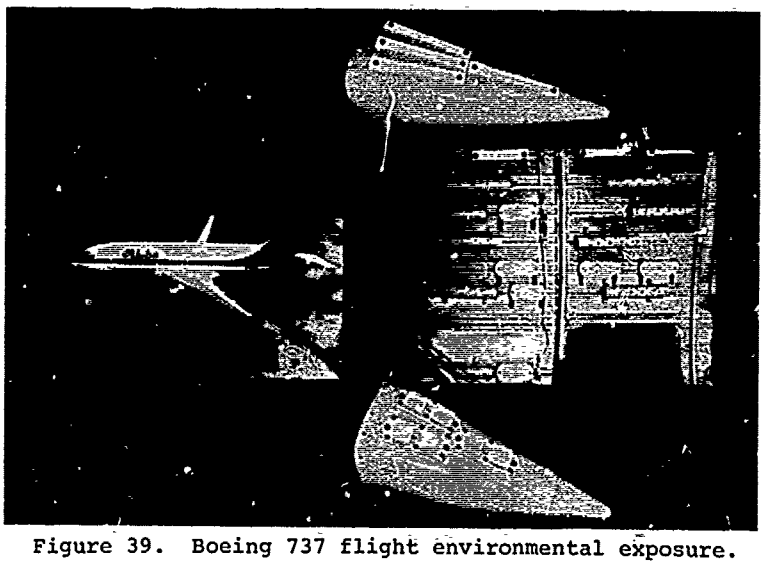

Figure 39. Boeing 737 flight environmental exposure.

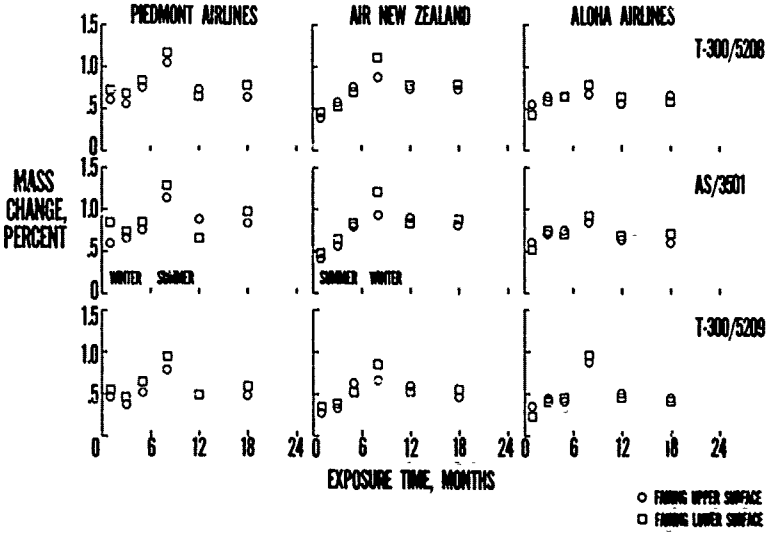

Figure 40. Composite mass change during flight exposure on Boeing 737.

TECHNICAL LIBRARY
ABBOTTAEROSPACE.COM

"Air Force Applications and In-Service Experience with Composite Structures"

Frank J. Fechek
Systems Support Division
Materials Laboratory
Air Force Wright Aeronautical Laboratories
Wright-Patterson AFB Ohio 45433

Summary: The chronology of the Air Force Materials Laboratory advanced composite development programs which contributed to the current capability to use these materials in primary and secondary structures on high performance military aircraft is described. Some of the concerns regarding the durability of these materials in actual service environments are being addressed by conducting a systematic, periodic non-destructive evaluation of selected composite structures in operational service. Whereas visual and x-radiographic inspection techniques have been found to be quite usable on composite structures in-the-field, inefficiencies using available, portable ultrasonic inspection equipment in the field environment have accentuated the need for the development of a semi-automated, ultrasonic inspection system specifically designed to be compatible with current, production composite aircraft structures. A system satisfying these needs has been shown to be feasible and is now in the prototype stage of development.

The Air Force Materials Laboratory has been instrumental in the growth of the advanced composites technology beginning with the fiber and resin/prepreg development, continuing through the period of structural design technique and configuration verification, and evolving into the manufacturing processes and cost effectiveness studies which eventually contributed to the commitment of this category of structure into production use in advanced aircraft airframes.

Beginning in 1961 the AFML sponsored the initial feasibility program to define the best chemical processes to produce boron fibers suitable for reinforcement in composite structures. As these filaments became available in sufficient quantities to verify the potential utility of high modulus reinforcements in polymeric resins, effort was initiated in 1963 to also refine the processes to produce high strength, high modulus graphite reinforcement fibers in useful quantities and at a reasonable cost. The availability of sufficient quantities of these fibers from pilot plant development programs in the mid 1960's made possible the initiation of structural hardware concept and development efforts beginning in 1964. At this time, the United States Air Force, by instituting the Composite Structures Advanced Development Program at the AFML, demonstrated its intention to solve the problems of transitioning this new technology from a demonstrated-to-be-feasible, laboratory curiosity into a viable, integrated structural materials industry. It was expected that the products of this new industry would make possible the redesigning of airframe structures along with achieving equivalent or increased airframe structural component performance with reduced weight. The approach taken to accomplish this transitioning goal was to select actual structural components of current or anticipated aircraft systems as technology demonstration items and then, through a series of design, fabrication, and test iterations, achieve a manufacturable component ready for flight service evaluation. Some of these development programs resulted in ground testing of one-of-a-kind structures, some resulted in limited production and in-service evaluation, and some have resulted in airframe structures which have been placed in routine production use. During the sixteen years since the first structural demonstration item program was initiated in 1964, many material system combinations, design concepts, structural configurations, and manufacturing techniques have been investigated. Table I depicts the chronological progress of the development of the advanced composite technology and its introduction into United States military aircraft systems. This table shows that the mid to late 1960's were used to refine, test, and confirm the evolving design methods and manufacturing capability to use composites as skin members in full depth honeycomb structures. The overriding design criteria during this period was to duplicate the static and dynamic response of the equivalent metal design which the composite part was to replace. This structural development period emphasized boron fibers, and although few articles of any individual design were produced, most were demonstration flight tested, and most exhibited weight savings in the 20% range.

The early 1970's were characterized by; A). high modulus graphite filaments becoming available to the designer, B). a series of programs directed at non-full depth honeycomb structural configurations, C), various attempts at non hand-layup manufacturing concepts, and, D). a continuing cautious attitude of the designers about incorporating composites into the substructure portions of the composite assemblies. This period continued to emphasize the manufacture of only a limited number of items of any single design, with no flight demonstration of them except in the case of the F-14, F-15, and F-111 production activity. In these latter instances, the technology of the 1960's, i.e. boron composite skins bonded to full depth aluminum honeycomb sandwich, was applied to production on a routine basis. The weight savings achieved by these production items was as predicted based upon the experience gained in the development programs.

The mid 1970's were characterized by a more aggressive and expanded use of this maturing technology by the airframe manufacturing community. Examples are; A). the many materials system combinations attempted in the earlier periods had evolved to a few, widely used systems, B). graphite fiber reinforced applications increased, C). composites as substructure were introduced, D). designs of increased sophistication were attempted, and E). prototype aircraft used composites as primary bill-of-materials with no alternate metal designs.

From the mid 1970's to the present, composites use has further increased in both numbers and types of application. The designs selected during this period emphasize: A). a more selective use of reinforcement materials for particular properties, B). a mixing of materials in a structure for both structural and economic reasons, C). introducing and evolving toward mechanically fastened concepts, and D). aggressive use of composites in strength critical designs.

TECHNICAL LIBRARY
ABBOTTAEROSPACE.COM

Thus, the current status of the continuing evolution of these materials is; A). that their use as secondary structures is routine, B). wing-type primary airframe loads and structures have been incorporated into the most recent systems, and C). the technological basis of information and data have been obtained to permit the future application of this technology into fuselage type applications. Current development programs are addressing both the wing/fuselage intersection requirements and the concerns about the long term reliability and durability of these materials and design concepts.

Table II contains a summary of those military aircraft systems which have incorporated the use of advanced composites as airframe structure on a routine, production basis. This table shows that a considerable amount of in-service experience has been achieved in the past ten years, measured either in calendar time or accumulated fleet or individual aircraft flighthours. Also shown in this table is the status of one of the advanced development effort structures. It is shown here both for comparison purposes, because it is graphite/epoxy, and because it is included in an in-service monitoring effort. Not included are more recent applications of this technology, where extensive amounts of graphite/epoxy composites have been used. The F-18 and the AV-8B are examples. These have been omitted because they are relatively new and have not yet accumulated comparable fleet flighthours and environmental experience.

The AFML, in 1976, initiated a non-destructive inspection monitoring program of selected composite structures in service with the objective of establishing some basic information on the durability of these structures in an actual service environment. In this effort, standard NDE techniques are used to periodically monitor the condition of a few selected structures. This effort is not intended to measure, nor statistically indicate, the actual condition of the structures in the fleet at any point in time. Rather, it is intended to establish a baseline of experience and data which could be used to plan future fleetwide inspection programs, should this become necessary, and/or to develop the information which would be used to establish the criteria against which a portable, reliable, semi-automated in-the-field inspection system could be developed. The composite structures on two aircraft systems were selected. These are the composite structure portions of the empennage of the F-15 and the composite outer wing panels on several A-7D aircraft. The details of this program are indicated below.

Three locations were selected to visit annually to monitor F-15 aircraft. They are Edwards AFB, California, Luke AFB, Arizona, and Langley AFB, Virginia. The two aircraft at Edwards AFB were selected because they are the second and eighth airframes manufactured in this program, thus they have been in the service environment the longest calendar time (although they have not necessarily accumulated the most flight hours). The three aircraft inspected annually at Luke AFB are of interest primarily because they are exposed to a desert environment, whereas the three aircraft inspected annually at Langley AFB experience a typical seashore environment throughout the year. The structures inspected on the F-15's are the vertical and horizontal stabilizer torque boxes and the rudders. All are full depth aluminum honeycomb construction bonded to boron/epoxy skins. Typical construction is shown in Figure 1. Disbonds or delaminations in the area of the skin to titanium step splice joints at the periphery of the skins or moisture incursion into the honeycomb core are the two primary effects expected upon the composite structures as a result of either the ambient climatological environment or the flight loads. Thus, ultrasonic testing and x-radiography were chosen as the in-the-field techniques to be used on this program. Because of the configuration of the skin to titanium close out joint in the torque boxes, a pulse-echo technique is very tedious. Because of this, a through transmission technique has been adopted in which the signal generated passes through the boron/titanium joint of the upper skin, through the honeycomb core, and again through a similar boron to titanium joint before being received by another transducer. Failure of the generated signal to be received is the indication of a disbond or delamination and such areas are further evaluated using pulse-echo techniques with a single transducer. For the structural configurations tested to date, 0.375 inch, 2.25 MHz transducers are used in conjunction with a Branson 301 portable ultrasonic instrument and have been found to be adequate. A typical inspection involves completely inspecting the entire periphery of both horizontal stabilizers and the periphery of the lower two thirds of each vertical torque box using this technique. The bonds are interrogated at one half inch centers and a total length of bonded steps of 1070 inches can typically be completed by a two person team in four hours.

In checking for moisture incursion, in order to restrict the inspection time required to a reasonable amount, it has been assumed that the most likely areas which would ingest moisture would be those where the skins were relatively thin. Thus, only the outboard 30 inches of each of the stabilizers and the complete planform of each rudder are radiographed. Using a focal distance of 30 feet for the vertical stabilizers and rudders and 13 feet for the horizontal stabilizers and exposing the structures to 125 kv at 5 ma for between 1.5 and 7.5 minutes (depending upon structure thickness and focal distance) results in obtaining good quality radiographs using Kodak Industrex AA ready pack film. This procedure results in films which contain a minimum amount of honeycomb image foldover so that either liquid moisture or evidence of moisture presence in the past (i.e. cell wall distortion) can be detected. Exposing 28 14x17 inch films per aircraft takes a two person team 5 hours, including set up and take down time.

During the 43 months of this program, no delaminations or disbonds have been discovered in the composite to titanium bonded joint areas. Likewise, only subtle evidence of moisture incursion into the honeycomb has been discovered and this in an insignificant percentage of the area examined.

The physical configuration of the A-7D composite outer wing panel is shown in Figure 2. Twelve of these structures were manufactured in 1976 as part of a manufacturing technology effort. The objective of this in-service experience program is to monitor the performance of a representative graphite/epoxy construction in both a desert and seashore environment with Air National Guard aircraft. Four composite outer wing panels (COWP's) have been stationed at Kirtland AFB New Mexico, and three at McEntire ANGB, Columbia, South Carolina.

The A-7D in-service inspection effort differs from the F-15 program in the following ways: A). only seven structures are included in the program (all the other wing tips in the fleet are metal), B). the COWP's are a hybrid construction including B/E, Ti, fiberglas, and Gr/E, C). the assembly is sandwich skin mechanically fastened and bonded to a composite rib/spar substructure, and D). x-radiography is unsuitable as an inspection technique and the return signals from this complex structural arrangement makes the use of

TECHNICAL LIBRARY
ABBOTTAEROSPACE.COM

ultrasonic techniques of marginal utility. Thus, visual inspection is the primary technique used on these structures, a boroscope being used on the interior of the structure. A Branson 301 portable ultrasonic unit in the pulse-echo mode, using a 0.375 inch, 2.25 MHz transducer has been used to check skin to substructure suspect areas. To date, since mid-1977, the semi-annual inspections have recorded no major degradation attributable to the in-service environment. The following have been experienced, however; A). some minor cracks in cut edges of the panels at the radii of access panel hole frames, and B). some minor damage where edge damage impact can occur. No structural disbonds and no damage attributable to in-service abuse have been discovered. Additionally, no extra maintenance has been required on these structures (in fact, they require less than the comparable metal structures) and no repair actions have been required. In summary, the performance of these graphite/epoxy structures in service has been quite satisfactory.

An additional experiment is being conducted in conjunction with the COWP's on the A-7D's. This involves installing unstressed 4x6 inch panels on racks on the underside of COWP access doors. The objective of this experiment is to monitor the change in physical and mechanical properties which these materials experience when exposed to real time environmental exposure identical to that of the wing structures. The parameters being compared are geographical location (i.e. low vs high ambient humidity), coated vs uncoated, and various material systems. Table III summarizes some of the properties measured during the first 24 months of this continuing effort.

A general summary of the observations resulting from these in-service inspection monitoring efforts is: A). the boron/epoxy structures appear to be quite inert to their service environment. They have not experienced any degradation resulting from either their flight loads or their typical ground handling environments and procedures. The structural bonds in the skin to titanium step splice appear to be similarily degradation resistant. Only an extremely few occurrences of possible moisture entry and minimal core damage have been observed. Of these, the seashore stationed items acquired most of the occurrences, although a small percentage were discovered on aircraft stationed in the desert. Recorded moisture in seashore aircraft "vanished" after these aircraft were transferred to the desert location. B). the graphite/epoxy structures generally likewise seem to be inert to the loads and ground handling environment. However, in the case of the specific structures inspected, some minor delaminations have been experienced and some cracking at cut edge corners has been discovered. It is not evident whether these few isolated events are problems peculiar to this individual design or a basic materials system inadequacy, C). in-service ultrasonic inspection of aircraft using off the shelf equipment and techniques is time-consuming and prohibitively expensive if anything other than small surface areas are to be inspected, D). observed changes in "flaw" size using ultrasonic testing is very subjective and operator dependent, especially when attempting to compare findings from one year to the next, E). off the shelf NDE ultrasonic equipment suitable to. in the field use is not capable of providing a printed permanent record usable for future reference.

Thus, a secondary conclusion from this effort has been that a need exists for a more efficient NDE tool to inspect this category of aircraft structure in-the-field.

Toward satisfying this need, the AFML, in 1978, initiated a program to define the feasibility of, and then develop, a portable, reliable in-service ultrasonic inspection system capable of in-the-field use. This system, as conceived, would; A). enable the operator to rapidly scan the structure, B). automatically detect flaws by comparing the ultrasonic signal against some predefined standard, C). store in computer memory the flaw locations, D). indicate, in real time, where the flaw locations were and which portions of the structure had not yet been interrogated, E). provide, in near real time, a permanent record printout of scanned area, flaw locations, and a computed flaw depth and, F). upon operator command, digitize the RF signal of the flaws and store in computer memory. This program is called "In Service Inspection System (ISIS)." The basic functional elements of the ISIS concept are shown in Figure 3. These elements have been organized into various assemblies as follows; A). Transducer Assembly--this hand held unit is composed of the transducer, the solid or liquid delay line, a couplant dispensor, a sound emitter, push button to activate the wave form digitizer, and a signal loss alarm light, B). Position Sensing Assembly--this apparatus positions the two, point source microphones which send the signals to the graphpen digitizer which in turn computes in rectangular coordinates the position of the transducer within the 24x24 inch operational inspection area and transmits this information to the CPU, D). Ultrasonic Assembly--currently a Sonic Mark IV (Sonic Instruments, Inc, Trenton, N.J.) has been modified to incorporate a dual flaw gate, a flaw amplitude digitizer, and waveform digitizer and is used for these functions, E). Data Acquisition/Processor Assembly--a Motorola MC 6800 Microprocessor with a 16 K byte ROM and a 48 byte RAM is used as the CPU for this system. The ROM contains the system level software. It contains 16 parallel I/O channels. F). Data Display Assembly--a Techtronics TEK 4025 Graphics Display is used to input instructions to the system and display in near real time the ultrasonic scan completion status and flaw locations on the CRT. It can also be used to display digitized waveforms, and G). Data Recording Assembly--this Hewett Packard 9876 A Printer/Plotter will provide permanent copies of C scan recordings, digitized RF waveforms, and coordinate/amplitude listings.

The ISIS block diagram, Figure 4 shows the relationships of the various functions. The operational procedure of the unit is; A). the outline of the area to be interrogated is projected on the CRT display based upon information fed to the CPU by placing the transducer assembly at the corners of the perimeter of the area of interest and activating a button on this assembly, B). each possible data point 0.1 inch by 0.1 inch in the area to be inspected is illuminated by a dot on the CRT, C). the reflected ultrasonic signal is identified with its location, then analyzed against predefined criteria and recorded in memory, D). if the interrogated area is a flaw, the display dot increases in brightness and if it is not, the dot is extinguished, thus, when the complete surface has been scanned, only flaw locations are illuminated, E). the flaw areas are automatically recorded and the printer plotter will produce a permanent copy of the results of the scan showing those areas which have and have not been scanned, F). for a given flaw, the operator can activate the waveform digitizer and record and print the digitized representation of the RF waveform, G). this information can also be used to automatically compute the depth of the flaw by ratioing the flaw reflection time to the difference between the near side reflection time and the far side reflection time.

A typical printer plotter representation of an inspected surface is shown in Figure 5.

TECHNICAL LIBRARY
ABBOTTAEROSPACE.COM

In summary, the ISIS feasibility has been demonstrated and currently the prototype system is being evaluated under actual in-service conditions in order to further define those operating characteristics which will be most appropriate for routine use. These findings will be incorporated into two units which will then be placed into service at two Air Force Logistics Centers for use in the routine inspection and maintenance of the composite structures on Air Force production aircraft.

THIS DOCUMENT PROVIDED BY THE ABBOTT
TECHNICAL LIBRARY
ABBOTTAEROSPACE.COM

Table I

Chronology of Advanced Composite Aircraft Applications

Component	Year Structure Completed	Aircraft System	Material System: Fiber / Resin	Construction	Application: Structure	Application: Other	Application: Substructure	Application: Skins	Purpose of Program: Structure Development	Purpose of Program: Mf'g & Processing	Purpose of Program: Prototype	Purpose of Program: Production	Was Structure Flight Tested?	Quantity Produced	% Weight Reduction	% Composite in Str.
Air Deflector Door	66	F-111	Boron 5505	F. D.[1] Sandwich	X						X		Yes	2	24	
Main Landing Gear Door	67	F-111	Boron 5505	F. D. Sandwich	X						X		Yes	2	9	
Wing Trailing Edge Panel	67	F-111	Boron 5505	F. D. Sandwich	X						X		Yes	24	13	
Rudder	68	F-4	Boron 5505	F. D. Sandwich	X						X	X	Yes	53	35	15
Wing Trailing Edge Flap	68	A-4	Boron 5505	F. D. Sandwich	X	X					X		Yes	4	22	
Rudder	68	F-15	Boron 5505	F. D. Sandwich	X						X		Yes	3		
Landing Gear Strut Door	68	F-5	Boron 5505	F. D. Sandwich	X						X		Yes	?	29	
Wing Tip Box	69	F-111	Boron 5505	Sandwich	X	X					X		No	1	17	
Horizontal Stabilizer	69	F-111	Boron 5505	F. D. Sandwich	X						X		Yes	6	26	22
Aft Rotor Blede	69	CH-47	Boron 5505	F. D. Sandwich	X	X					X	X	Yes	4		
Leading Edge Slat	70	C-5A	Boron 5505	Sandwich		X					X		Yes	13	21	25
Landing Gear Strut Door	70	F-5	HTS 3002	F. D. Sandwich	X						X		No	2	22	
Leading Edge Slat	70	C-5A	Mod II ER 279	Sandwich	X	X						X	No	1	30	
Horizontal Stabilizer	70	F-14	Boron 5505	F. D. Sandwich	X						X	X	Yes	860	18	19
Rudder	71	F-15	Boron 5505	F. D. Sandwich	X							X	Yes	1008		
Vertical Stabilizer	71	F-15	Boron 5505	F. D. Sandwich	X						X	X	Yes	1008	25	30
Horizontal Stabilizer	71	F-15	Boron 5505	F. D. Sandwich	X						X	X	Yes	1008	22	25
Landing Gear Strut Door	71	F-5	HTS 3002	F. D. Sandwich	X							X	No	3	22	
Wing	71	F-100	Boron 5505	Bolted Panel	X						X		No	1		
Speed brake	71	F-5	Mod II E 293	Molded	X						X		No	4		
Wing Trailing Edge Flap	71	F-5	HTS 3002	F. D. Sandwich	X						X		No	5	25	
Wing Leading Edge	71	F-5	HMG-50 4617	Filament Wound	X						X	X	No	2		
Aft Fuselage	71	F-111	Gr & Boron Epoxy & Al	Sandwich/ Stfn'd Panel	X	X					X		No	1		
Horizontal Stabilizer	71	F-5	HTS 3002	F. D. Sandwich	X						X		No	2		
Wing Pivot Fitting Doubler	72	F-111	Boron 5505	Panel			X				X	X	Yes	824		
Underwing Fairing	72	F-111	AS-1 3501	F. D. Sandwich	X						X	X	Yes	824		
Landing Gear Wheel Door	72	F-5	HTS 3002	F. D. Sandwich	X						X	X	No	9	28	

1 F. D. - Full depth honeycomb sandwich

THIS DOCUMENT PROVIDED BY THE TECHNICAL LIBRARY
ABBOTTAEROSPACE.COM

Table I (Cont'd)

Chronology of Advanced Composite Aircraft Applications

Component	Year Structure Completed	Aircraft System	Material System	Fiber / Resin	Construction	Application	Purpose of Program	Structure Development	Mfg'g Processing	Prototype	Production	Was Structure Flight Tested?	Quantity Produced	% Weight Reduction	% Composite in Str.
						Skins	Substructure	Other							
Wing	73	BQM-34	PRD-49-3 CE3305		F. D. Sandwich	X			X			No	1		
Aft Fuselage	73	F-5	Boron/T300 5505/5208		Stfn'd Panel	X	X		X			No	1	15	90
Dorsal Longeron	73	B-1	Boron 5505		Metal Doubler			X	X	X		Yes	5		
Horizontal Stabilizer	73	A-4	Gr 5206		Panel Skin Sdwich/Substr	X	X		X			No	2	28	
Center Wing Box	73	C-130	Boron 5505		Metal Doubler			X	X	X		Yes	3	13	
Vertical Stabilizer	74	YF-16	T300 5208		Panel	X				X		Yes	2		
Horizontal Stabilizer	74	YF-16	T300 5208		F. D. Sandwich	X				X		Yes	4		
Outer Wing Torque Box	74	A-7D	Boron/AS 5505/3501		Bolted Sandwich	X	X		X	X		Yes	12	11	
Doors, Panels Control Surfaces	74	YF-17	AS 3501		F. D. Sandwich, Panels	X				X		Yes	2ss		
Wing Torque Box	75	F-15	Boron/AS 5505/SP286		Sandwich	X	X		X	X		No	1	17	39
Speed brake	75	F-15	T300 5208		F. D. Sandwich	X			X	X	X X	Yes	462	28	60
Over Wing Fairing	75	F-14	Boron/AS 5505/3501		Stfn'd Hybrid Sandwich	X				X		Yes	10	25	47
Landing Gear Door	75	F-14	AS 3501		F. D. Sandwich	X				X		Yes	7	8	
Wing Trailing Edge Flap	75	B-1	AS 3501-5		F. D. Sandwich	X	X		X			No	3		
Weapons Bay Door	75	B-1	AS 3501-5		F. D. Sandwich	X	X		X	X		No	8		
Avionics Bay Door	75	B-1	AS 3501-5		F. D. Sandwich	X			X			No	2		
Leading Edge Slat	75	B-1	Boron/AS 5505/3501-5		Sandwich	X			X			No	3		
Forward Fuselage	76	F-16	Kevlar/T300 5208		Stfn'd Panel	X	X		X			No	1	21	
Vertical Stabilizer	76	F-16	T300 5208		Bolted Panel	X					X	Yes	100		
Horizontal Stabilizer	76	F-16	T300 5208		F. D. Sandwich	X					X	Yes	200		
Horizontal Stabilizer	77	B-1	Boron/AS-1 5505/3501-5A		Bolted Panel	X	X		X			No	4	19	
Vertical Stabilizer	77	B-1	AS 3501		Bolted Panel	X	X		X			No	2	17	65
Vert/Horiz Stabilizer	78	F-18	AS 3501		F. D. Sandwich	X					X	Yes	34ea		
Wing	78	F-18	AS 3501		Bolted Panel	X					X	Yes	34		
Doors/Panels	78	F-18	AS 3501		F. D. Sandwich	X	X				X	Yes	17ss		
Wing	78	AV-8B	AS 3501		Bolted Panel	X	X			X		Yes	3		
Wing Fixed Leading Edge	79	C-141	G1/AS 7SDE141/3501-6		Stfn'd Skin	X	X		X	X		Yes	12		

TECHNICAL LIBRARY
ABBOTTAEROSPACE.COM

Table II

Summary

Military Aircraft using Composite Structures in Production

Aircraft System	F-111	F-14	F-15	F-16	A-7D
Date - First Flight	Aug '73[1]	Dec '70	July '72	Feb '74	June '77[1]
Total Aircraft	412[2]	349/80[3]	483/21[3]	100	7[4]
Cumulative Airframe Flighthours	377,200	255,000	224,600	9854	4324
Maximum Flighthours per Airframe	2085[1]	1469	1200	892	727[1]
Cumulative Composite Component Flighthours	1,508,800	510,000	1,347,600[5]	49,270	4324
Composite Component(s)	wing root pivot fitting doubler underwing fairing	horizontal stabilizer	horizontal and vertical stabilizers and rudder	horizontal and vertical stabilizers, vert. leading edge and rudder	Composite outer wing panel

1 with composite structures
2 currently flying with composite doublers
3 Foreign sales - no data
4 only aircraft with COWP's
5 excluding speedbrake

Table III

Percent Weight Gain vs. Exposure Time vs. Surface Protection

Surface Protection Technique	Months Since Installation	EXPOSURE LOCATION Kirtland AFB New Mexico	McEntire ANG Base South Carolina	Wright-Patterson AFB Ohio[1]
None	6-8	0.18	0.40	0.41
	11-14	0.22	0.59	0.80
	18-20	0.34	0.70	0.81
	23-26	0.32	0.79	1.03
Polurethane Paint one surface	6-8	0.06	0.38	0.46
	11-14	0.10	0.52	0.81
	18-20	0.16	0.63	0.78
	23-26	0.25	0.70	1.01
Polurethane Paint both surfaces	6-8	0.02	0.35	0.44
	11-14	0.06	0.46	0.78
	18-20	0.09	0.56	0.70
	23-26	0.16	0.68	0.94
Aluminum Foil (bonded) one surface	6-8	0.11	2	0.30
	11-14	0.11		0.59
	18-20	0.17		0.67
	23-26	0.13		0.91
Aluminum Foil (bonded) both surfaces	6-8	0.02	2	0.25
	11-14	0.02		0.51
	18-20	0.03		0.66
	23-26	0.02		0.88

1 rooftop exposure (in shade)
2 specimens lost in aircraft crash

TECHNICAL LIBRARY
ABBOTTAEROSPACE.COM

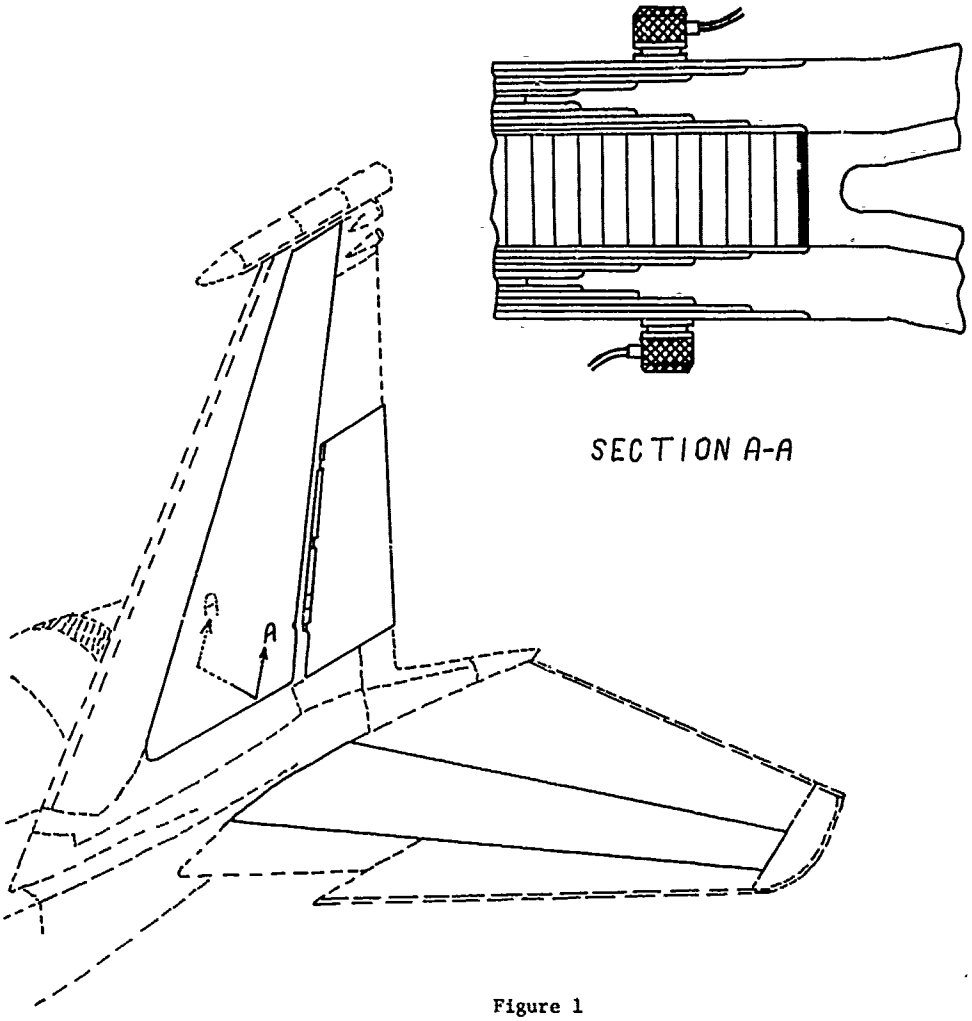

Figure 1

Typical F-15 Construction

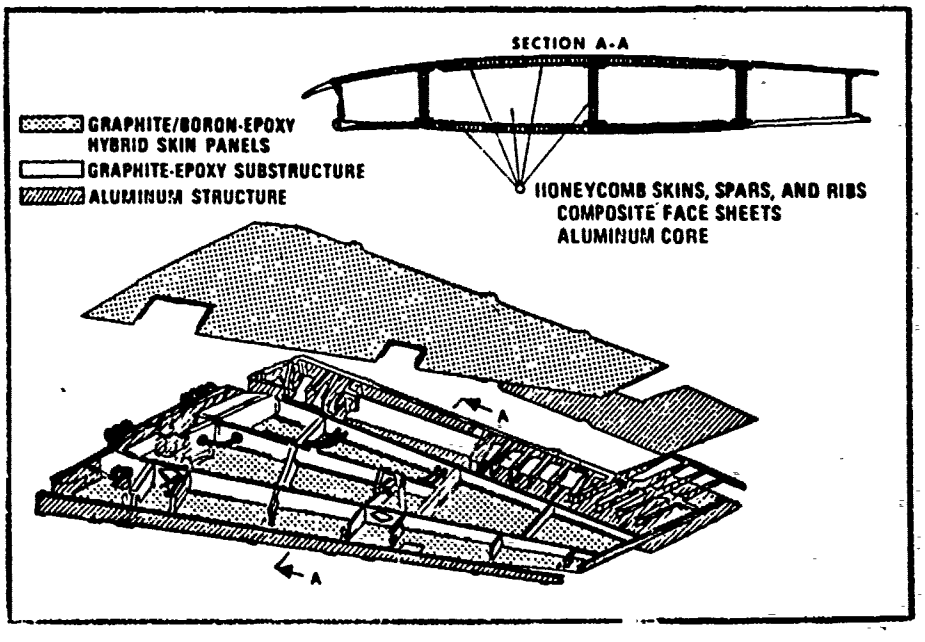

Figure 2

A-7D Composite Outer Wing Panel

TECHNICAL LIBRARY
ABBOTTAEROSPACE.COM

ISIS – CONCEPT

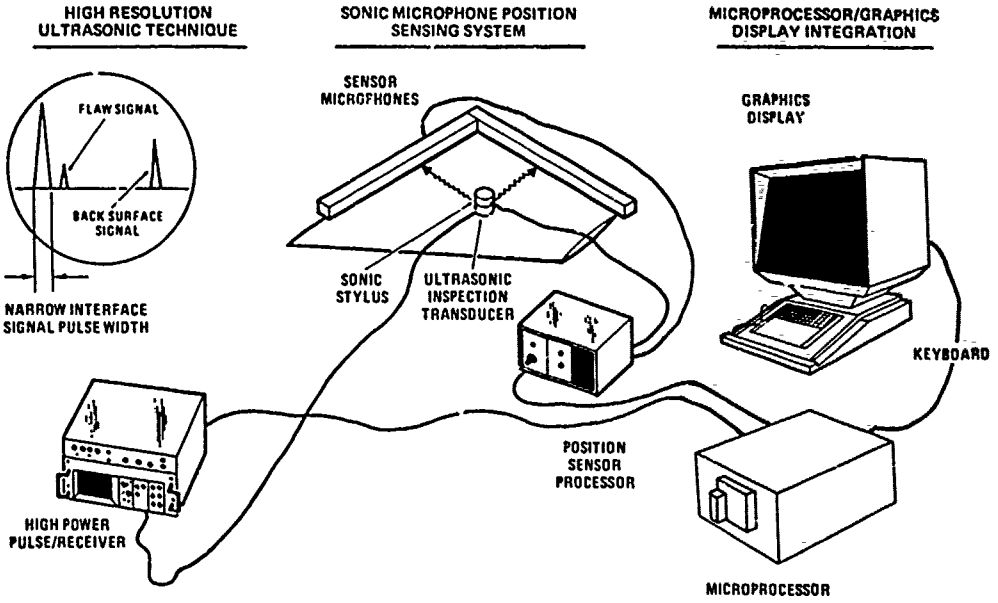

Figure 3

Functional Elements of ISIS

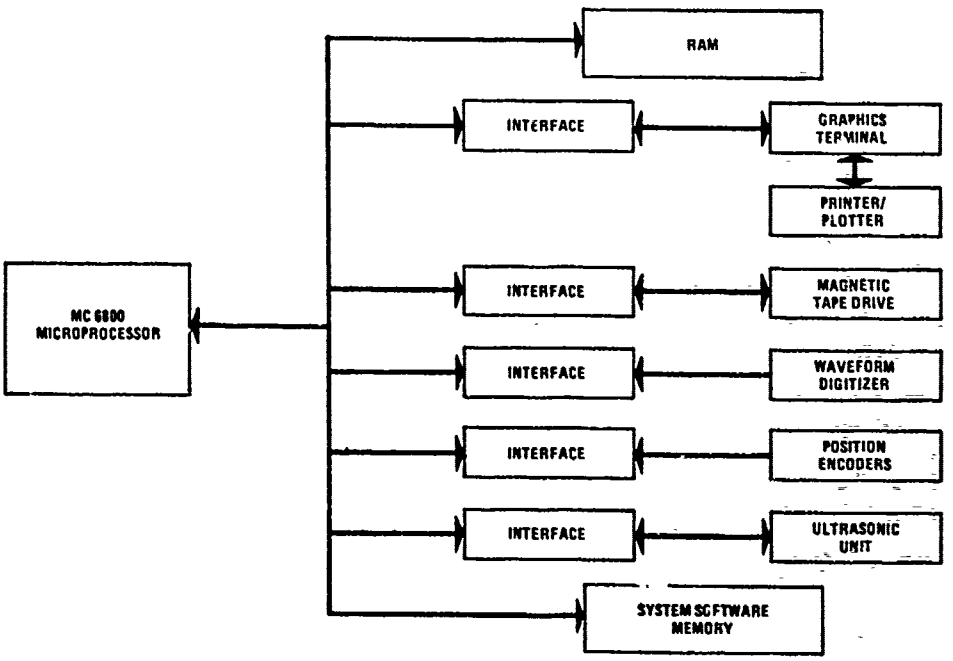

Figure 4

ISIS Block Diagram

TECHNICAL LIBRARY
ABBOTTAEROSPACE.COM


```
INSPECTION STATION GD FT WORTH DIV
INSPECTOR J. BELL
DATE (MO/DA/YR) 01/13/80
AIRCRAFT TYPE  N/A
PART NAME/SERIAL NO.  F16 HORZ STAB TEST

CALIBRATION LIST
REFERENCE STD. NO.  N/A
TRANSDUCER SER. NO.  V103
FREQUENCY (MHZ) 5
LOGIC NEG
GAIN SETTING
  COARSE 80
  FINE   05
DEC SLOPE (%)
DEC RANGE
FRONT SURF GATE (USEC/10) 26
MAX STEP (PLIES) 2
OPERATING MODE 1
```

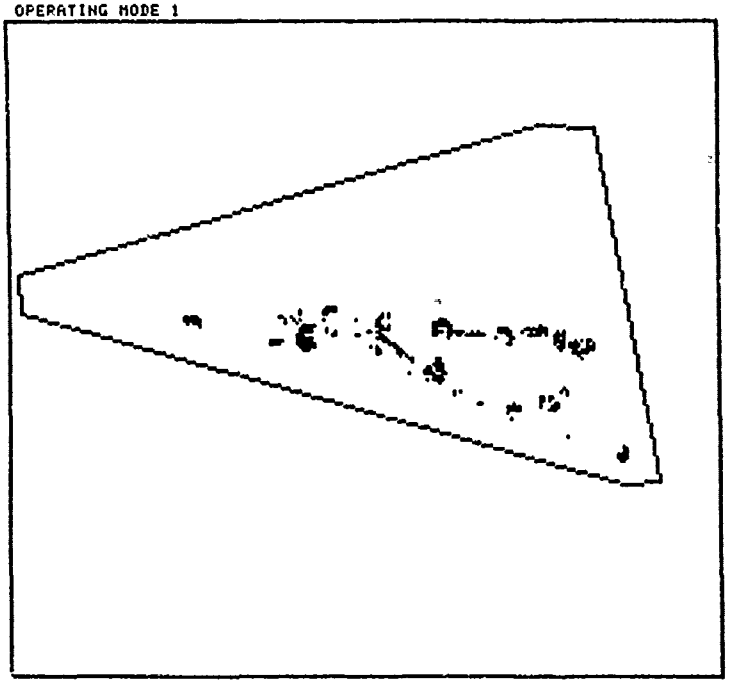

Figure 5

Typical ISIS Printer/Plotter Representation of Flawed Surface

TECHNICAL LIBRARY
ABBOTTAEROSPACE.COM

U. S. NAVY SERVICE EXPERIENCE WITH ADVANCED COMPOSITES

by
A. Somoroff, M. Dubberly, J. M. McGinn, and M. Tarricone
Naval Air Systems Command, Washington, D. C. 20361
and
A. Manno, Naval Air Development Center, Warminster, Pa. 18974

1. INTRODUCTION

The U. S. Navy is entering into a period of expanding composites use in major aircraft systems. These application committments, made several years ago, were based upon clear advantages in structural efficiency or cost and expectations of good service durability. The well known corrosion resistance and generally outstanding material fatigue behavior of composites coupled with limited but largely positive actual service experiences supported these expectations. Of course, it has been recognized that composites exhibit environmental sensitivities and other characteristics which differ markedly from conventional metallic behavior and which must be accommodated in design and service support. As might be expected, present designs reflect generally conservative judgments on expected lifetime environmental exposures. As actual long term operational experience accumulates, the distillate of this experience can be expected to shape the nature and extent of future composite applications as well as the supporting design development and fleet maintenance practices.

Obviously and unfortunately, 20 years of real-time service experience cannot be obtained in less than 20 years, but the earliest possible gathering of service durability information is clearly advantageous. Towards this end, the Navy, other Department of Defense agencies, and NASA are engaged in systematic acquisition of lifetime durability information encompassing laboratory programs, exposure of ground specimens and observation of flight structures. Within this broad background of activity, the Navy has of course concentrated on gaining information in the specific conditions characterizing the Navy/Marine physical and support environment. The discussions which follow later in this paper cover experience with composite structures which are in production or intended for production as well as others specifically developed to acquire service data. For the most part, observations made on the production composite structures have been gathered as part of normal maintenance and support activities. The specific structures discussed include the F-14 horizontal stabilizer and the H-46 rotor blade which are in production, and the YAV-8B wing developed for production on the AV-8B. Also discussed are S-3 spoilers and F-4 access doors which were developed exclusively to acquire service data.

Before proceeding with discussions of experiences with the above components, it is noted that the F-18 aircraft which is now in full scale development makes extensive use of graphite-epoxy composites in primary wing, horizontal stabilizer and vertical stabilizer skin structure. Composite applications on the F-18 have been described in some detail in reference (1) and no specific discussion of the F-18 is included below in this paper. However, by way of update, as of the end of February 1980, eleven F-18 development aircraft are engaged in flight test evaluation. A cumulative total of more than 900 flight hours have been accumulated with the highest number of flight hours for an individual aircraft being 214 and the longest calendar service time for an individual aircraft being 18 months. During this period the graphite-epoxy structure has performed well and without incident.

2. F-14 HORIZONTAL STABILIZER

The F-14 horizontal stabilizer was the first production application of composites in flight critical structure. As shown in Figure (1), the stabilizer is composed of boron/epoxy skins over full depth aluminum honeycomb core. The skins vary from 56 plys at the root, where they are bonded to a titanium splice plate, to 7 plys at the tip.

2.1 Horizontal Stabilizer Service Experience

The F-14 entered service in 1971 and since that time over 400 aircraft have been produced. To date, the horizontal tail has been relatively trouble free, with the only serious damage being due to mishandling, such as:

a. Dropping a heavy object (e.g. the stabilizer actuator or a tool).

b. Ramming the stabilizer into a wall or ground support equipment.

c. Dropping the stabilizer when it is removed from the aircraft.

A review of all maintenance data from Mid-1976 to late 1979 shows the majority of the damage to be cosmetic in nature such as repair of the paint, corrosion of the aluminum lightning protection strips and dents in the leading/trailing edges and tip assembly. Minor damage is repaired by squadron personnel while major punctures are returned to the depot. Typical examples of minor and major damage are shown in Figures (2) and (3), respectively. This review also shows that an average of four stabilizers are damaged beyond the fleet repair capabilities (2" diameter hole) each

TECHNICAL LIBRARY
ABBOTTAEROSPACE.COM

year. Approximately 30% of these units are repairable by the depot. Since the damage is being caused by handling as opposed to a design or manufacturing problem these trends are expected to continue.

A program which will increase the depot repair capability to deal with 6 in. diameter holes is about half way completed. Initial tests have shown that the repair concept being employed will recover in excess of design ultimate load capability. Further fatigue and environmental testing will begin soon. The test specimens and test set-up are shown in Figures (4) and (5), respectively.

2.2 Laboratory Reexamination of Service Stabilizer

The Navy recently removed from service a horizontal stabilizer that had seen approximately five years of service use in the fleet. This stabilizer is being subjected to an extensive laboratory examination to determine the effects of service use (real-time loading. temperature, humidity, etc.). The examination consists of both non-destructive and destructive testing including testing approximately 200 specimens cutout from the skins. While the study is not yet complete the results to date have shown minor damage such as dents and areas of honeycomb core corrosion. Tests of moisture content and mechanical properties are becoming available. In thinner laminate sections (20 plies or less), beneath the lightning protection strips, resin moisture content varies from approximately 1.5 to 2.1 percent of resin weight. For thicker sections (40 to 48 plies) resin moisture content was about 1 percent. Between the lightning protection strips, resin moisture content was found to be somewhat less. No significant differences were found between laminate specimens taken from the upper and lower surfaces of the stabilizer. Measurements of the resin content of all laminate specimens ranged from 25 to 29 percent by weight and were within original manufacturing requirements.

The evaluation of other properties is continuing and a final results should be available in approximately 6 months. Additionally, a full scale static test is planned for the near future as another quantitative check for any potential service degradation.

3. H-46 COMPOSITE ROTOR BLADE

As a result of major maintenance problems with the metal H-46 rotor blade, the Naval Air Systems Command initiated a contract with the Boeing Vertol Co. in early 1975 to develop and produce a replacement composite rotor blade. The primary objective of the composite blade program was to provide a significant improvement in the reliability and maintainability of rotor blades for the H-46. The design concept was similar to main rotor blades developed by Boeing Vertol for the Army CH-47, YUH-61 and HLH.

3.1 Metal Blade Problems

The existing H-46 metal rotor blade has been a source of continuing maintenance expense. The major cause of H-46 metal blade failures in service were undetected manufacturing defects, atmospheric and fretting corrosion, mechanical damage, and gunfire. The lack of tolerance to defects resulted in the necessity for many blade inspections in service and a high rate of return to depots for inspection and repair. A sealed spar pressure crack detection system was developed and retrofitted to monitor conditions in service. Malfunctions of this crack detection system added to an already low reliability level and increased the unscheduled removal rates. The attrition rate of metal blades due to corrosion is substantial.

3.2 Composite Blade Description

The H-46 composite rotor blade is shown in Figure (6). The rotor blade consists of a fiberglass "D" spar terminating in a two-pin, four-lug, wrap-around root end retention. Graphite is located along the spar vertical heel web to increase flapwise stiffness and section torsional stiffness. A titanium/nickle leading edge nose cap provides all-weather erosion capability for the blades, some torsional stiffness, lightning protection, and FOD protection for the composite leading edge. Titanium was selected in this application because of its formability and fatigue strength which makes it compatible with the fiberglass/graphite.

This construction concept is expected to be corrosion resistant and insensitive to small defects with soft failure propagation exhibiting a change in stiffness warning. This behavior allows pre-flight visual inspection only. Manufacturing process repeatability is expected to reduce blade tracking and balance time. Aerodynamically and dynamically the fiberglass blade is the same as the current metal blade. Qualified material systems include NARMCO 5209/T300 graphite; SP250/E and S2, and NARMCO 5216/E and S2 fiberglass and Ti-6AL-4V. E glass fibers are PPG 1062K and Owens Corning 456G, and S-2 glass fibers are Owens Corning 463.

3.3 The Composite Blade Program

The composite rotor blade program [Program schedule shown in Figure (7)] was designed to replace attrited metal blades by providing a replacement that satisfied vibration and load constraints established by the existing airframe and its dynamic

TECHNICAL LIBRARY
ABBOTTAEROSPACE.COM

components. During the course of the development, considerable effort was expended to establish production techniques that were cost effective. The composite blade program consisted of three phases as follows:

3.3.1 Phase I Development

This phase consisted of preliminary blade design, production blade design, tool design and fabrication; fabrication of tool proover and 14 test blades; reliability development/qualification via fatigue and whirl tests; and a flight test program.

3.3.2 Phase II Pilot Production and Reliability Demonstration

This phase consisted of tooling and minor design updating from the initial blade fabrication, fabrication of a pilot-production quantity of 72 blades, a reliability demonstration test utilizing ten flight aircraft in a closed cycle contractor supported program, and a flight demonstration of blade interchangeability.

The Phase II [Figure (8)] reliability testing was a key element of the development plan and was conducted from May 1978 to May 1979 under a variety of fleet operating conditions by four squadrons at four different locations. Sixty blades were utilized and a total of 18,658.8 blade flight hours were accumulated with no returns to depot required. The average hours per blade during the evaluation demonstration was 311 hours and the high time blades-six accumulated 778 hours. All blades continue in operation. Figure (9) provides data showing the cumulative blade hours for the program. Fourteen accountable repairs were accomplished by organizational or intermediate level maintenance. The problem areas (i.e. de-ice blanket wiring harness, inboard and outboard rubber closure rib) were identified early and timely corrective actions (i.e. manufacturing changes, design improvements, maintenance procedures) were initiated. It should be noted that the structural integrity of the blade was unaffected by any of the problems encountered and that no significant design defects were manifested. Approximately 200 pilots flew the H-46 with fiberglass blades during the evaluation. The vast majority of pilots rated flight performance good to excellent for all maneuvers.

Ultrasonic inspections were conducted at scheduled intervals throughout the program as shown in Figure (8). Blade areas inspected included the spar area covered by the titanium cap as well as the inboard end of the spar, trailing edge and the trim tab. The results of these inspections were compared to original inspection records made at the time of manufacture. Comparisons indicated a few areas of minor disbond growth or new disbond indications after the original inspections with no further changes found in later inspections. Based upon testing of representative blade specimens with similar NDI indications, none were of structural significance.

The development and implementation of practical repair concepts was a primary objective of the maintainability program. Field level repairs and materials were identified and developed. Sixteen typical repairs, Figure (10), were made to an outboard blade fatigue test specimen prior to test. Fatigue testing confirmed the adequacy of the repairs.

When fiberglass rotor blades were reinstalled following removal for maintenance, no new tracking adjustments were required. No difficulties with rotor blade interchangeability have been reported.

The experience from the service reliability program was used to maximize the likelihood that problems were identified and corrected prior to full scale production commitments. Approval for service use was granted in November 1979 and production rotor blades are being delivered for use on fleet aircraft.

3.3.3 Phase III Rate Production

Production and delivery of blades for the fleet is now underway with 339 delivered through the end of 1979. Nearly 50,000 rotor blade flight hours have been accumulated through the end of 1979. Service experience continues to be excellent. Rate production will continue for several years until metal blade attrition requirements are satisfied.

Although service experience is very limited, experience to date indicates the H-46 composite blade may well provide a solution to every major problem existing with the H-46 metal rotor blade. Cost studies indicate that composite blades will cost no more than metal blades in production. With reduced spares requirements, seemingly excellent repairability in the field and higher reliability in service, the admittedly still limited information supports the likelihood of a much lower overall cost of ownership.

4. GRAPHITE/EPOXY STRUCTURE ON THE YAV-8B

The YAV-8B Flight Demonstration Aircraft is a high performance, transonic, light attack V/STOL aircraft built by the McDonnell Douglas Corporation with the British Aerospace Corporation. The AV-8B is an advanced derivative of the Harrier V/STOL aircraft now in field service with the United States Marine Corps as the AV-8A/TAV-

TECHNICAL LIBRARY
ABBOTTAEROSPACE.COM

8A. Two YAV-8B aircraft have been built as flight test vehicles in support of the AV-8B Advanced Harrier full scale development aircraft.

4.1 Structural Description

The YAV-8B aircraft is characterized by a continuous carry-through shoulder mounted super critical wing and a swept stabilator, both with marked anhedral; a single vertical fin and rudder, and four vectored thrust nozzles, two on each side of the fuselage. As described in references (1) and (2), extensive use of graphite epoxy composites is made in the wing structure, Figure (11), which is composed of a main torque box, ailerons, trailing edge flaps and flap doors, (all embodying advanced composite structure), metal leading edge, wing tips, and pylons. The inboard portion of the main torgue box is sealed and serves as an integral fuel tank. The wing is configured to accept six pylons; inboard and intermediate stations contain external fuel provisions. A reaction control system (RCS) duct extends through the wing leading edge to valves located in the wing tips. The wing is attacked to the fuselage by three fittings on each side between the wing fuselage rib and the fuselage.

The 28 foot span wing torque box is a multi-spar design. The upper and lower covers are simple monolithic solid laminates of AS/3501-6 unidirectional graphite/epoxy, continuous from tip-to-tip and variable in thickness and orientation to provide for the many different loading conditions. The substructure is primarily sinewave construction fabricated with T300/3501-6 woven graphite/epoxy broadgoods. Metal fittings have been used at all significant load introduction points and where substantial out-of-plane loads exist. Assembly of the torque box is accomplished by bolts and nuts and no secondary bonding has been attempted.

The flaps and ailerons are of similar construction as the torque box except that channel type spares and ribs are used in most locations due to the lesser thickness of these components. Due to its very shallow thickness, the flap door is a full depth honeycomb design, with aluminum honeycomb core and graphite/epoxy skins. The outrigger and overwing fairings are relatively lightly loaded components and are fabricated as syntactic sandwich construction and are further stiffened with either cocured hat section stiffeners or separately cured stiffeners, subsequently bolted on. Three wings have been built, two for flight aircraft and one for static structural testing which has been successfully completed.

4.2 Experiences With Composite Wing

Fabrication of the graphite/epoxy wing and subsequent flight testing of the two YAV-8B prototype aircraft has provided some limited experience living with graphite/epoxy structure. Several observations from this experience are as follows:

- As with any new material, manufacturing personnel were somewhat apprehensive and cautious when first introduced to graphite/epoxy but as they gained experience in drilling holes, trimming edges, etc., they gained confidence in working with it and soon acquired a feel for it as a practical structural material.

- Early experience in repair came with the assembly of the substructure for the wing. Several holes were drilled at an improper location and had to be relocated to the correct position. The repair for this problem was to fill the hole with a chopped fiber/epoxy mix. When the filler was cured, (at room temperature), the hole was re-drilled at the proper location. The low design strain levels provided a structure generally tolerant to this type of typical manufacturing anomaly.

- Well into the assembly of the wing, it was discovered that additional shear strength was required in a portion of one rib. Since the lower skin was already attached to this member, removal was impractical. An auxiliary rib section was fabricated and installed adjacent to the existing rib much as a doubler would have been installed on a metal rib.

- A development program provided for evaluation of bolted repairs for graphite/epoxy structures. Part of the evaluation involved patching holes in sections representative of the YAV-8B wing skins, with titanium plates and bolts. Shortly after the YAV-8B made its first flight, it was discovered that access to the aft center wing tank was necessary. No access was available, so an elliptical hole was cut in the upper skin, the necessary modification was accomplished, and the hole patched with a titanium plate and bolts. Figure (12a) shows the elliptical hole in the wing skin together with the external patch plate and fastener pattern. Figure (12b) shows the external plate as well as the internal plates used to attach and locate the nut plates. The aircraft has since been through a flight test program that included approximately 190 flights with load factors as high as +7.0 g's. No problems or fuel leaks have occurred associated with the patch.

- During the flight test program, there were several instances of fuel leaks at fasteners through the graphite/epoxy skins, Figure (13). None of these leaks were attributed to the graphite/epoxy, but rather, faulty O-rings, loose fasteners or bad holes. All leaks were repaired.

TECHNICAL LIBRARY
ABBOTTAEROSPACE.COM

- A porosity condition on a fuel tank spar web which did not infringe on structural adequacy but which allowed fuel seepage was readily resolved. A partial vacuum was applied to the fuel tank and epoxy was painted on the external surface of the spar webs, which was then drawn into the porous areas - resolving the problem.

- In the course of various maintenance and inspection operations, personnel frequently walked and sat on the upper skin of the torque box. No special precautions or limitations were imposed against this and no damage was ever observed. The overwing fairing and engine bay access doors were also walked on and although they are considerably more flexible, no damage was observed.

- The Lift Improvement Devices (LIDS) fence and the graphite/epoxy strakes, Figure (14), are subject to impact damage from objects blown about during vertical landings and takeoffs and during power nozzle braking. No such damage was observed.

- Flight testing and service experience of the YAV-8B to date has revealed no problems attributable to the composite materials.

5. S-3A SPOILERS AND F-4 ACCESS DOORS

These secondary structural components were selected for composite demonstration specifically to acquire service exposure information. Following ground testing, limited numbers of these components were manufactured and placed on operational aircraft as direct replacements for metal components.

5.1 Structural Description Of Spoilers

The S-3A spoilers are surfaces hinged off the rear spar of the wing. They function as roll control devices and speedbrakes. Each wing half has four spoilers - three upper and one lower. The lower spoiler, which was selected for composite application, is located on the wing underside as shown in Figure (15), and is a simple beam supported by two hinge fittings and positioned by a push rod attached to each fitting. The lower spoiler planform is quadrilateral about 85 in. long, 8 in. wide at the outboard end, and 15 in. wide at the inboard end.

The spoiler is composed of twenty parts including a slightly contoured graphite-epoxy outer skin of variable thickness, a glass-reinforced-plastic honeycomb core, a pan shaped graphite-epoxy variable thickness inner skin and two metal hinge fittings that are attached to the surface with inserts bonded into the core. The complete assembly, including the trailing edge seal, is shown in Figure (16).

A low-temperature cure graphite reinforced epoxy system was used in order to reduce processing costs and to utilize a high strength/high peal adhesive for bonding. The material system selected was 5209/T300. Adhesives used were METALBOND M-1113 and 3M AF126 film. These materials have a 260°F during temperature with service application temperature limits of 180°F which is suitable for the spoiler environment. Lightning protection is provided by an aluminum wire mesh screen bonded to the external skin during cure of the laminate.

Construction details being evaluated in service are low temperature cure laminates and adhesive, thin skin honeycomb construction, potted insert attachments and wire mesh lightning protection.

5.2 Service Evaluation Of Spoilers

Fourteen ship sets of composite spoilers were fabricated. Ten were placed in service and four were held as spares. One ship set was installed on a test aircraft in April, 1975, to undergo flight testing at the Naval Air Test Center, Patuxent River, MD and has remained on the aircraft since then. The remaining nine ship sets were installed in February, 1977. Six were assigned to a Pacific Coast squadron and three were assigned to an Atlantic Coast squadron. Accompanying the spoilers were NDI standards and inspection/repair instructions. As of 30 November 1979, a total of 331 service months and 10,060 flight hours have been accumulated. Spoilers assigned to the Pacific Coast squadron have been deployed aboard carriers.

Several incidents have occurred to the spoilers related to installation, maintenance, or logistics. The first incident occurred during installation of the spoilers. One of the spoilers was dropped on the runway during high wind conditions and sustained delaminations and a chipped corner. The second incident occurred during routine maintenance of the aircraft. Both surfaces were penetrated by one of the push rods which had not been connected to the upper metal spoiler. The entrance damage is shown in Figure (17) and the exist damage in Figure (18). A thin skinned metal spoiler would have sustained comparable damage in a similar incident. The third incident occurred during ground handling in which several spare spoilers were dropped into the water during a loading operation. One spoiler sustained a crack across the compression skin and a chipped corner. Another spoiler had a chipped corner and several shallow gouges. Metal spoilers dropped in the same incident also incurred damage which was qualitatively judged to be less significant. All damage to the spoilers has been repaired or is in the process of being repaired. Routine visual and tap inspections of all composite spoilers have revealed no damage to spoilers other than described above.

TECHNICAL LIBRARY
ABBOTTAEROSPACE.COM

One ship set of spoilers was removed after 30 months of service for laboratory evaluation. The spoilers were first inspected using ultrasonic C-scan and X-ray. No delaminations, unbonded areas, or signs of water infiltration were detected. One spoiler was static tested identically to previous tests performed during preflight ground testing. Deflection characteristics, failure load and failure location were essentially the same as obtained in previous tests indicating no detrimental structural effects occurred as a result of the 30 months service environment. The spoiler will be dissected, inspected, cut into small specimens, and tested to determine any changes in material properties. Other spoilers will remain in service for a period of five years during which time several ship sets will be removed and laboratory tests performed.

5.3 F-4J Access Doors

This program, described in detail in reference (3), has been devoted to testing of composites in a carrier environment through installation of graphite-epoxy access doors on F-4J aircraft. The principal objectives of this program were to verify corrosion prevention methods used in graphite-epoxy/metal combinations, and determine the amount and rate of water absorption in graphite/epoxy composites on naval aircraft. Materials selected and corrosion prevention methods considered are those which are intended for application on the F-18 and AV-8B.

Two types of F-4J doors were selected for replacement with graphite/epoxy test doors: 1) an electrical access door, approximately 19 x 15 in.; and 2) a fuel access door, 8 in. in diameter. The locations of these doors on the F-4J are shown in Figure (19). As door orientation when installed on the aircraft could affect water retention, a vertical and a horizontal door were selected.

Eight graphite-epoxy test doors, four electrical access and four fuel access, were fabricated. These doors contained various test specimens which were attached to the inside of the doors. The test specimens consisted of various combinations of graphite/epoxy, aluminum (core and sheet), titanium, and Nomex core either adhesively bonded and/or mechanically fastened to their interior surfaces. Each door also contained twenty-four graphite-epoxy tabs for moisture content monitoring. Twelve were bare and twelve were painted. All tabs were twelve plys thick.

During February and March of 1977, the eight test doors were installed on four carrier-based F-4J aircraft, one set (an electrical and a fuel access door) per aircraft. Two of these aircraft were assigned to the Atlantic Fleet and two to the Pacific Fleet.

During service, these doors were inspected bimonthly. Door attachments were examined for evidence of corrosion and one painted and one unpainted tab were removed and sent to MCAIR, St. Louis for moisture content measurements. No corrosion was found on any attachments or fasteners during two years of monitoring. The moisture content was consistently higher for painted than for unpainted tabs and cycled with the seasons, being higher in the summer when it was hot and humid and lower in the winter. Typical moisture content variations are shown in Figure (20).

Six of the eight doors, four from the Atlantic and two from the Pacific Fleet, were removed in February 1979 for final examination. Visual, radiographic and ultrasonic inspections indicated the doors to be in generally good condition. Comparisons of specimens with baseline specimens fabricated in the same autoclave runs as the doors and subsequently exposed to either ambient environment or to accelerated environmental conditioning will be made. Final results are expected later this calendar year.

6. SUMMARY

A still limited but growing body of information is being accumulated on composites in actual service environments. To date, experience with production components has been largely "uneventful". Undoubtedly, as has been the case with most other aircraft structural materials in the past, there are lessons to be learned. But increasingly it appears that these lessons will relate to specific types of construction, design details and stress levels, or to fleet support methods rather than general widespread degradation of the carefully evaluated composite material systems now finding use. Further, experience suggests that successful expansion of composites in service will rest on stringent quality control in manufacture; traceability of components for obvious precautionary reasons and putting into place the required depot and fleet support capabilities.

REFERENCES

1. Weinberger, Somoroff and Riley, "U.S. Certification of Composite Wings for the F-18 and Advanced Harrier Aircraft", AGARD Report No. 660, April 1977.

2. Riley, B.L., "Composite Wing Technology on the AV-8B Advanced Aircraft", presented at the 34th Annual National Forum of the American Helicopter Society, Washington, D.C., May 1978.

3. Carrier Testing of Graphite Composites in Contact with Metals on F-4; Report Number NADC-76009-30, June 1979.

TECHNICAL LIBRARY
ABBOTTAEROSPACE.COM

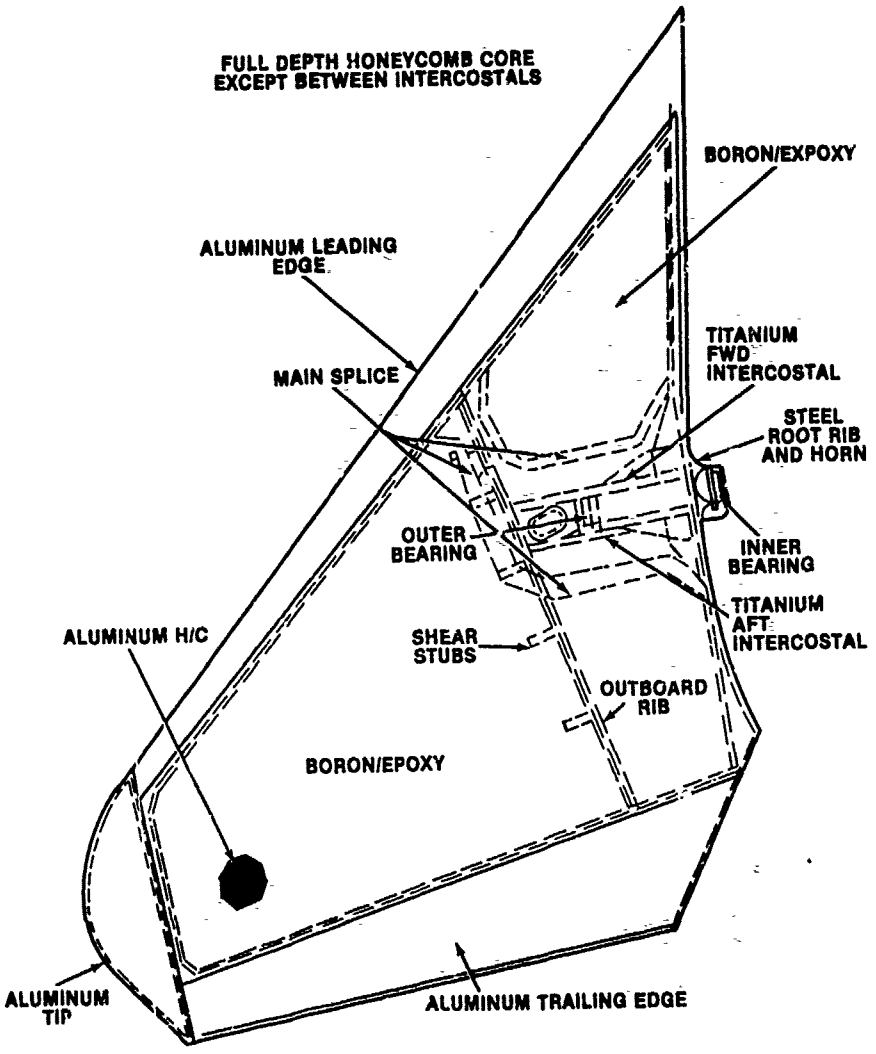

FIGURE 1—F-14 COMPOSITE STABILIZER

FIGURE 2—MINOR ABRASIVE DAMAGE

THIS DOCUMENT PROVIDED BY THE ABBOTT AEROSPACE
TECHNICAL LIBRARY
ABBOTTAEROSPACE.COM

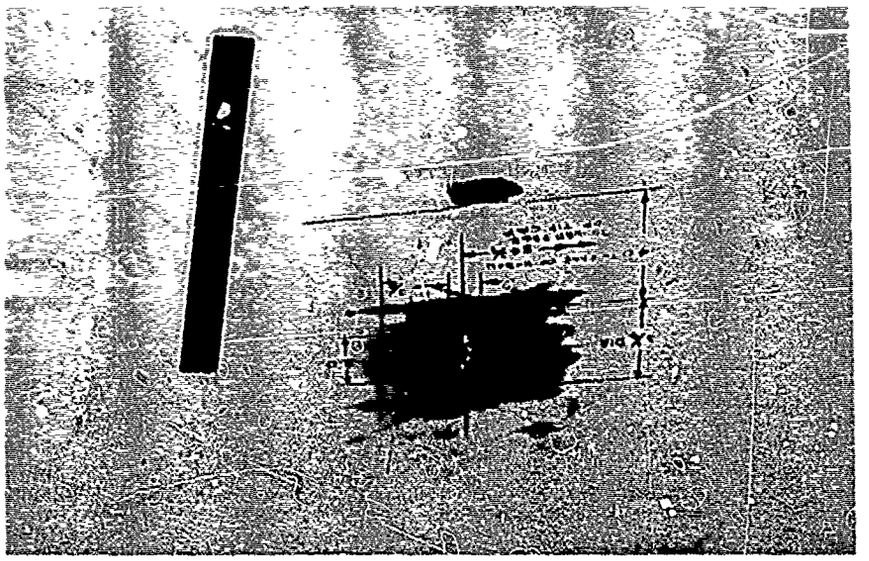

FIGURE 3—SKIN PENETRATION DAMAGE

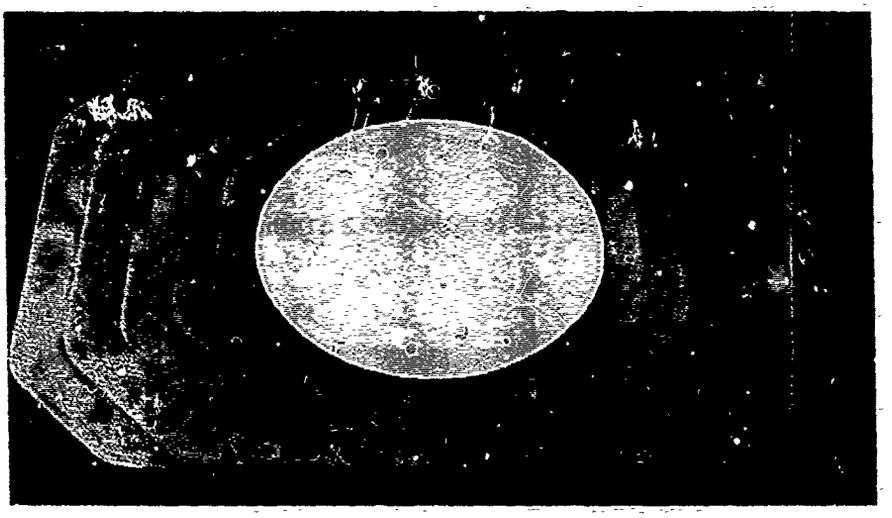

REPAIR SITE TERRACES

REPAIRED TEST ELEMENT

FIGURE 4—REPAIR TEST SPECIMENS FOR 6 INCH DAMAGE

TECHNICAL LIBRARY
ABBOTTAEROSPACE.COM

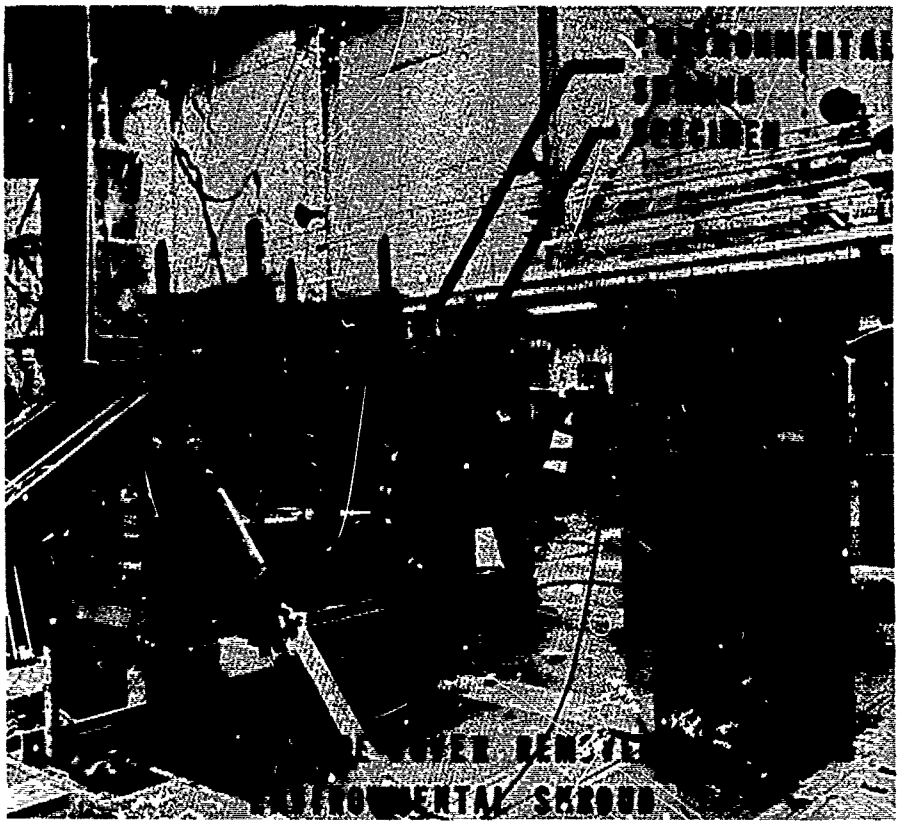

FIGURE 5—STATIC/FATIGUE SETUP WITH ENVIRONMENTAL SHROUD

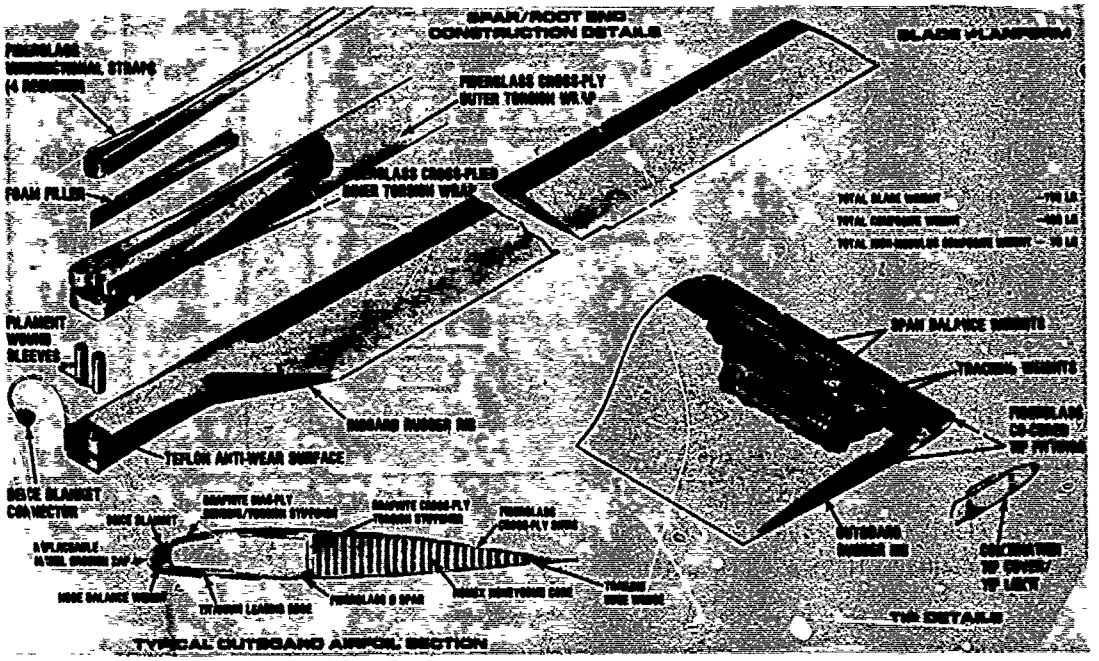

FIGURE 6—H-46 COMPOSITE ROTOR BLADE

THIS DOCUMENT PROVIDED BY THE ABBOTT AEROSPACE
TECHNICAL LIBRARY
ABBOTTAEROSPACE.COM

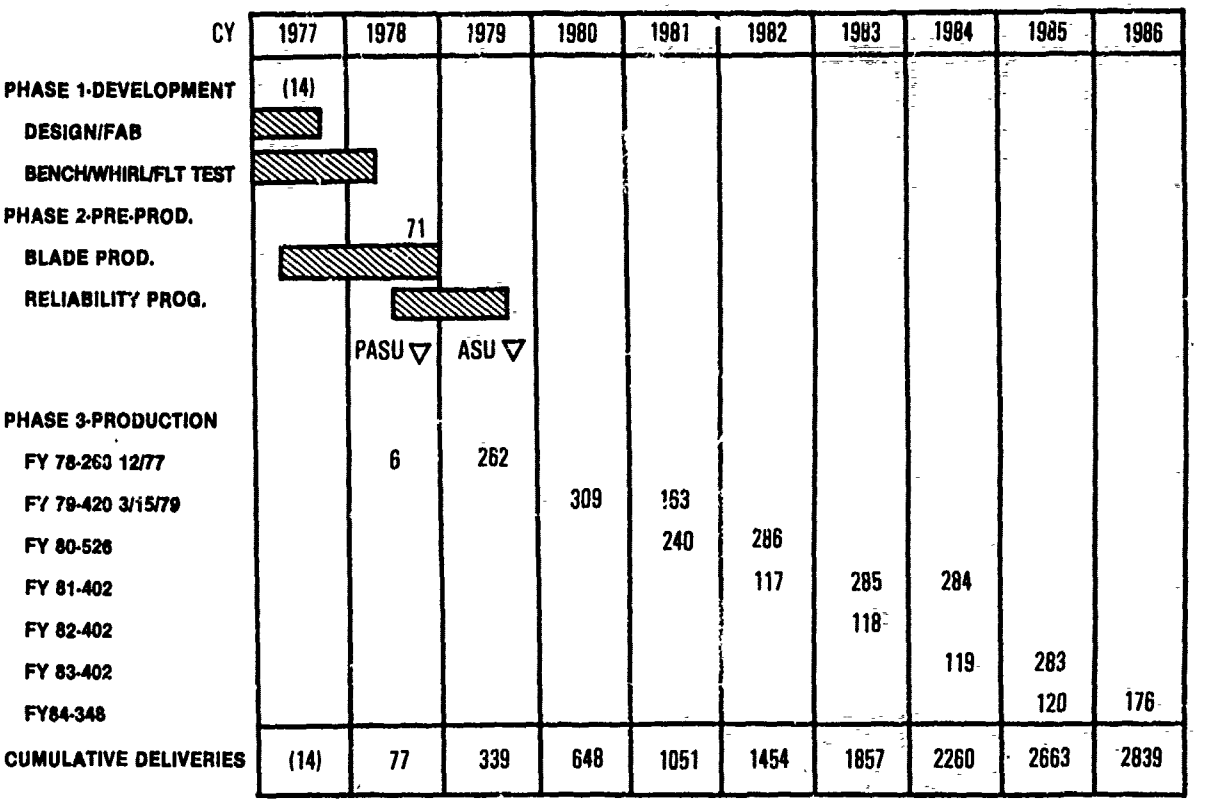

FIGURE 7—H-46 COMPOSITE ROTOR BLADE PROGRAM SCHEDULE

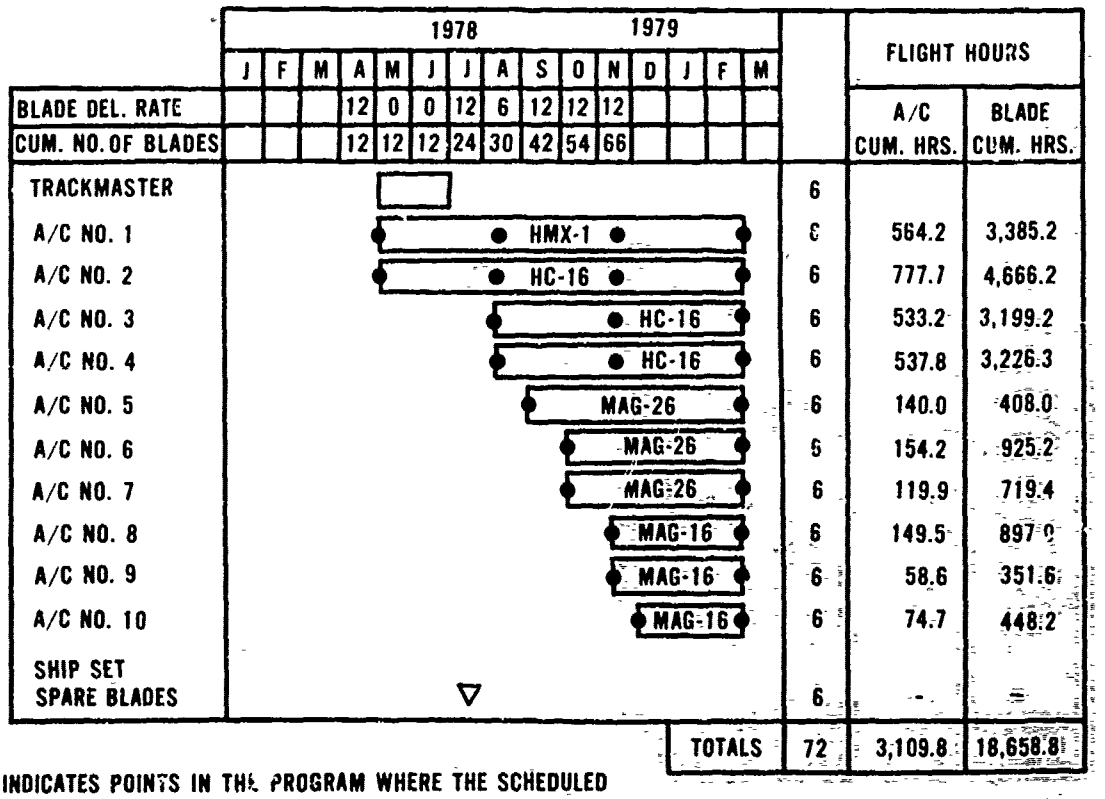

● INDICATES POINTS IN THE PROGRAM WHERE THE SCHEDULED NDT BLADE INSPECTIONS ARE CONDUCTED.

FIGURE 8—RELIABILITY DEMONSTRATION TEST PROGRAM BLADE ALLOCATION AND FLIGHT SCHEDULE

TECHNICAL LIBRARY
ABBOTTAEROSPACE.COM

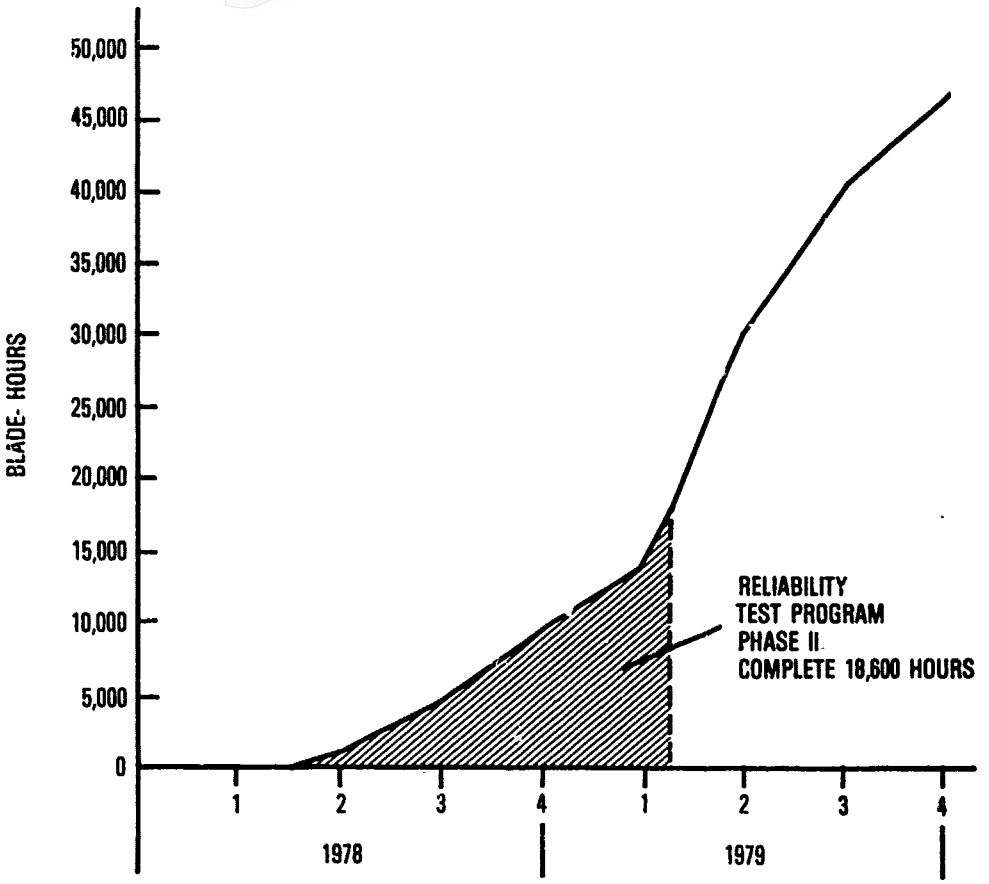

FIGURE 9—COMPOSITE ROTOR BLADE FLIGHT HOURS

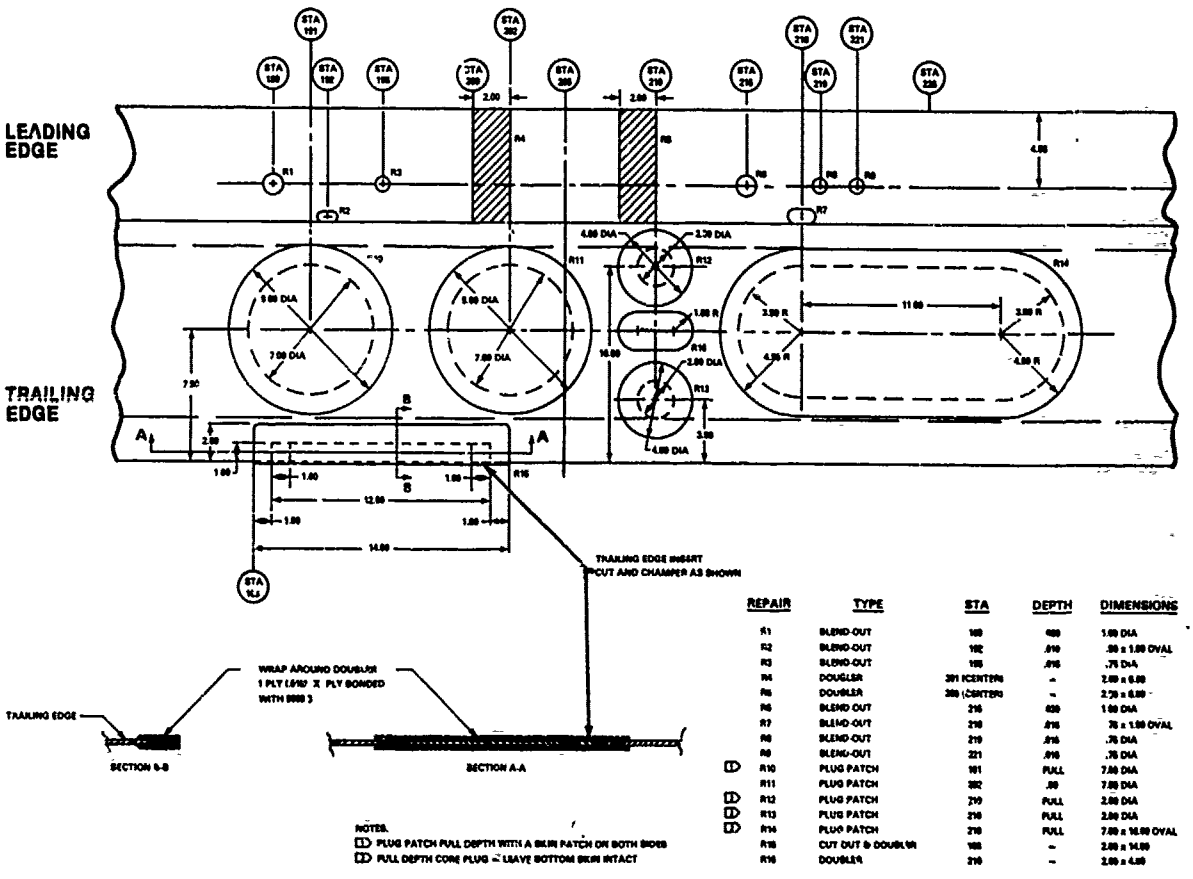

REPAIR	TYPE	STA	DEPTH	DIMENSIONS
R1	BLEND-OUT	160	020	1.00 DIA
R2	BLEND-OUT	192	.010	.50 x 1.00 OVAL
R3	BLEND-OUT	195	.015	.75 DIA
R4	DOUBLER	201 (CENTER)	–	2.00 x 6.00
R5	DOUBLER	209 (CENTER)	–	2.20 x 6.00
R6	BLEND OUT	216	020	1.00 DIA
R7	BLEND-OUT	216	.015	.75 x 1.00 OVAL
R8	BLEND-OUT	219	.015	.75 DIA
R9	BLEND-OUT	221	.015	.75 DIA
R10	PLUG PATCH	161	FULL	7.00 DIA
R11	PLUG PATCH	202	.00	7.00 DIA
R12	PLUG PATCH	219	FULL	2.00 DIA
R13	PLUG PATCH	216	FULL	2.00 DIA
R14	PLUG PATCH	216	FULL	7.00 x 16.00 OVAL
R15	CUT OUT & DOUBLER	188	–	2.00 x 14.00
R16	DOUBLER	216	–	2.00 x 4.00

FIGURE 10—H-46 COMPOSITE BLADE REPAIRS

THIS DOCUMENT PROVIDED BY THE
TECHNICAL LIBRARY
ABBOTTAEROSPACE.COM

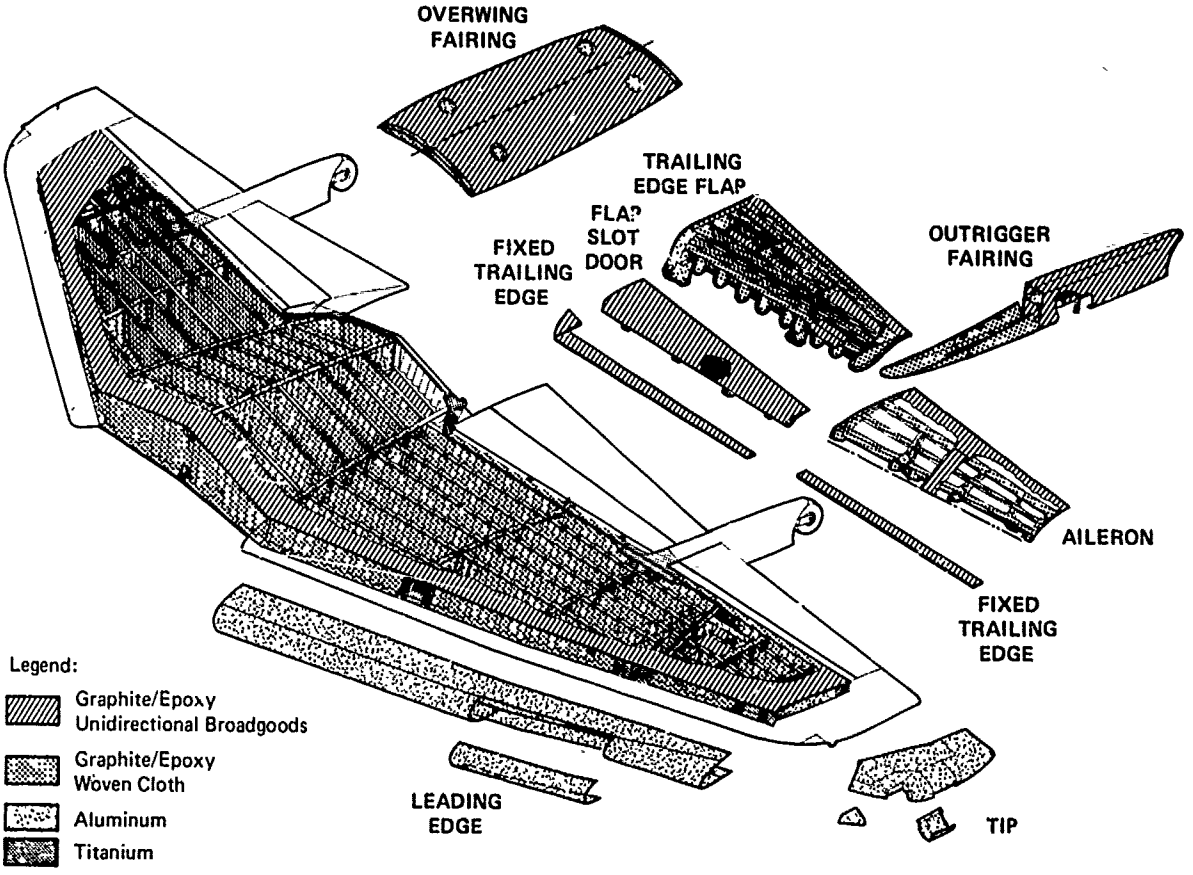

FIGURE 11—YAV-8B COMPOSITE WING

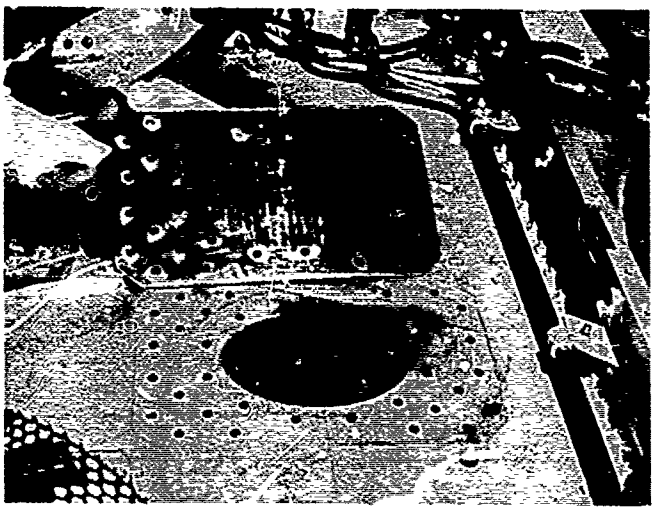

FIGURE 12A—BOLTED REPAIR ON YAV8B WING SKIN

FIGURE 12B—BOLTED REPAIR PARTS

TECHNICAL LIBRARY
ABBOTTAEROSPACE.COM

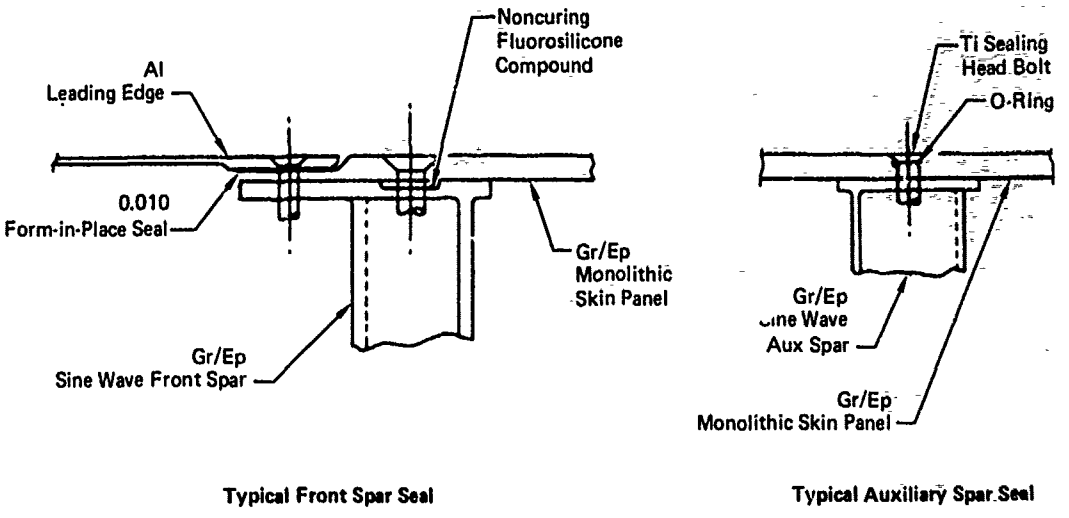

Typical Front Spar Seal

Typical Auxiliary Spar Seal

FIGURE 13—WING FUEL TANK SEALED SKIN SECTION

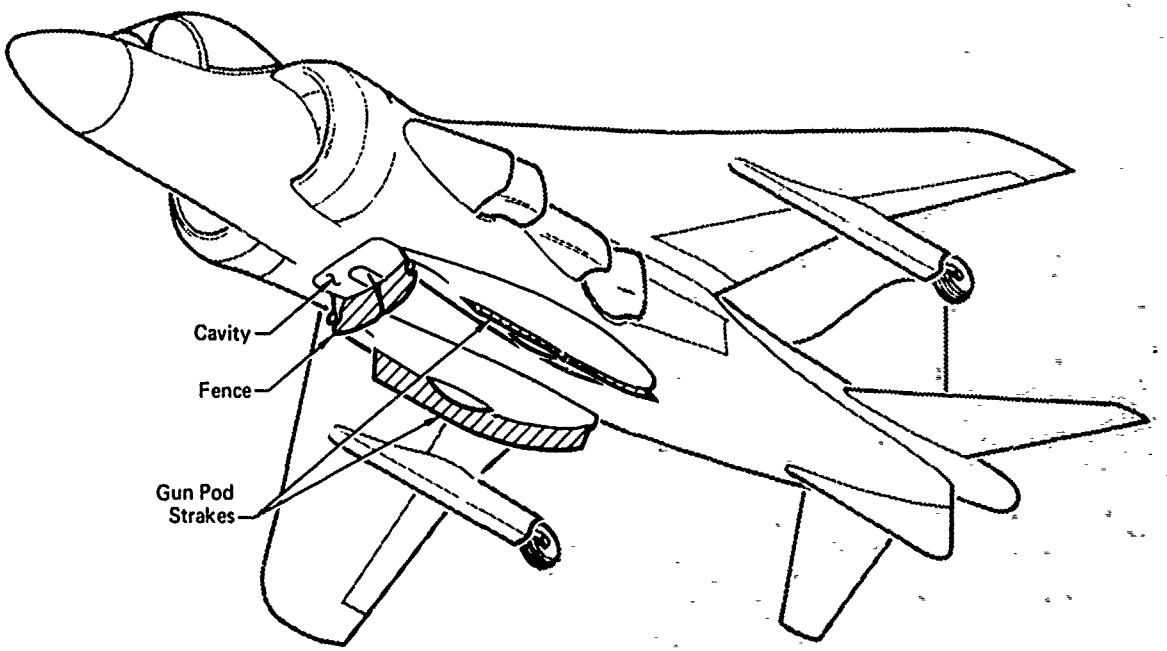

FIGURE 14 AV—8B LIFT IMPROVEMENT DEVICES

TECHNICAL LIBRARY
ABBOTTAEROSPACE.COM

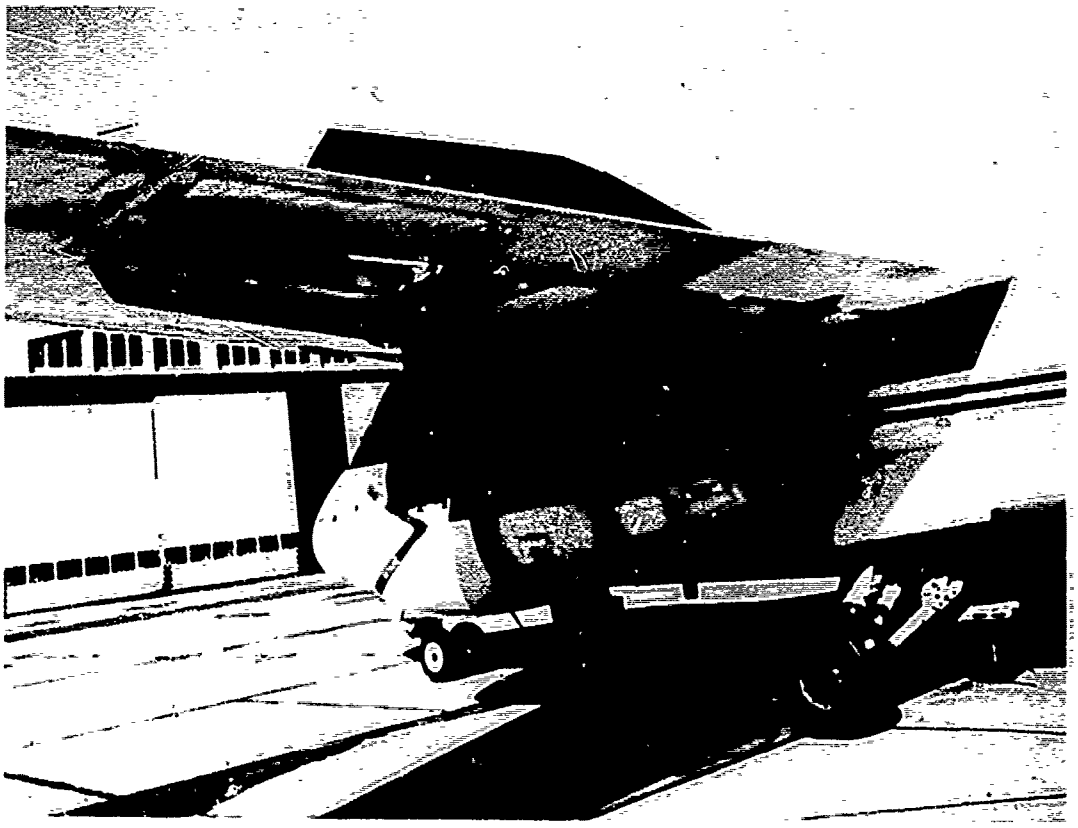

FIGURE 15—COMPOSITE LOWER SPOILER ON S-3A

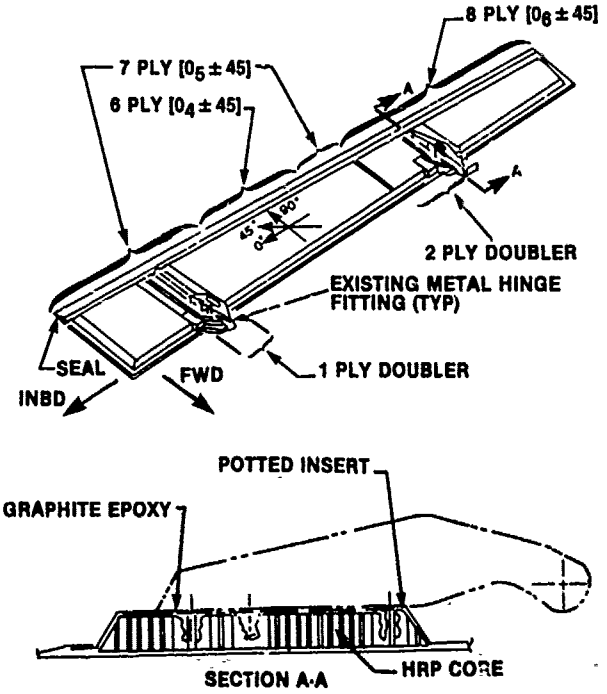

FIGURE 16—S-3A COMPOSITE SPOILER ASSEMBLY

TECHNICAL LIBRARY
ABBOTTAEROSPACE.COM

FIGURE 17—ENTRANCE DAMAGE ON S-3A COMPOSITE SPOILER

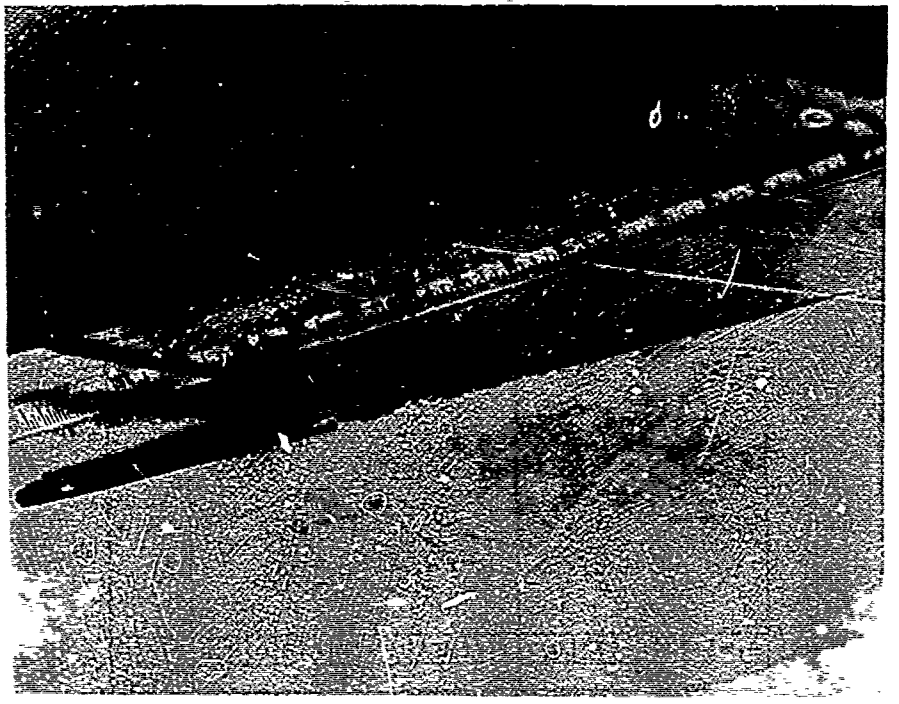

FIGURE 18—EXIT DAMAGE ON S-3A COMPOSITE SPOILER

TECHNICAL LIBRARY
ABBOTTAEROSPACE.COM

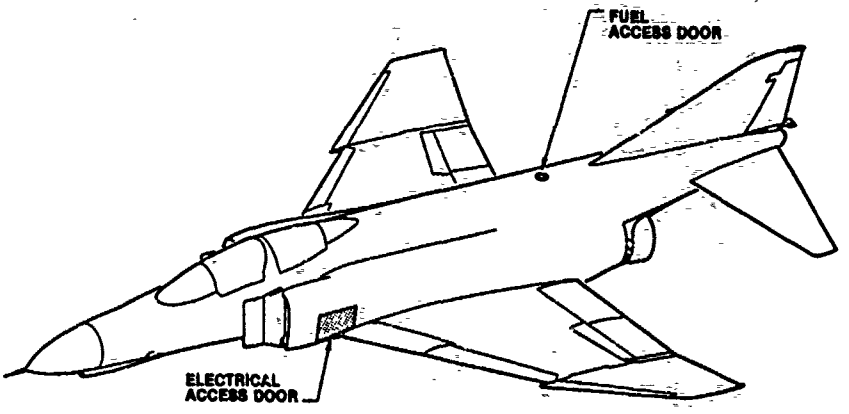

FIGURE 19—LOCATION OF SELECTED F-4J DOORS

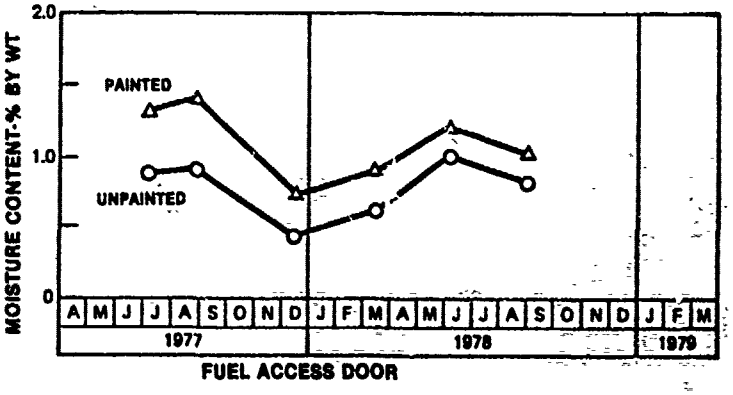

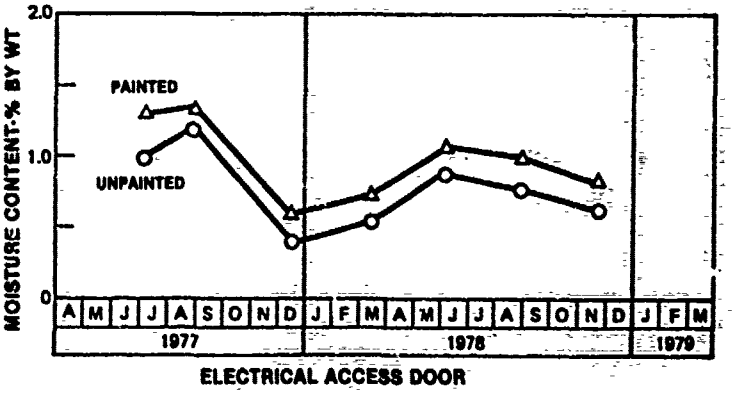

FIGURE 20—MOISTURE CONTENT OF GRAPHITE EPOXY TABS TAKEN FROM DOOR SET (ATLANTIC FLEET)

TECHNICAL LIBRARY
ABBOTTAEROSPACE.COM

EXPOSE DU RAPPORTEUR

SESSION V – ETUDES DE CASE D'EXPERIENCE EN SERVICE

par

J-M.Fehrenbach
Centre D'Essais Aeronautique de Toulouse (C.E.A.T.)
23 Avenue Henri Guillaumet
31056 Toulouse Cedex
France

Cinq papiers ont été présentés dans le cadre de cette session relative à l'expérience en service. Les deux premiers concernent les pales d'hélicoptères tandis que les trois autres présentent un panorama asses général de l'expérience en service aux Etats-Unis sur avions civils et militaires, avec une allusion plus limitée au cas des hélicoptères.

Le présent rapport a pour objet de souligner les thèmes qui ont été relevés comme particulièrement significatifs au cours de cette session, en tenant compte au mieux des éléments apportés par la discussion qui a suivi.

Le Dr BARNARD a présenté d'une manière très didactique l'intérêt des composites pour la structure des pales d'hélicoptères ainsi que les méthodes de qualification employées par Westland. Il a souligné que les méthodes employées ont permis de disposer de pales à durée de vie "non limitée", l'expérience en service n'ayant pas amené de remise en cause de cette approche. Son exposé a largement développé la philosophie des essais tant en ce qui concerne les essais sur "éléments structuraux" que ceux effectuée sur des pales ou tronçons de pales.

Westland considère que l'expérience acquise devrait permettre à l'avenir une réduction des facteurs de sécurité actuellement utilisés pour tenir compte de la dispersion des caractéristiques du matériau.

Une question a été posée concernant la corrélation entre les résultats d'essais sur éléments et sur tronçons de pales. Il arrive en effet que les modes de rupture, dans les conditions d'essai réalisées en labo soient différents de ceux de pièces réelles. Toutefois, les durées de vie "non limitées" obtenues ne remettent pas en cause la méthode.

Un programme d'exposition aux intempéries est en cours afin de permettre une évaluation du vieillissement à long terme des pales sous l'effet de l'environnement.

Mr K. BRUNSCH s'est appuyé sur l'expérience importante en service déjà accumulée sur le BO 105 pour souligner à son tour l'intérêt du matériau verre-époxy pour les pales d'hélicoptères : certaines pales, en service depuis 9 ans, approchent les 6 000 heures de vol, et les conditions d'environnement auxquelles elles sont soumises couvrent un très large domaine, depuis le golfe du Mexique jusqu'aux zones polaires. Les résultats apparaissent très positifs : en résistance comme en rigidité, des éléments ayant accumulé des milliers d'heures de vol présentent peu d'évolution des caractéristiques. La sensibilité aux endommagements (délaminage, impact...) apparaît peu critique.

Toutefois, la longue expérience de MBB a mis en évidence :

- les problèmes d'érosion en extrémité de pale pour lesquels la remise en état de la protection n'a pas encore atteint un stade de définition satisfaisant.
- les difficultés de réparation par l'utilisateur pour les pièces relativement sophistiquées que sont les pales d'hélicoptères.

Les exposés de MM. DEXTER, FECHEK et DUBBERLY (remplaçant de M. SOMOROFF) sont apparus très complémentaires.

La NASA étudie les effets de l'environnement sur les composites dans le cadre de plusieurs programmes d'activité :

- Evaluation des composites en service sur appareils de transport et hélicoptères civils.
- Développement des technologies ayant un impact sur les économies d'énergie (programme ACEE).
- Investigation extensive de l'effet de l'environnement sur coupons élémentaires.

Ce travail, commencé dès los années 1970, représente aujourd'hui une importante expérience accumulée (200 éléments en vol, totalisant 2,5 millions heure x composant).

TECHNICAL LIBRARY
ABBOTTAEROSPACE.COM

L'analyse des résultats a mis en évidence le faible niveau de dégradation constaté au terme de plusieurs années en service. Le "niveau de confiance" obtenu progressivement amène à étendre à une part plus grande de la structure l'usage des matériaux composites. Cette démarche se concrétise dans le cadre du remplacement du métallique par du composite sur des avions anciens ou par une utilisation extensive de la technologie composite pour l'ensemble des éléments mobiles ou démontables pour des projets nouveaux (B. 767).

L'U.S.A.F. a largement introduit l'usage des composites sur ses avions au cours de la dernière décennie. Des travaux systématiques ont été entrepris en laboratoire, au sol, en vol, pour évaluer le vieillissement en service des composites. Une phase importante actuellement en cours vise au développement d'un matériel de contrôle par ultra-sons fortement intégré, pour mise en oeuvre sur les bases par les utilisateurs (programme ISIS).

Des dommages ont été constatés en service, des réparations ont été mises au point et on a constaté généralement la faible évolution dans le temps des dégradations observées.

Le niveau de confiance obtenu a conduit a étudier l'emploi des composites pour des structures de fuselages (F 5, F 16).

L'US NAVY a également développé l'usage des composites sur ses appareils, avec des éléments importants sur F 14 et F 18 et le remplacement des pales métalliques du H 46.

Là encore, l'expérience accumulée apparaît très satisfaisante : les endommagements en service sur stabilisateurs F 14 n'ont pas posé de problèmes particuliers à la NAVY. Des méthodes satisfaisantes de réparation (restaurant les caractéristiques initiales) ont été développées et vérifiées.

L'expérience acquise sur le F 18 reste actuellement plus limitée par le faible nombre d'heures de vol.

Le niveau de confiance obtenu amène au projet de voilure composite "monobloc" pour le Y AV 8 B.

D I S C U S S I O N

Certaines questions ont été relevées comme présentant un intérêt majeur :

a - Le contrôle de la qualité a été souligné à plusieurs reprises comme étant un problème important pour l'emploi des composites dans les structures primaires. Ce problème revêt plusieurs aspects :

  - la qualité doit être assurée à tous les niveaux de la production et bien sûr contrôlée avec soin compte tenu de la sensibilité des caractéristiques à la précision du processus industriel

- le niveau d'exigence quant aux performances des moyens de contrôle dépend largement du caractère critique ou non critique des pièces concernées. Pour des pièces dimensionnées en rigidité (éléments mobiles sur avions), le seuil de détection de défauts peut être relativement large. Il n'en est pas de même pour des pièces vitales dimensionnées en résistance.

- le contrôle en service présente des caractéristiques semblables.

- il faut admettre que certains cas constatés peuvent encore poser des problèmes d'interprétation aux ingénieurs responsables : quels défauts peut-on tolérer en production ou en service pour des pièces vitales fortement sollicitées ?

TECHNICAL LIBRARY
ABBOTTAEROSPACE.COM

b - Les réparations sur composites ne paraissent pas présenter de difficultés majeures. Toutefois, si des réparations par l'utilisateur s'envisagent aisément sur des pièces sandwich dimensionnées en rigidité, il n'en est sans doute pas de même pour des pièces vitales plus sophistiquées.

c - L'expérience acquise paraît déjà très significative sur les pales d'hélicoptères. En ce qui concerne les avions, les données recueillies permettent d'étendre peu à peu l'usage de cette nouvelle technologie avec un bon niveau de confiance. Il faut cependant souligner le fait qu'on ne dispose à ce jour que d'une expérience très limitée sur des pièces vitales de dimensions appréciables, dimensionnées en résistance et travaillant à haut niveau de contrainte.

TECHNICAL LIBRARY
ABBOTTAEROSPACE.COM

REPORT DOCUMENTATION PAGE

1. Recipient's Reference	2. Originator's Reference	3. Further Reference	4. Security Classification of Document
	AGARD-CP-288	ISBN 92-835-0273-6	UNCLASSIFIED

5. Originator Advisory Group for Aerospace Research and Development
North Atlantic Treaty Organization
7 rue Ancelle, 92200 Neuilly sur Seine, France

6. Title

EFFECT OF SERVICE ENVIRONMENT ON COMPOSITE MATERIALS

7. Presented at

the 50th Meeting of the AGARD Structures and Materials Panel, held in Athens, Greece on 14–17 April 1980.

8. Author(s)/Editor(s)	9. Date
Various	August 1980
10. Author's/Editor's Address	**11. Pages**
Various	338

12. Distribution Statement This document is distributed in accordance with AGARD policies and regulations, which are outlined on the Outside Back Covers of all AGARD publications.

13. Keywords/Descriptors

Composite materials
Service life
Wear
Erosion
Fatigue (materials)
Damage
Weathering
Lightning
Environmental tests

14. Abstract

This meeting consisted of 21 presentations divided into 5 sessions:

- Physico-Chemical Effects of Environment
- Environment Superimposed on Stressing
- Mechanical Effects and Hazards
- Physical Hazards (lightning, rain erosion . . .)
- Case Studies of Service Experience.

The effects of humidity and of impacts, particularly when tests were made in compression, were emphasized. Damage due to lightning appeared to be less serious than had previously been supposed.

Some theories were propounded for the calculation of erosion, for the prediction of properties in a vacuum and for fatigue damage.

Service experience, on the other hand, proves to be extremely favourable and has not shown, up until now, any evidence of disturbing phenomena.

AGARD Conference Proceedings No.288 Advisory Group for Aerospace Research and Development, NATO EFFECT OF SERVICE ENVIRONMENT ON COMPOSITE MATERIALS Published August 1980 338 pages This meeting consisted of 21 presentations divided into 5 sessions: – Physico-Chemical Effects of Environment – Environment Superimposed on Stressing – Mechanical Effects and Hazards – Physical Hazards (lightning, rain erosion . . .) – Case Studies of Service Experience. P.T.O.	AGARD-CP-288 Composite materials Service life Wear Erosion Fatigue (materials) Damage Weathering Lightning Environmental tests	AGARD Conference Proceedings No.288 Advisory Group for Aerospace Research and Development, NATO EFFECT OF SERVICE ENVIRONMENT ON COMPOSITE MATERIALS Published August 1980 338 pages This meeting consisted of 21 presentations divided into 5 sessions: – Physico-Chemical Effects of Environment – Environment Superimposed on Stressing – Mechanical Effects and Hazards – Physical Hazards (lightning, rain erosion . . .) – Case Studies of Service Experience. P.T.O.	AGARD-CP-288 Composite materials Service life Wear Erosion Fatigue (materials) Damage Weathering Lightning Environmental tests
AGARD Conference Proceedings No.288 Advisory Group for Aerospace Research and Development, NATO EFFECT OF SERVICE ENVIRONMENT ON COMPOSITE MATERIALS Published August 1980 338 pages This meeting consisted of 21 presentations divided into 5 sessions: – Physico-Chemical Effects of Environment – Environment Superimposed on Stressing – Mechanical Effects and Hazards – Physical Hazards (lightning, rain erosion . . .) – Case Studies of Service Experience. P.T.O.	AGARD-CP-288 Composite materials Service life Wear Erosion Fatigue (materials) Damage Weathering Lightning Environmental tests	AGARD Conference Proceedings No.288 Advisory Group for Aerospace Research and Development, NATO EFFECT OF SERVICE ENVIRONMENT ON COMPOSITE MATERIALS Published August 1980 338 pages This meeting consisted of 21 presentations divided into 5 sessions: – Physico-Chemical Effects of Environment – Environment Superimposed on Stressing – Mechanical Effects and Hazards – Physical Hazards (lightning, rain erosion . . .) – Case Studies of Service Experience. P.T.O.	AGARD-CP-288 Composite materials Service life Wear Erosion Fatigue (materials) Damage Weathering Lightning Environmental tests

TECHNICAL LIBRARY
ABBOTTAEROSPACE.COM

The effects of humidity and of impacts, particularly when tests were made in compression, were emphasized. Damage due to lightning appeared to be less serious than had previously been supposed.

Some theories were propounded for the calculation of erosion, for the prediction of properties in a vacuum and for fatigue damage.

Service experience, on the other hand, proves to be extremely favourable and has not shown, up until now, any evidence of disturbing phenomena.

Papers presented at the 50th Meeting of the AGARD Structures and Materials Panel, held in Athens, Greece on 14–17 April 1980.

ISBN 92-835-0273-6

The effects of humidity and of impacts, particularly when tests were made in compression, were emphasized. Damage due to lightning appeared to be less serious than had previously been supposed.

Some theories were propounded for the calculation of erosion, for the prediction of properties in a vacuum and for fatigue damage.

Service experience, on the other hand, proves to be extremely favourable and has not shown, up until now, any evidence of disturbing phenomena.

Papers presented at the 50th Meeting of the AGARD Structures and Materials Panel, held in Athens, Greece on 14–17 April 1980.

ISBN 92-835-0273-6

The effects of humidity and of impacts, particularly when tests were made in compression, were emphasized. Damage due to lightning appeared to be less serious than had previously been supposed.

Some theories were propounded for the calculation of erosion, for the prediction of properties in a vacuum and for fatigue damage.

Service experience, on the other hand, proves to be extremely favourable and has not shown, up until now, any evidence of disturbing phenomena.

Papers presented at the 50th Meeting of the AGARD Structures and Materials Panel, held in Athens, Greece on 14–17 April 1980.

ISBN 92-835-0273-6

The effects of humidity and of impacts, particularly when tests were made in compression, were emphasized. Damage due to lightning appeared to be less serious than had previously been supposed.

Some theories were propounded for the calculation of erosion, for the prediction of properties in a vacuum and for fatigue damage.

Service experience, on the other hand, proves to be extremely favourable and has not shown, up until now, any evidence of disturbing phenomena.

Papers presented at the 50th Meeting of the AGARD Structures and Materials Panel, held in Athens, Greece on 14–17 April 1980.

ISBN 92-835-0273-6

TECHNICAL LIBRARY
ABBOTTAEROSPACE.COM

TECHNICAL LIBRARY
ABBOTTAEROSPACE.COM

B138
4

AGARD
NATO OTAN
7 RUE ANCELLE · 92200 NEUILLY-SUR-SEINE
FRANCE
Telephone 745.08.10 · Telex 610176

DISTRIBUTION OF UNCLASSIFIED AGARD PUBLICATIONS

AGARD does NOT hold stocks of AGARD publications at the above address for general distribution. Initial distribution of AGARD publications is made to AGARD Member Nations through the following National Distribution Centres. Further copies are sometimes available from these Centres, but if not may be purchased in Microfiche or Photocopy form from the Purchase Agencies listed below.

NATIONAL DISTRIBUTION CENTRES

BELGIUM
Coordonnateur AGARD – VSL
Etat-Major de la Force Aérienne
Quartier Reine Elisabeth
Rue d'Evere, 1140 Bruxelles

CANADA
Defence Science Information Services
Department of National Defence
Ottawa, Ontario K1A OK2

DENMARK
Danish Defence Research Board
Østerbrogades Kaserne
Copenhagen Ø

FRANCE
O.N.E.R.A. (Direction)
29 Avenue de la Division Leclerc
92320 Châtillon sous Bagneux

GERMANY
Fachinformationszentrum Energie,
Physik, Mathematik GmbH
Kernforschungszentrum
D-7514 Eggenstein-Leopoldshafen 2

GREECE
Hellenic Air Force General Staff
Research and Development Directorate
Holargos, Athens

ICELAND
Director of Aviation
c/o Flugrad
Reykjavik

ITALY
Aeronautica Militare
Ufficio del Delegato Nazionale all'AGARD
3, Piazzale Adenauer
Roma/EUR

LUXEMBOURG
See Belgium

NETHERLANDS
Netherlands Delegation to AGARD
National Aerospace Laboratory, NLR
P.O. Box 126
2600 A.C. Delft

NORWAY
Norwegian Defence Research Establishment
Main Library
P.O. Box 25
N-2007 Kjeller

PORTUGAL
Direcção do Serviço de Material
da Força Aerea
Rua da Escola Politécnica 42
Lisboa
Attn: AGARD National Delegate

TURKEY
Department of Research and Development (ARGE)
Ministry of National Defence, Ankara

UNITED KINGDOM
Defence Research Information Centre
Station Square House
St. Mary Cray
Orpington, Kent BR5 3RE

UNITED STATES
National Aeronautics and Space Administration (NASA)
Langley Field, Virginia 23365
Attn: Report Distribution and Storage Unit

THE UNITED STATES NATIONAL DISTRIBUTION CENTRE (NASA) DOES NOT HOLD STOCKS OF AGARD PUBLICATIONS, AND APPLICATIONS FOR COPIES SHOULD BE MADE DIRECT TO THE NATIONAL TECHNICAL INFORMATION SERVICE (NTIS) AT THE ADDRESS BELOW.

PURCHASE AGENCIES

Microfiche or Photocopy
National Technical
Information Service (NTIS)
5285 Port Royal Road
Springfield
Virginia 22161, USA

Microfiche
Space Documentation Service
European Space Agency
10, rue Mario Nikis
75015 Paris, France

Microfiche
Technology Reports
Centre (DTI)
Station Square House
St. Mary Cray
Orpington, Kent BR5 3RF
England

Requests for microfiche or photocopies of AGARD documents should include the AGARD serial number, title, author or editor, and publication date. Requests to NTIS should include the NASA accession report number. Full bibliographical references and abstracts of AGARD publications are given in the following journals:

Scientific and Technical Aerospace Reports (STAR)
published by NASA Scientific and Technical
Information Facility
Post Office Box 8757
Baltimore/Washington International Airport
Maryland 21240, USA

Government Reports Announcements (GRA)
published by the National Technical
Information Services, Springfield
Virginia 22161, USA

Printed by Technical Editing and Reproduction Ltd
Harford House, 7–9 Charlotte St, London W1P 1HD

ISBN 92-835-0273-6